Quantifizierung von Proteinaggregaten zur Diagnose neurodegenerativer Erkrankungen mit der sFIDA-Technologie

Inaugural-Dissertation

zur Erlangung des Doktorgrades
der Mathematisch-Naturwissenschaftlichen Fakultät
der Heinrich-Heine-Universität Düsseldorf

vorgelegt von

Lara Anna Blömeke
aus Volkmarsen

Warburg, Februar 2023

aus dem Institut für Physikalische Biologie
der Heinrich-Heine-Universität Düsseldorf

Gedruckt mit der Genehmigung der
Mathematisch-Naturwissenschaftlichen Fakultät der
Heinrich-Heine-Universität Düsseldorf

Berichterstatter:

1. Prof. Dr. Dieter Willbold
2. Prof. Dr. Henrike Heise
3. Prof. Dr. Heinrich Sticht

Tag der mündlichen Prüfung: 26.03.2024

Eidesstattliche Erklärung

Hiermit erkläre ich an Eides statt, dass ich die vorliegende Dissertation selbstständig verfasst und keine anderen als die von mir angegebenen Quellen und Hilfsmittel verwendet und Zitate kenntlich gemacht habe.
Ferne erkläre ich, dass ich in keinem anderen Dissertationsverfahren mit oder ohne Erfolg versucht habe, diese Dissertation einzureichen.

Warburg, den

_____

(Lara Blömeke)

Danksagung

Viele Menschen haben mich während meiner Arbeit unterstützt, bei denen ich mich von Herzen bedanken möchte.

Mein besonderer Dank gilt Herrn Prof. Dr. Dieter Willbold für die Möglichkeit, meine Dissertation in seinem Institut am Forschungszentrum in Jülich und der Heinrich-Heine-Universität durchführen zu können und für die vielen spannenden Projekte, die ich im Rahmen meiner Promotion bearbeiten durfte. Außerdem danke ich ihm für die zahlreichen fachlichen Diskussionen und den Freiraum bei der Planung und Durchführung der Projekte, die mir zusammen mit seiner fortlaufenden Unterstützung und Ermutigung in meiner persönlichen Entwicklung sehr geholfen haben.

Außerdem möchte ich Frau Prof. Dr. Henrike Heise und Herrn Prof. Dr. Heinrich Sticht für die Übernahme der Zweit- und Drittgutachten danken.

Ein besonderer Dank gilt insbesondere Dr. Oliver Bannach, der ab dem ersten Tag immer für Fragen offen war und der mich durch seine optimistische Art immer wieder dazu ermutigt hat, an mich und meine Ergebnisse zu glauben. An dieser Stelle möchte ich mich auch bei der gesamten sFIDA-Gruppe, insbesondere bei Marlene Pils und Victoria Kraemer-Schulien bedanken, die mir so viel beigebracht haben und sowohl fachlich als auch persönlich immer an meiner Seite standen. Anne Cousin und Sandra Kienast danke ich für die tolle Unterstützung im Labor und dass man sich immer auf sie verlassen kann. Bei Dr. Andreas Kulawik und Fabian Rehn bedanke ich mich dafür, dass sie mich bei der Statistik und Datenauswertung unterstützt und mich dafür begeistert haben. Dr. Tuyen Bujnicki und Prof. Dr. Gültekin Tamgüney danke ich für die fachliche Unterstützung und die vielen Ideen. Prof. Dr. Oliver Peters danke ich für die erfolgreiche und interessante Kooperation im Rahmen der DELCODE-Studie und die Bereitstellung der Plasmaproben.

Außerdem möchte ich mich bei meinen Freunden, Eltern und Geschwistern für ihren Rückhalt und ihr Vertrauen bedanken. Mein größter Dank gilt Benny, der immer hinter mir stand und mich fortlaufend motiviert und mir immer den Rücken freigehalten hat!

Vielen Dank euch allen!

Gender-Hinweis

Die in dieser Arbeit verwendeten Personenbezeichnungen beziehen sich immer gleichermaßen auf alle Geschlechter, sofern nicht anderweitig kenntlich gemacht. Auf eine Doppelnennung und gegenderte Bezeichnungen wird zugunsten einer besseren Lesbarkeit verzichtet.

Publikationsliste

- **Blömeke L.**, Pils M., Kraemer-Schulien V., Dybala A., Schaffrath A., Kulawik A., Rehn F., Cousin A., Nischwitz V., Willbold J., Zack R., Tropea TF., Bujnicki T., Tamgüney G., Weintraub D., Irwin D., Grossman M., Wolk DA., Trojanowski JQ., Bannach O., Chen-Plotkin A., Willbold D. (2022) Quantitative detection of α-Synuclein and Tau oligomers and other aggregates by digital single particle counting. *NPJ Parkinsons Disease (veröffentlicht)*

- Kutzsche J.*, Schemmert S.*, Bujnicki T.*, Zafiu C., Halbgebauer S., Kraemer-Schulien V., Pils M., **Blömeke L.**, Post J., Kulawik A., Jürgens D., Rossberg W., Hümpel M., Bannach O., Otto M., Araujo J., Antje Willuweit A., Willbold D. (2023) Oral treatment with the all-D-peptide RD2 enhances cognition in aged beagle dogs – a model of sporadic Alzheimer's disease. *Heliyon (veröffentlicht)*

- **Blömeke L.*,** Rehn F.*, Kraemer-Schulien V.*, Kutzsche J., Pils M., Bujnicki T., Lewczuk P., Kornhuber J., Freiesleben S., Schneider L., Preis L., Priller J., Spruth E., Altenstein A., Lohse A., Schneider A., Fliessbach K., Wiltfang J., Hansen N., Rostamzadeh A., Düzel E., Glanz W., I. Incesoy E., Butryn M., Buerger K., Janowitz D., Ewers M., Perneczky R., Rauchmann B., Teipel S., Kilimann I., Goerss D., Laske C., Munk M., Sanzenbacher C., Spottke A., Roy-Kluth N., T. Heneka M., Brosseron F., Wagner M., Wolfsgruber S., Kleineidam K., Stark M., Schmid M., Jessen F., Bannach O., Willbold D., Peters O. (2023) Aβ oligomers peak in early stages of Alzheimer's disease preceding Tau pathology. *Alzheimer's & Dementia (veröffentlicht)*

- **Blömeke L.**, Rehn F., Pils M., Kraemer-Schulien V., Cousin A., Kutzsche J., Bujnicki T., Freiesleben S., Schneider L., Preis L., Priller J., Spruth E., Altenstein S., Schneider A., Fliessbach K., Wiltfang J., Hansen N., Rostamzahdeh A., Düzel E., Glanz W., Incesoy E., Buerger K., Janowith D., Ewers M., Perneczky R., Rauchmann B., Teipel S., Kilimann I., Laske C., Munk M., Spottke A., Roy N., Heneka M., Brosseron F., Wagner M., Roeske S., Raminez A., Schmid M., Jessen F., Bannach O., Peters O., Willbold D. (2023) Blood-based quantification of Aβ oligomers indicates impaired clearance from the brain in ApoE ε4 positive subjects. *Communications Medicine (im Review)*

- Pils M., Dybala A., Schaffrath A., Rehn F., Kutzsche J., **Blömeke L.**, Tusche M., Bujnicki T., Kraemer-Schulien V., Fink G., Gramespacher H., Barbe M., Onur Ö., Tamgüney G., Bannach O., Willbold D. (2023) Elevated Aβ aggregates in feces from Alzheimer's disease patients: a proof-of-concept study. *Alzheimer's Research and Therapy (im Review)*

- Schaffrath A., Schleyken S., Seger A., Jergas H., Özdüzenciler P., Pils M., **Blömeke L.**, Cousin A., Willbold J., Bujnicki T., Bannach O., Fink GR., Willbold D., Sommerauer M., Barbe MT., Tamgüney G. (2023) Patients with isolated REM-sleep behavior disorder have elevated levels of alpha-synuclein aggregates in stool. *NPJ Parkinsons Disease (veröffentlicht)*
- Pils M., Dybala A., Rehn F., **Blömeke L.**, Bujnicki T., Kraemer-Schulien V., Riesner D., Willbold D., Bannach O. (2023) Development and Implementation of an Internal Quality Control Sample to Standardize Oligomer-Based Diagnostics of Alzheimer's Disease. *Diagnostics (veröffentlicht)*
- Eberle, R., Coronado M., Gering I., Korostov K., Stefanski, A., Stühler K., Kraemer-Schulien V., **Blömeke L.**, Bannach O., Willbold D. (2023) Tau protein aggregation associated with SARS-CoV-2 main protease. *PLOS ONE (veröffentlicht)*

* Autoren sind gleichberechtigt

Inhaltsverzeichnis

Abkürzungsverzeichnis

Aβ	Amyloid Beta
AD	Alzheimer-Demenz, Alzheimer-Krankheit
AD-K	Alzheimer-Kontinuum
ApoE	Apolipoprotein E
APP	Amyloid-Vorläuferprotein (*amyloid precursor protein*)
αSyn	Alpha Synuclein
BSA	Bovines Serumalbumin
BSE	Bovine spongiforme Enzephalopathie
CBD	Corticobasale Degeneration
CD7	*Celldiscoverer 7* (Fluoreszenzmikroskop von Zeiss)
CJD	Creutzfeld-Jakob-Krankheit
CSF	Cerebrospinalflüssigkeit
CVD	Cerebrovaskuläre Demenz
DELCODE	*DZNE-longitudinal cognitive impairment and dementia study*
DGN	Deutsche Gesellschaft für Neurologie
DGPPN	Deutsche Gesellschaft für Psychiatrie und Psychotherapie, Psychosomatik und Nervenheilkunde
DLB	Demenz mit Lewy Körperchen (*dementia with lewy bodies*)
EDTA	Ethylendiamintetraacetat
ELISA	Enzymgekoppelter Immunadsorptionstest (*enzyme linked immunosorbent assay*)
EMCCD	*Electron multiplying charge-coupled device*
FTD	Frontotemporale Demenz
ICP-MS	Massenspektrometrie mit induktiv-gekoppeltem Plasma
iRBD	Idiopathische REM-Schlaf-Verhaltensstörung (*idiopathic rapid eye movement (REM) sleep behavior disorder*)
ISF	Interstitialflüssigkeit
K_D	Dissoziationskonstante
LLOQ	Quantifizierungsgrenze (*lower limit of quantification*)
LOD	Detektionsgrenze (*limit of detection*)
MCI	Milde kognitive Einschränkung (*mild cognitive impairment*)
MDS	*Movement disorder society*

MRT	Magnetresonanztomographie
MSA	Multiple Systematrophie
NFT	Neurofibrilläre Bündel (*neurofibrillary tangles*)
PD	Parkinson-Krankheit
PET	Positronen-Emissions-Tomographie
PHF	Gepaarte helikale Filamente (*paired helical filaments*)
PSP	*Progressive supranuclear palsy*
SCD	Subjektive kognitive Einschränkung (*subjective cognitive decline*)
SF	*Straight filament*
sFIDA	*Surface-based fluorescence intensity distribution analysis*
SiNaP	Silika-Nanopartikel
SPECT	Einzelphotonen-Emissionscomputertomotraphie (*single photon emission computed tomography*)
TDM	Therapeutisches Drug Monitoring
TDP-43	*Transactivation response DNA binding protein 43*
TIRF	Interne Totalreflexionsfluoreszenzmikroskopie (*Total internal reflection fluorescence microscopy*)
UPDRS	Skala zur Verlaufbeobachtung bei PD (*Unified Parkinson's Disease Rating Scale*)
VD	Vaskuläre Demenz

Tabellenverzeichnis

Abbildungsverzeichnis

Kurzfassung

Der Begriff neurodegenerative Erkrankungen umfasst eine Vielzahl von Krankheiten wie die Alzheimer- (AD) oder die Parkinson-Krankheit (PD), die durch Proteinablagerungen und das fortschreitende Absterben von Nervenzellen charakterisiert sind. Weniger häufige, allerdings in ihrer Symptomatik ähnliche Erkrankungen sind z.B. die Lewy-Körperchen-Demenz (DLB) und die progressive supranukleäre Blickparese (PSP). Da das Alter der wichtigste Risikofaktor für das Auftreten dieser Erkrankungen darstellt, nimmt die Prävalenz und dadurch sowohl die persönliche als auch die ökonomische Bedeutung der neurodegenerativen Erkrankungen durch den demographischen Wandel weiter zu. Zum jetzigen Zeitpunkt können die Erkrankungen allerdings weder geheilt noch das Fortschreiten gestoppt werden. Eine Ursache für die fehlenden Therapien sind u.a. ungenaue und zu späte Diagnosestellungen.

Als direkte Zwischenstufen auf dem Weg zu den unlöslichen Proteinablagerungen bilden sich lösliche Oligomere, die bereits in Frühstadien auftreten können und als neurotoxisch gelten. Die Quantifizierung dieser Oligomere stellt daher einen direkten Biomarker dar, der sowohl eine frühzeitige Diagnose als auch die Entwicklung neuer Therapieansätze unterstützen kann. Während bei PSP Ablagerungen des Tau-Proteins vorherrschend sind, finden sich bei der Alzheimer-Erkrankung sowohl Amyloid Beta- (Aβ) als auch Tau-Ablagerungen. Im Gegensatz dazu sind PD und DLB durch die Anwesenheit von Lewy-Körperchen gekennzeichnet, die vor allem aus dem Protein alpha Synuclein (αSyn) bestehen.

Die sFIDA-Technologie (*surface-based fluorescence intensity distribution analysis*) wurde entwickelt, um die löslichen Oligomere dieser Proteine quantitativ nachzuweisen. Diese Arbeit diente der Weiterentwicklung der Technologie in Hinblick auf die Quantifizierung in verschiedenen Körperflüssigkeiten wie der Cerebrospinalflüssigkeit (CSF), Blutplasma oder Stuhl. Ein weiteres Augenmerk lag auf dem zeitgleichen Nachweis zweier Proteine in CSF und der Weiterentwicklung von Kalibrationsstandards und Qualitätskontrollen wie rekombinanten Aggregaten.

Die entwickelten Assays wurden zunächst hinsichtlich ihrer analytischen Sensitivität und Selektivität getestet. Hier zeigte sich je nach Analyten und Matrix eine geringe Nachweisgrenze (atto- bis femtomolar) und keine Beeinflussung durch Matrixbestandteile wie monomere Proteine oder heterophile Antikörper. Als Qualitätskontrolle wurden rekombinant hergestellte Proteinaggregate verwendet, wobei insbesondere der Charakterisierung der Aβ-Aggregate ein eigenes Kapitel gewidmet wurde. Im Anschluss an

die Entwicklung der Assays wurden die Oligomerkonzentrationen in Patientenproben u. a. der DELCODE-Kohorte bestimmt.

CSF-Analysen ergaben erhöhte Aβ-Oligomerkonzentrationen bei Patienten mit neuropathologischer AD in Frühstadien der Erkrankung wie milder kognitiver Beeinträchtigung (MCI) und subjektiver kognitiver Einschränkung (SCD), während die Tau-Oligomerkonzentrationen über den Erkrankungsverlauf hinweg unverändert waren. Im Gegensatz dazu waren die Aβ-Oligomerkonzentrationen im Plasma von AD-Patienten reduziert gegenüber den Kontrollen. Unter Berücksichtigung der Amyloid-Pathologie, genetischen Risikofaktoren und Korrelationsanalysen zwischen CSF und Plasma ist eine eingeschränkte Clearance der Oligomere als Erklärung für die geringeren Konzentrationen im Plasma naheliegend. Messbare Aβ-Oligomerkonzentrationen wurden außerdem im Stuhl von Patienten nachgewiesen, wobei AD-Patienten erhöhte Konzentrationen gegenüber den Kontrollen zeigten. Außerdem wurde ein Einfluss des anti-Oligomeren Medikaments RD2 auf die Tau-, allerdings nicht auf die Aβ-Oligomerkonzentrationen im CSF von behandelten Hunden gefunden.

Für die Synucleinopathien PD und DLB wurden erhöhte αSyn-Oligomerkonzentrationen im CSF und für DLB außerdem erhöhte Tau-Oligomerkonzentrationen im CSF festgestellt. Im Gegensatz dazu waren die αSyn-Oligomerkonzentrationen im Stuhl bei Patienten mit idiopathischer Traum-Schlaf-Verhaltensstörung (*REM sleep behaviour disorder*, iRBD), einer Vorstufe von PD, allerdings nicht bei PD-Patienten selbst erhöht.

Mit dieser Arbeit konnte die sFIDA-Technologie weiterentwickelt werden und gezeigt werden, dass die Technologie sensitiv und selektiv Oligomere verschiedener Proteine in unterschiedlichen Körperflüssigkeiten nachweisen kann. Außerdem wurde die Relevanz der Proteinoligomere sowohl für die Diagnose und die Entwicklung von Therapien als auch für die Erforschung der Pathologie neurodegenerativer Erkrankungen, insbesondere in CSF, gezeigt. Vertiefende Bildanalysen, der Austausch oder das Hinzufügen von Antikörpern und die Messung longitudinaler Proben und Proben derselben Patienten in unterschiedlichen Matrices stellen mögliche zukünftige Projekte dar. Diese können zum Verständnis der gemessenen Oligomerkonzentrationen in verschiedenen Körperflüssigkeiten und Erkrankungen beitragen und bei der gezielten Optimierung der Verfahren helfen.

Abstract

Neurodegenerative diseases include a variety of diseases such as Alzheimer's disease (AD) or Parkinson's disease (PD), which are characterized by protein deposition and neuronal loss. Less common diseases but similar in symptomatology are dementia with Lewy bodies (DLB) and progressive supranuclear palsy (PSP). As age is the most important risk factor for these diseases, the prevalence and thus both the personal and economic burden of neurodegenerative diseases continues to increase due to demographic change. However, the diseases can still not be cured, or their progression stopped. One reason for missing therapies is an inaccurate and late diagnosis.

On the way to insoluble protein deposits, soluble intermediates called oligomers form, which can already exist in early progression stages. Therefore, quantification of these oligomers presents a direct biomarker which can support both early diagnosis and the development of new therapies. While deposits of Tau protein are predominant in PSP, Amyloid beta (Aβ) as well as Tau deposits are markers of AD. In contrast, PD and DLB are characterized by the presence of Lewy bodies which are primarily composed of the protein alpha synuclein (αSyn).

The sFIDA (*surface-based fluorescence intensity distribution analysis*) technology was developed for quantification of soluble oligomers of these proteins. This work aimed to further develop the technology with respect to detection in various body fluids including cerebrospinal fluid (CSF), blood plasma, or stool. Further attention was given to the simultaneous detection of two proteins in CSF and the optimization of calibration standards and quality controls such as recombinant aggregates.

The developed assays were first tested regarding their analytical sensitivity and selectivity. Here, depending on the analytes and matrix, a low detection limit (atto- to femtomolar LOD) and no interference by matrix components like monomeric proteins or heterophilic antibodies was shown. Aggregates of recombinant protein were used as quality control, with a separate chapter focusing on the characterization of Aβ-aggregates. Following assay development, oligomer concentrations were determined in patient samples from the DELCODE cohort and others.

CSF analyses revealed increased Aβ oligomer concentrations in CSF from patients with neuropathological AD in early stages of the disease, such as mild cognitive impairment (MCI) and subjective cognitive decline (SCD), whereas Tau oligomer concentrations were not altered dependent on progression stages. In contrast, plasma Aβ oligomer concentrations in AD patients were reduced compared to control samples. Considering amyloid pathology, genetic risk factors, and correlation analyses between CSF and plasma,

impaired clearance of oligomers may explain lower concentrations in plasma. Measurable oligomer concentrations were also found in the stool samples of patients, with AD patients showing increased concentrations compared to healthy controls. In addition, an effect of the anti-oligomeric compound RD2 was found on Tau, but not Aβ oligomer concentrations in CSF from treated dogs.

αSyn oligomer concentrations in CSF were increased for the synucleinopathies PD and DLB with DLB showing increased Tau oligomer concentrations in CSF as well. In contrast, fecal αSyn oligomer concentrations were elevated in patients with idiopathic REM sleep behavior disorder (iRBD), a precursor of PD, but not in PD patients themselves.

This work further developed the sFIDA technology and demonstrated that the technology can sensitively and selectively detect oligomers of various proteins in different body fluids. Furthermore, the relevance of protein oligomers for both diagnosis and development of therapies as well as for the study of the pathology of neurodegenerative diseases, especially in CSF, was demonstrated. More in-depth image analysis, replacement or addition of antibodies, and measurement of longitudinal samples and samples from the same patients in different matrices represent possible future projects. These projects may contribute to the understanding of the measured oligomer concentrations in different body fluids and diseases and help to specifically optimize the methods.

1 Einleitung

Neurodegenerative Erkrankungen stellen aufgrund ihrer steigenden Prävalenz und des Fehlens kausativer Therapien eine große Herausforderung sowohl für Betroffene und Angehörige als auch für das Gesundheitssystem dar [1]. Unter neurodegenerativen Erkrankungen versteht man eine Gruppe von Krankheiten des zentralen Nervensystems, die durch Ablagerungen von intra- oder extrazellulären Proteinaggregaten und damit zusammenhängend dem Verlust von Neuronen charakterisiert sind [2]. Die Einteilung der neurodegenerativen Erkrankungen kann dabei entweder anhand ihrer klinischen Erscheinung, z.B. in Demenzen wie die Alzheimer-Demenz (AD), Parkinsonismus wie die Parkinson-Erkrankung (PD) und Motoneuronerkrankungen wie die Amyotrophe Lateralsklerose, oder anhand der maßgeblich beteiligten aggregierten Proteine erfolgen. Eine Auswahl über die aggregierten Proteine und den damit zusammenhängenden Erkrankungen ist in Tabelle 1 aufgeführt [3, 4]. Im Folgenden werden zunächst die Erkrankungen, die in der vorliegenden Arbeit thematisiert wurden, näher erläutert. Im Anschluss daran wird genauer auf die beteiligten aggregierten Proteine und die sFIDA-Technologie eingegangen.

Tabelle 1 Aggregierte Proteine und assoziierte neurodegenerative Erkrankungen

Protein	**Erkrankung**
Amyloid-β (Aβ)	Alzheimer-Demenz (AD)
Tau	Alzheimer-Demenz Progressive supranukleäre Blickparese (PSP) Frontotemporale Demenz (FTD) Corticobasale Degeneration (CBD) Chronisch-traumatische Enzephalopathie (CTE)
α-Synuclein (αSyn)	Parkinson Erkrankung (PD) Multiple Systematrophie (MSA) Demenz mit Lewy-Körperchen (DLB)
Prion-Protein	Creutzfeldt-Jakob-Erkrankung (CJD) Bovine spongiforme Enzephalopathie (BSE) Chronic Wasting Disease (CWD) Scrapie/Traberkrankheit
Transactivation response DNA binding protein 43 (TDP-43)	Frontotemporale Demenz Amyotrophe Lateralsklerose

1.1 Neurodegenerative Erkrankungen

In dieser Arbeit wurde insbesondere mit Proben von Alzheimer- und Parkinson-Patienten gearbeitet. Zusätzlich wurden Proben von DLB und PSP-Patienten gemessen, die eine ähnliche klinische Ausprägung wie PD-Patienten zeigen können und daher als atypische Parkinsonerkrankungen bezeichnet werden.

1.1.1 Alzheimer-Demenz

Überblick

Die Alzheimer-Demenz (AD) ist mit ca. 60 % aller Demenzen die häufigste Form der Demenz und mit weltweit 44 Millionen Betroffenen die häufigste neurodegenerative Erkrankung [1, 2, 5]. In Deutschland lag die Prävalenz (die Häufigkeit von Alzheimer in einer bestimmten Bevölkerungsgruppe) im Jahr 2021 bei den über 65-jährigen bei 8,5 % [6] und wird durch die höhere Lebenserwartung – Kalkulationen zufolge – bis zum Jahr 2060 auf 34 % steigen [7, 8]. Das erste Mal beschrieben wurde die Erkrankung im Jahr 1906 von Alois Alzheimer, der im Gehirn einer Patientin Ablagerungen der Proteine Aβ („Plaques“) und Tau („Neurofibrillen“) gefunden hat [9].

Für die Alzheimer-Demenz gibt es verschiedene Definitionen: im klinischen Alltag wird AD als Erkrankung definiert, die sich primär durch kognitive Beeinträchtigungen des Patienten äußert, insbesondere in Bezug auf das Erinnerungsvermögen, die Orientierung, Sprachstörungen und Beeinträchtigungen des logischen Denkens [10, 11]. In den letzten Jahren hat sich die Definition von AD, besonders im Forschungsrahmen, von einer symptomatischen zu einer biologischen Betrachtung gewandelt, sodass für die Diagnose einer Alzheimer-Erkrankung Evidenz für Aβ (Kapitel 1.2.1) und Tau-assoziierte Ablagerungen (Kapitel 1.2.2) in Form von Biomarkern vorliegen müssen (s. Einteilung) [12].

Durch den progressiven Verlauf der Erkrankung und der daraus resultierenden Pflegebedürftigkeit in fortgeschrittenen Stadien hat die Erkrankung nicht nur eine hohe persönliche Beeinträchtigung zur Folge, sondern beeinflusst auch das Leben von Angehörigen und Pflegenden und hat einen großen ökonomischen Einfluss [13]. Einer Studie aus dem Jahr 2021 aus den USA zufolge liegen die jährlichen Kosten für das Gesundheitssystem bei Demenz-Patienten mehr als dreimal höher als bei Patienten ohne Demenz [8].

Pathophysiologie

AD ist aus pathologischer Sicht durch die Ablagerung von extrazellulären Aβ-Plaques und intrazellulären neurofibrillären Bündeln des Tau-Proteins (NFTs) charakterisiert, die bereits 15 Jahre vor dem ersten Auftreten von Symptomen nachgewiesen werden können. Diese Ablagerungen zeigen je nach Stadium der Erkrankung eine unterschiedliche Ausbreitung im Gehirn. Aβ-Ablagerungen breiten sich von der Großhirnrinde über das limbische System in den Hirnstamm und ins Kleinhirn aus, zeigen aber keinen Zusammenhang mit der Kognition des Patienten. Tau-Ablagerungen treten im Vergleich zu Aβ-Ablagerungen verzögert zunächst im entorhinalen Cortex, im weiteren Verlauf im Hippocampus und in Bereichen des limbischen Systems und bei vollständig ausgeprägter AD in der Großhirnrinde auf und korrelieren stärker mit der Symptomatik [14-16].

Ablagerungen von Aβ und Tau sind zwar charakteristisch für AD, als toxische Komponenten werden allerdings die Vorstufen, lösliche Aβ- und Tau-Oligomere, verantwortlich gemacht. Für Aβ-Oligomere konnte gezeigt werden, dass sie die synaptische Weiterleitung zwischen Neuronen und damit das Erinnerungsvermögen und die Verarbeitung neuer Informationen beeinflussen. Außerdem können Aβ-Oligomere direkt, z.B. durch Permeabilisierung von Zellmembranen, oder indirekt durch die Aktivierung von Mikrogliazellen und Astrozyten die Zerstörung von Neuronen und Entzündungsreaktionen im Gehirn herbeiführen. Zusätzlich werden durch Aβ-Oligomere die Hyperphosphorylierung und die Aggregation von Tau ausgelöst [17].

Trotz der Einigkeit über die Rolle von Aβ und Tau bei der Entwicklung und dem Fortschreiten der Erkrankung, wird die Ursache für die Aggregation von Aβ und die Entstehung der Erkrankung kontrovers diskutiert. Im Allgemeinen werden zwei Formen von AD unterschieden: ca. 1 % der Patienten leiden unter einer genetisch bedingten, früh auftretenden Form von AD, wohingegen die sporadische Form am häufigsten ist und meist ab dem 65. Lebensjahr auftritt [13]. Bei der genetisch bedingten, früh auftretenden Form von AD kommt es aufgrund verschiedener Mutationen zu einer vermehrten Bildung von Aβ (s. Produktion). Im Gegensatz dazu ist die Produktion von Aβ bei sporadischer AD nicht beeinflusst, vielmehr wird eine reduzierte Reinigung des Gehirns (Clearance) als Ursache für erhöhte Konzentrationen und die Aggregation von Aβ diskutiert [18]. Der bekannteste genetische Risikofaktor für die Entstehung von sporadischer AD ist das Apolipoprotein E (ApoE), dass in drei verschiedenen Ausprägungen (ε2, ε3, ε4) vorkommen kann, wobei das ε4-Allel mit einem erhöhten und das ε2-Allel mit einem reduzierten Risiko für die Entwicklung von AD einhergeht. ApoE gehört zu den Aβ-bindenden Lipoproteinen und beeinflusst sowohl die Aggregation als auch die Reinigung von Aβ aus dem Gehirn [16, 19].

Diagnose

Durch die beiden unterschiedlichen Definitionen von AD nach klinischem Erscheinungsbild und neurobiologischen Biomarkern ergeben sich auch Unterschiede in Bezug auf die Diagnose. Die routinemäßige Diagnostik beruht primär auf der klinischen Erscheinung und den Symptomen des Patienten, wohingegen im Rahmen von klinischen Forschungen Evidenz für pathologische Veränderungen im Gehirn in Form von Biomarkern im CSF oder bildgebenden Verfahren vorliegen müssen [12]. Aufgrund des aktuellen Wandels in der Eingruppierung von Patienten und dem Einfluss auf die gemessenen Proben in dieser Arbeit, sollen im Folgenden beide Herangehensweisen erläutert werden.

In Deutschland werden Empfehlungen bezüglich Diagnose, aber auch Therapiemöglichkeiten in den Leitlinien der Fachgesellschaften auf Grundlage aktueller wissenschaftlicher Empfehlungen zusammengefasst und richten sich primär an Ärztinnen und Ärzte und weiteres Fachpersonal, welche mit der jeweiligen Erkrankung zu tun haben. Im Jahr 2016 wurde die aktuelle Fassung der S3-Leitlinie „Demenzen“ veröffentlicht, bei der die „deutsche Gesellschaft für Psychiatrie und Psychotherapie, Psychosomatik und Nervenheilkunde“ (DGPPN) und die „deutsche Gesellschaft für Neurologie“ (DGN) federführend waren. Diese Leitlinie beschreibt unter anderem aktuelle Empfehlungen zur Diagnose und Therapie von AD im klinischen Alltag [11].

Zur allgemeinen klinischen Diagnose einer Demenz wird zunächst eine Anamnese durchgeführt, die eine Zusammenfassung aus dem bisherigen Verlauf, den Erstsymptomen, psychopathologischen Befunden und eine Medikamentenanamnese umfasst. Anschließend wird eine körperliche und psychopathologische Untersuchung durchgeführt, um z.B. kardiovaskuläre, metabolische oder endokrinologische Ursachen auszuschließen. Außerdem werden kognitive und im Fall einer unklaren Ausprägung auch neuropsychologische Tests angewandt. Eine Demenz wird dann diagnostiziert, wenn Veränderungen in mindestens zwei der folgenden Bereiche auftreten: Erinnerungsvermögen, Aufmerksamkeit und Urteilsvermögen, visuell-räumliche Wahrnehmung, Sprache und der Persönlichkeit bzw. des Verhaltens. In einem zweiten Schritt erfolgt die Abgrenzung von AD gegenüber anderen Demenzen wie DLB, vaskulärer Demenz (VD) oder FTD. Körperliche und anamnestische Untersuchungen fokussieren sich dabei auf kardiovaskuläre Risikofaktoren als mögliche Ursache einer vaskulären Demenz, Verhaltensänderungen bei FTD oder Schlaf- und Bewegungsstörungen bei DLB bzw. PD. Im Gegensatz hierzu äußert sich AD primär durch Einschränkungen des Erinnerungsvermögens. Erschwert wird die Diagnose durch das Vorliegen von Co-Pathologien, z.B. VD und AD [10, 11, 20].

Die Bestimmung von Neurodegenerationsmarkern in der Cerebrospinalflüssigkeit (CSF) und bildgebenden Verfahren wie Magnet-Resonanz-Tomographie (MRT) und Positronen-Emissions-Tomographie (PET) werden im klinischen Alltag nur in Ausnahmefällen, z.B. bei einer unklaren Diagnose, und nur in Zusammenhang mit der klinischen Anamnese empfohlen [11, 12, 20].

Im Gegensatz dazu sind diese Marker die Grundlage für die Diagnosestellung im Forschungsalltag. Die Neurodegenerationsmarker umfassen die Bestimmung der 42-Aminosäuren langen Form von Aβ ($Aβ_{1-42}$), Gesamt-Tau (tTau) und phosphoryliertem Tau (pTau) im CSF. Im Rahmen von AD kommt es u.a. aufgrund vom Zelltod von Aβ-produzierenden Neuronen und der Akkumulation von Aβ in Aggregaten im Laufe der Erkrankung zu einer Abnahme von $Aβ_{1-42}$ bzw. des Verhältnisses von $Aβ_{1-42}$ zu $Aβ_{1-40}$ im CSF. Im Gegensatz dazu nimmt die Konzentration von tTau durch den Zelltod von Neuronen und pTau durch die Bildung von NFTs im Verlauf der Erkrankung zu. tTau wird dabei als allgemeiner Neurodegenerationsmarker verwendet, wohingegen pTau ein Marker für die Bildung von AD-assoziierten NFTs ist [13, 21-23].

Mit Hilfe der bildgebenden Verfahren können Aussagen über die Ausbreitung neurodegenerativer Veränderungen im Gehirn getroffen werden. Im MRT können entzündliche, aber auch strukturelle Veränderungen sichtbar gemacht werden. Entsprechend dient das MRT nicht nur dem Ausschluss anderer Ursachen, wie Tumoren oder entzündlichen Hirnerkrankungen, sondern kann, besonders bei wiederholten Messungen, Auskunft über neurodegenerative Veränderungen geben, die sich durch eine Abnahme der Hirnmasse in verschiedenen Gehirnregionen äußert [24].

Bei PET-Aufnahmen können bestimmte Stoffwechselprozesse, aber auch Aβ und Tau-Ablagerungen sichtbar gemacht werden. Hierfür werden dem Patienten radioaktiv-markierte Liganden gespritzt, deren Verteilung im Gehirn anschließend gemessen wird. Drei verschiedene Formen des PET haben sich zur Diagnose der AD etabliert: Bei verringerter neuronaler Aktivität nimmt die Stoffwechselaktivität in bestimmten Gehirnregionen ab. Diese Stoffwechselaktivitäten lassen sich durch reduzierte Aufnahme von radioaktiv markierter Glukose im ^{18}F-Fluorodeoxyglukose-PET (FDG-PET) sichtbar machen. Im Amyloid-PET werden radioaktive Liganden wie Florbetapir, Florbetaben oder Flutemetamol verabreicht, die sich spezifisch an Amyloid-Plaques anlagern und dadurch AD-assoziierte Veränderungen im Gehirn sichtbar machen. Beim Tau-PET hingegen werden NFTs markiert, die stärker mit dem Erkrankungsstadium und der kognitiven Verfassung des Patienten korrelieren, allerdings auch bei anderen neurodegenerativen Erkrankungen vorkommen können [24-26].

Die Genauigkeit von Biomarkern wird durch die Kennzahlen Sensitivität und Spezifität beschrieben. Die Sensitivität gibt den Prozentsatz der korrekt als erkrankt erkannten Patienten an (richtig positiv), während die Spezifität beschreibt, ob bzw. zu welchem Prozentsatz gesunde Patienten die richtige Diagnose erhalten haben (richtig negativ) (Tabelle 2) [27]. Je höher die Sensitivität und Spezifität eines Verfahrens, desto besser ist es für eine Diagnosestellung geeignet.

Tabelle 2 Beispiel für die Erklärung der Begriffe Spezifität und Sensitivität

	erkrankt	**nicht erkrankt**
Diagnose erkrankt	85	9
Diagnose gesund	15	91
	➔ 85 % Sensitivität	➔ 91 % Spezifität

Die Spezifität und Sensitivität der verschiedenen Biomarker im CSF und der bildgebenden Verfahren wurde im letzten Jahrzehnt eingehend untersucht und in verschiedenen Meta-Analysen zusammengefasst (Tabelle 3). Zwar können AD-Patienten mit hoher Genauigkeit (Spezifität > 80 %) von Gesunden abgegrenzt werden, bei der Abgrenzung zu anderen Formen der Demenz ist die Anzahl falsch-diagnostizierter Patienten allerdings erhöht. Verschiedene Analysen zeigen, dass Spezifität und Sensitivität durch die Kombination verschiedener Biomarker, z.B. Aβ und Tau oder dem Verhältnis von $A\beta_{1\text{-}42}/A\beta_{1\text{-}40}$, oder durch Kombination von Biomarker- und bildgebenden Verfahren erhöht werden können [24, 28-30].

Tabelle 3 Spezifität und Sensitivität von CSF-Biomarkern ($A\beta_{1\text{-}42}$, tTau und pTau) und bildgebenden Verfahren (MRT, PET) für die Unterscheidung von AD zu Gesunden (CI: Konfidenzintervall)

	Spezifität	**Sensitivität**	**Quelle**
$A\beta_{1\text{-}42}$	84 % (95 % CI: 82-87 %)	84 % (95 % CI: 82-86 %)	[31]
tTau	90 % (95 % CI: 86-93 %)	82 % (95 % CI: 76-87 %)	[28]
pTau	83 % (95 % CI: 75-88 %)	80 % (95 % CI: 70-87 %)	[28]
FDG-PET	86 % (95 % CI: 79-91 %)	91 % (95 % CI: 68-94 %)	[26]
Amyloid-PET	84 % (95 % CI: 71-91 %)	90 % (95 % CI: 83-94 %)	[32]
Tau-PET	88 % (95 % CI: 71-95 %)	94 % (95 % CI: 67-97 %)	[25]
MRT	84 % (95 % CI: 80-90 %)	84 % (95 % CI: 81-87 %)	[25]

Jedes der vorgestellten Verfahren hat Vor- und Nachteile. Während CSF aufgrund der direkten Interaktion mit der Interstitialflüssigkeit pathophysiologische Veränderungen im Gehirn widerspiegelt, handelt es sich bei der Liquorentnahme um ein invasives Verfahren mit den damit verbundenen Risiken und Unannehmlichkeiten für den Patienten (s. Probenmatrix). Bildgebende Verfahren hingegen sind zum einen mit hohen Kosten verbunden, zum anderen nur limitiert verfügbar und aufgrund der radioaktiven Strahlung bzw. Anwendung starker Magnetfelder nicht für jeden Patienten geeignet, was eine routinemäßige Anwendung in der AD-Diagnostik einschränkt. Veränderungen im Gehirn treten außerdem viele Jahre vor dem Auftreten erster Symptome ein, sodass eine routinemäßige Diagnosestellung im asymptomatischen Stadium aufgrund fehlender Therapiemöglichkeiten auch ethisch betrachtet fragwürdig ist. Eine Bestimmung von CSF-Biomarkern und bildgebenden Verfahren wird daher im klinischen Alltag nur bei Verdacht auf AD, aber unklarer Diagnosestellung angewendet [24, 25].

Einteilung

Ähnlich wie bei der Definition und Diagnose von AD, hängt auch die Einteilung der Erkrankung vom Anwendungsfeld ab. Im klinischen Alltag wird AD anhand der Schwere der kognitiven Einschränkung in milde, moderate und fortgeschrittene AD eingeteilt. Als Vorstadien der Demenz haben sich die Einteilung in subjektive kognitive Einschränkung (*subjective cognitive decline,* SCD) und milde kognitive Beeinträchtigung (*mild cognitive impairment,* MCI) durchgesetzt. Patienten mit SCD und MCI haben ein erhöhtes Risiko an AD zu erkranken, die Symptome können allerdings auch stabil bleiben oder sich sogar zurückbilden. Außerdem können der kognitiven Einschränkung andere Ursachen der Demenz zugrunde liegen, z.B. DLB oder FTD. Während verminderte kognitive Leistungsfähigkeit bei SCD auf der eigenen, subjektiven Einschätzung beruht, durch neuropsychologische Testverfahren aber nicht nachgewiesen werden kann, lässt sich bei MCI eine messbare Beeinträchtigung in diesen Tests gegenüber einer gleichaltrigen Kontrollgruppe finden. Sobald Tätigkeiten des täglichen Lebens durch die Demenz eingeschränkt sind, spricht man von AD [10, 12, 20, 33].

Im Forschungsalltag hingegeben erfolgt die Einteilung in das Alzheimer-Kontinuum (AD-K), nicht-AD assoziierte Demenzen und unauffällig nach dem Biomarker-Profil (normal) (Abbildung 1). Hierfür wurde der AT(N)-Score entwickelt, wobei A auf abnormes Aβ (Aβ-Plaques gemessen durch Amyloid-PET oder reduziertes $A\beta_{1\text{-}42}$ in CSF), T für abnormes Tau (gemessen durch pTau in CSF oder Tau-PET) und N für Neurodegeneration steht und durch MRT, FDG-PET oder tTau im CSF bestimmt werden kann. Ein auffälliger Amyloid-Status (A+) ist dabei entscheidend für eine Eingruppierung in das AD-Kontinuum.

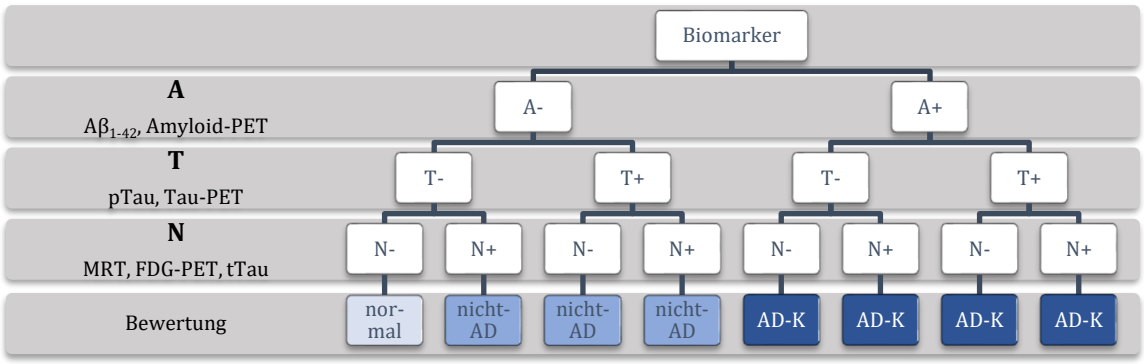

Abbildung 1 Einstufung der Demenzen in Abhängigkeit des Biomarker-Profils
Entscheidend für die Eingruppierung eines Patienten in das Alzheimer-Kontinuum (AD-K) sind Ablagerungen von Aβ (A), die durch reduziertes $A\beta_{1\text{-}42}$ oder Amyloid-PET nachgewiesen werden können. Liegt gleichzeitig eine Tau-Pathologie (T) vor, wird eine AD diagnostiziert. Sind die Amyloid-Biomarker unauffällig, Tau-Biomarker oder Biomarker für Neurodegeneration (N) hingegen auffällig, liegen nicht-AD assoziierte pathologische Veränderungen (nicht-AD) vor. Bei unauffälligen A, T und N-Biomarkern spricht man von einem normalen AD-Biomarker-Profil. Abbildung angelehnt an [12].

Da Veränderungen des Tau-Proteins verzögert zum Aβ auftreten, spricht man bei einem unauffälligem Tau-Status von einem Frühstadium im Alzheimer-Kontinuum, wohingegen eine ausgeprägte Tau-Pathologie (T+) für die vollständige AD-Diagnose entscheidend ist. Eine vorliegende Neurodegeneration (N+) bei unauffälligem Tau-Status (T-) deutet auf eine nicht-AD assoziierte pathologische Veränderung hin, die unabhängig (A-) oder als Co-Pathologie zusätzlich zur Eingruppierung im AD-Kontinuum auftreten kann (A+) [12]. Eine symptomatische Einteilung in sechs verschiedene Stadien kann im Anschluss an die Biomarkereinteilung und nur für Patienten mit auffälligen AD-Biomarkern erfolgen (Abbildung 2). Die Bezeichnung der Gruppen ist hier analog zur Einteilung von AD im klinischen Alltag. Aufgrund der positiven Amyloid-Biomarker liegt allerdings eine zusätzliche Evidenz für AD vor. Die Vorstadien werden deshalb häufig mit dem Zusatz „Alzheimer-Erkrankung", z.B. Alzheimer-Erkrankung mit MCI, gekennzeichnet [12, 33].

Abbildung 2 Symptomatische Einteilung von AD
Innerhalb des Alzheimer-Kontinuums (Patienten mit Amyloid-Pathologie) kann eine weitere Eingruppierung der Patienten in sechs Stufen in Abhängigkeit der kognitiven Einschränkung erfolgen. Während bei normalen Patienten (Stufe 1) weder eine selbst-beobachtete noch eine messbare kognitive Einschränkung festgestellt werden kann, berichten SCD-Patienten (Stufe 2) von einer kognitiven Einschränkung, die im Gegensatz zu MCI-Patienten (Stufe 3) allerdings in kognitiven Tests nicht nachweisbar ist. Abhängig vom Grad der Einschränkung der täglichen Aktivitäten und der Selbstständigkeit der Patienten unterscheidet man innerhalb der AD milde (Stufe 4), moderate (Stufe 5) und fortgeschrittene AD (Stufe 6). Abbildung angelehnt an [33].

Therapie

In Deutschland sind bisher nur Hemmstoffe der Acetylcholinesterase (Donezepil, Rivastagmin und Galantamin) und ein Antagonist des NMDA-Rezeptors (Memantin) zur Therapie von AD zugelassen, die die Symptomatik verringern sollen, aber keinen Einfluss auf das Fortschreiben der Erkrankung haben [11].

Da Aβ und Tau als toxische Komponenten der Erkrankung und möglicherweise auch als Ursache für die Entstehung von AD diskutiert werden, ist eine therapeutische Adressierung dieser Targets naheliegend. Aktuell befinden sich mehrere Medikamente in der klinischen Entwicklung, die verschiedene Strategien verfolgen [21, 34]:

- Verringerung der Produktion von Aβ durch Hemmung der β- und γ-Sekretase
- Erhöhung des Abbaus von Aβ durch Aβ-abbauende Enzyme
- Eliminierung von Aβ-Oligomeren durch kleine Moleküle oder Antikörper
- Aktivierung der Immunantwort durch aktive oder passive Immunisierung
- Therapien gegen Tau

Von diesen Therapieansätzen, die nicht nur die Symptomatik beeinflussen sollen, sondern auch in den Erkrankungsverlauf eingreifen (*Disease modifiying drugs*) wurde im Jahr 2021 der monoklonale Antikörper Aducanumab in den USA für die Therapie von MCI und leichter AD zugelassen. Für diesen Antikörper konnte durch PET-Analysen gezeigt werden, dass Aβ-Plaques im Gehirn aufgelöst werden, wobei die Ergebnisse auf die Verbesserung der Kognition nicht eindeutig waren [35]. Zusätzlich wurden in den Jahren 2022 und 2023 je eine Phase 3 Studie der humanisierten monoklonalen Antikörpers Lecanemab und Donanemab abgeschlossen, in denen für beide Antikörper sowohl eine Verlangsamung des Voranschreitens von kognitiven Symptomen als auch eine Abnahme der Amyloid-Ablagerungen im Gehirn erreicht werden konnte. Im Januar 2023 wurde auch Lecanemab im beschleunigten Zulassungsverfahren in den USA zugelassen [36, 37]. Allerdings zeigten alle drei Antikörper ein erhöhtes Aufkommen von Hirnödemen (*amyloid related imaging abnormality edema*, ARIA-E), insbesondere zu Beginn der Erkrankung, die in den meisten Fällen symptomlos verliefen, in Einzelfällen aber tödlich enden können [37, 38].

Im Gegensatz zu den monoklonalen Antikörpern wird das am Forschungszentrum Jülich entwickelte D-enantiomere Peptid RD2 (Synonyme: PRI-002, Contraloid) oral verabreicht. Für RD2 konnte in präklinischen Studien und Studien der Phase 1 eine Stabilisierung der Aβ-Monomere, ein Auflösen der Aggregate und eine Verbesserung der Kognition in Mäusen gezeigt werden [39]. Außerdem zeigte das Medikament bei Verabreichung in Menschen wenig Nebenwirkungen [40].

Insgesamt können 68 % der in klinischer Phase 3 befindlichen Medikamente zu den *Disease modifying drugs* gezählt werden, 29 % davon mit Aβ als Target. In der klinischen Phase 2 gehören 87 % zu den *Disease modifying Drugs,* wobei 16 % Aβ und 13 % Tau adressieren [41].

Viele getestete Ansätze haben sich in klinischen Studien am Ende als nicht wirksam bezüglich der Verbesserung der kognitiven Leistungsfähigkeit erwiesen oder haben zu große Nebenwirkungen gezeigt. Mögliche Ursachen für den vorherigen Misserfolg der *Disease modifying drugs* sind vielfältig: Zum einen adressierten frühere Therapieansätze monomeres Aβ bzw. Aβ-Plaques, wobei mittlerweile die Oligomere als toxische Komponenten gesehen werden. Außerdem ist die Penetration großer Moleküle, wie z.B. Antikörper, ins Gehirn behindert. Weitere Gründe liegen u.a. in heterogenen Patientengruppen und einem zu späten Therapiebeginn, da pathologische Veränderungen bereits Jahre vor den ersten Symptomen auftreten [34]. In neueren Studien wie der von Aducanumab und Lecanemab konnten durch die Rekrutierung von Patienten in Frühstadien der Erkrankung mit vorliegender Amyloid-Pathologie und durch Adressierung der toxischen Oligomere erste Studien erfolgreich abgeschlossen werden.

1.1.2 Parkinson-Erkrankung

Überblick

Nach der Alzheimer-Demenz ist die Parkinson-Krankheit (PD) die zweithäufigste neurodegenerative Erkrankung und betrifft > 3 % der über 65-jährigen, wobei Männer doppelt so häufig erkranken wie Frauen [42-44]. Das erste Mal beschrieben wurde die „Schüttellähmung“ vor über 200 Jahren von James Parkinson in seinem Werk „An Essay of the shaking palsy“ [45] und erst später in „Morbus Parkinson“ umbenannt. Die Erkrankung äußert sich bereits Jahre oder Jahrzehnte vor der Diagnose durch unspezifische, nicht-motorische Symptome wie Schlafstörungen, Geruchsstörungen und Verstopfung. In der Regel wir die Erkrankung erst nach dem Eintreten motorischer Symptome wie verlangsamte Bewegungen (Bradykinese), Zittern (Tremor) und Muskelsteife (Rigor) diagnostiziert [44].

Pathophysiologie

PD ist durch den Verlust von Dopamin-produzierenden Neuronen in der *Substantia Nigra* und durch intraneuronale αSyn-Ablagerungen in Form von Lewy-Körperchen charakterisiert (s. Kapitel 1.2.3) [44].

Als Ausgangspunkt für die Aggregation von αSyn wird neben dem zentralen (*brain-first)* auch das periphere Nervensystem (*gut-first*) diskutiert, bei dem αSyn-Aggregate im enterischen Nervensystem bzw. im Riechkolben entstehen und über den Vagus-Nerv ins Gehirn wandern. Während bei dem Ursprung im zentralen Nervensystem erste Veränderungen im Gehirn, v.a. der *Substantia Nigra* auftreten, äußert sich die Erkrankung bei Patienten mit Ursprung in der Peripherie zunächst durch Störungen des autonomen peripheren Nervensystems und erst im späteren Verlauf durch den Verlust dopaminerger Neurone. Die Ursprungshypothese beruht u.a. auf dem Zusammenhang von präsymptomatischer PD mit Schlafstörungen in der *Rapid Eye Movement* (REM)-Phase, die als iRBD bezeichnet werden. Normalerweise sind die Muskeln während des REM-Schlafes und des Träumens gelähmt (Atonie), bei iRBD-Patienten hingegen ist diese Atonie im Schlaf gestört, was sich durch starke Bewegungen äußert. Fast alle iRBD-Patienten haben nach 15 Jahren entweder PD, DLB oder multiple Systematrophie (MSA) entwickelt, zeigen aber erst mit Fortschreiten der Erkrankung Veränderungen im dopaminergen System [46].

Viele PD-Patienten entwickeln im Laufe der Erkrankung außerdem kognitive Einschränkungen bis hin zur Demenz, die sich durch das Ausbreiten der αSyn-Pathologie bis in den Cortex erklären lassen. Bis zu 50 % dieser Parkinson-Demenz-Patienten zeigen Aβ-Plaques und NFTs als charakteristische Ablagerungen einer Co-Pathologie mit AD [47, 48].

Diagnose

Die Diagnose von PD erfolgt i.d.R. erst nach dem Auftreten motorischer Symptome und beruht auf einer Kombination aus der klinischen Symptomatik und weiteren Einschluss- oder Ausschlusskriterien. Aus klinischer Sicht ist die Verlangsamung von Bewegungen in Kombinationen von entweder einem Ruhetremor oder Rigor entscheidend. Außerdem sprechen Parkinson-Patienten im Gegensatz zu Patienten mit PSP sehr gut auf die Gabe des Medikaments L-Dopa, einer Vorstufe vom Dopamin, an. Unterstützt werden kann die Diagnose durch Visualisierung der Dichte an Dopamintransportern durch Einzelphotonen-Emissionscomputertomographie (SPECT) oder durch PET-Analysen mit markiertem L-Dopa. Durch die Verwendung von Liganden, die dem Noradrenalin ähneln, kann eine Denervation im Herzmuskel sichtbar gemacht werden, die typisch für PD ist (MIBG-Herzmuskel-Szintigraphie) [44, 49]. Außerdem müssen andere Ursachen für Parkinsonismus, z.B. atypischer Parkinsonismus und medikamentenausgelöster Parkinsonismus, ausgeschlossen werden. Zu den atypischen Parkinsonismus-Syndromen gehören DLB, PSP, MSA und die cortikobasale Degeneration [50]. CSF-Biomarker wie monomeres αSyn haben bisher keine ausreichende Sensitivität und Spezifität für PD gezeigt

und werden daher ebenso wie genetische Analysen nicht zur Unterstützung der Diagnose empfohlen [44, 47]. Die Genauigkeit der Diagnose wird auf ca. 80 % geschätzt, wobei die häufigsten Fehldiagnosen MSA, PSP und in seltenen Fällen auch corticobasale Degeneration (CBD) sind [44, 51].

Einteilung

2003 wurde von Braak und Kollegen eine Einteilung der PD anhand der pathologischen Veränderungen in verschiedenen Hirnarealen in sechs Stufen vorgeschlagen. Erste Veränderungen in den Neuronen des unteren Hirnstamms in den Stadien I und II werden durch den Eintritt von Pathogenen über den Vagus-Nerv oder das olfaktorische System hervorgerufen und verlaufen asymptomatisch. In den Stadien III und IV kommt es durch die Beteiligung des Mittelhirns und basalen Vorderhirns zu den typischen Bewegungsstörungen von PD. Im weiteren Verlauf in den Stadien V und VI sind limbische und neokortikale Strukturen betroffen, wodurch es zusätzlich zur PD-Symptomatik zu kognitiven Einschränkungen kommen kann [44, 52].

Neben der Einteilung nach dem möglichen Ursprungsort im zentralen oder peripheren Nervensystem und der Ausbreitung im Gehirn erfolgt die Einteilung und die Beurteilung von Therapieeffekten im klinischen Alltag anhand der Symptome. Hierfür sind insbesondere die Hoehn & Yahr Skala und die *Unified Parkinson's Disease Rating Scale* (UPDRS) gebräuchlich [50].

Tabelle 4 Einteilung der Parkinson-Erkrankung nach Hoehn & Yahr (aus [53])

Grad	Beschreibung
I	Streng einseitige Symptome mit minimaler oder fehlender funktioneller Behinderung
II	Bilaterale Beteiligung ohne Gleichgewichtsstörung
III	Bilaterale Erkrankung: leichte oder mäßige Behinderung mit Einschränkung posturaler Reflexe (pathologischer Pull-Test), noch körperlich selbstständig
IV	Schwer behindernde Erkrankung, Patient noch in der Lage, ohne fremde Hilfe zu stehen oder zu gehen
V	Ohne fremde Hilfe an Rollstuhl gebunden oder bettlägerig

Während die Hoehn & Yahr Skala (Tabelle 4) einfach in der Anwendung ist, sich aber auf posturale Störungen begrenzt, ist die international gültige UPDRS-Skala und besonders deren Weiterentwicklung der Movement Disorder Society (MDS-UPDRS) deutlich umfangreicher in der Anwendung und umfasst vier Teile (Tabelle 5) [53].

Tabelle 5 MDS-UPDRS-Skala (modifiziert aus [53])

Teil	Inhalt
1	Erfahrungen des täglichen Lebens – nicht motorische Aspekte, u.a. Kognition, Halluzinationen, Stimmung, Antrieb
2	Auswirkung motorischer Symptome auf die Aktivitäten des täglichen Lebens
3	Schweregrad motorischer Symptome
4	Motorische Komplikationen

Therapie

Ebenso wie bei AD ist für PD bisher keine ursächliche Therapie oder Heilung der Erkrankung möglich. Die klassische symptomatische Therapie umfasst die Gabe von L-Dopa, das in den noch funktionsfähigen Neuronen zu Dopamin gespalten wird. Um die Spaltung und Inaktivierung in der Peripherie zu verhindern, wird L-Dopa immer in Kombination mit einem Decarboxylasehemmer verabreicht. Zusätzlich können Dopaminagonisten zum Ausgleich des Dopaminmangels und verschiedene Medikamente mit nicht-dopaminergen Targets, wie Acetylcholinesterasehemmer zur Verbesserung der kognitiven Symptome oder Medikamente gegen die autonomen Symptome wie orthostatischer Hypotension, Inkontinenz oder Obstipation gegeben werden [44]. Im Jahr 2021 befanden sich 56 *Disease modifying drugs* in klinischer Erprobung, drei davon in klinischer Phase III [54].

1.1.3 Demenz mit Lewy-Körperchen

Überblick

DLB gehört ebenso wie PD und PD mit Demenz zu den Lewy-Körperchen-Erkrankungen. Die Prävalenz bei den über 65-Jährigen liegt bei 0,4 % und ist nach der AD die zweithäufigste neurodegenerative Demenzform [55]. Die Erkrankung äußert sich durch eine stark fluktuierende kognitive Einschränkung, die besonders das Benennen von Objekten, die Wortflüssigkeit und die optisch-räumliche Wahrnehmung betrifft. Außerdem kann es zu visuellen Halluzinationen und den typischen Parkinsonismus-Symptomen wie Bradykinese, Tremor und Rigor kommen, wobei Gedächtnisstörungen wie bei AD erst in späteren Stadien auftreten. Häufig zeigten DLB-Patienten in der Vergangenheit iRBD-Symptome [47, 55].

Pathophysiologie

Analog zur Parkinson-Erkrankung treten bei DLB αSyn-Ablagerungen in Form von sogenannten Lewy-Körperchen und Lewy-Neuriten im Cortex und im Hirnstamm auf, die zum Verlust dopaminerger Neurone in der *Substantia Nigra* führen. Im Endstadium der Erkrankung ist weder aus klinischer noch aus neurochemischer oder morphologischer Sicht eine Unterscheidung zur Demenz infolge einer Parkinson-Erkrankung möglich. Bei vielen DLB-Patienten zeigt sich eine Co-Pathologie mit AD, sodass ein Drittel bis die Hälfte der AD-Patienten Lewy-Pathologie im Gehirn zeigen. Die Erkrankung äußert sich bei diesen Patienten unterschiedlich und erschwert die Diagnose [47, 55].

Diagnose

Die Basisdiagnostik richtet sich wie bei PD nach den klinischen Symptomen und kann durch erweiterte bildgebende Verfahren wie SPECT, PET-Analysen und Untersuchungen im Schlaflabor unterstützt werden. Für die Abgrenzung von DLB gegenüber der Parkinson-Demenz ist die zeitliche Abfolge der Symptome entscheidend. Bei DLB treten erste Anzeichen der Demenz gleichzeitig oder zeitlich vor den Parkinsonismus-Symptomen auf, während bei der Parkinson-Demenz die Demenz erst bei fortgeschrittener PD eintritt. Auch zur Diagnose der DLB haben sich CSF-Biomarker bisher nicht etabliert [47].

Einteilung

Die Einteilung der Erkrankung erfolgt anhand ihrer Wahrscheinlichkeit: Zeigt der Patient mindestens zwei typische klinische Symptome wie wechselnde kognitive Einschränkung, visuelle Halluzinationen, spontane extrapyramidale Motorsymptome oder iRBD in der Vergangenheit oder nur eins dieser Symptome mit gleichzeitiger Evidenz für DLB in einem bildgebenden Verfahren, gilt die Diagnose als wahrscheinlich. Zeigt sich hingegen nur ein klinisches Symptom ohne Biomarker-Evidenz oder nur Biomarker ohne klinische Symptomatik, gilt die Diagnose als möglich [47].

Therapie

Die Therapie erfolgt rein symptomatisch mit Acetylcholinesteraseinhibitoren gegen die Demenzsymptome, Memantin gegen Verhaltenssymptome, L-Dopa gegen die motorischen Einschränkungen und atypische Neuroleptika bei Psychosen. Eine ursächliche Therapie ist derzeit noch nicht möglich.

1.1.4 Progressive supranukleäre Blickparese

Überblick

Die progressive supranukleäre Blickparese (PSP) ist eine schnell fortschreitende, neurodegenerative Erkrankung und gehört wie DLB zu den atypischen Parkinsonsyndromen. Die Prävalenz liegt bei 5-10 Betroffenen pro 100 000 Einwohnern mit einem durchschnittlichen Alter bei Diagnosestellung von ca. 65 Jahren [55, 56].

Klinisch kann sich PSP unterschiedlich äußern. Bei ca. 40 % der Patienten liegt die typische Symptomatik, genannt Richardson-Syndrom, mit früh auftretender Haltungsinstabilität, Stürzen und Störungen der Augenmotorik bis hin zur namensgebenden Blicklähmung vor. Bei weiteren 20 % der Patienten äußert sich PSP mit den klassischen Parkinsonsymptomen, wobei die charakteristische Blickparese erst in späteren Stadien auftritt. Weitere Ausformungen von PSP äußern sich durch Sprachstörungen, Verhaltensstörungen oder Gangblockaden (Akinesie) [4, 55-57].

Pathophysiologie

Pathophysiologisch kommt es bei PSP zu Ablagerungen von Tau als NFTs in Neuronen, als *coiled bodies* in Oligodendrozyten und als *tufts* in Astrogliazellen. Letztere dienen auch der Abgrenzung von PSP gegenüber CBD, einer weiteren, aber deutlich selteneren Tauopathie. Die Tau-Ablagerungen unterscheiden sich nicht nur in ihrer Morphologie im Vergleich zu AD, sondern auch in der Primärstruktur des Proteins (s. Kapitel Tau) [4, 55-57].

Diagnose

Die Diagnosestellung erfolgt in der Regel 3-4 Jahre nach dem ersten Auftreten von Symptomen mit einer hohen Spezifität von 85-90 % [58]. Die Diagnostik beruht auf dem klinischen Erscheinungsbild des Patienten im Hinblick auf eine verlangsamte Augenmotorik, Haltungsschwäche, Akinesie und kognitiver Dysfunktion [56]. Im Jahr 2017 wurden die Diagnosekriterien für PSP angepasst, um Patienten mit PSP ohne Richardson-Syndrom besser einzuschließen. Dadurch konnte die Sensitivität von 45,5 % auf 87,9 % verbessert werden [58]. Zusätzlich zur symptomatischen Betrachtung des Patienten können MRT-Aufnahmen zur Visualisierung einer Mittelhirn- und Frontalhirnatrophie, PET-Aufnahmen mit speziellen Tracern für die entsprechende Tau-Struktur und FDG-PET oder unterschiedliche SPECT-Aufnahmen zum Nachweis dopaminerger Denervierung oder einer Degeneration im Striatum durchgeführt werden [57]. Im Gegensatz zur AD sind die CSF-Werte für pTau und tTau bei PSP unverändert oder sogar leicht reduziert [59, 60] und werden routinemäßig nicht untersucht.

Einteilung

Eingeteilt werden kann PSP entweder anhand der Wahrscheinlichkeit der Erkrankung in suggestiv, möglich, wahrscheinlich und sicher oder anhand der Ausprägung der klinischen Symptomatik u.a. in Richardson-Syndrom oder PSP mit prädominanter Parkinson-Symptomatik [55, 56].

Therapie

Eine Heilung der PSP ist aktuell noch nicht möglich, sodass die durchschnittliche Lebenserwartung von PSP-Patienten nach Diagnose bei ca. 8 Jahren liegt. Die Patienten versterben in der Regel an Lungenentzündungen infolge vom Verschlucken. Die Behandlung erfolgt symptomatisch zur Verbesserung der Bewegungsstörungen, der Augenmotorik und neuropsychologischer Symptome [55].

1.2 Proteinaggregate in neurodegenerativen Erkrankungen

Trotz der unterschiedlichen Symptomatik der verschiedenen neurodegenerativen Erkrankungen und der verschiedenen Größen, Strukturen und Sequenzen der beteiligten Proteine, ähneln sich diese bezüglich der Fehlfaltung, Aggregation und Ablagerung im Gehirn [3]. Nach der Beschreibung eines allgemein gültigen Aggregationsmechanismus, soll im Folgenden auf die Proteine Aβ, Tau und αSyn bezüglich der Produktion, Aggregation und Clearance genauer eingegangen werden.

Die Aggregation ist ein mehrschrittiger Prozess (Abbildung 3), der mit der Keimbildungsphase (*nucleation phase*) beginnt, in der sich ein erstes stabiles Oligomer bildet [3]. Oligomere sind definiert als lösliche Vorstufen der Fibrillen, die aus zwei bis hin zu mehreren hundert Monomereinheiten bestehen können [3]. Ausgelöst wird diese Oligomerisierung vermutlich zufällig, kann aber durch Mutationen in der Proteinsequenz oder durch Erhöhung der Proteinkonzentration, z.B. durch vermehrte Produktion aufgrund genetischer Veränderungen oder verringertem Abtransport durch altersabhängige Beeinträchtigung der Reinigungsprozesse, begünstigt werden [61]. Auf die Keimbildungsphase folgt eine schnelle Elongationsphase, bei der sich monomeres Protein an die Oligomere anlagert, wodurch Protofibrillen und Fibrillen entstehen (*seeding*). Fibrillen wiederrum können direkt an ihrer Oberfläche die Bildung von neuen Oligomeren katalysieren (sekundäre Nukleation) oder durch weitere Anlagerung von Monomeren wachsen, fragmentieren und neue Keime bilden, wodurch ein exponentielles Fibrillenwachstum ausgelöst wird. Fibrillen können außerdem mit sich selbst interagieren und größere, unlösliche Ablagerungen, sogenannte Amyloid-Plaques bilden (stationäre Phase). Monomere, Oligomere und (Proto-)Fibrillen stehen im Gleichgewicht miteinander, wobei Oligomere noch einmal eingeteilt werden in On- und Off-Pathway-Oligomere, abhängig von ihrer Fähigkeit, Fibrillen zu bilden [3, 62, 63].

Die Fibrillen in neurodegenerativen Erkrankungen zeigen eine charakteristische Cross-β-Struktur. In dieser Struktur lagern sich die β-Stränge der Proteine zunächst in einem Abstand von ca. 4,7 Å entlang der Fibrillenachse zu β-Faltblättern übereinander und bilden das strukturelle Rückgrat der Protofilamente. Weiter entwickelte, reife Fibrillen bestehen aus einem oder mehreren dieser Protofilamente mit einem Abstand von ca. 10 Å und werden allgemein als Amyloid-Fibrillen bezeichnet, unabhängig davon, ob es sich um fehlgefaltete Proteinaggregate oder um Fibrillen mit normaler biologischer Aktivität handelt [62, 64, 65].

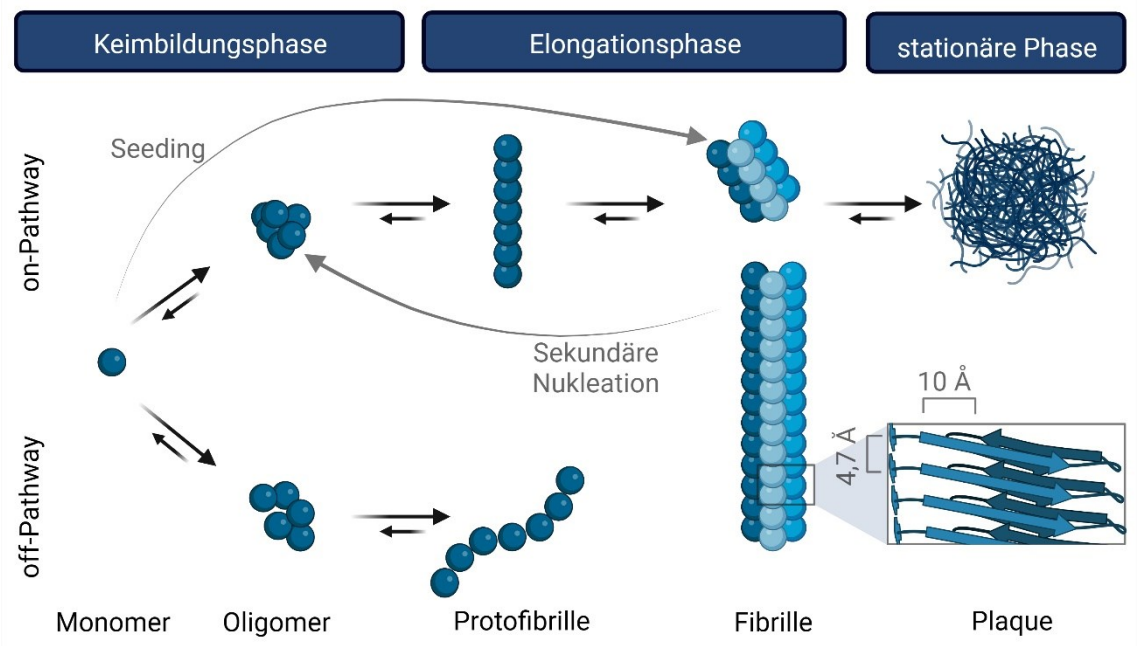

Abbildung 3 Schematische Abbildung der Protein-Aggregation
Während der Keimbildungsphase bildet sich ein erstes stabiles Oligomer, das in der Elongationsphase zunächst zu Protofibrillen und anschließend zu Amyloid-Fibrillen und Plaques (stationäre Phase) wachsen kann. Innerhalb einer Fibrille zeigen die β-Faltblätter eines Protofilaments einen charakteristischen Abstand von 4,7 Å und zwischen den Protofilamenten einen Abstand von 10 Å. An der Oberfläche der Fibrillen kann es zur Bildung neuer Oligomere (sekundäre Nukleation) oder zur Anlagerung von Monomeren an die Fibrille (*seeding*) kommen. Off-Pathway-Oligomere bilden keine Fibrillen. *Erstellt mit BioRender.com*

Trotz der vielen Gemeinsamkeiten der Amyloid-Fibrillen, unterscheiden sich die Fibrillen bei unterschiedlichen Erkrankungen, selbst wenn sie aus dem gleichen Protein entstanden sind. Mögliche Ursachen hierfür sind unterschiedliche Bedingungen für die Aggregation oder unterschiedliche Orte und Mutationen, z.B. Punktmutationen, die die Primärstruktur und damit das Aggregationsverhalten verändern [62].

Neben der Struktur der Fibrillen teilen die verschiedenen Aggregate die Fähigkeit, ihre Fehlfaltung auf andere, monomere Proteine zu übertragen. Dadurch wird sowohl eine Ausbreitung im Gehirn als auch eine Übertragung zwischen Individuen ermöglicht. An diesem Verhalten angelehnt wurde der Begriff Prionen als Bezeichnung für proteinartige, infektiöse Partikel eingeführt. Proteine, die diese Eigenschaft mit dem Prion-Protein teilen, werden als prionenartige Proteine bezeichnet, auch wenn eine Übertragung zwischen Menschen bisher nur für das Prion-Protein selbst nachgewiesen wurde [3, 62, 66].

1.2.1 Amyloid-β

Ablagerungen des Proteins Amyloid-β (Aβ) werden mit der Alzheimer-Demenz (AD) in Zusammenhang gebracht und können bereits 15-20 Jahre vor dem ersten Auftreten von Symptomen im Gehirn nachgewiesen werden [16].

Produktion und Struktur

Aβ ist ein 37-49 Aminosäuren langes Protein, dass durch proteolytische Spaltung aus dem Amyloidvorläuferprotein (APP) gebildet wird. APP wird in verschiedenen Geweben, vor allem in den Synapsen von Neuronen, exprimiert und besteht aus einem extrazellulärem N-Terminus, einem membranständigen Mittelteil und dem kürzeren C-Terminus.

Für die Spaltung zu Aβ gibt es zunächst zwei Wege (Abbildung 4): APP kann entweder durch die α-Sekretase (nicht amyloidogener Weg) oder durch die β-Sekretase (amyloidogener Weg) zu löslichem, nicht-toxischem APPα (sAPPα) bzw. APPβ (sAPPβ) und dem membranständigen Amyloid-Teil gespalten werden.

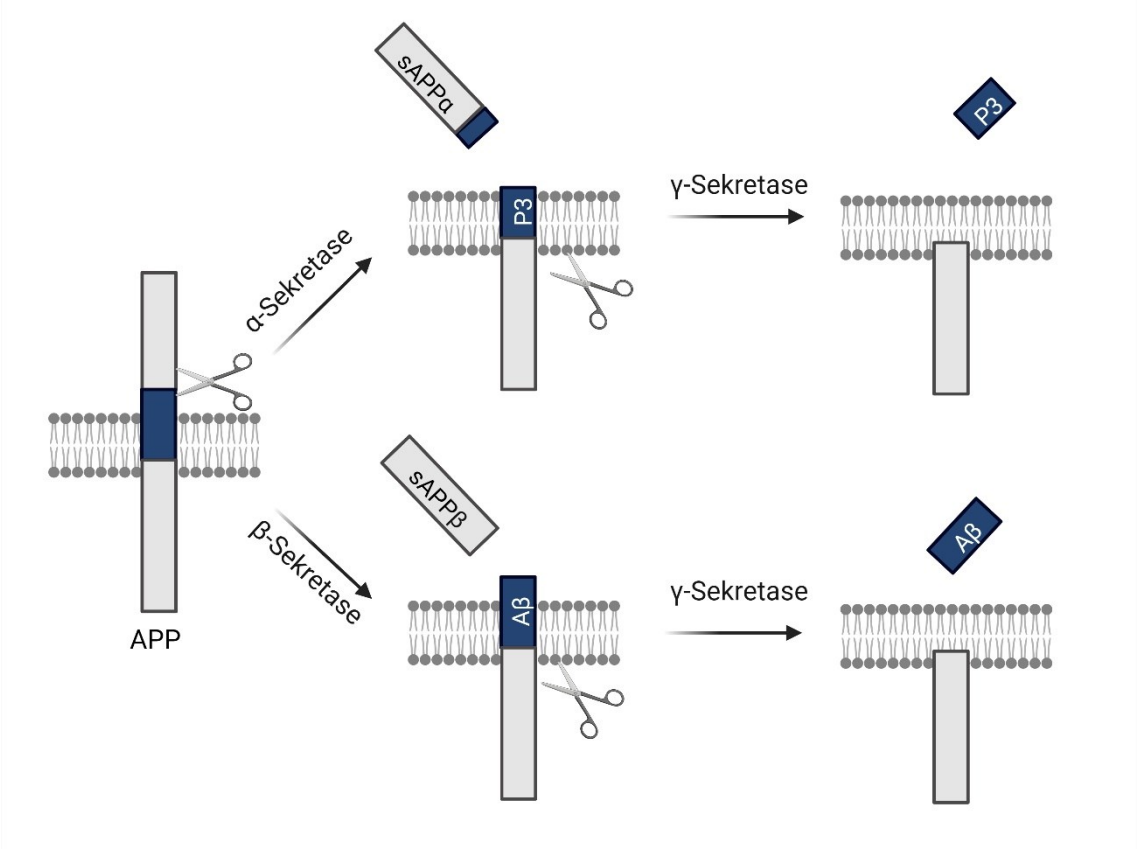

Abbildung 4 Proteolytische Spaltung von APP zu Aβ
Das Amyloid-Vorläuferprotein APP kann entweder über den nicht-amyloidogenen Weg zunächst durch die α-Sekretase und anschließend über die γ-Sekretase zum P3-Fragment und einem membranständigen Fragment gespalten werden. Beim amyloidogenen Weg wird das APP im ersten Schritt von der β-Sekretase und im zweiten Schritt analog zum nicht-amyloidogenen Weg von der γ-Sekretase prozessiert, wodurch das Aβ-Fragment entsteht. *Erstellt mit BioRender.com*

Im zweiten Schritt schneidet die γ-Sekretase den membranständigen Amyloid-Teil: Erfolgte die erste Prozessierung mit der α-Sekretase, entsteht das nicht-toxische P3-Fragment; wurde das APP im ersten Schritt hingegen mithilfe der β-Sekretase gespalten, entsteht durch die γ-Sekretase das toxische Aβ-Fragment. Das Aβ-Fragment kann je nach genauer Aminosäuresequenz vom APP unterschiedlich lang sein, für AD sind besonders die beiden Fragmente mit 40 bzw. 42 Aminosäuren relevant ($A\beta_{1-40}$ bzw. $A\beta_{1-42}$). Mutationen im APP-Gen und den Genen Presinilin 1 und 2, die für die γ-Sekretase codieren, führen zu einer vermehrten Bildung von Aβ bei früh-auftretender AD. Die dabei entstandenen Aβ-Fragmente werden entweder in den Extrazellularraum entlassen oder verbleiben an der Zellmembran assoziiert [16, 21].

Aggregation

Sowohl $A\beta_{1-40}$ als auch $A\beta_{1-42}$ sind per se nicht toxisch und unter anderem für die Signalweiterleitung in Neuronen verantwortlich. Neuere Erkenntnisse weisen darauf hin, dass Zwischenprodukte auf dem Weg zu den Aβ-Plaques, die löslichen Oligomere, das höchste toxische Potenzial haben und für den Zelltod von Neuronen, Störungen in der Signalweiterleitung zwischen Neuronen und der Langzeitpotenzierung verantwortlich sind [17, 67].

Aβ-Oligomere können definiert werden als lösliche Zusammenlagerungen von Einzelproteinen, die nicht durch Hochgeschwindigkeitszentrifugation pelletiert werden können [16, 17]. Besonders kleine Oligomere mit zwei bis drei Untereinheiten werden als Low-Molecular-Weight-Oligomere bezeichnet, während Oligomere über 100 kDa High-Molecular-Weight-Oligomere heißen und den Übergang zu Protofibrillen und Fibrillen darstellen. Diese wiederum können sich zu unlöslichen Aβ-Plaques zusammenlagern, die in Gehirnen von Alzheimer-Patienten nachgewiesen werden können [17, 21].

Das Aggregationsverhalten von Aβ wird sowohl von der Sequenz als auch von posttranslationalen Modifikationen beeinflusst. Da das längere $A\beta_{1-42}$ zwei zusätzliche, hydrophobe Aminosäuren aufweist, neigt dieses Fragment besonders zur Aggregation. Ebenso bewirken N-terminale Verkürzungen und N-terminales Pyroglutamat eine reduzierte Löslichkeit von Aβ und fördern dadurch, ebenso wie Phosphorylierungen am Serin an Position 8, die Aggregation. Im Gegensatz dazu resultiert das Anhängen von Zuckerresten oder die Nitrierung von Tyrosin an Position 10 in einer verminderten Aggregationsneigung [16, 21, 68].

Aβ in der Peripherie zeigt eine deutlich geringere Aggregationsneigung im Vergleich zum Gehirn. Hierfür kommen verschiedene Ursachen infrage: In der Peripherie produziertes Aβ liegt in der Regel in der verkürzten, weniger zur Aggregation neigenden

Form $A\beta_{1-40}$ vor. Außerdem ist der freie, ungebundene Anteil von Aβ im Blut deutlich reduziert, zum einen aufgrund der insgesamt geringeren Konzentration von Aβ im Blut, zum anderen aufgrund der Bindung an Plasmaproteine: Im Blut sind 89 % des Aβ an Albumin, 5 % an Lipoproteine wie High-Density-Lipoprotein (HDL) und Low-Density-Lipoprotein (LDL) und ein weiterer Anteil an Erythrozyten gebunden. Die Bindung an Albumin erfolgt in einer 1:1 Stöchiometrie [18, 69].

In vivo vorliegende Oligomere unterscheiden sich nicht nur hinsichtlich ihrer Struktur, der Anzahl, Sequenz und posttranslationaler Modifikation der Monomereinheiten, sondern auch in ihrer Toxizität. Für unterschiedliche Strukturen wurden variierende Einflüsse auf die Permeabilisierung von Membranen, die Auslösung von Entzündungsprozessen, die Anregung von Down-Stream-Prozessen wie die Tau-Aggregation oder die Auslösung von oxidativem Stress beschrieben, wobei noch keine Einigkeit darüber besteht, ob und welche Oligomerstrukturen für die Pathologie von AD verantwortlich sind [67, 70].

Transport und Clearance

Im menschlichen Gehirn befinden sich vier verschiedene Flüssigkeitssysteme: die Intrazellulärflüssigkeit, die Interstitialflüssigkeit (ISF), die die Neurone und andere Gehirnzellen umgibt, die Cerebrospinalflüssigkeit (CSF) und das Blut, wobei die Intrazellulärflüssigkeit mit > 60 % der Gesamtflüssigkeit im Gehirn den größten Teil ausmacht. Aβ liegt nur zu geringen Teilen intrazellulär vor und kann dort primär über das Ubiquitin-Proteasom-System (UPS) oder das Autophagie-Lysosom-System (ALS) (Abbildung 5) abgebaut werden [71, 72].

Nach der Synthese wird Aβ größtenteils in den interstitiellen Raum des Gehirns sezerniert, wo es zur Aggregation und Ablagerung in Plaques kommen kann. Die Ausbreitung der Oligomere im Gehirn erfolgt über einen prionenartigen Mechanismus. Im Gegensatz zu primären Prionen-Erkrankungen wie der Creutzfeldt-Jakob-Krankheit (CJD) oder der bovinen spongiformen Enzephalopathie (BSE), gibt es für Aβ keine epidemiologische Evidenz für ein infektiöses Übertragen der Oligomere zwischen Individuen [62, 70, 73].

Extrazelluläres Aβ im Gehirnparenchym kann über Proteasen wie Neprilysin oder das Insulin-Degradierungs-Enzym und über Phagozytose durch Mikrogliazellen abgebaut werden (Abbildung 5). Vom Interstitium kann Aβ sowohl ins Blut als auch ins CSF übertragen werden. Der direkte Transport von Substanzen aus dem Interstitium ins Blut erfolgt über die Blut-Hirn-Schranke und ist durch *tight junctions* – dichte Zell-Zell-Verbindungen – reglementiert. Kleine, lipophile Substanzen können direkt durch die Plasmamembranen der Epithel- und Endothelschicht zwischen dem Blut und dem

Gehirnparenchym passieren, während größere, hydrophilere Substanzen über spezielle Transporter transportiert werden. Der Transport von Aβ aus dem Gehirn erfolgt über den regulierten Weg über Transporter wie z.B. P-Glykoprotein oder *low density lipoprotein receptor- related protein* (LRP). Der umgekehrte Weg von Aβ aus dem Blut ins Gehirn wird u.a. über den *receptor for advanded glycation endproducts* (RAGE) kontrolliert. Der Übergang vom ISF zum CSF ist im Gegensatz zur Blut-Hirn-Schranke nur wenig begrenzt und kann durch die Zellzwischenräume der Ependymzellen erfolgen. Der Weitertransport von Aβ aus dem CSF ins Blut hingegen wird über die Blut-CSF-Schranke über ähnliche Mechanismen wie die Blut-Hirn-Schranke kontrolliert und kann in beide Richtungen – ins CSF und ins Blut – erfolgen [71, 72, 74, 75].

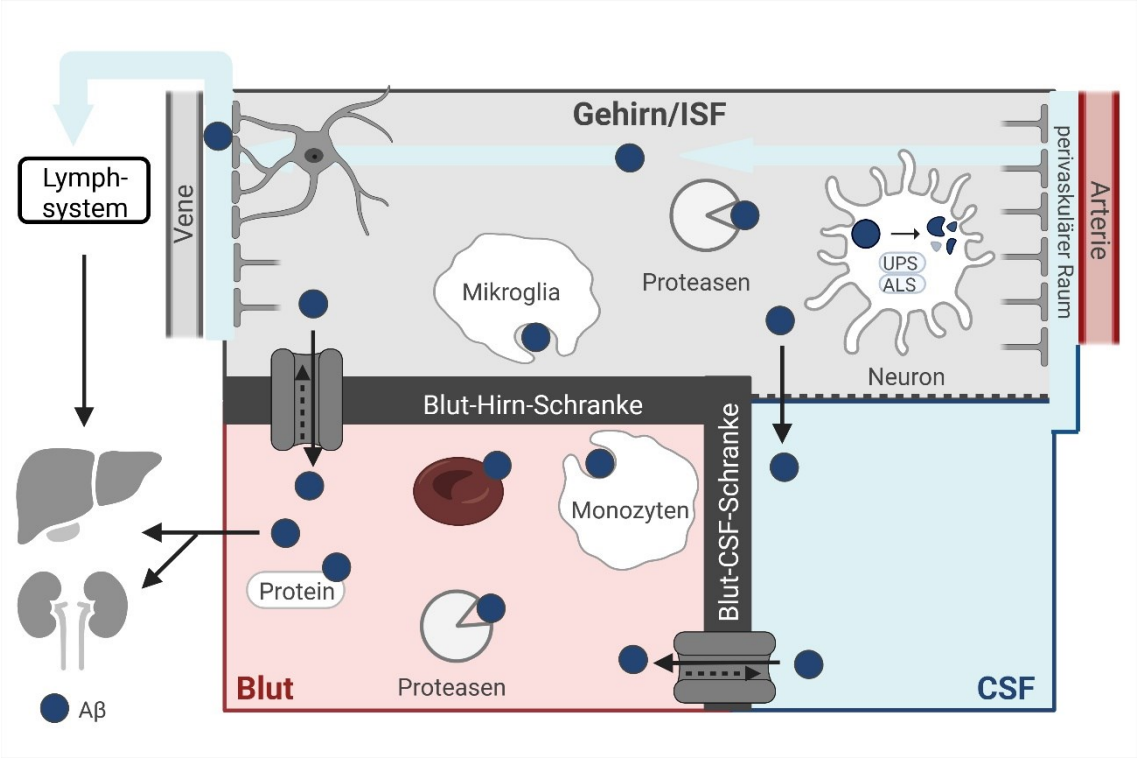

Abbildung 5 Transport und Clearance von Aβ
Aβ liegt im Gehirn als extrazelluläres Protein vor und kann im ISF direkt durch Proteasen oder in den Neuronen oder Mikrogliazellen abgebaut werden. Außerdem kann Aβ ins CSF und von dort über die Blut-CSF-Schranke oder direkt aus dem Gehirn über die Blut-Hirn-Schranke über spezielle Transporter ins Blut transportiert werden. Hier liegt Aβ zu > 95 % gebunden an Plasmaproteine und Erythrozyten vor. Der Abbau im Blut erfolgt über Proteasen, Monozyten und Makrophagen. Aβ kann neben dem direkten Transport über das Blut über den glymphatischen Reinigungsmechanismus und das Lymphsystem in periphere Organe wie die Leber und die Niere gelangen, wo ein weiterer Abbau und die Ausscheidung über die Galle, den Stuhl und Urin erfolgt.

Zusätzlich gibt es um die Blutgefäße herum einen schmalen, mit CSF gefüllten Raum, den sogenannten Virchow-Robin-Raum oder perivaskulären Raum. Die Begrenzung für diesen Raum wird durch die Endfüße von Astrozyten gebildet, die den Übergang von CSF zum Gehirnparenchym kontrollieren.

Das beim Übergang ins Gehirnparenchym entstehende CSF-ISF-Gemisch kann über einen hydrostatischen Druckgradienten und die pulsartigen Bewegungen der Arterienwände von der arteriellen zur venösen Seite gelangen, in den dortigen perivaskulären Raum aufgenommen und zu den Lymphgefäßen der Hirnhäute oder den Lymphknoten im Hals transportiert werden (Abbildung 5). Dadurch kann gelöstes Aβ-Monomer, aber auch Aβ-Oligomere aus dem Interstitium ausgespült werden, wobei die Effektivität dieses Reinigungsmechanismus mit der Größe der vorliegenden Oligomere abnimmt. Dieser Transportweg wird aufgrund der Beteiligung der Gliazellen und der Ähnlichkeit mit dem peripheren lymphatischen System als glymphatisches System bezeichnet [67, 72, 74, 76]. Beeinträchtigungen der Funktion der Blut-Hirn-Schranke und eine Reduktion der Aktivität des glymphatischen Systems werden als Ursache für erhöhte Aβ-Konzentrationen im Gehirn und die damit verbundene Aggregation diskutiert [18].

Der Transport von Aβ über die Blut-Hirn-Schranke in die Peripherie macht über die Hälfte des Transports und der Clearance von Aβ aus dem Gehirn aus. Im Blut wird Aβ entweder an Proteine (insbesondere Albumine) und rote Blutkörperchen gebunden, über Proteasen, Monozyten und Makrophagen abgebaut oder weiter in periphere Organe transportiert, wo die Ausscheidung von Aβ z.B. über die Leber in die Galle und den Stuhl oder über die Niere in den Urin erfolgen kann [71, 77].

1.2.2 Tau

Ein weiteres Hauptmerkmal der AD sind pathologische Ablagerungen des Tau-Proteins in NFTs. Die Aggregation des Tau-Proteins wird außerdem verantwortlich gemacht für primäre Tauopathien wie PSP oder CBD. Ablagerungen von Tau werden aber auch in anderen Erkrankungen wie den Lewy-Körperchen-Erkrankungen gefunden [78].

Produktion und Struktur

Tau ist im Gegensatz zu Aβ ein intrazelluläres Protein, das in erster Linie von Neuronen, aber auch von Gliazellen gebildet wird und in monomerer Form für die Stabilität von Mikrotubuli und den axonalen Transport verantwortlich ist [79, 80].

Das Tau-Protein lässt sich in vier verschiedene Bereiche einteilen: die N-terminale Projektionsdomäne, die prolinreiche Region, die Mikrotubuli-Bindestelle und den C-Terminus [81, 82]. Im menschlichen Gehirn sind sechs verschiedene Tau-Isoformen

präsent, die durch alternatives Spleißen entstehen und in zwei Gruppen eingeteilt werden: 3R und 4R-Tau, abhängig davon, ob drei oder vier Wiederholungen in der Mikrotubuli-Bindestelle eingebaut sind. Tau-Ablagerungen in unterschiedlichen Erkrankungen, die mit Tau assoziiert sind, wie AD, PSP oder FTD, zeigen nicht nur unterschiedliche Morphologien und sind in unterschiedlichen Zelltypen im Gehirn zu finden, auch die Splicing-Formen unterscheiden sich [81]. Während bei AD ein ähnliches Verhältnis von 4R und 3R-Tau zu finden ist, überwiegt bei PSP das 4R-Tau und bei FTD 3R-Tau [82]. Innerhalb vom 3R und 4R-Tau unterscheidet man drei weitere Splicing-Varianten innerhalb der N-terminalen Projektionsdomäne, die durch 0, 1 oder 2 N-Insertionen gekennzeichnet sind. Abhängig von der Spleißvariante besteht das Tau-Protein aus 352 bis 441 Aminosäuren [82]. Tau liegt physiologisch entweder als ungefaltetes Protein oder in einer sogenannten *paperclip*-Struktur vor (Abbildung 6). Diese bildet sich aufgrund der ungleichen Ladungsverteilung im Protein mit einem sauren N-Terminus, einem basischen Mittelteil und einem neutralen C-Terminus und schützt möglicherweise vor Aggregation [80].

Alle Tau-Isoformen unterliegen vielfältigen posttranslationalen Veränderungen, wobei u.a. Phosphorylierungen, Trunkierungen und Glykierungen die Aggregationsneigung erhöhen, wohingegen Nitrierungen, Acylierungen und Methylierungen vor Aggregation schützen [68].

Aggregation

Im Gegensatz zu Aβ neigt Tau nicht zur spontanen Aggregation, sondern benötigt Kofaktoren, z.B. Polyanionen, freie Fettsäuren oder bestehende Oligomere oder Aggregate, an die es sich anlagern kann. Tau muss sich dabei zunächst von den Mikrotubuli lösen, um in freier Form und hoher Konzentration im Zytosol vorzuliegen. Da Phosphorylierungen zu einer reduzierten Bindung von Tau an Mikrotubuli führen, stehen diese in engem Zusammenhang mit der Aggregation, wobei noch nicht geklärt ist, ob Phosphorylierungen die Aggregation fördern oder Aggregate besonders anfällig für Phosphorylierungen sind [82, 83]. Für die Aggregation sind zwei Hexapeptidsequenzen, die sich in der Mikrotubuli-Bindestelle (R2 und R3) befinden, entscheidend. Die entstehenden Fibrillen und Ablagerungen unterscheiden sich abhängig von der Tau-Isoform und der assoziierten Erkrankung. Bei AD liegen die Tau-Filamente als gepaarte helikale Filamente (PHFs) oder, wenn die einzelnen Stränge nicht gegeneinander verdreht sind, als *straight filaments* (SF) vor, die sich als NFTs ablagern können (Abbildung 6) [81]. Für PSP sind zusätzlich spezielle Ablagerungen in den Oligodendrozyten (*coiled bodies*) und Astrogliazellen (*tufts*) charakteristisch [56].

Nach dem Absterben von Neuronen können die Tau-Filamente als *ghost tangles* im Extrazellulärraum verbleiben [82]. Ähnlich wie bei Aβ, werden auch bei Tau die Oligomere für die Ausbreitung der Erkrankung im Gehirn und die neurotoxischen Effekte verantwortlich gemacht [83, 84].

Transport und Clearance

Die Ausbreitung von Tau-Monomeren, aber auch Aggregaten im Gehirn erfolgt entweder durch Exo- und Endozytose, vesikelvermittelt oder durch direkten Transport durch die Membran. In der Zielzelle können Tau-Aggregate durch Elongation von monomerem Tau wachsen und sich weiterverbreiten [80].

Der intrazelluläre Abbau von Tau erfolgt ähnlich wie bei Aβ über das Ubiquitin-Proteasom-System und das Autophagie-Lysosom-System, allerdings können die dabei entstehenden Tau-Fragmente eine höhere Aggregationsneigung aufweisen. Extrazelluläres Tau kann über Proteasen oder Mikroglia-Phagozytose degradiert werden. Außerdem kann lösliches, extrazelluläres Tau über die Blut-Hirn-Schranke, die Blut-CSF-Schranke und über das glymphatische System ins Blut bzw. zu den Lymphknoten transportiert werden. In der Peripherie wurde Tau außerdem in Speicheldrüsen, im Darm, in der Leber und in der Haut gefunden, was auf einen Abbau in der Peripherie hindeutet [71].

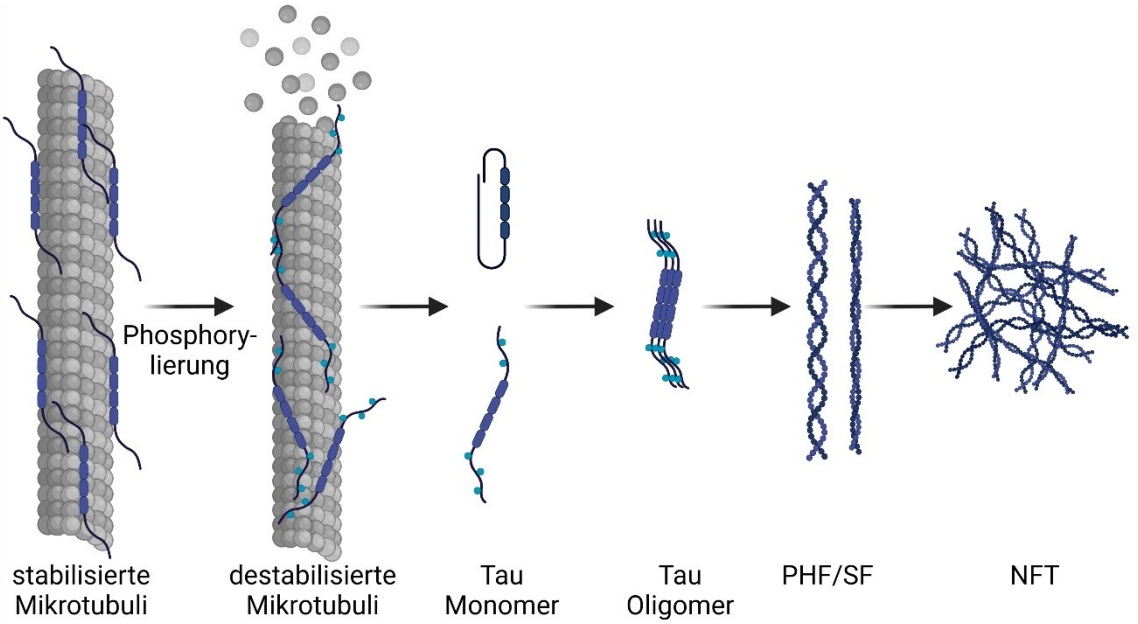

Abbildung 6 Aggregationskaskade von Tau am Beispiel von AD
Tau liegt in den Neuronen an Mikrotubuli gebunden vor. Durch Phosphorylierung von Tau löst sich die Bindung an die Mikrotubuli, sodass Tau in monomerer Form ungefaltet oder in der *paperclip*-Struktur vorliegt. Die aus den Monomeren gebildeten Oligomere können weiter aggregieren zu gepaarten helikalen Filamenten (PHF) oder geraden Filamenten (SF) und sich in Form von neurofibrillären Bündeln (NFTs) ablagern. *Erstellt mit BioRender.com*

1.2.3 Alpha Synuclein

Erkrankungen, die durch Ablagerungen des Proteins alpha Synuclein (αSyn) charakterisiert sind, werden allgemein als Synucleinopathien bezeichnet. Zu diesen Erkrankungen gehören PD, DLB und MSA [4].

Produktion und Struktur

αSyn ist ein 140 Aminosäuren langes Protein, dass auf dem SNCA-Gen codiert und primär in Neuronen des *Neocortex, Hippocampus, Thalamus, Cerebellum* und der *Substantia Nigra* exprimiert wird. Das Protein besteht aus drei Bereichen: die N-terminale Lipid-Bindestelle umfasst die Aminosäuren 1-60 und interagiert aufgrund der positiven Ladung mit Membranen. Die Aminosäuren 61-95 bilden die zentrale Domäne (*Non-amyloid component*, NAC-Domäne) und sind für die Aggregation von αSyn und die Ausbildung der Cross-β-Struktur entscheidend. Der saure C-Terminus reicht von Aminosäure 96-140 und hemmt abhängig vom pH-Wert durch Interaktion mit der NAC-Domäne die Aggregation [44, 85]. Abhängig von den Umgebungsbedingungen kann αSyn in verschiedenen Konformationen vorliegen, wie z.B. der ungefalteten Struktur unter physiologischen Bedingungen oder mit einem α-helicalen N-Terminus bei Interaktion mit Membranen [85-87].

αSyn ist in seiner monomeren Form an vielen physiologischen Funktionen wie dem intrazellulären Transport, der Freisetzung von Neurotransmittern und der mitochondrialen Funktion beteiligt und kann sowohl als Chaperon als auch als Antioxidans agieren [44]. Zusätzlich zum Gehirn wurde αSyn u.a. in roten Blutkörperchen, im Gastrointestinaltrakt, in der Haut und in Speicheldrüsen entdeckt [87, 88].

Aggregation

Für die Oligomerisierung und die weitere Aggregation ist eine hydrophobe, 12 Aminosäuren lange Sequenz in der NAC-Domäne entscheidend [87]. Die Aggregationskaskade läuft analog zu den anderen amyloidogenen Proteinen zunächst über lösliche On- oder Off-Pathway-Oligomere. On-Pathway-Oligomere können anschließend in der Elongationsphase exponentiell zu Protofibrillen und Fibrillen wachsen, wobei die Formen im Gleichgewicht miteinander stehen. Intrazelluläre Ablagerungen von αSyn werden je nach Form und Lokalisierung als Lewy-Körperchen oder Lewy-Neuriten bezeichnet. Diese Ablagerungen sind charakteristisch für Synucleinopathien wie die PD und DLB, bestehen neben αSyn auch aus Ubiquitin und anderen zellulären Proteinen und überlagern sich teilweise mit Tau-Ablagerungen [42, 89-92].

Das αSyn in den Lewy-Körperchen liegt zum großen Teil an Serin 129 phosphoryliert vor. Ob diese Phosphorylierung ursächlich für die Aggregation und Ablagerung ist, z.B. durch verminderten Abbau durch Proteasome, oder ob die Phosphorylierungen erst im fortgeschrittenem Erkrankungsstadium oder sogar nach der Ablagerung entstehen, wird noch diskutiert [93, 94]. Für die Toxizität, wie z.B. Entzündungsprozesse, Zerstörung von Membranen und Verlust der synaptischen Aktivität, werden, ähnlich wie bei Aβ und Tau, nicht die unlöslichen Lewy-Körperchen, sondern kleine, lösliche Oligomere verantwortlich gemacht [43, 89]. αSyn Oligomere unterscheiden sich hinsichtlich ihres Molekulargewichts, ihres Anteils an β-Faltblattstrukturen und ihrer Hydrophobizität [89]. Als Gründe für die unterschiedlichen Strukturen sind Mutationen im SNCA-Gen, posttranslationale Modifikationen und unterschiedliche Aggregationsbedingungen beschrieben [47, 92].

Transport und Clearance

Während die Toxizität von kleineren Oligomeren, möglicherweise < 100 nm ausgelöst wird, sind für die prionenartige Ausbreitung im Gehirn größere Oligomere und Fibrillen verantwortlich. Hierzu können die Aggregate entweder intra-axonal zwischen Gehirnregionen transportiert oder zunächst von der Zelle sekretiert und von einer anderen Zelle wieder aufgenommen werden, um dort die Aggregation von endogenem αSyn auszulösen [43, 44].

Sowohl Monomere als auch Oligomere können über das Ubiquitin-Proteasom-System oder über das Lysosom-System abgebaut werden. Da höheres Alter mit einer reduzierten Aktivität des Autophagie-Lysosom-Systems und des Ubiquitin-Proteasom-Systems einhergehen und diese Systeme außerdem durch αSyn-Oligomere gehemmt werden, kann es durch die Beeinflussung des Abbaus zur Anreicherung von αSyn im Gehirn kommen [44].

Extrazelluläres αSyn, das ebenfalls neurotoxisch ist und Entzündungsprozesse auslösen kann, wird entweder direkt durch Proteasen abgebaut oder zunächst in die Zellen aufgenommen und dort wie oben beschrieben eliminiert [93]. Zusätzlich kann αSyn über die Blut-CSF-Schranke zwischen CSF und Blut transportiert werden, wohingegen ein Transport über die Blut-Hirn-Schranke noch nicht nachgewiesen wurde [95].

Außerdem wurde ein Transport von αSyn von der Peripherie, z.B. dem Gastrointestinaltrakt über den Vagusnerv oder über das olfaktorische System ins Gehirn beobachtet, was zur Hypothese des peripheren Ursprungs der Lewy-Pathologie geführt hat (s. Parkinson-Erkrankung) [46]. Auch der umgekehrte Weg vom Gehirn in den Gastrointestinaltrakt wurde beobachtet [88].

1.3 sFIDA

1.3.1 Oligomere als Biomarker

Die Diagnose der meisten neurodegenerativen Erkrankungen erfolgt im klinischen Alltag anhand der Symptomatik des Patienten und dem Abschneiden in kognitiven Tests. Zur Abgrenzung und bei unklaren Fällen können außerdem bildgebende Verfahren hinzugezogen werden [10, 20, 44, 47, 56]. Das bisherige Vorgehen hat dabei im Wesentlichen zwei Nachteile: Eine Diagnose erfolgt häufig erst im fortgeschrittenen Stadium der Erkrankung, wenn Patienten eine Beeinträchtigung des täglichen Lebens feststellen. Zu diesem Zeitpunkt ist die Neurodegeneration im Gehirn allerdings schon weit fortgeschritten, wodurch eine therapeutische Intervention erschwert wird [96]. Außerdem ist die Diagnose bei Verwendung neuropsychiatrischer Tests zeitintensiv und bildgebende Verfahren sind teuer und limitiert in ihrer Verfügbarkeit [13, 96].

Da die Toxizität neueren Erkenntnissen zufolge bei allen beschriebenen neurodegenerativen Erkrankungen auf der Anwesenheit von löslichen Oligomeren beruht [16, 80, 89], stellen Veränderungen in der Oligomerkonzentration in Körperflüssigkeiten einen direkten Biomarker für die Diagnose der Erkrankungen, aber auch für die Therapie ebendieser dar [34, 97]. Eine Quantifizierung der Oligomere kann dabei helfen, Patienten mit erhöhten Oligomer-Konzentrationen für klinische Studien auszuwählen (Selektion bzw. Stratifizierung der Patienten) [97], da diese Patienten möglicherweise besonders von einer anti-Oligomeren Therapie profitieren. Außerdem kann der Effekt der Therapie auf die Konzentration der Oligomere beobachtet und damit die Effektivität des Medikaments beurteilt werden (*Target Engagement*). Zusätzlich ermöglicht die regelmäßige Bestimmung der Oligomere eine individuell angepasste Therapie (Therapeutisches Drug Monitoring) [34], was zu einem höheren Therapieerfolg mit gleichzeitig geringeren Nebenwirkungen führen kann.

Aufgrund der geringen Konzentration von Oligomeren in Körperflüssigkeiten und des Einflusses an Monomer erfordert die Quantifizierung von Oligomeren extrem sensitive und spezifische Verfahren. Erschwerend kommt hinzu, dass Oligomere in verschiedenen Größen, Strukturen und posttranslationalen Modifikationen vorliegen, wobei noch nicht abschließend geklärt ist, welche der Strukturen für die jeweiligen Erkrankungen relevant sind [67].

Für die Quantifizierung von Oligomeren gibt es verschiedene Möglichkeiten, wobei die meisten Verfahren in mindestens einem der Schritte spezifische Antikörper verwenden. Um die Detektion von Monomeren zu vermeiden, können Antikörper gegen strukturspezifische

Epitope verwendet werden, die nur in Oligomeren vorkommen. Alternativ kann ein Sandwich-Assay aufgebaut werden, bei dem der Fängerantikörper (Captureantikörper) und der Detektionsantikörper gegen das gleiche Epitop gerichtet sind. Andere Verfahren, die z.B. auf der Verwendung von Massenspektrometrie oder Größenausschlusschromatographie beruhen, befinden sich ebenfalls in der Entwicklung [97]. In vorherigen Studien konnte durch verschiedene Verfahren bereits eine Erhöhung sowohl von αSyn-Oligomeren in CSF als auch von Aβ-Oligomeren in CSF und Plasma nachgewiesen werden [98-103]. Bisherige Verfahren sind allerdings oft wenig validiert und unterscheiden sich hinsichtlich der Methodik und des Kalibrationsstandards, was zu Unterschieden in den ermittelten Konzentrationen und der Sensitivität und Spezifität der Verfahren führt.

1.3.2 Prinzip und Präparation des sFIDA

Das sFIDA-Verfahren wurde entwickelt, um sensitiv und selektiv Oligomere in Körperflüssigkeiten nachzuweisen. sFIDA steht für *surface-based fluorescence intensity distribution analysis* und verwendet zur Quantifizierung von Oligomeren ein Verfahren mit Antikörpern gegen gleiche oder überlappende Epitope. Erste Anwendungen des Verfahrens dienten dem Nachweis von aggregiertem Prion-Protein in Hirnhomogenaten und der Cerebrospinalflüssigkeit von Scrapie-infizierten Hamstern und BSE-infizierten Rindern [104-106]. Weiterentwicklungen der Methode zielten auf die Anwendung in anderen neurodegenerativen Erkrankungen wie AD und anderen Körperflüssigkeiten wie Blut, einem höheren Durchsatz und der Entwicklung von Standardpartikeln zur Kalibrierung der Methode ab [107-115].

Das biochemische Prinzip des sFIDA ähnelt einem enzymgekoppelten Immunadsorptionstest (ELISA) mit Sandwich-Aufbau (Abbildung 7 - Präparation): Zunächst wird der Captureantikörper auf der Glasoberfläche immobilisiert. Da der Captureantikörper nicht alle potenziellen Bindestellen für Probenbestandteile lückenlos abdeckt, folgt auf die Immobilisierung des Captureantikörpers ein Blocking Schritt, für den in der Regel andere Proteine oder Proteingemische, z.B. bovines Serumalbumin (BSA), verwendet werden. Bei der anschließenden Probeninkubation wird die spezifische und sehr stabile Antikörper-Protein-Bindung ausgenutzt. Alle anderen Probenbestandteile, die nicht oder nur schwach an die Oberfläche binden, werden durch anschließende Waschschritte entfernt. Abschließend wird der Detektionsantikörper hinzugefügt, der mit einem Fluoreszenzfarbstoff markiert ist [116, 117].

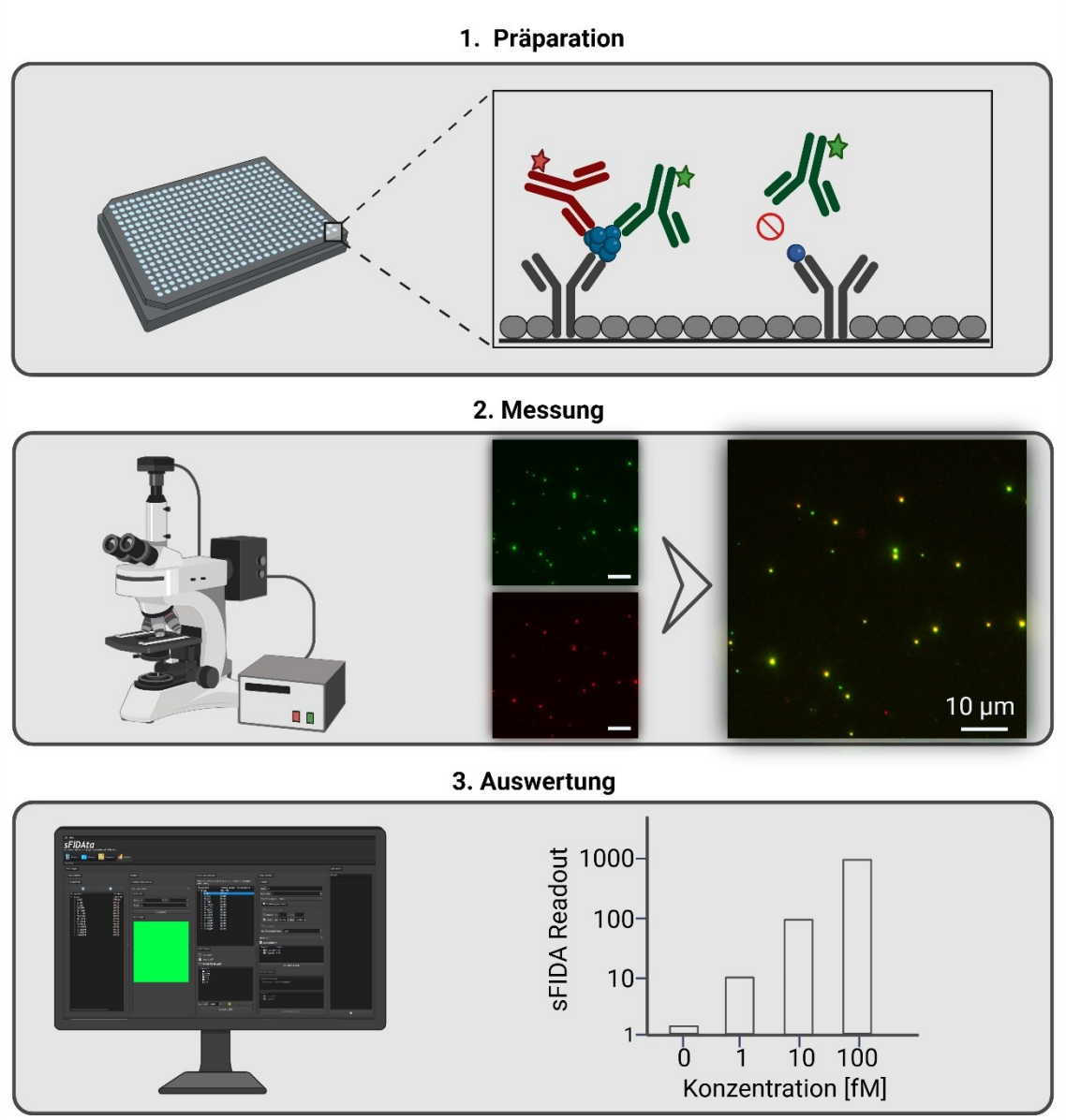

Abbildung 7 Prinzip und Ablauf des sFIDA
Der sFIDA-Assay gliedert sich in drei Abschnitte: die Präparation, die Messung und die Auswertung. Bei der Präparation wird im Sandwich-Verfahren zunächst der Capture-Antikörper auf der Oberfläche immobilisiert und anschließend freie Bindestellen im Blocking-Schritt abgesättigt. Im Probeninkubations-Schritt kann der Analyt an den Capture-Antikörper binden und im Detektionsantikörperschritt durch den gleichen oder einem mit dem Captureantikörper in der Epitopbindestelle überlappenden Antikörper nachgewiesen werden, wodurch die Detektion von Monomeren ausgeschlossen wird. Während der anschließenden Messung werden die fluoreszenzmarkierten Detektionsantikörper durch Laser- oder LED-Strahlung angeregt und Aufnahmen von der Oberfläche gemacht. Die dabei generierten Bilder können anschließend mithilfe der Software „sFIDAta“ ausgewertet werden. Als Ergebnis wird die Anzahl der Pixel in den Einzelkanälen (PixelCount) oder der Kolokalisation (sFIDA Readout) angegeben, die einen definierten Intensitätsschwellenwert überschreiten. *Erstellt mit BioRender.com*

Die Besonderheit des sFIDA liegt in der Bildaufnahme und Datenanalyse. Im Gegensatz zu einem normalen ELISA wird ein Fluoreszenzmikroskop gekoppelt mit einer hochauflösenden Kamera verwendet, die Aufnahmen von der Oberfläche macht. Bei der anschließenden Bildanalyse können einzelne Partikel gezählt werden, wodurch Einzelmolekülsensitivität erreicht werden kann (s. Messung und Auswertung) [115, 118].

Die Auswahl der Antikörper ist ein entscheidender Schritt in der Entwicklung des sFIDA: Sie bestimmt die Selektivität von Aggregaten gegenüber Monomeren und trägt zur Sensitivität des Verfahrens bei. Die Antikörper für den sFIDA werden dabei so ausgewählt, dass der Capture- und Detektionsantikörper die gleichen oder überlappende Epitope erkennen. So werden Monomere zwar über den Captureantikörper auf der Oberfläche immobilisiert, allerdings ist durch diesen Schritt die Bindestelle für den Detektionsantikörper bereits belegt, sodass die Monomere kein Signal geben.

Die Auswahl der Antikörper bzw. deren Affinität ist außerdem entscheidend für die Sensitivität des Assays. Die Affinität eines Antikörpers wird durch die Dissoziationskonstante (K_D) angegeben und beschreibt die Stärke der Wechselwirkung zwischen Protein und Ligand. Je kleiner der K_D-Wert, desto mehr liegt das Gleichgewicht auf der Seite des Antikörper-Antigen-Komplexes und desto stärker ist die Bindung. Für Immunoassays sollte der K_D-Wert der Antikörper nicht über 10 nmol/l liegen. Da die verwendeten IgG-Antikörper außerdem zwei Bindestellen für das Antigen aufweisen, ist die Gesamtbindungsstärke (Avidität) im Vergleich zu einer einzelnen Bindestelle exponentiell höher [116, 117, 119].

Die Selektivität des Assays kann weiter erhöht werden, indem nicht nur ein Detektionsantikörper, sondern zwei verschiedene Detektionsantikörper gegen das gleiche oder überlappende Epitope zugegeben werden [120]. Neben den Einzelkanälen kommt so eine zusätzliche Analyseoption hinzu, bei der nur die Pixel gezählt werden, bei denen beide Detektionsantikörper ein Signal geben. Dadurch können zum einen nur Analyten erkannt werden, die mindestens drei Bindestellen für die Antikörper besitzen (eine Bindestelle für den Capture- und zwei weitere für die Detektionsantikörper), zum anderen kann die Sensitivität des Assays erhöht werden (s. Auswertung). Da die Antikörper, die im sFIDA verwendet werden, lineare Epitope unabhängig von der Aggregatstruktur erkennen, kann im sFIDA die Gesamtheit der Aggregate detektiert werden.

Kalibration

Eine weitere Herausforderung bei der Entwicklung eines Assays ist die Auswahl eines geeigneten Kalibrationsstandards. Der Nachteil rekombinanter Aggregate ist die große strukturelle Diversität abhängig von den gewählten Aggregationsbedingungen wie Puffer

oder Temperatur und die fehlende Stabilität [120, 121]. Aus diesem Grund werden zur Kalibration des sFIDA keine rekombinanten Aggregate, sondern Silikananopartikel (SiNaPs) verwendet. Auf die Oberfläche von diesen SiNaPs kann das entsprechende Protein in mehrfacher Ausführung gekoppelt werden, sodass ein Aggregat nachgeahmt wird [113]. Der Vorteil dieser Partikel ist, dass sie eine einheitliche Größenverteilung aufweisen und über einen langen Zeitraum stabil sind [112]. Außerdem können die Partikel speziell für bestimmte Anwendungen synthetisiert werden, indem unterschiedliche Proteine mit definierter Anzahl auf einen SiNaP gekoppelt werden [112, 113, 115].

1.3.3 Messung

Die Oberfläche des sFIDA wird mit einem Fluoreszenzmikroskop, das an eine Kamera gekoppelt ist, vermessen. Hierbei werden die Fluorophore an den Detektionsantikörpern durch die Laser- oder LED-Strahlung angeregt. Fluoreszenzfarbstoffe unterscheiden sich von normalen Farbstoffen darin, dass die Energie nach Anregung nicht nur durch Wärmestrahlung und Bewegung, sondern auch durch die Emission von Lichtstrahlung abgegeben werden kann. Dabei ist das emittierte Licht immer langwelliger als das absorbierte, da ein Teil der Energie durch strahlungslose Prozesse verloren geht (Abbildung 8). Die Farbstoffe werden so ausgewählt, dass sich die Spektren nur wenig überlappen, um zu verhindern, dass sich die Farbstoffe gegenseitig anregen können.

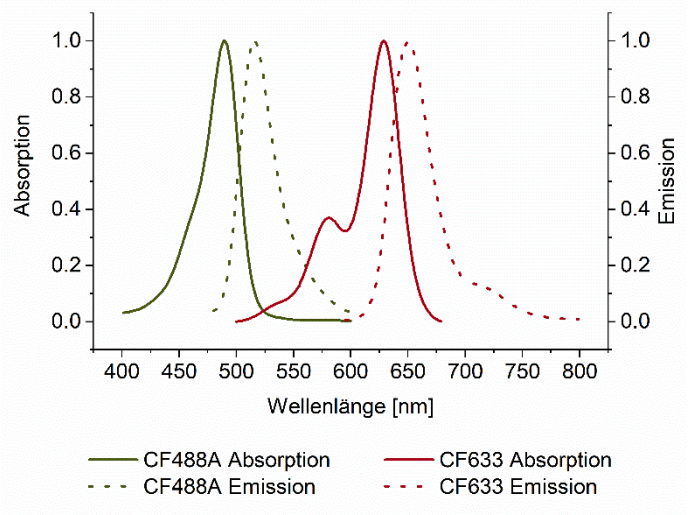

Abbildung 8 Absorptions- und Emissionsspektren des CF488A und CF633 Farbstoffes der Firma Biotium
Die im sFIDA verwendeten Farbstoffe CF488 und CF633 überlappen sich weder in den Absorptionsspektren (–) noch in den Emissionspektren (---), wodurch die Farbstoffe zeitgleich in einem Assay eingesetzt werden können, ohne sich gegenseitig zu beeinflussen.

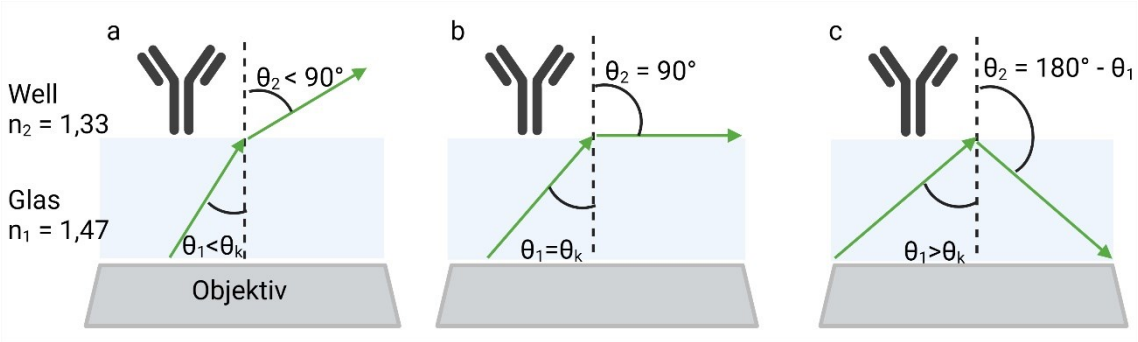

Abbildung 9 Abhängigkeit des Reflektionswinkels vom Einstrahlwinkel
Ist der Einstrahlwinkel θ_1 kleiner als der kritische TIRF Winkel θ_k, dringt der Laserstrahl in die Probe ein und kann ungerichtet Fluorophore in der Probe anregen (a). Entspricht der Einstrahlwinkel θ_1 dem kritischen TIRF Winkel θ_k, wird der Laserstrahl im 90° Winkel abgestrahlt (θ_2). Nur wenn der Einstrahlwinkel größer als der kritische TIRF-Winkel ist, kann der Lichtstrahl totalreflektiert werden, wodurch nur die elektrische Komponente des Lichts in die Probe eindringen und dadurch nur die Fluorophore an der Grenzfläche zwischen Glas und Well angeregt werden können. Abbildung in Anlehnung an [122]. *Erstellt mit BioRender.com*

Zusätzlich werden in Fluoreszenzmikroskopen in der Regel zwei Filter verbaut: der Anregungsfilter sorgt dafür, dass nur das Licht eines bestimmten Wellenlängenbereichs, z.B. 488 nm für den grünen Kanal, auf die Probe trifft, wohingegen der Emissionsfilter das emittierte Licht einer bestimmten Wellenlänge, allerdings nicht das Anregungslicht, an den Chip der Kamera weiterleitet [123]. Da die verwendete Laserstrahlung bei der in dieser Arbeit verwendeten TIRF-Mikroskopie (*Total internal reflection fluorescence microscopy*) bereits monochromatisch ist, ist hier im Gegensatz zu anderen Fluoreszenzmikroskopen, die LEDs verwenden, kein Anregungsfilter notwendig.

Im Gegensatz zur konfokalen Mikroskopie, wo der Laser- oder LED-Strahl durch die Probe geschickt wird, ist bei der TIRF-Mikroskopie der Einstrahlwinkel entscheidend: Ist der Einstrahlwinkel θ_1 kleiner als der kritische TIRF-Winkel θ_k, dringt der Laserstrahl in die Probe ein und regt dort die Fluorophore auf allen Ebenen an (Abbildung 9a). Entspricht der Einstrahlwinkel θ_1 dem kritischen TIRF-Winkel θ_k, wird der Laserstrahl im 90° Winkel abgestrahlt (θ_2, Abbildung 9b). Nur wenn der Einstrahlwinkel größer als der kritische TIRF-Winkel ist (Abbildung 9c), kann der Lichtstrahl totalreflektiert werden, wodurch nur die elektrische Komponente des Lichts in die Probe eindringen und ein elektromagnetisches Feld an der Grenzfläche zur Probe, das sogenannte evaneszente Feld bzw. die evaneszente Welle, bilden kann (Abbildung 10). Die Eindringtiefe der evaneszenten Welle in die Probe hängt von der Wellenlänge, dem Einstrahlwinkel und den Brechungsindizes der Medien (Glas und Probe) ab und beträgt bis zu 200 nm. Dabei ist die Intensität umso stärker, je näher sich die Probe an der Quelle der Energie befindet. In Abbildung 10 ist schematisch der Aufbau des sFIDA und die Position der Fluorophore dargestellt. Der Assayaufbau

erstreckt sich über einen Bereich von ca. 20-30 nm über der Glasoberfläche und liegt damit vollständig im evaneszenten Feld.

Der Vorteil der TIRF-Mikroskopie gegenüber konfokalen Mikroskopen liegt darin, dass nur Fluorophore, die sich an der Oberfläche des Glases befinden, angeregt werden, wodurch sich das Hintergrundrauschen reduziert und die Auflösung verbessert [122]. Die Auflösung in der Mikroskopie ist der Abstand, den zwei Objekte haben müssen, um noch getrennt voneinander dargestellt werden zu können. Die Auflösung ist von der numerischen Apertur des Objektivs, der Wellenlänge und dem Brechungsindex des Mediums abhängig. Beim TIRF-Mikroskop wird ein Ölimmersionsobjektiv verwendet. Da Öl einen höheren Brechungsindex (n = 1,55) als Wasser (n = 1,33) oder Luft (n = 1) hat, kann hierdurch die Auflösung verbessert werden. Die Auflösung lässt sich anhand der folgenden Formel (1) berechnen und beträgt für das TIRF-Mikroskop mit einer numerischen Apertur von 1,47 im grünen Fluoreszenzkanal 202 nm und im roten 263 nm [123, 124].

$$Auflösung[nm] = \frac{0{,}61*\lambda}{NA} \quad (1)$$

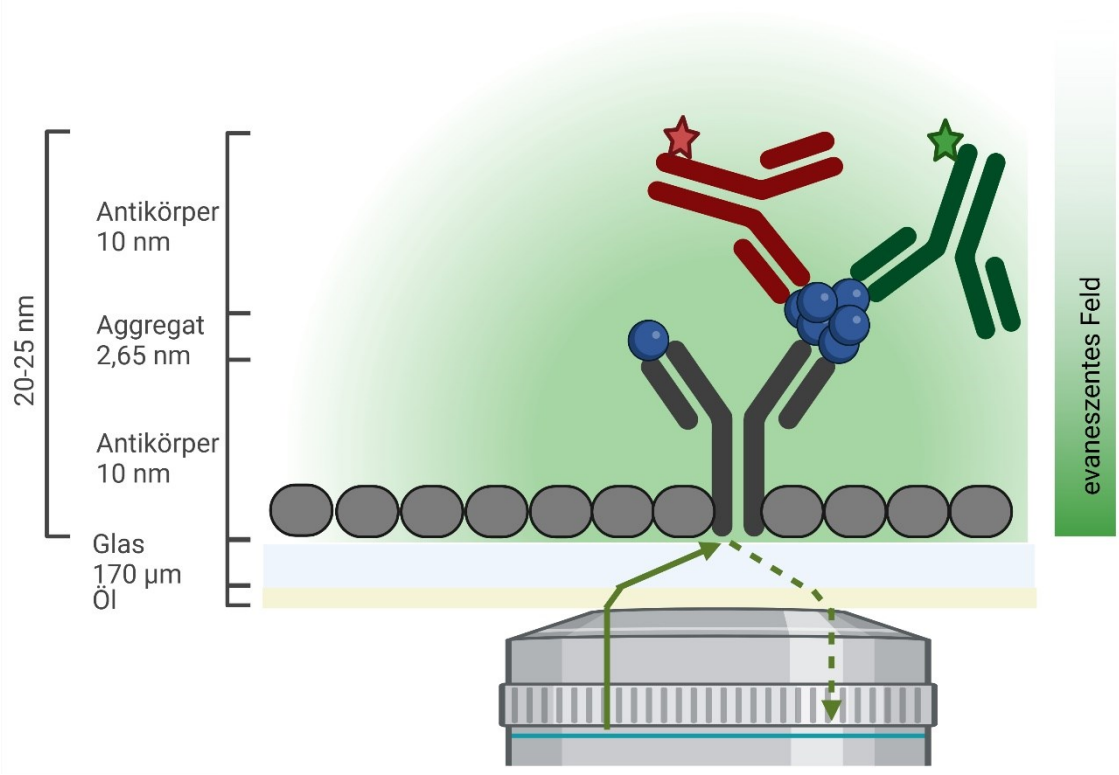

Abbildung 10 Prinzip der TIRF-Mikroskopie
Trifft der Lichtstrahl in einem Winkel größer als der kritische Winkel auf die Probe, wird das Licht reflektiert. Es bildet sich ein evaneszentes Feld, dass bis zu 200 nm tief in die Probe eindringen kann. Hierdurch werden nur Fluorophore an der Glasoberfläche angeregt, wodurch das Hintergrundrauschen reduziert und die Auflösung verbessert werden kann. *Erstellt mit BioRender.com*

Gekoppelt ist das TIRF-Mikroskop an eine *electron-multiplying charge-coupled device* (EMCCD)-Kamera, die Bildaufnahmen von der Oberfläche macht. Die Bilder haben eine Abmessung von 1000 x 1000 Pixeln und entsprechen bei einer 100 x Vergrößerung einer Bildfläche von 113,8 x 113,8 µm und einer Pixelkantenlänge von 113,8 nm.

Durch die Welleneigenschaft des Lichtes wird ein Lichtpunkt von Kreisen geringerer Intensität umgeben (sogenannte *Airy Discs* bzw. Beugungsringe). Für die Messung der Proteinaggregate im sFIDA bedeutet das, dass selbst bei Partikeln, die kleiner sind als ein Pixel, umgebende Pixel mit ausgeleuchtet werden können.

1.3.4 Auswertung

Für die Auswertung des sFIDA wurde die Software sFIDAta entwickelt. Die Auswertung erfolgt dabei auf Pixelebene und basiert für jeden Pixel auf der Entscheidung, ob die Intensität des Pixels über oder unter einem bestimmten Intensitätsschwellenwert, dem sogenannten *cutoff* liegt. Abbildung 11 zeigt beispielhaft die Abhängigkeit der digitalen Entscheidung vom gewählten *cutoff*: Je höher der *cutoff*, desto weniger Pixel erreichen diesen Schwellenwert. Der *cutoff* wird idealerweise so gewählt, dass Negativ- und Positivkontrolle die beste Differenzierung aufweisen. Ein zu niedriger *cutoff* (Abbildung 11a) führt dazu, dass zu viele unspezifische Pixel gezählt werden (Hintergrundrauschen der Kamera oder Hintergrund durch unspezifische Bindung der Antikörper an die Assayoberfläche), während bei einem zu hohen *cutoff* (c) viele Pixel den Schwellenwert nicht mehr erreichen, obwohl sie auf einer spezifischen Bindung des Antikörpers basieren. Der verwendete *cutoff* wird anhand der Negativkontrolle definiert und ist der Intensitätsschwellenwert, bei dem in der Negativkontrolle eine definierte Anzahl an Pixeln diesen Schwellenwert überschreiten. Die Anzahl an Pixeln über dem *cutoff* wird als PixelCount bezeichnet.

Bei Verwendung von mehr als einem Detektionsantikörper kann als zusätzliche Auswerteoption der *sFIDA Readout* verwendet werden. Der sFIDA Readout ist dabei erneut eine Pixelanzahl, allerdings wird ein Pixel nur dann gezählt, wenn er in allen Fluoreszenzkanälen den entsprechenden individuellen Intensitätsschwellenwert überschreitet. Der sFIDA Readout ist entsprechend die Anzahl kolokalisierter Pixel in einem Bild. Während die unspezifische Bindung der Antikörper an der Assayoberfläche zufällig erfolgt und dadurch stochastisch bedingt nur in Einzelfällen kolokalisert ist, ist die Bindung an den Analyten spezifisch und zu einem größeren Anteil kolokalisiert. Der Vorteil des sFIDA-Readouts liegt sowohl in einer höheren Sensitivität aufgrund eines reduzierten Hintergrundrauschens und einer verbesserten Differenzierung in den niedrigen

Konzentrationen als auch in einer höheren Selektivität, da einzelne unspezifisch gebundene Antikörper die Analyse nicht beeinflussen.

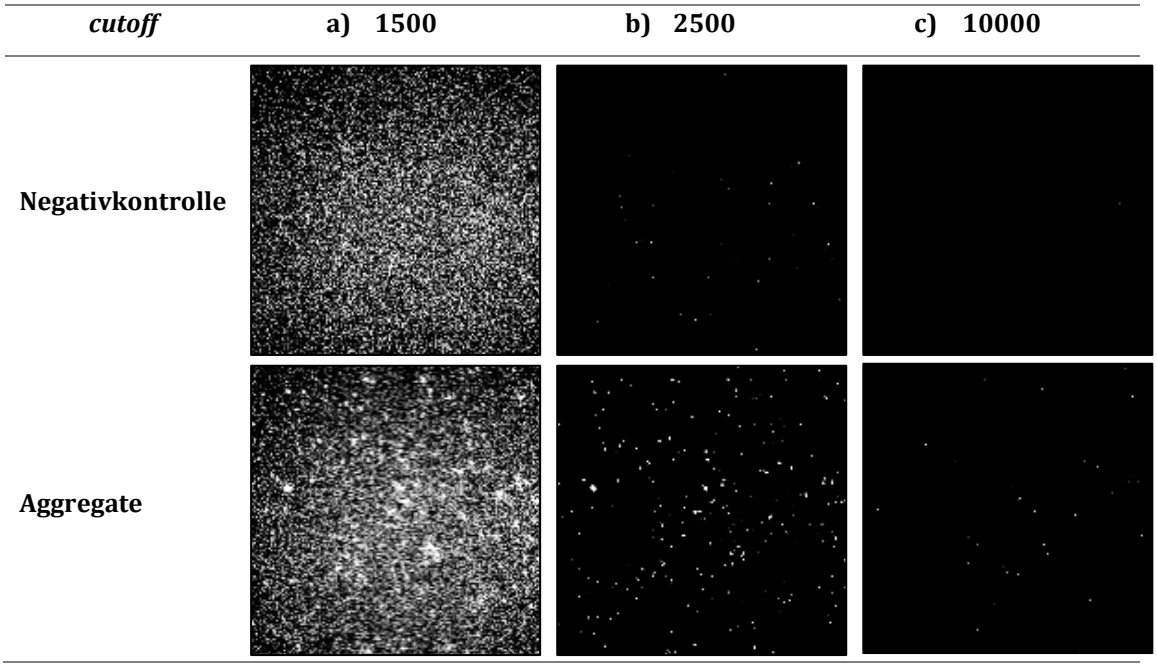

Abbildung 11 Binäre Darstellung einer Negativkontrolle und von Aβ-Aggregaten in Abhängigkeit des gewählten *cutoffs*
Pixel mit Intensitäten über dem *cutoff* werden weiß dargestellt, Pixel mit geringerer Intensität als der *cutoff* schwarz (die Summe der weißen Pixel entspricht dem PixelCount). Die Differenzierung der Negativkontrolle (Plasma) und einer Konzentration von 250 pM Aggregaten (in Plasma, Konzentration bezogen auf die Monomereinheiten) ist abhängig vom gewählten cutoff.

1.3.5 Probenmatrix

Der Nachweis der Proteinaggregate mittels sFIDA kann in verschiedenen Körperflüssigkeiten (Matrices) erfolgen. Präanalytische Faktoren, z.B. Zentrifugieren und Zeit bis zum Einfrieren, die Probenqualität, z.B. Material der Probengefäße oder Hämolyse, und die Zusammensetzung der jeweiligen Matrix (z.B. Proteinkonzentration oder heterophile Antikörper) können die Quantifizierung der Oligomere beeinflussen. In der vorliegenden Arbeit wurde mit CSF-, Plasma- und Stuhlproben gearbeitet.

CSF

Bei der Cerebrospinalflüssigkeit (*Liquor cerebrospinalis*, CSF) handelt es sich um eine klare, proteinarme (0,16-0,38 g/l) und fast zellfreie Flüssigkeit (1 Leukozyt/µl CSF). Die gesamte Menge an CSF im Gehirn liegt bei 150-160 ml, wobei täglich ca. 400 ml durch Filtration von Blut zwischen den Kapillaren und der Interstitialflüssigkeit und im *Plexus Choroideus* in den Hirnventrikeln produziert werden. Die Aufgaben vom CSF liegen in dem Schutz von Gehirn und Rückenmark vor mechanischen Einwirkungen, dem Ausgleich des

Blutvolumens während eines Herzschlags und der Beseitigung von Abfallstoffen aus dem Gehirn [72, 74, 125]. Durch die Nähe zum Gehirnparenchym stellt CSF eine geeignete Matrix dar, um Veränderungen im Proteinmetabolismus im Gehirn zu messen [23].

Die Gewinnung von CSF erfolgt üblicherweise über eine Lumbalpunktion zwischen dem dritten und fünften Lendenwirbeldornfortsatz. In seltenen Fällen, z.B. aufgrund von Kontraindikationen, kann eine subokzipitale Punktion im Bereich der Halswirbelsäule durchgeführt werden. Häufige Nebenwirkungen der Liquorpunktion sind leichte Blutungen, lokale Schmerzen an der Punktionsstelle und das postpunktionelle Syndrom, bei dem es sich um einen orthostatischen Kopfschmerz handelt, der mit Übelkeit, Erbrechen und Lichtempfindlichkeit einhergehen kann [126].

Die Entnahme der CSF-Probe sollte in ein Gefäß aus Polypropylen erfolgen, um eine Wechselwirkung des Analyten mit der Gefäßwand zu vermeiden. Außerdem kann das Volumen und bei mehrere Aliquots deren Reihenfolge die Konzentration der Biomarker beeinflussen, da die Proteinkonzentration im CSF mit steigender Fraktion abnehmen kann. Nach der Entnahme kann CSF zentrifugiert werden, um Zellen, u.a. rote Blutkörperchen durch Blutkontamination des CSF, zu entfernen. Die Lagerung der Proben sollte bei -80°C erfolgen [127].

Plasma

Eine weniger invasive Matrix stellt das Blutplasma dar. Im menschlichen Körper fließen 6-7 Liter Blut, das für den Transport von Sauerstoff, zur Pufferung und für die Immunabwehr zuständig ist. Eine wichtige Aufgabe liegt außerdem im Transport von Proteinen, u.a. Aβ. Blut besteht dabei aus einem zellulären Anteil, dem sogenannten Hämatokrit, der größtenteils aus Erythrozyten, aber auch Leukozyten und Thrombozyten besteht und bei Männern 40-54 % und bei Frauen 37-47 % des Gesamtblutvolumens ausmacht. Der flüssige Anteil wird als Blutplasma bzw. Blutserum bezeichnet und kann durch Abzentrifugieren der Blutzellen gewonnen werden (Abbildung 12) [128].

Um Blutplasma zu gewinnen, muss direkt nach der Blutabnahme ein Blutgerinner (Antikoagulanz) zugesetzt werden. Hierfür können entweder Ethylendiamintetraacetat (EDTA) oder Citrat verwendet werden, die durch Komplexierung von Calcium die Blutgerinnung verhindern, oder Heparin, das durch Bindung an Antithrombin Gerinnungsfaktoren wie Faktor X oder Thrombin hemmt [114]. Lässt man Blut ohne Zusatz von Gerinnungshemmern gerinnen, erhält man nach der Zentrifugation Blutserum, dass im Gegensatz zum Plasma keine Gerinnungsfaktoren mehr enthält. Nach dem Überführen des Überstandes sollten Plasma- oder Serumproben zur Lagerung bei -80°C eingefroren werden

[129, 130]. In der vorliegenden Arbeit wurde ausschließlich mit EDTA-Plasma gearbeitet, das im Folgenden als Plasma bezeichnet wird.

Im Plasma sind Salze, Fette, Aminosäuren, Kohlenhydrate und Proteine, insbesondere Albumin und Globuline, enthalten. Albumin macht mit ca. 60 % der Gesamtproteine und einer Konzentration von 43 g/l den Hauptbestandteil der Plasmaproteine aus. Neben der Aufrechterhaltung des onkotischen Drucks ist Albumin ein Transportprotein und bindet u.a. Fettsäuren, Hormone, Medikamente aber auch andere Proteine wie Aβ. Unter die Globuline fallen neben den Antikörpern auch die Lipoproteine und Gerinnungsproteine [69, 74, 125, 128].

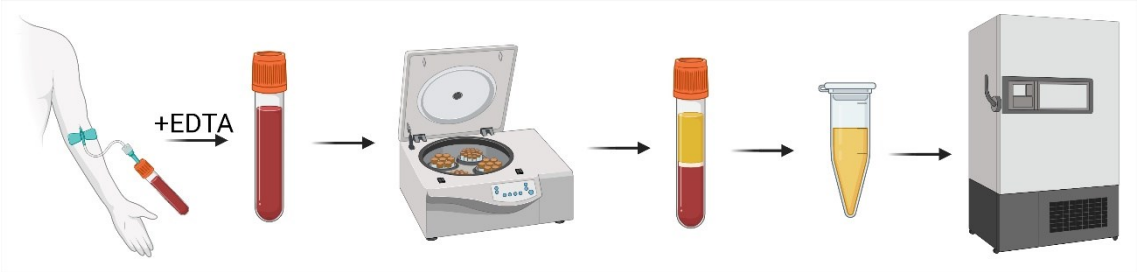

Abbildung 12 Gewinnung von Plasma
Die Blutabnahme erfolgt in Röhrchen mit einem Antikoagulanz, z.B. EDTA, dass die Blutgerinnung verhindert. Bei der anschließenden Zentrifugation des Blutes erfolgt eine Trennung in die festen Bestandteile (Hämatokrit, rot) und das Blutplasma (gelb). Das Blutplasma wird abgenommen und bis zur Vermessung bei -80°C gelagert.

Stuhl

Die Gewinnung von Stuhl ist im Gegensatz zu Plasma und CSF ein nicht-invasives Verfahren und eignet sich daher besonders als Matrix für die Bestimmung von Biomarkern [131]. Die tägliche Stuhlmenge liegt bei durchschnittlich 150-200 g pro Tag, ist aber ebenso wie die Stuhlzusammensetzung von der Nahrung abhängig [125, 131, 132].

Stuhl besteht zu ca. 75 % aus Wasser und 25 % aus festen Bestandteilen wie Proteinen, Kohlenhydraten und Fetten, wobei die bakterielle Biomasse mit 25-54 % der gesamten festen Bestandteile den größten Anteil hat. Der Proteinanteil setzt sich aus endogenem und bakteriellem Protein zusammen. Die Form des Stuhls wird anhand der Bristol-Stuhlformskala in sieben Kategorien eingeteilt, wobei der Stuhl in der ersten Kategorie als einzelne, harte, nussförmige Kügelchen vorliegt und die siebte Kategorie flüssigen Stuhl ohne feste Bestandteile umfasst [132]. Die Stuhlproben werden vor Verwendung homogenisiert und zentrifugiert, um u.a. die Proteine zu extrahieren und unlösliche Bestandteile abzutrennen.

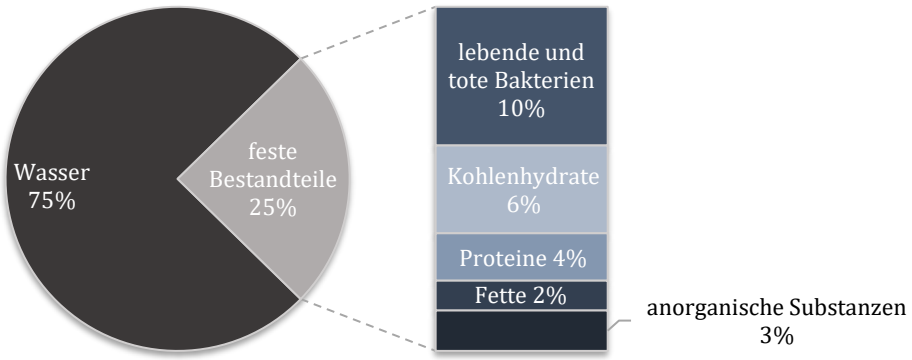

Abbildung 13 Zusammensetzung von Stuhl
Stuhl besteht zum größten Teil aus Wasser. Die festen Bestandteile setzen sich in absteigenden Anteilen aus lebenden und toten Bakterien, Kohlenhydraten, Proteinen, anorganischen Substanzen und Fetten zusammen, wobei die genaue Zusammensetzung individuell sehr verschieden ist und z.B. von der Ernährung abhängt.

Matrixeffekte

Als Matrixeffekte können alle Interferenzen in einem Immunoassay verstanden werden, die durch die Matrix, z.B. durch Plasma und CSF, ausgelöst werden. Messungen in Plasma sind dabei aufgrund des hohen Proteinanteils anfälliger für Matrixeffekte als z.B. CSF.

Als Ursache für Matrixeffekte kommen Analyt-spezifische Interferenzen wie Autoantikörper und Analyt-unspezifische Interferenzen wie heterophile Antikörper oder die Maskierung des Analyten infrage. Bei einem Sandwich-Aufbau können Matrixeffekte im Allgemeinen zwei Folgen haben: Proben, die keinen Analyten enthalten, geben ein positives Signal (falsch positiv) oder Proben geben trotz der Anwesenheit des Analyten kein Signal (falsch negativ) (Abbildung 14). Von besonderer Relevanz bei der Messung von Plasmaproben ist die Anwesenheit heterophiler Antikörper, insbesondere humaner Anti-Maus-Antikörper (HAMAs). Aufgrund der bivalenten Struktur der Antikörper können HAMAs in einem Sandwich-Aufbau zu einer Quervernetzung von Capture- und Detektionsantikörper führen und ein falsch-positives Signal bewirken. Falsch negative Signale können durch direkte Blockierung der Assay-Antikörper oder durch die Maskierung der Epitopbindestelle hervorgerufen werden, z.B. durch Bindung des Analyten an Matrixbestandteile wie Albumin oder Fett [117, 133].

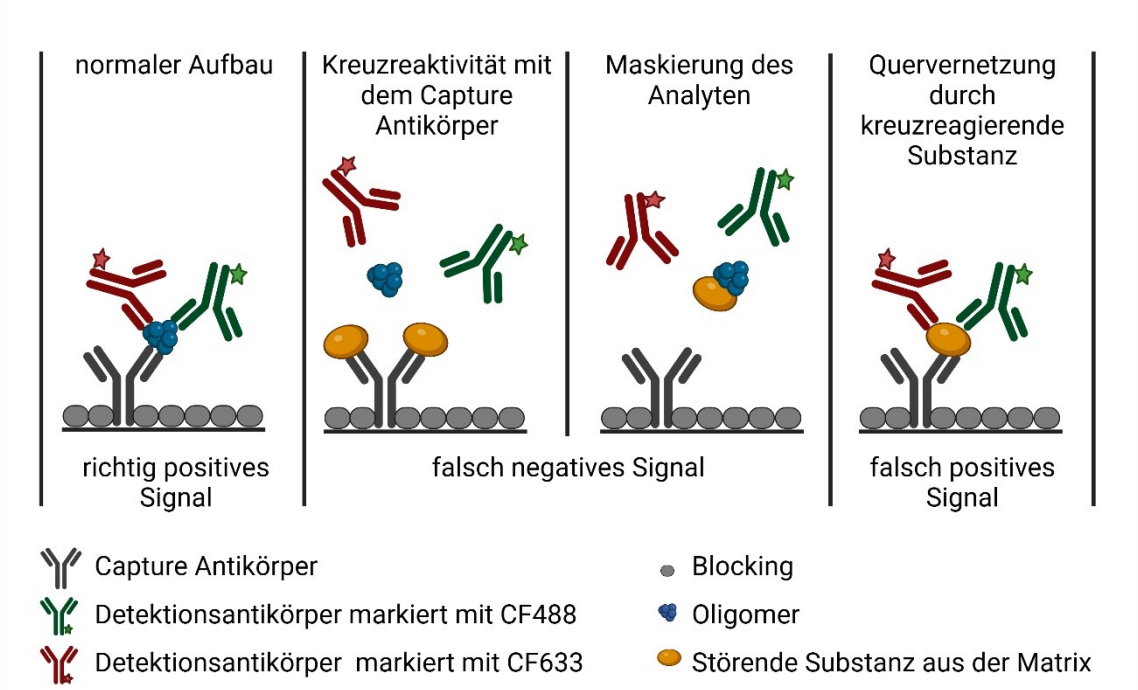

Abbildung 14 Einfluss von Matrixeffekten auf das Signal im sFIDA
Probenbestandteile können durch unspezifische Bindung an den Captureantikörper entweder die Bindung des Analyten blockieren und zu falsch-negativen Signalen führen oder durch Quervernetzung des Capture- und Detektionsantikörpers (z.B. durch heterophile Antikörper) falsch-positive Signale hervorrufen. Außerdem können Probenbestandteile an den Analyten binden und die Epitopbindestelle abdecken oder aus sterischen Gründen eine Immobilisierung oder Detektion verhindern und dadurch ebenfalls falsch-negative Signale auslösen. Abbildung in Anlehnung an [117].

2 Zielsetzung

Allen neurodegenerativen Erkrankungen ist die Beteiligung aggregierter Proteine, insbesondere der löslichen, neurotoxischen Oligomere, gemein. Aufgrund des direkten Zusammenhangs der Oligomere mit der Erkrankung stellen diese Oligomere einen idealen Biomarker für die Diagnose neurodegenerativer Erkrankungen dar. Für den sFIDA konnte in vorherigen Studien gezeigt werden, dass eine verlässliche Quantifizierung durch die Verwendung von stabilen proteinkonjugierten SiNaPs möglich ist und dass Oligomere in CSF von AD-Patienten gegenüber Kontrollen erhöht sind.

Das Ziel der vorliegenden Arbeit war zunächst eine Weiterentwicklung bestehender Assays bezüglich der analytischen Sensitivität und Selektivität zum Nachweis von Oligomeren in CSF für verschiedene neurodegenerative Erkrankungen. Ein besonderer Fokus lag hier auf dem zeitgleichen Nachweis verschiedener aggregierter Proteine wie αSyn und Tau bzw. Aβ und Tau, um eine Abhängigkeit sowohl zwischen den Proteinen als auch zwischen verschiedenen Erkrankungen zu eruieren. Hierzu wurden in zwei großen Probenpanels die Konzentrationen von αSyn und Tau-Oligomeren in verschiedenen neurodegenerativen Erkrankungen und von Aβ- und Tau-Oligomeren in unterschiedlichen Stadien von AD bestimmt. Hierdurch sollen zum einen Rückschlüsse über die Eignung des sFIDA zur Quantifizierung der Proteinaggregate in neurodegenerativen Erkrankungen getroffen werden, zum anderen soll diese Arbeit damit zur Fragestellung beitragen, ob die Bestimmung der Proteinoligomere und Aggregate einen geeigneten Biomarker für die Diagnose neurodegenerativer Erkrankungen darstellt.

Die Analyse von Proteinaggregaten in CSF hat den großen Vorteil der direkten Verbindung von CSF mit der Interstitialflüssigkeit und dem Gehirnparenchym, sodass pathophysiologische Veränderungen im Gehirn auch im CSF nachgewiesen werden können. Allerdings kann eine Liquorpunktion aufgrund der Invasivität und der Notwendigkeit der direkten Weiterverarbeitung von CSF nicht standardmäßig in Hausarztpraxen durchgeführt werden. Ein weniger invasives Verfahren, z.B. der Nachweis der Oligomere in Stuhl oder in Plasma, würden ein routinemäßiges Screening ermöglichen. Die Herausforderung dieser Körperflüssigkeiten liegt in der komplexeren Matrix und den geringeren Konzentrationen der Biomarker, was noch sensitivere und weniger störanfällige Verfahren erfordert. Außerdem gibt es bisher wenig Evidenz für die Eignung dieser explorativen Biomarker in Körperflüssigkeiten außerhalb des CSF.

Das Hauptaugenmerk im zweiten Teil dieser Arbeit lag daher zunächst in der Entwicklung eines sensitiven und spezifischen Tests zur Quantifizierung von Aβ-Oligomeren in Blutplasma. Durch die Anwendung dieses Tests in Plasmaproben von AD-

Patienten sollte anschließend geklärt werden, ob sich Aβ-Oligomere in Plasma in Abhängigkeit des Erkrankungsfortschritts verändern und damit einen möglichen minimalinvasiven Biomarker darstellen.

3 Manuskripte

3.1 Quantitative Detection of α-Synuclein and Tau oligomers and other aggregates by Digital Single Particle Counting

Autoren:	Lara Blömeke, Marlene Pils, Victoria Kraemer-Schulien, Alexandra Dybala, Anja Schaffrath, Andreas Kulawik, Fabian Rehn, Anne Cousin, Volker Nischwitz, Johannes Willbold, Rebecca Zack, Thomas F. Tropea, Tuyen Bujnicki, Gültekin Tamgüney, Daniel Weintraub, David Irwin, Murray Grossman, David A. Wolk, John Q. Trojanowski, Oliver Bannach, Alice Chen-Plotkin, Dieter Willbold
Journal:	npj parkinson's disease (veröffentlicht)
DOI:	10.1038/s41531-022-00330-x
Impact-Faktor:	8,7 (2022)
Beitrag:	Eigenanteil: 70 % Entwicklung des Assays Messung und Auswertung der Proben Anfertigung der Abbildungen Statistische Auswertung Hauptverfasserin des Manuskripts
Anhang zum Manuskript	Kapitel 7.1

npj | parkinson's disease

www.nature.com/npjparkd

ARTICLE OPEN

Check for updates

Quantitative detection of α-Synuclein and Tau oligomers and other aggregates by digital single particle counting

Lara Blömeke[1,2], Marlene Pils[2,3], Victoria Kraemer-Schulien[1], Alexandra Dybala[2,3], Anja Schaffrath[1], Andreas Kulawik[1,2,3], Fabian Rehn[1], Anneliese Cousin[1], Volker Nischwitz[4], Johannes Willbold[1], Rebecca Zack[5], Thomas F. Tropea[5,6], Tuyen Bujnicki[1], Gültekin Tamgüney[1,3], Daniel Weintraub[6,7,8], David Irwin[5,6], Murray Grossman[5,6], David A. Wolk[5], John Q. Trojanowski[6,9], Oliver Bannach[1,2,3], Alice Chen-Plotkin[5,6] and Dieter Willbold[1,3]✉

The pathological hallmark of neurodegenerative diseases is the formation of toxic oligomers by proteins such as alpha-synuclein (aSyn) or microtubule-associated protein tau (Tau). Consequently, such oligomers are promising biomarker candidates for diagnostics as well as drug development. However, measuring oligomers and other aggregates in human biofluids is still challenging as extreme sensitivity and specificity are required. We previously developed surface-based fluorescence intensity distribution analysis (sFIDA) featuring single-particle sensitivity and absolute specificity for aggregates. In this work, we measured aSyn and Tau aggregate concentrations of 237 cerebrospinal fluid (CSF) samples from five cohorts: Parkinson's disease (PD), dementia with Lewy bodies (DLB), Alzheimer's disease (AD), progressive supranuclear palsy (PSP), and a neurologically-normal control group. aSyn aggregate concentration discriminates PD and DLB patients from normal controls (sensitivity 73%, specificity 65%, area under the receiver operating curve (AUC) 0.68). Tau aggregates were significantly elevated in PSP patients compared to all other groups (sensitivity 87%, specificity 70%, AUC 0.76). Further, we found a tight correlation between aSyn and Tau aggregate titers among all patient cohorts (Pearson coefficient of correlation $r = 0.81$). Our results demonstrate that aSyn and Tau aggregate concentrations measured by sFIDA differentiate neurodegenerative disease diagnostic groups. Moreover, sFIDA-based Tau aggregate measurements might be particularly useful in distinguishing PSP from other parkinsonisms. Finally, our findings suggest that sFIDA can improve pre-clinical and clinical studies by identifying those individuals that will most likely respond to compounds designed to eliminate specific oligomers or to prevent their formation.

npj Parkinson's Disease (2022)8:68 ; https://doi.org/10.1038/s41531-022-00330-x

INTRODUCTION

Tauopathies and synucleinopathies are characterized by abnormal aggregation of microtubule-associated protein tau (Tau) and alpha-synuclein (aSyn), respectively. From the clinical perspective there is some overlap in the phenotypic presentation of the resulting diseases, with parkinsonism characterizing multiple diseases, including Parkinson's disease (PD), dementia with Lewy bodies (DLB), and progressive supranuclear palsy (PSP)[1,2]. While protein aggregation is the pathological key event in these disorders, ultimately resulting in the formation of aSyn and Tau deposits, the neurotoxic effect is thought to be exerted by small oligomeric intermediates within the aggregation pathway[3–5]. Consequently, a number of drug candidates have been designed to interfere with the aggregation pathway aiming to eliminate existing oligomers or to prevent their formation[6]. Since aggregate formation reflects pathophysiological changes inside the brain, oligomers have also been proposed as promising biomarker candidates[7–9]. However, quantitative measurement of oligomers is technically challenging and mainly hampered by three technical issues. First, the minute amount of oligomers in human biofluids such as cerebrospinal fluid (CSF) requires extreme sensitivity. Secondly, the presence of a vast excess of monomers demands high selectivity for oligomers over monomeric species. Quantitation of oligomeric aSyn by ELISA-like techniques, which employ overlapping epitopes or antibody probes directed against structural motifs, render these assays insensitive towards monomers[10]. Our previously developed sFIDA technology (surface-based fluorescence intensity distribution analysis) employs a similar biochemical setup using the same capture and detection antibody (Fig. 1) but features single-particle sensitivity through a microscopy-based readout[11]. Thirdly, the structural diversity of aggregates renders their detection technically challenging[12]. sFIDA uses linear epitopes and therefore detects and counts all subtypes of aggregated protein irrespectively of higher-ordered structures, while assays using structural epitopes only determine a subfraction of oligomers, fibrils, or other aggregates from a heterogeneous pool of structures. Because the assay itself is not yet discriminating between small oligomers and larger, but still soluble assemblies, like protofibrils, seeding competent fibrillar oligomers or fibrils, we refer to the analytes measured by sFIDA as aggregates, irrespectively, whether they are on or off pathway to fibrils[13].

While our prior work establishes the technical concept of sFIDA[11,14,15], its utility in clinical samples from neurodegenerative

[1]Institute of Biological Information Processing (Structural Biochemistry: IBI-7), Forschungszentrum Jülich, 52428 Jülich, Germany. [2]attyloid GmbH, 40225 Düsseldorf, Germany. [3]Institut für Physikalische Biologie, Heinrich-Heine-Universität Düsseldorf, 40225 Düsseldorf, Germany. [4]Central Institute for Engineering, Electronics and Analytics, Analytics (ZEA-3), Forschungszentrum Jülich, 52428 Jülich, Germany. [5]Department of Neurology, Perelman School of Medicine, University of Pennsylvania, Philadelphia, PA, USA. [6]Center for Neurodegenerative Disease Research, Perelman School of Medicine, University of Pennsylvania, Philadelphia, PA, USA. [7]Department of Psychiatry, Perelman School of Medicine, University of Pennsylvania, Philadelphia, PA, USA. [8]Parkinson's Disease and Mental Illness Research, Education, and Clinical Centers, Philadelphia Veterans Affairs Medical Center, Philadelphia, PA, USA. [9]Department of Pathology and Laboratory Medicine, Perelman School of Medicine, University of Pennsylvania, Philadelphia, PA, USA.
✉email: d.willbold@fz-juelich.de

Published in partnership with the Parkinson's Foundation

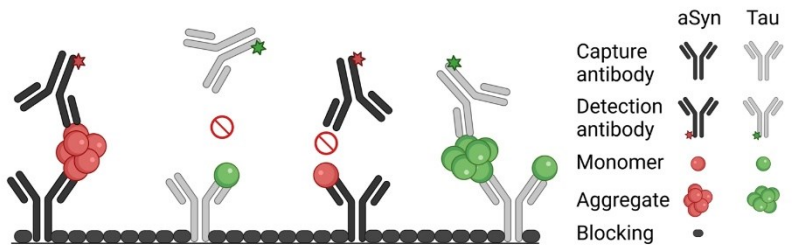

Fig. 1 Scheme of the sFIDA assay. Antibodies directed against linear epitopes of aSyn (211) or Tau (Tau5) are immobilized on the glass surface of a microtiter plate. Monomers and aggregates of the sample can bind to the capture antibodies, but only aggregates are detected with fluorescently labeled probes (211 CF633 and Tau5 CF488A) because capture and detection antibodies bind the same epitope. For monomeric protein, this epitope is masked by the capture antibody and can therefore not be bound by a probe antibody. Finally, the assay surface is imaged by dual-color fluorescence microscopy and single particles on the well surface are counted by image-data analysis. *Created with BioRender.com*.

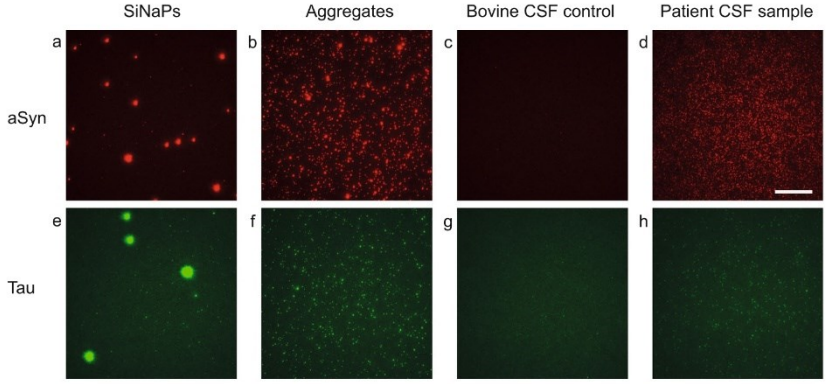

Fig. 2 TIRFM images of aSyn and Tau SiNaPs, synthetic aggregates, and samples. Shown are characteristic TIRFM images for the red fluorescence channel (211 CF633) of **a** 629 fM aSyn SiNaPs in buffer, **b** 8 nM aSyn aggregates in buffer (the concentration is based on the monomer concentration), **c** a bovine CSF control, **d** a CSF sample of a PD patient as well as for the green fluorescence channel (Tau5 CF488) of **e** 645 fM Tau SiNaPs in buffer, **f** 200 nM Tau aggregates in buffer (the concentration is based on the monomer concentration), **g** a bovine CSF control, **h** a CSF sample of a PSP patient. The scale bar is 25 µm. For illustration of the 14-bit images, the contrast was adjusted to a maximum grayscale value of 5000.

disease patients is yet to be established. In the present work, we apply sFIDA to quantitate aSyn and Tau aggregates in CSF from 237 individuals, demonstrating its applicability in clinical settings and drug development.

RESULTS

In this work, we have developed an sFIDA assay for simultaneous quantification of aSyn and Tau aggregates. Development and validation of immunoassays require determination of crucial parameters including limit of detection (LOD), coefficient of variation, inter-assay and inter-laboratory correlation and cross reactivity, which are described in the first part of the results chapter.

sFIDA displays low intra-assay variance for measurements of SiNaPs and samples

The sFIDA technology was used to determine the concentrations of aggregated aSyn and aggregated Tau in a total of 237 CSF samples. Due to the high number of assay points, the measurements were performed on a total of eight 384 well microtiter plates. For calibration of the samples and determination of the LOD, we used our previously developed silica nanoparticle (SiNaP) standard[14] (TEM image and size distribution in Supplementary Fig. 1). Exemplary images of SiNaPs, aggregates, bovine CSF and patient samples are shown in Fig. 2. The intra-assay variance among all experiments was calculated from the pixel counts of the four replicates. The intra-assay variance for the calibration standard was 15.8% for aSyn SiNaPs and 19.1% for Tau SiNaPs for the concentrations included in the calibration range. The intra-assay variance of the samples was 16.8% for aSyn aggregates and 13.0% for Tau aggregates, respectively (individual results for each experiment in Supplementary Table 1).

Independent measurements of aSyn and Tau aggregates in CSF samples yield comparable results

The inter-assay variance was studied in 20 samples on two different runs that were executed at a four-month interval. We analyzed each sample in four replicates and determined an intra-assay variation for the 20 CSF samples of 22.6% for aSyn aggregates and 20.4% for Tau aggregates. A linear correlation between the two measurements was observed for the detection of aSyn aggregates with a Pearson coefficient of correlation of $r = 0.964$. Although the concentration of Tau aggregates was less than that of aSyn aggregates and very close to the LOD, the two

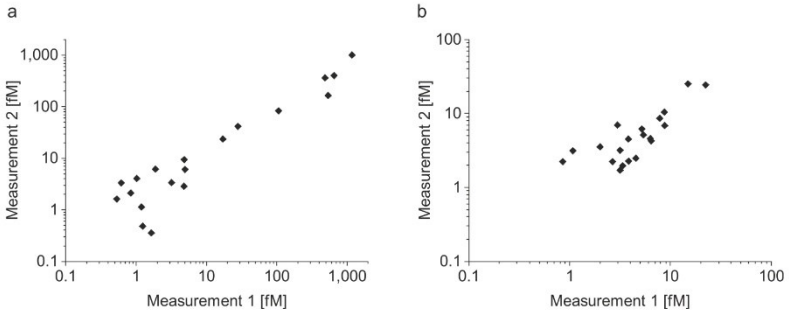

Fig. 3 Repeated measurements of aSyn and Tau aggregates in CSF yield highly reproducible results. We tested the inter-assay variance of the sFIDA assay for **a** aSyn and **b** Tau aggregates. Two independent measurements of 20 CSF samples by the same technician in the same laboratory on different days were highly reproducible with a Pearson coefficient of correlation of $r = 0.96$ for aSyn aggregates and $r = 0.92$ for Tau aggregates.

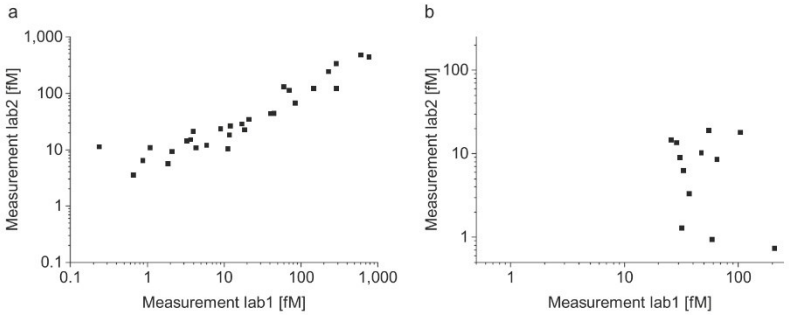

Fig. 4 Measurements of aSyn but not Tau aggregates in CSF correlated well when measured in a different laboratory. The CSF samples were measured by sFIDA by two different technicians in two different laboratories. The first sFIDA experiment was prepared and run by a technician at the Forschungszentrum Jülich, while the second sFIDA was performed by another technician at the Heinrich-Heine-Universität Düsseldorf. **a** Concentrations of aSyn aggregates correlated well between both experiments with a Pearson coefficient of correlation of $r = 0.95$, **b** while for Tau aggregates no correlation was observed ($r = 0.03$).

measurements showed a significant correlation with a Pearson coefficient of correlation of $r = 0.920$ (Fig. 3).

The inter-laboratory variance was studied in a laboratory at the Forschungszentrum Jülich and another laboratory at the Heinrich-Heine-Universität in Düsseldorf. The calibrated results for the detection of aSyn aggregates showed a high correlation with a Pearson coefficient of correlation of $r = 0.950$. In this study, no correlation for Tau aggregates was observed (Pearson coefficient of correlation of $r = 0.033$, Fig. 4).

sFIDA features femtomolar sensitivity for the detection of aSyn and Tau SiNaPs

We determined the sensitivity of the assay based on aSyn and Tau SiNaPs. After application of t-test, Mann-Whitney U test, LOD and standardization of the calibration range for all experiments, the upper limit of the calibration curve was 1.99 pM for aSyn and 2.04 pM for Tau SiNaPs, and the lower limit was set to 63 fM and 204 fM for aSyn and Tau SiNaPs, respectively. In all experiments a linear correlation between pixel count and concentration with a mean coefficient of determination of 0.98 for aSyn and 0.96 for Tau SiNaPs was observed. The calibration resulted in a mean LOD of 6.72 fM for the detection of aSyn SiNaPs and a mean LOD of 33.7 fM for the detection of Tau SiNaPs (individual LOD values for each experiment are shown in Supplementary Table 2). For aSyn aggregates, 66% of samples were above the LOD of the individual experiment and for Tau aggregates 44% (Supplementary Table 3).

sFIDA shows negligible cross reactivity for measurements of aSyn, amyloid beta, and Tau

To determine the selectivity of the sFIDA assay, amyloid beta SiNaPs with a concentration of 6 pM were used as a control. The amyloid beta SiNaPs were coated with amino acid residues 1–15 of the amyloid beta protein. We observed a very low cross reactivity with 0.1% of the signal for amyloid beta SiNaPs when compared to the signal obtained with aSyn SiNaPs and 0.2% of the signal obtained with Tau SiNaPs when used at a comparable concentration (data not shown). Detection of synthetic Tau aggregates with the 211 antibody and detection of synthetic aSyn aggregates with the Tau5 antibody resulted in a pixel count as negligible as for the buffer control (Fig. 5). The pixel count of the buffer control (BC) showed an increased background signal compared to the CSF control for aSyn (capture and detection antibody: 211) and Tau (capture and detection antibody: Tau5) (Fig. 5). Therefore, the CSF control was used as negative control for the calibration of the samples. The buffer control showed no autofluorescence signal (data not shown). The recovery of aSyn SiNaPs spiked in bovine CSF was 79%. For Tau SiNaPs the recovery in CSF was 36%. Another control was to run the assay without a capture antibody, which is an indication for unspecific binding of silica nanoparticles or proteins to the surface, and is described as the signal compared to the same concentration of silica nanoparticles/protein on an antibody surface. For aSyn, the signal originating from 6 pM silica nanoparticles without the use of a

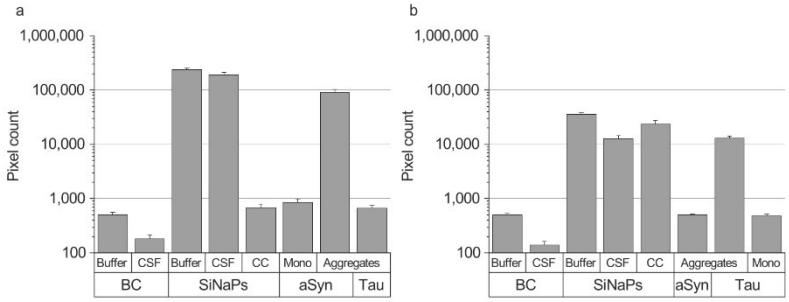

Fig. 5 Pixel counts of assay controls for the detection of aSyn and Tau aggregates. a aSyn SiNaPs showed a recovery of 79% in CSF, whereas **b** Tau SiNaPs showed a recovery of 36% in CSF. Synthetic aSyn and Tau aggregates served as positive controls. The pixel counts of the aSyn aggregates when detected with the Tau5 antibody as well as the pixel counts of the Tau aggregates when detected with the 211 antibody were as low as the blank control (BC). The pixel count of 8 nM monomeric (Mono) aSyn as well as 200 nM monomeric Tau was reduced by 99.5% compared to the same concentration of monomer units in aggregated aSyn or Tau. When the capture antibody was omitted (capture control, CC), no signal was detected for aSyn SiNaPs, whereas the signal for Tau SiNaPs was still at 67%. Standard deviation was calculated from the four replicates.

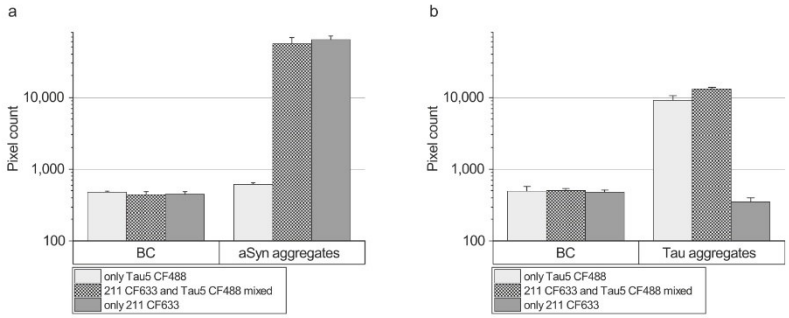

Fig. 6 Analysis of probe interference. To analyze the effect of detection probe interference on the signal, we performed an additional experiment in which we added either only one detection antibody or both detection antibodies. Using only the relevant antibody probe did not show an increased pixel count for the detection of aggregated aSyn (**a**, 211 CF633) or Tau (**b**, Tau5 CF488), respectively. Standard deviation was calculated from the four replicates.

capture antibody was below 0.1% of that when a capture antibody was used. For Tau, the signal was still at 67% without a capture antibody and, presumably, originating from large particles which non-specifically stick to the glass surface. Furthermore, we investigated the effect of monomeric aSyn and Tau on the sFIDA readout.

We found that the pixel counts of both aSyn and Tau monomers, respectively, were decreased by about 99.5% compared to the signal of aSyn or Tau aggregates indicating that endogenous monomers in the CSF samples have a neglectable effect on the sFIDA readout (Fig. 5).

To address the question whether addition of the mixture of two antibodies might impair assay sensitivity, we added just the relevant detection antibody or a mixture of both detection antibodies, and compared the correspondent sFIDA readouts. As shown in Fig. 6, applying just a single detection antibody did not increase the readout. Moreover, absence of confounding autofluorescence signals was demonstrated, because aggregated aSyn and Tau did not show any non-specific signal when the relevant antibody probe was not applied.

aSyn and Tau aggregates are removed by immunodepletion

To show that the signal measured by sFIDA is specifically attributed to aSyn and Tau aggregates and not to matrix interference, we performed immunodepletion in five CSF samples and the silica nanoparticle standard. To remove the analytes, samples were incubated in presence of magnetic beads linked to 211 antibody, Tau5 antibody or no antibody. After magnetic separation, the supernatants were subjected to sFIDA analysis. For aSyn, 211-depleted samples showed a mean decrease of the readout by 97.0% (Fig. 7b), while in the controls without 211 antibody, the readout was not reduced (−0.6%). Although the readout for Tau aggregates in the samples was comparatively low and close to that of the bovine CSF control, depletion with Tau5 decreased the readout by 38.6% (Fig. 7c, d). Incubation of the samples with magnetic beads alone led to an average decrease of the pixel count by only 19.5% (Fig. 7d). Still, the less efficient reduction in the samples compared to the standards can be attributed to a lower signal-to-noise ratio. The Tau-coated silica nanoparticle standard was depleted even without Tau5 antibody, suggesting non-specific adherence to the surface as observed in the capture control experiment (Fig. 5b).

Analysis of potential heterophilic anti-mouse antibodies (HAMAs) interference

Although one may expect absence of high antibody titers in CSF, we investigated whether HAMAs could possibly compromise the sFIDA assay result, and whether this is potentially relevant for the interpretation of the study results. HAMAs are a well-described interfering factor in immunoassays especially for blood-based

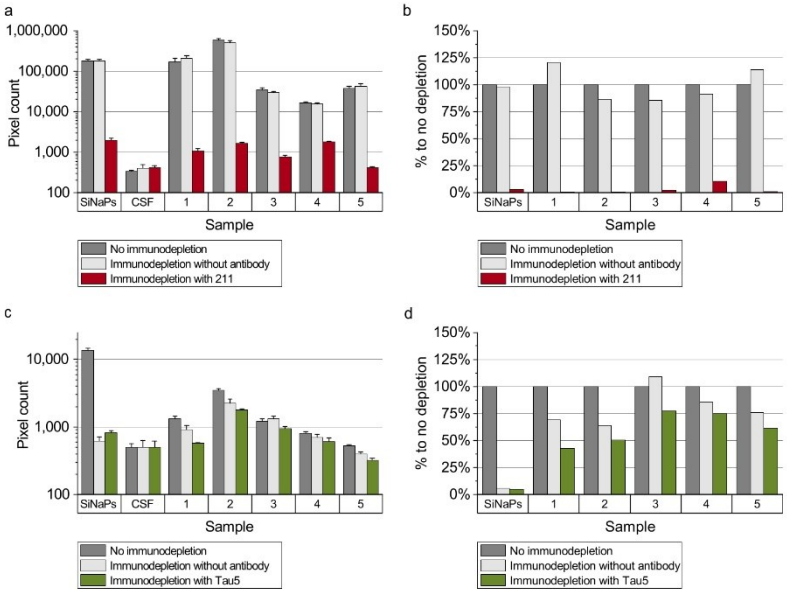

Fig. 7 Immunodepletion of aSyn and Tau in CSF samples. The SiNaP standard and five CSF samples were subjected to immunodepletion with magnetic beads with and without antibody. **a**, **b** Immunodepletion of samples with 211 antibody decreased the pixel counts for aSyn on average by 97%, while incubation with magnetic beads without antibody did not affect the signal. **c**, **d** For aggregated Tau, incubation with magnetic beads without antibody decreased the pixel count by 94% for Tau SiNaPs and on average by 19.5% for samples. Using Tau5 antibody, the decrease of the pixel count for Tau SiNaPs was 95% and for samples 38.6%, respectively. The *% to no depletion* value (Fig. 7 **b**, **d**) was calculated by the ratio the pixel counts of depleted to non-depleted samples. Standard deviation was calculated from the four replicates.

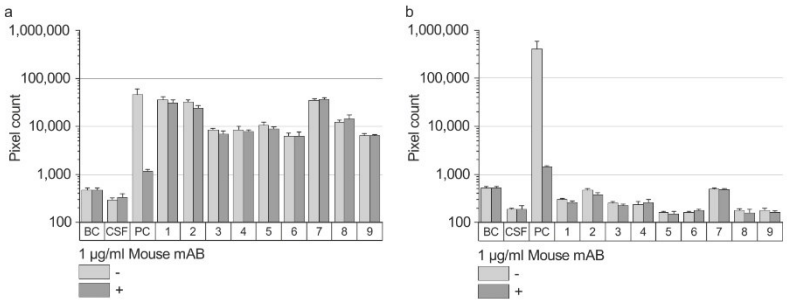

Fig. 8 Influence of heterophilic anti-mouse antibodies. To test, if the signal obtained by sFIDA was possibly caused by heterophilic anti-mouse antibodies, nine CSF samples were incubated with or without 1 µg/ml MOPC-21. As a HAMA model and positive control (PC), we used a goat anti-mouse antibody. The interference of this anti-mouse antibody was reduced by about 98.4% for aSyn (211 CF633, **a**) and 99.7% for Tau (Tau5 CF488, **b**) when adding MOPC-21 while for the CSF samples the signal remains unaffected. Standard deviation was calculated from the four replicates.

assays[16,17]. HAMAs can crosslink capture and detection mouse antibodies leading to false positive signals. Recent research indicates, that HAMAs can also interfere with measurements of CSF samples[18,19]. To analyze HAMA interference in our assay, we used an anti-mouse antibody as a HAMA model. As expected, sFIDA analysis of a blank control spiked with the anti-mouse antibody shows an increased signal in both detection channels (Fig. 8, PC). Addition of the same concentration of a competitor mouse antibody (MOPC-21) reduces the signal by 98.4% for 211 CF633 and by 99.7% for Tau5 CF488. Additionally, we tested nine CSF samples, which yielded high sFIDA readouts, for possible presence of HAMAs. Incubation of the samples with MOPC did not influence sFIDA readouts (p-value of two-sided Mann-Whitney-U for 211 CF633: 0.470, Tau5 CF488: 0.800) suggesting that the observed signal indeed originates from aggregate-bound probes and is not due to HAMA interference.

Contamination with blood did not affect the quantification of aSyn and Tau aggregates in CSF

As blood shows an increased concentration of total aSyn, the contamination of CSF even with low amounts of blood can interfere with the detection of aSyn monomers in CSF[20,21]. To investigate, whether the results in sFIDA were affected by blood contamination as well, we classified the samples into five groups according to their contamination level. Most of the samples (57%)

Table 1. Demographic information on patients and controls that donated CSF samples.

	PD	AD	DLB	PSP	*N*
Number	115	28	19	30	45
Female	41 (36%)	10 (36%)	5 (26%)	15 (50%)	20 (44%)
Age [years]	65.7 (±7.6)	68.2 (±6.3)	69.7 (±7.2)	67.5 (±6.2)	69.0 (±8.9)
Education [years]	16.3 (±2.3)	14.9 (±3.2)	15.5 (±2.8)	15.2 (±2.7)	16.6 (±3.6)
Deceased	17%	32%	32%	37%	13%

PD Parkinson's disease, *AD* Alzheimer's disease, *DLB* Dementia with Lewy bodies, *PSP* Progressive supranuclear palsy, *N* Normal control.

showed no contamination with blood (negative test result), 11% were classified to contamination level 1 (~10 Ery/µL), 7% to level 2 (~25 Ery/µL), and 8% to level 3 (~50 Ery/µl). A contamination of level 4 (> 250 Ery/µL) was observed in 18% of CSF. We further investigated, whether there is a correlation between high read-outs in sFIDA and the blood contamination level. We could not observe a significant increase of aSyn ($p = 0.776$) or Tau ($p = 0.628$) aggregate concentrations in CSF contaminated with blood using Kruskal-Wallis ANOVA (scatterplot in Supplementary Fig. 2). Therefore, no samples were excluded from analysis.

Descriptive analysis of the patient and control cohorts

The samples comprised five diagnostic groups (Table 1). Applying the Kruskal-Wallis test, no significant differences between groups was found for age and gender. For education, PD patients received longer education than AD patients, and normal controls received longer education than the AD and PSP cohorts. Individual information and results of each patient are listed in Supplementary Table 4.

aSyn and Tau aggregate levels distinguish patients with different neurodegenerative diseases

First, we tested the calibrated results of all groups for normal distribution. As the data showed non-normal distributions (*p*-value < 0.05, Supplementary Table 5), statistical analysis was performed using non-parametric tests like the Kruskal-Wallis or Mann-Whitney U test. The results of the Kruskal-Wallis test showed significant differences between the diagnostic groups for aggregated aSyn ($p = 6.92*10^{-3}$) as well as for aggregated Tau ($p = 2.17*10^{-6}$). The results of pairwise comparisons are shown in Table 2. Concentrations of aSyn aggregates in CSF samples of PD patients were significantly increased compared to the control group. Moreover, patients with DLB showed elevated levels of aSyn aggregates in their CSF. Interestingly, CSF samples of AD patients also showed significantly increased levels of aSyn aggregates compared to normal controls. In the scatterplot (Fig. 9a) as well as in the receiver operating characteristic (ROC) curve (Fig. 9c) we observed a great overlap between synucleinopathies like PD and DLB and the control group (sensitivity and specificity values and AUC in Table 3).

The concentrations of Tau aggregates in PSP samples were significantly elevated compared to all other groups (PD, DLB, AD and controls; Fig. 9b). ROC analysis (Fig. 9d) for this model showed a sensitivity and specificity of 87 and 70% (AUC 0.76) for distinguishing PSP from all other subjects based on Tau sFIDA alone. Moreover, patients with DLB had elevated levels of Tau aggregates compared to the control group ($p = 0.006$) and to PD patients ($p = 0.024$). Interestingly, no significant increase in Tau aggregate concentration for AD patients was observed. The performance of ROC analysis for the tauopathies PSP and AD versus non-tauopathies (DLB, PD, N) revealed a decreased sensitivity and specificity compared to PSP alone. AD alone showed no distinguishability to PD, DLB, and N (Table 2).

Table 2. *P*-values of two-sided Mann-Whitney U test for pairwise comparisons of measured aSyn and of Tau aggregate concentrations.

		PD	DLB	PSP	AD	*N*
aSyn	PD	1				
	DLB	0.992	1			
	PSP	0.292	0.326	1		
	AD	0.811	0.887	0.561	1	
	N	$3.6*10^{-4}$	0.007	0.109	0.010	1
Tau	PD	1				
	DLB	0.024	1			
	PSP	$2.0*10^{-6}$	0.022	1		
	AD	0.418	0.167	$3.4*10^{-4}$	1	
	N	0.243	0.006	$9.7*10^{-6}$	0.123	1

PD Parkinson's disease, *AD* Alzheimer's disease, *DLB* Dementia with Lewy bodies, *PSP* Progressive supranuclear palsy, *N* Normal control.

Aggregate concentrations show comparable discrimination to conventional biomarkers

In CNS biomarker research and clinical routine, total Tau protein (tTau) and phosphorylated Tau protein (pTau) are frequently used as a measure of neurodegeneration. For the present study, we received pTau and tTau concentrations of 88% of the CSF samples and compared sensitivity, specificity and AUC values for each biomarker alone and as combination of three biomarkers (for PD and DLB: pTau, tTau and aSyn aggregates, for AD and PSP: pTau, tTau and Tau aggregates). For PD vs. N, tTau, aSyn aggregates and the combination of pTau, tTau and aSyn aggregates showed nearly the same AUC but differences in specificity and sensitivity (Fig. 10 and Table 4). Due to the reduced number of samples and adaption of the method for the analysis of DLB vs. N, the AUC for aSyn aggregates was decreased compared to the first analysis with all samples (Fig. 9 and Table 3). Consequently, in this analysis, discrimination is only possible based on tTau values. Like in the first analysis, Tau aggregate levels did not discriminate AD vs. N, while AD patients showed increased concentrations of pTau and tTau and can be discriminated with an AUC of 0.78 and 0.75, respectively. For PSP vs. N, pTau and Tau aggregates separated the diseases with an AUC of 0.74 and 0.73. Here, the combination of the three biomarkers showed the largest AUC of 0.80.

aSyn and Tau aggregate concentrations significantly correlate between all patient cohorts

As a correlation between total aSyn (t-aSyn) and total Tau (tTau) has been reported in many studies[8,22–24], we investigated the correlation between aggregated forms of aSyn and Tau, respectively. A significant correlation between Tau and aSyn aggregate concentrations was observed for the whole data set (Pearson coefficient of correlation: $r = 0.81$, $p = 3.8*10^{-57}$), as well as for each individual diagnostic group (Fig. 11a). The greatest correlation was observed

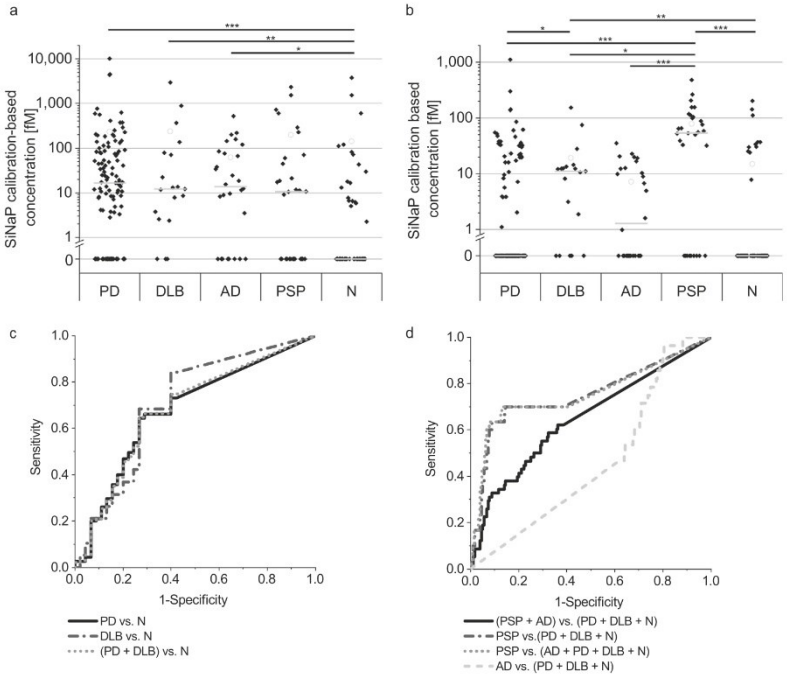

Fig. 9 Calibrated sFIDA results (a, b) and receiver operating characteristic (ROC) analysis (c, d) for the detection of aSyn and Tau aggregates in CSF samples. a For aSyn aggregates, PD, DLB, and AD samples were significantly elevated compared to normal controls (N). **c** In ROC analysis, discrimination of PD patients versus normal controls (N) showed a specificity of 73% and a sensitivity of 64% with an AUC of 0.68, while discrimination of DLB patients versus normal controls showed a specificity of 60% and a sensitivity of 84% with an AUC of 0.71. In combination, synucleinopathies (PD and DLB) can be differentiated from normal controls with a specificity of 73% and a sensitivity of 65% with an AUC of 0.68. **b**, **d** For Tau aggregates, the tauopathy PSP but not AD can be discriminated from non-tauopathies (for PSP vs. non-tauopathies: 86% specificity and 70% sensitivity with an AUC of 0.75; for other specificity and sensitivity values s. Table 3). DLB samples showed significantly increased Tau aggregate concentrations compared to normal controls and PD patients (*p*-values of Mann-Whitney U test for aSyn and Tau aggregates are shown in Table 2). Values below the LOD were set to 0. "-" indicates the median and "○" the mean. Significant differences between cohorts were calculated with Mann-Whitney U test and signed with * ($*p = 0.01–0.05$; $**p = 0.001–0.01$; $***p < 0.001$). Please, note the logarithmic concentration scales.

Table 3. Results of ROC analysis for specificity, sensitivity and area under the curve (AUC) for aSyn and Tau aggregates in CSF.

		Specificity	Sensitivity	AUC
aSyn	PD vs. N	73.3%	64.3%	0.678
	DLB vs. N	60.0%	84.2%	0.705
	(PD + DLB) vs. N	73.3%	64.9%	0.682
Tau	(PSP + AD) vs. (PD + DLB + N)	67.6%	58.6%	0.649
	PSP vs. (PD + DLB + N)	85.5%	70.0%	0.753
	PSP vs. (AD + PD + DLB + N)	87.0%	70.0%	0.755
	AD vs. (PD + DLB + N)	19.6%	96.4%	0.462

PD Parkinson's disease, *AD* Alzheimer's disease, *DLB* Dementia with Lewy bodies, *PSP* Progressive supranuclear palsy, *N* Normal control, *AUC* Area under the curve.

for DLB samples with a Pearson coefficient of correlation of 0.98 ($p = 8.5*10^{-13}$). PD ($r = 0.87$, $p = 6.5*10^{-36}$), PSP ($r = 0.74$, $p = 3.4*10^{-6}$), and normal control ($r = 0.90$, $p = 2.5*10^{-17}$) CSF samples also showed a positive correlation. For AD patients, the correlation was weaker ($r = 0.52$, $p = 0.005$).

Age, sex and disease duration do not correlate with aggregate concentrations in CSF

As age and gender are risk factors for PD, AD, DLB and PSP[25], the correlation between the concentration of aSyn and Tau aggregates to age and sex are interesting parameters. Across all cohorts, there was no detectable significant effect specific to age, sex, or disease duration (Pearson coefficient of correlation in Supplementary Table 6). For Tau, we observed an inverse correlation between aggregate concentration and education.

DISCUSSION

Our study explored the ability of the sFIDA technology to detect and quantitate aSyn and Tau aggregates in CSF samples and its applicability for the diagnosis of neurodegenerative diseases. aSyn oligomers are thought to be the major toxic species in synucleinopathies like PD and DLB[4,26] but the detection of such oligomers in human biofluids is still challenging due to the low concentration of oligomers and the interference with monomers. The principle of sFIDA allows the sensitive detection and quantitation of oligomers and other aggregates in the presence of monomers with an LOD in the low femtomolar region. Approximately 66% of the CSF samples tested here showed concentrations above the LOD with a wide concentration range of up to 10 pM. Most samples harbored concentrations of aSyn

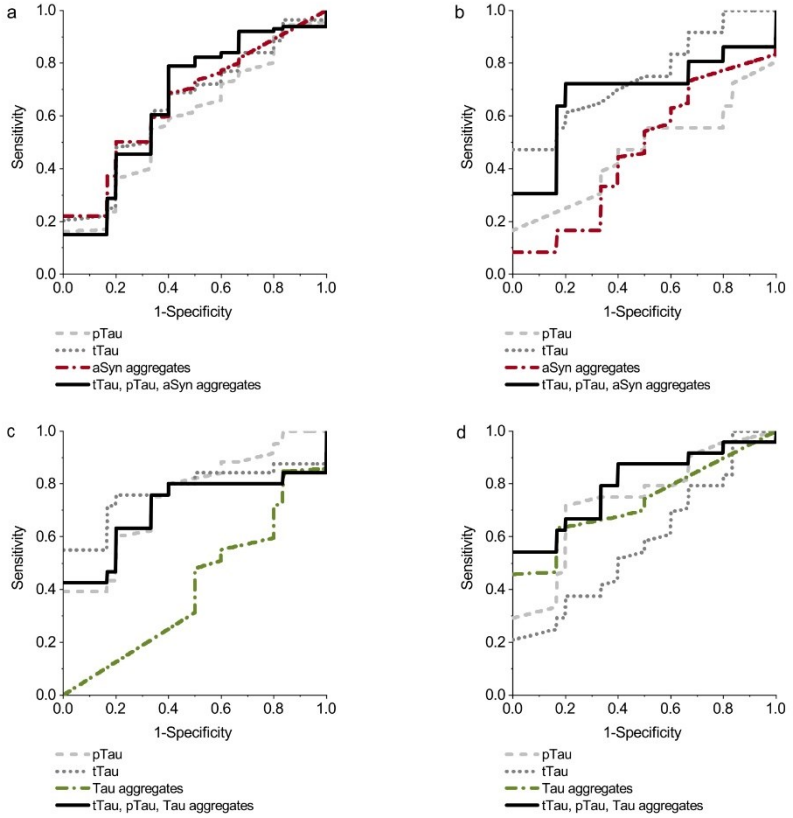

Fig. 10 ROC of pTau, tTau, aSyn and Tau aggregates and their combination. We compared the performance of different biomarkers and analyzed, if the combination of biomarkers improves the discrimination of neurodegenerative diseases compared to normal control (**a**: PD vs. N, **b**: DLB vs. N, **c**: AD vs. N, **d**: PSP vs. N). Sensitivity, Specificity and AUC values are listed in Table 4.

aggregates between 5 fM and 500 fM. For Tau aggregates, 44% of the CSF samples were above the LOD. It has to be considered that a single SiNaP led on average to more pixels with fluorescence above the cutoff value than compared to the average aggregate from real samples. This is presumably due to a higher amount of accessible binding sites for detection antibodies or due to agglomeration of our silica nanoparticle standard. Probably, both aspects influence the average apparent size distribution of our standard particles. With the term size, we therefore do not refer to the actual size, as all particles can be expected to be below the optical resolution limit, but instead to the number of pixels that are illuminated above the cutoff value. The evaluation accounts at least partially for that, because the exact fluorescence intensity of a pixel is not affecting the readout, only the digital decision, whether the fluorescence intensity of a pixel is above the cutoff threshold or not. Nevertheless, the differences in particle size may influence the calibration, so we described the calibrated concentrations as *SiNaP calibration-based concentration*. In this study, we calculated an average apparent particle size of 11.2 pixels per particle for aSyn SiNaPs (obtained from the 63 fM calibration), while for aggregated aSyn in patient samples, the apparent average particle size was 5.2 pixels. For Tau, 204 fM SiNaPs and samples yielded an average apparent particle size of 10 pixels and 2.6 pixels, respectively.

As expected, CSF samples of PD and DLB patients harbored significantly elevated levels of aSyn aggregates compared to normal controls. This is in agreement with several other studies quantifying aSyn oligomers in CSF[8,27,28]. But there is also a large overlap between synucleinopathies and normal controls, which is congruent with some previous studies aimed at discriminating both populations (Majbour: sensitivity 89%, specificity 52%[8], Tokuda: sensitivity 75%, specificity 88%[27]). The combination of aSyn aggregates with other predictive values like total aSyn (t-aSyn), phosphorylated aSyn (p-aSyn), tTau, phosphorylated Tau (pTau), or age may improve the discrimination of synucleinopathies from normal controls, as investigated in other studies[8,21,29]. In this work, we have tested the combination of aSyn aggregates as biomarker with pTau and tTau. The combination of the three biomarkers did not improve the predictive power of the analysis, but for PD vs N, aSyn aggregates alone showed the highest performance of the three biomarkers. We hypothesize that the combination with t-aSyn probably has a higher impact on the AUC, but information on total aSyn levels was not available for the samples tested in this study.

Interestingly, we found elevated levels of aSyn aggregates also in AD patients with concentrations comparable to that of PD or DLB patients. The role of aSyn in AD is still under investigation. Many studies have reported the presence of Lewy bodies in AD brains[30–33] as well as increased t-aSyn concentrations in CSF[24],

Table 4. Results of ROC analysis for specificity, sensitivity and area under the curve (AUC) for pTau, tTau, aSyn or Tau aggregates in CSF and their combination.

		Specificity	Sensitivity	AUC
PD vs. N	tTau	60.0%	68.5%	0.645
	pTau	66.6%	55.0%	0.589
	aSyn aggregates	80.0%	50.2%	0.656
	pTau + tTau + aSyn aggregates	60.0%	78.8%	0.663
DLB vs. N	tTau	100.0%	47.2%	0.752
	pTau	100.0%	16.7%	0.468
	aSyn aggregates	100.0%	8.3%	0.468
	pTau + tTau + aSyn aggregates	80.0%	72.2%	0.689
AD vs. N	tTau	80.0%	75.8%	0.775
	pTau	66.6%	74.7%	0.753
	Tau aggregates	16.6%	84.7%	0.409
	pTau + tTau + Tau aggregates	80.0%	63.3%	0.708
PSP vs. N	tTau	100.0%	20.8%	0.586
	pTau	80.0%	71.7%	0.743
	Tau aggregates	83.3%	63.2%	0.734
	pTau + tTau + Tau aggregates	100.0%	54.2%	0.800

and in an autopsy study based at UPenn, where our CSF samples were collected, more than 52% of individuals with a diagnosis of AD showed considerable Lewy body burden on neuropathology[34]. However, prior biomarker studies have also reported no difference in aSyn monomer concentrations in CSF of AD patients compared to normal controls[21], or even decreased levels of aSyn oligomers in CSF of AD and PSP compared to PD patients[27,35], which is in contrast to our results. Differences in study results might be ascribed to differences in (1) the makeup of patients recruited at different clinical sites, (2) preanalytical aspects related to sample collection or handling, or (3) quantification methods[36]. In this context, we note that all samples used in this study were single-use aliquots collected under strict standard operating procedures. For PSP, we did not measure a significant increase in aSyn aggregate concentration compared to normal controls, which agrees with other studies[21,27].

To date, limited evidence exists regarding the detectability of Tau aggregates in CSF for the diagnosis of neurodegenerative diseases. Increased Tau oligomer concentrations in postmortem PSP brain samples have been reported by Gerson et al.[37]. This is in agreement with our study, where PSP patients showed increased levels of Tau aggregates compared to all other diseases, with sensitivity and specificity of 87 and 70%, respectively. Although there is a consensus about the certainty of tTau and pTau for diagnosis of AD[38] and the presence of Tau oligomers in AD brains[9], we did not observe a statistically significant increase in the concentration of Tau aggregates in CSF samples of these patients. Up to now, most studies are focusing on the presence of tTau and pTau in neurodegenerative diseases. For PSP and AD, quite different concentrations are found in CSF: AD shows significantly increased levels of tTau and pTau[23], whereas PSP samples show no difference or even a decrease in Tau monomer concentrations[23,39]. These observations match our data showing that pTau and tTau were increased for AD, but decreased for PSP (for pTau). For PSP, Tau aggregates alone can differentiate between PSP and normal control group similar to pTau, and the combination of the biomarkers improves the specificity and AUC, which underlines the role of Tau aggregates in PSP as possible biomarker. Wagshal et al. postulate that differences between AD and PSP can probably be ascribed to differences in Tau isoforms, as PSP is known as a 4R-tauopathy, whereas AD shows equal ratios of 4 R and 3 R Tau. Different isoforms of Tau are differentially released from neuronal and glial cells and have differing affinities to antibodies[39,40]. These differences could also be relevant in interpreting our present results, which suggest that aggregated Tau species discriminate PSP vs. AD.

The importance of Tau protein in PD and DLB is still under investigation. Many studies have reported the presence of neurofibrillary tangles in PD and DLB brains[30,31,41,42] but no increase in tTau or pTau in CSF samples of PD patients[8,21]. Our study implicates no relation of increased Tau aggregate concentrations in CSF and the presence of PD. Interestingly, DLB samples showed elevated levels of Tau aggregates compared to those of normal controls and compared to PD patients, but less than those observed in PSP samples.

We also correlated aSyn and Tau aggregate concentrations in CSF samples between individual groups. For correlation of t-aSyn and tTau evidence in the literature is inconcise. Parnetti et al. reported an inverse correlation of aSyn and Tau[29], while several others have observed a positive correlation[22–24]. For aSyn and Tau aggregates, we observed a highly significant positive correlation (Fig. 11a), which is in agreement with several other studies showing the coexistence of the two proteins in Lewy bodies[30,41] and even the existence of hetero-aggregates[33]. Despite substantial overlap, median values of the individual disease groups suggest a mixed pathology ranging from rather pure aSyn pathology in PD via AD and DLB to PSP which shows decreased aSyn and increased Tau pathology (Fig. 11b). Additional correlations with other potential biomarkers, e.g. Amyloid beta and TDP43 aggregates, may further complement the view on these diseases on the molecular level. Determining whether aSyn-Tau hetero-aggregates might be detected by sFIDA in human biofluids is a promising area of future investigation that might add to our understanding on the molecular basis of phenotypic overlap among neurodegenerative diseases.

Naturally occurring oligomers and other aggregates differ in size, morphology and posttranscriptional modifications[4,43]. For detection and quantification, we used the same capture and detection antibody directed against linear epitopes that are expected to be accessible in all aggregated species, in order to quantitate all isoforms, irrespectively of their structural conformation. In future studies, we will further characterize the exact nature of the analytes by introducing size standards and structural probes. Possibly, not all aSyn assemblies in human brain are neurotoxic or disease-specific, and it was strongly discussed if aSyn physiologically occurs as a globular tetramer or as an intrinsically disordered monomer[4,44,45]. Future research will show, if the complex pathology of neurodegenerative diseases limits the diagnostic specificity of measuring the whole soluble aggregate fraction. Nevertheless, we are convinced that the possibility to finally measure aggregate concentrations is essential not only in understanding the underlying pathology, but also for developing therapeutic compounds against these species. Here we showed, that total aggregate concentrations differentiate i.e. PD or PSP from normal control, which further emphasizes the usefulness of quantifying aggregates in CSF for diagnosis of neurodegenerative diseases. For sufficient accuracy, surely, sensitivity and specificity need to be improved, i.e., by combining the concentration of aSyn or Tau aggregates with other biomarkers like t-aSyn, tTau, pTau, or Aβ1-42. Taking further into consideration that perhaps not all naturally occurring aggregates are disease-relevant, it might be interesting to compare or combine the results of total aggregates measured by sFIDA with seeding assays like the RT-QuIC or assays that measure a specific fraction of aggregates.

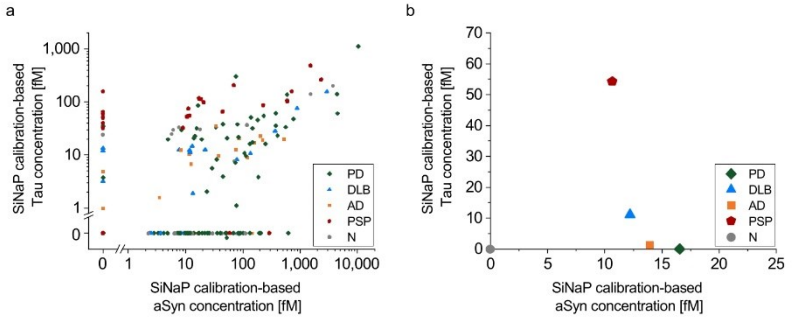

Fig. 11 Correlation of aSyn and Tau aggregate concentration. a aSyn and Tau aggregate concentrations measured by sFIDA show a highly significant correlation across all samples tested (Pearson coefficient of correlation $r = 0.81$, $p = 3.8*10^{-57}$) as well as for each individual cohort. Correlation of the median values for the disease groups is plotted in **b**.

Moreover, we note that, aside from diagnostic applications, sFIDA may be a valuable tool in clinical studies, to select, stratify, and monitor patients for therapies targeting aSyn or Tau oligomers, since sFIDA allows for direct assessment of the mechanism of action and is able to measure target engagement, irrespectively of the structural conformation. Finally, treatment success can be validated on the molecular level by monitoring aggregate titers over the course of medication.

METHODS

Synthesis of protein-coated silica nanoparticles

For assay calibration we have developed a nanoparticle calibration standard based on a silica core[14]. These silica nanoparticles (SiNaPs) were synthesized via Stöber process and afterwards modified with 3-aminopropyl(triethoxysilane) (APTES, Sigma-Aldrich, St. Louis, USA) to generate an aminated surface. Proteins were crosslinked to the aminated surface by maleimido hexanoic acid (MIHA, abcr GmbH, Karlsruhe, Germany). After activation with 200 mM 1-ethyl-3-(3-dimethylaminopropyl)carbodiimide (EDC, Sigma Aldrich, St. Louis, USA) and 50 mM N-hydroxysuccinimid (NHS, Sigma Aldrich, St. Louis, USA) for 10 min at room temperature (RT), the carboxy group of MIHA was coupled covalently to the amines of the silica nanoparticles. Following incubation for 1 h at RT, the resulting SiNaPs were centrifuged (7000 x *g*, 2 min) and redispersed in PBS and 10% dimethylformamid (DMF, Sigma Aldrich, St. Louis, USA). The washing step was repeated three times, where after the pellet was redispersed in PBS containing 10% DMF and 50 mM ethylendiamintetraacetic acid disodium salt (Na_2EDTA, AppliChem, Darmstadt, Germany) in the last step. Protein fragments of aSyn (aa115-130, Peptides and Elephants, Henningsdorf, Germany) and Tau (aa 210-230, Peptides and Elephants, Henningsdorf, Germany) are functionalized with cysteamine on the C-terminus to enable reacting with the maleimide group of the SiNaPs. For synthesis of protein-conjugated silica nanoparticles, 10% of the possible binding sites were functionalized by adding protein to the redispersed SiNaPs. The dispersion was shaken at RT and 650 rpm. After 1 h, 50 µL of 1 M Tris-(2-carboxyethyl)-phosphine (TCEP, abcr GmbH, Karlsruhe, Germany) was added to prevent oxidation of the protein. The reaction was quenched by adding 20 µL of a 1 M 2-mercaptoethanol solution. The functionalized SiNaPs were washed two times by centrifugation (10,000 x *g*, 4 min) and redispersed in ddH_2O. Finally, the silicon concentration was determined using ICP-MS (inductively coupled plasma – mass spectrometry) and the resulting molar SiNaPs concentration was calculated based on size, density as well as particle shape. Prior to use, the protein-conjugated silica nanoparticles were subjected to ultra-sonification for 10 min.

Tau and aSyn monomers were isolated prior to sFIDA measurement using size exclusion chromatography (Bio SEC3, pore size 150 Å, Agilent, Santa Clara, USA) to ensure that the sample does not contain any aggregates. After SEC purification, we determined the monomer concentration using UV-Vis spectroscopy. We calculated the signal reduction of monomers versus aggregates as described in Eq. (1):

$$Signal\ reduction[\%] = \left(1 - \frac{pixel\ count_{monomer} - pixel\ count_{BC}}{pixel\ count_{aggregates} - pixel\ count_{BC}}\right) * 100\% \quad (1)$$

Characterization of silica nanoparticles

Size and particle shape of the aminated silica nanoparticles were analyzed using transmission electron microscopy (TEM) as previously described by Hülsemann et al.[14]. Mean particle size was 18.5 nm for the aminated silica core (TEM image and size distribution in Supplementary Fig. 1).

Finally, the silicon concentration was determined using inductively coupled plasma – mass spectrometry (ICP-MS). SiNaPs were diluted in 3% nitric acid and analyzed in helium collision cell mode with an Agilent 7500 (Agilent Technologies, Japan). External calibration with rhodium as the internal standard was performed using NIST traceable commercial standard solution (VWR International, PA, USA). Complete dissociation of silica nanoparticles in the plasma without the need for digestion prior to analysis was shown in earlier studies up to a particle diameter of 500 nm[46–48]. The molar SiNaPs concentration was calculated based on the silicon concentration determined by ICP-MS and the known size, density as well as shape of the particles.

Labeling of antibodies

For microscopic detection of aggregates, we used fluorescent antibodies. The mouse anti-aSyn monoclonal antibody 211 (Santa Cruz Biotechnology, Inc., Dallas, USA) was labeled with CF633 (Biotium, Freemont, USA), whereas the anti-tau Tau5 antibody (Biolegend, San Diego, USA) was labeled with CF488A (Biotium, Freemont, USA). The labeling process was performed as described in the manufacturer's protocol. The dyes were activated as succinimidyl esters to react covalently with the amines of the antibody in carbonate buffer. For purification of each labeled antibody, a polyacrylamide bead suspension (Bio-Gel P-30 Gel, Bio-Rad Laboratories, Inc., Hercules, USA) was used. The concentration and the degree of labeling was determined according to the manufacturer's protocol.

Assay protocol

The biochemical principle of the sFIDA assay was previously described by Kravchenko et al., and Herrmann et al.[11,49]. In the present study, we used Nunc MicroWell 384-Well plates (Thermo Fisher Scientific, Waltham, USA) functionalized with 211 and Tau5 antibodies as captures, each at 5 µg/mL in 1 x PBS buffer. After washing five times with 80 µL TBS-T (1x TBS (Serva, Duisburg, Germany) and 0.05% Tween20 (AppliChem, Darmstadt, Germany)) and afterwards five times with 1 x TBS, the wells were blocked with 1% BSA (AppliChem, Darmstadt, Germany) in TBS containing 0.03% ProClin (Sigma Aldrich, Missouri, USA) for 1.5 h at RT. The plate was washed again with TBS-T and TBS (see above) and 20 µl protein-conjugated SiNaPs diluted in TBS-ProClin containing 0.5% BSA and 0.05% Tween, and 20 µl of the samples were incubated for 2 h at RT. After washing five times with TBS and changing the buffer to TBS-ProClin, the wells were incubated for 2 h

with the fluorescent detection antibodies 211-CF633 (0.4 µg/mL) and Tau5-CF488 (4 µg/mL) in TBS, after which the wells were washed with TBS again. For measurement, the buffer in the wells was changed against TBS-ProClin. Each concentration and sample were pipetted fourfold. All washing steps were carried out by an automated microplate washer (405 LS Microplate Washer, BioTek, VT, USA).

Inter-assay and inter-laboratory measurements

For inter-assay measurement of the calibration curve and the samples, the same assay was repeated four months later by the same technician with the same antibodies and materials but minor changes in washing conditions, such as the use of a different microplate washer and washing and blocking reagents with a different manufacturing date. Repeatedly assayed samples were subjected to an additional freeze-thaw cycle.

For inter-laboratory analysis, the assay was prepared and measured by a different operator in a different laboratory. The first measurement took place at the Forschungszentrum Jülich, and the second measurement at the Heinrich-Heine-Universität in Düsseldorf two months after the first measurement with the same changes as described above for inter-assay analysis.

Immunodepletion

For immunodepletion, 211 and Tau5 antibody were covalently coated to carboxylated magnetic dynabeads (Invitrogen, Waltham, USA) according to the manufacturer's protocol. Shortly, dynabeads were washed twice with 2.5 mM 2-(N-morpholino)ethanesulfonic acid (MES, pH 5, Roth, Karlsruhe, Germany) and applied to a magnet to remove the supernatant. Carboxy groups were activated with 50 µg/ml EDC and 50 µg/ml NHS in MES for 30 min at RT while rotating. After activation, the dynabeads were washed again with MES and coated with 211 or Tau5 antibody to a concentration of 20 µg/ml dynabeads, respectively. To ensure that signal loss is not due to unspecific binding of sample components to dynabeads, we run a third synthesis without antibody. After incubation for 1 h at RT, dynabeads were washed again and quenched with 50 mM ethanolamine in MES for 1 h at RT followed by a last washing step.

For immunodepletion, we applied 0.5 mg of antibody coated dynabeads to the magnet and removed the supernatant. 100 µl sample were added and incubated for 1 h at RT while rotating. After incubation, dynabeads were applied to the magnet again and the supernatant was transferred to a fresh tube. The immunodepleted samples were analyzed using sFIDA as described above. To consider for possible effects of magnetic beads on the pixel count, we normalized the signals by using an individual cutoff based on the CSF control. Please, note that the CSF control used for immunodepletion and HAMA interference experiments differed from the CSF control used for calibrating the results of the big data set of the study and showed an increased fluorescence signal for Tau5 CF488.

Influence of heterophilic antibodies

The potential influence of heterophilic antibodies, specifically anti-mouse antibodies (HAMAs), was analyzed using the purified mouse IgG isotype control MOPC-21 as a competitor (Biolegend, San Diego, USA). Possibly existing HAMAs in CSF can bind to MOPC instead to the assay antibodies which prevents false positive signals. A total of nine samples that yielded high sFIDA signals were spiked with 1 µg/ml MOPC-21. As positive control, we used buffer spiked with 1 µg/ml goat anti-mouse IgG (Thermo Fisher Scientific, Waltham, USA) with or without MOPC-21.

Determination of blood contamination

Contamination of CSF samples with blood was determined semi-quantitatively using Combur10-Test-Analysis (Hoffmann-La Roche, Basel, Switzerland) as described in Barkovits et al.[20]. Test stripes were incubated with 50 µL CSF for 60 s and the amount of contamination was analyzed according to the manufacture's protocol.

Image-data acquisition

Imaging was performed on a total internal reflection microscope (TIRFM, Leica DMI6000B, Wetzlar, Germany) as previously described by Kravchenko et al.[49] (excitation: 635 nm, emission filter: 705/22 nm; excitation: 488 nm, emission filter: 525/36 nm; exposure time: 1000 ms; gain: 1300). A total of 25 images per well with 1000 × 1000 pixels each were measured, which covers 3.14% of the total area per well. For unbiased and automated image-data analysis, we have used our previously developed sFIDAta software tool[15]. The analysis includes the automated detection and elimination of artefact containing images and counting of aggregate indicating pixels. The *pixel count* is referred to as the average number of pixels in an image that exceed a pre-defined cutoff value. The *cutoff* is defined as the grey-scale value at which the ratio of the positive versus the total number of pixels in the buffer control equals a pre-defined value. The cutoff is used to compensate fluctuations in the absolute fluorescence intensities among experiments and different conditions within one experiment (i.e., antibody dilutions) and is determined for each experiment based on a buffer control sample. To further ensure that differences in fluorescence intensity do not affect assay robustness, we run a calibration in each 384-microtiter plate and converted pixel counts into SiNaP calibration-based fM concentrations.

For inter-assay measurement, a cutoff of 0.001% was chosen, while the cutoff for the analysis of the whole dataset of 237 samples was 0.05%. This difference is due to a new lot of detection antibodies with a lower degree of labeling. To further ensure that all artificial images are excluded from the analysis, min-max filtering was applied, which removed 10% of the images per well with the highest and 10% of the images per well with the lowest pixel counts.

Statistics

General statistics. Statistical analysis was performed using OriginPro 2020 SR1 (OriginLab Corporation, MA, USA) and matlab2019b (The MathWorks, MA, USA) software. Mean and standard deviation was calculated based on the pixel counts of the four replicates. Intra-assay variation is described by the CV% value. To determine inter-assay and inter-laboratory variation, the Pearson coefficient of correlation was calculated for the replicate measurements of the samples.

Calibration. For calculation of the calibration curve, only the concentrations of the silica nanoparticle standard were included that significantly differed from the blank control and were above the limit of detection (LOD). To this end, a one-sided Mann-Whitney U test was carried out with a confidence interval of 5%. After calculation of the calibration range for each experiment, a universal calibration range for all of the experiments was established. The LOD is defined based on Eq. (2):

$$LOD[pixel] = pixel\,count(blank\,control) * 2\sigma \quad (2)$$

For linear regression, the pixel counts were weighted with 1/readout. The bovine CSF control was used as a negative control for the calibration as well as for calculation of the LOD.

Logistic regression and ROC analysis. Logistic regression was performed to evaluate the ability of each biomarker to classify the diagnostic groups. To this end, we used scikit-learn library (version 1.0.2). Since the use of multiple features increases the risk of overfitting, the k-fold cross-validation method was used to generate Fig. 10, in order to provide unbiased results. Deviations between Fig. 9 and Fig. 10 can be explained not only by the modified method but also by a divergent data basis. Since tTau and pTau values were not available for all samples, these were excluded for the creation of the Fig. 10. By forming the average of the k results, a single receiver operating characteristic (ROC) curve was generated. The optimal combination of sensitivity and specificity for a ROC curve was calculated with a maximized Youden's index.

Patient samples

Patients were recruited from the University of Pennsylvania (UPenn) Parkinson's Disease and Movement Disorder Center (PDMDC), Alzheimer's Disease Center (ADC), or Frontotemporal Dementia Center (FTDC). Written, informed consent was obtained from each study participant at enrollment and biofluids were collected and stored for future research as approved by the UPenn Institutional Review Board (FWA00004028). Participants were diagnosed with Parkinson's disease (PD, $n = 115$), Alzheimer's disease (AD, $n = 28$), progressive supranuclear palsy (PSP, $n = 30$), or dementia with Lewy bodies (DLB, $n = 19$) according to clinical criteria as previously described[50]. Participants with no known neurological disorder were also enrolled (normal control, N, $n = 45$). Cerebrospinal fluid (CSF) was collected by trained neurologists via lumbar puncture, and aliquots of 0.5 mL were stored at −80 °C until analysis. Demographic information was collected by trained research staff. Samples were collected between August of 2005 and November 2019, with the exception of one sample, which was

collected in March of 1999. Samples included in the analysis were matched for age across diagnosis groups. Initially, a subset of PSP ($n = 30$), PD ($n = 30$), and N ($n = 30$) samples were analyzed as an exploratory cohort. The remainder of the samples were analyzed to investigate differences between disease groups. Researchers were blinded to clinical data at the time of sFIDA measurement.

Concentrations of pTau and tTau were measured using Luminex xMAP immunoassay platform (Luminex, Austin, USA)[51,52] and provided by Integrated Neurodegenerative Disease Database (INDD).

After unblinding, the data points of each group were first tested for normal distribution (Shapiro Wilk, Lilliefors, Kolmogorov-Smirnov, Anderson Darling). Afterwards, a Kruskal-Wallis test was executed to identify differences between the groups. In case of significant differences ($p < 0.05$) a pairwise comparison using the two-sided Mann-Whitney U test with a confidence interval of 0.05 was performed.

DATA AVAILABILITY

The authors confirm that the data supporting the findings of this study are available within the article and its supplementary materials.

CODE AVAILABILITY

For image data analysis, we used the sFIDAta software tool, which can be made available upon request from the corresponding author.

Received: 27 November 2021; Accepted: 10 May 2022;
Published online: 02 June 2022

REFERENCES

1. Dickson, D. W. Parkinson's disease and parkinsonism: neuropathology. *Cold Spring Harb. Perspect Med.* **2**, https://doi.org/10.1101/cshperspect.a009258 (2012).
2. Foguem, C. & Manckoundia, P. Lewy Body Disease: Clinical and Pathological "Overlap Syndrome" Between Synucleinopathies (Parkinson Disease) and Tauopathies (Alzheimer Disease). *Curr. Neurol. Neurosci. Rep.* **18**, 24 (2018).
3. Haass, C. & Selkoe, D. J. Soluble protein oligomers in neurodegeneration: lessons from the Alzheimer's amyloid beta-peptide. *Nat. Rev. Mol. Cell Biol.* **8**, 101–112 (2007).
4. Bengoa-Vergniory, N., Roberts, R. F., Wade-Martins, R. & Alegre-Abarrategui, J. Alpha-synuclein oligomers: A new hope. *Acta Neuropathol.* **134**, 819–838 (2017).
5. Prots, I. et al. alpha-Synuclein oligomers induce early axonal dysfunction in human iPSC-based models of synucleinopathies. *Proc. Natl Acad. Sci. USA* **115**, 7813–7818 (2018).
6. Willbold, D. & Kutzsche, J. Do we need anti-prion compounds to treat Alzheimer's Disease? *Molecules* **24**, https://doi.org/10.3390/molecules24122237 (2019).
7. Majbour, N. K. et al. Cerebrospinal alpha-Synuclein oligomers reflect disease motor severity in DeNoPa longitudinal cohort. *Mov. Disord.* https://doi.org/10.1002/mds.28611 (2021).
8. Majbour, N. K. et al. Oligomeric and phosphorylated alpha-synuclein as potential CSF biomarkers for Parkinson's disease. *Mol. Neurodegener.* **11**, 7 (2016).
9. Sengupta, U. et al. Tau oligomers in cerebrospinal fluid in Alzheimer's disease. *Ann. Clin. Transl. Neurol.* **4**, 226–235 (2017).
10. Kulenkampff, K., Wolf Perez, A.-M., Sormanni, P., Habchi, J. & Vendruscolo, M. Quantifying misfolded protein oligomers as drug targets and biomarkers in Alzheimer and Parkinson diseases. *Nat. Rev. Chem.* **5**, 277–294 (2021).
11. Herrmann, Y. et al. Nanoparticle standards for immuno-based quantitation of alpha-synuclein oligomers in diagnostics of Parkinson's disease and other synucleinopathies. *Clin. Chim. Acta* **466**, 152–159 (2017).
12. Alam, P., Bousset, L., Melki, R. & Otzen, D. E. alpha-synuclein oligomers and fibrils: A spectrum of species, a spectrum of toxicities. *J. Neurochem.* **150**, 522–534 (2019).
13. Willbold, D., Strodel, B., Schroder, G. F., Hoyer, W. & Heise, H. Amyloid-type protein aggregation and prion-like properties of amyloids. *Chem. Rev.* **121**, 8285–8307 (2021).
14. Hülsemann, M. et al. Biofunctionalized Silica nanoparticles: Standards in amyloid-beta oligomer-based diagnosis of Alzheimer's Disease. *J. Alzheimers Dis.* **54**, 79–88 (2016).
15. Kühbach, K. et al. Application of an Amyloid Beta Oligomer Standard in the sFIDA Assay. *Front Neurosci.* **10**, 8 (2016).
16. Bolstad, N. et al. Heterophilic antibody interference in commercial immunoassays; a screening study using paired native and pre-blocked sera. *Clin. Chem. Lab Med.* **49**, 2001–2006 (2011).
17. Vanderstichele, H., Stoops, E., Vanmechelen, E. & Jeromin, A. Potential sources of interference on Abeta immunoassays in biological samples. *Alzheimers Res. Ther.* **4**, 39 (2012).
18. Ishii, R. et al. Decrease in plasma levels of alpha-synuclein is evident in patients with Parkinson's disease after elimination of heterophilic antibody interference. *PLoS One* **10**, e0123162 (2015).
19. Sehlin, D. et al. Interference from heterophilic antibodies in amyloid-beta oligomer ELISAs. *J. Alzheimers Dis.* **21**, 1295–1301 (2010).
20. Barkovits, K. et al. Blood Contamination in CSF and Its Impact on Quantitative Analysis of Alpha-Synuclein. *Cells* **9**, https://doi.org/10.3390/cells9020370 (2020).
21. Mollenhauer, B. et al. alpha-Synuclein and tau concentrations in cerebrospinal fluid of patients presenting with parkinsonism: a cohort study. *Lancet Neurol.* **10**, 230–240 (2011).
22. Forland, M. G. et al. The value of cerebrospinal fluid alpha-synuclein and the tau/alpha-synuclein ratio for diagnosis of neurodegenerative disorders with Lewy pathology. *Eur. J. Neurol.* **27**, 43–50 (2020).
23. van Steenoven, I. et al. alpha-Synuclein species as potential cerebrospinal fluid biomarkers for dementia with lewy bodies. *Mov. Disord.* **33**, 1724–1733 (2018).
24. Slaets, S. et al. Increased CSF alpha-synuclein levels in Alzheimer's disease: Correlation with tau levels. *Alzheimers Dement* **10**, S290–S298 (2014).
25. Savica, R., Grossardt, B. R., Bower, J. H., Ahlskog, J. E. & Rocca, W. A. Incidence and pathology of synucleinopathies and tauopathies related to parkinsonism. *JAMA Neurol.* **70**, 859–866 (2013).
26. Winner, B. et al. In vivo demonstration that alpha-synuclein oligomers are toxic. *Proc. Natl Acad. Sci. USA* **108**, 4194–4199 (2011).
27. Tokuda, T. et al. Detection of elevated levels of alpha-synuclein oligomers in CSF from patients with Parkinson disease. *Neurology* **75**, 1766–1772 (2010).
28. Park, M. J., Cheon, S. M., Bae, H. R., Kim, S. H. & Kim, J. W. Elevated levels of alpha-synuclein oligomer in the cerebrospinal fluid of drug-naive patients with Parkinson's disease. *J. Clin. Neurol.* **7**, 215–222 (2011).
29. Parnetti, L. et al. Differential role of CSF alpha-synuclein species, tau, and Abeta42 in Parkinson's Disease. *Front. Aging Neurosci.* **6**, 53 (2014).
30. Wakabayashi, K. et al. The Lewy body in Parkinson's disease and related neurodegenerative disorders. *Mol. Neurobiol.* **47**, 495–508 (2013).
31. Irwin, D. J. & Hurtig, H. I. The Contribution of Tau, Amyloid-Beta and Alpha-Synuclein Pathology to Dementia in Lewy Body Disorders. *J. Alzheimers Dis. Parkinsonism* **8**, https://doi.org/10.4172/2161-0460.1000444 (2018).
32. Hamilton, R. L. Lewy bodies in Alzheimer's disease: a neuropathological review of 145 cases using alpha-synuclein immunohistochemistry. *Brain Pathol.* **10**, 378–384 (2000).
33. Galpern, W. R. & Lang, A. E. Interface between tauopathies and synucleinopathies: A tale of two proteins. *Ann. Neurol.* **59**, 449–458 (2006).
34. Robinson, J. L. et al. Neurodegenerative disease concomitant proteinopathies are prevalent, Age-related and APOE4-associated. *Brain* **141**, 2181–2193 (2018).
35. Hansson, O. et al. Levels of cerebrospinal fluid alpha-synuclein oligomers are increased in Parkinson's disease with dementia and dementia with Lewy bodies compared to Alzheimer's disease. *Alzheimers Res. Ther.* **6**, 25 (2014).
36. Abdi, I. Y. et al. Preanalytical stability of CSF Total and Oligomeric Alpha-Synuclein. *Front. Aging Neurosci.* **13**, 638718 (2021).
37. Gerson, J. E. et al. Characterization of tau oligomeric seeds in progressive supranuclear palsy. *Acta Neuropathol. Commun.* **2**, 73 (2014).
38. Olsson, B. et al. CSF and blood biomarkers for the diagnosis of Alzheimer's disease: A systematic review and meta-analysis. *Lancet Neurol.* **15**, 673–684 (2016).
39. Wagshal, D. et al. Divergent CSF tau alterations in two common tauopathies: Alzheimer's disease and progressive supranuclear palsy. *J. Neurol. Neurosurg. Psychiatry* **86**, 244–250 (2015).
40. Karch, C. M., Jeng, A. T. & Goate, A. M. Extracellular Tau levels are influenced by variability in Tau that is associated with tauopathies. *J. Biol. Chem.* **287**, 42751–42762 (2012).
41. Zhang, X. et al. Tau pathology in Parkinson's Disease. *Front Neurol.* **9**, 809 (2018).
42. Irwin, D. J., Lee, V. M. & Trojanowski, J. Q. Parkinson's disease dementia: Convergence of alpha-synuclein, tau and amyloid-beta pathologies. *Nat. Rev. Neurosci.* **14**, 626–636 (2013).
43. Ingelsson, M. Alpha-Synuclein Oligomers-Neurotoxic Molecules in Parkinson's disease and other Lewy body disorders. *Front. Neurosci.* **10**, 408 (2016).
44. Bartels, T., Choi, J. G. & Selkoe, D. J. alpha-Synuclein occurs physiologically as a helically folded tetramer that resists aggregation. *Nature* **477**, 107–110 (2011).
45. Fauvet, B. et al. alpha-Synuclein in central nervous system and from erythrocytes, mammalian cells, and Escherichia coli exists predominantly as disordered monomer. *J. Biol. Chem.* **287**, 15345–15364 (2012).
46. Heroult, J., Nischwitz, V., Bartczak, D. & Goenaga-Infante, H. The potential of asymmetric flow field-flow fractionation hyphenated to multiple detectors for the quantification and size estimation of silica nanoparticles in a food matrix. *Anal. Bioanal. Chem.* **406**, 3919–3927 (2014).

47. Dubascoux, S. et al. Field-flow fractionation and inductively coupled plasma mass spectrometer coupling: History, development and applications. *J. Anal. At. Spectrom.* **25**, 613–623 (2010).
48. Meermann, B. & Nischwitz, V. ICP-MS for the analysis at the nanoscale – a tutorial review. *J. Anal. At. Spectrom.* **33**, 1432–1468 (2018).
49. Kravchenko, K. et al. Analysis of anticoagulants for blood-based quantitation of amyloid beta oligomers in the sFIDA assay. *Biol. Chem.* **398**, 465–475 (2017).
50. Toledo, J. B. et al. A platform for discovery: The University of Pennsylvania Integrated Neurodegenerative Disease Biobank. *Alzheimer's Dement* **10**, 477–484 e471 (2014).
51. Irwin, D. J. et al. CSF tau and beta-amyloid predict cerebral synucleinopathy in autopsied Lewy body disorders. *Neurology* **90**, e1038–e1046 (2018).
52. Berlyand, Y. et al. An Alzheimer's Disease-Derived Biomarker Signature Identifies Parkinson's Disease Patients with Dementia. *PLoS One* **11**, e0147319 (2016).

ACKNOWLEDGEMENTS

We received funding from the European Union Seventh Framework Program (FP7/2007-2013) under grant agreement 602999 (SYMPATH project), the Federal Ministry of Education and Research within the projects VIP (03V0641), KNDD (01GI1010A), JPND/BIOMARKAPD (01ED1203H), and NEUROALLIANZ (16GW0099). We were also supported by the programs "Biomarkers Across Neurodegenerative Diseases I + II" of The Alzheimer's Association, Alzheimer's Research UK and the Weston Brain Institute (11084 and BAND-19-614337). We are also grateful for support from The Michael J. Fox Foundation for Parkinson's Research (14977, 009889), from the ALS Association and from the Packard Center (19-SI-476). We further received funding from the Deutsche Forschungsgemeinschaft (INST 208/616-1 FUGG, INST 208/794-1 FUGG) and the Helmholtz Association (HVF0079). TFT is additionally funded by the NIH (K23-NS11416). In memoriam of John Q. Trojanowski.

AUTHOR CONTRIBUTIONS

LB, MP, and VK developed the assay. LB performed the experiments and analyzed the data, VK, AC and VN assisted in validation of the method. AK, FR and JW helped carry out the statistics and analysis. LB wrote the manuscript together with OB, DW and GT. OB, DW, and ACP supervised the project. DWe, DI, MG, DAW, JQT, TFT, and ACP recruited the patients. RZ, TFT, and ACP selected appropriate samples and organized the clinical data. AD, AS and TB contributed to the discussion of the results and provided critical feedback. JQT reviewed the manuscript and all data before his passing on February 8, 2022.

FUNDING

Open Access funding enabled and organized by Projekt DEAL.

COMPETING INTERESTS

The Authors declare no competing non-financial interests but the following competing financial interests: DW, OB, and AK are shareholders of attyloid GmbH. All other authors declare no competing financial interests related to this work.

ADDITIONAL INFORMATION

Supplementary information The online version contains supplementary material available at https://doi.org/10.1038/s41531-022-00330-x.

Correspondence and requests for materials should be addressed to Dieter Willbold.

Reprints and permission information is available at http://www.nature.com/reprints

Publisher's note Springer Nature remains neutral with regard to jurisdictional claims in published maps and institutional affiliations.

3.2 Aβ oligomers peak in early stages of Alzheimer's disease preceding Tau pathology

Autoren:	Lara Blömeke*, Fabian Rehn*, Victoria Kraemer-Schulien*, Janine Kutzsche, Marlene Pils, Tuyen Bujnicki, Piotr Lewczuk, Johannes Kornhuber, Silka D. Freiesleben Luisa-Sophie Schneider, Lukas Preis, Josef Priller, Eike J. Spruth, Slawek Altenstein, Andrea Lohse, Anja Schneider, Klaus Fliessbach, Jens Wiltfang, Niels Hansen, Ayda Rostamzadeh, Emrah Düzel, Wenzel Glanz, Enise I. Incesoy, Michaela Butryn, Katharina Buerger, Daniel Janowitz, Michael Ewers, Robert Perneczky, Boris-Stephan Rauchmann, Stefan Teipel, Ingo Kilimann, Doreen Goerss, Christoph Laske, Matthias H. Munk, Carolin Sanzenbacher, Annika Spottke, Nina Roy-Kluth, Michael T. Heneka, Frederic Brosseron, Michael Wagner, Steffen Wolfsgruber, Luca Kleineidam, Melina Stark, Matthias Schmid, Frank Jessen, Oliver Bannach, Dieter Willbold, Oliver Peters *Autoren sind gleichberechtigt
Journal:	Alzheimer's and Dementia- Diagnosis, Assessment & Disease Monitoring (veröffentlicht)
DOI:	10.1002/dad2.12589
Impact-Faktor:	16,655 (2021)
Beitrag:	Eigenanteil: 25 % Entwicklung des Assays Auswertung der Ergebnisse Anfertigung der Abbildungen Verfassen des Manuskripts
Anhang zum Manuskript	Kapitel 7.2

Received: 19 December 2023 | Revised: 11 March 2024 | Accepted: 15 March 2024

DOI: 10.1002/dad2.12589

RESEARCH ARTICLE

Alzheimer's & Dementia® Diagnosis, Assessment & Disease Monitoring

Aβ oligomers peak in early stages of Alzheimer's disease preceding tau pathology

Lara Blömeke[1,2,3] | Fabian Rehn[1,2,3] | Victoria Kraemer-Schulien[1] | Janine Kutzsche[1] | Marlene Pils[1,2,3] | Tuyen Bujnicki[1] | Piotr Lewczuk[4] | Johannes Kornhuber[4] | Silka D. Freiesleben[5,6] | Luisa-Sophie Schneider[5] | Lukas Preis[5] | Josef Priller[5,6,7,8] | Eike J. Spruth[5,6] | Slawek Altenstein[5,6] | Andrea Lohse[5] | Anja Schneider[9,10] | Klaus Fliessbach[9,10] | Jens Wiltfang[11,12,13] | Niels Hansen[12] | Ayda Rostamzadeh[14] | Emrah Düzel[15,16] | Wenzel Glanz[15] | Enise I. Incesoy[15,16,17] | Michaela Butryn[15] | Katharina Buerger[18,19] | Daniel Janowitz[19] | Michael Ewers[18,19] | Robert Perneczky[18,20,21,22] | Boris-Stephan Rauchmann[20,23,24] | Stefan Teipel[25,26] | Ingo Kilimann[25,26] | Doreen Goerss[25,26] | Christoph Laske[27,28] | Matthias H. Munk[27,29] | Carolin Sanzenbacher[27] | Annika Spottke[9,30] | Nina Roy-Kluth[9] | Michael T. Heneka[31] | Frederic Brosseron[9] | Michael Wagner[9,10] | Steffen Wolfsgruber[9,10] | Luca Kleineidam[9,10] | Melina Stark[10] | Matthias Schmid[9,32] | Frank Jessen[9,14,33] | Oliver Bannach[1,2] | Dieter Willbold[1,2,3] | Oliver Peters[5,6]

[1]Institute of Biological Information Processing (Structural Biochemistry: IBI-7), Forschungszentrum Jülich GmbH, Jülich, Germany

[2]attyloid GmbH, Düsseldorf, Germany

[3]Institut für Physikalische Biologie, Heinrich-Heine-Universität Düsseldorf, Düsseldorf, Germany

[4]Department of Psychiatry and Psychotherapy, Universitätsklinikum Erlangen and Friedrich-Alexander-Universität Erlangen-Nürnberg, Erlangen, Germany

[5]Department of Psychiatry and Psychotherapy, Charité, Berlin, Germany

[6]German Center for Neurodegenerative Diseases (DZNE), Berlin, Germany

[7]School of Medicine, Department of Psychiatry and Psychotherapy, Technical University of Munich, Munich, Germany

[8]University of Edinburgh and UK DRI, Edinburgh, UK

[9]German Center for Neurodegenerative Diseases (DZNE), Bonn, Germany

[10]Department of Neurodegenerative Disease and Geriatric Psychiatry/Psychiatry, University of Bonn Medical Center, Bonn, Germany

[11]German Center for Neurodegenerative Diseases (DZNE), Göttingen, Germany

[12]Department of Psychiatry and Psychotherapy, University Medical Center Göttingen, University of Göttingen, Göttingen, Germany

[13]Department of Medical Sciences, Neurosciences and Signaling Group, Institute of Biomedicine (iBiMED), University of Aveiro, Aveiro, Portugal

[14]Department of Psychiatry, Medical Faculty, University of Cologne, Cologne, Germany

[15]German Center for Neurodegenerative Diseases (DZNE), Magdeburg, Germany

[16]Institute of Cognitive Neurology and Dementia Research (IKND), Otto-von-Guericke University, Magdeburg, Germany

[17]Department for Psychiatry and Psychotherapy, University Clinic Magdeburg, Magdeburg, Germany

[18]German Center for Neurodegenerative Diseases (DZNE, Munich), Munich, Germany

Lara Blömeke, Fabian Rehn, and Victoria Kraemer-Schulien contributed equally to this study.

[19]Institute for Stroke and Dementia Research (ISD), University Hospital, LMU Munich, Munich, Germany

[20]Department of Psychiatry and Psychotherapy, University Hospital, LMU Munich, Munich, Germany

[21]Munich Cluster for Systems Neurology (SyNergy) Munich, Munich, Germany

[22]Ageing Epidemiology Research Unit (AGE), School of Public Health, Imperial College London, London, UK

[23]Sheffield Institute for Translational Neuroscience (SITraN), University of Sheffield, Sheffield, UK

[24]Department of Neuroradiology, University Hospital LMU, Munich, Germany

[25]German Center for Neurodegenerative Diseases (DZNE), Rostock, Germany

[26]Department of Psychosomatic Medicine, Rostock University Medical Center, Rostock, Germany

[27]German Center for Neurodegenerative Diseases (DZNE), Tübingen, Germany

[28]Section for Dementia Research, Hertie Institute for Clinical Brain Research and Department of Psychiatry and Psychotherapy, University of Tübingen, Tübingen, Germany

[29]Department of Psychiatry and Psychotherapy, University of Tübingen, Tübingen, Germany

[30]Department of Neurology, University of Bonn, Bonn, Germany

[31]Luxembourg Centre for Systems Biomedicine (LCSB), University of Luxembourg, Belvaux, Luxemburg

[32]Institute for Medical Biometry, University Hospital Bonn, Bonn, Germany

[33]Excellence Cluster on Cellular Stress Responses in Aging-Associated Diseases (CECAD), University of Cologne, Köln, Germany

Correspondence
Oliver Peters, Charité – Universitätsmedizin Berlin, Klinik für Psychiatrie und Psychotherapie CBF, Hindenburgdamm 30, 12203 Berlin, Germany.
Email: oliver.peters@charite.de

Oliver Bannach, attyloid GmbH, Merowingerplatz 1a, 40225 Düsseldorf, Germany.
Email: o.bannach@attyloid.com

Dieter Willbold, Institute of Biological Information Processing (IBI-7), Forschungszentrum Jülich, Wilhelm-Johnen-Straße, 52428 Jülich, Germany.
Email: d.willbold@fz-juelich.de

Funding information
"Biomarkers Across Neurodegenerative Diseases I + II" of The Alzheimer's Association; Alzheimer's Research UK and the Weston Brain Institute, Grant/Award Numbers: 11084, BAND-19-614337; The Michael J. Fox Foundation for Parkinson's Research, Grant/Award Numbers: 14977, 009889; ALS Association, Grant/Award Number: 19-SI-476; Packard Center, Grant/Award Number: 19-SI-476; Deutsche Forschungsgemeinschaft, Grant/Award Numbers: INST 208/616-1 FUGG, INST 208/794-1 FUGG; Helmholtz Association, Grant/Award Number: HVF0079

Abstract

INTRODUCTION: Soluble amyloid beta (Aβ) oligomers have been suggested as initiating Aβ related neuropathologic change in Alzheimer's disease (AD) but their quantitative distribution and chronological sequence within the AD continuum remain unclear.

METHODS: A total of 526 participants in early clinical stages of AD and controls from a longitudinal cohort were neurobiologically classified for amyloid and tau pathology applying the AT(N) system. Aβ and tau oligomers in the quantified cerebrospinal fluid (CSF) were measured using surface-based fluorescence intensity distribution analysis (sFIDA) technology.

RESULTS: Across groups, highest Aβ oligomer levels were found in A+ with subjective cognitive decline and mild cognitive impairment. Aβ oligomers were significantly higher in A+T− compared to A−T− and A+T+. *APOE* ε4 allele carriers showed significantly higher Aβ oligomer levels. No differences in tau oligomers were detected.

DISCUSSION: The accumulation of Aβ oligomers in the CSF peaks early within the AD continuum, preceding tau pathology. Disease-modifying treatments targeting Aβ oligomers might have the highest therapeutic effect in these disease stages.

KEYWORDS
Alzheimer's disease, *APOE*, AT(N) classification, Aβ, cerebrospinal fluid, oligomers, preclinical, prodromal, sFIDA, tau

Highlights

- Using surface-based fluorescence intensity distribution analysis (sFIDA) technology, we quantified Aβ oligomers in cerebrospinal fluid (CSF) samples of the DZNE-Longitudinal Cognitive Impairment and Dementia (DELCODE) cohort
- Aβ oligomers were significantly elevated in mild cognitive impairment (MCI)
- Amyloid-positive subjects in the subjective cognitive decline (SCD) group increased compared to the amyloid-negative control group

- Interestingly, levels of Aβ oligomers decrease at advanced stages of the disease (A+T+), which might be explained by altered clearing mechanisms

1 | BACKGROUND

Alzheimer's disease (AD) is a neuropathological disorder accompanied by abnormal protein deposits such as amyloid plaques and neurofibrillary tangles (NFTs)[1] which may occur up to 20 years before the onset of clinical symptoms.[2,3]

Soluble amyloid beta (Aβ) oligomers are neuro- and synaptotoxic Aβ aggregates implicated in triggering AD-related Aβ pathology that are derived from the sequential cleavage of the transmembrane amyloid precursor protein (APP).[4,5] A growing body of research indicates that deficient clearing mechanisms prevent Aβ oligomer degradation and facilitate the accumulation of Aβ species into insoluble plaques.[4,6–9] Furthermore, the formation of toxic Aβ oligomers and fibrils in the cerebrospinal fluid (CSF) has been associated with a decreased ratio of Aβ42/Aβ40, and an increased amyloid plaque burden as measured by positron emission tomography (PET).[10,11] Thus, increased Aβ oligomer levels and increasing Aβ plaque burden might act as a surrogate marker for deficient Aβ monomer clearance. Furthermore, in a series of experiments that included human brain autopsy and rat models, tau pathology measured by phosphorylated tau (pTau) in the CSF or by PET was found to act downstream of synaptic Aβ oligomer accumulation.[12] Consequently, examining potential differences in Aβ oligomer concentrations in different biomarker profiles across the AD spectrum might help identify individuals in the earliest stages of AD, thereby allowing to identify a unique window of opportunity for effective therapeutic intervention.[13] Yet, little is known how the levels of Aβ oligomers in the CSF correlate with the stages of AD, or whether they could serve as reliable biomarkers for disease progression.[14] In order to investigate the role of Aβ oligomer concentrations, the National Institute on Aging and the Alzheimer's Association (NIA-AA) research framework provide a unified biological definition of Alzheimer's disease, capable of identifying early pathological changes and biomarker interactions related to the disease.[1,15]

According to the NIA-AA research framework, individuals can be placed on the Alzheimer continuum once pathological Aβ aggregation (ie, A+) arises, regardless of their cognitive status.[1,15] In the revised NIA-AA research framework, six symptom stages of AD are defined,[16] with stages 1 and 2 characterizing individuals with preclinical AD that are cognitively unimpaired (CU).[15,16] In stage 1, experiencing subjective cognitive decline (SCD) has to be absent, whereas individuals can experience SCD or newly acquired neurobehavioral symptoms in stage 2.[16] Stages 3, 4, 5, and 6 correspond to mild cognitive impairment (MCI), and mild, moderate and severe AD dementia, respectively. Although the revised research framework is closely linked to the AT(N) (A, amyloid; T, tau; N, neurodegeneration) classification system for AD biomarkers, the presence of pTau pathology (ie, T+) is not essential to be placed on the AD continuum, as pTau pathology has been suggested to be a downstream event of amyloid pathology, and may therefore arise at later disease stages.[1] Consequently, individuals on the AD continuum can have varying biomarker profiles (eg, A+T− or A+T+), where A+T− indicates early pathologic change, whereas full-blown AD pathology (ie, the presence of both pathological amyloid and pTau deposition; A+T+) might occur at a later time[1].

Accordingly, the present study aims to elucidate the role of CSF Aβ and tau oligomers in individuals along the AD continuum stratified for different biomarker profiles (ie, A−T−, A−T+, A+T−, and A+T+), assuming that these different cross-sectional profiles reflect the temporal evolution of AD, with subjects being in one of these biological disease stages. Using surface-based fluorescence intensity distribution analysis (sFIDA), a platform technology for the quantitation of protein aggregates in biofluids,[17–21] we specifically aimed to investigate whether oligomer titers differ between biomarker profiles, and whether there is an association between amyloid positivity (ie, A+), oligomer concentrations, and diagnostic status. Lastly, as carrying the ε4 allele of the apolipoprotein E (*APOE*) gene is the most important genetic risk factor in sporadic AD,[22] we examined whether the concentrations of Aβ and tau oligomers are increased in *APOE* ε4 carriers.

2 | METHODS

2.1 | Samples and design

In the present study, demographic and clinical information and CSF baseline samples from 526 participants of the DZNE-Longitudinal Cognitive Impairment and Dementia (DELCODE) study[23] were included. Details on the overall DELCODE study design, definition of patient groups including criteria for patient enrollment, and execution of cognitive, neuropsychological tests as well as biomaterial sampling, *APOE*-genotyping, PET, magnetic resonance imaging (MRI) and CSF biomarker assessment are described in Jessen et al.[23] All participants provided their written informed consent. Only participants with a minimum of 18 points on the Mini-Mental State Examination (MMSE) qualified for the AD group in the DELCODE study.[23] In short, participants were recruited from 10 memory clinics throughout Germany and allocated to 5 participant groups, that is, the cognitively unimpaired control (C) group, SCD, MCI, mild AD dementia, and healthy first-degree relatives of AD patients (REL). To increase the number of controls in the present study, the REL were integrated into the control group. In order to classify participants according to the AT(N) classification system, we used cutoffs established within the DELCODE cohort, that is, Aβ42 ≤ 638.7 pg/mL, total tau (tTau) > 510.9 pg/mL,

and pTau ≥ 73.65 pg/mL.[24] CSF samples were stored at −80°C and did not undergo a freeze-thaw cycle. All 526 samples were blinded at the timepoint of sFIDA measurement.

2.2 | Oligomer measurement using sFIDA

We previously developed sFIDA to specifically and sensitively measure protein oligomers and aggregates in biofluids.[17–19] sFIDA uses a sandwich-like biochemistry employing the same capture and detection antibodies with linear epitopes to reliably measure the whole fraction of Aβ or tau oligomers and larger, but still soluble, aggregates even in the presence of excessive monomers. Due to the use of fluorescence microscopy and sophisticated image analysis, sFIDA yields single particle sensitivity.

2.3 | Synthesis of protein conjugated silica nanoparticles

For assay development and as assay control we used our previously developed silica nanoparticle (SiNaP) standard standard.[25,26] Aβ SiNaPs were coated with amino acids 1−15 of the Aβ protein (peptides and elephants, Henningsdorf, Germany) as described in Blömeke et al.[19] Shortly, SiNaPs were synthetized using the Stöber process and afterwards aminated using (3-aminopropyl)triethoxysilane (APTES, Sigma-Aldrich, St. Louis, MO, USA).[25,26] In the next step, activated maleimidohexanoic acid (MIHA, abcr GmbH, Karlsruhe, Germany) was allowed to react covalently with the amines. Finally, Aβ1−15 functionalized with cysteamine at the C-terminus was added to react with the maleimide groups of the particles.

Tau SiNaPs were coated with full-length tau protein (2N4R). Here, we used a different approach which was previously described in Hülsemann et al.[25] In this approach, synthesized and aminated SiNaPs were further functionalized with succinic anhydride (Sigma-Aldrich). To enable reaction, the pellet of aminated SiNaPs was redispersed in 0.1 M succinic acid anhydride in N,N-dimethylformamide anhydrous (DMF) and incubated for 2 hours at 70°C and afterwards for 2 days at room temperature (RT) when stirring. The carboxylated SiNaPs were washed three times with ddH_2O by centrifugation (7 minutes at 10,000 × *g*) and redispersion. For biofunctionalization, carboxylated SiNaPs were activated with 20 mM 1-ethyl-3-(3-dimethylaminopropyl)carbodiimide (EDC; Sigma-Aldrich) and 5 mM N-hydroxysuccinimide (NHS; Sigma-Aldrich) in a buffer of 0.1 M 2-(N-Morpholino)ethanesulfonic acid (MES; Carl Roth, Karlsruhe, Germany) while shaking for 1 hour at RT. After two washing steps (centrifugation at 18,200 × *g* for 10 minutes) and redispersion in phosphate-buffered saline (PBS), full-length tau protein was added. The next day, biofunctionalized SiNaPs were washed twice with ddH_2O as described before.

SiNaPs were characterized based on particle size and shape as previously described.[19,25] Size and shape of the particles were determined using transmission electron microscopy while concentrations were determined using inductively coupled plasma-mass spectrometry (ICP-MS).

RESEARCH IN CONTEXT

1. **Systematic review**: Aβ oligomers are the most toxic Aβ species. They disrupt synaptic communication and may thereby initiate neurodegeneration in Alzheimer's disease (AD). In order to elucidate the temporal order of amyloid (A) and tau (T) pathology along the AD continuum, we quantified cerebrospinal fluid (CSF) Aβ and tau oligomers in different disease stages.
2. **Interpretation**: CSF Aβ oligomers were significantly higher in participants with subjective cognitive decline (stage 2) and mild cognitive impairment (stage 3) classified as A+. Interestingly, A+T+ showed comparably lower Aβ oligomer levels, which might be due to increased binding to amyloid plaques over time.
3. **Future directions**: Further research examining the underlying mechanisms of the rise and fall of Aβ oligomers along the AD continuum is needed.

2.4 | Labeling of antibodies

To detect oligomers in samples, we labeled the antibodies Nab228 (Sigma-Aldrich) and Tau12 (BioLegend, San Diego, CA, USA) with the fluorescent dyes CF633 (Sigma-Aldrich) and CF488A (Sigma-Aldrich) according to manufacturer's protocol. The principle of reaction, the purification, and the determination of concentration and degree of labeling were previously described.[19]

2.5 | Assay protocol

The biochemical principle of sFIDA has been reported elsewhere.[27,28] In the present study, we used Nunc MicroWell 384-well plates for each experiment (Thermo Fisher Scientific, Waltham, MA, USA) functionalized with N-terminal monoclonal antibodies Nab228 (Sigma-Aldrich) and Tau12 (BioLegend) at a concentration of 2.5 µg/mL in 0.1 M NaHCO3. After overnight incubation at 4°C, we washed the plates five times with 80 µL tris-buffered saline (TBS)-T (1×TBS; Serva Electrophoresis, Duisburg, Germany) containing 0.05% Tween20 (AppliChem, Darmstadt, Germany) and afterwards five times with TBS (405 LS Microplate Washer, BioTek, VT, USA). To block remaining binding sides of the glass surface, 1% bovine serum albumin (BSA; AppliChem) in TBS with 0.03% ProClin (Sigma-Aldrich) were incubated for 1.5 h at RT. After washing five times with TBS-T and TBS as described above, we diluted a mix of Aβ and tau SiNaPs in PBS (Sigma-Aldrich) containing 0.5% BSA and 0.05% Tween (dilution factor 1:2) and applied 20 µL of each dilution and 20 µL of undiluted samples to the plate. The plate was incubated for 2 hours at RT and thereafter washed five times with TBS. Then 20 µL of fluorescent detection antibodies Nab228 CF633 (0.156 µg/mL) and Tau12 CF488A

(0.312 µg/mL) diluted in TBS were applied and incubated for 1 hour at RT. Finally, the plate was washed five times with TBS and the buffer was exchanged against TBS-ProClin. In order to obtain a sufficient number of replicates, each dilution and all samples were applied in a quadruple determination.

2.6 | Image data acquisition

For imaging of the assay surface, we used total internal reflection microscopy (TIRF-M; Leica, Wetzlar, Germany)[27] (excitation: 635 nm, emission filter: 705/22 nm; excitation: 488 nm, emission filter: 525/36 nm; exposure time: 1500 ms; gain: 800). In total, 25 images per well were measured with 1000 × 1000 pixels each.

2.7 | Quantification and statistical analyses

Quantification and general statistical analyses were carried out using Python 3.9.7 (Python software foundation, Wilmington, USA; packages: scipy version 1.7.3) and Origin 2020 (OriginLab Corporation, Northampton, USA). Data were further analyzed for normal distribution and in the case of not normally distributed data, nonparametric tests, for example, Spearman correlation or Mann–Whitney *U*-test, were used for further analyses.

2.8 | Image data analysis

For analysis of the images, the in-house developed software tool sFIDAta was used including the detection and elimination of artefact-containing images.[26,27] The analysis itself is based on the number of pixels above a defined cutoff value, which is defined as the pixel count. The cutoff is defined as the grayscale value at which the blank control exceeds a number of 100 pixels (0.01% of total pixels). The cutoff value is determined for each experiment individually. Moreover, 10% of images per well with the highest and lowest pixel counts were excluded from analysis to ensure that no artificial images influence the readouts.[28,29] Given pixel counts were calculated as the mean of the four sample wells.

2.9 | Analytical validation

To assess intra-assay variability of SiNaPs and samples, the coefficient of variation (CV) percentage of the four test replicates within the same run was calculated (Table S1). Furthermore, analytical selectivity of the assay was investigated applying different assay control setups as described previously.[18,19,30] In this study, we investigate if 2 pM of Aβ or tau SiNaPs interfere with the assay surface in the absence of capture antibodies (capture control), show false-positive signals due to autofluorescence component of the used assay buffers (autofluorescence control, no detection probe), or show cross-reactivity with anti-α-synuclein detection antibodies. In addition, the selectivity of the used assay antibodies was analyzed using equimolar concentrations of α-synuclein-coated SiNaPs. Since monomeric species of Aβ and tau are present in excess compared to synthetic oligomers and therefore can falsify the measurement signals, we have additionally compared equimolar concentrations of monomeric as well as oligomeric species, that is, 1 nM of synthetic Aβ oligomers[30] and 250 pM tau oligomers[19] (Figure S1). Afterward, the signal reduction of each assay control was calculated based on the normalized pixel counts according to Equation (1).

$$\text{Signal reduction } [\%] = \left(1 - \frac{\text{pixel count}_{\text{assay control}} - \text{pixel count}_{\text{blank control}}}{\text{pixel count}_{\text{reference}} - \text{pixel count}_{\text{blank control}}}\right) \times 100\% \quad (1)$$

2.10 | Data scaling

Since oligomer levels in samples were lower than suggested, not enough data points of the SiNaPs concentration series were available to create a suitable calibration curve. However, as it was not possible to use the raw data directly without distorting the statistical results, a scaling method was used to compensate for differences between the experiments. This method was based on the samples of the control group and was carried out separately for Aβ and tau oligomers. For each oligomer type, a cross-plate median *globalMedian* of all control group samples was calculated. Subsequently, a separate medium *plateMedian* was formed for each plate *p*. Using these values, a scaling factor (Table S2) was calculated for each plate *p* according to Equation (2).

$$\text{scaleFacto}\, r_p = \frac{\text{globalMedian}}{\text{plateMedian}_p} \quad (2)$$

Finally, all measurement results of a plate were multiplied by the corresponding scaleFactor_p. The scaled pixel counts for Aβ and tau oligomers, in the following referred to as Aβ and tau oligomer pixel counts, were used for all analyses. Figure S2 and Figure S3 show the data before and after scaling, respectively.

2.11 | Descriptive analysis

Using Spearman correlations and two-sided Mann–Whitney *U*-tests, we examined the association of oligomer pixel counts with demographic variables and known risk factors for AD, including age, sex, and *APOE* status,[31,32] as well as associations with further CSF biomarkers.

2.12 | Differences in Aβ and tau oligomer levels

To test for differences between participant groups, we performed a two-sided Mann–Whitney *U*-test. For this purpose, we regrouped the samples stepwise, based first on clinical diagnosis. However, symptoms used for the clinical diagnosis of AD can also be caused by other

forms of dementia, which leads to a clinical diagnosis not necessarily being free of errors. Therefore, we subsequently subdivided the four clinically defined groups based on the amyloid status using Aβ42 biomarker data. Afterward, the samples were analyzed independently of their clinical diagnosis using the AT(N) classification. To this end, cutoffs established within the study of Jessen et al.[24] can be used to classify the participants according to AT(N) system. In the present study, the cut-offs for Aβ42 (≤ 638.7 pg/mL), pTau (≥ 73.65 pg/mL) and tTau (> 510.9 pg/mL) positivity were applied to determine amyloid positivity or tau positivity or neurodegeneration. In addition, we also regrouped the samples based on *APOE* status with carrying at least one *APOE* ε4 allele defining *APOE* positivity (ε2/ε4, ε3/ε4, or ε4/ε4) since the *APOE* ε4 allele is an important genetic risk factor for AD.[22]

2.13 | Modeling Aβ oligomer levels in the AD continuum

In an effort to model levels of Aβ oligomers in the course of AD, a regression pipeline was designed to anticipate the Aβ oligomers utilizing Aβ42 and pTau monomers as features. The pipeline is made up of a standard scaler and a bagging model, the latter comprising three support vector regression models with radial basis function (RBF) kernels that are trained on various data subsets. Given the presumption that the relationship between the features and target might vary depending on the *APOE* ε4 status, three different instances of this pipeline were created using solely *APOE* ε4 carrier data, *APOE* ε4 noncarrier data, and all-encompassing data.

To generate continuous oligomer curves describing the progression of AD with these pipelines, it is necessary to establish a probable trajectory of Aβ42 and pTau monomers throughout the AD stages. In order to exclude bias arising from disproportionate representation of AT groups, equal numbers of samples were randomly chosen from the A−T−, A+T−, and A+T+ sets. Following this, data were scaled employing a min-max scaler, centered, and aligned to the antidiagonal. The trajectory was finally ascertained by applying a second-degree polynomial regression, and subsequently reverse transformed. The resulting trajectory was utilized as input to predict oligomer curves for *APOE* ε4 carrier, *APOE* ε4 noncarrier, and all data by the three system instances, which were later refined by a moving average. Given their relationship to Aβ42 and pTau, these curves can be integrated into other models. With this feature in mind, the curves were deliberately superimposed on a biomarker model for AD progression.[33]

All of the above was achieved using the scikit-learn Python package, version 1.0.2.

3 | RESULTS

The aim of the present study was to investigate Aβ and tau oligomer levels in human CSF samples of patients across the clinical and neurobiological continuum of AD.

3.1 | Descriptive analysis of patient and control groups

In the present study, 526 CSF samples from DELCODE, that is, 137 samples from controls, 211 samples from SCD participants, 112 samples from MCI patients, and 66 samples from AD patients, were screened for Aβ and tau oligomer levels. Demographic and clinical information for these four groups on age, gender, neuropsychological tests, amyloid-, tau-, and *APOE* ε4-status is available in Table 1.

To avoid misinterpretation of the statistical results due to demographic characteristics, we checked for correlations of age and gender with oligomer levels. Since the Shapiro–Wilk test showed that neither Aβ nor tau oligomer values were normally distributed ($p = 9.22 \times 10^{-42}$ and 1.44×10^{-34}, respectively), nonparametric tests were used. No significant Spearman correlation was found between age and oligomer pixel counts (Aβ: $r = .033$, $p = .446$; tau: $r = .016$, $p = .709$). Results from two-sided Mann–Whitney *U*-tests showed that Aβ and tau oligomer pixel counts did not significantly differ between genders, even if the significance is nearly reached for Aβ oligomers ($p = .063$; tau $p = .973$). Furthermore, as age and gender are equally distributed for all combinations of groupings by AT(N) classification as well as *APOE* ε4 genotpye, it can be assumed that there is no respective bias for the analysis.

3.2 | Clinically diagnosed MCI patients showed significantly higher levels of Aβ oligomers compared to controls

First, we investigated if Aβ and tau oligomer levels differ between clinical diagnosis groups, using two-tailed Mann–Whitney *U*-tests (Figure 1). In the case of MCI patients, significantly higher Aβ oligomer levels were found compared to the control group ($p = .017$, Figure 1A). Although Aβ and tau oligomer levels showed a highly significant correlation (Spearman $r = .541$, $p = 2.7 \times 10^{-41}$), no increase of tau oligomer levels regarding the disease stage was observed (Figure 1B).

Next, we divided the four clinical groups based on presence of amyloid pathology into amyloid negative (A−) and amyloid positive (A+) cases to analyze if differences in Aβ oligomer levels are due to underlying AD pathology. When comparing these refined groups with the A− control group, it became apparent that SCD ($p = .014$) and MCI ($p = .003$) participants with underlying amyloid pathology, but not those without evidence for AD, showed significantly increased Aβ oligomer levels (Figure 1C). Furthermore, SCD participants with amyloid positive states showed elevated Aβ oligomer levels compared to SCD individuals without diagnosed amyloid pathology ($p = .048$). However, even after the additional breakdown by A, there was no difference in tau oligomer levels (Figure 1D).

3.3 | Differences in Aβ oligomer levels based on AT(N) profiles and *APOE* ε4 status

As the results of Section 3.2 indicate the importance of the underlying pathologies for increases of Aβ oligomers, we regrouped and analyzed

TABLE 1 Demographic information and study characteristics of participants grouped by clinical diagnosis.

	Control	SCD	MCI	AD
Number	137	211	112	66
Age, years (SD)	68.2 (4.9)	71.4 (5.8)	72.3 (5.4)	75.5 (6.3)
Female	54%	43%	43%	65%
MMSE (SD)	29.3 (0.9)	29.1 (1.1)	27.5 (1.9)	23.2 (3.1)
A+	27.7%	40.8%	72.3%	92.4%
T+	7.3%	15.2%	37.5%	68.2%
APOE ε4[a]	27.6%	34.6%	50.5%	64.5%

Abbreviations: A+, amyloid pathology above cut-off; AD, Alzheimer's disease; *APOE* ε4, apolipoprotein E ε4 allele; MCI, mild cognitive impairment; MMSE, Mini-Mental State Examination; SCD, subjective cognitive decline; SD, standard deviation; T+, tau pathology above cut-off.
[a]No *APOE* data were available for 17 participants.

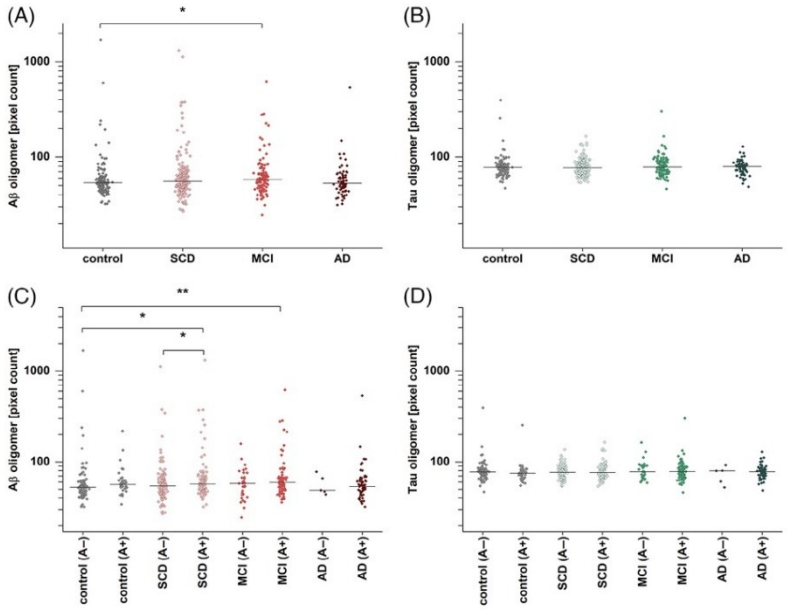

FIGURE 1 Amyloid beta (Aβ) and tau oligomer pixel count based on amyloid pathology (A+/A−). (A) Aβ oligomer pixel counts in mild cognitive impairment (MCI) are significantly increased compared to the controls ($p = .017$). (B) By contrast, no significant changes were detected for tau oligomer pixel count. (C) After dividing groups along amyloid status, significantly higher levels in subjective cognitive decline (SCD) (A+) and MCI (A+) compared to controls (A−) were observed ($p = .014$ and $p = .0028$, respectively). Furthermore, SCD (A+) is significantly elevated compared to SCD (A−) ($p = .048$). (D) Tau oligomers in subgroups show no significant differences when divided in A+ and A−. Effect sizes for the significantly differing groups are provided in Table S3, while receiver operating characteristic curves and area under the curve scores are presented in Figure S4 and Table S5. Horizontal lines indicate the median; y-axis scales are logarithmic. A two-sided Mann–Whitney *U*-test (confidence interval = .05) was carried out to investigate differences between the groups. Abbreviation: AD, Alzheimer's disease. $^{*}p \leq .05$, $^{**}p \leq .01$.

the results based on the AT classification proposed by the NIA-AA research framework and the currently established cutoff values by Jessen et al. for Aβ42 and pTau[24] (Figure 2). Furthermore, demographic information was regrouped based on AT classification (Table 2). Since again no differences in tau oligomer levels between the sample groups were observed, the subsequent analyses were only described with respect to Aβ oligomer levels.

Applying this classification, samples of participants with amyloid pathology without tau pathology (A+T−) had significantly increased levels of Aβ oligomers compared to A+T+ participants with amyloid and tau pathology ($p = 5.8 \times 10^{-5}$). This applied to participants with (A+T−N+) and without (A+T−N−), a concomitant non-Alzheimer's pathologic change (A+T−N+: $p = .032$; A+T−N−: $P = 1.8 \times 10^{-4}$). Aβ oligomer levels of participants classified as A+T+ did not differ

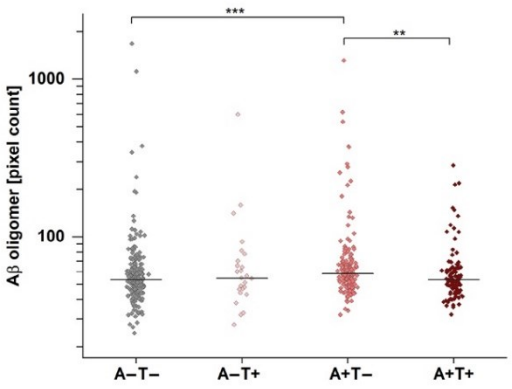

FIGURE 2 Amyloid beta (Aβ) oligomers in quantified cerebrospinal fluid (CSF) samples after AT (amyloid/tau) classification. Aβ oligomer pixel counts in CSF of A+T− patients are significantly increased compared to the reference group A−T− ($p = 5.8 \times 10^{-5}$) and to A+T+ ($p = .0026$). Effect sizes for the significantly differing groups are provided in Table S3, while receiver operating characteristic curves and area under the curve scores are presented in Figure S4 and Table S5. Horizontal lines indicate the median; y-axis scale is logarithmic. A two-sided Mann–Whitney *U*-test (confidence interval = .05) was carried out to investigate differences between the groups. $^{**}p \leq .01$, $^{***}p$ value $\leq .001$.

significantly from control group participants but compared to A+T− participants ($p = .0026$).

Because the *APOE* ε4 allele is an important genetic risk factor for AD,[22] we also investigated Aβ oligomer levels in *APOE* ε4 carriers. Here, significantly increased Aβ oligomer levels were found compared *APOE* ε4 noncarriers independent of the disease stage ($p = .02$). For further evaluation, receiver operating characteristic (ROC) curves, area under the curve (AUC) scores, and effect sizes were presented in Figure S4, Tables S3 and S4.

3.4 | Aβ oligomer levels are elevated in early disease stages

To investigate how Aβ oligomers fit into the AD continuum, we established a regression model that predicts Aβ oligomer levels based on monomeric Aβ42 and pTau concentrations. This model was validated by normalized mean absolute error (Table S5) and by comparing the binned raw data and the binned regression model predictions (Figure S5). As displayed in Figure 3A, increased oligomer levels were only found at low Aβ42 and pTau concentrations in early AD stages. Furthermore, we also investigated if the observed increase and later decrease of Aβ oligomer levels depends on *APOE* ε4 status. To this end, we classified samples into *APOE* ε4 carriers (Figure 3B) and noncarriers (Figure 3C). The predicted Aβ oligomer levels in context of different *APOE* ε4 states indicated that the levels of Aβ oligomers are increased in *APOE* ε4 carriers, and that the peak shifted to higher pTau concentrations (red areas in Figure 3B,C). To provide a more specific statement about the probable level of the Aβ oligomer in the AD continuum, the prediction was reduced to the most likely trajectory of Aβ42 and pTau monomer through the AD stages, as described in 2.3.6 and displayed in Figure 4A. The model of Jack et al.[33] supplemented by the modeled Aβ oligomer curves revealed that in *APOE* ε4

TABLE 2 Demographic information of participants based on the AT classification.

Characteristic	A−T−	A−T+	A+T−	A+T+
number	234	26	163	103
Age, years (SD)	69.62 (5.61)	73.08 (5.15)	71.61 (6.00)	74.08 (5.78)
Female	48.7%	53.8%	61.0%	51.5%
MMSE (SD)	29.1 (1.3)	28.3 (2.9)	28.2 (2.4)	25.7 (3.4)
Aβ42, pg/mL (SD)	960.9 (212.2)	1218.9 (471.2)	445.3 (122.9)	419.8 (116.4)
Aβ42/40 ratio (SD)	0.108 (0.015)	0.094 (0.029)	0.071 (0.023)	0.046 (0.009)
pTau, pg/mL (SD)	47.7 (10.9)	102.2 (45.3)	46.4 (16.3)	108.3 (35.8)
tTau, pg/mL (SD)	333.0 (120.2)	696.8 (361.0)	353.0 (153.3)	849.8 (273.3)
APOE ε4[a]	20.0%	23.1%	48.1%	73.0%
Clinical diagnosis in percentage of subgroups				
Control	39.7%	23.1%	20.9%	3.9%
SCD	48.3%	46.2%	40.5%	19.4%
MCI	10.7%	23.1%	27.6%	35.0%
AD	1.3%	7.7%	11.0%	41.7%
	100%	100%	100%	100%

Abbreviations: A+, amyloid pathology above cut-off; Aβ, amyloid beta; AD, Alzheimer's disease; *APOE* ε4, apolipoprotein E ε4 allele; AT, amyloid/tau; MCI, mild cognitive impairment; MMSE, Mini-Mental State Examination; SCD, subjective cognitive decline; SD, standard deviation; T+, tau pathology above cut-off.
[a]No *APOE* data were available for 17 participants.

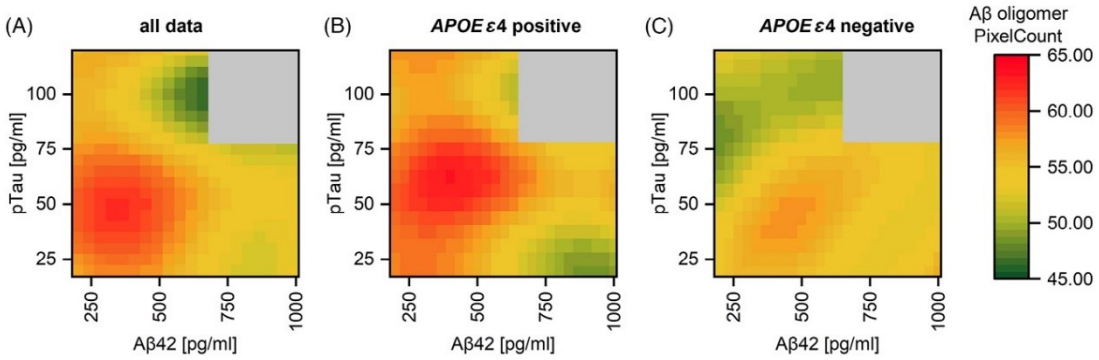

FIGURE 3 Regression model for the interrelationship of amyloid beta (Aβ) oligomers pixel count, Aβ42, and phosphorylated tau (pTau) in cerebrospinal fluid (CSF). Based on Aβ42, pTau, and Aβ oligomer levels in CSF, regression models for prediction of Aβ oligomers pixel count were performed. Highest Aβ oligomer levels can be expected in patients with low Aβ42 while pTau is relatively low in (A) all patients, (B) apolipoprotein E (*APOE*) gene ε4 allele carriers, and (C) *APOE* ε4 noncarriers. Aβ42 oligomer levels in *APOE* ε4-positive participants are overall higher and shifted toward higher pTau concentrations compared to those who were *APOE* ε4 negative.

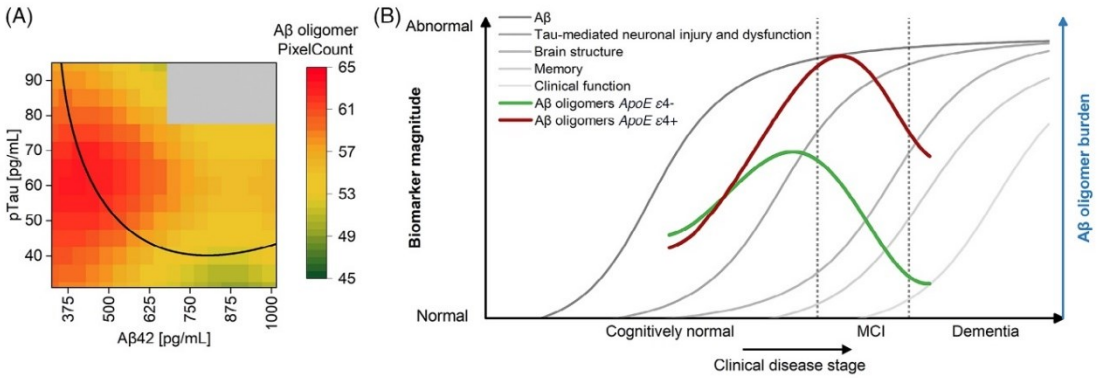

FIGURE 4 Hypothetical model of amyloid beta (Aβ) oligomers in cerebrospinal fluid (CSF) within the Alzheimer's disease (AD) continuum. (A) Along the trajectory of biomarkers during AD progression from high Aβ42 and low pTau (A−T−) to lowered Aβ42 first (A+T−) followed by elevated pTau (A+T+), Aβ oligomers start to rise until a turning point is reached. Soon after pTau starts to increase, Aβ oligomer concentrations decrease. This panel is a zoomed-in portion of Figure 3B. Data are represented in a binned form. (B) Hypothetical changes of Aβ oligomers during disease progression are transferred to the model of AD biomarker changes according to Jack et al.[1] Apolipoprotein E (*APOE*) gene ε4 allele carriers show higher oligomer concentrations with a peak at a more advanced disease stage but still in the early stages of the disease. Due to the high age of the cohort (60+) and the absence of persons with advanced AD, it was not possible to cover the entire x-axis with the curves. For validation of the model, Figure S5 shows a comparison between the measured oligomer level and the oligomer level determined by regression. Figure modified after Jack et al.[33]

noncarriers the peak is reached during the SCD stage, whereas in *APOE* ε4 carriers it is reached at the MCI stage (Figure 4B). Regardless of the *APOE* ε4 status, Aβ oligomer levels already decrease within the MCI stage.

4 | DISCUSSION

In the present study we measured Aβ oligomers in CSF aiming to allocate the presence of these most neurotoxic Aβ species within the neurobiological continuum of AD and thereby elucidate the temporal sequence of Aβ oligomers in AD pathology. Our work provides novel evidence for the importance of Aβ oligomers in early biological and symptomatic disease stages, as we found the highest levels of Aβ oligomers in participants with the clinical diagnosis of MCI. However, 59.8% of SCD and 27.7% of MCI participants did not have evidence for amyloid pathology and might therefore not suffer from AD. Stratification for amyloid positivity (ie, A+ vs A−) alone yielded significant differences within the SCD group and enhanced the discrimination of SCD and MCI to controls. Strikingly, stratification of participants by A/T

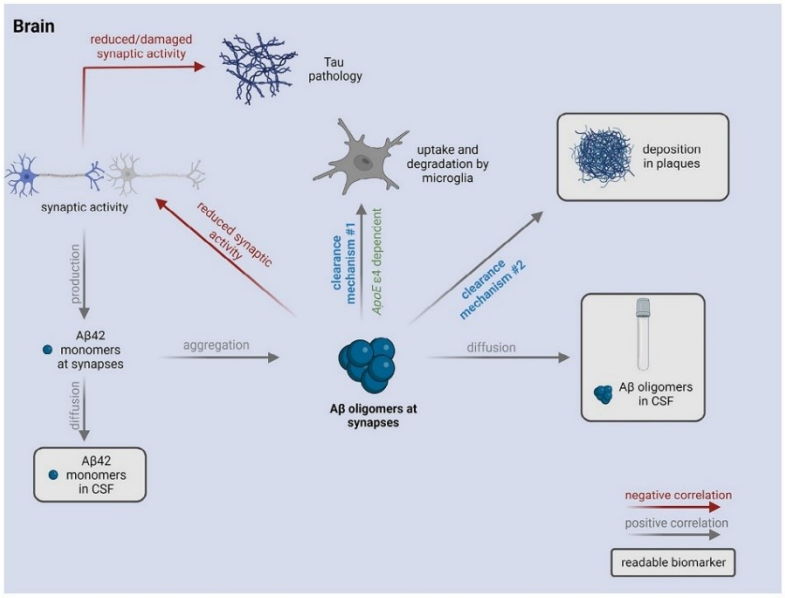

FIGURE 5 Proposed clearance mechanisms for amyloid beta (Aβ) oligomers and the influence on the use of Aβ oligomers as biomarker. Hypothetic scenario: Aβ monomer production at synapses is dependent on synaptic activity. At a certain time point, aggregation of Aβ monomers leads to the formation of toxic Aβ oligomers which can be cleared by different mechanisms. Aβ oligomers can be degraded by microglia (clearance mechanism #1), diffuse into cerebrospinal fluid (CSF), or be deposited into plaques (clearance mechanism #2) as soon as there are plaques. Formation of plaques in patients with amyloid pathology allows oligomers to be deposited there (clearance mechanism #2), which may well become the preferred fate of Aβ oligomers. Figure created with BioRender.com. *APOE* ε4, apolipoprotein E ε4 allele.

biomarker profiles, thereby also taking tau pathology as reflected by CSF pTau into account, yielded significantly elevated Aβ oligomer levels in individuals with an A+/T− biomarker profile compared to participants with nonpathological AD biomarkers (A−/T−) on the one hand, and full-blown AD neuropathological changes (A+/T+ profile) on the other. Consequently, Aβ oligomers in our cohort peak in early disease stages, where tau pathology is still inconspicuous (A+T−). Intuitively, one may assume that while Aβ aggregation is increasing in the brain during early disease stages, the Aβ oligomer level is also rising in the CSF. That is exactly what we observed in the present study when comparing A−T− with A+T− subjects. Rather surprisingly, we observed reduced Aβ oligomer levels in the more advanced disease stage A+T+ compared to the earlier A+T− stage. Deposition of oligomer species into plaques or breakdown of active clearance mechanisms from brain to CSF are just two of many possible explanations (Figure 5). To elucidate the relationship of Aβ oligomers, Aβ42, and pTau (Figure 3), we calculated a chronological sequence of Aβ oligomer levels based on the regression model and superimposed it to key biomarkers of AD as depicted in Figure 4. With respect to the limited range of disease stages within our cohort, lacking very early and advanced disease stages, no statements about oligomer levels over the whole spectrum of disease stages can be made. A limitation of the study is the low number of samples from stage 1 of AD to determine the age at which Aβ oligomer levels start to rise. According to our model, Aβ oligomers start to rise approximately at the beginning of stage 2 and reach their peak early in stage 3 before the oligomer level decreases again, which is in line with previous studies.[34,35] However, other studies, which did not include early stages, reported increased Aβ oligomer concentrations in CSF samples of demented patients compared to the control group[21,34,36] or no differences between dementia or MCI and controls.[37] In addition to differences in patient preanalytical variables such as freeze-thaw cycles, storage period, or centrifugation of the samples,[38] different results may be caused by the choice of assay setups, especially regarding the selection of antibodies,[35] targeting different epitopes and oligomer structures. More recent publications focused on blood-based detection reported increased Aβ oligomer levels in plasma over the course of the disease or a correlation with amyloid-PET positivity.[39–41]

We further investigated the effect of *APOE* ε4 positivity on Aβ oligomer levels. As can be seen in the regression model (Figure 3) and the hypothetical model of Aβ oligomer changes (Figure 4), *APOE* ε4 carriers showed higher oligomer levels. Notably, in *APOE* ε4 carriers, the Aβ oligomer level in CSF peaks further right of the peak in *APOE* ε4 noncarriers. This is not later in time, but further down in disease progression strengthening the view that *APOE* ε4 carriers start earlier into the Alzheimer's continuum.[22,42]

Although Aβ and tau oligomers show a highly significant correlation, no differences of tau oligomers with respect to the biomarker

profile or the clinical syndrome were observed, which is in line with previous findings from our lab.[19] In the present study, we investigated patients who were at mild disease stages when enrolled in the DELCODE study.[23] Presumably, tau oligomers in CSF might be increased and detectable in late stages of dementia. Indeed, a previous study from Sengupta et al. reported elevated tau oligomers only at moderate to severe dementia.[43]

Our results emphasize the relevance of the biologically based definition of Alzheimer's disease, as Aβ oligomers, which are thought to be the major toxic species in the disease, are only increased in patients with abnormal Aβ42. Moreover, we have previously demonstrated that sFIDA is now a robust method to quantitate aggregates from tau, α-synuclein, and Aβ in body fluids.[17–20,30] To further understand the differences between assay outcomes and investigate setups or antibodies which are best suited for diagnosis, it will be of great interest to measure a pool of samples with diverse Aβ oligomer assays. Probably, the combination of different oligomer biomarkers improves the understanding of the underlying pathology and the diagnostic accuracy as calculated by the probability analysis of Lewczuk et al.[44] In particular, longitudinal analysis of Aβ and tau oligomer concentrations over a longer period of time may support our model of Aβ oligomer concentration changes and add to our understanding about which patients at a predementia stage will develop AD in the future. Besides the diagnostic aspects, Aβ oligomers measured by sFIDA are promising biomarkers for clinical drug development to easily monitor their effects.[20]

AUTHOR CONTRIBUTIONS

Victoria Kraemer-Schulien, Lara Blömeke, and Marlene Pils developed the assay. Victoria Kraemer-Schulien performed the experiments together with Lara Blömeke and Marlene Pils. Fabian Rehn, Victoria Kraemer-Schulien, and Lara Blömeke analyzed the data and carried out the statistics. Lara Blömeke, Fabian Rehn, and Victoria Kraemer-Schulien wrote the manuscript together with Oliver Peters, Marlene Pils, Oliver Bannach, and Dieter Willbold. Oliver Bannach, Dieter Willbold, and Oliver Peters supervised the project. Piotr Lewczuk and Johannes Kornhuber were involved in the establishment of the assay. Janine Kutzsche, Tuyen Bujnicki, Luisa-Sophie Schneider, Silka D. Freiesleben, and Michael Wagner carefully revised the manuscript. Lukas Preis, Josef Priller, Eike J. Spruth, Slawek Altenstein, Anja Schneider, Klaus Fliessbach, Jens Wiltfang, Frank Jessen, Wenzel Glanz, Katharina Buerger, Daniel Janowitz, Robert Perneczky, Boris-Stephan Rauchmann, Stefan Teipel, Ingo Kilimann, Doreen Goerss, Christoph Laske, Matthias H. Munk, Michael Ewers, Emrah Düzel, Andrea Lohse, Niels Hansen, Ayda Rostamzadeh, Enise I. Incesoy, Michaela Butryn, Carolin Sanzenbacher, Matthias Schmid were responsible for the management of the DELCODE study at the various sites. Oliver Peters, Frank Jessen, Annika Spottke, Nina Roy-Kluth, Michael T. Heneka, Frederic Brosseron, Steffen Wolfsgruber, Luca Kleineidam, Melina Stark, Michaela Butryn, and Emrah Düzel were responsible for methodological core central data management and quality control of the DELCODE study.

ACKNOWLEDGMENTS

We received funding from the programs "Biomarkers Across Neurodegenerative Diseases I + II" of The Alzheimer's Association, Alzheimer's Research UK and the Weston Brain Institute (11084 and BAND-19-614337). We are also grateful for support from The Michael J. Fox Foundation for Parkinson's Research (14977, 009889), from the ALS Association, and from the Packard Center (19-SI-476). We further received funding from the Deutsche Forschungsgemeinschaft (INST 208/616-1 FUGG, INST 208/794-1 FUGG) and the Helmholtz Association (HVF0079).

Open access funding enabled and organized by Projekt DEAL.

CONFLICTS OF INTERESTS STATEMENT

Dieter Willbold and Oliver Bannach are co-founders and shareholders of attyloid GmbH. This had no influence of the interpretation of the data. All other authors declare no competing interests related to this work. The sFIDA method is protected by patents EP3271724A1, EP3014279B1 and EP2794655B1. Author disclosures are available in the supporting information.

CODE AVAILABILITY STATEMENT

For image data analysis, we used the sFIDAta software tool which can be made available upon request.

DATA AVAILABILITY STATEMENT

The authors confirm that the data supporting the findings of this study are available within the article and its supplementary materials.

CONSENT STATEMENT

All local institutional review boards and ethical committees approved the study protocol. All participants gave written informed consent before inclusion in the study. DELCODE is registered at the German clinical trials register (drks00007966) (04/may/2015).

REFERENCES

1. Jack CR Jr, Bennett DA, Blennow K, et al. NIA-AA Research framework: toward a biological definition of Alzheimer's disease. *Alzheimer's Dement*. 2018;14:535-562.
2. Jack CR Jr, Holtzman DM. Biomarker modeling of Alzheimer's disease. *Neuron*. 2013;80:1347-1358.
3. Villemagne VL, Burnham S, Bourgeat P, et al. Amyloid beta deposition, neurodegeneration, and cognitive decline in sporadic Alzheimer's disease: a prospective cohort study. *Lancet Neurol*. 2013;12:357-367.
4. Tolar M, Hey J, Power A, Abushakra S. Neurotoxic soluble amyloid oligomers drive Alzheimer's pathogenesis and represent a clinically validated target for slowing disease progression. *Int J Mol Sci*. 2021;22(12):6355.
5. Larson ME, Lesné SE. Soluble Aβ oligomer production and toxicity. *J Neurochem*. 2012;120(supp l):125-139.
6. Brinkmalm G, Hong W, Wang Z, et al. Identification of neurotoxic cross-linked amyloid-beta dimers in the Alzheimer's brain. *Brain*. 2019;142:1441-1457.
7. Gaspar RC, Villarreal SA, Bowles N, Hepler RW, Joyce JG, Shughrue PJ. Oligomers of beta-amyloid are sequestered into and seed new plaques in the brains of an AD mouse model. *Exp Neurol*. 2010;223:394-400.
8. Iljina M, Garcia GA, Dear AJ, et al. Quantitative analysis of co-oligomer formation by amyloid-beta peptide isoforms. *Sci Rep*. 2016;6:28658.

9. O'Brien RJ, Wong PC. Amyloid precursor protein processing and Alzheimer's disease. *Annu Rev Neurosci*. 2011;34:185-204.
10. Olsson B, Lautner R, Andreasson U, et al. CSF and blood biomarkers for the diagnosis of Alzheimer's disease: a systematic review and meta-analysis. *Lancet Neurol*. 2016;15:673-684.
11. Lewczuk P, Lukaszewicz-Zajac M, Mroczko P, Kornhuber J. Clinical significance of fluid biomarkers in Alzheimer's disease. *Pharmacol Rep*. 2020;72:528-542.
12. Bilousova T, Miller CA, Poon WW, et al. Synaptic amyloid-β oligomers precede p-Tau and differentiate high pathology control cases. *Am J Pathol*. 2016;186:185-198.
13. Hefti F, Goure WF, Jerecic J, Iverson KS, Walicke PA, Krafft GA. The case for soluble Aβ oligomers as a drug target in Alzheimer's disease. *Trends Pharmacol Sci*. 2013;34:261-266.
14. Hayden EY, Teplow DB. Amyloid β-protein oligomers and Alzheimer's disease. *Alzheimer's Res Ther*. 2013;5:60.
15. Kiselica AM. Empirically defining the preclinical stages of the Alzheimer's continuum in the Alzheimer's disease neuroimaging initiative. *Psychogeriatrics*. 2021;21:491-502.
16. Knopman DS, Haeberlein SB, Carrillo MC, et al. The National Institute on Aging and the Alzheimer's Association Research Framework for Alzheimer's disease: perspectives from the research roundtable. *Alzheimer's Dement*. 2018;14:563-575.
17. Pils M, Rutsch J, Eren F, et al. Disrupted-in-schizophrenia 1 (DISC1) protein aggregates in cerebrospinal fluid are elevated in first-episode psychosis patients. *Psychiatry Clin Neurosci*. 2023;77:665-671.
18. Schaffrath A, Schleyken S, Seger A, et al. Patients with isolated REM-sleep behavior disorder have elevated levels of alpha-synuclein aggregates in stool. *NPJ Parkinson's Dis*. 2023;9:14.
19. Bloemeke L, Pils M, Kraemer-Schulien V, et al. Quantitative detection of alpha-synuclein and Tau oligomers and other aggregates by digital single particle counting. *NPJ Parkinsons Dis*. 2022;8:68.
20. Kass B, Schemmert S, Zafiu C, et al. Abeta oligomer concentration in mouse and human brain and its drug-induced reduction ex vivo. *Cell Rep Med*. 2022;3:100630.
21. Wang-Dietrich L, Funke SA, Kuhbach K, et al. The amyloid-beta oligomer count in cerebrospinal fluid is a biomarker for Alzheimer's disease. *J Alzheimer's Dis*. 2013;34:985-994.
22. Yamazaki Y, Zhao N, Caulfield TR, Liu CC, Bu G. Apolipoprotein E and Alzheimer disease: pathobiology and targeting strategies. *Nat Rev Neurol*. 2019;15:501-518.
23. Jessen F, Spottke A, Boecker H, et al. Design and first baseline data of the DZNE multicenter observational study on predementia Alzheimer's disease (DELCODE). *Alzheimer's Res Ther*. 2018;10:15.
24. Jessen F, Wolfsgruber S, Kleineindam L, et al. Subjective cognitive decline and stage 2 of Alzheimer disease in patients from memory centers. *Alzheimer's Dement*. 2022;19(2):487-497.
25. Hülsemann M, Zafiu C, Kühbach K, et al. Biofunctionalized silica nanoparticles: standards in amyloid-beta oligomer-based diagnosis of Alzheimer's disease. *J Alzheimer's Dis*. 2016;54:79-88.
26. Kühbach K, Hülsemann M, Herrmann Y, et al. Application of an amyloid beta oligomer standard in the sFIDA assay. *Front Neurosci*. 2016;10:8.
27. Kravchenko K, Kulawik A, Hülsemann M, et al. Analysis of anticoagulants for blood-based quantitation of amyloid beta oligomers in the sFIDA assay. *Biol Chem*. 2017;398:465-475.
28. Herrmann Y, Bujnicki T, Zafiu C, et al. Nanoparticle standards for immuno-based quantitation of alpha-synuclein oligomers in diagnostics of Parkinson's disease and other synucleinopathies. *Clin Chim Acta*. 2017;466:152-159.
29. Herrmann Y, Kulawik A, Kuhbach K, et al. sFIDA automation yields sub-femtomolar limit of detection for Aβ aggregates in body fluids. *Clin Biochem*. 2017;50:244-247.
30. Pils M, Dybala A, Rehn F, et al. Development and implementation of an internal quality control sample to standardize oligomer-based diagnostics of Alzheimer's disease. *Diagnostics*. 2023;13:1702.
31. Vermunt L, Sikkes SAM, van den Hout A, et al. Duration of preclinical, prodromal, and dementia stages of Alzheimer's disease in relation to age, sex, and APOE genotype. *Alzheimer's Dement*. 2019;15:888-898.
32. Alzheimer's Association. 2022 Alzheimer's disease facts and figures. *Alzheimer's Dement*. 2022;18:700-789.
33. Jack CR, Knopman DS, Jagust WJ, et al. Hypothetical model of dynamic biomarkers of the Alzheimer's pathological cascade. *The Lancet Neurology*. 2010;9:119-128.
34. Holtta M, Hansson O, Andreasson U, et al. Evaluating amyloid-beta oligomers in cerebrospinal fluid as a biomarker for Alzheimer's disease. *PLOS ONE*. 2013;8:e66381.
35. Yang T, O'Malley TT, Kanmert D, et al. A highly sensitive novel immunoassay specifically detects low levels of soluble Aβ oligomers in human cerebrospinal fluid. *Alzheimer's Res Ther*. 2015;7:14.
36. Savage MJ, Kalinina J, Wolfe A, et al. A sensitive Aβ oligomer assay discriminates Alzheimer's and aged control cerebrospinal fluid. *J Neurosci*. 2014;34:2884-2897.
37. Jongbloed W, Bruggink KA, Kester MI, et al. Amyloid-beta oligomers relate to cognitive decline in Alzheimer's disease. *J Alzheimer's Dis*. 2015;45:35-43.
38. Dulewicz M, Kulczynska-Przybik A, Mroczko P, Kornhuber J, Lewczuk P, Mroczko B. Biomarkers for the diagnosis of Alzheimer's disease in clinical practice: the role of CSF biomarkers during the evolution of diagnostic criteria. *Int J Mol Sci*. 2022:23:8598.
39. Babapour Mofrad R, Scheltens P, Kim S, et al. Plasma amyloid-beta oligomerization assay as a pre-screening test for amyloid status. *Alzheimer's Res Ther*. 2021;13:133.
40. Liu L, Kwak H, Lawton TL, et al. An ultra-sensitive immunoassay detects and quantifies soluble Aβ oligomers in human plasma. *Alzheimer's Dement*. 2022;18:1186-1202.
41. Shea D, Colasurdo E, Smith A, et al. SOBA: development and testing of a soluble oligomer binding assay for detection of amyloidogenic toxic oligomers. *Proc Natl Acad Sci U S A*. 2022;119:e2213157119.
42. Leoni V. The effect of apolipoprotein E (ApoE) genotype on biomarkers of amyloidogenesis, tau pathology and neurodegeneration in Alzheimer's disease. *Clin Chem Lab Med*. 2011;49:375-383.
43. Sengupta U, Portelius E, Hansson O, et al. Tau oligomers in cerebrospinal fluid in Alzheimer's disease. *Ann Clin Transl Neurol*. 2017;4:226-235.
44. Lewczuk P, Wiltfang J, Kornhuber J, Verhasselt A. Distributions of Aβ42 and Aβ42/40 in the cerebrospinal fluid in view of the probability theory. *Diagnostics*. 2021;11:2372.

SUPPORTING INFORMATION

Additional supporting information can be found online in the Supporting Information section at the end of this article.

How to cite this article: Blömeke L, Rehn F, Kraemer-Schulien V, et al. Aβ oligomers peak in early stages of Alzheimer's disease preceding tau pathology. *Alzheimer's Dement*. 2024;16:e12589. https://doi.org/10.1002/dad2.12589

3.3 Oral treatment with all-D-peptide RD2 enhances cognition in aged beagle dogs – a model of sporadic Alzheimer's disease

Autoren:	Janine Kutzsche*, Sarah Schemmert*, Tuyen Bujnicki*, Christian Zafiu, Steffen Halbgebauer, Victoria Kraemer-Schulien, Marlene Pils, Lara Blömeke, Julia Post, Andreas Kulawik, Dagmar Jürgens, Wolfgang M. Rossberg, Michael Hümpel, Oliver Bannach, Markus Otto, Joseph A. Araujo, Antje Willuweit, Dieter Willbold *Autoren sind gleichberechtigt
Journal:	Heliyon (veröffentlicht)
DOI:	10.1016/j.heliyon.2023.e18443
Impact-Faktor:	3,776 (2022)
Beitrag:	Eigener Anteil: 5 % Entwicklung des sFIDA-Assays Diskussion der Ergebnisse Prüfen des Manuskripts
Anhang zum Manuskript	Kapitel 7.3

Heliyon 9 (2023) e18443

Contents lists available at ScienceDirect

Heliyon

journal homepage: www.cell.com/heliyon

Oral treatment with the all-D-peptide RD2 enhances cognition in aged beagle dogs – A model of sporadic Alzheimer's disease

Janine Kutzsche [a,1], Sarah Schemmert [a,1], Tuyen Bujnicki [a,1], Christian Zafiu [a], Steffen Halbgebauer [b], Victoria Kraemer-Schulien [a], Marlene Pils [a,g], Lara Blömeke [a,c], Julia Post [a,c], Andreas Kulawik [a], Dagmar Jürgens [a], Wolfgang M. Rossberg [d], Michael Hümpel [e], Oliver Bannach [a,c,g], Markus Otto [b], Joseph A. Araujo [f], Antje Willuweit [h], Dieter Willbold [a,c,*]

[a] *Institute of Biological Information Processing, Structural Biochemistry (IBI-7), Forschungszentrum Jülich, Jülich, Germany*
[b] *Institute of Experimental Neurology, Ulm University Hospital, Ulm, Germany*
[c] *Institut für Physikalische Biologie, Heinrich-Heine-Universität Düsseldorf, Düsseldorf, Germany*
[d] *ConsultWMR, Potsdam, Germany*
[e] *KAIROSmetics UG, Berlin, Germany*
[f] *InterVivo Solutions, Fergus, Canada*
[g] *attyloid GmbH, Düsseldorf, Germany*
[h] *Institute of Neuroscience and Medicine, Medical Imaging Physics (INM-4), Forschungszentrum Jülich, Jülich, Germany*

ARTICLE INFO

Keywords:
Alzheimer's disease
Aβ oligomers
Tau oligomers
Cognitively impaired aged Beagle dogs
Sporadic AD animal model
Disease-modifying therapy
Pharmacokinetics
Pharmacodynamics

ABSTRACT

Disease-modifying therapies to treat Alzheimer's disease (AD) are of fundamental interest for aging humans, societies, and health care systems. Predictable disease progression in transgenic AD models favors preclinical studies employing a preventive study design with an early pre-symptomatic treatment start, instead of assessing a truly curative approach with treatment starting after diagnosed disease onset. The aim of this study was to investigate the pharmacokinetic profile and efficacy of RD2 to enhance short-term memory and cognition in cognitively impaired aged Beagle dogs - a non-transgenic model of truly sporadic AD. RD2 has previously demonstrated pharmacodynamic efficacy in three different transgenic AD mouse models in three different laboratories. Here, we demonstrate that oral treatment with RD2 significantly reduced cognitive deficits in cognitively impaired aged Beagle dogs even beyond the treatment end, which suggests in combination with the treatment dependent CSF tau oligomer decrease a disease-modifying effect of RD2 treatment.

1. Introduction

Alzheimer's disease is the most common form of dementia and accounting for 60–70% of the more than 44 million people with dementia worldwide [1]. Cognitively impaired aged Beagle dogs are one of the very few non-transgenic AD animal models that may

* Corresponding author. Forschungszentrum Jülich GmbH Institute of Biological Information Processing, Structural Biochemistry (IBI-7), 52425, Jülich, Germany.
E-mail address: d.willbold@fz-juelich.de (D. Willbold).
[1] Authors contributed equally.

https://doi.org/10.1016/j.heliyon.2023.e18443
Received 24 January 2023; Received in revised form 14 July 2023; Accepted 18 July 2023
Available online 29 July 2023

simulate the situation of spontaneous late onset AD, i.e. sporadic AD, which is the most common form of AD in humans. Pathophysiologically, the decline in cognitive proficiency, including memory and learning deficits, is attributed to structural and functional changes in the aging canine brain that reflects AD-like neurodegeneration [2]. Affected dogs exhibit, similar to human AD patients, progressive accumulation of amyloid beta (Aβ) deposits that manifest as cortical diffuse plaques and cerebral amyloid angiopathy (CAA) [2]. Additionally, reduced neurogenesis [3], increased neuronal death [4] and cerebral atrophy [5] have been described. In contrast to human AD patients, development of neurofibrillary tangle pathology has not been described in Beagle dogs; however, they exhibit hyperphosphorylated tau that possibly represents pre-tangle pathology [6].

Age-related cognitive impairment of the dogs parallels the cognitive symptomology of AD. The earliest deficits are most evident in performance on tasks involving working (short-term) memory and complex learning [7]. Affected dogs additionally develop deficits in discrimination learning as well as behavioral changes [8]. In conclusion, these characteristics suggest that aged Beagle dogs are an appropriate AD model for testing disease-modifying effects of new drug candidates for the treatment of AD.

The novel drug candidate RD2 is currently under clinical development for the treatment of AD [9]. RD2 is an all D-enantiomeric peptide, which was designed to directly destabilize, disassemble and ultimately eliminate toxic Aβ oligomers via direct disruption into native Aβ monomers, rather than by relying on the immune system for their degradation. This mechanism of action (MoA) was confirmed by successfully demonstrating target engagement *in vitro, ex vivo* and *in vivo* [10–13]. RD2 has also proven pharmacodynamic activity in three different transgenic mouse models in independent studies conducted in three different laboratories. Treatment with orally applied RD2 enhanced the cognitive performance in two different AD mouse models (APP_{swe}/PS1ΔE9 and APP_{SL}) [10,11,14]. Efficacy was even demonstrated in aged AD mice with fully developed AD-associated pathology at the beginning of treatment resulting in cognition and behavior, which was indistinguishable from that of healthy wild type littermates at the end of treatment [10]. Furthermore, oral treatment with RD2 led to significant deceleration in the development of the motor neurodegenerative phenotype in transgenic TBA2.1 mice expressing human pyroglutamate-Aβ [15]. The aim of the current study was to investigate the pharmacokinetic profile and the efficacy of RD2 on cognition and biomarkers in a non-transgenic AD animal model - aged cognitively impaired Beagle dogs - that is not based on mutations of human early onset familial AD cases and thus is much closer to the situation of sporadic AD in humans. In addition, the cognitive tests were continued beyond the treatment end to be able to discriminate between acute and disease modifying effects.

2. Results

Two separate studies have been carried out. One study was designed as a pharmacokinetic (PK) study to obtain time dependent RD2 levels in blood and cerebrospinal fluid (CSF). The other study was designed as a placebo-controlled interventional study with a low and high once daily dose of RD2 to investigate pharmacodynamic parameters in aged dogs with three months of treatment and two more months after treatment end, "follow up phase". In both studies study dogs were returned to the colony after completion of the study. Sample collection is therefore limited to blood and CSF samples.

2.1. Tolerability of treatment with RD2 and its pharmacokinetics

In the PK study, single intravenous (i.v.) doses of 3 mg/kg and oral (p.o.) doses of 20 mg/kg or 50 mg/kg of RD2 to each of six dogs were overall well tolerated. Intravenous administration of 3 mg/kg of RD2 resulted in hypersalivation in all dogs and trembling in a subset of dogs. After the 20 mg/kg oral dose, one dog demonstrated fasciculation of neck muscles. The events resolved without intervention. No remarkable findings were noted at the 50 mg/kg oral dose level.

The PK study yielded time-dependent plasma and CSF levels of RD2 after single i.v. and p.o. dosing (Fig. 1A–C).

Following intravenous injection of 3 mg RD2 acetate/kg, a total clearance of 1.16 ml/min/kg and an apparent volume of distribution at steady-state of 0.66 l/kg was calculated from the mean AUC (area under the curve) of 28600 ng*h/ml. Plasma levels decreased rapidly from a C_{max} (0.05 h post administration) of 32000 ng/ml to 37 ng/ml. Disposition was in three phases for which half-lives of 0.05, 2.9, and 71 h were estimated. 93% of total AUC was covered by the half-life of 2.9 h, whereas the long terminal phase only covered 3.4% of the total AUC. Following the oral administration of 20 mg RD2 acetate/kg (50 mg RD2 acetate/kg, respectively)

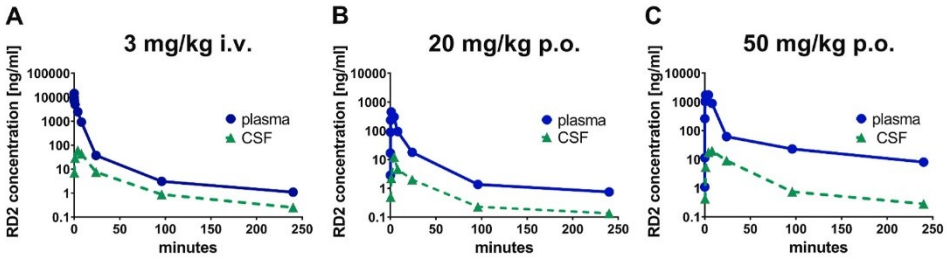

Fig. 1. Concentration-time profiles of RD2 in plasma and CSF following single (A) 3 mg/kg i.v., (B) 20 mg/kg p.o. and (C) 50 mg/kg p.o. administration of RD2 to young dogs (1.7–1.8 years of age). Data are presented as mean; n = 6.

maximum plasma levels of 567 ± 427 ng/ml (2380 ± 2280 ng/ml) were obtained at T_{max} of 2.0 ± 1.6 h (2.7 ± 2.9 h). The AUC was calculated to 3340 ± 1370 ng*h/ml (19800 ± 19700 ng*h/ml) leading to an MRT of 40.0 ± 15 h (35 ± 10 h) and an absolute oral bioavailability of 2.0 ± 0.78% (5.5 ± 4.5%). The half-life of the disposition phase β was estimated from the mean plasma level to be 0.56 h (2.9 h). More than 75% of the total AUC is eliminated with these half-lives of 3 h or shorter and less than 25% of the dose is eliminated with the much longer half-life of the disposition phase γ of 62 h (77 h). There was a more than dose-proportional increase in peak concentrations and AUC from 20 mg/kg to 50 mg/kg oral dosing. The dogs dosed with 50 mg/kg exhibited 2.65 times higher oral bioavailability compared with the mean value of the dogs exposed to 20 mg/kg.

The obtained PK parameters are shown in Table 1 for plasma and in Table 2 for CSF.

The results of the pharmacokinetic evaluation (non-compartment analysis) for RD2 in CSF are given in Table 2. The mean peak CSF level of RD2 in animals treated intravenously with 3 mg RD2/kg was 71 ng/ml 0.05 h post administration. Mean $AUC_{0\text{-tlast}}$ value was 961 h ng/ml and mean residence time 39 h. The mean peak CSF level of RD2 in animals treated orally with 20 mg/kg was 13 ng/ml at 8.0 h post administration and with 50 mg/kg 21 ng/ml at 8.7 h post administration. Mean $AUC_{0\text{-tlast}}$ value were 180 h ng/ml for the 20 mg/kg treated animals and 614 h ng/ml for the 50 mg/kg treated animals. An AUC based CSF/plasma ratio of 0.031 (3 mg/kg iv) to 0.066 (20 mg/kg po) shows that RD2 is able to penetrate the brain.

Most importantly for the following treatment study is that the oral bioavailability of RD2 was between 2.0 and 5.5%. Elimination upon oral application followed a fast phase with a half-live between 0.6 and 2.9 h and a slow phase, which accounts for about 25% of the AUC, with a half-live of about 70 h. RD2 crossed the blood-brain-barrier with a ratio of AUCs in CSF and blood between 2.5 and 6.6%. High inter-individual differences in RD2 levels in the dogs of the PK study have been observed.

During the 3-month treatment phase of the interventional study (Fig. 3A), on day 80, one dog had to be euthanized. Unblinding revealed that this dog was in the placebo cohort. On day 123 (30 days after treatment end), another dog needed to be euthanized. Unblinding revealed that the dog was in the low dose (3 mg/kg/day) cohort. The causes of morbidity (forelimb paralysis and progressing vestibular disease, respectively) were considered consequences of underlying age-related background diseases in these old dogs. All other dogs survived the study and were returned to the colony at study conclusion.

In the therapeutic study (Fig. 3A) blood samples were collected before and after three months of oral treatment for hematological (complete blood count) and clinical chemistry analyses including liver function tests (Tables S1, S2 and S3). In addition, RD2 levels in plasma (Fig. 2A) and CSF (Fig. 2B) were determined before and after one, two and three months of treatment.

Increases of triglyceride and CK-MB concentrations after 3 mg/kg and 30 mg/kg RD2 p.o. compared to in-group baseline values, although statistically significant, were minor and comparable with the changes in the placebo group (Figs. S1 and S2). Another remarkable finding was the presence of Döhle bodies in neutrophils of three out of 12 dogs after three months treatment with 30 mg/kg (once daily). The occurrence of Döhle bodies is often interpreted as a marker for inflammatory processes in dogs [16]. In the absence of changes in neutrophil, total white blood cell and platelet counts, this occurrence was most probably not of toxicological relevance.

2.2. Efficacy parameters

The treatment study was designed to investigate RD2's efficacy on cognitive outcome measures as the primary endpoint, as cognitive impairment is the predominant and most relevant symptom in human AD patients.

2.2.1. RD2 significantly decreased cognitive deficits compared to baseline even beyond the end of treatment

Dogs were tested on a variable-delay paradigm of the DNMP (delayed non-matching to position) test using delays of 20 s and 90 s. The task was performed in 5-day intervals to assess spatial working memory. Testing occurred during baseline and subsequently once a month - at three time points during the treatment phase and at two time points after treatment end (Fig. 3A). The mean performance

Table 1
Pharmacokinetic parameters for RD2 in plasma after single administration of RD2.

Parameter	3 mg/kg (i.v.) Mean ± SD	20 mg/kg (p.o.) Mean ± SD	50 mg/kg (p.o.) Mean ± SD
t_{max} (h)		2.0 ± 1.6	2.7 ± 2.9
C_{max} (ng/ml)	32000 ± 18200	567 ± 427	2380 ± 2280
$t_{1/2\ \alpha}$ (h)	0.046	n.c.	n.c.
[1]% of AUC	3.6	n.c.	n.c.
$t_{1/2\ \beta}$ (h)	2.9	0.56	2.9
[2]% of AUC	93	78	76
$t_{1/2\ \gamma}$ (h)	71	62	77
[a]% of AUC	3.4	22	25
$AUC_{0\text{-tlast}}$ (h·ng/ml)	29900 ± 4230	3340 ± 1370	19800 ± 19700
$AUC_{0\text{-inf}}$ (h·ng/ml)	28600 ± 2540	3890 ± 1120	26000 ± 21900
CL_{total} (ml/min·kg)	1.2 ± 0.11		
MRT (h)	9.4 ± 1.0	40 ± 15	35 ± 10
V_{ss} (ml/kg)	659 ± 140		
F (%)	100	2.0 ± 0.78	5.5 ± 4.5

n.c. denotes not calculable, [1]% of AUC covered by $t_{1/2\ \alpha}$, [2]% of AUC covered by $t_{1/2\ \beta}$.
[a] % of AUC covered by $t_{1/2\ \gamma}$.

Table 2
Pharmacokinetic parameters for RD2 in CSF after single administration.

Parameter	3 mg/kg (i.v.) Mean ± SD	20 mg/kg (p.o.) Mean ± SD	50 mg/kg (p.o.) Mean ± SD
t_{max} (h)	4.2 ± 2.2	8.0 ± 8.0	8.7 ± 7.8
C_{max} (ng/ml)	71 ± 32	13 ± 15	21 ± 18
Apparent $t_{1/2}$ (h)[a]	80 ± 5.6	190 ± 93	119 ± 37
$AUC_{0\text{-tlast}}$ (h·ng/ml)	961 ± 373	180 ± 77	614 ± 592
$AUC_{0\text{-inf}}$ (h·ng/ml)	990 ± 383	242 ± 47	659 ± 605
$MRT_{0\text{-inf}}$ (h)	39 ± 4.0	155 ± 131	97 ± 47
CSF/Plasma $AUC_{0\text{-inf}}$	0.031 ± 0.011	0.066 ± 0.021	0.025 ± 0.020

[a] half-life is estimated from the last 2 time points and thus may not be accurate.

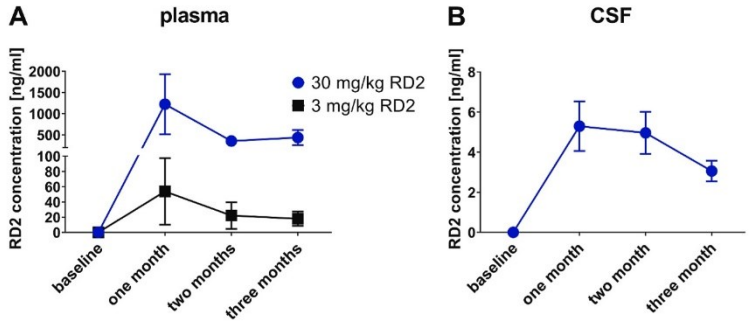

Fig. 2. Concentration-time profiles of RD2 in (A) plasma and (B) CSF following daily oral administration of 3 mg/kg or 30 mg/kg of RD2 for three months. CSF-values of 3 mg/kg treated animals were below the lower limit of quantification (LLOQ) of 0.5 ng/mg and were therefore excluded from the graph. Data is presented as mean±SEM; n = 11 to 12.

accuracy across delays (20 s and 90 s combined) was analyzed using two-way repeated-measure ANOVA with testing time-point serving as a within-subject measure (Fig. 3B). The dogs in all three cohorts exhibited a practicing effect due to the repeated performance of the test. While this seemed to be a small tendency in the placebo group, dogs in the treatment cohorts showed a significant cognitive enhancement relative to their baseline level, which even extended beyond the end of the treatment period in the high dose group. Significantly enhanced cognitive performance was reached in dogs treated for only one month with high doses (30 mg/kg) of RD2, leading to RD2 levels of 5 ng/ml on average in CSF (Fig. 2B), or two months with low doses (3 mg/kg) of RD2. The results obtained in the DNMP test suggested a benefit of RD2 on working memory. After the follow up period of one and two months after treatment end, dogs previously treated with 30 mg/kg daily maintained significant increase in performance in DNMP accuracy compared to baseline.

As second cognitive task, variable discrimination testing with variable oddity was performed in order to assess selective attention performance of the dogs during treatment. As impairment in tasks involving complex learning develops earlier than in simple discrimination learning [8,17–19], the conditions with none or one distractor were excluded from analysis. RD2 enhanced learning on the more difficult conditions (two or three distractors) of the variable discrimination task in the low dose group at two months of treatment and in the high dose group at three months of treatment compared to baseline, but had no effect on the easier conditions. Percent accuracy was analyzed using a two-way repeated-measure ANOVA with test time-points serving as within subject measures. No significant learning effect of placebo treated Beagle dogs was found (Fig. 3C).

2.2.2. Analysis of neuropathological biomarkers in CSF and plasma

Neuropathological biomarkers were longitudinally assessed by analysis of Aβ42, total tau, GFAP, NfL and β-synuclein in CSF samples and for NfL in plasma (Fig. 4). Significant differences between the treatment groups were found only in total Aβ42 concentrations. Significantly lower concentrations were observed in placebo compared to 3 mg/kg RD2 treated animals at baseline, after 3 months of treatment and two months follow up and to 30 mg/kg RD2 treated animals after 3 months of treatment.

2.2.3. Analysis of Aβ oligomers and tau oligomers in CSF

Aβ oligomer and tau oligomer levels were assessed in CSF before and after three-month treatment by means of the oligomer-specific sFIDA assay [13,20–24]. In the surface-based fluorescence intensity distribution analysis (sFIDA) assay, Aβ and tau oligomers were captured on a glass surface by a monoclonal anti-Aβ antibody directed against the N-terminus of Aβ and a monoclonal anti-tau antibody directed against the proline rich region P2. After immobilization, the captured oligomers were detected by the same antibodies, which were fluorescence-labeled. Therefore, fluorescence-labelling of capture-bound Aβ or tau monomers was excluded, thus rendering the assay insensitive for monomeric Aβ and tau. The assay surface was imaged by a multi-color total internal reflection

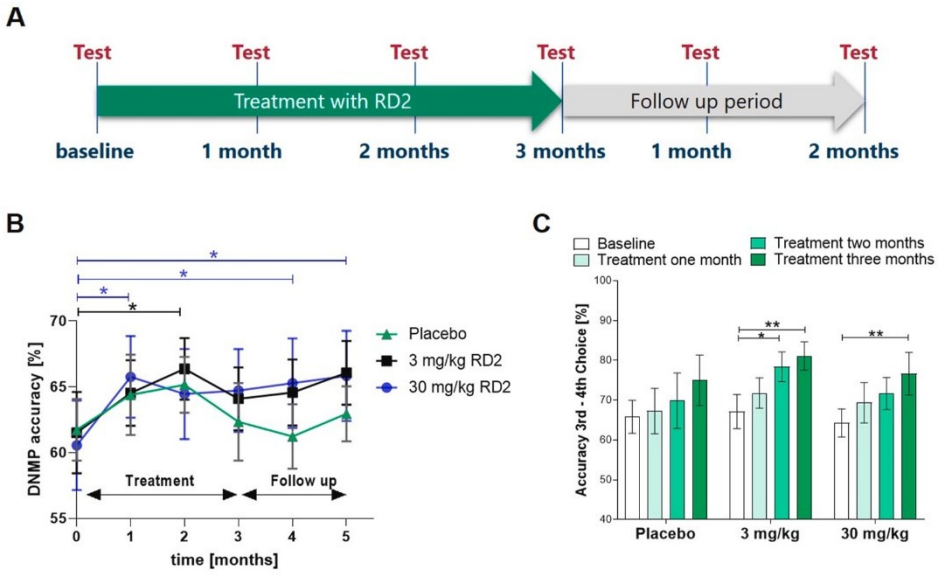

Fig. 3. Study design and cognitive testing outcomes. A: Treatment and cognitive testing time scheme of the interventional study. B: Percent mean performance accuracy in the DNMP assay combined at 20 s and 90 s delay in placebo versus low (3 mg/kg daily) and high oral RD2 dosed (30 mg/kg daily) dogs. Two-way RM-ANOVA (followed by Fisher post hoc test) revealed significantly enhanced performance ($p < 0.05$) after one month of treatment compared to baseline in the high dose cohort and after two months treatment in the low dose cohort. The significant treatment effect (*$p < 0.05$) in the high dose group was maintained two months upon treatment end. Data is presented as mean ± SEM; n = 11 to 12. C: Percent mean performance accuracy on the selective attention - variable oddity performance combined across the 2 and 3 distractor conditions in placebo vs. low dose and high dose dogs treated with RD2. A two-way RM ANOVA (followed by Fisher post hoc test) revealed a significantly enhanced cognitive performance after three months of treatment of both treatment groups (**$p < 0.01$), and 3 mg/kg after two months of treatment (*$p < 0.05$). Data is presented as mean ± SEM; n = 11 to 12.

fluorescence (TIRF) microscope. The number of pixels above a given background cutoff in each fluorescence channel directly correlates with the concentration of Aβ oligomers (Fig. 5A–C) or tau oligomers (Fig. 5D–F) in the sample.

No significant changes in Aβ oligomer concentrations were found neither between baseline and the three-month treatment time point in the treatment groups (Fig. 5A–C) nor between the treatment groups (Fig. 5D). However, the treatment with 30 mg/kg RD2 led to a stagnation, if not a reduction, of the tau oligomer concentrations ($p = 0.073$) (Fig. 5G), while tau oligomer concentrations in 3 mg/kg RD2 (Fig. 5F) and placebo treated groups (Fig. 5E) increased significantly during the three months period (3 mg/kg $p = 0.0043$; placebo $p = 0.027$). In addition, the comparison between the treatment groups showed significant differences between 30 mg/kg RD2 and both other treatment groups (Fig. 5H, $p = 0.016$ for placebo vs. 30 mg/kg RD2, $p = 0.0051$ for 3 mg/kg vs. 30 mg/kg).

2.2.4. Correlation of RD2 plasma levels with CSF Aβ oligomer and tau oligomer concentrations

Because the treatment study was designed to investigate RD2′s efficacy on cognitive outcome measures as the primary endpoint, recruitment of the 36 dogs for the study was based on age and their cognitive status measured in three baseline cognitive tests (discrimination learning, delayed non-matching to position (DNMP) and attention as described in the methods). It was not based on typical human AD biomarker concentrations in CSF, like Aβ42 and tau, or brain imaging data. Thus, it must be expected that recruitment included not only dogs into the study that were cognitively impaired solely due to AD-like pathology, but also due to a reasonable fraction of other age- or non-age-related diseases or other constraints. To take this important background information into account, correlation analyses were carried out, which are able to reveal dose-response relationships based on individual drug plasma and exposure levels of the dogs.

We examined the correlations of RD2 concentrations in plasma with Aβ oligomer (Fig. 6A) and tau oligomer (Fig. 6B) concentrations in CSF after three months of treatment by performing Spearman correlation analyses. Whereas both analyses yielded inverse correlations as expected, the RD2 plasma level correlation with Aβ oligomer concentrations did not become significant (Fig. 6A, Spearman −0.234, p-value 0.170). The correlation of RD2 plasma levels with tau oligomer concentrations after three months of treatment, however, was strong and significant (Fig. 6B, Spearman −0.530, p-value 0.00090). Thus, as expected from a successful treatment, also the correlation between RD2 plasma levels and the changes of tau oligomer concentrations (three months treatment vs. baseline) was inverse, strong and significant (Fig. 6D, Spearman −0.493, p-value 0.0024).

In humans, the most reliable biomarker for AD is the longitudinal decrease of total Aβ42 in CSF. In the here described treatment study, we observed a significant difference between the 30 mg/kg dose group and the placebo group after 3 months treatment, which

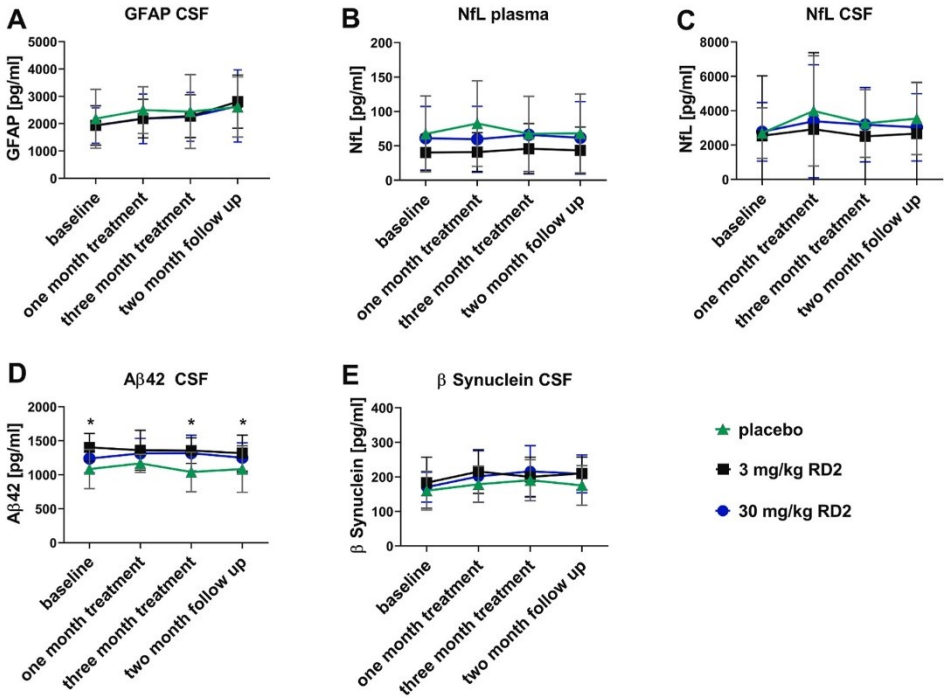

Fig. 4. CSF and blood based biomarkers. (A) Concentrations of GFAP in CSF, (B) NfL in plasma, (C) NfL in CSF (D) Aβ42 in CSF, and (E) β-synuclein concentrations in CSF of placebo, 3 mg/kg and 30 mg/kg treated animals with RD2 were longitudinally determined. Statistical calculations were conducted using a two-way RM ANOVA (followed by Fisher post hoc test). A significant difference between placebo and 3 mg/kg RD2 treated animals (marked by *) was shown for Aβ42 levels at baseline ($p = 0.004$), after 3 months of treatment ($p = 0.004$) and two months after treatment end ($p = 0.031$) and between placebo and 30 mg/kg RD2 treated after 3 months of treatment ($p = 0.009$). Data is presented as mean ± SEM; n = 11 to 12; *$p < 0.05$; **$p < 0.01$.

was not significant at baseline (Fig. 4D). Because groups have not been randomized for Aβ42 levels in CSF, and the 3 mg/kg dose group had Aβ42 CSF levels significantly higher than placebo already at baseline, the overall significant and positive correlation between Aβ42 CSF levels and RD2 plasma levels may be interesting (Fig. 6C, Spearman 0.407, p-value 0.017).

Most remarkably, treatment-dependent changes of DNMP accuracy were found at three months of treatment as shown by the positive and significant correlation of RD2 plasma levels with the changes of DNMP accuracy at three months treatment versus baseline (Fig. 6E, Pearson 0.37, p-value 0.0262). This positive correlation did not disappear two months after treatment end, but became even stronger and more significant (Fig. 6F, Pearson 0.457, p-value 0.0066) suggesting a disease modification.

2.2.5. Correlation of CSF Aβ oligomer concentrations and selective attention

We examined the correlation of changes (after three months treatment versus baseline) of CSF Aβ oligomer concentration with changes of selective attention (Fig. 7). Changes of CSF Aβ oligomer concentrations inversely correlated with changes of selective attention for all animals (Fig. 7D; Spearman −0.412, p-value 0.0127). Separate analyses yielded significant and negative correlations between the individual changes in absolute Aβ oligomer concentrations and individual changes in selective attention for both RD2 treated cohorts (Fig. 7 B, C), but not for the placebo cohort (Fig. 7A). Thus, the more RD2-dependent reduction or stagnation of Aβ oligomer concentrations, the more the dogs did improve in the cognitive tests. The absence of this correlation in the placebo group may indicate that cognitive deficits indeed are not solely due to Aβ pathology, but some dogs had cognition deficits due to other reasons. Treatment effects with RD2, however, may drive cognition enhancements strong enough in the responsive fraction of dogs in the treated cohorts in order to outweigh the effects of non-responders. Such an effect is, of course, not present in the placebo group.

2.2.6. Correlation between CSF Aβ oligomer and tau oligomer concentrations

We found a significant and positive correlation between Aβ oligomer and tau oligomer concentrations, at baseline (Fig. 7A, Spearman 0.505, p-value 0.0018), after three months of treatment with RD2 or placebo (Fig. 7B, Spearman 0.306, p-value 0.029), and for the individual differences between both time points (Fig. 7C, Spearman 0.371, p-value 0.026). This indicates a robust correlation between Aβ oligomer and tau oligomer concentrations in CSF. To our knowledge, this is the first report of such a correlation in dogs.

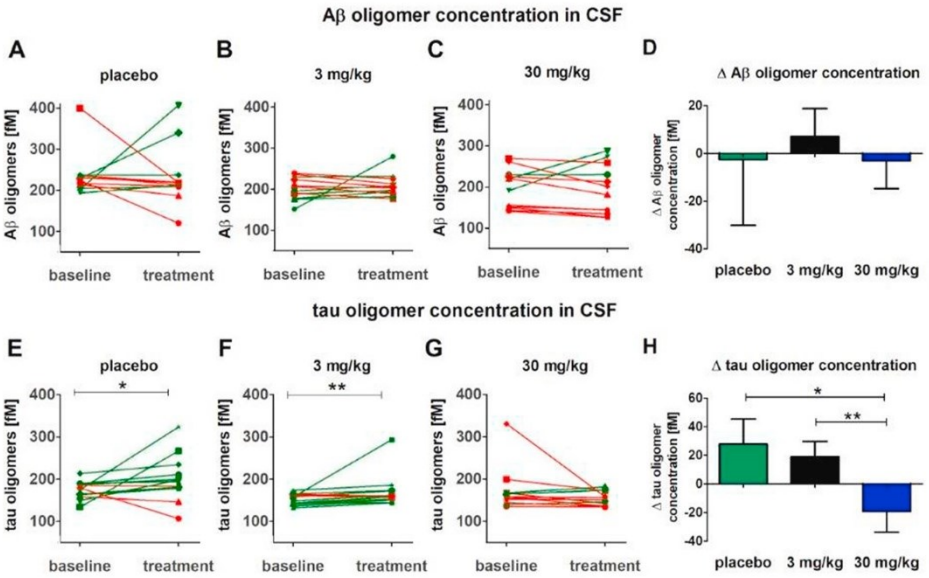

Fig. 5. Aβ oligomer and tau oligomer concentrations in CSF. Aβ oligomer (A–C) and tau oligomer concentrations (E–G) in CSF of placebo, 3 mg/kg and 30 mg/kg treated animals with RD2 were determined with sFIDA assay. A green connection line indicates a positive change and a red line indicates a negative change. Pairwise comparison with one-sided Wilcoxon signed-rank test showed no significant difference between baseline and three-month treatment in Aβ oligomer concentrations in any of the treatment groups (A–C), and in tau oligomer concentration in the 30 mg/kg RD2 group (G). In placebo (E) and 3 mg/kg RD2 (F) treated animals the tau oligomer concentration is significantly increased after three-month treatment compared to baseline. Changes (Δ) of Aβ oligomer (D) and tau oligomer (H) levels were calculated by subtracting baseline values from three-month treatment values. A negative change indicates a reduction of oligomer concentration, and a positive change indicates an increasing of oligomer concentration after treatment. A Mann-Whitney *U* test revealed a significant difference in Δ tau (H) between the 30 mg/kg RD2 group and both other treatment groups. *$p < 0.05$, **$p < 0.01$. Data is presented as mean ± SEM; $n = 12$. (For interpretation of the references to color in this figure legend, the reader is referred to the Web version of this article.)

3. Discussion

Among the numerous transgenic AD animal models, none is able to exert the full spectrum of human AD pathology together with typical cognition deficits observed in human AD patients. Our interventional study in cognitively impaired aged Beagle dogs is thus an unprecedented effort to show efficacy of a drug candidate, which was developed for disease modification and for beneficial effects on AD-relevant cognitive impairment, in a non-transgenic animal model of AD.

The pharmacokinetic study yielded an oral bioavailability of RD2 in blood between 2.0 and 5.5%. Elimination upon oral application was observed in two phases with a terminal half-live of about 70 h, very similar as was found for humans [9]. RD2 did cross the blood-brain-barrier with CSF-blood ratios between 2.5 and 6.6% indicating that the compound reaches its target organ, the brain. Orally administered RD2, at single doses of 20 mg/kg or 50 mg/kg in the PK study and at daily doses of 3 mg/kg and 30 mg/kg over three months in the interventional study, was well tolerated by the dogs. Also, the single intravenous dose of 3 mg/kg did not result in signs of intolerability. Laboratory investigations (hematology and blood clinical chemistry) as part of the 3-month efficacy study revealed no signs of severe adverse effects.

The interventional study was designed to investigate RD2′s efficacy on cognitive outcome measures as the primary endpoint, since cognitive decline is the major symptom in human AD patients. Recruitment of the study dogs was, therefore, based on age and the extent of cognitive deficits and not based on CSF biomarkers, like Aβ42 and tau, or brain imaging data. As a consequence, it must be expected that a reasonable fraction of dogs had their cognitive impairments due to other age- or non-age-related causes and not solely due to AD-like pathology. This is important to keep in mind, when analyzing the outcome the study. One way to deal with the unknown ratios of animals with or without AD-like pathology in the respective treatment cohorts would be to analyze only “responders” to the study drug for efficacy. For reasons of transparency, however, and because a responder analysis is not possible in the placebo group, we additionally carried out correlation analyses between several measures in order to account for potential non-responders within the treatment cohorts. Such correlation analyses can be used to explore expected dose-response relationships, because they consider the high inter-individual differences in drug exposure at a given oral dose. Thus, especially the correlations of any outcome measure with RD2 plasma levels can be expected to provide valuable results on dose-response relationships.

For assessment of deficits in working memory before and during the study, a delayed non-matching-to-position (DNMP) task was

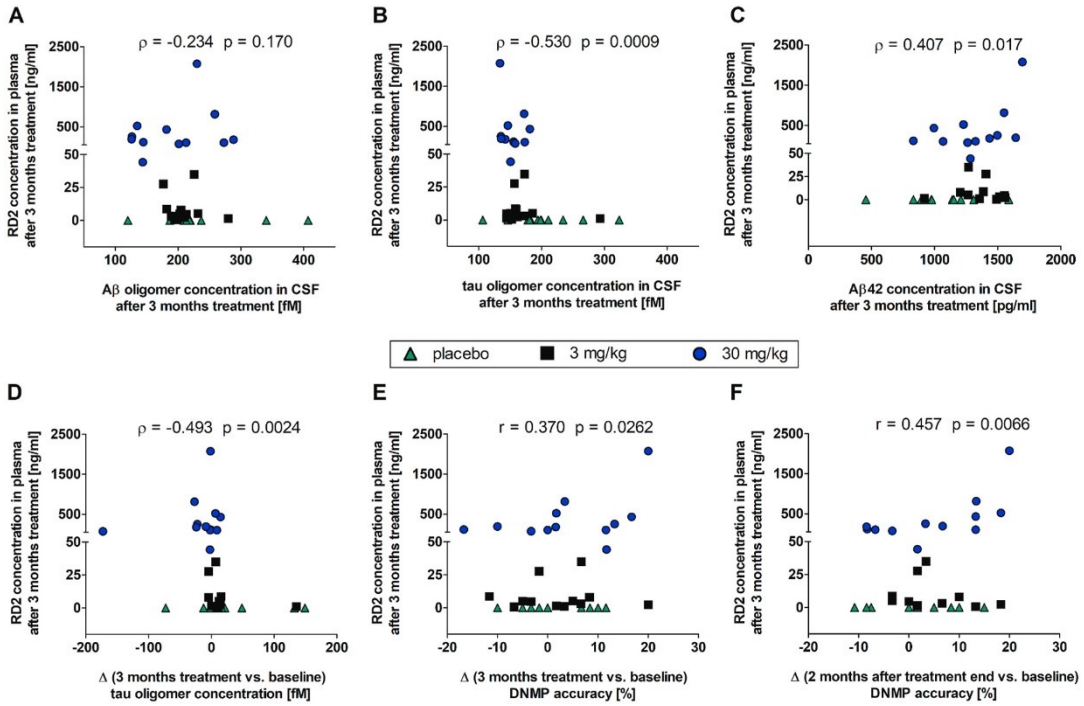

Fig. 6. Dose-response relationships. Correlations of RD2 concentration in plasma with Aβ oligomer, tau oligomer and Aβ42 concentration and with DNMP accuracy. A–C: Correlations of RD2 concentration in plasma with Aβ oligomer (A), tau oligomer (B) and Aβ42 (C) concentrations in CSF after 3 months treatment. D: Correlation of RD2 concentration in plasma with changes of tau oligomer concentration. E, F: Correlation of RD2 concentration in plasma with treatment-dependent changes of DNMP accuracy. Changes (Δ) were calculated by subtracting baseline value from three-month treatment value (D, E) or from two-month after treatment end value (F). Correlations of RD2 in plasma with all parameters except Aβ oligomer concentration were statistically significant. Correlation was performed with Pearson (r) and Spearman (ρ) analysis at alpha level 0.05 with n = 11 to 12.

performed. To assess complex learning the variable discrimination learning task was conducted. Small positive practicing effects on the DNMP outcome during the first two months were observed in all groups but did not become significant in the placebo group. Significant increase of DNMP accuracy compared to baseline was observed in the high dose (30 mg/kg once daily) and the low dose (3 mg/kg once daily) group after one or two months, respectively. The significant increase in DNMP performance in the RD2 dosed groups suggests beneficial effects of RD2 on working memory. The effect was still present one- and two-months after treatment end in dogs treated with high dose RD2. In dogs treated with the low dose a prolonged impact on cognitive performance beyond treatment stop was also visible, but did not reach statistical significance ($p = 0.06$). This suggests a dose-dependent and disease-modifying effect on neuroprotection from Aβ oligomer induced toxicity (Fig. 3B). This is further supported by the positive and significant correlation of DNMP difference (three months treatment values versus baseline values) with RD2 plasma levels at month three with respect to a dose-response relationship (Fig. 6E).

RD2 treatment enhanced learning compared to baseline in the variable discrimination task in the low and the high dose group from two and three months of treatment onward, respectively, which implies a benefit of treatment on complex learning (Fig. 3C). Because reversal learning was assessed after the three months test, which required subjects to respond to their non-preferred object, the variable discrimination task was not useable to evaluate changes in selective attention during the follow up period. We found a significant and positive correlation between the results of the DNMP and the selective attention tests in the dogs of the placebo cohort at all time points available (Fig. S3F). This indicates that both tests are robustly measuring memory and cognition deficits in dogs.

Longitudinal monitoring of neuropathological biomarkers in the different treatment groups were assessed by ELISA analysis of CSF and blood samples (Fig. 4). None of the biomarkers was significantly different between the groups, except Aβ42 levels, which were different between groups at some time points, including baseline, reflecting the high inter-individual variability of the dogs.

RD2′s mode of action (MoA) is to stabilize Aβ monomers in their native intrinsically disordered protein (IDP)-like conformation, thereby destabilizing Aβ oligomers to ultimately disassemble them into Aβ monomers. This MoA was confirmed by respective successful target engagement *in vitro* [11] *ex vivo* [13] and *in vivo* in brain homogenates from RD2-treated versus placebo-treated transgenic mice using sFIDA analysis [10]. Therefore, also in the present study, Aβ oligomer, but also tau oligomer levels, were determined by sFIDA analysis in CSF from the dogs at baseline and after three months of treatment. No significant changes in Aβ

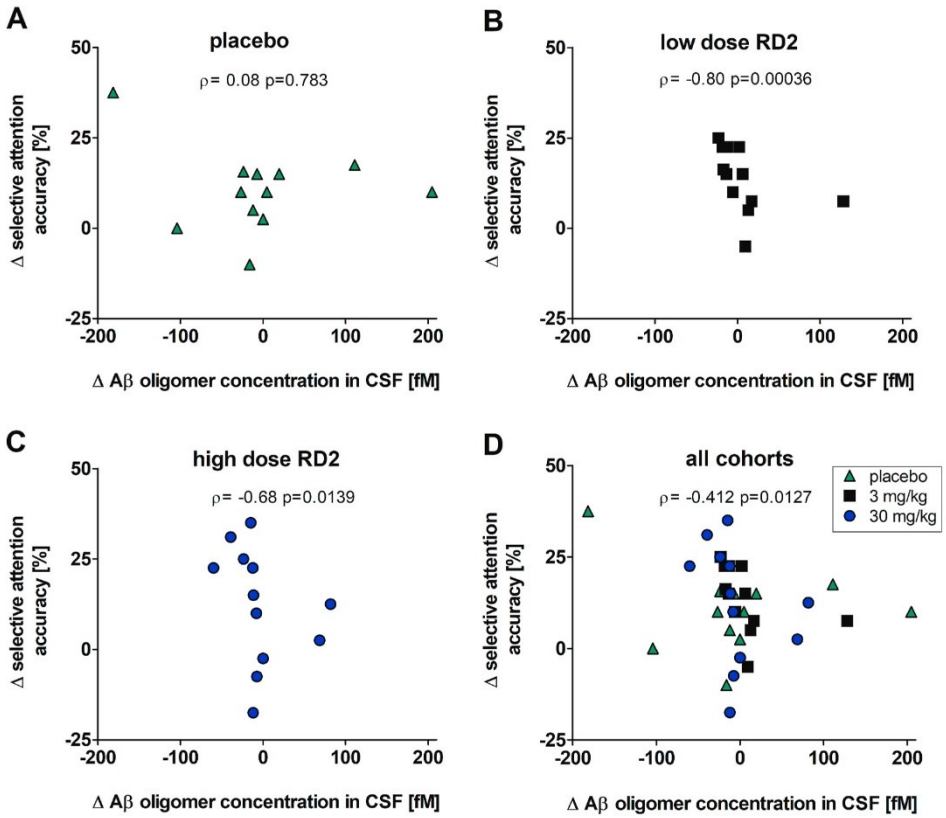

Fig. 7. RD2 treatment dependent Aβ oligomer concentration change and its correlation with selective attention outcome. Correlation of changes of CSF Aβ oligomer concentrations with changes of selective attention accuracy. A: Correlation for placebo group. B: Correlation for low dose treated animals with 3 mg/ml RD2. C: Correlation for high dose treated animals with 30 mg/ml RD2. D: Correlation for all groups (placebo, low dose and high dose) together. Changes (Δ) were calculated by subtracting baseline value from three-month treatment value. Correlations of the low dose group, high dose group and all cohorts were significant. No significant correlation was found for the placebo group. Correlation was performed with Spearman (ρ) analysis at alpha level 0.05 with n = 11 to 12.

oligomer levels, however, were observed in any of the groups during three months of treatment (Fig. 5A, B, C) or between the groups (Fig. 5D).

In contrast, tau oligomer levels in CSF increased significantly during the treatment duration in the placebo and low dose groups, while high dose treatment led to an overall stagnation of the tau oligomer levels (Fig. 5 E, F, G). Most individuals of this group showed even a reduction of tau oligomer levels in CSF upon treatment leading to statistical significance between the high dose and the other groups (Fig. 5H). There was a correlation between the Aβ and tau oligomer levels at baseline and at three months treatment (Figs. S3A and B). Why RD2 treatment in cognitively impaired Beagle dogs yielded significant reduction of tau oligomers but not of Aβ oligomers, at least under the described dosing and recruitment regime as well as the treatment duration, remains to be investigated. There are more and more data which suggest that the progression of AD may be driven by the synergistic interaction between tau and Aβ species [25,26]. Thus, targeting Aβ oligomers may possibly lead to effects on downstream targets like tau oligomers. The significant inverse correlation of RD2 plasma concentrations and tau oligomer levels after three months of treatment (Fig. 6B) supports this hypothesis.

Adding on the discussion above concerning the certainly suboptimal recruitment conditions, it is interesting to look again at the significant correlations between the individual changes in absolute Aβ oligomer concentrations (three-month treatment values minus baseline values) and individual changes in selective attention (three-month treatment values minus baseline values) for both RD2 treated cohorts (Fig. 7 B, C), but there was no such correlation for the placebo cohort (Fig. 7A). This is not only suggesting that RD2 treatment led to reduction or stagnation of CSF Aβ oligomer concentrations, but the absence of this correlation in the placebo group suggests that cognitive deficits in the recruited animals are not solely due to Aβ pathology but also due to other reasons. Treatment effects with RD2, however, may drive cognition enhancements strong enough in the responsive fraction of dogs to outweigh the effects of non-responders (Fig. 7D). Such an effect, of course, cannot be expected and was not found in the placebo group.

The here presented study, which investigated the pharmacokinetic profile and the efficacy of RD2 on cognition and AD-relevant

biomarkers, especially Aβ oligomers and tau oligomers in CSF, using aged cognitively impaired Beagle dogs as a non-transgenic model of sporadic AD has certainly limitations concerning the recruitment strategy. Anyway, we demonstrate that RD2, with its unique MoA of disassembling Aβ oligomer complexes into Aβ monomers, crosses the blood-brain barrier in dogs and exerts beneficial effects on cognition and tau oligomer levels in CSF after oral administration. This has promising implications for the ongoing clinical development of RD2. Apart from the treatment results, the study shows that tau pathology is present in cognitively impaired old Beagle dogs, even if not in the form of tau tangles, but as tau oligomers in the CSF. The fact that their levels correlate with the levels of Aβ oligomers may be another relevant finding for dogs in general, and for this animal model for sporadic AD.

4. Methods

4.1. Study compound

The all-D-peptide RD2 (sequence: ptlhthnrrrrr, CBL Patras, Patras, Greece) consists of 12 D-enantiomeric amino acid residues with its C-terminus being amidated.

4.1.1. Test article and administration

Different batches of the acetate salt of RD2 were used as the test article in the canine studies. The compound was maintained at ultracold temperatures but thawed to room temperature for preparation of the dosing formulations.

Two separate studies have been carried out. One study was designed as a pharmacokinetic study to obtain time-dependent RD2 levels in blood plasma and CSF. The second study was designed as an interventional study to investigate pharmacodynamics parameters during three months of treatment and two more months after treatment end. The latter two months period is sometimes referred to as the "follow up phase".

For oral application in the pharmacokinetic (PK) study, RD2 acetate was dissolved in sterile aqueous 0.9% NaCl, the pH was adjusted to 7.0 to 7.4 with NaOH. Solutions were prepared one day prior to dosing and kept refrigerated until 30 min prior to administration. The solutions contained 10 mg/ml or 25 mg/ml of RD2 acetate and were administered by oral gavage with a volume of 2 ml/kg (final dose 20 or 50 mg/kg). For the dosing procedure, the gavage tube was inserted into the stomach and 5 ml of tap water was flushed to ensure proper positioning. Then the test product was administered via syringe through the tube followed by 10 ml tap water.

For intravenous administration in the PK study, RD2 acetate was dissolved as described above. The solution contained 3 mg/ml and was administered by a single intravenous injection over 30 s with a dosing volume of 1 ml/kg. Injection was through a cephalic vein catheter that was flushed with 1 ml of sterile saline.

For oral application during the interventional study, RD2 acetate was administered as powder without excipients in hard gelatin/hypromellose (HPMC) capsules (Torpac, size 00). Empty capsules were used as placebo control. Amounts in the capsules were adjusted to the RD2 acetate dose of 3 or 30 mg/kg body weight (low or high dose). Prepared capsules were kept refrigerated until required for administration. On each assessment or collection day, dosing was staggered such that dogs were dosed 1 h (±15 min) prior to their cognitive assessment or 1-h (±10 min) prior to cerebrospinal fluid (CSF) collections. When none of these procedures were applied, the animals were dosed at approximately the same time daily.

4.2. Animals

Male and female Beagle dogs were obtained from the InterVivo Solutions Inc. colony. For the PK study 4 male and 4 female dogs and for the cognitive assessment study 12 male and 24 females were included. At study initiation, the age of the dogs for the PK study ranged from 1.7 to 1.8 years (1.8 ± 0.05). The age of the dogs for the interventional study ranged from 7 to 15 years (9.8 ± 2.5 years). Animals were included in the study after passing a general health evaluation.

4.2.1. Test site and approval

All animal experiments were performed at the site of InterVivo Solutions, Fergus, Canada, in accordance with principles of the Animal for Research Act of Ontario and the guidelines of Canadian Council on Animal Care (CCAC) and were approved by the Study Facility's Institutional Animal Care and Use Committee (IACUC) (approval number VRI108-17182-CE).

4.2.2. Pharmacokinetic (PK) study

The study was a randomized, non-blinded, preclinical study using a within-subject, incremental dose, design. The objective of the study was to evaluate the pharmacokinetic parameters of RD2, following a single intravenous or oral administration of RD2 acetate to Beagle dogs. Doses of 3 mg/kg (Day 0) were used for intravenous administration; 20 mg/kg (day 12) and 50 mg/kg (day 28 were used for oral administration. The concentration of RD2 was determined in serially collected blood plasma samples (3, 5, 10, and 20 min post dose, and 1, 4, 8, 24, 96, and 240 h post dose). Cerebrospinal fluid (CSF) samples were also serially collected (20 min post dose, and 1, 4, 8, 24, 96, and 240 h post dose) from the cisterna magna of the dogs while under isoflurane anesthesia.

A total of six (three male and three female) dogs were used to test each dose level. A washout period of at least 11 days was allowed before the same animal were treated with another dose. For serial sample collection procedures, animals were held in metabolic cages for observational purposes. Dogs were fed a standard commercial dry diet. Food consumption was not recorded. Water was provided ad libitum, except within 30 min prior to the start of anaesthetic procedures. Animal body weights were determined with a certified, verified scale prior to the beginning of each treatment arm. The recorded weights were used to determine individual treatment doses.

Dosing sequence was started with 3 mg/kg intravenous (n = 6), followed by 20 mg/kg oral (n = 6) and 50 mg/kg oral (n = 6).

4.2.3. Study for evaluation of RD2 treatment-dependent cognitive parameters and CSF levels of Aβ and tau oligomers

This blinded preclinical study employed a controlled, parallel matched-group design. Following a baseline study phase including cognitive assessment, animals were allocated to one of three treatment groups (n = 12 dogs per group) balanced for initial cognitive performance to the extent possible. One group was assigned to receive a high oral dose of RD2 acetate (30 mg/kg once daily), while a second group received a low oral dose of RD2 acetate (3 mg/kg once daily). The third group was assigned to receive placebo. RD2 acetate or the placebo were administered orally once a day for three months. Test product and placebo were washed in for 17 days prior to initiation of treatment phase cognitive assessments. Following approximately three months of administration (93 days), cognitive function tests were repeated following two and six weeks of treatment washout.

For allocation of animals to treatment groups, the baseline phase cognitive status of the dogs was used to balance cognitive groups. Animals meeting the inclusion/exclusion criteria were ranked in descending order based on the three baseline cognitive tests (discrimination learning, delayed non-matching to position (DNMP) and attention), such that the best performing animals on each test received a rank of 1, and the poorest performing animals received a rank of 36. In the event that two or more animals had the same score, these subjects were ranked equally using the median rank according to the number of animals (i.e. if two animals had an equal score for ranks 4 and 5, then both were assigned a rank of 4.5 on the test; if three animals had an equal score for ranks 4, 5 and 6, then all three animals were assigned a rank of 5 on the test). The rank scores across the three tests were summed up for each animal and the rank sum was then used to rank dogs from highest performing to lowest performing using the procedures described above for animals with identical rank sums. Subsequently, subjects were then allocated to treatment groups based on rank sums such that rank sums 1, 2 and 3 were placed into treatment groups 1, 2 and 3 and rank sums 4, 5 and 6 were placed into treatment groups 3, 2 and 1, respectively. Dogs with identical rank sums were allocated to groups based on alphabetical order. Once all subjects had been allocated to groups in this manner, the allocation of individual subjects was adjusted to ensure that treatment groups were balanced to the extent possible across all applicable cognitive tests.

The study was blinded to all personnel in the investigation with the exception of the person(s) involved in administration of the experimental product and placebo, the person responsible for performing allocation and the Scientific Director. The treatment given to each animal was not revealed to the people collecting data.

Thirty-six dogs were screened on baseline cognitive tests, physical/neurological tests, hematology and blood biochemistry and that met the inclusion criteria were selected for the treatment phase. Dogs were maintained at the animal facility and group-housed in pens or rooms in compliance with the recommendations of the Canadian Council on Animal Care. Environmental management including lighting, ventilation, temperature, and humidity regulation were maintained and controlled according to standard operating procedures. All animals were fed according to the facilities standard operating procedures, using a standard commercial diet to maintain body condition (Purina ProPlan Savor Adult, Chicken and Rice Formula). Animals were fed at the end of each day following completion of any testing or sample collection procedures. Water was provided ad libitum.

During the 3-month treatment phase of the interventional study (Fig. 1A), on day 80, one dog needed to be euthanized. Unblinding revealed that this dog was in the placebo cohort. On day 123 (30 days after treatment end), another dog needed to be euthanized. Unblinding revealed that the dog was in the low dose (3 mg/kg/day) cohort. The causes of morbidity (forelimb paralysis and progressing vestibular disease, respectively) were considered consequences of underlying age-related background diseases in these old dogs. All other dogs survived the study and were returned to the colony at study conclusion.

4.3. Behavioral assessments

4.3.1. Discrimination Learning

Discrimination learning was performed over three weeks during baseline (days −38 to −17) in order to assess learning ability and executive function as well as to prepare the subjects for cognitive tasks that would be completed during the treatment phase. Initially, on the first day of testing, animals participated in a 10-trial preference test using two objects differing in size, shape and color (i.e. green block and yellow banana). Following this test, each dog's preferred object was used as the rewarded stimulus for subsequent learning sessions during which selection of the preferred object was required in order to obtain a reward. The subsequent daily sessions consisted of 20 trials and were carried out according to standard operating procedures. Animals were tested until they successfully passed a two-stage criterion as follows: Stage 1: 90% or greater on one session or a minimum of 80% over two consecutive sessions; Stage 2: 70% or greater over two consecutive sessions.

4.3.2. Variable delayed non-matching to position (DNMP)

The DNMP task was performed in 5-day intervals in order to assess spatial working memory. Testing occurred during baseline (days −16 to −12), at three time points during the treatment phase (days 23–27, 46 to 50 and 74 to 78) and at two time points during follow up (days 114–118 and 142 to 146). Testing was performed according to standard operating procedures. Briefly, subjects were initially presented with a single object (i.e. white block) on a sliding tray. The block was positioned over one of three possible food-well locations and the animal was required to displace the block with its nose in order to uncover a food reward. The tray was then removed from the dog's sight and a delay was initiated. Following the delay, the subject was presented with two white blocks - one in the original location and one in a new location. The dog was required to select the block in the new (non-matching) location in order to obtain a reward. On each designated testing day, animals participated in a single session, regardless of score, with delays of 20 and 90 s equally divided among 12 trials. During the treatment phase, testing was performed 1 h following dosing (±15 min).

4.3.3. Variable discrimination (selective attention task)

Variable discrimination testing was performed in 4-day intervals in order to assess selective attention. Testing occurred during baseline (days −11 to −8), at three time points during the treatment phase (days 17–20, 40 to 43 and 68 to 71) and at two time points during follow up (days 107–110 and 135 to 138). Animals were tested on the designated days regardless of score. During the treatment phase testing was performed 1 h following dosing (±15 min) according to standard operating procedures. This task was similar to discrimination learning; however, the preferred object was presented with either 0, 1, 2, or 3 negative stimuli (non-preferred objects) to serve as distractors. There were 20 trials per session.

4.3.4. Discrimination reversal

Discrimination reversal testing was carried over ten days in the treatment phase (days 81–90). This task occurred following all other treatment phase testing. The task was performed as described for Discrimination Learning; however, the non-preferred object from the baseline preference test was now rewarded. Animals were tested once daily regardless of score according to standard operating procedures.

4.4. Plasma and cerebrospinal fluid (CSF) collection

Whole blood collections were performed immediately following each CSF collection time point. Approximately 4 ml of blood were collected from a suitable vein according to standard operating procedures. Blood was placed into K3EDTA tubes and within 15 min of collection, plasma was isolated by centrifugation at 1500×*g* for 15 min at 4 °C.

CSF was collected at baseline (day −2), at three time points during the treatment phase (days 28, 51, and 93) and twice after treatment end (days 120 and 148) for determination of RD2 levels and biomarkers. Using sterile techniques, samples were obtained from the cisterna magna while the animals were anesthetized. Anesthesia was induced with Propofol (8 mg/kg, intravenous) to effect. Subjects were intubated and anesthesia was maintained with an isoflurane/oxygen mixture for the duration of the procedure. If a suitable vein could not be accessed for Propofol injection, masking the animal with the isoflurane/oxygen mixture was used as an alternative. In each treatment arm, CSF was collected 1 h following dosing (±10 min). Samples were collected and subsequently processed by centrifugation (within 15 min of collection) at 2000×*g* for 10 min at 4 °C to remove potential red blood cell contamination.

RD2 plasma and CSF concentrations were quantified using an ultra-high-pressure liquid chromatography method combined with mass spectrometric detection using a QTRAP6500 in positive MRM mode (TNO, Zeist, Netherlands). The method had been validated (in accordance with the EMA guidelines on bioanalytical method validation) in terms of reproducibility, specificity, robustness and precision. The lower limit of quantification (LLOQ) was 0.5 ng/ml. Plasma concentrations for each dose level following single i.v. or oral doses of RD2 were used to calculate the following pharmacokinetic parameters: maximum concentration (C_{max}) and time to reach it (T_{max}), area under the plasma concentration versus time curve between 0 and t, and from 0 to infinity ($AUC_{0\text{-}tlast} + AUC_{0\text{-}inf}$), terminal half-life ($t_{1/2\alpha,\beta,\gamma}$), and total plasma clearance (CL_{total}) using TOPFIT 2.0 program [27].

4.5. Hematology and blood clinical chemistry

Whole blood collections were conducted on days −41 and −2 (baseline) as well as on day 93 of the treatment phase.

Complete blood count (CBC) and clinical chemistry analysis was performed by Antech Diagnostics (Mississauga, Ontario, Canada). CBC analysis included the blood parameters white blood cells (WBC), red blood cells (RBC), hemoglobin, hematocrit, mean corpuscular volume (MCV), mean corpuscular hemoglobin (MCH), mean corpuscular hemoglobin concentration (MCHC), platelet count, platelet estimate, neutrophils, lymphocytes, monocytes, eosinophils and basophils.

Clinical chemistry analysis included the blood parameters total protein, albumin, globulin, calculated ratio of albumin to globulin (A/G ratio), aspartate aminotransferase (AST), alanine transaminase (ALT), alkaline phosphatase (ALP), gamma-glutamyl transpeptidase (GGTP), total bilirubin, blood urea nitrogen (BUN), creatinine, BUN/creatinine ratio, phosphorus, glucose, calcium, magnesium, sodium, potassium, sodium/potassium ratio, chloride, cholesterol, triglycerides, amylase, lipase, creatine phosphokinase (CPK) and creatine kinase isozymes (CK-MM, CK-MB, and CK-BB).

4.6. Biomarker analysis

4.6.1. Aβ42 and total tau ELISA

Aβ42 and total tau ELISAs were purchased from Innotest (Fujirebio Germany GmbH, Hannover, Germany) and performed according to the manufacturer's protocol with CSF. Antibodies used for the specific detection of Aβ1-42 were 3D6, which recognizes amino acid residues 1 to 5 and 21F12, which recognizes amino acid residues 33 to 42 leading to a negligible cross reactivity for Aβ 1–40. Antibodies used for the detection of total tau were AT120, HT7 and BT2, all antibodies which are specific for the mid-domain region of the tau protein. All samples were measured in duplicates. Most of the tau concentration values were lower than the lower limit of quantification (50 pg/ml). Therefore, no further analysis of the data was performed.

4.6.2. Albumin ELISA

Albumin ELISA was purchased from Bethyl Laboratories (Montgomery, Alabama, USA) and performed according to the manufacturer's protocol with CSF and plasma. All samples were measured as duplicates.

4.6.3. GFAP and NfL single molecule array

GFAP and NfL single molecule arrays (Simoa) were purchased from Quanterix (Quanterix, Billerica, Massachusetts, USA) and performed according to the manufacturer's protocol with CSF on a Simoa HD-1 Analyzer (Quanterix, Billerica, Massachusetts, USA). All samples were measured as duplicates.

4.6.4. Surface-based fluorescence intensity distribution analysis (sFIDA) assay

Surface-based fluorescence intensity distribution analysis (sFIDA) assays were performed in 384 flat-bottom square well microplates with a glass bottom (ThermoFisher, Waltham, Germany) as previously described [19]. 2.5 μg/ml of Nab228 monoclonal antibody (mAB) (Sigma-Aldrich, Missouri, USA) and 2.5 μg/ml of Tau5 mAB (Biolegend, San Diego, USA) in $NaHCO_3$, pH 8 were added directly to the wells and incubated overnight at 4 °C. The plate was washed five times each with TBS (Serva, Duisburg, Germany) + 0.1 % Tween 20 (AppliChem, Darmstadt, Germany) (TBST) and TBS. Each of the wells was blocked with 1% BSA (AppliChem, Darmstadt, Germany) in TBS for 1 h at room temperature (RT). After washing the wells five times each with TBST and TBS, CSF samples and oligomer standard were added to the plate and were incubated overnight at 4 °C. The next day, after washing the excessive sample away five times with TBS, 0.2 μg/ml Nab228, labeled with CF-488 dye and 2 μg/ml Tau5, labeled with CF-633 dye, (both: Sigma-Aldrich, Missouri, USA), both ultra-centrifuged (100,000×*g*, 1 h, 4 °C), were added to the wells and incubated for 1 h. After incubation, the excessive detection antibodies were washed away five times with TBS. All washing steps were carried out by an automated microplate washer (405 LS Microplate Washer, Agilent, Santa Clara, USA). For measurement, the buffer in the wells was changed against TBS with 0.03% ProClin (Sigma Aldrich, Missouri, USA) and the plate was sealed with a plastic foil and transferred to a Leica multi-color TIRF total internal reflection fluorescence system (AMTIRF MC, Leica Microsystems, Wetzlar, Germany). The TIRF system operated with an automated stage and a × 100 oil immersion objective (1.47 oil CORRTIRF Leica). Images were recorded consecutively with Ex/Em = 633/705 and 488/525 nm with a 1000 ms exposure time and a gain of 1000 for both color channels at a penetration depth of 200 nm. The microscope took 5 × 5 images per well in each channel, which corresponds to app. 3% of the well's surface. Each image consisted of 1000 × 1000 pixels with a lateral resolution of 116 nm (pixel to pixel) and an intensity resolution of 14 bit (gray scale). Image analysis was performed using sFIDAta, a custom-made software. The cutoff values were calculated for each channel based on the buffer blank. The software then applied the cutoff values to the sample results and counted the pixels that were higher than the cutoff for each channel (pixelcount). All samples were measured in triplicates.

The calibration standard for Aβ and tau oligomers were silica nanoparticles (SiNaPs) with a diameter of 20 nm with covalently attached epitopes for the detection antibodies, Aβ(1–15) and tau(210–230). These Aβ(1–15)-tau(210–230)-SiNaPs have been prepared as described previously [21], with the following modifications: Aβ and tau peptides, which were functionalized with cysteamine on the C-terminus (Peptides and Elephants, Henningsdorf, Germany) were crosslinked to the aminated surface of the SiNaPs by maleimido hexanoic acid (MIHA, abcr GmbH, Karlsruhe, Germany).

4.7. Statistical analysis

All statistical calculations were performed using SigmaPlot Version 11 (Systat Software, Germany) or OriginPro 2019 (OriginLab Corporation, USA). Normal distribution of data was tested using Kolmogorov-Smirnov-test. Statistical calculations were conducted using two-way RM ANOVA followed by Fisher post hoc test. Pairwise comparisons were performed with one-sided Wilcoxon signed-rank test for dependent data and Mann-Whitney *U* test for independent data. Correlations were first calculated with Pearson and then with Spearman analysis at alpha level 0.05 with n = 11 to 12.

Author contribution statement

Janine Kutzsche, Dieter Willbold: Conceived and designed the experiments; Analyzed and interpreted the data; Wrote the paper.

Sarah Schemmert, Wolfgang M. Rossberg, Michael Hümpel, Antje Willuweit: Analyzed and interpreted the data.

Tuyen Bujnicki: Conceived and designed the experiments; Performed the experiments; Analyzed and interpreted the data; Wrote the paper.

Christian Zafiu, Steffen Halbgebauer, Markus Otto, Joseph A. Araujo: Conceived and designed the experiments; Performed the experiments.

Victoria Kraemer-Schulien: Performed the experiments.

Marlene Pils, Lara Blömeke, Julia Post, Andreas Kulawik: Contributed reagents, materials, analysis tools or data.

Dagmar Jürgens, Oliver Bannach: Conceived and designed the experiments.

Data availability statement

The datasets generated and/or analyzed during the current study are available from the corresponding author on reasonable request.

Declaration of competing interest

The authors declare the following financial interests/personal relationships which may be considered as potential competing interests:

Dieter Willbold reports a relationship with Priavoid GmbH that includes: board membership. Dieter Willbold has patent issued to Priavoid GmbH. Co-founder and co-owner of Priavoid GmbH.

Acknowledgments

D.W. was supported by the Technology Transfer Fund of the Forschungszentrum Jülich, Germany. D.W. was supported by "Portfolio Drug Research" of the "Impuls und Vernetzungs-Fonds der Helmholtzgemeinschaft", Germany. Additional funding was received from Part the Cloud: Translational Research Funding for Alzheimer's Disease (PTC) Award Number: 18PTC-19-605853 from the Alzheimer's Association, US. We received funding from the European Union Seventh Framework Program (FP7/2007–2013), European Union, under grant agreement 602999 (SYMPATH project), the Federal Ministry of Education and Research, Germany, within the projects VIP (03V0641), KNDD (01GI1010A), JPND/BIOMARKAPD (01ED1203H), and NEUROALLIANZ (16GW0099). We were also supported by the programs "Biomarkers Across Neurodegenerative Diseases I + II" of The Alzheimer's Association, Alzheimer's Research UK and the Weston Brain Institute, Canada (11084 and BAND-19-614337). We are also grateful for support from The Michael J. Fox Foundation, US, for Parkinson's Research (14977), from the ALS Association, US, and from the Packard Center, US, (19-SI-476). We further received funding from the Deutsche Forschungsgemeinschaft, Germany (INST 208/616-1 FUGG, INST 208/794-1 FUGG) and the Helmholtz Association, Germany (HVF0079).

Appendix A. Supplementary data

Supplementary data to this article can be found online at. https://doi.org/10.1016/j.heliyon.2023.e18443.

References

[1] X. Li, et al., Global, regional, and national burden of Alzheimer's disease and other dementias, 1990–2019, Front. Aging Neurosci. (2022) 14.
[2] E. Head, A canine model of human aging and Alzheimer's disease, Biochim. Biophys. Acta 1832 (9) (2013) 1384–1389.
[3] C.T. Siwak-Tapp, et al., Neurogenesis decreases with age in the canine hippocampus and correlates with cognitive function, Neurobiol. Learn. Mem. 88 (2) (2007) 249–259.
[4] C.T. Siwak-Tapp, et al., Region specific neuron loss in the aged canine hippocampus is reduced by enrichment, Neurobiol. Aging 29 (1) (2008) 39–50.
[5] P.D. Tapp, et al., Frontal lobe volume, function, and beta-amyloid pathology in a canine model of aging, J. Neurosci. 24 (38) (2004) 8205–8213.
[6] M. Pugliese, et al., Diffuse beta-amyloid plaques and hyperphosphorylated tau are unrelated processes in aged dogs with behavioral deficits, Acta Neuropathol. 112 (2) (2006) 175–183.
[7] E. Head, et al., Spatial learning and memory as a function of age in the dog, Behav. Neurosci. 109 (5) (1995) 851–858.
[8] N.W. Milgram, et al., Landmark discrimination learning in the dog, Learn. Mem. 6 (1) (1999) 54–61.
[9] J. Kutzsche, et al., Safety and pharmacokinetics of the orally available antiprionic compound PRI-002: a single and multiple ascending dose phase I study, Alzheimers Dement. (N Y) 6 (1) (2020), e12001.
[10] S. Schemmert, et al., Abeta oligomer elimination restores cognition in transgenic Alzheimer's mice with full-blown pathology, Mol. Neurobiol. 56 (3) (2019) 2211–2223.
[11] T. van Groen, et al., The Abeta oligomer eliminating D-enantiomeric peptide RD2 improves cognition without changing plaque pathology, Sci. Rep. 7 (1) (2017), 16275.
[12] T. Zhang, et al., Toward the mode of action of the clinical stage all-d-enantiomeric peptide RD2 on Aβ42 aggregation, ACS Chem. Neurosci. 10 (12) (2019) 4800–4809.
[13] B. Kass, et al., Aβ oligomer concentration in mouse and human brain and its drug-induced reduction ex vivo, Cell Rep. Med. 3 (5) (2022), 100630.
[14] J. Kutzsche, et al., Large-scale oral treatment study with the four most promising D3-derivatives for the treatment of Alzheimer's disease, Molecules 22 (10) (2017).
[15] S. Schemmert, et al., Deceleration of the neurodegenerative phenotype in pyroglutamate-Abeta accumulating transgenic mice by oral treatment with the Abeta oligomer eliminating compound RD2, Neurobiol. Dis. 124 (2019) 36–45.
[16] L. Bau-Gaudreault, C.N. Grimes, Effect of time and storage on toxic or pseudo-toxic change in canine neutrophils, Vet. Clin. Pathol. 48 (3) (2019) 400–405.
[17] N.W. Milgram, et al., Cognitive functions and aging in the dog: acquisition of nonspatial visual tasks, Behav. Neurosci. 108 (1) (1994) 57–68.
[18] P.D. Tapp, et al., Size and reversal learning in the beagle dog as a measure of executive function and inhibitory control in aging, Learn. Mem. 10 (1) (2003) 64–73.
[19] P.D. Tapp, et al., Effects of age on measures of complex working memory span in the beagle dog (Canis familiaris) using two versions of a spatial list learning paradigm, Learn. Mem. 10 (2) (2003) 148–160.
[20] Y. Herrmann, et al., sFIDA automation yields sub-femtomolar limit of detection for Aβ aggregates in body fluids, Clin. Biochem. 50 (4–5) (2017) 244–247.
[21] M. Hülsemann, et al., Biofunctionalized silica nanoparticles: standards in amyloid-β oligomer-based diagnosis of Alzheimer's disease, J. Alzheimers Dis. 54 (1) (2016) 79–88.
[22] A. Kulawik, et al., Advancements of the sFIDA method for oligomer-based diagnostics of neurodegenerative diseases, FEBS Lett. 592 (4) (2018) 516–534.
[23] L. Wang-Dietrich, et al., The amyloid-β oligomer count in cerebrospinal fluid is a biomarker for Alzheimer's disease, J. Alzheimers Dis. 34 (4) (2013) 985–994.
[24] L. Blömeke, et al., Quantitative detection of α-Synuclein and Tau oligomers and other aggregates by digital single particle counting, NPJ Parkinsons Dis. 8 (1) (2022) 68.
[25] J.P. Guo, et al., Abeta and tau form soluble complexes that may promote self aggregation of both into the insoluble forms observed in Alzheimer's disease, Proc. Natl. Acad. Sci. U. S. A. 103 (6) (2006) 1953–1958.
[26] Y. Miller, B. Ma, R. Nussinov, Synergistic interactions between repeats in tau protein and Aβ amyloids may Be responsible for accelerated aggregation via polymorphic states, Biochemistry 50 (23) (2011) 5172–5181.
[27] G. Heinzel, R. Woloszczak, P. Thomann, TopFit : Pharmacokinetic and Pharmacodynamic Data Analysis System for the PC, G. Fischer, Stuttgart, 1993.

3.4 Blood-based quantification of Aβ oligomers indicates impaired clearance from brain in ApoE ε4 positive subjects

Autoren:	Lara Blömeke, Fabian Rehn, Marlene Pils, Victoria Kraemer-Schulien, Anne Cousin, Janine Kutzsche, Tuyen Bujnicki, Silke Dawn Freiesleben, Luisa-Sophie Schneider, Lukas Preis, Josef Priller, Eike Jakob Spruth, Slawek Altenstein, Anja Schneider, Klaus Fliessbach, Jens Wiltfang, Niels Hansen, Ayda Rostamzahdeh, Emrah Düzel, Wenzel Glanz, Enise I. Incesoy, Katharina Buerger, Daniel Janowitz, Michael Ewers, Robert Perneczky, Boris-Stephan Rauchmann, Stefan Teipel, Ingo Kilimann, Christoph Laske, Matthias H. Munk, Annika Spottke, Nina Roy, Michael T. Heneka, Frederic Brosseron, Michael Wagner, Sandra Roeske, Alfredo Raminez, Matthias Schmid, Frank Jessen, Oliver Bannach, Oliver Peter, Dieter Willbold
Journal:	Communications Medicine (im Review)
DOI:	/
Impact-Faktor:	Gegründet 2021, noch kein Impact-Faktor verfügbar
Beitrag:	Eigenanteil: 75 % Entwicklung des Assays Synthese und Weiterentwicklung der Silikananopartikel Planung, Durchführung und Auswertung der Validierungsexperimente Durchführung und Auswertung der Plasmaprobenmessungen Anfertigung der Abbildungen Statistische Auswertung Hauptverfasserin des Manuskripts
Anhang zum Manuskript	Kapitel 7.4

Blood-based quantification of Aβ oligomers indicates impaired clearance from brain in ApoE ε4 positive subjects

Lara Blömeke[1,2], Fabian Rehn[1,2], Marlene Pils[1,2], Victoria Kraemer-Schulien[1], Anneliese Cousin[1], Janine Kutzsche[1], Tuyen Bujnicki[1], Silka D. Freiesleben[3,4], Luisa-Sophie Schneider[4], Lukas Preis[4], Josef Priller[3,4,5,6], Eike J. Spruth[3, 4], Slawek Altenstein[3,4], Anja Schneider[7,8], Klaus Fliessbach[7,8], Jens Wiltfang[9,10,11], Niels Hansen[10], Ayda Rostamzadeh[12], Emrah Düzel[13,14], Wenzel Glanz[13], Enise I. Incesoy[13,14,15], Katharina Buerger[16,17], Daniel Janowitz[17], Michael Ewers[16, 17], Robert Perneczky[16,18,19,20], Boris-Stephan Rauchmann[18,21,22], Stefan Teipel[23,24], Ingo Kilimann[23,24], Christoph Laske[25,26], Matthias H. Munk[25,27], Annika Spottke[7,9], Nina Roy[7], Michael T. Heneka[28], Frederic Brosseron[7], Michael Wagner[7,8], Sandra Roeske[7], Alfredo Ramirez[7,8,29,30,31], Matthias Schmid[7,32], Frank Jessen[7,10,29], Oliver Bannach[1,2], Oliver Peters[3,4], Dieter Willbold[1,2,33*]

[1]Institute of Biological Information Processing (Structural Biochemistry: IBI-7), Forschungszentrum Jülich, 52428 Jülich, Germany

[2]attyloid GmbH, 40225 Düsseldorf, Germany

[3]German Center for Neurodegenerative Diseases (DZNE), 10117 Berlin, Germany

[4]Department of Psychiatry and Psychotherapy, Charité, 10117 Berlin, Germany

[5]School of Medicine, Technical University of Munich; Department of Psychiatry and Psychotherapy, 81675 Munich, Germany

[6]University of Edinburgh and UK DRI, Edinburgh, UK

[7]German Center for Neurodegenerative Diseases (DZNE), Bonn, 53127 Bonn, Germany

[8]University of Bonn Medical Center, Dept. of Neurodegenerative Disease and Geriatric Psychiatry/Psychiatry, 53127 Bonn, Germany

[9]German Center for Neurodegenerative Diseases (DZNE), 37075 Goettingen, Germany

[10]Department of Psychiatry and Psychotherapy, University Medical Center Goettingen, University of Goettingen, 37075 Goettingen, Germany

[11]Neurosciences and Signaling Group, Institute of Biomedicine (iBiMED), Department of Medical Sciences, University of Aveiro, 3810-193 Aveiro, Portugal

[12]Department of Psychiatry, University of Cologne, Medical Faculty, 50924 Cologne, Germany

[13]German Center for Neurodegenerative Diseases (DZNE), 39120 Magdeburg, Germany

[14]Institute of Cognitive Neurology and Dementia Research (IKND), Otto-von-Guericke University, 39106 Magdeburg, Germany

[15]Department for Psychiatry and Psychotherapy, University Clinic Magdeburg, 39120 Magdeburg, Germany

[16]German Center for Neurodegenerative Diseases (DZNE, Munich), 81377 Munich, Germany

[17]Institute for Stroke and Dementia Research (ISD), University Hospital, LMU Munich, 81377 Munich, Germany

[18]Department of Psychiatry and Psychotherapy, University Hospital, LMU Munich, 81377 Munich, Germany

[19]Munich Cluster for Systems Neurology (SyNergy) Munich, 81377 Munich, Germany

[20]Ageing Epidemiology Research Unit (AGE), School of Public Health, Imperial College London, London, UK

[21]Sheffield Institute for Translational Neuroscience (SITraN), University of Sheffield, Sheffield, UK

[22]Department of Neuroradiology, University Hospital LMU, 81377 Munich, Germany

[23]German Center for Neurodegenerative Diseases (DZNE), 18147 Rostock, Germany

[24]Department of Psychosomatic Medicine, Rostock University Medical Center, 18147 Rostock, Germany

[25]German Center for Neurodegenerative Diseases (DZNE), 72076 Tübingen, Germany

[26]Section for Dementia Research, Hertie Institute for Clinical Brain Research and Department of Psychiatry and Psychotherapy, University of Tübingen, 72076 Tübingen, Germany

[27]Department of Psychiatry and Psychotherapy, University of Tübingen, 72076 Tübingen, Germany

[28]Luxembourg Centre for Systems Biomedicine (LCSB), University of Luxembourg, L-4367 Belvaux, Luxembourg

[29]Excellence Cluster on Cellular Stress Responses in Aging-Associated Diseases (CECAD), University of Cologne, 50931 Cologne, Germany

[30]Division of Neurogenetics and Molecular Psychiatry, Department of Psychiatry and Psychotherapy, Faculty of Medicine and University Hospital Cologne, University of Cologne, 50931 Cologne, Germany

[31]Department of Psychiatry & Glenn Biggs Institute for Alzheimer's and Neurodegenerative Diseases, San Antonio, TX, USA

[32]Institute for Medical Biometry, University Hospital Bonn, 53127 Bonn, Germany

[33]Institut für Physikalische Biologie, Heinrich-Heine-Universität Düsseldorf, 40225 Düsseldorf, Germany

***Corresponding Author:**

Prof. Dr. Dieter Willbold, Institute of Biological Information Processing (IBI-7), Forschungszentrum Jülich, Wilhelm-Johnen-Straße, 52428 Jülich, Germany

Tel.: +49 2461 61 2100; E-Mail: d.willbold@fz-juelich.de

Abstract

Quantification of Amyloid beta (Aβ) oligomers in plasma enables early diagnosis of Alzheimer's Disease (AD) and improves our understanding of underlying pathologies. However, quantification necessitates an extremely sensitive and selective technology because of very low Aβ oligomer concentrations and possible interference from matrix components. In this report, we developed and validated a surface-based fluorescence distribution analysis (sFIDA) assay for quantification of Aβ oligomers in plasma. The blood-based sFIDA assay delivered a sensitivity of 1.8 fM, an inter- and intra-assay variation below 20% for oligomer calibration standards and no interference with matrix components. Quantification of Aβ oligomers in 359 plasma samples from the DELCODE cohort revealed lower oligomer concentrations in subjective cognitive decline and AD patients than healthy Control participants. Correlation analysis between CSF and plasma oligomer concentrations indicates an impaired clearance of Aβ oligomers that is dependent on the ApoE ε4 status.

Introduction

Although Alzheimer's Disease (AD) is the most prominent neurodegenerative disorder affecting 50 million people worldwide [1], there remains a lack of therapeutic options and diagnostic tools, such as a blood-based test suitable for use in primary care. As increasing evidence supports the role of Amyloid Beta (Aβ) oligomers as the most toxic component in AD progression [2-4], these oligomers represent a promising biomarker candidate for diagnosis of AD and drug development. The level of Aβ oligomers in the brains of AD patients are higher and, because of the direct connection to brain parenchyma and liquor [5], also in cerebrospinal fluid (CSF), as supported by previous studies [6-9]. Moreover, more than 50% of monomeric brain Aβ is transferred and cleared in the periphery [10], reaching the blood via blood-brain-barrier (BBB), blood-CSF barrier (BCSFB) or perivascular and glymphatic clearance [11].

Although the exact clearance mechanisms of Aβ oligomers from the brain and CSF to plasma remain largely unknown, earlier studies have confirmed the presence of Aβ oligomer species in plasma samples [12].

However, disease progression may lead to a reduction in Aβ oligomers in plasma samples because of their deposition in amyloid plaques and impaired clearance from the brain into the blood stream [13]. For example, an inverse correlation between efficiency of glymphatic clearance and oligomer size has been described [2]. Additionally, transport of Aβ across the BBB is affected in AD patients, especially in carriers of the AD risk gene allele apolipoprotein E (ApoE) ε4 [2,14]. Quantification of Aβ oligomer concentrations in plasma samples, especially in early disease stages, and in-depth analysis of dependencies between Aβ oligomers and different biomarkers will improve our understanding of the role of amyloid pathology in AD.

Previous studies have reported higher oligomer concentrations in AD patients [13,15-17]. All of the methods applied in these studies detect specific subtypes of Aβ oligomers, depending on the respective antibody used. For Aβ oligomers derived from the brain, a broad range of species was described, ranging from small molecular weight oligomers like dimers and trimers via 56mers and spherical oligomers like Aβ derived diffusible ligands (ADDLs) to high-molecular weight oligomers and protofibrils [18,19]. For these species, differences have been claimed for their neurotoxicity and

pathologic mechanisms, like impairment of mitochondrial dysfunction, Ca^{2+} homeostasis dysregulation and induction of tau pathology [18].

The most widely described method for detection of Aβ oligomers in plasma is the multimer detection system (MDS) which uses $Aβ_{1-42}$ to amplify the signal and is therefore a tool to measure the oligomerization tendency of on-pathway oligomers. Using this method, AD patients showed significantly increased MDS signal compared to the control group [15,20,21] and the correlation with cognitive decline using neuropsychological tests like MMSE and CERAD [20,22,23]. Other methods used oligomer specific antibodies to quantify those oligomer species that are recognized by the respective specific antibody [12,17,24]. A third method claimed to quantify the alpha-sheet content of oligomers in plasma using specifically designed alpha-sheet peptides [25].

In contrast to these methods, the surface-based fluorescence intensity distribution analysis (sFIDA) technology aims to quantify all oligomer species, irrespective of their conformation, morphology and size, all of them potentially relevant for disease development and progression. sFIDA is a versatile platform for quantification of protein aggregates in biofluids that features single particle sensitivity due to a microscopy-based readout and selectivity for aggregated Aβ because of the use of antibodies with overlapping or even identical linear epitopes at the N-terminus of Aβ (principle of sFIDA in Fig. 1a). Quantifying the total amount of oligomeric species is crucial for quantitation of target engagement in the development of anti-oligomeric drugs. New therapies aim to eliminate Aβ oligomers. Using a diagnostic tool that captures all oligomer species may show the effect of this anti-oligomeric drug irrespective of the exact mechanism of action and the target oligomer species.

As calibration standard for oligomer-based assay, we previously established protein conjugated silica nanoparticles (SiNaPs) [26-28]. Additionally, we demonstrated that sFIDA sensitively and specifically detects alpha synuclein (αSyn), Tau and Aβ oligomers in CSF samples [9,29]. Nonetheless, the reliable quantification of Aβ oligomers in plasma samples poses an even greater challenge, as plasma typically contains a 200-fold higher total protein concentration than CSF [5]. This high protein background can lead to false negative readouts because of epitope masking, or false positive readouts because of interferences with human anti-mouse-antibodies [30]. Moreover,

Aβ oligomer concentrations are expected to be in the low femto- to even attomolar range [31], thus requiring an extremely sensitive method for detection.

In this report, an sFIDA assay for quantification of Aβ oligomers in plasma samples was developed and validated as a basic research project. We intended to quantitate the total Aβ oligomer levels in plasma samples of the DELCODE cohort to investigate the development of their concentrations during disease progression and their dependency from the ApoE4 status of the donors.

Results

Initially, we validated the sFIDA assay using our $A\beta_{1-15}$-coated silica nanoparticle (SiNaPs) standard [28]. Additionally, Aβ aggregates were used to simulate a positive plasma sample, referred to as "internal quality control" (IQC). To this end, control plasma samples were spiked with different concentrations of Aβ oligomers. The synthesis and characterization of these aggregates is described in Pils et al. including a setup image in the supplement [32].

Additionally, we confirmed the sensitivity and selectivity of the assay for Aβ oligomers in a validation cohort comprising 20 plasma samples of control subjects (Control), mild cognitive impairment (MCI) and AD patients. Exemplary raw data images for the red and green fluorescence channels and colocalization are shown in Fig. 1b. We then applied the assay to a larger set of plasma samples of the DELCODE cohort, which comprises a control group, subjective cognitive decline (SCD), MCI, AD patients and first-degree relatives of AD patients.

sFIDA features high sensitivity and precision

Analytical sensitivity: Quantification of Aβ oligomers in plasma requires extreme sensitivity. Therefore, we initially investigated analytical sensitivity of sFIDA using $A\beta_{1-15}$-coated SiNaPs spiked in plasma and calculated a limit of detection (LOD) of 1.8 fM for the colocalization (Fig. 1c). Dilution linearity of SiNaPs was demonstrated between 2 fM to 8 pM with a mean dilution linearity of 100.6% and coefficient of determination of 0.994. Moreover, an upper limit of quantification (ULOQ) for SiNaPs was determined to be 256 pM, showing a 5-log dynamic range of sFIDA (data not shown). For recombinant Aβ aggregates as IQC, an LOD of 1.9 pg/ml (monomer unit

158 concentration) and a mean dilution linearity of 98.2% was calculated (Fig. 1d). Colocalization
159 enhances the analytical sensitivity by two-fold for SiNaPs and ten-fold for recombinant aggregates
160 compared to the individual channels red and green (Supplementary Fig. 1). Thus, colocalization
161 was used unless otherwise stated. In a small proof-of-concept study including 20 plasma samples
162 of healthy Control, MCI and AD patients, we measured Aβ oligomer concentrations ranging from 0
163 to 500 fM, confirming sufficient sensitivity of sFIDA for *in vivo* Aβ oligomers (sFIDA readouts in
164 Supplementary Fig. 2a). Moreover, these oligomers showed a similar size distribution and amount
165 of colocalization compared to synthetic Aβ-SiNaPs and aggregates (Fig. 1b). Pre-analytical studies
166 indicated that tube transfers and freeze-thaw-cycles should be avoided (Supplementary Fig. 3).
167 **Intra-assay precision:** Mean intra-assay variation of SiNaPs among all concentrations was 9.4%
168 for the red fluorescence channel (IC16 CF633), 4.9% for the green fluorescence channel
169 (Nab228 CF488) and 15.5% for colocalization based on four replicates (Fig. 1c). Recombinant
170 aggregates showed a mean intra-assay variation of 19.1% for the colocalization (Fig. 1d).
171 **Inter-assay precision:** Repeated measurements of SiNaPs spiked in plasma yielded a mean inter-
172 assay variation of 19.3% for all concentrations tested (Fig. 2a). Calibrated concentrations of BC,
173 two IQC and seven plasma samples showed a mean inter-assay variation of 41.9%. Using repeated
174 measures ANOVA, the individual experiments for measurement of SiNaPs, IQC and plasma
175 samples did not differ significantly (*p*-value >0.05).

176 Aβ oligomer quantification is not influenced by endogenous substances

177 **Recovery and dilution linearity:** We spiked three concentrations of SiNaPs in plasma samples
178 from three individual patients to investigate matrix effects and calculated a mean percent recovery
179 of 92% (excluding one concentration/sample) (Supplementary Fig. 4a, b). Additionally, the
180 calibrated concentrations of SiNaPs and aggregates spiked in plasma were not affected by dilution
181 with buffer (Supplementary Fig. 4c, d). The observed negligible effects of the sample matrix in both
182 experiments showed that quantification of Aβ oligomers in individual plasma samples is accurate.
183 **Monomers:** In plasma, concentrations of approximately 300 pg/ml $Aβ_{1-40}$ and 20 pg/ml $Aβ_{1-42}$ have
184 been determined [33]. Interference from Aβ monomers on sFIDA measurements was investigated by
185 spiking 452 pg/ml Aβ monomers in a blank plasma sample. As a positive control, the same

concentration of aggregated $A\beta_{1-42}$ was used. Monomer samples yielded a signal equivalent to the non-spiked blank control, whereas $A\beta_{1-42}$ aggregates yielded a nearly 100x stronger signal (Fig. 2d), indicating negligible interference from monomeric Aβ at physiologically relevant concentrations in our assay.

HAMA: In sandwich ELISAs, heterophilic antibodies (HA) can crosslink capture and detection antibodies, causing false-positive signals [30]. By changing the capture antibody Nab228, which gave false positive signals at concentrations of 10 ng/ml or higher (Fig. 2e), to bapineuzumab (humanized equivalent to 3D6 [34]), interference from the spiked anti-mouse antibody was reduced to <0.005% at the highest concentration tested. Although a false-positive signal was observed at 1000 ng/ml HA, such concentrations are unlikely to be present in human plasma [35].

Cross-reaction with αSyn and Tau aggregates: We next investigated whether other protein aggregates composed of Tau or αSyn cross-reacted with our Aβ-specific detection system. The presence of αSyn or Tau aggregates gave no false-positive (BC spiked with αSyn or Tau aggregates) or false-negative signals ($A\beta_{1-42}$ aggregates spiked with αSyn or Tau aggregates), as all signals were ±20% from the non-spiked sample (Supplementary Fig. 2b).

Haemolytic plasma: During blood donation, erythrocytes may be damaged, leading to the release of haemoglobin through haemolysis [36]. As erythrocytes bind Aβ [37], their disruption may affect the sFIDA readout. This potential interference was examined by spiking a non-haemolytic sample with different concentrations of haemolytic plasma. Concentrations of 0.5% and 1% of haemolytic plasma produced a higher background signal, but did not affect aggregate detection (Fig. 2e). However, haemolytic plasma at a concentration of 0.5% gave a visibly reddish colour, indicating that these samples should be excluded from analysis.

sFIDA readouts in plasma samples are solely attributed to Aβ oligomers

Immunodepletion: Immunodepletion was used to further demonstrate that the sFIDA-based Aβ oligomer signal does not originate from the plasma matrix. We removed Aβ species using magnetic beads coated with bapineuzumab, and used magnetic beads that were not coated with antibodies as a control. Non-specific immunodepletion reduced the signal for the recombinant aggregates (IQC-1) by 93.1% and on average by 79.8% for patient samples. In contrast, immunodepletion with

bapineuzumab reduced the signal for Aβ aggregates by 99.3% and that of the clinical samples by 94.9% for samples above LOD. Moreover, specific immunodepletion with bapineuzumab yielded a lower signal compared to unspecific immunodepletion for almost every sample tested with a mean signal reduction of 50.3% (Fig. 2c).

Detection probe control: The validation cohort was subjected to sFIDA in the absence of detection antibodies to exclude false-positive signals because of plasma sample autofluorescence. The autofluorescence signal was below the LOD for each sample tested with a mean signal reduction of >99% compared to the signal with detection antibodies (data not shown). Possible matrix interferences with IgG detection antibodies in general was investigated by probing plasma samples with an IgG isotype control (MOPC CF633) and an anti-αSyn antibody (211 CF488). The signals of the 20 plasma samples with these non-Aβ-specific probes were also reduced by >97% for the individual channels and colocalization (values of the colocalization are plotted in Supplementary Fig. 2a). Assay specificity was further increased by choosing an assay setup with two different anti-Aβ-probes and analysing only colocalized pixels.

Capture control: As non-specific adherence of Aβ oligomers to surfaces was reported previously [38], we investigated the unspecific binding of the analyte to the sFIDA assay surface by introducing a control where we skip the capture antibody (capture control).

binding of the analyte to the sFIDA assay surface. In the absence of a capture antibody, SiNaPs and aggregates spiked in plasma showed a signal of 33.5% and 54.7%, respectively. However, the signals of SiNaPs and aggregates spiked in buffer were reduced by >99.9% in absence of a capture antibody (data not shown), indicating that surface binding is mediated by plasma matrix components. Similar to the calibration standards, five plasma samples tested showed non-specific binding of the analyte to the assay surface, indicated by a signal still at 77.2% (data not shown).

Aβ oligomer concentrations in plasma samples are in the low femtomolar range

After analysing the sensitivity and selectivity of the analytical assay and investigating differences among the 20-sample validation cohort, we examined the disease-relevance and correlation with

other AD-related biomarkers. Thus, we subjected 359 plasma samples from the DELCODE cohort to sFIDA analysis.

Like the validation cohort, Aβ oligomer concentrations determined in the samples from the DELCODE cohort spanned three orders of magnitude, ranging from 0.4 to 400 fM. Unexpectedly, AD (p-value: 0.037) and SCD (p-value: 0.023) subjects showed a significantly lower plasma Aβ oligomer concentrations compared to control.subjects using Mann-Whitney-U test, whereas samples of first-degree relatives and MCI patients did not show any significant differences (Fig. 3a). Interestingly, after subdividing groups according to their CSF amyloid pathology status (A+/A-, based on CSF $A\beta_{1-42}/A\beta_{1-40}$ ratio [39]), it became evident that oligomer concentrations are reduced in amyloid positive SCD, MCI and AD patients only (Fig. 3b).

Correlations of Aβ oligomers in CSF and plasma depend on cognitive staging, amyloid pathology and ApoE status

We performed several correlation analyses to explore the pathophysiological basis for determining Aβ oligomer concentrations in plasma. We performed bootstrapping (re-sampling with replacement, see statistics) to enhance the reliability of our correlation analysis. Moreover, we grouped Control, relatives and SCD patients as well as MCI and AD patients for correlation analysis to enhance clarity and meaningfulness of our statistical analyses. No correlations of Aβ oligomers with Aβ monomers in plasma or with age or MMSE were observed (Supplementary Table 1). In contrast, Aβ oligomers in plasma of MCI and AD patients showed a significant correlation with monomeric Aβ in CSF. We also analysed the correlation of Aβ oligomer concentrations in plasma versus CSF, which were recently measured by sFIDA (yet unpublished observation). Although oligomer concentrations in Control, relatives and SCD patients showed a direct correlation between CSF and plasma, oligomer concentrations in MCI and AD patients showed an inverse correlation (Fig. 4a). In AD, clearance of Aβ species from the brain is hypothesised to be impaired [2], which is probably dependent on the ApoE ε4 status or TREM-2 mutations affecting microglia activity [40,41]. Thus, we examined the dependency of Aβ oligomers in CSF and plasma on amyloid pathology or ApoE ε4 status. For both Control, relatives and SCD and MCI and AD patient groups, significant correlations were only observed for amyloid negative and ApoE ε4 negative patients, respectively.

In contrast, when patients are ApoE ε4 positive or amyloid positive (A+), no significant correlations were found (Fig. 4b, c).

Discussion

In the present study we adapted the sFIDA technology to quantify Aβ oligomers in human plasma samples. We demonstrated femtomolar sensitivity and low inter- and intra-assay variations for SiNaPs spiked in plasma. In contrast, plasma samples showed an increased inter-assay variation suggesting a yet unknown, possibly pre-analytical influence. However, taking into consideration the inherently high inter-assay variations at low concentrations [42], the 3-log difference between individual samples and the limited effect on the individual ranking of the samples, intra-assay variation was considered to be acceptable currently. Nevertheless, intra- and inter-assay variation may be improved in the future, by in-depth analyses of pre-analytical influences, and by applying full automation of the sFIDA assay to avoid human operator dependent variations, as has been partially applied previously [43].

Investigation of possible interfering factors, such as monomers and HAMAs, and analysis of patient plasma samples from the validation cohort confirmed the sensitivity and selectivity of the sFIDA assay for quantification of Aβ oligomers. Although non-specific binding of Aβ oligomers to experimental surfaces did not influence the interpretation of the results, future efforts aim to reduce this issue to avoid signal loss in pre-analytical steps.

As the validation experiments showed the suitability of sFIDA to sensitively and specifically quantitate Aβ oligomers in plasma samples, we investigated Aβ oligomer concentrations in 359 plasma samples of the DELCODE cohort. Remarkably, we observed significantly reduced oligomer concentrations in SCD and AD patients compared to the Control group, which is in contrast to previous studies reporting increased Aβ oligomer concentrations in the plasma of AD patients [13,21,25] and a correlation of plasma Aβ oligomer concentration with SCD symptoms [44]. SCD is a heterogeneous condition with many potentially underlying causes – one of them is an early stage of AD [45]. In our cohort, 35.6% of SCD patients were amyloid positive and therefore fulfilling the NIA-AA research framework criteria for an underlying AD [46]. Although at a very early stage of AD,

296 presumably the same mechanisms apply as with MCI and AD patients as discussed below. To
297 interpret the differences to previous studies, it is important to point out, that most of these previous
298 studies detected various oligomeric sub-species because of the use of structure-specific antibodies
299 [17,24], detection of seeding-competent oligomers [21] or α-sheet content [25], whereas sFIDA quantifies
300 the total amount of Aβ oligomers in plasma. It can be hypothesized that the Aβ oligomer
301 subfractions examined by other studies might be subject to different formation and clearing
302 mechanism compared to those described in the present study. Exploring whether differences in
303 patient enrolment or pre-analytical aspects are responsible for these inconsistencies or alternative
304 subpopulations of Aβ oligomers are measured by different assays is essential, and comparative
305 studies using the same set of samples should be conducted. These varying outcomes across
306 different assay setups emphasize the importance of such investigations.
307 This study aimed to quantify and better understand the potential origin of total Aβ oligomer
308 concentrations in plasma samples. We observed that monomeric Aβ in plasma did not correlate
309 with Aβ oligomers in plasma, whereas a correlation with CSF monomers and oligomers was
310 observed. This observation indicates that Aβ oligomers, at least partially, originate from CSF (Fig.
311 5 clearance mechanism #4) or directly from the brain (Fig. 5 clearance mechanism #3). Therefore,
312 it is possible that elevated oligomer concentrations in plasma may result from an increase in
313 oligomer concentrations in CSF. Indeed, we observed a positive correlation of Aβ oligomers
314 between CSF and plasma in Controls, relatives and SCD patients. However, this correlation was
315 only evident for patients without amyloid pathology (A-, classification based on CSF $A\beta_{1-42}/A\beta_{1-40}$
316 ratio [39]) or without the genetic risk factor. We hypothesize that once amyloid positivity becomes
317 evident (A+), Aβ oligomers are preferentially deposited in plaques (clearance mechanism #2),
318 leading to a reduced clearance via other pathways (clearance mechanisms #1, #3, #4). This may
319 explain the absence of a correlation between Aβ oligomers in the CSF and plasma, and the
320 decrease in oligomer concentrations in the plasma of amyloid positive patients. Additionally,
321 impaired clearance mechanisms for Aβ monomers across the BBB, BCSFB and perivascular
322 drainage, and impaired degradation by microglia, have been reported for ApoE ε4 carriers
323 (clearance mechanisms #1 and probably #3 and #4) [10,41]. Assuming similar pathological effects for
324 oligomers, the most likely clearance mechanism in ApoE ε4 carriers is the deposition of Aβ

oligomers into plaques (clearance mechanism #2), which limits the transport and results in a weaker correlation between CSF and plasma.

When interpreting correlations of Aβ oligomers between CSF and plasma in MCI and AD patients, it is important to consider previous sFIDA studies that have quantified Aβ oligomers in CSF. These studies have shown that Aβ oligomer concentrations in CSF are highest in the early stages of the disease and decrease as the disease progresses, particularly in ApoE ε4 carriers who have a higher Aβ oligomer burden during the early stages of the disease (yet unpublished observation). Decreasing concentrations of oligomers in CSF in advanced disease stages may arise from negative feedback mechanisms initiated by Aβ oligomers at synapses, resulting in reduced synaptic activity and consequently reduced production of Aβ monomers and replenishment of Aβ oligomers. Additionally, enhanced clearance through other pathways, such as deposition in plaques (clearance mechanism #2) or transport to the blood in a CSF-independent manner, may also contribute to reduced oligomer concentrations in CSF. We observed an inverse correlation of Aβ oligomer concentrations in CSF and plasma indicating an impaired clearance via CSF pathways (clearance mechanism #4) and an uncoupling of Aβ oligomer concentrations in blood and CSF. Moreover, this correlation was not observed for ApoE ε4 carriers, which supports the idea that ApoE ε4 plays a role in transporting Aβ oligomers from the brain and thus an increase in oligomer concentrations in CSF for these carriers. However, these are only a few factors that influence Aβ oligomer clearance. Activation of microglia have also been associated with TREM-2 variants [40], which should be analyzed in future studies, as well as the weakly pronounced differences in oligomer concentrations and correlations, which has previously been observed in studies measuring plasma Aβ monomer concentrations [47]. Moreover, monomer concentrations in plasma were reported to depend on co-pathologies like hypertension, dyslipidemia, diabetes, liver function and chronic kidney disease [48]. These co-pathologies might be determinants of Aβ oligomer concentrations in plasma and should be considered in future studies.

Full interpretation of the results requires a better understanding of how Aβ oligomers are distributed and cleared from the brain and peripheral tissues during disease progression. Although the developed assay accurately measures total Aβ oligomer concentrations in plasma, the potential for

using Aβ oligomers as a diagnostic biomarker has not been fully exploited and warrants further research and development. In particular, concentration and distribution analysis of different body fluids, such as novel matrices like stool [49], may improve our understanding of oligomer distributions in peripheral tissues. Owing to their central role in AD pathology, oligomers are an attractive therapeutic target to prohibit disease progression or even cure AD [50]. In pre-clinical and clinical development of anti-oligomer compounds, sFIDA is well suited to determine target engagement and to monitor therapeutic success at the molecular level.

Acknowledgements

We thank Dr. Carsten Korth (Institute of Neuropathology, Universitätsklinikum Düsseldorf, 40225 Düsseldorf, Germany) who kindly provided the IC16 antibody. We thank Dr. Volker Nischwitz (Central Institute of Engineering, Electronics and Analytics (ZEA-3), Forschungszentrum Jülich, 52428 Jülich, Germany) for ICP-MS measurements of silica nanoparticles. We thank Dr. Andrew Dingley for proof-reding the manuscript.

This work was supported by the Helmholtz Association [grant number HVF0079].

Author contributions

LB developed the assay with support of MP. LB performed the experiments and LB and FR analysed the data and carried out the statistics. VK, AC and TB aid in experimental work and evaluation of the data. JK supported organization of the samples. LB, OB and DW wrote the manuscript. OB, DW and OP supervised the project.

OP, SDF, LSS, LP, JP, EJS, SA, AS, KL, JF, NH, FJ, AR, ED, WG, EII, KB, DJ, MW, RP, BSR, ST, IK, CL, MHM, AS, NR, MTH, FB, MW, SR, AR, MS were responsible for overall design, implementation and collection of data for the DELCODE study at the respective study sites.

All authors approved the final version of this manuscript.

Disclosure

DW and OB are co-founders and shareholders of attyloid GmbH. This affiliation had no influence of the interpretation of the data. All other authors declare no competing interests related to this work.

Online Methods

SiNaPs

We used our previously developed silica nanoparticle standard (SiNaPs) as an assay control and for calibration. SiNaPs are small, spherical particles with a diameter of ~18.5 nm, which are functionalized with amino acids 1–15 of the Aβ peptide. Synthesis and characterization of the particles have been described previously [28,29] (Supplementary Fig. 5). The silica core of the particles was synthesized via the Stöber process and subsequently modified with APTES (3-aminopropyl(triethoxysilane), Sigma-Aldrich, St. Louis, USA) to create an aminated surface. As a crosslinker between protein and aminated particles, we used maleimido hexanoic acid (MIHA, abcr, Karlsruhe, Germany), which was activated using EDC (1-ethyl-3-(3-dimethylaminopropyl)carbodiimide, Sigma-Aldrich) and NHS (N-hydroxysuccinimide, Sigma-Aldrich). After washing, $A\beta_{1-15}$ (Peptides and Elephants, Henningsdorf, Germany) functionalized with cysteamine at the C-terminus was reacted with the maleimide group of SiNaPs to form a covalent attachment. $A\beta_{1-15}$ was added to achieve a theoretical protein load of ~18 $A\beta_{1-15}$ peptides per SiNaP. After 1 h, TCEP (Tris-(2-carboxyethyl)-phosphine, abcr, Karlsruhe, Germany) was added to prevent oxidation of the cysteamine-functionalized protein, and 1 h later, the reaction was terminated by adding 2-mercaptoethanol. SiNaPs were washed twice with ddH_2O. Prior to use, SiNaPs were subjected to ultrasonication for 15 s at 50% amplitude with a 1 s pulse - 1 s pause cycle.

Aggregates

Aβ aggregates: $A\beta_{1-42}$ was purchased from Bachem AG (Bubendorf, Switzerland). 50 µg aliquots of $A\beta_{1-42}$ were dissolved in 1,1,1,3,3,3-hexafluoroisopropanol (HFIP, Sigma-Aldrich) and divided in 5 µg aliquots. HFIP was then evaporated in a vacuum concentrator (Vacufuge concentrator, Eppendorf, Hamburg, Germany) and stored at RT. 5 µg of $A\beta_{1-42}$ was dissolved in 5 µl dimethyl sulfoxide (DMSO, Sigma-Aldrich) for 10 min with shaking at 650 rpm (Thermomixer, Eppendorf). PBS and 1% sodium azide (AppliChem, Darmstadt, Germany) were added to achieve a

concentration of 10 µM $A\beta_{1-42}$ containing 0.04% sodium azide. $A\beta_{1-42}$ was allowed to aggregate for 16 h at RT with shaking at 650 rpm. Aggregates were used directly or stored at –80 °C in 5 µl aliquots. Aβ aggregates have previously been characterized in Pils et al. using Thioflavin T assay (THT) and atomic force microscopy (AFM). Aggregates showed a monodisperse size distribution with a mean diameter of 2.7 nm [32]. We focused on $A\beta_{1-42}$ to prepare artificial aggregates, because in our hands their preparation is more robust and reproducible, and, because the capture and detection antibodies used here do not discriminate between $A\beta_{1-40}$ and $A\beta_{1-42}$.

αSyn aggregates: αSyn (expressed and purified in-house) was dissolved to 1 mg/ml in 20 mM Tris-HCl containing 100 mM sodium chloride (pH 7.4) and incubated for seven days at 37 °C with shaking at 1000 rpm. Aggregates were then sonicated for 60 s in 15 s intervals with a 1 s sonication pulse and a 1 s pause. Aggregates were aliquoted and stored at –80 °C. Preparation of α-Syn aggregates was based on Lohmann et al. 2019 [51]. For characterization, AFM measurements were used [51].

Tau aggregates: Full-length Tau (expressed and purified in-house) was dissolved in TBS buffer (Serva, Duisburg, Germany) containing 10-fold excess TCEP. Tau was centrifuged at 18213 *g* for 1 h at RT and the Tau concentration in the supernatant was determined using UV-Vis spectroscopy. For aggregation, 8 µM heparin and 0.05% sodium azide were added to 15 µM Tau. The mixture was incubated at 37 °C with shaking at 300 rpm every 10 min for 10 days. Tau aggregates were characterized previously including AFM measurement and THT [52].

Fluorescent antibodies

Fluorescently labelled detection antibodies were used for detection of SiNaPs and aggregates. IC16 (Heinrich-Heine-Universität Düsseldorf) was labelled with a red-fluorescent dye (CF633, Sigma-Aldrich), whereas Nab228 (Sigma-Aldrich) was labelled with a green-fluorescent dye (CF488, Sigma-Aldrich). The labelling process, the determination of concentration and degree of labelling are described in the manufacturer's protocol. Purification was carried out with a polyacrylamide bead suspension (Bio-Gel P-30, Bio-Rad Laboratories, Hercules, USA).

Assay setup

Greiner BioOne 384 well plates (Kremsmünster, Austria) were used to ensure an adequate sample and replicate number within one assay. The biochemical principle of sFIDA was described previously[27]. The time course of the sFIDA workflow was illustrated in Fig. 6. For capturing, 40 µl of the humanized monoclonal antibody bapineuzumab (ProteoGenix, Schiltigheim, France) was used at a concentration of 0.625 µg/ml in 0.1 M carbonate buffer (Carl Roth, Karlsruhe, Germany) overnight at 4 °C. Wells were washed using an automated microplate washer (405 LS Microplate Washer, BioTec, VT, USA), with five washing cycles with 80 µl TBS-T (TBS (Serva) containing 0.05% Tween (AppliChem)) and five washing cycles with 80 µl TBS. Washing with TBS-T and TBS was performed after each incubation step. After washing, the remaining binding sites were blocking using 0.5% BSA (AppliChem) in TBS containing 0.03% ProClin (Sigma-Aldrich) for 1.5 h at RT. After washing, we first applied 15 µl of LowCross buffer strong (Candor Bioscience, Wangen, Germany) to the wells to reduce matrix effects and then added 15 µl sample or SiNaPs and aggregates spiked in plasma. Samples were centrifuged at 2500 *g* for 5 min prior to analysis. The supernatant was transferred to a new tube and incubated on the plate for 2 h at RT. Fluorescently labelled IC16 CF633 and Nab228 CF488, each at 0.625 µg/ml in TBS containing 0.03% ProClin were first diluted in 0.1% BSA and 0.05% Tween and then centrifuged for 1 h at 100'000 xg. For detection, 20 µl per well of the probes were incubated for 1 h at RT. The TBS buffer was exchanged with 80 µl TBS-ProClin prior to measurement to prevent bacterial growth during measurement and storage. Calibration standards (SiNaPs and aggregates) were spiked and analysed in plasma to prevent plasma matrix effects on the calibration of the results.

Influence of monomeric $A\beta_{1-40}$ and $A\beta_{1-42}$: $A\beta_{1-40}$ was dissolved at 0.1 µg/ml in HFIP, whereas $A\beta_{1-42}$ was dissolved to 10 µM (approximately 45 µg/ml) and shaken for 24 h at RT and 600 rpm. Prior to analysis, monomeric Aβ was diluted to 25 nM in LowCross buffer strong and then to 100 pM in plasma.

Influence of heterophilic anti-mouse antibodies (HAMA): HAMA interference was analysed by spiking different concentrations of goat anti-mouse antibody (Thermo Fisher Scientific, Waltham, USA) in neat plasma. In addition to the capture antibody bapineuzumab, the Nab228 antibody was

462 coated at 2.5 µg/ml in 0.1 M carbonate buffer to the glass surface to compare their HAMA
463 interference in sFIDA.
464 **Influence of haemolysis:** Non-haemolytic plasma was spiked with different concentrations of
465 haemolytic plasma to examine the effects of red blood cell haemolysis on assay results. Haemolytic
466 plasma was prepared by freezing whole blood at –80 °C for 24 h and centrifugation at 1200 *g* for
467 15 min after thawing. Plasma prepared using this procedure is referred to as 100% haemolytic.

468 Measurement

469 Measurement of the sFIDA assay surface was performed using total internal reflection microscopy
470 (TIRF-M, Leica DMI6000B, Wetzlar, Germany) with 100x magnification, as described previously
471 (excitation: 635 nm, emission filter: 705 nm; excitation: 488 nm, emission filter: 525 nm; exposure
472 time both channels: 1000 ms; gain 1300) [43]. Each image consisted of 1,000,000 pixels
473 (1,000 x 1,000 pixels) and in total, 100 images per sample (25 images per well) were measured,
474 which covers 3.14% of the total well surface.
475 For measurement and calibration of the DELCODE cohort plasma samples, a third fluorescence
476 channel was added (excitation: 405 nm, emission filter: 450 nm) for automated detection and
477 elimination of artificial pixels, as described in statistics.
478

479 sFIDAta

480 The in-house software tool sFIDAta was used for analysis of the images. sFIDAta enables
481 automated detection and elimination of artefact-containing images and counting of pixel above a
482 cutoff value. The cutoff value is defined as the grey-scale value, at which a predefined number of
483 pixels in the blank control are counted and is determined individually for each fluorescence channel
484 and for each experiment to compensate for fluorescence fluctuations. For analysis, a cutoff value
485 of 0.05% (blank control exceeds 500 pixel) was chosen. PixelCount refers to the average number
486 of pixels in an image above the cutoff value for each fluorescent channel, whereas the sFIDA
487 readout describes the number of colocalized pixels that exceed the cutoff value in both

fluorescence channels. Min-max filtering was applied to prevent possible remaining artificial images influencing outcomes after artefact detection. Min-max filtering excluded 10% of images per well with the highest fluorescence and 10% of images per well with the lowest PixelCounts [29].

The measurement procedure was extended by an additional step for analysis of DELCODE cohort samples and for inter-assay measurements. After using a red laser (635 nm) and a green laser (488 nm) to detect the IC16 CF633 and Nab228 CF488 antibodies, respectively, a blue laser (405 nm) was used, which does not target any specific antibody. By comparing the colocalized signals with the signals resulting from the blue laser, artificial autofluorescence signals can be detected and removed. This was performed by subtracting the number of autofluorescence pixels above the calculated cutoff from the number of colocalized pixels (corrected sFIDA readouts).

Statistics

Statistical analyses were performed using Excel 2020 (Microsoft corporation, Redmond, USA), Matlab 2019b (The MathWorks, Natick, USA), OriginPro 2020 (OriginLab Corporation, Northhampton, USA) and python 3.9.7 (Python software foundation, Wilmington, USA; packages: pandas 1.3.4, scipy 1.7.1, seaborn 0.11.2).

Intra-assay precision: The PixelCount, coefficient of variation (CV %) and the sFIDA readout were calculated based on the mean value and standard deviation of the four replicates.

Calibration: Linear regression was performed for dilution experiments and to determine the concentration of aggregates in plasma samples. To this end, PixelCounts of the silica nanoparticles and the aggregate standards were weighted with 1/readout.

Corrected sFIDA readouts were used for calibration of DELCODE plasma samples: Based on these adjusted PixelCounts, the calibration of the samples was carried out using the SiNaPs dilution series between 0 and 125 fM for each of the six plates. After regression, the y-intercept of the regression models was subtracted from the respective calibrated values.

The limit of detection (LOD) and die lower limit of quantification (LLOQ) is described in Eq. (1) and (2) and subsequently converted to a molar concentration using linear regression.

$$LOD\ [pixel] = PixelCount\ (blank\ control) + 1\sigma \quad (1)$$

$$LLOQ\ [pixel] = PixelCount\ (blank\ control) + 10\sigma \quad (2)$$

Analysis of the assay controls is mainly based on colocalization (sFIDA readout).

Inter-assay precision: Inter-assay precision was calculated among six individual experiments. Inter-assay variation for SiNaPs was calculated based on the mean coefficient of variation (CV %) for each concentration and thereafter by calculating the mean among the whole calibration curve. For inter-assay variation of aggregates and samples, we first determined the molar concentrations and afterwards proceeded as described above for inter-assay variation of SiNaPs. The potential significance of experimental differences was further examined by performing ANOVA of repeated measurements for SiNaPs, aggregates and samples with a 5% level of significance.

Dilution linearity: Two-fold dilutions were performed to analyse the influence of dilution on the calibration standard and a simulated plasma sample (aggregates spiked in plasma). sFIDA readouts were calibrated to molar concentrations and corrected by the dilution factor.

Tube transfer: For analysis of the effect of repeated tube transfers on sFIDA readout, 100 µl of plasma were transferred to a new tube, incubated for 5 min at RT and transferred once again (repeated according to the number of tube transfers).

Spike and recovery: A blank plasma sample (reference) and three plasma samples of Control, MCI or AD patients were analysed directly (unspiked) and after spiking with a low (31.3 fM), medium (250 fM) and high (2 pM) concentration of $A\beta_{1-15}$ SiNaPs. Recovery was calculated based on Eq. 3:

$$Recovery[\%] = \frac{sFIDA\ Readout_{spiked\ sample} - sFIDA\ Readout_{non-spiked\ sample}}{sFIDA\ Readout_{spiked\ BC} - sFIDA\ Readout_{non-spiked\ BC}} \quad (3)$$

Pre-analytical and selectivity studies: The effect of freeze-thaw cycles was evaluated using aliquots of six plasma samples, which were thawed repeatedly for 2 h at RT and frozen again [53]. The remaining signal (recovery) and signal reduction for sFIDA readouts of tube transfer, capture control (CC), autofluorescence control (AF), other probes (OP) and immunodepletion (IP) was calculated according to Eq. 4 and Eq. 5 directly, whereas PixelCounts were initially normalized with the blank control.

$$Recovery\ and\ remaining\ signal\ [\%] = \frac{sFIDA\ readout_{assay\ control}}{sFIDA\ readout_{reference}} * 100\% \quad (4)$$

$$signal\ reduction\ [\%] = 100\% - remaining\ signal[\%] \quad (5)$$

DELCODE plasma samples: After calibration, samples below the LOD were set to zero. Calibrated concentrations were first tested for normal distribution. For non-normally distributed data, non-parametric tests like Mann-Whitney-U test and Spearman correlation tests were performed.

Bootstrapping: For testing the significance of the Spearman correlation, bootstrapping was applied to all samples with Aβ oligomer concentrations above LOD. This was achieved by performing 5000 replications of the bootstrapping with replacement and calculating the mean Spearman *r* value of the results. After normalization of the standard deviation, bootstrapping *p*-values were calculated using a normal distribution.

Plasma samples

Plasma of validation cohort: Samples of Control, MCI and AD patients were kindly provided by the working group of Oliver Peters at Charité Berlin from patients. Plasma samples were centrifuged, aliquoted to 500 µl and stored at –80 °C. Samples did not undergo a freeze-thaw cycle prior to analysis. Written, informed consent was obtained from all participants. The number for ethical approval of the Charité Berlin was EA2/118/15.

Plasma of DELCODE cohort: Plasma samples were collected as part of the multicentre DZNE-Longitudinal Cognitive Impairment and Dementia Study (DELCODE) at ten clinical centres in Germany, according to a standard operating procedure. After processing, plasma samples were stored at –80 °C [39]. The project was approved by the ethical committee of the Charité Berlin (EA1/074/21 and EA4/066/17).

We received plasma samples from 429 patients, including healthy Controls (*n* = 44), SCD (*n* = 148), MCI (*n* = 92), AD patients (*n* = 52) and first-degree relatives of AD patients (*n* = 30). Sixty-two samples were excluded from analysis because of contamination in one experiment, one sample was excluded because of missing data and seven samples were excluded because of haemolysis. Besides testing cognitive function using different neuropsychological tests (i.e., mini mental state

examination (MMSE), Alzheimer's disease assessment scale (ADAS), clinical dementia rating), CSF and plasma biomarkers like $A\beta_{1-40}$, $A\beta_{1-42}$, tau phosphorylated at threonine 181 (pTau) and total tau (tTau) were determined. Information on patient selection, sampling of blood and CSF, neuropathological tests and biomarker quantification are described in Jessen et al. [39]. Subdivision of patient groups by amyloid pathology is based on the $A\beta_{1-42}/A\beta_{1-40}$ ratio with previously established limits [54].

References

1 Cummings, J. *et al.* Alzheimer's disease drug development pipeline: 2022. *Alzheimers Dement (N Y)* **8**, e12295 (2022). https://doi.org:10.1002/trc2.12295

2 Cline, E. N., Bicca, M. A., Viola, K. L. & Klein, W. L. The Amyloid-β Oligomer Hypothesis: Beginning of the Third Decade. *J Alzheimers Dis* **64**, S567-s610 (2018). https://doi.org:10.3233/jad-179941

3 Hampel, H. *et al.* The Amyloid-β Pathway in Alzheimer's Disease. *Molecular Psychiatry* **26**, 5481-5503 (2021). https://doi.org:10.1038/s41380-021-01249-0

4 Mroczko, B., Groblewska, M., Litman-Zawadzka, A., Kornhuber, J. & Lewczuk, P. Amyloid beta oligomers (AbetaOs) in Alzheimer's disease. *J Neural Transm (Vienna)* **125**, 177-191 (2018). https://doi.org:10.1007/s00702-017-1820-x

5 Hladky, S. B. & Barrand, M. A. Mechanisms of fluid movement into, through and out of the brain: evaluation of the evidence. *Fluids Barriers CNS* **11**, 26 (2014). https://doi.org:10.1186/2045-8118-11-26

6 Holtta, M. *et al.* Evaluating amyloid-beta oligomers in cerebrospinal fluid as a biomarker for Alzheimer's disease. *PLoS One* **8**, e66381 (2013). https://doi.org:10.1371/journal.pone.0066381

7 Savage, M. J. *et al.* A sensitive abeta oligomer assay discriminates Alzheimer's and aged control cerebrospinal fluid. *J Neurosci* **34**, 2884-2897 (2014). https://doi.org:10.1523/JNEUROSCI.1675-13.2014

8 Herskovits, A. Z., Locascio, J. J., Peskind, E. R., Li, G. & Hyman, B. T. A Luminex assay detects amyloid beta oligomers in Alzheimer's disease cerebrospinal fluid. *PLoS One* **8**, e67898 (2013). https://doi.org:10.1371/journal.pone.0067898

9 Wang-Dietrich, L. *et al.* The amyloid-beta oligomer count in cerebrospinal fluid is a biomarker for Alzheimer's disease. *J Alzheimers Dis* **34**, 985-994 (2013). https://doi.org:10.3233/JAD-122047

10 Xin, S. H., Tan, L., Cao, X., Yu, J. T. & Tan, L. Clearance of Amyloid Beta and Tau in Alzheimer's Disease: from Mechanisms to Therapy. *Neurotox Res* **34**, 733-748 (2018). https://doi.org:10.1007/s12640-018-9895-1

11 Wang, J., Gu, B. J., Masters, C. L. & Wang, Y. J. A systemic view of Alzheimer disease - insights from amyloid-β metabolism beyond the brain. *Nat Rev Neurol* **13**, 612-623 (2017). https://doi.org:10.1038/nrneurol.2017.111

12 Liu, L. *et al.* An ultra-sensitive immunoassay detects and quantifies soluble Aβ oligomers in human plasma. *Alzheimers Dement* **18**, 1186-1202 (2022). https://doi.org:10.1002/alz.12457

13 Xia, W. *et al.* A specific enzyme-linked immunosorbent assay for measuring beta-amyloid protein oligomers in human plasma and brain tissue of patients with Alzheimer disease. *Arch Neurol* **66**, 190-199 (2009). https://doi.org:10.1001/archneurol.2008.565

14 Kurz, C., Walker, L., Rauchmann, B. S. & Perneczky, R. Dysfunction of the blood-brain barrier in Alzheimer's disease: Evidence from human studies. *Neuropathol Appl Neurobiol* **48**, e12782 (2022). https://doi.org:10.1111/nan.12782

15 An, S. S. A. *et al.* Dynamic changes of oligomeric amyloid β levels in plasma induced by spiked synthetic Aβ(42). *Alzheimers Res Ther* **9**, 86 (2017). https://doi.org:10.1186/s13195-017-0310-6

16 Dominguez, J. C. *et al.* Multimer Detection System-Oligomerized Amyloid Beta (MDS-OAβ): A Plasma-Based Biomarker Differentiates Alzheimer's Disease from Other Etiologies of Dementia. *Int J Alzheimers Dis* **2022**, 9960832 (2022). https://doi.org:10.1155/2022/9960832

17 Santos, A. N., Simm, A., Holthoff, V. & Boehm, G. A method for the detection of amyloid-beta1-40, amyloid-beta1-42 and amyloid-beta oligomers in blood using magnetic beads in combination with Flow cytometry and its application in the diagnostics of Alzheimer's disease. *J Alzheimers Dis* **14**, 127-131 (2008). https://doi.org:10.3233/jad-2008-14201

18 Huang, Y. R. & Liu, R. T. The Toxicity and Polymorphism of β-Amyloid Oligomers. *Int J Mol Sci* **21** (2020). https://doi.org:10.3390/ijms21124477

19 Fändrich, M. Oligomeric intermediates in amyloid formation: structure determination and mechanisms of toxicity. *J Mol Biol* **421**, 427-440 (2012). https://doi.org:10.1016/j.jmb.2012.01.006

20 Meng, X. *et al.* Association between increased levels of amyloid-β oligomers in plasma and episodic memory loss in Alzheimer's disease. *Alzheimers Res Ther* **11**, 89 (2019). https://doi.org:10.1186/s13195-019-0535-7

21 Wang, M. J. *et al.* Oligomeric forms of amyloid-β protein in plasma as a potential blood-based biomarker for Alzheimer's disease. *Alzheimers Res Ther* **9**, 98 (2017). https://doi.org:10.1186/s13195-017-0324-0

22 Lee, J. C., Kim, S. J., Hong, S. & Kim, Y. Diagnosis of Alzheimer's disease utilizing amyloid and tau as fluid biomarkers. *Experimental & Molecular Medicine* **51**, 1-10 (2019). https://doi.org:10.1038/s12276-019-0250-2

23 Babapour Mofrad, R. *et al.* Plasma amyloid-β oligomerization assay as a pre-screening test for amyloid status. *Alzheimers Res Ther* **13**, 133 (2021). https://doi.org:10.1186/s13195-021-00873-w

24 Zhou, L. *et al.* Plasma amyloid-β oligomers level is a biomarker for Alzheimer's disease diagnosis. *Biochem Biophys Res Commun* **423**, 697-702 (2012). https://doi.org:10.1016/j.bbrc.2012.06.017

25 Shea, D. *et al.* SOBA: Development and testing of a soluble oligomer binding assay for detection of amyloidogenic toxic oligomers. *Proc Natl Acad Sci U S A* **119**, e2213157119 (2022). https://doi.org:10.1073/pnas.2213157119

26 Kulawik, A., Heise, H., Zafiu, C., Willbold, D. & Bannach, O. Advancements of the sFIDA method for oligomer-based diagnostics of neurodegenerative diseases. *FEBS Lett* **592**, 516-534 (2018). https://doi.org:10.1002/1873-3468.12983

27 Herrmann, Y. *et al.* Nanoparticle standards for immuno-based quantitation of alpha-synuclein oligomers in diagnostics of Parkinson's disease and other synucleinopathies. *Clin Chim Acta* **466**, 152-159 (2017). https://doi.org:10.1016/j.cca.2017.01.010

28 Hülsemann, M. *et al.* Biofunctionalized Silica Nanoparticles: Standards in Amyloid-beta Oligomer-Based Diagnosis of Alzheimer's Disease. *J Alzheimers Dis* **54**, 79-88 (2016). https://doi.org:10.3233/JAD-160253

29 Bloemeke, L. *et al.* Quantitative detection of alpha-Synuclein and Tau oligomers and other aggregates by digital single particle counting. *NPJ Parkinsons Dis* **8**, 68 (2022). https://doi.org:10.1038/s41531-022-00330-x

30 Sehlin, D. *et al.* Interference from heterophilic antibodies in amyloid-beta oligomer ELISAs. *J Alzheimers Dis* **21**, 1295-1301 (2010). https://doi.org:10.3233/jad-2010-100609

31 Kulenkampff, K., Wolf Perez, A.-M., Sormanni, P., Habchi, J. & Vendruscolo, M. Quantifying misfolded protein oligomers as drug targets and biomarkers in Alzheimer and Parkinson diseases. *Nature Reviews Chemistry* **5**, 277-294 (2021). https://doi.org:10.1038/s41570-021-00254-9

32 Pils, M. *et al.* Development and Implementation of an Internal Quality Control Sample to Standardize Oligomer-Based Diagnostics of Alzheimer’s Disease. *Diagnostics* **13**, 1702 (2023). https://doi.org:10.3390/diagnostics13101702

33 Janelidze, S. *et al.* Plasma β-amyloid in Alzheimer's disease and vascular disease. *Sci Rep* **6**, 26801 (2016). https://doi.org:10.1038/srep26801

34 Miles, L. A., Crespi, G. A., Doughty, L. & Parker, M. W. Bapineuzumab captures the N-terminus of the Alzheimer's disease amyloid-beta peptide in a helical conformation. *Sci Rep* **3**, 1302 (2013). https://doi.org:10.1038/srep01302

35 Mohammadi, M. M. & Bozorgi, S. Investigating the presence of human anti-mouse antibodies (HAMA) in the blood of laboratory animal care workers. *Journal of Laboratory Medicine* **43**, 87-91 (2019). https://doi.org:doi:10.1515/labmed-2018-0084

36 Hsieh, S.-Y., Chen, R.-K., Pan, Y.-H. & Lee, H.-L. Systematical evaluation of the effects of sample collection procedures on low-molecular-weight serum/plasma proteome profiling. *PROTEOMICS* **6**, 3189-3198 (2006). https://doi.org:https://doi.org/10.1002/pmic.200500535

37 Kuo, Y. M. *et al.* Amyloid-beta peptides interact with plasma proteins and erythrocytes: implications for their quantitation in plasma. *Biochem Biophys Res Commun* **268**, 750-756 (2000). https://doi.org:10.1006/bbrc.2000.2222

685 38 Willemse, E. *et al.* How to handle adsorption of cerebrospinal fluid amyloid β (1-42) in laboratory
686 practice? Identifying problematic handlings and resolving the issue by use of the Aβ(42)/Aβ(40)
687 ratio. *Alzheimers Dement* **13**, 885-892 (2017). https://doi.org:10.1016/j.jalz.2017.01.010
688 39 Jessen, F. *et al.* Design and first baseline data of the DZNE multicenter observational study on
689 predementia Alzheimer's disease (DELCODE). *Alzheimers Res Ther* **10**, 15 (2018).
690 https://doi.org:10.1186/s13195-017-0314-2
691 40 Gratuze, M., Leyns, C. E. G. & Holtzman, D. M. New insights into the role of TREM2 in
692 Alzheimer's disease. *Mol Neurodegener* **13**, 66 (2018). https://doi.org:10.1186/s13024-018-
693 0298-9
694 41 Yamazaki, Y., Zhao, N., Caulfield, T. R., Liu, C. C. & Bu, G. Apolipoprotein E and Alzheimer
695 disease: pathobiology and targeting strategies. *Nat Rev Neurol* **15**, 501-518 (2019).
696 https://doi.org:10.1038/s41582-019-0228-7
697 42 Horwitz, W. & Albert, R. The Horwitz ratio (HorRat): A useful index of method performance with
698 respect to precision. *J AOAC Int* **89**, 1095-1109 (2006). https://doi.org:10.1093/jaoac/89.4.1095
699 43 Herrmann, Y. *et al.* sFIDA automation yields sub-femtomolar limit of detection for Abeta
700 aggregates in body fluids. *Clin Biochem* **50**, 244-247 (2017).
701 https://doi.org:10.1016/j.clinbiochem.2016.11.001
702 44 Kim, K. Y. *et al.* Plasma amyloid-beta oligomer is related to subjective cognitive decline and
703 brain amyloid status. *Alzheimer's Research & Therapy* **14**, 162 (2022).
704 https://doi.org:10.1186/s13195-022-01104-6
705 45 Jessen, F. *et al.* The characterisation of subjective cognitive decline. *Lancet Neurol* **19**, 271-278
706 (2020). https://doi.org:10.1016/s1474-4422(19)30368-0
707 46 Jack, C. R., Jr. *et al.* NIA-AA Research Framework: Toward a biological definition of Alzheimer's
708 disease. *Alzheimers Dement* **14**, 535-562 (2018). https://doi.org:10.1016/j.jalz.2018.02.018
709 47 Olsson, B. *et al.* CSF and blood biomarkers for the diagnosis of Alzheimer's disease: a
710 systematic review and meta-analysis. *Lancet Neurol* **15**, 673-684 (2016).
711 https://doi.org:10.1016/S1474-4422(16)00070-3
712 48 O'Bryant, S. E., Petersen, M., Hall, J. & Johnson, L. A. Medical comorbidities and ethnicity
713 impact plasma Alzheimer's disease biomarkers: Important considerations for clinical trials and
714 practice. *Alzheimers Dement* (2022). https://doi.org:10.1002/alz.12647

49 Schaffrath, A. *et al.* Patients with isolated REM-sleep behavior disorder have elevated levels of alpha-synuclein aggregates in stool. *npj Parkinson's Disease* **9**, 14 (2023). https://doi.org:10.1038/s41531-023-00458-4

50 Kutzsche, J. *et al.* Safety and pharmacokinetics of the orally available antiprionic compound PRI-002: A single and multiple ascending dose phase I study. *Alzheimers Dement (N Y)* **6**, e12001 (2020). https://doi.org:10.1002/trc2.12001

51 Lohmann, S. *et al.* Oral and intravenous transmission of α-synuclein fibrils to mice. *Acta Neuropathol* **138**, 515-533 (2019). https://doi.org:10.1007/s00401-019-02037-5

52 Altendorf, T. *et al.* Stabilization of Monomeric Tau Protein by All D-Enantiomeric Peptide Ligands as Therapeutic Strategy for Alzheimer's Disease and Other Tauopathies. *Int J Mol Sci* **24** (2023). https://doi.org:10.3390/ijms24032161

53 Andreasson, U. *et al.* A Practical Guide to Immunoassay Method Validation. *Front Neurol* **6**, 179 (2015). https://doi.org:10.3389/fneur.2015.00179

54 Jessen, F. *et al.* Subjective cognitive decline and stage 2 of Alzheimer disease in patients from memory centers. *Alzheimers Dement* (2022). https://doi.org:10.1002/alz.12674

55 Lucey, B. P. & Bateman, R. J. Amyloid-β diurnal pattern: possible role of sleep in Alzheimer's disease pathogenesis. *Neurobiology of Aging* **35**, S29-S34 (2014). https://doi.org:https://doi.org/10.1016/j.neurobiolaging.2014.03.035

56 Lucey, B. P. *et al.* Effect of sleep on overnight cerebrospinal fluid amyloid β kinetics. *Ann Neurol* **83**, 197-204 (2018). https://doi.org:10.1002/ana.25117

Figures and Tables

Table 1 Demographic information and biomarker concentrations of participants from the DELCODE cohort (mean ± standard deviation; SCD: subjective cognitive decline, MCI: mild cognitive impairment, AD: Alzheimer's Disease)

	Controls	Relatives	SCD	MCI	AD
Patient information					
number	44	30	146	88	51
% female	45%	63%	42%	45%	67%
Age [years]	68.7 ± 5.2	65.7 ±5.0	70.8 ± 6.0	71.4 ± 5.0	75.9 ± 5.7
Education [years]	14.5 ± 2.5	14.4 ± 2.7	15.2 ± 2.8	13.6 ±2.8	13.1 ± 3.1
MMSE	29.6 ± 0.6	29.2 ± 1.1	29.2 ± 1.1	27.5 ± 2.0	23.2 ± 3.3
ApoE ε4 positive	8 (18.2%)	11 (36.7%)	46 (31.5%)	40* (46.0%)	31 (60.8%)
ε2/4	0	1 (3.3%)	4 (2.7%)	3* (3.4%)	2 (3.9%)
ε3/4	8 (18.2%)	10 (33.3%)	39 (26.7%)	32* (36.8%)	21 (41.2%)
ε 4/4	0	0	3 (2.1%)	5* (5.7%)	8 (15.7%)
CSF biomarkers					
$A\beta_{1-40}$ [pg/ml]	9321.1 ± 2617.7	8675.0 ± 2412.6	8679.5 ± 2213.3	8158.6 ± 2378.5	8179.5 ± 2475.2
$A\beta_{1-42}$ [pg/ml]	875.2 ± 344.4	903.6 ± 353.1	808.6 ± 355.3	604.7 ± 309.7	426.6 ± 211.9
$A\beta_{1-42}/A\beta_{1-40}$	0.094 ± 0.024	0.103 ± 0.024	0.092 ± 0.028	0.075 ± 0.030	0.053 ± 0.018
tTau [pg/ml]	413.3 ± 185.1	333.0 ± 135.9	379.1 ± 194.3	532.5 ± 287.4	744.2 ± 344.2
pTau [pg/ml]	54.9 ± 22.6	49.8 ± 20.3	55.9 ± 24.1	69.7 ± 43.3	89.7 ± 34.1
Plasma biomarkers					
$A\beta_{1-40}$ [pg/ml]	76.9 ± 18.7	74.6 ± 19.0	84.3 ± 20.0	86.1 ± 20.8	94.5 ± 28.0
$A\beta_{1-42}$ [pg/ml]	8.8 ± 1.9	8.5 ± 1.7	9.1 ± 1.9	8.5 ± 2.1	9.1 ± 2.5
$A\beta_{1-42}/A\beta_{1-40}$	0.117 ± 0.022	0.115 ± 0.013	0.110 ± 0.015	0.099 ± 0.014	0.094 ± 0.019

*data not available for one patient

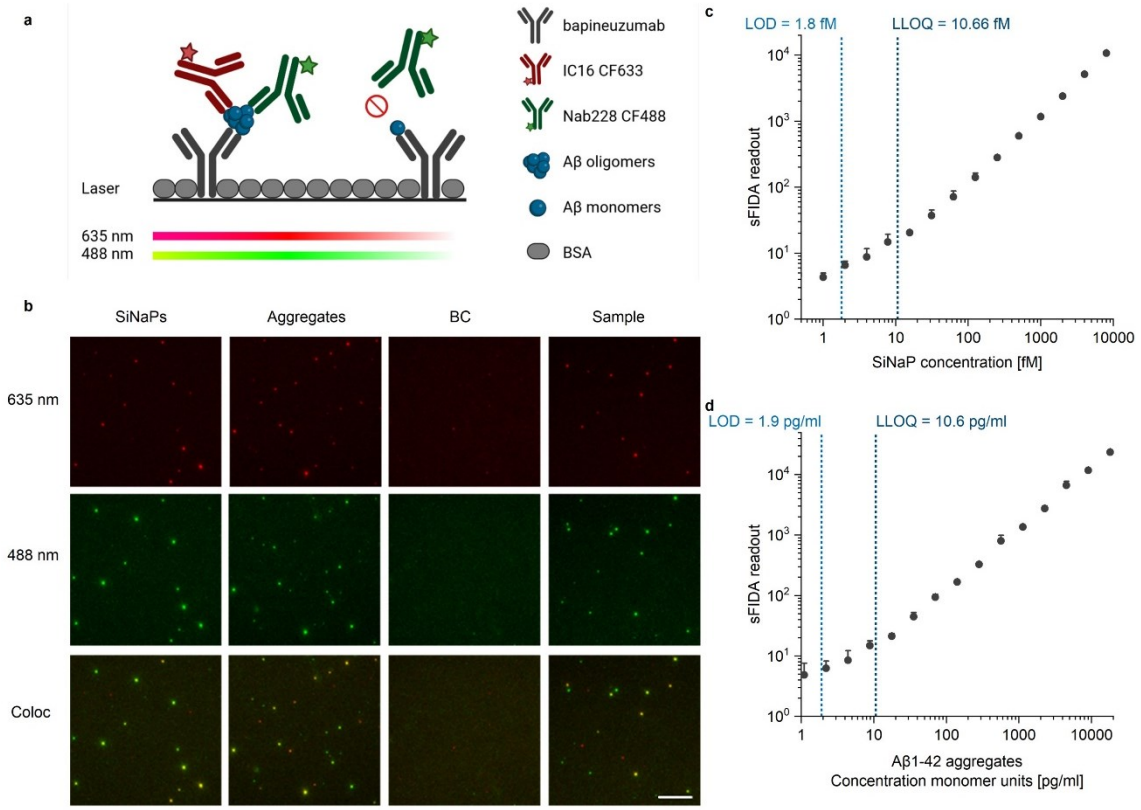

743

744 **Fig. 1 Principle of sFIDA setup, imaging and calibration. a** The biochemical principle of sFIDA is
745 similar to a sandwich ELISA with capture and detection antibodies directed against overlapping epitopes
746 of the Aβ N-terminus. Therefore, monomers can be captured but not detected as the epitope is already
747 occupied. After preparation, the assay surface is imaged using dual colour fluorescence microscopy
748 (635 and 488 nm, respectively). *Created with biorender.com* **b** Exemplary images of 500 fM SiNaPs
749 coated with $A\beta_{1-15}$, aggregates composed of 564 pg/ml $A\beta_{1-42}$, a blank plasma (blank control, BC) and
750 an AD plasma sample for the red (illumination with 635 nm) and green (illumination with 488 nm)
751 fluorescence channels and colocalization. For imaging, the gray-scale value of 14-bit images was
752 adjusted to min and max values of 750 and 7500, respectively. The scale bar is 50 µm. **c** Calibration
753 curve of 1 fM to 8 pM $A\beta_{1-15}$ SiNaPs for the colocalization. **d** Dilution series of $A\beta_{1-42}$ aggregates
754 consisting of 1.1 to 18,060 pg/ml $A\beta_{1-42}$ monomers. The standard deviation was calculated across the
755 four replicates. Limit of detection (LOD) and lower limit of quantification (LLOQ) were calculated as BC
756 with a single- or ten-fold standard deviation. Please note the logarithmic scale.

757

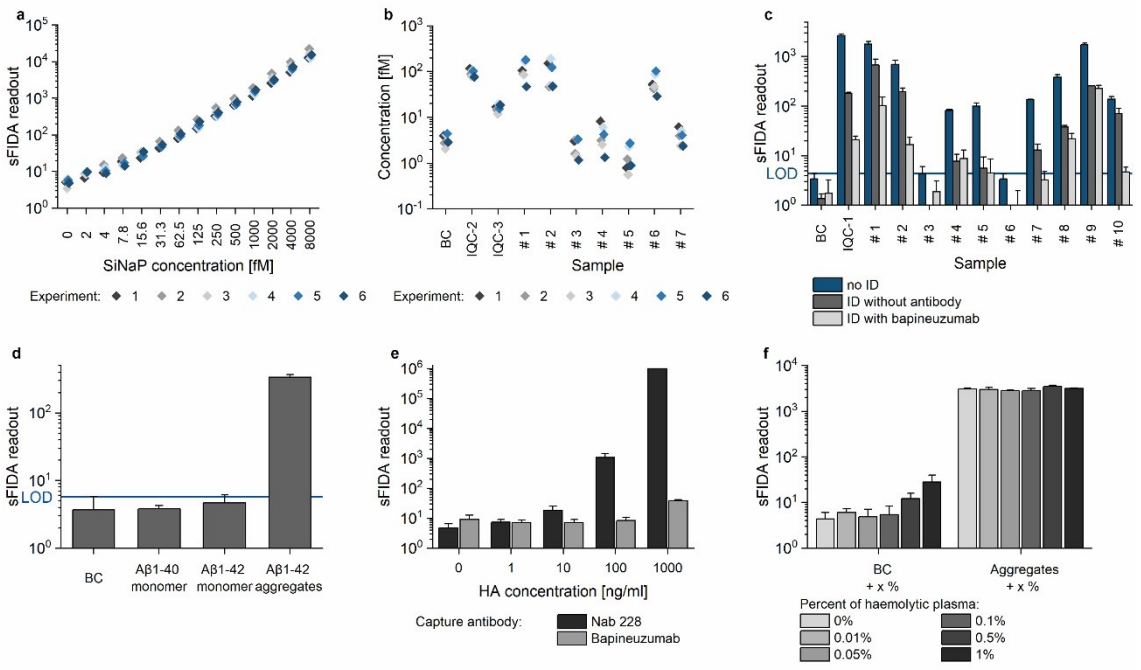

758

759 **Fig. 2 Inter-assay variation (a, b) and specificity controls for Aβ oligomer quantification in plasma**
760 **(c-f). a** Repeated preparation of SiNaP calibration in six individual experiments showed an inter-assay
761 variation of 19.3%. **b** Repeated measurements of seven samples of the validation cohort, a blank plasma
762 (BC) and two internal quality controls (IQC, refers to aggregates at 141 pg/ml (IQC-2) and 17.6 pg/ml
763 $A\beta_{1-42}$ monomers (IQC-3), respectively) were calibrated and mean inter-assay variation was calculated
764 as 41.9%. **c** A blank control, $A\beta_{1-42}$ aggregates (IQC-1 with 18 ng/ml $A\beta_{1-42}$ monomer concentration)
765 and 10 plasma samples of Control, MCI and AD patients were subjected to immunodepletion (ID).
766 Unspecific ID (beads without antibody conjugation) resulted in a signal reduction to 6.9% for IQC-1 and
767 to 20.2% for plasma samples for signals above the LOD (limit of detection). However, with specific
768 immunodepletion using bapineuzumab, the signal of IQC-1 was eliminated (signal <1% compared to the
769 non-depleted sample) and that of the samples was reduced on average to 5.1%. **d** Blank plasma (BC)
770 was spiked with 452 pg/ml of $A\beta_{1-40}$, $A\beta_{1-42}$ monomer and aggregates formed from 452 pg/ml $A\beta_{1-42}$
771 monomer. Samples were analysed by sFIDA. **e** Plasma was spiked with different concentrations of
772 heterophilic antibody (HA) and analysed in two different assay setups, i.e., with monoclonal mouse
773 antibody Nab228 as the capture antibody or with monoclonal humanized antibody bapineuzumab,
774 respectively, to investigate heterophilic antibody interference. **f** Blank plasma and 18 ng/ml Aβ
775 aggregates (concentration based on the monomer unit concentration) were spiked with haemolytic
776 plasma and the effect on detection of aggregates was analysed. Standard deviations were calculated
777 across the four replicates. Please, note the logarithmic scaling.

778

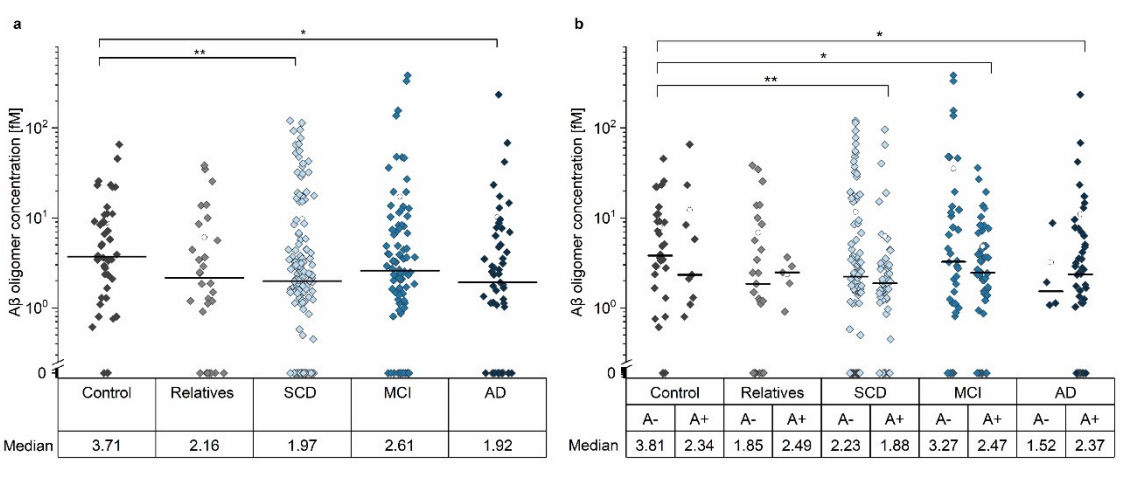

779 **Fig. 3 Concentrations of Aβ oligomers in plasma samples. a** Aβ oligomer concentrations in plasma
780 decreased significantly in SCD and AD patients compared to the Control group. **b** After subdivision by
781 amyloid pathology (A, , based on CSF $A\beta_{1-42}/A\beta_{1-40}$ ratio [39]), SCD, MCI and AD patients positive for
782 amyloid pathology (A+) showed significantly decreased Aβ oligomer concentrations in plasma compared
783 to the amyloid negative (A-) Control group. Please note the logarithmic scale. Samples that fell below
784 LOD were set to zero. For reasons of clarity, the median Aβ oligomer concentrations are given for each
785 analysis group below *the logarithmically scaled* figures (Median; values in fM). SCD: subjective cognitive
786 decline; MCI: mild cognitive impairment; AD: Alzheimer's disease; open circle: mean; line: median, * *p*-
787 value of Mann-Whitney-U test 0.01 - 0.05; ** *p*-value of Mann-Whitney-U test 0.001 - 0.01.

788

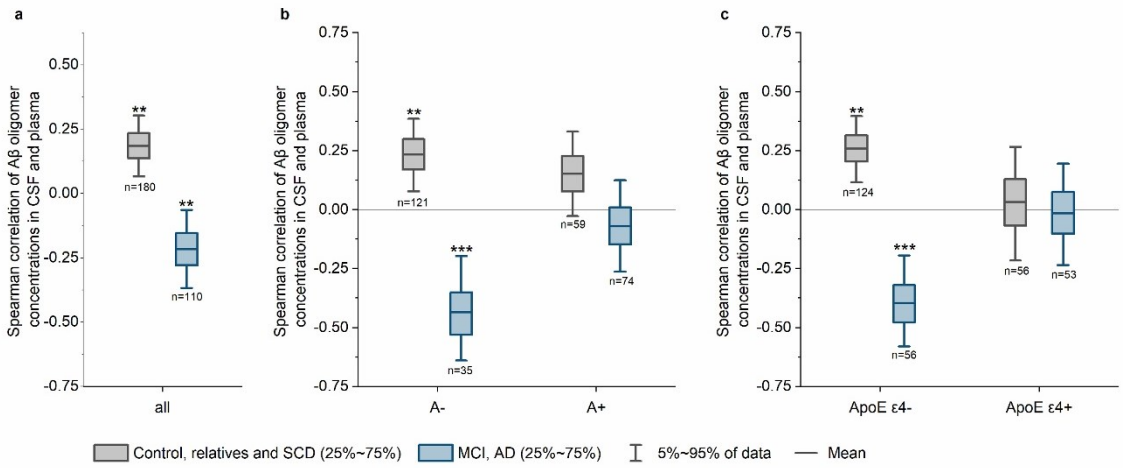

789 **Fig. 4 Box plots for the bootstrap distribution of the Spearman coefficient of correlation r**
790 **between Aβ oligomer levels in CSF and plasma. a** The combined group of Controls, relatives and
791 SCD patients (grey) showed a weak, but significant direct correlation of Aβ oligomer levels in CSF and
792 plasma (Spearman r = 0.164), whereas MCI and AD patients (blue) showed an inverse correlation (blue,
793 Spearman r = -0.157). **b** The groups were sub-divided by the presence of CSF amyloid pathology (A-
794 /A+) based on the ratio of $A\beta_{1-42}/A\beta_{1-40}$. **c** The groups were sub-divided based on their ApoE ε4 status
795 where carrying at least one ApoE ε4 allele defines positivity (ApoE ε4+). Only for amyloid negative (A-)
796 or ApoE ε4 negative patients, significant correlations between oligomers in CSF and plasma were
797 observed with the Control, relatives and SCD patients showing a direct correlation and MCI and AD
798 patients an inverse correlation. p-value of Spearman r distribution: * p-value 0.01 – 0.05, ** p-value
799 0.001 – 0.01, *** p-value <0.001

800

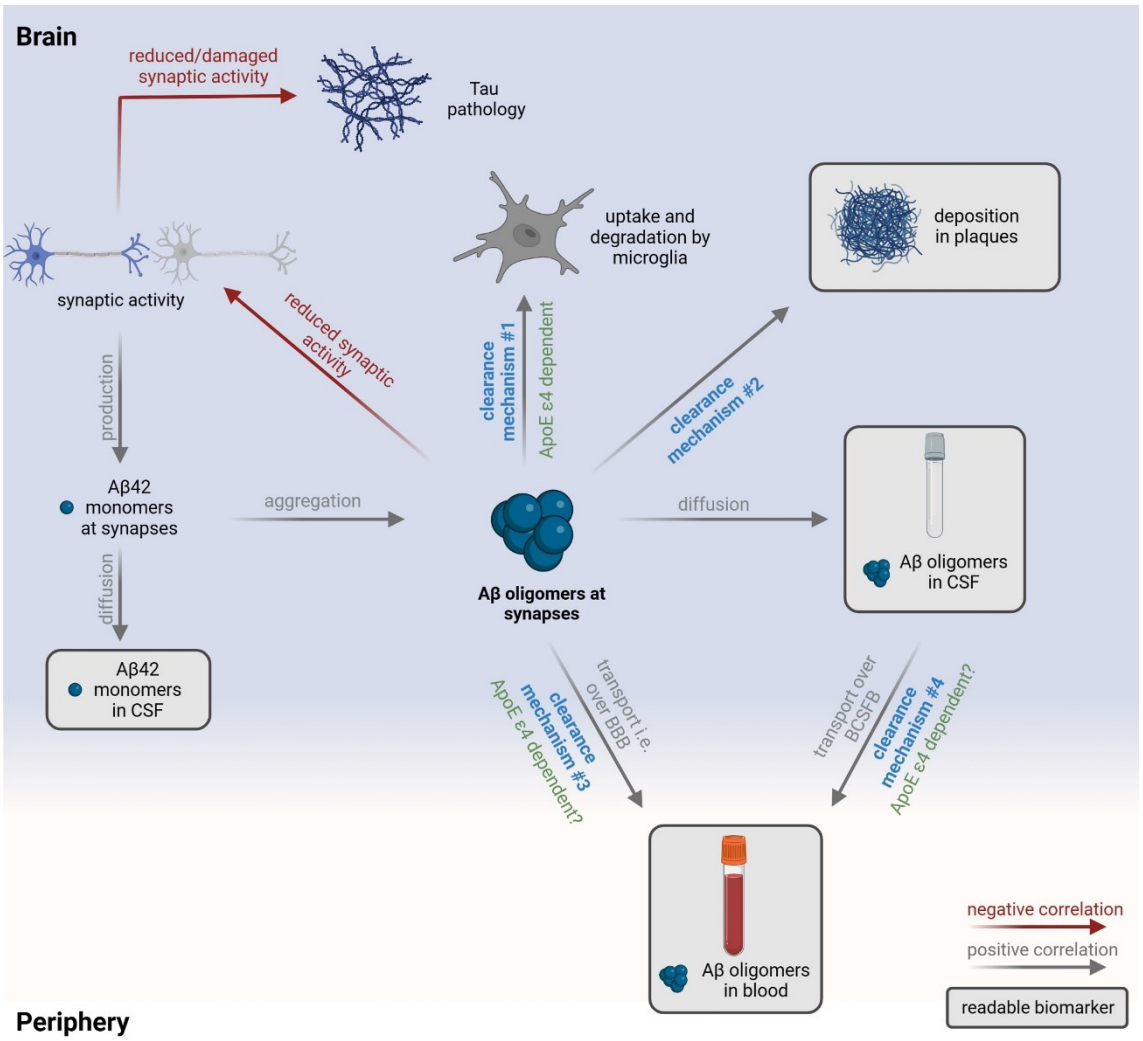

Fig. 5 Model of the clearance mechanisms for Aβ oligomers and the influence on the use of Aβ oligomers as biomarker. Aβ monomer production at synapses is dependent on synaptic activity [55,56]. At a certain time point, aggregation of Aβ monomers leads to the formation of toxic Aβ oligomers that can be cleared by different mechanisms: Aβ oligomers can be degraded by microglia (clearance mechanism #1), diffuse into CSF or deposited into plaques (clearance mechanism #2). Moreover, Aβ oligomers may be transported to blood either directly across the BBB via glymphatic clearance or interstitial flow (clearance mechanism #3), or after diffusion into CSF and reaching blood via BCSFB (clearance mechanism #4). Formation of plaques in patients with amyloid pathology allows oligomers to be deposited (clearance mechanism #2), which may become the preferred fate of Aβ oligomers. This may lead to reduced clearance to blood and reduced Aβ oligomer concentrations in plasma. Additionally, transport of Aβ oligomers from the brain and CSF to plasma may be inefficient in ApoE ε4 carriers influencing correlation analysis. *Created with BioRender.com*

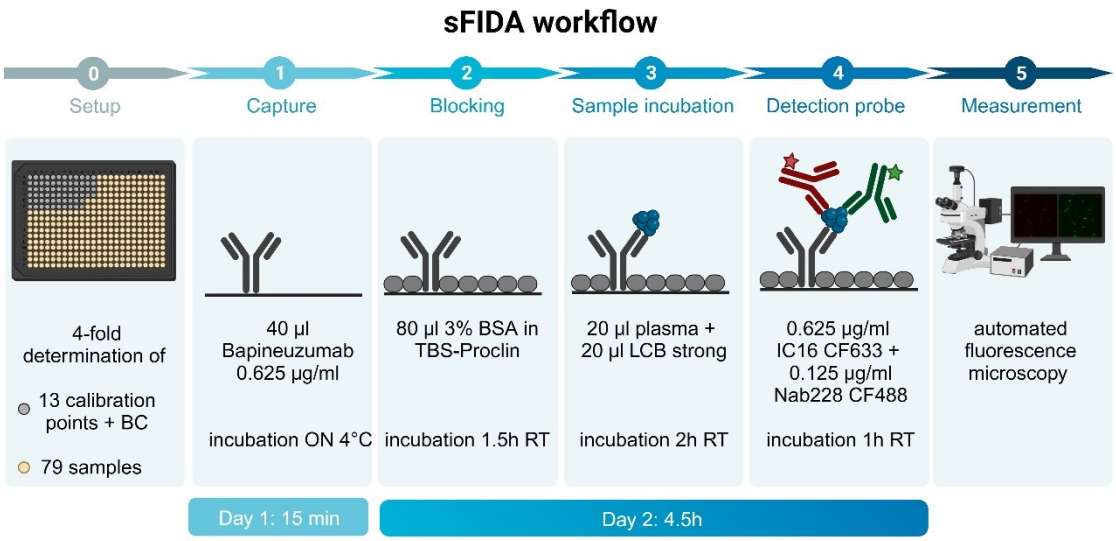

814

815 **Fig. 6 Time course of the sFIDA workflow.** The use of 384 well plates allow a close-meshed
816 concentration series and the determination of 79 patient samples on one plate in 4-fold replicate
817 determination. The individual steps consist of an over night (ON) incubation of the capture antibody at
818 4°C, a 1.5 h blocking step at room temperature (RT) followed by 2 h incubation of the plasma samples
819 and 1 h incubation of detection antibodies. The final measurement is conducted by an automated
820 fluorescence microscope. *Created with BioRender.com*

821

3.5 Elevated Aβ aggregates in feces from Alzheimer's disease patients: a proof-of-concept study

Autoren:	Marlene Pils, Alexandra Dybala, Anja Schaffrath, Fabian Rehn, Janine Kutzsche, Lara Blömeke, Markus Tusche, Pelin Özdüzenciler, Tuyen Bujnicki, Victoria Kraemer-Schulien, Hannes Gramespacher, Maximilian H.T. Schmieschek, Michael T. Barbe, Oezguer A. Onur, Gereon R. Fink, Gültekin Tamgüney, Oliver Bannach und Dieter Willbold
Journal:	Alzheimer's Research and Therapy (im Review)
DOI:	/
Impact-Faktor:	9.0 (2022)
Beitrag:	Eigenanteil: 10 % Etablierung des Aggregationsprotokolls und des Protokolls für die Immunodepletion im sFIDA Unterstützung bei der analytischen Validierung und Statistik Diskussion der Ergebnisse Prüfung des Manuskripts
Anhang zum Manuskript	Kapitel 3.5

Elevated Aβ aggregates in feces from Alzheimer's disease patients: a proof-of-concept study

Marlene Pils [1,2], Alexandra Dybala [3], Anja Schaffrath [1], Fabian Rehn [1,2], Janine Kutzsche [1], Lara Blömeke [1], Markus Tusche [1], Pelin Özdüzenciler [1], Tuyen Bujnicki [1], Victoria Kraemer-Schulien [1], Hannes Gramespacher[4], Maximilian H.T. Schmieschek[4], Michael T. Barbe[4], Oezguer A. Onur[4,5], Gereon R. Fink[4,5], Gültekin Tamgüney[1,3], Oliver Bannach[1,2] and Dieter Willbold[1,2,3*]

Affiliations

[1] Institute of Biological Information Processing, Structural Biochemistry (IBI-7), Forschungszentrum Jülich, Jülich, 52428, Germany
[2] attyloid GmbH, Düsseldorf, 40225, Germany
[3] Institut für Physikalische Biologie, Heinrich-Heine-Universität Düsseldorf, Düsseldorf, 40225, Germany
[4] Department of Neurology, Faculty of Medicine and University Hospital Cologne, University of Cologne, Köln, 50923, Germany
[5] Cognitive Neuroscience, Institute of Neuroscience and Medicine (INM-3), Jülich Research Centre, Jülich, 52428, Germany

*Correspondence:
Prof. Dr. Dieter Willbold
Institute of Biological Information Processing (IBI-7)
Forschungszentrum Jülich,
Wilhelm-Johnen-Straße, 52428 Jülich
Germany
E-Mail: d.willbold@fz-juelich.de
Phone.: +492461612100
Fax: +492461612023

Abstract

Background

Misfolding and aggregation of amyloid β (Aβ), along with neurofibrillary tangles consisting of aggregated Tau species, are pathological hallmarks of Alzheimer's disease (AD) onset and progression. In this study, we hypothesized the clearance of Aβ aggregates from the brain and body into the gut.

Methods

To investigate this, we used surface-based fluorescence intensity distribution analysis (sFIDA) to determine the Aβ aggregate concentrations in feces from 26 AD patients and 31 healthy controls (HC).

Results

Aβ aggregates were detectable in human feces and their concentrations were elevated in AD patients compared to HC (specificity 90.3%, sensitivity 53.8%).

Conclusion

Thus, fecal Aβ aggregates constitute a non-invasive biomarker candidate for diagnosing AD. Whether digestion-resistant Aβ aggregates in feces are secreted via the liver and bile or directly from the enteric neuronal system remains to be elucidated.

Keywords: amyloidosis, Aβ oligomer quantitation, sFIDA, brain-gut-microbiota axis, leaky gut, fecal/stool sampes, clearance

Background

Alzheimer's disease (AD) is the most prevalent age-related cause of dementia, characterized by neurodegenerative processes ultimately leading to neuronal loss in the hippocampus and cerebral cortex. Due to neurodegeneration, a progressive decline of cognitive functions, especially learning and memory, is observed [1]. AD is neuropathologically characterized by the progressive accumulation of extracellular senile plaques composed of fibrillar amyloid β (Aβ) peptides and of intracellular neurofibrillary tangles composed of tau proteins [2, 3]. Furthermore, recent evidence indicates that smaller soluble Aβ protein and tau aggregates like oligomers cause and promote pathological processes due to neurotoxicity [3, 4].

Based on various aspects, including disturbances along the brain-gut-microbiota axis [5-9], liver-mediated Aβ clearance and elimination by bile [10-12], and the consequences of a disturbed blood-brain barrier and a permeable intestinal barrier [6, 7, 13, 14], the presence of Aβ aggregates in feces can be assumed. Initial studies have confirmed an association between AD and increased intestinal or fecal Aβ concentrations, irrespectively of conformational structure [15-18]. Protein aggregation occurs in various neurodegenerative disorders, and it often precedes the appearance of clinical symptoms for several years or even decades [19]. Therefore, we hypothesized that clearance mechanisms must exist that reduce the aggregate load in the brain and body by disposing Aβ aggregates via gut. Consequently, fecal Aβ aggregates may also serve as a biomarker candidate for non-invasive AD diagnosis.

We previously developed surface-based fluorescence intensity distribution analysis (sFIDA), a platform technology for quantitating single protein aggregates [20]. While the biochemical setup of the sFIDA assay is similar to a sandwich ELISA (Figure 1), the readout is microscopy-based featuring sub-femtomolar sensitivity [20, 21]. To avoid monomer interference, sFIDA uses capture and detection antibodies directed against the same or overlapping epitopes. After probing, the glass surface is imaged by total internal reflection fluorescence microscopy (TIRFM), illuminating fluorescence-labeled detection antibodies bound to the captured aggregates. Individual particles are counted by image-data analysis of pixels with fluorescence intensities above background noise. Our previous work established the technical concept of sFIDA [21-23] and demonstrated that sFIDA is useful for diagnosing neurodegenerative diseases [24-26] and drug development [27].

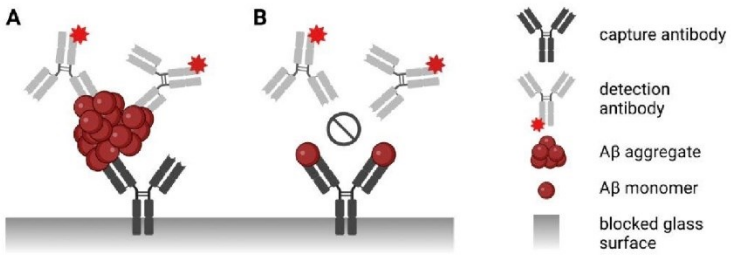

Figure 1. Scheme of sFIDA principle. In sFIDA, capture antibodies directed against a linear epitope on Aβ (Nab228, directed against epitope amino acids 1−11) are immobilized on a glass surface, and unoccupied surface area is blocked with bovine serum albumin to reduce unspecific binding events. During sample incubation, monomeric and aggregated Aβ species are bound to the capture antibody. (A) Because sFIDA uses the same or overlapping epitopes for capture and detection, only Aβ aggregates are subsequently detected with fluorescence-labeled antibodies (IC16-CF633, directed against epitope amino acids 2−8). (B) For monomeric Aβ, this epitope is already masked by the capture antibody and cannot be bound by the detection antibody. Afterward, the assay surface is imaged by fluorescence microscopy, and pixels above a defined cutoff threshold are counted by image-data analysis (called pixel count). Finally, pixel-based readouts are calibrated into molar particle concentrations using silica nanoparticles (SiNaPs) coated with Aβ as calibration standards. Created with BioRender.com.

The present study aimed to investigate the fecal concentrations of Aβ aggregates in AD patients and healthy controls (HC). Therefore, we developed and analytically validated the sFIDA assay to detect and quantify Aβ aggregates in human fecal samples. We also assessed its applicability as an explorative biomarker for non-invasive AD diagnosis in a small proof-of-concept study including samples from 26 AD patients and 31 HC.

Methods

Human fecal samples

The Ethics Commission of the Faculty of Medicine of the University of Cologne approved patient recruitment (19-1644). In total, 26 AD patients (amyloid positivity as part of the clinical workup by cerebrospinal fluid (CSF) or Amyloid positron emission tomography and impaired cognitive function, 48−84 years of age at sample collection), i.e., 22 patients with mild cognitive impairment (MCI), and four patients with dementia were enrolled between October 2019 and June 2022. HC (n = 31, 26−78 years of age at sample collection) were recruited by advertisement. For ethical reasons, fecal sample tubes of HC were handled anonymously, thus we could not match the sample with the respective donor. HC had

no known neurological disease and were not subjectively cognitively impaired. Informed consent was obtained from each participant.

Sample collection

Fecal samples were collected using polypropylene sample tubes with a screwcap-integrated spoon (megro, Wesel, Germany) and a paper-based collection aid (Med Auxil analysis aids, Seesen, Germany) to avoid contamination. In order not to endanger sample stability, samples were stored and transported on ice. After receiving the fecal samples, samples were classified according to their consistency and shape using the Bristol scale [28] and were aliquoted into polypropylene protein low-binding tubes (Sarstedt, Nümbrecht, Germany). Samples were stored at −80 °C until further use.

Homogenization of fecal samples for sFIDA analysis

In this study, we used Tris buffer (20 mM Tris and 250 mM NaCl, both AppliChem, Darmstadt, Germany, pH 8.3), which was previously applied to quantify Aβ aggregates in homogenized brain tissue using sFIDA technology [27]. To reduce non-specific binding of Aβ aggregates to the homogenization tubes, we added 1% bovine serum albumin (BSA, AppliChem). Furthermore, the properties of glycerol (Carl Roth, Karlsruhe, Germany) were used to further stabilize the analyte, especially during repeated freezing and thawing [29], using a concentration of 5%. As during homogenization release of proteases and phosphatases cannot be excluded, we added cOmplete EDTA-free protease inhibitor and PhosStop phosphatase inhibitor (both Roche, Basel, Switzerland). Because about a quarter of the solid fecal components comprises bacteria and other microorganisms that may still be viable [30, 31], we added NaN_3 (AppliChem) at a concentration of 0.05%.

Various feces homogenization methods are described in the literature, with the required sample quantity being determined either by weighing or using tubes with an integral dosing system [32-36]. We decided to use such a dosing system, i.e., Simplix tubes (polypropylene, Gaudlitz, Coburg, Germany), allowing for simple, clean, and fast sample handling and accurate dosing. The homogenization procedure used in this study was adapted by combining already established instructions of *in-vitro* diagnostics (IVDs) using feces as sample matrix for the quantification of other biomarkers, e.g., fecal IgA, hemoglobin, or calprotectin [32, 33, 35, 36]. Briefly, Simplix tubes were prefilled with cold 1300 µL homogenization buffer. Afterward, thawed fecal samples were applied on a sample stick, whereby the integrated dosing system ensured a sample weight of approximately 17 mg. Due to the liquid consistency, fecal samples with Bristol scale seven were weighted into Simplix tubes. Samples were homogenized completely using

a vortex mixer, incubated for 10 min at RT, and transferred into 2 mL polypropylene low-binding tubes (Eppendorf, Hamburg, Germany). However, since dead bacteria can also show autofluorescence, these and solid components, e.g., undigested food residues, were mechanically separated from the liquid phase by centrifugation (5 min, 3000× *g*, 4 °C). Finally, the supernatants were transferred into fresh 1.5 mL polypropylene low-binding tubes and stored at −80 °C before sFIDA analysis.

sFIDA Assay

Synthesis of Aβ1−15 coated silica nanoparticles

For assay calibration, we have previously introduced silica nanoparticle (SiNaP) standards coated with multiple Aβ-derived epitopes to mimic Aβ aggregates [22]. To this end, bare SiNaPs were synthesized via the Stöber process, functionalized, and activated as described previously by Blömeke et al. [24]. Briefly, synthesized SiNaPs were silanized with 3-aminopropyl(triethoxysilane) (APTES, Sigma-Aldrich, St. Louis, MO, USA) to functionalize the surface with primary amino groups. Afterward, crosslinking of Aβ1−15 peptides to aminated SiNaPs surface was enabled using maleimido hexanoic acid (MIHA, abcr GmbH, Karlsruhe, Germany), preactivated with 1-ethyl-3-(3-dimethylaminopropyl)carbodiimide (EDC, Sigma-Aldrich) and N-hydroxysuccinimid (NHS, Sigma-Aldrich). Using C-terminal functionalized Aβ1−15 peptides with cysteamine, crosslinking between Aβ and maleimide groups was enabled. Finally, molar concentration of Aβ-coated SiNaPs was calculated based on silicon concentration determined by inductively coupled plasma-mass spectrometry, density of SiNaPs and size and shape of the particles, as determined by transmission electron microscopy.

Aβ1−42 oligomer-based IQC sample

We have previously introduced synthetic Aβ1−42 oligomers as internal quality control (IQC) sample [23]. To this end, 5 µg of monomeric Aβ1−42 (Bachem, Bubendorf, Switzerland) was dissolved in 1,1,1,3,3,3-hexafluoro-2-propanol (HFIP, Sigma-Aldrich) and evaporated. Afterward, the Aβ pellet was resolved with 5 µL dimethyl sulfoxide (DMSO, Sigma-Aldrich), agitated for 10 min at 650 rpm at RT and diluted with 1× PBS containing 0.04% NaN_3 to a final stock concentration of 10 µM. Following an overnight incubation on a shaker at 650 rpm and RT, the IQC sample was sonicated for 20 min in an ultrasonic bath before dilution and use in sFIDA assay.

157 Labeling of antibody

158 For detection of captured Aβ aggregates, fluorescence-labeled anti-Aβ antibody IC16 (directed against
159 epitope amino acid 2−8, kindly provided by Carsten Korth, Universitätsklinikum Düsseldorf, Germany)
160 [37] was applied on the assay surface. To this end, the antibody was labeled according to the
161 manufacturer's protocol using CF633 dye (Biotium, Freemont, CA, USA). In carbonate buffer, the
162 succinimidyl ester groups of the preactivated dye bind covalently to the amines of the IC16 antibody.
163 Purification was performed using a polyacrylamide bead suspension (Bio-Gel P-30 Gel, Bio-Rad
164 Laboratories Inc, Hercules, CA, USA), and afterward, concentration and degree of labeling of the probe
165 were calculated as described in manufacturer's protocol. Finally, the detection probe was stored at 4 °C,
166 diluted, and centrifuged for 1 h at 4 °C and 100,000× *g* just before usage.

167 Assay protocol

168 The biochemical principle of sFIDA was reported previously [21, 22, 24]. In this study, 384-well-plates
169 (SensoPlate plus, Greiner Bio-One, Frickenhausen, Germany) were functionalized with 40 µL of Nab228
170 monoclonal anti-Aβ antibody (Sigma-Aldrich, St. Louis, MO, USA) at 2.5 µg/mL in 0.1 M $NaHCO_3$. After
171 overnight incubation at 4 °C, the wells were washed five times with TBST (1× Tris-buffered saline, TBS
172 (Serva, Duisburg, Germany), 0.05% Tween20 (AppliChem, Darmstadt, Germany)) and five times with
173 TBS. Non-coated glass area was blocked with 0.5% BSA (AppliChem) in TBS-ProClin (TBS with 0.03%
174 ProClin (Sigma-Aldrich)) for 1.5 h at RT. After washing five times with TBST and TBS, 20 µL samples
175 were applied in 4-fold determination and incubated for 2 h at RT. For this, Aβ-coated SiNaPs as
176 calibration standard and synthetic Aβ1−42 oligomers as IQC were diluted in sample buffer (1×
177 phosphate-buffered saline (PBS, Sigma-Aldrich), 0.05% Tween, 0.095% NaN_3 (AppliChem) and 0.5%
178 BSA). For fecal samples, an assay-specific 1:5 dilution in sample buffer was performed. After washing
179 five times with TBS, 20 µL of IC16-CF633 (0.625 µg/mL in TBST + 0.1% BSA) were applied and
180 incubated for 1 h at RT. Finally, wells were washed five times with TBS, and buffer was changed against
181 TBS-ProClin.

182 Image data acquisition

183 Using TIRFM (Leica DMI6000B, Leica microsystems, Wetzlar, Germany), 3.15% of the well surface
184 were imaged at 25 different positions (14-bit grayscale, excitation: 635 nm, emission filter: 705/72 nm,
185 exposure time: 1000 ms, gain: 1000). Each image consists of 1000 × 1000 pixels and represents an
186 area of 113.76 × 113.76 µm.

Quantification and statistical analysis

Analysis of image data

Image data analysis was performed using the in-house developed software sFIDAta [21, 24]. All images containing artifacts or images that were out of focus were excluded from analysis. For the exclusion of background signal, an intensity cutoff was determined at which 0.001% of all pixels remain positive in the blank control (unspiked sample buffer, BC). The number of pixels above the respective cutoff is referred to as pixel count. sFIDAta calculated the mean value, standard deviation, and coefficient of variation (CV%) for each sample based on the four replicates. Statistical analyses were performed using OriginPro (OriginLab Corporation, Northampton, MA, USA) and matlab2019b (The MathWorks, Natick, MA, USA) were used for calculations and graphs.

Calibration

To convert pixel counts into femtomolar particle concentration, we used readouts of Aβ-coated SiNaPs to calculate the calibration curve. To this end, only those Aβ-coated SiNaPs concentrations which significantly differed from BC and were within linear range were included in the calculation. A one-sided Mann−Whitney U test with a confidence interval of 5% was performed to investigate significant differences. Linear regression was executed with matlab2019b software, where pixel counts were weighted with 1/readout.

Preanalytics

Reproducibility of preanalytical procedures

Due to the complex and individually varying composition of feces, we tested the reproducibility of homogenization and sample dilution using three fecal samples with an initial low, intermediate, and high readout. To this end, six homogenates of each of the three samples were prepared, whereby the weight of the sample was additionally calculated based on the previously recorded empty weight (homogenization tube with buffer). Based on these data, the sample dosage's precision and trueness were calculated. Each homogenate was subjected to sFIDA assay in quadruplicates. In addition, the reproducibility of sample dilution was investigated by preparing four dilutions from one homogenate of each sample and assaying them also in quadruplicate within sFIDA. Afterward, pixel counts of individual replicates of each sample were normalized based on Eq.1. Values within the tolerance range of ± 25% indicated sufficient reproducibility.

(1) $$\text{Normalized pixel count } [\%] = \frac{\text{pixel count}_{\text{replicate x}}}{\text{pixel count}_{\text{mean all replicates}}} \times 100\ \%$$

Dilution linearity

In this study, the dilution linearity of Aβ-coated SiNaPs and IQC in dilution buffer was investigated. Before calculating the dilution linearity of both targets, background correction was performed by subtracting the BC value from each value. Subsequently, the percent dilution linearity of each calibration or IQC sample was calculated using Eq.2. Dilution linearity was accepted when the mean percent dilution linearity was between 80−120%.

(2) $$\text{Dilution linearity or parallelism } [\%] = \frac{\text{observed concentration}}{(\text{previous observed value}/\text{dilution factor})} \times 100\ \%$$

For investigating parallelism, two fecal samples with high endogenous concentrations of Aβ aggregates were homogenized and diluted 1:5 with sample dilution buffer. Subsequently, these samples were serially diluted four times by a factor of two, and all prepared dilutions were applied on sFIDA surface. Because parallelism and dilution linearity are conceptually similar [38], the percent parallelism of each dilution step was also calculated using Eq.2. In the case of fecal samples, acceptance criteria for the mean dilution linearity were increased up to ± 25%.

Sample stability

To assess thermostability, three crude fecal samples with low, intermediate, and high readouts were stored at −20 °C, 4 °C, or 20 °C for 3, 6, or 18 h to simulate sample transport and bench top conditions, respectively. To this end, nine Simplix tubes were prefilled with the respective fecal sample, and the individual homogenization tubes were stored according to the storage condition mentioned above. At the end of each storage period, the aliquots were frozen at −80 °C. As a reference, another Simplix tube was prefilled with the corresponding sample and stored directly at −80 °C. On the day of the sFIDA experiment, all Simplix tubes were thawed simultaneously, the homogenization tubes were filled with homogenization buffer, and the samples were homogenized and diluted 1:5 with sample dilution buffer. Finally, all samples were measured by sFIDA, and the normalized pixel counts were calculated (Eq.1), where values within a tolerance range of ± 25% were accepted. Values outside the tolerance range indicated that sample stability was compromised.

For CSF samples, it is known that repeated thawing and refreezing can drastically reduce the measurable concentration of Aβ [39]. In order to test whether similar effects can be observed in crude

244 and already homogenized fecal samples, the effect of multiple freeze-thaw cycles (none, one, two, three,
245 five, or seven) on the stability of the three samples was investigated according to Andreasson et al. [38].
246 To this end, six Simplix tubes each were prefilled with the respective crude sample and then stored at
247 −80 °C. In contrast, for the investigation of fecal homogenates, homogenates of three samples were
248 prepared at the beginning of the stability study, whereby the supernatant obtained after centrifugation
249 was divided into six aliquots of 100 µL each. For this purpose, 1.5 mL polypropylene low-binding
250 Eppendorf reaction tubes were used as containers, and all aliquots were frozen at −80 °C. Subsequently,
251 the individual Simplix tubes and the fecal homogenates were thawed successively, while the reference
252 aliquots did not undergo a thaw-freezing process during the study. After an incubation time of 2 h at RT,
253 samples were frozen again for at least 12 h at −80 °C. At the end of the study period, all aliquots were
254 thawed simultaneously and diluted 1:5 with sample buffer, while the crude fecal samples were first
255 homogenized. The data acquisition and analysis of the image data were carried out analogously to the
256 thermostability study.

257 Analytical validation

258 *Assay selectivity – investigation of assay controls*

259 To determine the selectivity of the sFIDA assay, Aβ-coated SiNaPs (molar particle concentration of
260 10.26 pM), IQC sample (100 nM, Aβ monomer subunit concentration), and three fecal samples were
261 applied on different sFIDA setups. To exclude unspecific binding of Aβ to the blocking agent, a capture
262 control (CC) was performed in which no capture antibody was added to the surface. The assay was
263 performed without adding any fluorescent probes to exclude autofluorescence (AF) events from assay
264 components or samples. In addition, we also tested the cross-reactivity of anti-α-synuclein antibodies
265 (detection antibody 211) against the immobilized Aβ species. For each assay control setup, the ratio of
266 observed and expected (standard assay setup) values and the percentage amount of reduced signal
267 were calculated according to Eq.3. Values between 80−120% were accepted for Aβ-coated SiNaPs and
268 IQC sample. In comparison, the tolerance range for fecal samples was increased up to ± 25%.

269 (3) $$\text{Signal reduction}\,[\%] = \left(1 - \frac{\text{observed readout assay control}}{\text{readout reference}} \times 100\%\right)$$

270 *Assay selectivity – immunodepletion*

271 Immunodepletion was performed to demonstrate that the observed pixel counts by sFIDA can be
272 specifically attributed to Aβ aggregates. To this end, the Nab228 antibody was covalently coated on the

surface of carboxylated magnetic dynabeads (Invitrogen, Waltham, USA), as previously described by Blömeke et al. [24]. Briefly, the dynabeads were washed twice with 2.5 mM 2-(N-morpholino)ethanesulfonic acid (MES, pH 5.0, Carl Roth, Karlsruhe, Germany) before being applied to a magnet to remove the supernatant. Afterward, carboxy groups of the dynabeads were activated for 30 min at RT using 50 µg/mL EDC and 50 µg/mL NHS in MES, and the dynabeads were rewashed with MES and coated with Nab228 antibody to a concentration of 20 µg/mL dynabeads. The control dynabeads were coated with an α-synuclein-specific antibody 211 to investigate Aβ specificity of the depletion protocol. After antibody incubation for 1 h at RT, coated dynabeads were rewashed, and still activated carboxy groups were quenched with 50 mM ethanolamine in MES for 1 h at RT, followed by a final washing step. We applied 0.5 mg of antibody-coated dynabeads to the magnet for immunodepletion and removed the supernatant. 100 µL sample (10.26 pM Aβ-coated SiNaPs, 100 nM synthetic Aβ1−42 oligomers, and three fecal samples, which were diluted 1:5 in sample buffer before depletion) were added and incubated for 1 h at RT while rotating. After incubation, dynabeads were applied to the magnet again and the supernatant was transferred into a fresh tube and stored at −80 °C until sFIDA analyses. To assess assay selectivity, the efficiency of the immunodepletion was calculated according to Eq.3. The acceptance criteria were the same as for the assay control setup described above.

Assay selectivity – detection of Aβ using ELISA

For the qualitative detection of Aβ species in feces, two samples were analyzed using a human amyloid β (1−42) ELISA Assay kit (IBL international, Hamburg, Germany) according to the manufactures protocol. For sample preparation, 15 mg of each sample were transferred into a low binding Eppendorf tube, which was prefilled with 20 µL ddH_2O containing protease inhibitor. After homogenization using vortex mixer, homogenates were incubated for 10 min at 95 °C at 600 rpm. To separate insoluble digestive residues, homogenates were centrifuged for 5 min at 3000× *g*, 4 °C, and supernatants were used for ELISA analysis. To enrich Aβ from the sample matrix, samples were subjected to immunoprecipitation. To this end, protein-G magnetic dynabeads (Invitrogen, Waltham, USA) were functionalized with IC16 antibody and samples were precipitated according to manufactures protocol. Afterward, Aβ was eluted using 10 mM acetic acid, resuspended in ddH_2O containing protease inhibitor and supernatants were used for ELISA analysis. We also attempted to increase signal by seeding by spiking 100 pg/µL synthetic Aβ1−42 to the homogenates prior to immunoprecipitation. Afterward, the supernatants were also analyzed in ELISA. Finally, ELISA readouts were translated into pg/mL concentration based on the calibration curve ($y = 0.0228x$, $R^2 = 0.994$).

Influence of Bristol scale

Recent studies have demonstrated that microbiome composition and species richness change during AD progression and might impact cognition [9, 40-42]. Microbiome composition and species richness also affect feces consistency. Therefore, changes in both water content and pH value are directly reflected in the Bristol scale [28, 43]. The latter may also act as a non-analyte-specific interfering factor [44], altering the quantification of the analyte through dilution or pH-dependent changes in assay kinetics. At sample receipt, all samples were assessed according to their consistency and shape using the Bristol scale. We performed a Mann−Whitney U test and a Spearman correlation analysis to determine whether the Bristol scale influences the fecal Aβ aggregate concentration or whether a cognition-based influence is present.

Influence of matrix components

The presence of interfering endogenous substances in fecal samples may falsely alter assay results, either false positive or negative [45, 46]. Because disturbances of the brain-gut-microbiota axis, including gut inflammation and increased permeability of the intestinal barrier, may contribute to AD pathology [7], levels of fecal biomarkers indicating pathological processes of the gut, i.e., fecal albumin, hemoglobin, α-1-antitrypsin, calprotectin, IgA, lipids, and bile acid were determined for a set of 15 fecal samples (AD n = 7, HC n = 8). Biomarker analyses were performed by the Medizinisches Versorgungszentrum Limbach (Heidelberg, Germany). Afterward, Spearman correlation was conducted to investigate possible interfering effects of those biomarkers on fecal Aβ aggregate concentrations. In addition, Mann−Whitney U tests were used to determine whether levels of all seven biomarkers differ in AD patients and HC.

Intra- and inter-assay variability

In this study, we determined CV% values to measure intra-assay variability. For synthetic Aβ species such as Aβ-coated SiNaPs and IQC sample, values below 20% were accepted, while for naturally occurring Aβ species from fecal samples, the tolerance range was increased up to ± 25%. The Spearman coefficient of correlation was calculated for two independent measurements to determine inter-assay variability.

Calculation of LoD

In order to describe the smallest concentration of Aβ aggregates that can be measured reliably with the sFIDA assay, the limit of detection (LoD) was estimated for each experiment by measuring 24 replicates

of BC. First, LoD was calculated according to Armbruster et al. using Eq.4 [47] and then calibrated into femtomolar concentrations using the determined calibration line.

$$\text{Limit of detection (LoD)} = \text{pixel count}_{BC} + 2\sigma \quad (4)$$

Proof-of-concept study

For the proof-of-concept, the whole set of 57 fecal samples was subjected to sFIDA. At the time of measurements, all patient-related data and samples were anonymized, and researchers were aware of the clinical data at the time of the sFIDA measurements. Pixel counts were generated and calibrated. Data of fecal samples were subsequently tested for normal distribution using Shapiro−Wilk, Lilliefors, Kolmogorov Smirnov, and Anderson−Darling tests. In the case of non-normally distributed data, non-parametric tests, e.g., the Mann−Whitney U test or Spearman correlation, were conducted for further analyses. A receiver operating characteristic (ROC) analysis was performed to evaluate the effectiveness of fecal Aβ aggregates as diagnostic biomarker to differentiate between AD patients and HC. Using maximized Youden's index, the optimal combination of sensitivity and specificity and the area under the curve (AUC) were calculated.

Results

Homogenization and sample dilution of fecal samples are reproducible

Because fecal samples must be homogenized before they are subjected to sFIDA, we first established a suitable homogenization buffer and protocol. Due to the complex and individually varying composition of feces, we tested the reproducibility of homogenization and sample dilution (1:5 in sample buffer) using normalized pixel counts of three fecal samples (initial low, intermediate, high readout) to calculate percentage reproducibility. Figure S1 demonstrates that the homogenization and sample dilution resulted in a high degree of reproducibility, as most of the normalized pixel counts fell within the predefined tolerance range of ± 25%. Only two of the observed values have exceeded the tolerance range with a slight deviation of ± 0.8% (Figure S1A).

sFIDA features dilution linearity of Aβ-coated SiNaPs, IQC Samples, and fecal samples

Next, we analyzed dilution linearity by subjecting an Aβ-coated SiNaPs and IQC dilution series to sFIDA analysis, ranging from 0.32 fM−10 pM (molar particle concentration) and 3.2 pM−31 nM (total Aβ concentration), respectively. The percent dilution linearity was determined using blank-corrected pixel counts and was accepted within a tolerance range of 80−120%. The results showed high dilution linearity

for both targets, with an average linearity of 107% for Aβ-coated SiNaPs and 97.6% for IQC samples. Furthermore, for two fecal samples possessing high endogenous Aβ aggregate concentrations, high parallelism of 99.9% and 85.2%, respectively, as depicted in Figure S2.

Repeated freeze-thaw cycles do not affect stability of homogenized fecal samples

In order not to compromise the sample stability during transport or assay preparation, we first performed a thermostability study. The results indicated that a temperature of 4 °C or lower did not compromise sample stability for up to 18 h, as depicted in Figure S3. In addition, we investigated the influence of freeze/thawing on crude and homogenized fecal samples since repeated freezing and thawing of clinical samples is known to compromise sample stability [38, 39, 48]. To this end, we subjected three fecal samples to repeated freeze-thaw cycles and determined the level of Aβ aggregates. As shown in Figure 2, the stability of the crude fecal samples was indeed affected by multiple thawing and freezing but remained intact in the homogenized fecal samples. In detail, for the crude control sample (sample 1, low readout), neither a signal reduction due to decreased sample stability nor a signal increase was observed. In contrast, a decreasing effect of the number of freeze-thaw cycles on the signal was determined for samples 2 and 3. In particular, repetitive freeze-thaw cycles dramatically reduced the stability of high-readout sample 3. Compared to the reference (no freeze-thaw cycle), a signal loss of 57% was recorded for this sample after thawing and freezing seven times. Considering crude sample 2, an out-of-tolerance value was also recorded at the seventh freeze-thaw cycle, with the measured signal dropping by 31% compared to the reference. In contrast to the crude fecal samples, no signal decrease was observed for the homogenized samples over all freeze-thaw cycles indicating high sample stability after homogenization.

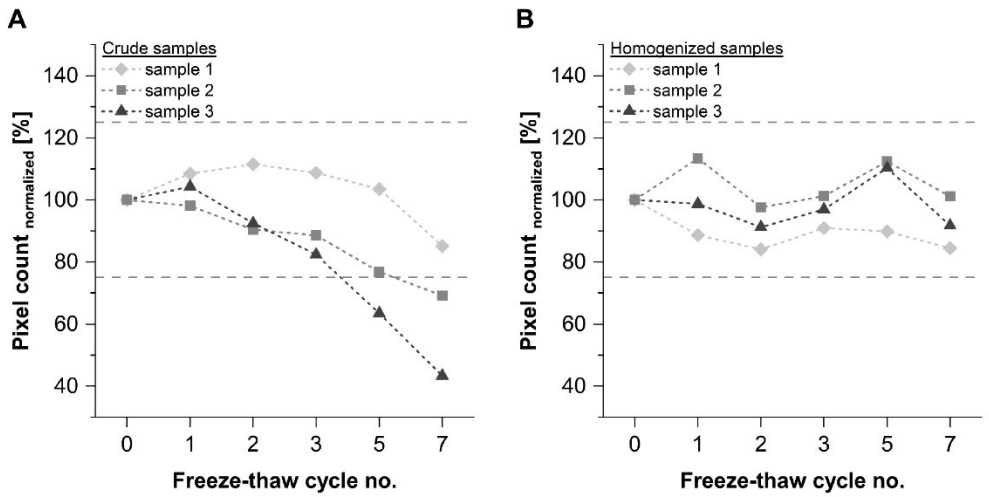

Figure 2. Influence of repeated freeze-thaw cycles on the stability of Aβ aggregates. Normalized pixel counts of three crude (A) or homogenized (B) fecal samples (sample 1 = diamonds, low readout; sample 2 = square, intermediate readout; sample 3 = triangle, high readout) were plotted against freeze-thaw cycles. The tolerance range of ± 25% is depicted as dashed gray lines.

sFIDA is selective for aggregated Aβ species

To evaluate the selectivity of the sFIDA assay in detecting Aβ-coated SiNaPs, IQC samples, and three fecal samples with intermediate to high readouts, we measured the percent signal reduction of capture, autofluorescence, and cross-reactivity control, and compared it to a standard assay setup (Figure 3A). In this analysis, the sFIDA assay showed a selectivity of about 100% for both Aβ-coated SiNaPs and IQC samples. Thus, unspecific interference with the used blocking agent, autofluorescent components, and cross-reactivity can be excluded for both targets. In contrast, a selectivity of about 77% was determined for fecal Aβ aggregates. Both capture and cross-reactivity control showed about 19.2% and 24.8% remaining pixel counts, respectively. However, since the absence of the detection probe from the fecal samples also led to a comparable result (24.3% of remaining pixels), higher background intensities of the matrix and no interference with assay surface or cross-reactivity with α-synuclein directed antibodies can be assumed. Despite this increased background noise, the signal reduction down to 25% remaining pixels in the fecal samples was still sufficient.

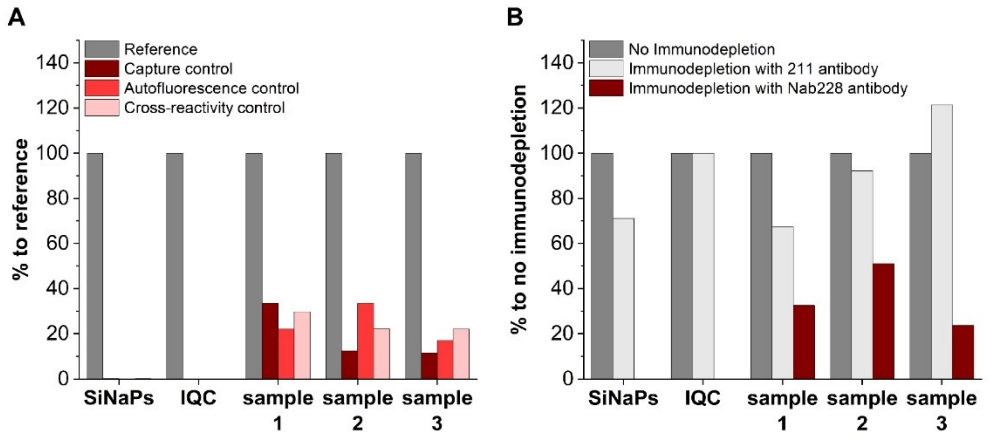

Figure 3. Percent signal reduction of different assay controls for the assessment of assay selectivity. (**A**) Aβ-coated SiNaPs, IQC, and Aβ aggregates in three fecal samples were analyzed by sFIDA. Based on the observed pixel counts, the percent signal reduction of each assay control (no capture antibody: capture control, dark red; no detection probe: autofluorescence control, light red; detection probe against α-synuclein: cross-reactivity control, rose) in comparison to reference (standard assay setup) were calculated. (**B**) All samples were subjected to immunodepletion using magnetic beads linked to Aβ-specific antibody (Nab228) and control beads linked to α-synuclein-specific antibody (211). Based on the observed pixel counts of non-depleted (dark gray), 211-depleted (light gray), and Nab228-depleted (red) samples, percent signal reduction was calculated.

Assay readouts are specifically attributed to Aβ

Immunodepletion was performed on three fecal samples with intermediate to high readouts, Aβ-coated SiNaPs, and IQC samples to determine if the observed pixel counts were specifically attributed to Aβ aggregates and not to interfering fecal matrix components. Following Aβ immunodepletion, supernatants were subjected to sFIDA analysis, and depletion effectivity was calculated by the percent signal reduction compared to non-depleted sample (reference). Nab228-depleted Aβ-coated SiNaPs and IQC showed depletion-dependent signal reduction close to 100% (Figure 3B), whereas, for Nab228-depleted fecal samples, a mean signal reduction of 72.6% was determined. As a control, α-synuclein immunodepletion with 211-coated magnetic beads was performed, resulting in only negligible signal reduction of IQC (0%) and fecal samples (6.5%). However, for Aβ-coated SiNaPs a signal reduction of 28.9% was observed, suggesting some non-specific adherence of Aβ-coated SiNaPs to bead surface since cross-reactivity between 211 and Aβ-coated SiNaPs was previously excluded (Figure 3A). To qualitatively confirm the presence of Aβ in human fecal samples, we detected Aβ species in two fecal samples (HC and AD) using a commercial ELISA kit (Figure S4). However, differentiation of fecal Aβ

levels between the two subjects was only achievable after complex and sample-consuming pretreatment including homogenization, immunoprecipitation, and spiking.

Independent measurements yield comparable results

We investigated the inter-assay variability of Aβ-coated SiNaPs, IQC samples, and 13 fecal samples in two different assays (Figure 4). All three targets showed high comparability, indicated by Spearman's coefficient of correlations (*r*-value: 1.0 for Aβ-coated SiNaPs and IQC samples and *r*-value: 0.929 (*p*-value: 8.63×10^{-4}) for fecal samples).

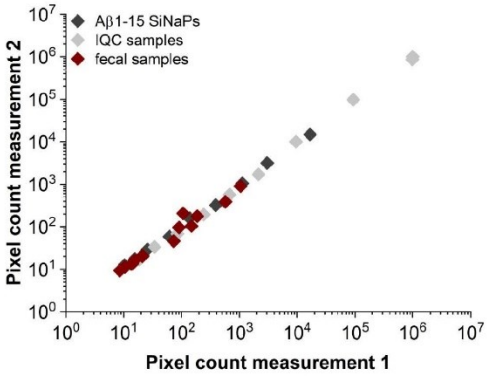

Figure 4. Independent measurements of Aβ yield high comparability. For Aβ-coated SiNaPs (dark grey), IQC sample (light gray), and 13 fecal samples (red), pixel counts of the second measurement were plotted against pixel counts of the first measurement. Because the second measurement was carried out months later, there were minor changes in used reagent lots, e.g., manufacturing date of washing buffers, and the used homogenized fecal samples were subjected to an additional freeze-thaw cycle. NOTE. The logarithmic scaling.

Aβ aggregates are present in fecal samples and are elevated in AD patients

After completion of preanalytical and selectivity studies, a proof-of-concept study was performed using dilution series of Aβ-coated SiNaPs for calibration and LoD calculation, a dilution series of IQC samples and 57 fecal samples comprising two diagnostic groups (Table 1). In detail, we quantified fecal Aβ aggregate concentrations of HC subjects having no subjective cognitive decline (n = 31) and patients diagnosed with clinical AD (n = 26). Because the data mainly did not show normal distribution (Table S1), we performed statistical analysis using non-parametric tests like the Mann−Whitney U test or Spearman correlation.

448 **Table 1. Demographic and clinical information on AD patients and HC that donated fecal**
449 **samples.**

Characteristics	AD	HC
Number	26	31
Female	42.3%	64.5%
Age [years ± SD]	71.1 ± 8.6	49.2 ± 16.4
Bristol scale [score ± SD]	4.4 ± 0.9	5.1 ± 0.8

450 [a]Abbreviations: AD, Alzheimer's disease; HC, healthy controls; SD, standard deviation.

451 Due to the high number of assay points, the measurements were performed on two 384-well microtiter
452 plates (experiment 1: 48 samples, experiment 2: 9 samples), each carrying both a dilution series of Aβ-
453 coated SiNaPs for calibration and LoD calculation and a dilution series of IQC samples, respectively.
454 We determined a femtomolar mean LoD of 1.68 fM for Aβ-coated SiNaPs, indicating high analytical
455 sensitivity. The mean CV% for Aβ-coated SiNaPs was 13.4% and 11.1% for IQC samples. A mean intra-
456 assay variability of 18.7% was observed for fecal samples (for individual results of each experiment see
457 Table S2). Representative TIRFM images of Aβ-coated SiNaPs, IQC sample, patient sample and the
458 sample buffer control are shown in Figure 5A.

459 Using Aβ-coated SiNaPs standards, pixel counts of fecal samples were calibrated into molar particle
460 concentrations (Table S3). We determined Aβ aggregate concentrations ranging from 1.3 fM−3.4 pM
461 (Figure 5B). Despite a substantial overlap between both groups, Aβ aggregate levels of AD patients
462 were significantly elevated (*p*-value: 0.009). ROC curve were determined to evaluate the use of fecal
463 Aβ aggregates as a diagnostic biomarker (Figure 5C). Discrimination of AD patients versus HC showed
464 a specificity of 90.3% and a sensitivity of 53.8% with an AUC of 0.703.

465 Since HC samples were collected anonymously, we could not match the sample with the demographic
466 information of the respective donor. Thus, only the mean age and proportion of female donors was
467 calculated. Therefore, a direct correlation to the determined fecal Aβ aggregate concentration could only
468 be established for the AD cohort. Since we are aware that the samples used from HC do not match with
469 samples of AD patients (Table 1), we investigated for the AD cohort whether fecal Aβ aggregate
470 concentrations might be influenced by age or sex. However, no correlation between AD patients' age
471 and Aβ aggregate concentration was found using Spearman correlation (*r*-value: 0.163, *p*-value: 0.426).

In addition, no difference was found in Aβ aggregate concentrations in fecal samples from male and female AD patients using a two-sided Mann−Whitney U test with a confidence interval of 5% (*p*-value: 0.959).

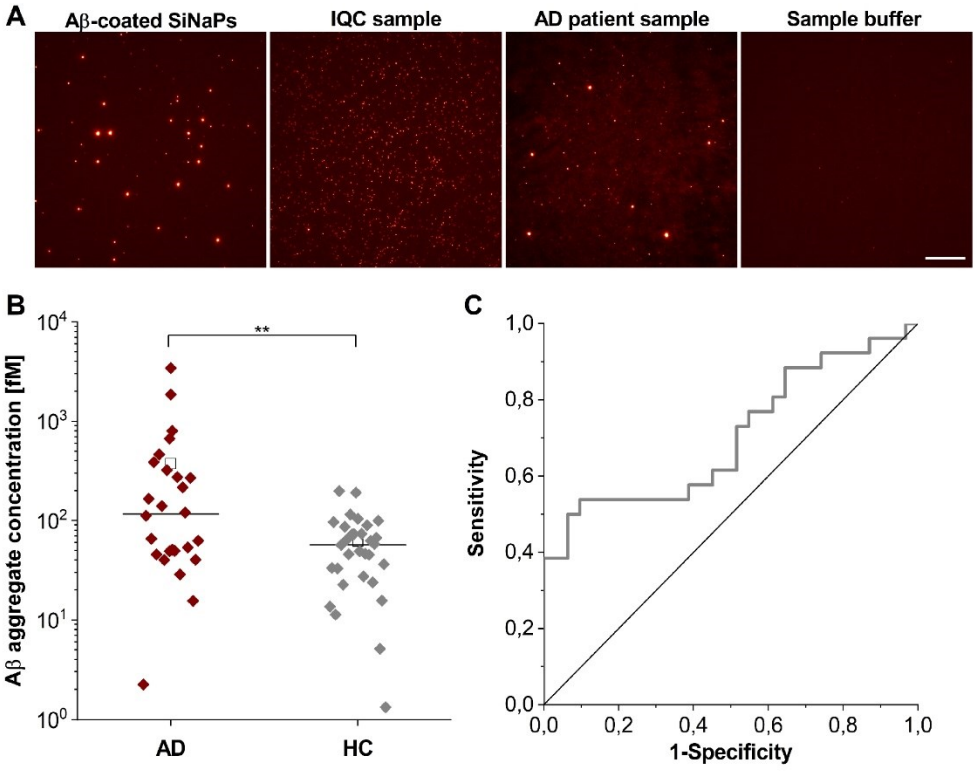

Figure 5. Representative TIRFM images, molar particle concentration of fecal Aβ aggregates and receiver operating characteristic. (**A**) Representative TIRFM images for the red channel (IC16-CF633, excitation 635 nm, emission 705 nm, exposure time 1000 ms, gain 1000) of 1 pM Aβ-coated SiNaPs, 100 pM synthetic Aβ1−42 oligomers (based on total Aβ concentration), fecal sample (AD patient) and sample buffer control. For better illustration of 14-bit images, color and contrast were adjusted using ImageJ software (colormap: red hot, contrast: maximum grayscale value 8000). Scale bar: 20 µm. (**B**) Concentrations of fecal Aβ aggregates of AD patients were significantly elevated with a *p*-value of 0.009 compared to HC. Significant differences between both cohorts were calculated with a Mann−Whitney U test (**$p \leq 0.01$). NOTE. The logarithmic scaling (line = median, square = mean). (**C**) In receiver operating characteristic (ROC) analysis, discrimination of AD patients versus HC showed a specificity of 90.3% and a sensitivity of 53.8% with an AUC of 0.703.

Aβ aggregate quantification is not affected by sample consistency or endogenous substances

To investigate whether the feces consistency, indicated by Bristol scale, affects the measured fecal Aβ aggregate concentrations, we performed a Spearman correlation for all 57 samples. Here, we did not

find a significant correlation, indicating that the quantification was not affected by feces consistency (*r*-value: −0.176, *p*-value: 0.191). Since we found significant differences in feces consistency between AD patients and HC (*p*-value: 0.003, Table 1), we performed additional Spearman correlation for HC and AD patient groups separately. Here, we also did not find any correlation between the Bristol scale and the signals of fecal Aβ-aggregate (AD patients: *r*-value: −0.087, *p*-value: 0.672; HC: *r*-value: 0.073, *p*-value: 0.696). Spearman correlation between fecal albumin, hemoglobin, calprotectin, IgA, bile acid, α-1-antitrypsin, lipids, and fecal Aβ aggregate concentrations were investigated to assess interfering effects. As shown in Table S4, Spearman correlation coefficients between −0.38 and +0.36 were observed. However, since they were not significant, only minute interfering effects of endogenous substances on quantification can be assumed. In addition, we investigated whether the levels of all seven biomarkers could be attributed to AD patients or HC. As shown in Table S5, no significant differences between both cohorts were observed.

Discussion

AD is the most common age-related cause of dementia and among the most critical public health problems in industrialized countries due to increasing life expectancy [49]. In AD pathology, small soluble Aβ oligomers are the most toxic Aβ species that damage neurons and compromise synaptic function. Aβ oligomers form probably decades before clinical symptoms of AD manifest in humans. We hypothesized that clearance mechanisms are likely to exist to protect the brain from toxic effects. The deposition of Aβ oligomers into amyloid plaques is likely just one clearance mechanism, while the sequestration of Aβ oligomers out of the brain could be another mechanism [10, 11, 14]. Given that the liver plays a crucial role in detoxifying the blood, it is reasonable to assume that Aβ oligomers are sequestered from the bloodstream by the liver and then transported to the gut via bile. We and others have provided compelling evidence indicating that disturbances along the brain-gut-microbiota axis may substantially contribute to the pathogenesis of neurodegenerative diseases such as AD because gastrointestinal metabolic, endocrine, neuronal, and immunological pathways are critical for the maintenance of brain homeostasis [5-9]. Although the bidirectional communication between the brain and gut and its microbiome is not yet fully understood, it is clear that changes in the gut microbiome can induce an immune activation resulting in a systematic inflammation, which in turn may compromise the intestinal barrier (leaky gut) and the blood-brain barrier [6-9, 13]. Combined with a dysregulated Aβ homeostasis, brain-derived Aβ aggregates could thus directly enter the enteric nervous system by

520 crossing the blood-brain barrier or by neuron-to-neuron, distal neuron spreading, or other cells like
521 astrocytes, fibroblasts, microglia and immune system cells [7]. Conversely, Aβ species produced by
522 enteric neurons [16] may also enter the brain. Moreover, due to the permeability of the intestinal barrier
523 caused by systematic inflammation, it can be assumed that Aβ aggregates in blood or originating in
524 enteric neurons enter the intestinal lumen and are excreted with feces, as we have observed for α-
525 synuclein aggregates in patients with isolated rapid eye movement sleep behavior disorder, a prodromal
526 form of parkinsonism [26]. Besides, circulating Aβ is predominantly cleared by degradation in
527 hepatocytes and secreted into the gut in bile [10-12, 14], which in turn could increase intestinal and fecal
528 Aβ concentrations. Initial studies have confirmed this association between AD and increased intestinal
529 or fecal Aβ concentrations, irrespective of Aβ conformation [15-18]. One may assume, however, that
530 only Aβ species that are resistant to proteases in the gut may become observable in feces.

531 The clinical assessment of AD is supported by neurological evaluation, imaging, and biomarkers in
532 patients' CSF [1, 4]. Due to the invasiveness and burden of a lumbar puncture on patients, CSF is not
533 routinely collected [50, 51]. Identifying non-invasive biomarkers that can be used for sensitive detection
534 of AD years or even decades before clinical onset is of utmost importance [20, 52]. Therefore, we used
535 sFIDA technology to verify whether Aβ aggregates exist in feces and, more importantly, whether Aβ
536 aggregate concentrations in fecal samples of HC and AD differ.

537 As this was a pilot project to use sFIDA for the quantification of fecal Aβ aggregates, we first had to
538 overcome several preanalytical hurdles due to a complex sample matrix in addition to already existing
539 challenges of oligomer-based diagnostics. Because the fecal samples must be processed before they
540 are subjected to sFIDA, we first established a reproducible homogenization procedure. Various
541 homogenization methods for fecal samples are described in the literature, with the required sample
542 quantity being determined either by weighing or using tubes with an integral dosing system [32-36]. For
543 our study, we opted to use Simplix tubes, which facilitated simple, clean, and efficient sample handling,
544 and accurate dosing, as confirmed by our results.

545 The easiest way to overcome matrix effects in immunoassays is to dilute samples in a dilution buffer
546 that ensures high discrimination between negative and positive samples [53]. In this study, a 1:5 dilution
547 of the fecal homogenates was found optimal (data not shown) and reproducible in sFIDA assay
548 development. Furthermore, as dilution linearity or parallelism, respectively, were observed for Aβ-coated

549 SiNaPs, IQC sample, and fecal samples, we can exclude strong interferences due to, e.g., heterophilic
550 antibodies as these are typically reflected in insufficient dilution linearity [46]. Therefore, samples
551 containing high levels of endogenous fecal Aβ can be diluted within a linear range, and still yield reliable
552 outcomes.

553 Chemical, microbial, and physical factors influence an analyte's stability and measurable concentration
554 in a complex sample and can significantly falsify a measurement [38, 48]. Because our thermostability
555 study showed that incubation at temperatures above 4 °C did affect sample stability, we adjusted the
556 sFIDA procedure for fecal analysis accordingly. In addition, we have developed a homogenization buffer,
557 which combined with the homogenization process, leads to stable Aβ aggregates in feces, even when
558 they are exposed to several freeze-thaw cycles. In contrast, crude samples reacted to freeze-thaw
559 cycles with a signal reduction. These results are similar to those reported for CSF, where the stability of
560 Aβ42 was analyzed, and a signal loss of 20% was observed after three freeze-thaw cycles [39, 54].
561 Especially, the signal of Aβ aggregates was further reduced with increasing cycle numbers, which is in
562 accordance with our study in the case of crude fecal samples.

563 Despite complex matrix, using a suitable homogenization and sample dilution buffer ensured a high
564 consistency within the sample replicates implicated by low intra-assay variability. Furthermore, Aβ-
565 coated SiNaPs, IQC sample and fecal samples demonstrated low inter-assay variability, indicating a
566 highly precise assay. In particular, the comparability of both sample measurements of the inter-assay
567 study should be emphasized since the homogenates used for the second measurement were stored at
568 −80 °C for nine months. Thus, besides sufficient stability against freeze-thaw cycles, the
569 homogenization buffer also allows aggregate stability over an extended period. Additionally, the sFIDA
570 assay displayed a high level of selectivity for fecal Aβ aggregates.

571 After preanalytical and analytical validation, we determined the Aβ aggregate concentrations in the feces
572 of AD patients and HC. All feces contained Aβ aggregates in the femtomolar range, a few samples even
573 above. Although it is not clear whether the Aβ aggregates found in feces have been secreted by the
574 liver/bile system or have been directly secreted into the gut, e.g., from neurons of the enteric system,
575 this study supports the presence of clearance mechanisms that reduce Aβ oligomer concentration in the
576 body. Here, we demonstrated that sFIDA is suitable to measure low femtomolar (1.3 fM) to low
577 picomolar (3.4 pM) concentrations of Aβ aggregates in fecal samples, which is slightly higher than the

previously reported concentration range of Aβ aggregates in CSF (aM-fM) [55, 56]. We also demonstrated that fecal samples of AD patients with proven amyloid-positivity in the CSF or brain showed significantly elevated levels of Aβ aggregates compared to HC, which has been previously shown for Aβ aggregate concentrations in CSF [25, 55-59]. Due to a high specificity for aggregated Aβ species, the sFIDA assay developed in the present study could discriminate between fecal samples from HC and AD patients with a specificity of 90.3%. Because potential clearance mechanisms can be expected to yield increased Aβ aggregate concentrations also in (still) HC, not surprisingly, we observed an overlap between both cohorts, resulting in an assay sensitivity of only 54%, which limits the clinical use at the current stage of development. In this context, longitudinal samples may help to determine possible changes in the fecal Aβ aggregate concentration before and during disease. The correlation between fecal Aβ aggregate concentration and clinical symptoms within the AD cohort could not be thoroughly evaluated in this study, as it only involved four patients with dementia and 22 with MCI. However, if future studies indeed confirm a correlation between fecal Aβ aggregate concentrations and cognitive abilities, it will represent a significant advancement toward non-invasive early detection of AD.

Since this is a proof-of-concept study, there are certain limitations to our findings, primarily due to the restricted availability of samples, resulting in small sample sizes. While we could demonstrate statistically significant ($p < 0.01$) elevation of fecal Aβ aggregates in AD vs. HC, it is crucial to replicate this result in larger validation studies employing independent cohorts. While in this study we did not observe any correlation the age and Aβ aggregate concentration, we acknowledge that the samples obtained from HC were not matched in age with those from AD patients, which should be addressed in future work. Additionally, it would be intriguing to explore the link of fecal Aβ aggregates with additional biomarkers related to AD pathology, gut microbiota, and liver function (Figure 6). Additional data on these biomarkers in combination with a larger cohort of patients across the AD continuum have the potential to enhance our comprehension of the fundamental disease pathology and enable early diagnosis at a stage when clearance mechanisms may be starting to malfunction.

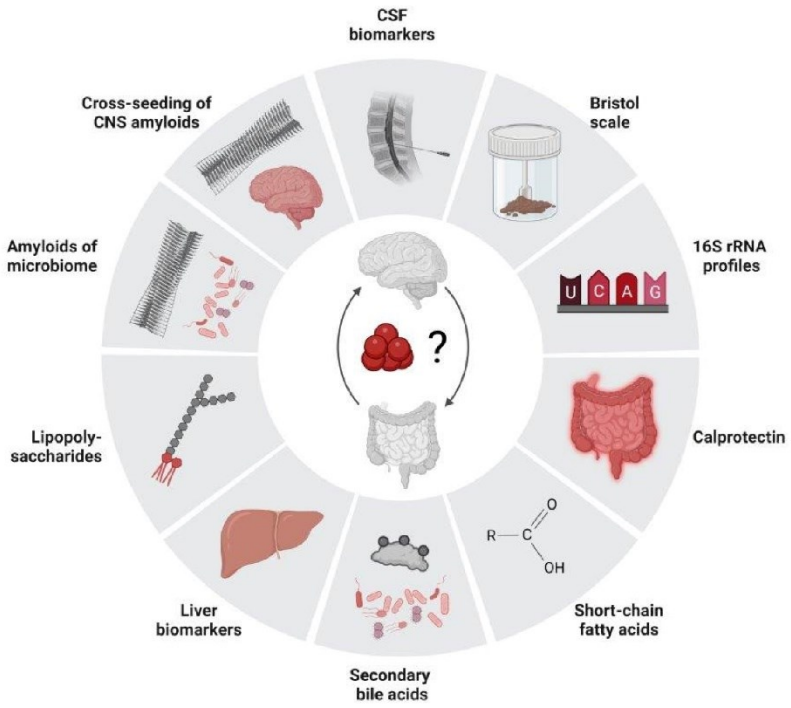

Figure 6. Association of fecal Aβ aggregates with additional biomarkers affecting AD pathology. The combination of fecal Aβ aggregates with further biomarkers may provide new insights into mechanism of brain-gut-microbiota axis and AD pathogenesis. Therefore, in addition to CSF biomarkers (Aβ40, Aβ42, phosphorylated and total Tau) and Bristol scale, 16S rRNA profiles fecal calprotectin, short-chain fatty acids, and secondary bile acids, liver biomarkers, and lipopolysaccharides should be determined in the future. Because amyloids produced by gut microbiome share similarities in tertiary structure with CNS amyloids, they may act in a prion-like manner and induce misfolding, aggregation, and deposition of Aβ and may cross-seed with neuronal amyloids once they have entered the brain due to increased permeability of the blood-brain barrier. Created with BioRender.com.

Conclusion

In conclusion, we developed a sFIDA assay for the quantitation of fecal Aβ aggregates, showing high reproducibility of preanalytical procedures, high analytical sensitivity, and specificity. In this work we delivered a proof-of-concept study, that Aβ aggregate are present in human feces and that AD patients exhibited elevated levels of fecal Aβ aggregate compared to HC. Future studies will need to confirm our results with more extensive cohort of participants, encompassing various AD stages, along with longitudinal samples and more comprehensive biomarker analysis. Finally, this work underscores the promising potential of fecal Aβ aggregates as a non-invasive biomarker for AD from which clinical routine and the development of therapeutic interventions might benefit in the future.

Abbreviations

Aβ	amyloid β
AD	Alzheimer's disease
AF	autofluorescence control
APTES	3-aminopropyl(triethoxysilane)
AUC	area under the curve
BC	blank control
BSA	bovine serum albumin
CC	capture control
CSF	cerebrospinal fluid
CV%	coefficient of variation
DMSO	dimethyl sulfoxide
EDC	1-ethyl-3-(3-dimethylaminopropyl)carbodiimide
HC	healthy controls
HFIP	1,1,1,3,3,3-hexafluoro-2-propanol
IQC	internal quality control
IVDs	*in-vitro* diagnostics
LoD	limit of detection
MCI	mild cognitive impairment
MES	2-(N-morpholino)ethanesulfonic acid
MIHA	maleimido hexanoic acid
NHS	N-hydroxysuccinimid
PBS 1	× phosphate-buffered saline
ROC	receiver operating characteristic
SD	standard deviation
sFIDA	surface-based fluorescence intensity distribution analysis
SiNaP	silica nanoparticle
TBS	1× Tris-buffered saline
TBST	1× Tris-buffered saline containing 0.05% Tween20
TIRFM	total internal reflection fluorescence microscopy

Additional file 1: Supplementary Information

Figure S1. Evaluation of the reproducibility of sample homogenization and dilution for three different fecal samples, related to Results. **Figure S2.** Parallelism of endogenous Aβ aggregates in fecal sample 1 and sample 2, related to Results. **Figure S3.** Evaluation of thermostability during transport or bench-top handling, related to Results and Figure 2. **Figure S4.** Schematic illustration of sample treatment and confirming the presence of fecal Aβ species in those samples using ELISA, related to Results. **Table S1.** Results of normal distribution tests for molar Aβ aggregate concentrations in fecal samples, related to Results. **Table S2.** The coefficient of variation, calculated calibration curve, coefficient of determination and the limit of detection of each experiment for Aβ-coated SiNaPs, IQC samples, and fecal samples, related to Results. **Table S3.** Clinical information, Bristol scale scores, and mean Aβ-aggregate concentrations with the standard deviation of the individual subjects, related to Results, Figure 5B and Figure 5C. **Table S4.** Spearman coefficient of correlation values for the analyses between fecal Aβ aggregate levels and seven fecal biomarkers indicating gut inflammation and increased permeability of intestinal membranes (bile acid, lipids, calprotectin, IgA, α-1-antitrypsin, hemoglobin, and albumin), related to Results. **Table S5.** p-values of two-sided Mann−Whitney U test for pairwise comparisons of measured fecal biomarker concentrations, related to Results.

Declarations

Ethics approval and consent to participate

The Ethics Commission of the Faculty of Medicine of the University of Cologne approved patient recruitment (19-1644).

Consent for publication

Not applicable

Availability of data and materials

All data generated or analysed during this study are included in this published article and its Supplementary Information. For image data analysis, we used the sFIDAta software application, which can be made available upon request.

678 **Competing Interests**

679 D.W. and O.B. are cofounders and shareholders of attyloid GmbH. D.W. is member of attyloid's
680 supervisory board. M.P., O.B., G.T. and D.W. are inventors of patent DE102020114278A1
681 (determination of disease-specific protein aggregates in fecal samples). These factors did not influence
682 the interpretation of the data. Remaining authors declare no conflicts of interest.

683 **Funding**

684 sFIDA was supported by the programs "Biomarkers Across Neurodegenerative Diseases I + II" of The
685 Alzheimer's Association, Alzheimer's Research UK, and the Weston Brain Institute [11084, BAND-19-
686 614337]. We are also grateful for support from The Michael J. Fox Foundation for Parkinson's Research
687 [14977, 009889], the ALS Association, and the Packard Center [19-SI-476]. We received further funding
688 from the Deutsche Forschungsgemeinschaft [INST 208/616-1 FUGG, INST 208/794-1 FUGG],
689 Helmholtz Association [HVF0079], Förderstiftung Dierichs, and Deutsche Alzheimer Gesellschaft e.V.
690 Selbsthilfe Demenz (DalzG). G.R.F. and O.A.O. were supported by the Marga and Walter Boll-
691 Foundation. H.G. was supported by the Cologne Clinician Scientist Program (CCSP) / Faculty of
692 Medicine / University of Cologne and received funding from Deutsche Forschungsgemeinschaft [DFG,
693 FI 773/15-1].

694 **Author contribution**

695 Conceptualization, M.P., O.B., D.W. and G.T.; Methodology, M.P.; Validation, M.P.; L.B., T.B. and V.K.;
696 Formal Analysis, M.P., L.B. and F.R.; Investigation, M.P. and M.T.; Resources, i.e., coordination of
697 sample collection, transport, and biobanking M.P., A.S., G.T., M.HT.S., H.G., G.R.F., M.T.B., and
698 O.A.O.; Writing – Original Draft, M.P.; Writing – Review & Editing, O.B., D.W., O.A.O, M.T.B., G.R.F.
699 and G.T; Visualization, M.P.; Supervision, O.B., G.T., J.K. and D.W.; Project Administration, O.B., D.W.
700 and G.T.; Funding Acquisition, O.B., G.T., D.W., G.R.F and O.A.O. All authors participated in the
701 discussion of the data, provided critical feedback, and contributed to the manuscript. All authors read
702 and approved the final manuscript.

703 **Acknowledgements**

704 The authors thank Carsten Korth (Institute of Neuropathology, Universitätsklinikum Düsseldorf, 40225
705 Düsseldorf, Germany) for providing the IC16 antibody. The authors Volker Nischwitz (Central Institute
706 for Engineering, Electronics and Analytics, Analytics (ZEA-3), Forschungszentrum Jülich, 52428, Jülich,

Germany) for determining the silicon concentration of the used Aβ-coated SiNaPs using inductively coupled plasma mass spectrometry. The authors confirm that these results have not currently been presented at any conference or reviewed or published in any other journal.

References

[1] Jack, C.R., Jr., et al., NIA-AA Research Framework: Toward a biological definition of Alzheimer's disease. *Alzheimers Dement*, 2018. **14**(4): p. 535-562.

[2] Brown, M.R., S.E. Radford, and E.W. Hewitt, Modulation of β-Amyloid Fibril Formation in Alzheimer's Disease by Microglia and Infection. *Front Mol Neurosci*, 2020. **13**: p. 609073.

[3] Hampel, H., et al., The Amyloid-β Pathway in Alzheimer's Disease. *Mol Psychiatry*, 2021. **26**(10): p. 5481-5503.

[4] Kulenkampff, K., et al., Quantifying misfolded protein oligomers as drug targets and biomarkers in Alzheimer and Parkinson diseases. *Nature Reviews Chemistry*, 2021. **5**(4): p. 277-294.

[5] Sun, M., et al., A Review of the Brain-Gut-Microbiome Axis and the Potential Role of Microbiota in Alzheimer's Disease. *J Alzheimers Dis*, 2020. **73**(3): p. 849-865.

[6] Leblhuber, F., et al., Elevated fecal calprotectin in patients with Alzheimer's dementia indicates leaky gut. *J Neural Transm* 2015. **122**(9): p. 1319-22.

[7] Kowalski, K. and A. Mulak, Brain-Gut-Microbiota Axis in Alzheimer's Disease. *J Neurogastroenterol Motil*, 2019. **25**(1): p. 48-60.

[8] Fink, A., G. Doblhammer, and G. Tamgüney, Recurring Gastrointestinal Infections Increase the Risk of Dementia. *Journal of Alzheimer's Disease*, 2021. **84**: p. 797-806.

[9] Ferreiro, A.L., et al., Gut microbiome composition may be an indicator of preclinical Alzheimer's disease. *Sci Transl Med*, 2023. **15**(700): p. eabo2984.

[10] Cheng, Y., D.Y. Tian, and Y.J. Wang, Peripheral clearance of brain-derived Aβ in Alzheimer's disease: pathophysiology and therapeutic perspectives. *Transl Neurodegener*, 2020. **9**(1): p. 16.

[11] Wang, J., et al., A systemic view of Alzheimer disease - insights from amyloid-β metabolism beyond the brain. *Nat Rev Neurol*, 2017. **13**(10): p. 612-623.

[12] Ullah, R., et al., Abnormal amyloid beta metabolism in systemic abnormalities and Alzheimer's pathology: Insights and therapeutic approaches from periphery. *Ageing Res Rev*, 2021. **71**: p. 101451.

[13] Jiang, C., et al., The Gut Microbiota and Alzheimer's Disease. *J Alzheimers Dis*, 2017. **58**(1): p. 1-15.

[14] Wu, S., et al., Excretion of Amyloid-β in the Gastrointestinal Tract and Regulation by the Gut Microbiota. *Journal of Alzheimer's Disease*, 2022. **90**: p. 1153-1162.

[15] Pellegrini, C., et al., Prodromal Intestinal Events in Alzheimer's Disease (AD): Colonic Dysmotility and Inflammation Are Associated with Enteric AD-Related Protein Deposition. *Int J Mol Sci*, 2020. **21**(10).

[16] Manocha, G.D., et al., Temporal progression of Alzheimer's disease in brains and intestines of transgenic mice. *Neurobiol Aging*, 2019. **81**: p. 166-176.

[17] Puig, K.L., G.D. Manocha, and C.K. Combs, Amyloid precursor protein mediated changes in intestinal epithelial phenotype in vitro. *PLoS One*, 2015. **10**(3): p. e0119534.

[18] Joachim, C.L., H. Mori, and D.J. Selkoe, Amyloid beta-protein deposition in tissues other than brain in Alzheimer's disease. *Nature*, 1989. **341**(6239): p. 226-30.

[19] Willbold, D., et al., Amyloid-type Protein Aggregation and Prion-like Properties of Amyloids. *Chem Rev*, 2021. **121**(13): p. 8285-8307.

[20] Kulawik, A., et al., Advancements of the sFIDA method for oligomer-based diagnostics of neurodegenerative diseases. *FEBS Lett*, 2018. **592**(4): p. 516-534.

[21] Herrmann, Y., et al., sFIDA automation yields sub-femtomolar limit of detection for Aβ aggregates in body fluids. *Clin Biochem*, 2017. **50**(4-5): p. 244-247.

[22] Hülsemann, M., et al., Biofunctionalized Silica Nanoparticles: Standards in Amyloid-β Oligomer-Based Diagnosis of Alzheimer's Disease. *J Alzheimers Dis*, 2016. **54**(1): p. 79-88.

[23] Pils, M., et al., Development and Implementation of an Internal Quality Control Sample to Standardize Oligomer-Based Diagnostics of Alzheimer’s Disease. *Diagnostics*, 2023. **13**(10): p. 1702.

[24] Blömeke, L., et al., Quantitative detection of α-Synuclein and Tau oligomers and other aggregates by digital single particle counting. *NPJ Parkinsons Dis*, 2022. **8**(1): p. 68.

[25] Wang-Dietrich, L., et al., The amyloid-β oligomer count in cerebrospinal fluid is a biomarker for Alzheimer's disease. *J Alzheimers Dis*, 2013. **34**(4): p. 985-94.

[26] Schaffrath, A., et al., Patients with isolated REM-sleep behavior disorder have elevated levels of alpha-synuclein aggregates in stool. *NPJ Parkinsons Dis*, 2023. **9**(1): p. 14.

[27] Kass, B., et al., Aβ oligomer concentration in mouse and human brain and its drug-induced reduction ex vivo. *Cell Rep Med*, 2022. **3**(5): p. 100630.

[28] Lewis, S.J. and K.W. Heaton, Stool form scale as a useful guide to intestinal transit time. *Scand J Gastroenterol*, 1997. **32**(9): p. 920-4.

[29] Vagenende, V., M.G. Yap, and B.L. Trout, Mechanisms of protein stabilization and prevention of protein aggregation by glycerol. *Biochemistry*, 2009. **48**(46): p. 11084-96.

[30] Rose, C., et al., The Characterization of Feces and Urine: A Review of the Literature to Inform Advanced Treatment Technology. *Crit Rev Environ Sci Technol*, 2015. **45**(17): p. 1827-1879.

[31] Stephen, A.M. and J.H. Cummings, The microbial contribution to human faecal mass. *J Med Microbiol*, 1980. **13**(1): p. 45-56.

[32] Phadia-AB. Stool Extraction Kit plus / Stool Extraction Buffer plus, instruction for use: 200/250/2500/5000-6665-020 / UK, version 2021-09-14. . 2021; Available on https://dfu.phadia.com/Data/Pdf/6130cb9570eec660e274806b.pdf [Accessed 23 January 2023].].

[33] ORGENTEC-Diagnostika-GmbH. Calprotectin, instruction for use: ORG 580_4, version ORG 580_IFU_EN_QM140866_2022-03-08_4. 2022; Available on https://products.orgentec.com/pdfs/ifu/ORG%20580_IFU_EN_QM140866_2022-03-08_4.pdf [Accessed 23 January 2023].].

[34] Bühlmann-Laboratories. Bühlmann Smart-Prep - Faecal sample preparation kit, Instruction for use: B-CAL-RD, version 2010-11-10. 2010; Available on https://www.buhlmannlabs.ch/wp-content/uploads/2015/01/B-CAL-RD_101110.pdf [Accessed 23 January 2023].].

[35] Immundiagnostik-AG. IDK Hemoglobin ELISA: For the in vitro determination of hemoglobin in stool, instruction for use: K 7816D, K7816D.20, version 2022-02-22. 2022; Available on https://www.immundiagnostik.com/media/pages/testkits/k-7816d/9a63870b70-1663639307/k7816d_2022-02-22_haemoglobin.pdf [Accessed 23 January 2023].].

[36] Demeditec-Diagnostics-GmbH. Calprotectin ELISA, instruction for use: DE849 V211014/DLB, version 2021-11-25. . 2021; Available on https://www.demeditec.de/de/produkte/calprotectin-elisa-de849/ifu-de849-calprotectin-elisa-211125-e.pdf [Accessed 23 January 2023].].

[37] Dornieden, S., et al., Characterization of a single-chain variable fragment recognizing a linear epitope of aβ: a biotechnical tool for studies on Alzheimer's disease? *PLoS One*, 2013. **8**(3): p. e59820.

[38] Andreasson, U., et al., A Practical Guide to Immunoassay Method Validation. *Front Neurol*, 2015. **6**: p. 179.

[39] Vanderstichele, H.M., et al., Optimized Standard Operating Procedures for the Analysis of Cerebrospinal Fluid Aβ42 and the Ratios of Aβ Isoforms Using Low Protein Binding Tubes. *J Alzheimers Dis*, 2016. **53**(3): p. 1121-32.

[40] Varesi, A., et al., The Potential Role of Gut Microbiota in Alzheimer's Disease: From Diagnosis to Treatment. *Nutrients*, 2022. **14**(3).

[41] Qian, X.H., et al., Mechanisms of Short-Chain Fatty Acids Derived from Gut Microbiota in Alzheimer's Disease. *Aging Dis*, 2022. **13**(4): p. 1252-1266.

[42] Vogt, N.M., et al., Gut microbiome alterations in Alzheimer's disease. *Sci Rep*, 2017. **7**(1): p. 13537.

[43] Vandeputte, D., et al., Stool consistency is strongly associated with gut microbiota richness and composition, enterotypes and bacterial growth rates. *Gut*, 2016. **65**(1): p. 57-62.

[44] Vanderstichele, H., et al., Potential sources of interference on Abeta immunoassays in biological samples. *Alzheimers Res Ther*, 2012. **4**(5): p. 39.

[45] Dimeski, G., Interference testing. *Clin Biochem Rev*, 2008. **29 Suppl 1**(Suppl 1): p. S43-8.

[46] Park, J.Y. and L.J. Kricka, *Chapter 5.3 - Interferences in Immunoassay*, in The Immunoassay Handbook (Fourth Edition), D. Wild, Editor. 2013, *Elsevier*: Oxford. p. 403-416.

[47] Armbruster, D.A. and T. Pry, Limit of blank, limit of detection and limit of quantitation. *Clin Biochem Rev*, 2008. **29 Suppl 1**(Suppl 1): p. S49-52.

[48] van de Merbel, N., et al., Stability: recommendation for best practices and harmonization from the Global Bioanalysis Consortium Harmonization Team. *Aaps j*, 2014. **16**(3): p. 392-9.

[49] Salvadores, N., et al., Detection of misfolded Aβ oligomers for sensitive biochemical diagnosis of Alzheimer's disease. *Cell Rep*, 2014. **7**(1): p. 261-8.

[50] Teunissen, C.E., et al., Blood-based biomarkers for Alzheimer's disease: towards clinical implementation. *Lancet Neurol*, 2022. **21**(1): p. 66-77.

[51] Paraskevaidi, M., et al., Diagnostic Biomarkers for Alzheimer's Disease Using Non-Invasive Specimens. *J Clin Med*, 2020. **9**(6).

[52] Lewczuk, P., et al., Clinical significance of fluid biomarkers in Alzheimer's Disease. *Pharmacol Rep*, 2020. **72**(3): p. 528-542.

[53] Minic, R. and I. Zivkovic, *Optimization, Validation and Standardization of ELISA*. 2020.

828 [54] Schoonenboom, N.S., et al., Effects of processing and storage conditions on amyloid beta (1-
829 42) and tau concentrations in cerebrospinal fluid: implications for use in clinical practice. *Clin*
830 *Chem*, 2005. **51**(1): p. 189-95.

831 [55] Yang, T., et al., A highly sensitive novel immunoassay specifically detects low levels of soluble
832 Aβ oligomers in human cerebrospinal fluid. *Alzheimers Res Ther*, 2015. **7**(1): p. 14.

833 [56] Savage, M.J., et al., A sensitive aβ oligomer assay discriminates Alzheimer's and aged control
834 cerebrospinal fluid. *J Neurosci*, 2014. **34**(8): p. 2884-97.

835 [57] Herskovits, A.Z., et al., A Luminex assay detects amyloid β oligomers in Alzheimer's disease
836 cerebrospinal fluid. *PLoS One*, 2013. **8**(7): p. e67898.

837 [58] Fukumoto, H., et al., High-molecular-weight beta-amyloid oligomers are elevated in
838 cerebrospinal fluid of Alzheimer patients. *Faseb j*, 2010. **24**(8): p. 2716-26.

839 [59] Hölttä, M., et al., Evaluating amyloid-β oligomers in cerebrospinal fluid as a biomarker for
840 Alzheimer's disease. *PLoS One*, 2013. **8**(6): p. e66381.
841

3.6 Patients with isolated REM-sleep behavior disorder have elevated levels of alpha-synuclein aggregates in stool

Autoren:	Anja Schaffrath, Sophia Schleyken, Aline Seger, Hannah Jergas, Pelin Özdüzenciler, Marlene Pils, Lara Blömeke, Annelise Cousin, Johannes Willbold, Tuyen Bujnicki, Oliver Bannach, Gereon R. Fink, Dieter Willbold, Michael Sommerauer, Michael T. Barbe, Gültekin Tamgüney
Journal:	npj parkinson's disease (veröffentlicht)
DOI:	10.1038/s41531-023-00458-4
Impact-Faktor:	8,7 (2022)
Beitrag:	Eigenanteil: 10 % Etablierung des Protokolls der Immundepletion im sFIDA Synthese der Silika-Nanopartikel Diskussion der Ergebnisse Prüfung des Manuskripts
Anhang zum Manuskript	Kapitel 7.6

npj | parkinson's disease

www.nature.com/npjparkd

ARTICLE OPEN

Check for updates

Patients with isolated REM-sleep behavior disorder have elevated levels of alpha-synuclein aggregates in stool

Anja Schaffrath[1], Sophia Schleyken[2], Aline Seger[2], Hannah Jergas[2], Pelin Özdüzenciler[1], Marlene Pils[1,3], Lara Blömeke[1,3], Anneliese Cousin[1], Johannes Willbold[1], Tuyen Bujnicki[1], Oliver Bannach[1,3,4], Gereon R. Fink[2,5], Dieter Willbold[1,4], Michael Sommerauer[2,5], Michael T. Barbe[2] and Gültekin Tamgüney[1,4]✉

Misfolded and aggregated α-synuclein is a neuropathological hallmark of Parkinson's disease (PD). Thus, α-synuclein aggregates are regarded as a biomarker for the development of diagnostic assays. Quantification of α-synuclein aggregates in body fluids is challenging, and requires highly sensitive and specific assays. Recent studies suggest that α-synuclein aggregates may be shed into stool. We used surface-based fluorescence intensity distribution analysis (sFIDA) to detect and quantify single particles of α-synuclein aggregates in stool of 94 PD patients, 72 isolated rapid eye movement sleep behavior disorder (iRBD) patients, and 51 healthy controls. We measured significantly elevated concentrations of α-synuclein aggregates in stool of iRBD patients versus those of controls ($p = 0.024$) or PD patients ($p < 0.001$). Our results show that α-synuclein aggregates are excreted in stool and can be measured using the sFIDA assay, which could support the diagnosis of prodromal synucleinopathies.

npj Parkinson's Disease (2023)9:14 ; https://doi.org/10.1038/s41531-023-00458-4

INTRODUCTION

Parkinson's disease (PD), dementia with Lewy bodies (DLB), and multiple system atrophy (MSA) are synucleinopathies characterized by the oligomerization and aggregation of α-synuclein into assemblies rich in cross-beta structure, which is a critical event in the pathogenesis of these diseases[1–6]. Because α-synuclein fibrils deposit in Lewy bodies and Lewy neurites in neurons in PD and DLB or in neuronal and glial cytoplasmic inclusions in MSA, small oligomeric intermediates of α-synuclein that are still soluble are thought to be the most toxic to neurons[7–9]. The diagnosis of synucleinopathies primarily relies on clinical assessment and brain imaging, which are either imprecise or costly, especially during early disease stages, highlighting the urgent need for a biomarker for early and reliable disease detection[10,11]. Also, for potential therapies to be most effective, detecting synucleinopathies at early stages may be advantageous when the burden of pathologic α-synuclein and neuronal loss are minimal. In the prodromal stage of synucleinopathies, non-motor symptoms, such as hyposmia and gastrointestinal dysfunction, can appear as early symptoms up to 20 years before cardinal motor symptoms manifest[10,12]. Also, most patients with isolated rapid eye movement (REM) sleep behavior disorder (iRBD), a parasomnia characterized by REM sleep without atonia and vivid dream enactment, convert to PD, DLB, or MSA within 10–20 years of diagnosis[13,14]. IRBD patients display many non-motor symptoms seen in PD patients including hyposmia, orthostatic hypotension, and gastrointestinal dysfunction[15]. Importantly, iRBD patients also accumulate pathologic α-synuclein assemblies in the central and peripheral nervous system[16,17]. Besides the nervous system and cerebrospinal fluid (CSF), α-synuclein aggregates have been detected in skin, olfactory mucosa, saliva, tears, urine, and blood of PD patients, which may all serve as potential sources for diagnosing synucleinopathies[18–26]. Histological findings also show that enteric neurons in the gastrointestinal submucosa of PD patients contain pathologic α-synuclein, even at prodromal stages[27–29]. Together with findings of pathological α-synuclein in the enteric nervous system (ENS) and the dorsal motor nucleus of the vagus nerve and the anterior olfactory bulb as the earliest lesion sites in PD, Braak and colleagues postulated the dual-hit hypothesis suggesting that α-synuclein pathology spreads from the olfactory bulb to the temporal lobes, and from the ENS via the vagus nerve to the CNS[30,31]. Further, several studies suggest that pathologic α-synuclein assemblies have prion-like properties, allowing them to multiply and propagate between neurons in the nervous system and to spread across large distances in the brain and body, including from the ENS to the CNS and vice versa[32–35].

Earlier findings in transgenic TgM83$^{+/-}$ mice expressing human α-synuclein demonstrated that α-synuclein fibrils used for an oral challenge could cross the mucosal barrier of the gastrointestinal tract after which they invaded the nervous system and triggered a synucleinopathy in these mice[36]. Here, we hypothesized that human pathologic α-synuclein assemblies released from, e.g., affected enteric neurons may traverse the mucosal lining of the gastrointestinal tract and be excreted in stool. This would involve a mechanism similar to the environmental shedding of prions in feces of deer and elk infected with chronic wasting disease or that of sheep and goats infected with scrapie[37,38].

It remains challenging to specifically detect protein aggregates in body fluids as the expected concentrations are very low, requiring a high sensitivity that standard techniques such as ELISA do not provide[39]. Moreover, monomers are present in great excess, necessitating that assays have a high selectivity for oligomers. To overcome these challenges in detecting aggregated α-synuclein assemblies, we used the sFIDA (surface-based fluorescence intensity distribution analysis) assay, which uses antibodies targeting overlapping or identical epitopes, enabling it to specifically detect

[1]Institute of Biological Information Processing (Structural Biochemistry: IBI-7), Forschungszentrum Jülich, 52428 Jülich, Germany. [2]Department of Neurology, Faculty of Medicine and University Hospital Cologne, University of Cologne, 50923 Köln, Germany. [3]attyloid GmbH, 40225 Düsseldorf, Germany. [4]Institut für Physikalische Biologie, Heinrich-Heine-Universität Düsseldorf, 40225 Düsseldorf, Germany. [5]Cognitive Neuroscience, Institute of Neuroscience and Medicine (INM-3), Forschungszentrum Jülich, 52428 Jülich, Germany. ✉email: erdem@fz-juelich.de

Published in partnership with the Parkinson's Foundation

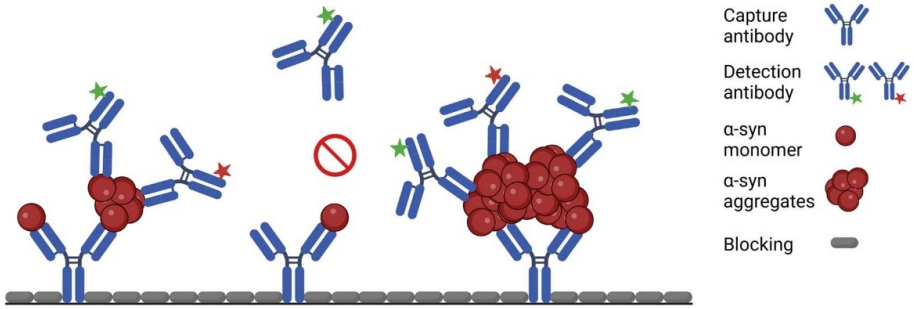

Fig. 1 Schematic figure of the sFIDA assay principle. The glass surface of a microtiter plate is coated with a capture antibody (Syn211) against amino acid residues 121–125 of α-synuclein. The capture antibody binds both α-synuclein monomers and aggregates in the sample. The detection antibody (Syn211), a 1:1 mixture of this antibody labeled with fluorescent dye CF633 or CF488A, can only detect aggregates since it is directed against the same epitope as the capture antibody. The epitope on the monomer bound to the capture antibody is masked by the capture antibody and can, thus, not be bound by the detection antibody. The microtiter plate wells are imaged by two-channel confocal fluorescence microscopy to detect single particles. Only particles decorated with at least two different detection antibodies (colocalized signal) contribute to the sFIDA readout signal. The image was created with BioRender.com.

Table 1. Demographic and clinical information on patients and controls that donated stool samples.

	PD	iRBD	HC	*p* (PD vs. HC)	*p* (PD vs. iRBD)	*p* (iRBD vs. HC)
Number	94	72	51	N/A	N/A	N/A
Female [number (percentage)]	29 (30.9)	10 (13.9)	31 (60.8)	0.001	n.s.	$p < 0.001$
Age [years ± SD]	64.5 ± 9.9	66.3 ± 6.4	56.4 ± 17.1	n.s.	n.s.	$p < 0.05$
Education [years ± SD]	15.4 ± 4.1	15.9 ± 4.0	16.0 ± 3.3	n.s.	n.s.	n.s.
Disease duration [years ± SD]	9.0 ± 5.8	7.4 ± 5.5	N/A	N/A	n.s.	N/A
DemTect [score ± SD]	13.8 ± 3.3	14.8 ± 2.3	15.9 ± 2.3	$p < 0.001$	n.s.	$p < 0.05$
MDS-UPDRS III [score ± SD]	24.1 ± 14.9	4.0 ± 2.7	N/A	N/A	$p < 0.001$	N/A
Non-Motor Symptoms Scale [score ± SD]	30.6 ± 23.1	16.2 ± 18.0	12.5 ± 14.4	$p < 0.001$	$p < 0.001$	n.s.
CCCSS [score ± SD]	4.1 ± 4.0	2.8 ± 2.7	2.5 ± 2.5	$p < 0.05$	$p < 0.05$	n.s.
Scent [score ± SD]	5.3 ± 2.6	6.6 ± 2.7	10.4 ± 1.7	$p < 0.001$	$p < 0.05$	$p < 0.001$
Screening questionnaire for parkinsonism [score ± SD]	5.6 ± 2.2	0.3 ± 0.8	0.3 ± 0.8	$p < 0.001$	$p < 0.001$	n.s.
IRBD screening questionnaire [score ± SD]	4.9 ± 3.0	9.0 ± 2.7	1.7 ± 1.6	$p < 0.001$	$p < 0.001$	$p < 0.001$
Hoehn and Yahr [score ± SD]	3.0 ± 0.9	N/A	N/A	N/A	N/A	N/A
Levodopa challenge test [% ± SD]	40 ± 20	N/A	N/A	N/A	N/A	N/A

PD Parkinson's disease, *iRBD* isolated rapid eye movement sleep behavior disorder, *HC* healthy control, *SD* standard deviation, *MDS-UPDRS III* Movement Disorder Society's Unified Parkinson's Disease Rating Scale Part III, *CCCSS* Cleveland Clinic Constipation Scoring System, *N/A* not available, *n.s.* not significant.

aggregates in the presence of monomers[40–43]. Here, the Syn211 antibody that recognizes amino acids 121–125 on α-synuclein is attached to a glass surface and captures α-synuclein species in stool homogenates[44]. Next, the captured α-synuclein species are detected with a blend of two Syn211 antibodies, each labeled with a different fluorescent dye, one green and one red (Fig. 1). The surface is then scanned by two-channel fluorescent confocal microscopy, yielding single particle sensitivity. Because the Syn211 antibody only recognizes a single linear epitope on α-synuclein, using the same Syn211 antibody to capture and detect α-synuclein species guarantees specific quantitation of only aggregated α-synuclein species. Monomers with a single linear epitope are captured but cannot be detected and are thus disregarded. Since the sFIDA assay in its current version does not differentiate between α-synuclein species from small oligomers to large fibrils, we refer to analytes measured in sFIDA as aggregates.

We recently used sFIDA to quantitate α-synuclein and tau aggregates in CSF of patients with PD, DLB, and other neurodegenerative diseases, showing that sFIDA is a reliable, highly sensitive, and robust assay for the diagnosis of neurodegenerative diseases and drug development[40]. The aim of this study was to detect and quantify α-synuclein aggregates in human stool and, more importantly, to demonstrate its possible use in a clinical setting and potentially for drug development. We adapted the sFIDA assay to quantify α-synuclein aggregates in stool samples of 217 subjects. We technically validated this assay by assessing parameters like the limit of detection (LOD), coefficient of variation (CV%), inter-assay correlation, and cross-reactivity to other aggregates.

RESULTS

Descriptive analysis of the patient and control groups

We collected stool samples of PD ($n = 94$) and iRBD patients ($n = 72$) and healthy controls (HC) without past or present neurological disorder ($n = 51$) to determine if and how much α-synuclein aggregates they contain. Demographic and clinical information for these three cohorts on sex, age, education, disease duration, memory, motor, non-motor, olfactory, constipation, and further information are available in Table 1, and for individual

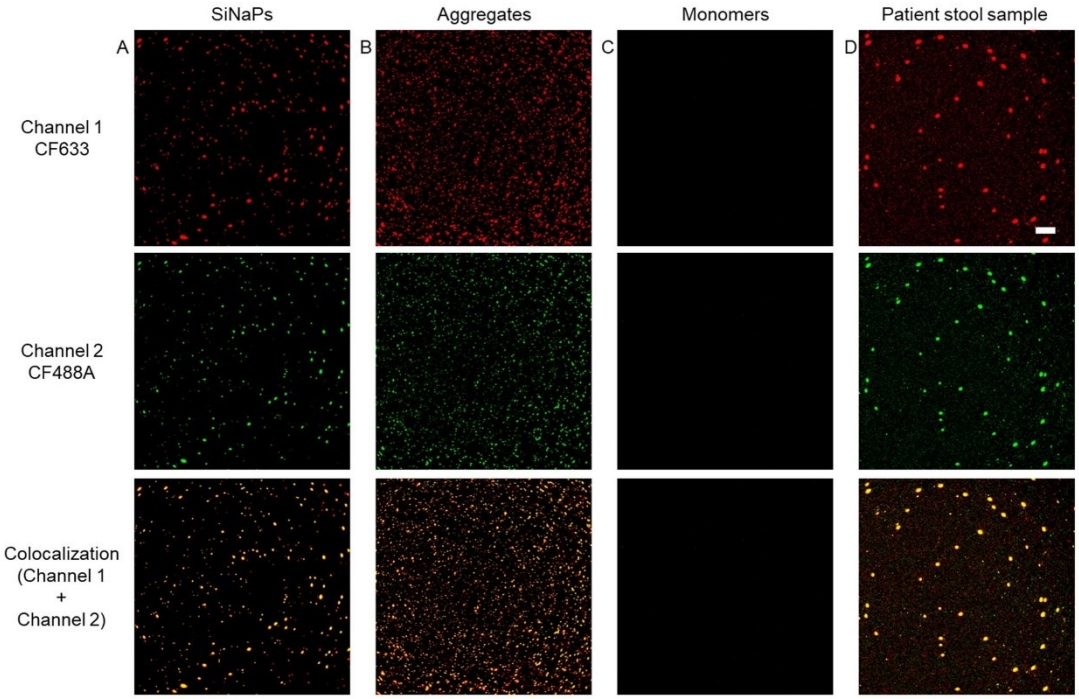

Fig. 2 Fluorescence images of α-synuclein SiNaPs, synthetic α-synuclein aggregates, monomers, and a PD stool sample. Shown are exemplary fluorescence images taken in the red fluorescence channel (channel 1, CF633), green fluorescence channel (channel 2, CF488A), and the colocalized fluorescence signal of both channels of **a** 0.32 pM α-synuclein SiNaPs in buffer **b** 1581 pM synthetic α-synuclein aggregates in buffer (concentration based on the deployed monomer concentration), **c** 1000 pM α-synuclein monomers in buffer, and **d** a stool sample of a PD patient. To better visualize the 16-bit images, the contrast and minimum/maximum values were adjusted. Scale bar: 30 µm.

patients and healthy controls in Supplementary Table 1. There was a gender bias towards men in the PD (69.1%) and more so in the iRBD (86.1%) cohort. In the control group, gender bias was slightly more towards women (60.8%). The age of PD (64.5 ± 9.9 years) and iRBD patients (66.3 ± 6.4 years) did not significantly differ, while healthy controls were on average 8–10 years younger (56.4 ± 17.1 years). We did not observe significant differences in the duration of education between the three groups. Disease duration in PD patients was 9.0 ± 5.8 years and in iRBD patients 7.4 ± 5.5 years. The cognitive performance (DemTect score) of healthy controls (15.9 ± 2.3) was significantly higher than that of PD (13.8 ± 3.3) and iRBD patients (14.8 ± 2.3, Supplementary Fig. 1a)[45]. PD patients (24.1 ± 14.9) scored significantly higher than iRBD patients (4.0 ± 2.7) on the Movement Disorder Society's Unified Parkinson's Disease Rating Scale Part III (MDS-UPDRS III)[46]. Equally, PD patients (30.6 ± 23.1) scored significantly higher on the Non-Motor Symptoms Scale (NMSS) for PD than iRBD patients (16.2 ± 18.0) or healthy controls (12.5 ± 14.4, Supplementary Fig. 1b)[47]. Also, PD patients (4.1 ± 4.0) were significantly more constipated than iRBD patients (2.8 ± 2.7) and healthy controls (2.5 ± 2.5), based on the Cleveland Clinic Constipation Scoring System (Supplementary Fig. 1c)[48]. PD patients (5.3 ± 2.6) also suffered more from hyposmia (Supplementary Fig. 1d), reflected in a significantly lower scent score, than iRBD patients (6.6 ± 2.7) or healthy controls (10.4 ± 1.7). In addition, PD patients (5.6 ± 2.2) scored significantly higher in the screening questionnaire for parkinsonism compared to iRBD patients (0.3 ± 0.8) and healthy controls (0.3 ± 0.8, Supplementary Fig. 1e)[49]. The results of the RBD screening questionnaire (RBDSQ, Supplementary Fig. 1f) also showed significant differences between iRBD (9.0 ± 2.7) and PD patients (4.9 ± 3.0) or healthy controls (1.7 ± 1.6), as well as between PD patients and healthy controls[50]. On average, PD patients scored 3.0 ± 0.9 on the Hoehn and Yahr scale and 40 ± 20% on the levodopa challenge test[51].

sFIDA measurements of α-synuclein silica nanoparticles (SiNaPs) and stool samples show a low intra-assay variance

As a standard for signal calibration and LOD calculation, we used silica nanoparticles (SiNaPs), each carrying multiple monomers of α-synuclein[42]. Figure 2 shows exemplary images of the α-synuclein SiNaPs standard, synthetic α-synuclein aggregates, the buffer control, and a PD stool sample for the red fluorescence channel (channel one), the green fluorescence channel (channel two), and the colocalized signal of both channels. For analysis, only colocalized pixels (sFIDA readout) were utilized. Because of the high number of samples, the measurements had to be performed on nine 384-well microtiter plates. For all experiments, the mean intra-assay coefficient of variation (CV%) was calculated from the sFIDA readout of the four replicates of each sample to be 28.4% for the α-synuclein SiNaPs standard and 26.3% for the stool samples (Supplementary Table 2).

Repeated sFIDA measurements of α-synuclein aggregates in stool samples show a low inter-assay variance

To assess the inter-assay variance between independent sFIDA assays, we repeatedly measured 50 randomly selected stool

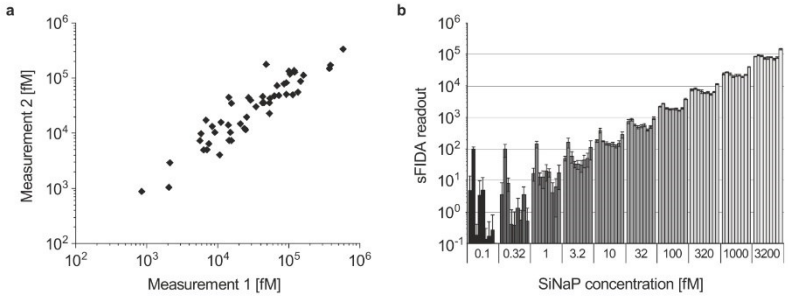

Fig. 3 Repeated measurements of α-synuclein aggregates in stool and of α-synuclein SiNaPs yield highly replicable results. We tested the inter-assay variance of the sFIDA assay for α-synuclein aggregates. **a** Repeated measurements of 50 randomly selected stool samples by the same operator in the same laboratory on different days were highly reproducible with a Spearman coefficient of correlation of $r = 0.916$ ($p = 0.2 \times 10^{-6}$). **b** Nine independent measurements of a dilution series of the α-synuclein SiNaPs used for calibration of the stool sample data set also showed highly replicable results for all concentrations with a Spearman coefficient of correlation of $r = 0.979$ ($p = 3.85 \times 10^{-62}$). Error bars indicate standard deviation.

samples on two different days. Both measurements showed a significant correlation with a Spearman correlation coefficient of $r = 0.916$ ($p = 0.2 \times 10^{-6}$) (Fig. 3a). Next, we confirmed the reproducibility of the assay by repeatedly measuring the α-synuclein SiNaPs standard used for calibrating all stool samples in nine independent assays (Fig. 3b). The repeated measurements yielded highly reproducible results with a Spearman correlation coefficient of $r = 0.979$ ($p = 3.85 \times 10^{-62}$).

sFIDA measurements of α-synuclein aggregates are highly selective

To further evaluate the sFIDA assay, we examined the ability of unspecific binding of synthetic α-synuclein aggregates or α-synuclein SiNaPs to the surface of the 384-well microtiter plate by comparing the readout in the presence and absence of a capture antibody. Relative to the readouts of α-synuclein aggregates and SiNaPs measured with a capture antibody, readouts without a capture antibody were reduced by 97% and 96%, respectively (Fig. 4a). We also measured samples in the absence of detection antibodies. This reduced the readout for synthetic α-synuclein aggregates fully (100%), which became indistinguishable from the generally low buffer control (BC) and for α-synuclein SiNaPs by 98%. Additionally, we tested the ability of the sFIDA assay to detect monomeric α-synuclein. As shown in Fig. 4b, the readout for α-synuclein monomers was as negligible as the BC readout and much lower than the readout of the positive control, which consisted of synthetic α-synuclein aggregates made from the same monomer concentration. Our results show that the potential presence of monomeric α-synuclein in stool, which most probably is degraded in this particular environment, did not influence the sFIDA readout. To determine the cross-reactivity of the sFIDA assay, we used the NAB228 antibody against amyloid-beta (Aβ) as a capture antibody and synthetic α-synuclein aggregates or SiNaPs as samples. This reduced the sFIDA readout for synthetic α-synuclein aggregates by 98% and that for α-synuclein SiNaPs by almost 100% (Fig. 4b).

At last, to determine the selectivity of the sFIDA assay, we measured synthetic Aβ aggregates and Aβ SiNaPs using the Syn211 antibody against α-synuclein for capture and detection. As a positive control for detecting Aβ aggregates and SiNaPs, we used NAB228 as a capture antibody and 6E10 and IC16 as detection antibodies. In contrast to this antibody combination specific for Aβ, antibodies specific for α-synuclein did not detect Aβ aggregates or Aβ SiNaPs (Fig. 4c).

Immunodepletion removes α-synuclein aggregates in samples

To prove that sFIDA measurements are selective for α-synuclein aggregates, we performed an immunodepletion. Samples were incubated with dynabeads coupled to the Syn211 antibody specific for α-synuclein to remove α-synuclein aggregates in stool or α-synuclein SiNaPs. As a further control, samples were also incubated with blank dynabeads not coupled to antibodies for mock immunodepletions. After immunodepletion, supernatants were analyzed with sFIDA. The sFIDA readout for immunodepleted stool samples was on average decreased by 73%, and for immunodepleted α-synuclein SiNaPs by 100% (Fig. 5a, b). Mock immunodepletion of the same samples resulted in a reduction of only about 7% compared to readouts without immunodepletion (Fig. 5b). This minimal reduction could have been caused by proteolytic digestion or disassembly of aggregates, or unspecific adhesion of aggregates to beads during incubation at room temperature.

sFIDA detects attomolar concentrations of α-synuclein SiNaPs

The sensitivity of the sFIDA assay was determined using the α-synuclein SiNaPs standard. To achieve this, a one-sided Mann-Whitney U test was applied to determine the lowest concentration significantly different from the buffer control for each SiNaPs standard to standardize the calibration range and determine the LOD. Based on these results, the lower limit of the calibration curve was set to 0.32 fM and the upper limit to 3200 fM. In all experiments, we observed a correlation between the sFIDA readout and the corresponding SiNaPs concentration with a Spearman correlation coefficient of $r = 0.979$ ($p = 3.85 \times 10^{-62}$). After calibration, the mean LOD was 0.3 fM for all experiments (for individual LOD values see Supplementary Table 3). For all measured samples, aggregate concentrations were above the LOD of the associated experiment (Supplementary Table 4).

α-Synuclein aggregate concentrations are elevated in stool of iRBD patients

We finally used the sFIDA assay to measure α-synuclein aggregate concentrations in stool of PD and iRBD patients, and healthy controls. Using the α-synuclein SiNaPs standard, we calibrated the sFIDA readout of all samples and calculated α-synuclein aggregate concentrations (Supplementary Table 1). Statistical analyses were performed using non-parametric tests because none of the three groups showed a normal distribution (p-value < 0.05, Supplementary Table 5). The median concentration of α-synuclein aggregates in stool samples of iRBD patients (9.2 fM) was significantly elevated compared to those of the control group (5.2 fM, $p = 0.024$) as well as

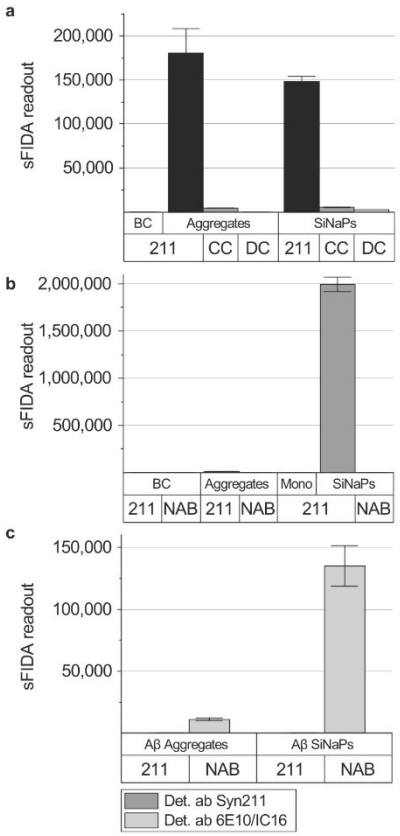

Fig. 4 sFIDA with antibodies against α-synuclein specifically detects α-synuclein aggregates and α-synuclein SiNaPs but not α-synuclein monomers, Aβ aggregates, or Aβ SiNaPs. a When either the capture antibody or the detection antibodies were omitted (capture control (CC), detection control (DC)), the sFIDA readout for the CC was reduced by 96% for α-synuclein SiNaPs and 97% for α-synuclein aggregates of the respective readout with a capture antibody. For the DC, the sFIDA readout was reduced by 98% for α-synuclein SiNaPs, and entirely for α-synuclein aggregates (100%), where the sFIDA readout was indistinguishable from the buffer control (BC). **b** The sFIDA readout of α-synuclein SiNaPs and α-synuclein aggregates, when captured with the NAB228 antibody against beta-amyloid (Aβ), was reduced by almost 100% for α-synuclein SiNaPs and 98% for synthetic α-synuclein aggregates compared to the signal with Syn211 capture antibody. The sFIDA readout of α-synuclein monomers (Mono) was reduced to the level of the BC compared to the same concentration of monomers in aggregated α-synuclein. **c** Additionally, Aβ aggregates and Aβ SiNaPs were captured and detected with the Syn211 antibody against α-synuclein. As a positive control, the same Aβ aggregates and Aβ SiNaPs were captured with antibodies specific to Aβ (capture antibody: NAB228, detection antibodies: 6E10/IC16). The graph shows that the Syn211 antibody does not detect Aβ aggregates or Aβ SiNaPs. Error bars indicate standard deviation.

those of PD patients (3.8 fM, $p < 0.001$) when using the Kruskal–Wallis *H* test (Fig. 6a). Our findings for the iRBD cohort remained significant when the two highest outliers in this cohort were ignored or when adjusted for sex ($p < 0.001$). No difference was detected between PD patients and the control group. Receiver operating characteristic (ROC) curves (Fig. 6b) revealed a high sensitivity (>75%) of the sFIDA assay in detecting α-synuclein aggregates in stool of iRBD patients versus healthy controls or PD patients but a lower specificity (iRBD vs. PD: 52.1%; iRBD vs. HC: 49.0%; Table 2). In contrast, the sFIDA assay was highly specific (96.1%) but much less sensitive (6.4%) in detecting α-synuclein aggregates in stool samples of PD patients versus healthy controls. We also observed a weak positive correlation with a Spearman coefficient between the DemTect score and α-synuclein aggregate concentrations ($r = 0.221$, $p < 0.05$), and between the RBDSQ score and α-synuclein aggregate concentrations ($r = 0.223$, $p < 0.05$), but no other correlations in stool of PD patients, iRBD patients or healthy controls (Supplementary Table 6).

DISCUSSION

We demonstrated that α-synuclein aggregates can be detected and quantified in stool, proving that not only α-synuclein aggregates are secreted from the body into the lumen of the gastrointestinal tract and excreted in stool, but also that the sFIDA assay can be applied to stool samples to reveal the existence of α-synuclein aggregates in a subgroup of humans. To investigate the origin and fate of α-synuclein aggregates in the gastrointestinal tract is essential in the future. Also, this provides opportunities to explore the concentration of α-synuclein aggregates in stool for the diagnosis of neurodegenerative diseases. By omitting the Syn211 capture or detection antibodies, changing the Syn211 capture antibody to one specific for Aβ, or changing the substrate to α-synuclein monomers, Aβ aggregates, or Aβ SiNaPs, we showed that the stool-adapted sFIDA assay measures α-synuclein aggregate and α-synuclein SiNaP concentrations very specifically and sensitively over a wide range of concentrations. We observed an overlap between patients and healthy controls, resulting in a specificity of 49.0% and a sensitivity of 76.4% for discriminating iRBD patients from healthy controls, and a specificity of 52.1% and a sensitivity of 80.6% for discriminating iRBD and PD patients. We were unable to discriminate PD patients from healthy controls. Our results are less specific but almost as sensitive as other studies aiming to discriminate α-synuclein aggregate concentrations in CSF samples of different synucleinopathies from healthy controls[40,52,53]. We are not aware of any other studies that have attempted to quantify α-synuclein aggregate concentrations in stool, making a comparison of our results with previous ones, e.g., in CSF is not straightforward. All measured stool samples showed concentrations above the determined LOD with values between 0.1 M and 100 pM, with the majority of the samples (87%) showing concentrations between 1 fM and 300 fM. Surprisingly, stool of iRBD patients showed significantly elevated levels of α-synuclein aggregates compared to healthy controls. In contrast to this, stool of PD patients not only showed significantly lower levels of α-synuclein aggregates than those of iRBD patients but also showed no difference to healthy controls (Fig. 6a). For CSF, it has previously been shown that α-synuclein aggregate concentrations are significantly elevated in PD and iRBD patients compared to healthy controls[24,40,52,54]. Further, several longitudinal studies in PD patients showed an increase of aggregated α-synuclein in CSF with disease progression[55,56]. One explanation of why we did not observe an increase of α-synuclein aggregate concentrations in stool of PD patients or a correlation with age or disease duration may be the recently proposed "brain-first" and "body-first" PD subtypes with different affection of the ENS, making it harder to observe a difference to healthy controls[57–59]. Still, separation of potential brain-first and body-first PD is most reliable in de novo PD using polysomnography to detect RBD. As we had mid-stage PD samples and only a questionnaire-based evaluation of RBD symptoms, we could not reliably separate our PD patient cohort in brain-first and body-first PD subtypes. Another explanation might be that levels of α-synuclein aggregates in stool of PD patients do not behave like those in CSF. More α-synuclein aggregates could be excreted in stool during prodromal and early phases of PD and

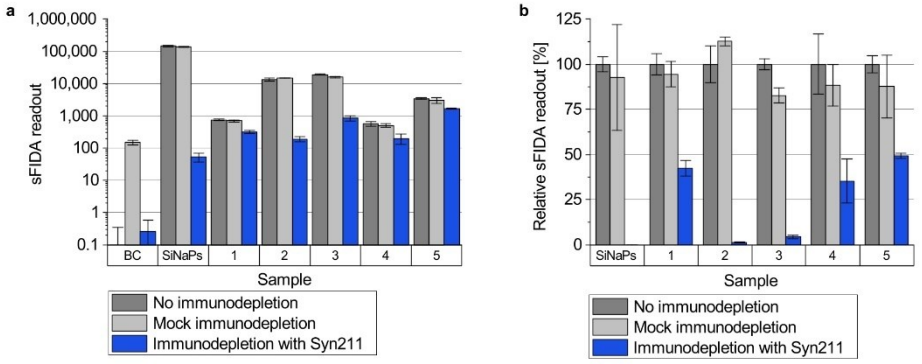

Fig. 5 Immunodepletion of α-synuclein SiNaPs and α-synuclein aggregates in stool samples. a The α-synuclein SiNaPs standard and five stool samples were immunodepleted with magnetic beads coupled to Syn211 antibodies and, as a mock immunodepletion, without coupled antibodies. Immunodepletion entirely eliminated the sFIDA readout for α-synuclein SiNaPs (100%) and reduced that for α-synuclein aggregates in stool samples on average by 73%, ranging from 51% to 99% for different samples. Mock immunodepletion did not significantly affect the sFIDA readout with a reduction of about 7% for stool samples and α-synuclein SiNaPs. **b** The relative sFIDA readout [%] value represents the percent ratio of the sFIDA readouts of (mock) depleted to non-depleted samples.

less in advanced stages, similar to decreases in CSF concentrations of $A\beta_{42}$ during the course of Alzheimer's disease[60]. One could also speculate that the α-synuclein aggregates in stool during very early disease stages may not exclusively be shed into the gastrointestinal tract by affected submucosal neurons but also by a systemic disposal mechanism for α-synuclein aggregates via liver and bile that becomes less efficient during later disease stages. This may explain why α-synuclein aggregate concentrations in stool and CSF correlate well during early disease stages but less in later stages. To better understand the dynamics of α-synuclein aggregate shedding or release into stool, concentrations in longitudinally collected stool samples of iRBD and PD patients need to be assessed.

Our data show that iRBD patients with a high risk of developing synucleinopathies have significantly higher levels of α-synuclein aggregates in stool compared to healthy controls, stressing the value of the sFIDA assay in early disease detection[13]. Stool, next to CSF, skin, and nasal mucosa, where α-synuclein aggregates accumulate in iRBD patients, is now an additional valuable and easily accessible resource with a potential for diagnostic purposes[52,61–63]. Whether iRBD patients with high concentrations of α-synuclein aggregates in stool are more likely to convert faster to PD, DLB, or MSA, or are more likely to develop a particular type of synucleinopathy remains to be determined. Interestingly, we also measured high α-synuclein aggregate concentrations in stool of some control subjects. This could be either due to prodromal iRBD/PD pathology or other factors in the gastrointestinal tract that may cause a disease-independent aggregation of α-synuclein. According to the presumption mentioned above, it could also mean that these subjects still do have a very efficient disposal system for α-synuclein aggregates into the stool. It will be essential to assess whether these individuals are showing other prodromal signs of PD and to monitor them longitudinally.

This study has several limitations. Due to the specificity of the Syn211 antibody, which recognizes epitopes 121–125 of α-synuclein, this sFIDA assay cannot detect aggregates that are solely composed of fragments missing the C-terminus with this epitope, or have this epitope masked due to posttranslational nitration or phosphorylation of tyrosine 125[44,64]. However, the abundance of α-synuclein aggregates where all α-synuclein molecules within one aggregate may be missing this particular epitope or have it masked is likely to be very small. Furthermore, more recent studies suggest that tyrosine 125 of α-synuclein may not be phosphorylated in PD and DLB[65]. Also, sFIDA does not distinguish between α-synuclein aggregates that are seeding-incompetent or harmless to neurons (off-pathway) and those that may be harmful to neurons (on-pathway)[66,67].

The sensitivity and specificity of this assay may be improved, for example, by combining measurements of aggregated α-synuclein with those of other potential biomarkers like phosphorylated α-synuclein, tau, glial fibrillary acidic protein, or neurofilament light chain that are expressed in the ENS and may be altered early in disease[68–71]. Another approach to improve this assay could be to extract and concentrate α-synuclein aggregates from stool samples, e.g., by immunoprecipitation, prior to their quantitation. Diet and the gut microbiome may likely affect the detection of α-synuclein aggregates in stool[72]. Stool has a complex matrix containing water, proteins, fatty acids, polysaccharides, bacterial biomass, undigested food residues, and bile that may inhibit antibody binding and mask α-synuclein aggregates from detection. Stool also contains proteases that may still be active during the preparation of the stool homogenates, which would mean that the measured values must be regarded as lower limits of the present α-synuclein aggregates. Also, using additional tissue and body fluid sources in combination with stool may further enhance the sensitivity and specificity of the sFIDA assay and improve diagnostic accuracy in discriminating between different patient cohorts and controls[52,61–63]. In summary, our results show that α-synuclein aggregates are excreted in stool and can be measured using the sFIDA assay, which may facilitate the diagnosis of prodromal synucleinopathies. This could be of value for developing therapies targeting early disease stages, which may result in better efficacy.

METHODS

Synthesis of protein-coated silica nanoparticles (SiNaPs)

SiNaPs were used for calibration and to test selectivity[40]. The body of the SiNaPs was synthesized via the Stöber process and the surface aminated with (3-aminopropyl)triethoxysilane. Functionalized α-synuclein peptide fragments (amino acids 115–130, Peptides and Elephants, Henningsdorf, Germany) or Aβ peptide fragments (amino acids 1–15, Peptides and Elephants, Henningsdorf, Germany) containing a cysteamine at the C-terminus were cross-linked to the surface of aminated SiNaPs functionalized with maleimidohexanoic acid, which was previously activated with 1-ethyl-3(3-dimethylaminopropyl)carbodiimide and N-hydroxysuccinimide (Sigma Aldrich, St. Louis, USA) to enable reaction of the cysteamine with the maleimide

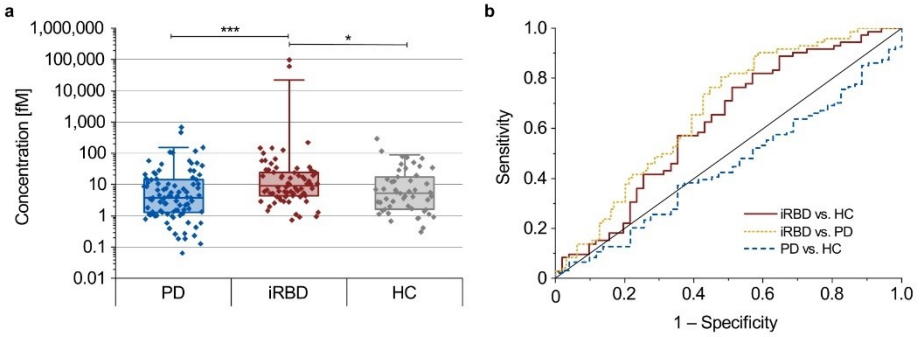

Fig. 6 Calibrated sFIDA results and receiver operating characteristic (ROC) analyses for detecting α-synuclein aggregates in stool samples. Median concentrations of α-synuclein aggregates in stool samples of iRBD patients (9.2 fM) were significantly elevated compared to those of healthy controls (HC, 5.2 fM, $p = 0.024$) or PD patients (3.8 fM, $p < 0.001$). PD patients did not significantly differ from healthy controls. Box plots indicate the lower (Q1) and upper (Q3) quartiles as boxes. Horizontal lines within boxes indicate medians. Whiskers indicate 1.5 times the interquartile range (Q3–Q1) above Q3 and below Q1. Data falling outside this range are plotted as outliers. Significant differences between groups were calculated using the Kruskal–Wallis H test. ***$p < 0.001$, **$0.001 \le p < 0.01$, *$0.01 \le p < 0.05$. Error bars indicate standard deviation. **b** In the ROC analyses, discrimination of PD patients versus healthy controls showed a specificity of 96.1% and a sensitivity of 6.4%, with an area under the curve (AUC) of 0.447. In comparison, discrimination of iRBD patients versus healthy controls showed a specificity of 49.0% and a sensitivity of 76.4% with an AUC of 0.622 (see Table 2 for other specificity and sensitivity values and significances).

Table 2. Results of the ROC analyses for specificity, sensitivity, and area under the curve with the respective p-value for α-synuclein aggregates in stool.

	Specificity [%]	Sensitivity [%]	AUC	p
iRBD vs. HC	49.0	76.4	0.622	0.021
iRBD vs. PD	52.1	80.6	0.670	1.81×10^{-4}
PD vs. HC	96.1	6.4	0.447	0.291

Parkinson's disease (PD), isolated rapid eye movement sleep behavior disorder (iRBD), healthy control (HC), area under the curve (AUC).

group. For synthesis of protein-conjugated SiNaPs, 10% of the possible binding sites were functionalized by adding protein to dispersed SiNaPs. Protein-coupled SiNaPs were subjected to ultrasonication for 10 min prior to each use. The same batches of α-synuclein or Aβ SiNaPs were used for all experiments. To serve as a calibration standard, the stock solution of α-synuclein SiNaPs was diluted in extraction buffer (EliA Calprotectin 2 Extraction Buffer (Phadia, Uppsala, Sweden) with 1× protease inhibitor cocktail (cOmplete EDTA-free Protease Inhibitor Cocktail, Roche, Basel, Switzerland)) in a half-logarithmic dilution series from 3200 to 0.1 fM.

Characterization of SiNaPs

The size and shape of the aminated SiNaPs were analyzed using transmission electron microscopy[73]. For the aminated silica core, a mean particle size of 18.5 nm was determined. Inductively coupled plasma–mass spectrometry (ICP-MS) was used to determine the silicon concentration. The molar concentration of the SiNaPs was calculated using the silicon concentration and the known size, density, and shape[40].

Labeling of antibodies

Fluorescent antibodies were used for microscopy-based detection of aggregates. The mouse monoclonal anti-α-synuclein Syn211 antibody (Santa Cruz Biotechnology, Inc., Dallas, USA) was labeled with CF633 and CF488A (Biotium, Freemont, USA) and the anti-Aβ IC16 (Heinrich-Heine University, Düsseldorf, Germany) antibody was labeled with CF633 (Biotium, Freemont, USA)[40,44]. The labeling process was performed according to the manufacturer's protocol. The dyes with activated succinimidyl esters were mixed with the antibody in carbonate buffer to react covalently with the amines of the antibody. The labeled antibody was purified using a polyacrylamide bead suspension (Bio-Gel P 30 Gel, Bio-Rad Laboratories, Inc., Hercules, USA). The concentration and degree of labeling were determined according to the manufacturer's protocol.

Patients and healthy controls

This study was approved by the Ethics Commission of the Faculty of Medicine of the University of Cologne (19–1644). PD and iRBD patients and healthy controls were enrolled at the Department of Neurology of the University Hospital Cologne. Informed consent was obtained from all human participants. All enrolled subjects completed a basic characteristics questionnaire providing information on items, such as age, sex, handedness, years of education, and medical history. All subjects completed the validated German version of the screening questionnaire for parkinsonism originally developed by Tanner and colleagues[49], the REM sleep behavior disorder screening questionnaire (RBDSQ)[50], for which a score of six was determined as a cut-off value for detecting iRBD[74], the Cleveland Clinics Constipation Scoring System (CCCSS)[48], the Ocular Surface Disease Index (OSDI)[75], the revised Beck Depression Inventory (BDI-II)[76], the Memory Assessment Clinic Questionnaire (MAC-Q)[77], and the Functional Activities Questionnaire (FAQ)[78].

PD patients were recruited from patient charts of our outpatient clinic or the ward when patients were admitted to the hospital. Patients were diagnosed with PD ($n = 94$) according to the Movement Disorder Society Clinical Diagnostic Criteria for Parkinson's disease[79]. Clinical and demographic information, including disease duration, were acquired based on an investigator's medical reports and careful anamnesis. In addition to the basic characteristics questionnaire, PD and iRBD patients were asked to complete the Non-Motor Symptoms Scale (NMSS) questionnaire for PD[46], and the Movement Disorder Society's (MDS) Unified Parkinson's Disease Rating Scale Part II (MDS-UPDRS II)[46]. Cognitive performance was assessed using DemTect[45]. Motor function was assessed with the MDS-UPDRS Part III[46]. The Hoehn and Yahr scale[51], and MDS-UPDRS Parts I and IV were rated by an investigator for each patient[46]. A smell test was performed for each subject according to a standardized procedure. Some but

not all PD patients received a DaTSCAN and a levodopa challenge test (LCT) outside of this study.

IRBD patients were part of an ongoing study ($n = 72$) recruiting a local prodromal PD cohort in Cologne through newspaper advertisements from the community. Following a structured telephone interview, subjects with a high likelihood of having iRBD were invited to undergo polysomnography (PSG). We used a mobile SOMNOscreenTM plus device for overnight PSG[80]. Visual PSG scoring was performed on 30 s epochs as well as diagnosis of iRBD according to the American Academy of Sleep Medicine's manual for the scoring of sleep and associated events, version 2.6[46].

Healthy controls ($n = 51$) were recruited by advertisement, and, in many cases, the caregivers of the PD patients agreed to participate in the study. Healthy controls were free of any neurological disease. In addition to the basic characteristics questionnaire (see above), healthy controls completed the NMSS questionnaire for PD, the RBDSQ, and a smell test. Healthy controls with an RBDSQ score greater than five were excluded from the analysis[74].

Stool samples from all subjects were collected between July 2020 and September 2021 using beakers with a screw cap and a removal spoon. Additionally, a paper towel stool catcher was used to avoid contamination. Stool samples were collected at various locations. If a stool sample was collected at home, in most cases, it was not older than two hours and stored in a plastic bag in a refrigerator until it was further processed. Pseudonymized samples were stored at −80 °C.

All patient-related data and samples were anonymized, and researchers were aware of the clinical data at the time of the sFIDA measurement. Data were subsequently tested for normal distribution (Shapiro Wilk, Lilliefors, Kolmogorov–Smirnov, Anderson Darling). A Kruskal–Wallis H test was used to identify differences between cohorts. If significant differences were determined, a pairwise comparison using a two-sided Mann–Whitney U test was conducted.

Sample preparation

Stool samples were collected at various time points using beakers with a screw cap and a removal spoon. Stool samples were thawed at room temperature (RT) for 15 min and homogenized according to the manufacturer's protocol of the EliA Stool Extraction Kit with minor changes (Phadia, Uppsala, Sweden). Using Simplix extraction tubes (Gaudlitz, Coburg, Germany), 17 mg stool were sampled and homogenized in 1300 µL cold extraction buffer through vortexing. The homogenate was centrifuged at $3000 \times g$ for 5 min at 4 °C to pellet non-soluble components. The supernatant was aliquoted and stored at −80 °C until further use.

Assay protocol

In the present study, we used SensoPlate Plus 384-well glass bottom microtiter plates (Greiner Bio-One I, Frickenhausen, Germany). The glass surface was incubated with the Syn211 antibody as capture at 7.5 µg/mL in 1x PBS buffer overnight at 4 °C. After washing five times with 80 µL TBS-T (TBS and 0.05% Tween20) and afterwards five times with TBS, the wells were blocked with 0.5% nonfat, dried milk powder in TBS-ProClin (TBS containing 0.03% ProClin) for 3 h at RT. The plate was washed again with TBS-T and TBS and 20 µL protein-conjugated SiNaPs diluted in extraction buffer, and 20 µL of the samples, thawed at RT for 15 min, were incubated for 1 h at RT. After washing five times with TBS, the wells were incubated for 1 h with the fluorescent detection antibodies Syn211-CF633 and Syn211-CF488A (each 0.625 µg/mL) in TBS-T containing 0.1% BSA, after which the wells were washed again with TBS. For measurement, the buffer in the wells was changed to TBS-ProClin. Each standard and sample were pipetted as four replicates. For detection of Aβ aggregates and Aβ SiNaPs, the NAB288 antibody (Sigma Aldrich, St. Louis, USA) was used at 2.5 µg/mL in PBS buffer for capture, and the fluorescent detection antibodies IC16-CF633 and 6E10-AF488 (Biolegend, San Diego, USA) each at 0.625 µg/mL for detection. All washing steps were carried out with an automated microplate washer (405 LS Microplate Washer, BioTek, VT, USA).

Inter-assay measurements

For inter-assay measurements of the calibration curve and samples, the same assay was repeated by the same person with the same antibodies and materials. Repeatedly assayed samples were subjected to an additional freeze–thaw cycle.

Immunodepletion

Immunodepletion was performed with magnetic Dynabeads Protein G (Invitrogen, Waltham, USA) to which the Syn211 antibody was bound via the Fc region according to the manufacturer's protocol. Shortly, dynabeads were washed twice with PBS-T (PBS and 0.05% Tween20) and applied to a magnet to remove the supernatant. After washing, the beads were incubated with 0.1 mg/mL Syn211 antibody (to reach a target load of 8 µg/mL beads), shaking at 650 rpm for 100 min at RT. After two more washing steps (see above), the coated beads were diluted in PBS-T to 20 µg/mL dynabeads, respectively. To ensure that a signal loss did not result from a non-specific binding of sample components to dynabeads, we also performed a synthesis without the antibody. For immunodepletion and mock immunodepletion, we applied 0.5 mg of antibody-coated and non-coated dynabeads to a magnet and removed the supernatant. Then, 100 µL sample was added and incubated for 1 h at RT while rotating. After incubation, the dynabeads were pelleted with a magnet and the supernatant was transferred to a fresh tube. All samples were analyzed using sFIDA as described above.

Image-data acquisition and analysis

Images were taken with an IRIS confocal fluorescence microscope (In Cell Analyzer 6500HS, GE Healthcare, Chicago, USA), using a 40× magnification objective with water immersion by two-channel imaging (channel one excitation: 642 nm, emission filter: 682.5/59 nm, exposure time: 3 s; channel two excitation: 488 nm, emission filter: 524.5/48 nm; exposure time: 4 s). A total of 16 images with 2040×2040 pixels each were acquired per well, covering 16% of the total well area. The acquired images were analyzed with the in-house developed sFIDAta software tool to ensure unbiased and automated image data analysis[40]. This included automatic detection and elimination of images containing artifacts and counting aggregate labeling pixels. In addition, a min-max filtering was applied, resulting in a removal of 10% of the images with the highest and lowest sFIDA readout per well. The sFIDA readout refers to the number of colocalized pixels of both channels. To reduce the background signal and compensate for fluctuations of the absolute fluorescence intensities, intensity cutoffs were determined for each experiment based on the buffer control. The cutoff is referred to as the gray-scale value of an image at which the rate of positive versus the total number of pixels in the buffer control equals a preset value[40,81]. By choosing a cutoff value, only pixels exceeding the cutoff value were considered for analysis. Additionally, we included a calibration in each measurement and converted the sFIDA readout to a SiNaP calibration-based concentration [fM] to ensure that differences in fluorescence intensity did not influence assay results. For inter-assay measurements, a cutoff value of 0.001% and, for the analysis of the stool samples, a cutoff value of 0.0003% were chosen.

Statistics

General statistics. Statistical analyses were performed using SigmaPlot 11.0, IBM SPSS Statistics 28.0.1.1 (15), OriginPro 2020 SR1, or JASP 0.14.1. Mean and standard deviation were calculated based on the

sFIDA readout of four replicates. The intra-assay variation is described by the coefficient of variation (CV%). To determine inter-assay variation, the Spearman coefficient of correlation was calculated for the replicate measurements of the samples.

Calibration. For calculating the calibration line, only concentrations of the SiNaPs standard were included that significantly differed from the blank control and were above the LOD. To this end, a one-sided Mann-Whitney U test was carried out. After calculating the calibration range for each experiment, a universal calibration range for all experiments was established. The LOD is defined based on Eq. (1):

$$LOD\ [pixel] = sFIDA\ readout\ (blank\ control) + 3\sigma \quad (1)$$

For linear regression, the sFIDA readouts were weighted with 1/readout. The buffer control was used as a negative control for the calibration and for calculating the LOD.

ROC analysis. A receiver operating characteristic (ROC) analysis was performed on the acquired dataset. The optimal combination of sensitivity and specificity for a ROC curve was calculated with a maximized Youden's index.

Reporting summary

Further information on research design is available in the Nature Research Reporting Summary linked to this article.

DATA AVAILABILITY

The authors confirm that the data supporting the findings of this study are available within the article and its supplementary materials.

CODE AVAILABILITY

For image data analysis, we used the sFIDAta software application, which can be made available upon request.

Received: 2 November 2022; Accepted: 16 January 2023;
Published online: 02 February 2023

REFERENCES

1. Schweighauser, M. et al. Structures of alpha-synuclein filaments from multiple system atrophy. *Nature* **585**, 464–469 (2020).
2. Yang, Y. et al. Structures of alpha-synuclein filaments from human brains with Lewy pathology. *Nature* **610**, 791–795 (2022).
3. Spillantini, M. G. et al. Alpha-synuclein in Lewy bodies. *Nature* **388**, 839–840 (1997).
4. Spillantini, M. G. et al. Filamentous alpha-synuclein inclusions link multiple system atrophy with Parkinson's disease and dementia with Lewy bodies. *Neurosci. Lett.* **251**, 205–208 (1998).
5. Spillantini, M. G., Crowther, R. A., Jakes, R., Hasegawa, M. & Goedert, M. alpha-Synuclein in filamentous inclusions of Lewy bodies from Parkinson's disease and dementia with lewy bodies. *Proc. Natl Acad. Sci. USA* **95**, 6469–6473 (1998).
6. Wakabayashi, K., Yoshimoto, M., Tsuji, S. & Takahashi, H. Alpha-synuclein immunoreactivity in glial cytoplasmic inclusions in multiple system atrophy. *Neurosci. Lett.* **249**, 180–182 (1998).
7. Fusco, G. et al. Structural basis of membrane disruption and cellular toxicity by alpha-synuclein oligomers. *Science* **358**, 1440–1443 (2017).
8. Cremades, N. et al. Direct observation of the interconversion of normal and toxic forms of alpha-synuclein. *Cell* **149**, 1048–1059 (2012).
9. Wong, Y. C. & Krainc, D. alpha-synuclein toxicity in neurodegeneration: mechanism and therapeutic strategies. *Nat. Med* **23**, 1–13 (2017).
10. Heinzel, S. et al. Update of the MDS research criteria for prodromal Parkinson's disease. *Mov. Disord.* **34**, 1464–1470 (2019).
11. Magalhaes, P. & Lashuel, H. A. Opportunities and challenges of alpha-synuclein as a potential biomarker for Parkinson's disease and other synucleinopathies. *NPJ Parkinsons Dis.* **8**, 93 (2022).
12. Schapira, A. H. V., Chaudhuri, K. R. & Jenner, P. Non-motor features of Parkinson disease. *Nat. Rev. Neurosci.* **18**, 509 (2017).
13. Postuma, R. B. et al. Risk and predictors of dementia and parkinsonism in idiopathic REM sleep behaviour disorder: a multicentre study. *Brain* **142**, 744–759 (2019).
14. Schenck, C. H., Bundlie, S. R. & Mahowald, M. W. Delayed emergence of a parkinsonian disorder in 38% of 29 older men initially diagnosed with idiopathic rapid eye movement sleep behaviour disorder. *Neurology* **46**, 388–393 (1996).
15. Fedorova, T. D. et al. Imaging progressive peripheral and central dysfunction in isolated REM sleep behaviour disorder after 3 years of follow-up. *Parkinsonism Relat. Disord.* **101**, 99–104 (2022).
16. Iranzo, A. et al. Neurodegenerative disease status and post-mortem pathology in idiopathic rapid-eye-movement sleep behaviour disorder: an observational cohort study. *Lancet Neurol.* **12**, 443–453 (2013).
17. Miglis, M. G. et al. Biomarkers of conversion to alpha-synucleinopathy in isolated rapid-eye-movement sleep behaviour disorder. *Lancet Neurol.* **20**, 671–684 (2021).
18. Nam, D. et al. Detection and assessment of alpha-synuclein oligomers in the urine of Parkinson's disease patients. *J. Parkinsons Dis.* **10**, 981–991 (2020).
19. Vivacqua, G. et al. Salivary alpha-synuclein in the diagnosis of Parkinson's disease and progressive supranuclear palsy. *Parkinsonism Relat. Disord.* **63**, 143–148 (2019).
20. Luan, M. et al. Diagnostic value of salivary real-time quaking-induced conversion in Parkinson's disease and multiple system atrophy. *Mov. Disord.* **37**, 1059–1063 (2022).
21. Hamm-Alvarez, S. F. et al. Levels of oligomeric alpha-Synuclein in reflex tears distinguish Parkinson's disease patients from healthy controls. *Biomark. Med* **13**, 1447–1457 (2019).
22. Wang, Z. et al. Skin alpha-synuclein aggregation seeding activity as a novel biomarker for Parkinson disease. *JAMA Neurol.* **78**, 1–11 (2020).
23. De Luca, C. M. G. et al. Efficient RT-QuIC seeding activity for alpha-synuclein in olfactory mucosa samples of patients with Parkinson's disease and multiple system atrophy. *Transl. Neurodegener.* **8**, 24 (2019).
24. Tokuda, T. et al. Detection of elevated levels of alpha-synuclein oligomers in CSF from patients with Parkinson disease. *Neurology* **75**, 1766–1772 (2010).
25. Kluge, A. et al. Detection of neuron-derived pathological alpha-synuclein in blood. *Brain* **145**, 3058–3071 (2022).
26. Bongianni, M. et al. Olfactory swab sampling optimization for alpha-synuclein aggregate detection in patients with Parkinson's disease. *Transl. Neurodegener.* **11**, 37 (2022).
27. Shannon, K. M. et al. Alpha-synuclein in colonic submucosa in early untreated Parkinson's disease. *Mov. Disord.* **27**, 709–715 (2012).
28. Braak, H., de Vos, R. A., Bohl, J. & Del Tredici, K. Gastric alpha-synuclein immunoreactive inclusions in Meissner's and Auerbach's plexuses in cases staged for Parkinson's disease-related brain pathology. *Neurosci. Lett.* **396**, 67–72 (2006).
29. Stokholm, M. G., Danielsen, E. H., Hamilton-Dutoit, S. J. & Borghammer, P. Pathological alpha-synuclein in gastrointestinal tissues from prodromal Parkinson disease patients. *Ann. Neurol.* **79**, 940–949 (2016).
30. Hawkes, C. H., Del Tredici, K. & Braak, H. Parkinson's disease: a dual-hit hypothesis. *Neuropathol. Appl. Neurobiol.* **33**, 599–614 (2007).
31. Hawkes, C. H., Del Tredici, K. & Braak, H. Parkinson's Disease. *Ann. N. Y. Acad. Sci.* **1170**, 615–622 (2009).
32. Woerman, A. L. & Tamgüney, G. Body-first Parkinson's disease and variant Creutzfeldt-Jakob disease—similar or different? *Neurobiol. Dis.* **164**, 105625 (2022).
33. Tamgüney, G. & Korczyn, A. D. A critical review of the prion hypothesis of human synucleinopathies. *Cell Tissue Res* **373**, 213–220 (2017).
34. Van Den Berge, N. et al. Evidence for bidirectional and trans-synaptic parasympathetic and sympathetic propagation of alpha-synuclein in rats. *Acta Neuropathol.* **138**, 535–550 (2019).
35. Arotcarena, M. L. et al. Bidirectional gut-to-brain and brain-to-gut propagation of synucleinopathy in non-human primates. *Brain* **143**, 1462–1475 (2020).
36. Lohmann, S. et al. Oral and intravenous transmission of alpha-synuclein fibrils to mice. *Acta Neuropathol.* **138**, 515–533 (2019).
37. Tamgüney, G. et al. Asymptomatic deer excrete infectious prions in faeces. *Nature* **461**, 529–532 (2009).
38. Terry, L. A. et al. Detection of prions in the faeces of sheep naturally infected with classical scrapie. *Vet. Res* **42**, 65 (2011).
39. Kulenkampff, K., Wolf Perez, A.-M., Sormanni, P., Habchi, J. & Vendruscolo, M. Quantifying misfolded protein oligomers as drug targets and biomarkers in Alzheimer and Parkinson diseases. *Nat. Rev. Chem.* **5**, 277–294 (2021).
40. Blömeke, L. et al. Quantitative detection of alpha-Synuclein and Tau oligomers and other aggregates by digital single particle counting. *NPJ Parkinsons Dis.* **8**, 68 (2022).

41. Kulawik, A., Heise, H., Zafiu, C., Willbold, D. & Bannach, O. Advancements of the sFIDA method for oligomer-based diagnostics of neurodegenerative diseases. *FEBS Lett.* **592**, 516–534 (2018).
42. Herrmann, Y. et al. Nanoparticle standards for immuno-based quantitation of alpha-synuclein oligomers in diagnostics of Parkinson's disease and other synucleinopathies. *Clin. Chim. Acta* **466**, 152–159 (2017).
43. Herrmann, Y. et al. sFIDA automation yields sub-femtomolar limit of detection for Abeta aggregates in body fluids. *Clin. Biochem.* **50**, 244–247 (2017).
44. Giasson, B. I. et al. A panel of epitope-specific antibodies detects protein domains distributed throughout human alpha-synuclein in Lewy bodies of Parkinson's disease. *J. Neurosci. Res.* **59**, 528–533 (2000).
45. Kalbe, E. et al. DemTect: a new, sensitive cognitive screening test to support the diagnosis of mild cognitive impairment and early dementia. *Int J. Geriatr. Psychiatry* **19**, 136–143 (2004).
46. Goetz, C. G. et al. Movement disorder society-sponsored revision of the Unified Parkinson's Disease Rating Scale (MDS-UPDRS): Process, format, and clinimetric testing plan. *Mov. Disord.* **22**, 41–47 (2007).
47. Chaudhuri, K. R. et al. The metric properties of a novel non-motor symptoms scale for Parkinson's disease: results from an international pilot study. *Mov. Disord.* **22**, 1901–1911 (2007).
48. Agachan, F., Chen, T., Pfeifer, J., Reissman, P. & Wexner, S. D. A constipation scoring system to simplify evaluation and management of constipated patients. *Dis. Colon Rectum* **39**, 681–685 (1996).
49. Pramstaller, P. P., Falk, M., Schoenhuber, R. & Poewe, W. Validation of a mail questionnaire for parkinsonism in two languages (German and Italian). *J. Neurol.* **246**, 79–86 (1999).
50. Stiasny-Kolster, K. et al. The REM sleep behavior disorder screening questionnaire–a new diagnostic instrument. *Mov. Disord.* **22**, 2386–2393 (2007).
51. Hoehn, M. M. & Yahr, M. D. Parkinsonism: onset, progression and mortality. *Neurology* **17**, 427–442 (1967).
52. Rossi, M. et al. Ultrasensitive RT-QuIC assay with high sensitivity and specificity for Lewy body-associated synucleinopathies. *Acta Neuropathol.* **140**, 49–62 (2020).
53. Compta, Y. et al. Correlates of cerebrospinal fluid levels of oligomeric- and total-alpha-synuclein in premotor, motor and dementia stages of Parkinson's disease. *J. Neurol.* **262**, 294–306 (2015).
54. Iranzo, A. et al. Detection of alpha-synuclein in CSF by RT-QuIC in patients with isolated rapid-eye-movement sleep behaviour disorder: a longitudinal observational study. *Lancet Neurol.* **20**, 203–212 (2021).
55. Hall, S. et al. Longitudinal Measurements of Cerebrospinal Fluid Biomarkers in Parkinson's Disease. *Mov. Disord.* **31**, 898–905 (2016).
56. Majbour, N. K. et al. Longitudinal changes in CSF alpha-synuclein species reflect Parkinson's disease progression. *Mov. Disord.* **31**, 1535–1542 (2016).
57. Borghammer, P. & Van Den Berge, N. Brain-first versus gut-first Parkinson's disease: a hypothesis. *J. Parkinsons Dis.* **9**, S281–S295 (2019).
58. Horsager, J. et al. Brain-first versus body-first Parkinson's disease: a multimodal imaging case-control study. *Brain* **143**, 3077–3088 (2020).
59. Berg, D. et al. Prodromal Parkinson disease subtypes—key to understanding heterogeneity. *Nat. Rev. Neurol.* **17**, 349–361 (2021).
60. Mattsson, N. et al. CSF biomarkers and incipient Alzheimer disease in patients with mild cognitive impairment. *J. Am. Med. Assoc.* **302**, 385–393 (2009).
61. Doppler, K. et al. Dermal phospho-alpha-synuclein deposits confirm REM sleep behaviour disorder as prodromal Parkinson's disease. *Acta Neuropathol.* **133**, 535–545 (2017).
62. Doppler, K. et al. Consistent skin alpha-synuclein positivity in REM sleep behavior disorder—a two center two-to-four-year follow-up study. *Parkinsonism Relat. Disord.* **86**, 108–113 (2021).
63. Stefani, A. et al. Alpha-synuclein seeds in olfactory mucosa of patients with isolated REM sleep behaviour disorder. *Brain* **144**, 1118–1126 (2021).
64. Schmid, A. W., Fauvet, B., Moniatte, M. & Lashuel, H. A. Alpha-synuclein post-translational modifications as potential biomarkers for Parkinson disease and other synucleinopathies. *Mol. Cell. Proteom.* **12**, 3543–3558 (2013).
65. Fayyad, M. et al. Investigating the presence of doubly phosphorylated alpha-synuclein at tyrosine 125 and serine 129 in idiopathic Lewy body diseases. *Brain Pathol.* **30**, 831–843 (2020).
66. Winner, B. et al. In vivo demonstration that alpha-synuclein oligomers are toxic. *Proc. Natl Acad. Sci. USA* **108**, 4194–4199 (2011).
67. Conway, K. A. et al. Acceleration of oligomerization, not fibrillization, is a shared property of both alpha-synuclein mutations linked to early-onset Parkinson's disease: implications for pathogenesis and therapy. *Proc. Natl Acad. Sci. USA* **97**, 571–576 (2000).
68. Clairembault, T. et al. Enteric GFAP expression and phosphorylation in Parkinson's disease. *J. Neurochem* **130**, 805–815 (2014).
69. Harapan, B. N. et al. No enhanced (p-) alpha-synuclein deposition in gastrointestinal tissue of Parkinson's disease patients. *Parkinsonism Relat. Disord.* **80**, 82–88 (2020).
70. Lionnet, A. et al. Characterisation of tau in the human and rodent enteric nervous system under physiological conditions and in tauopathy. *Acta Neuropathol. Commun.* **6**, 65 (2018).
71. Gries, M. et al. Parkinson mice show functional and molecular changes in the gut long before motoric disease onset. *Mol. Neurodegener.* **16**, 34 (2021).
72. Nerius, M., Doblhammer, G. & Tamgüney, G. GI infections are associated with an increased risk of Parkinson's disease. *Gut* **69**, 1154–1156 (2019).
73. Hulsemann, M. et al. Biofunctionalized silica nanoparticles: standards in amyloid-beta oligomer-based diagnosis of Alzheimer's disease. *J. Alzheimers Dis.* **54**, 79–88 (2016).
74. Nomura, T., Inoue, Y., Kagimura, T., Uemura, Y. & Nakashima, K. Utility of the REM sleep behavior disorder screening questionnaire (RBDSQ) in Parkinson's disease patients. *Sleep. Med* **12**, 711–713 (2011).
75. Walt, J., Rowe, M. & Stern, K. Evaluating the functional impact of dry eye: the ocular surface disease index. *Drug Inf. J.* **31**, b5 (1997).
76. Beck, A. T., Steer, R. A., Ball, R. & Ranieri, W. Comparison of Beck Depression Inventories -IA and -II in psychiatric outpatients. *J. Pers. Assess.* **67**, 588–597 (1996).
77. Crook, T. H. 3rd, Feher, E. P. & Larrabee, G. J. Assessment of memory complaint in age-associated memory impairment: the MAC-Q. *Int. Psychogeriatr.* **4**, 165–176 (1992).
78. Pfeffer, R. I., Kurosaki, T. T., Harrah, C. H. Jr., Chance, J. M. & Filos, S. Measurement of functional activities in older adults in the community. *J. Gerontol.* **37**, 323–329 (1982).
79. Postuma, R. B. et al. MDS clinical diagnostic criteria for Parkinson's disease. *Mov. Disord.* **30**, 1591–1601 (2015).
80. Doppler, C. E. J. et al. Microsleep disturbances are associated with noradrenergic dysfunction in Parkinson's disease. *Sleep* **44**, zsab040 (2021).
81. Kühbach, K. et al. Application of an amyloid beta oligomer standard in the sFIDA assay. *Front. Neurosci.* **10**, 8 (2016).

ACKNOWLEDGEMENTS

We thank Carsten Korth for providing the IC16 antibody and Volker Nischwitz for characterizing SiNaPs. Parts of this study were supported by the Parkinson's Foundation (PF-IMP-2022), the Else Kröner-Fresenius-Stiftung (2019_EKES.02), and the Köln Fortune Program, Faculty of Medicine, University of Cologne (453/2018). GRF is funded by the Deutsche Forschungsgemeinschaft (DFG, German Research Foundation—Project-ID 431549029—SFB 1451).

AUTHOR CONTRIBUTIONS

M.S., M.T.B., G.R.F., D.W., and G.T. supervised the project. S.S., H.J., M.T.B., and M.S. recruited and clinically assessed patients and control subjects, and collected patient samples. J.W. developed the sFIDAta software tool. A.C. expressed and purified protein. A.S. and M.P. developed the sFIDA assay for stool samples. A.S., M.P., and P.Ö. performed sFIDA experiments. A.S., M.P., L.B., T.B., O.B., D.W., and G.T. analyzed the data. A.S., M.S., M.T.B., and G.T. wrote the paper. All authors critically revised the paper.

FUNDING

Open Access funding enabled and organized by Projekt DEAL.

COMPETING INTERESTS

D.W. and O.B. declare no competing non-financial interests but the following competing financial interests: D.W. and O.B. are shareholders of attyloid GmbH. A.S., S.S., A.S., H.J., P.Ö., M.P., L.B., A.C., J.W., T.B., G.R.R., M.S., M.T.B., and G.T. declare no competing interests.

ADDITIONAL INFORMATION

Supplementary information The online version contains supplementary material available at https://doi.org/10.1038/s41531-023-00458-4.

Correspondence and requests for materials should be addressed to Gültekin Tamgüney.

Reprints and permission information is available at http://www.nature.com/reprints

Publisher's note Springer Nature remains neutral with regard to jurisdictional claims in published maps and institutional affiliations.

3.7 Development and Implementation of an Internal Quality Control Sample to Standardize Oligomer-Based Diagnostics of Alzheimer's Disease

Autoren:	Marlene Pils, Alexandra Dybala, Fabian Rehn, Lara Blömeke, Tuyen Bujnicki, Victoria Kraemer-Schulien, Wolfgang Hoyer, Detlev Riesner, Dieter Willbold und Oliver Bannach
Journal:	Diagnostics (veröffentlicht)
DOI:	10.3390/diagnostics13101702
Impact-Faktor:	3,6 (2022)
Beitrag:	Eigenanteil: 10 % Etablierung des Aggregationsprotokolls Diskussion der Ergebnisse Prüfung des Manuskripts
Anhang zum Manuskript	Kapitel 7.7

diagnostics

MDPI

Article

Development and Implementation of an Internal Quality Control Sample to Standardize Oligomer-Based Diagnostics of Alzheimer's Disease

Marlene Pils [1,2], Alexandra Dybala [1,3], Fabian Rehn [1,2], Lara Blömeke [1,2], Tuyen Bujnicki [2], Victoria Kraemer-Schulien [2], Wolfgang Hoyer [2,3], Detlev Riesner [1,3], Dieter Willbold [1,2,3] and Oliver Bannach [1,2,*]

[1] attyloid GmbH, Merowingerplatz 1a, 40225 Düsseldorf, Germany; m.pils@attyloid.com (M.P.); alexandra.ziemski@hhu.de (A.D.); f.rehn@attyloid.com (F.R.); l.bloemeke@attyloid.com (L.B.); detlev.riesner@hhu.de (D.R.); d.willbold@fz-juelich.de (D.W.)
[2] Institute of Biological Information Processing (Structural Biochemistry: IBI-7), Forschungszentrum Jülich, 52428 Jülich, Germany; t.bujnicki@fz-juelich.de (T.B.); v.kraemer-schulien@fz-juelich.de (V.K.-S.); wolfgang.hoyer@hhu.de (W.H.)
[3] Institut für Physikalische Biologie, Heinrich-Heine-Universität Düsseldorf, 40225 Düsseldorf, Germany
* Correspondence: o.bannach@attyloid.com; Tel.: +49-(0)-211-81-10377

Abstract: Protein misfolding and aggregation are pathological hallmarks of various neurodegenerative diseases. In Alzheimer's disease (AD), soluble and toxic amyloid-β (Aβ) oligomers are biomarker candidates for diagnostics and drug development. However, accurate quantification of Aβ oligomers in bodily fluids is challenging because extreme sensitivity and specificity are required. We previously introduced surface-based fluorescence intensity distribution analysis (sFIDA) with single-particle sensitivity. In this report, a preparation protocol for a synthetic Aβ oligomer sample was developed. This sample was used for internal quality control (IQC) to improve standardization, quality assurance, and routine application of oligomer-based diagnostic methods. We established an aggregation protocol for Aβ1–42, characterized the oligomers by atomic force microscopy (AFM), and assessed their application in sFIDA. Globular-shaped oligomers with a median size of 2.67 nm were detected by AFM, and sFIDA analysis of the Aβ1–42 oligomers yielded a femtomolar detection limit with high assay selectivity and dilution linearity over 5 log units. Lastly, we implemented a Shewhart chart for monitoring IQC performance over time, which is another important step toward quality assurance of oligomer-based diagnostic methods.

Keywords: Alzheimer's disease; diagnosis; dementia; biomarkers; amyloid-β peptide; oligomer-based diagnostics; immunoassays; internal quality control; atomic force microscopy; Shewhart chart

Citation: Pils, M.; Dybala, A.; Rehn, F.; Blömeke, L.; Bujnicki, T.; Kraemer-Schulien, V.; Hoyer, W.; Riesner, D.; Willbold, D.; Bannach, O. Development and Implementation of an Internal Quality Control Sample to Standardize Oligomer-Based Diagnostics of Alzheimer's Disease. *Diagnostics* **2023**, *13*, 1702. https://doi.org/10.3390/diagnostics13101702

Academic Editor: Agnieszka Kulczyńska-Przybik

Received: 30 March 2023
Revised: 5 May 2023
Accepted: 7 May 2023
Published: 11 May 2023

1. Introduction

Alzheimer's disease (AD) is a progressive brain disease that causes increasing deterioration of mental abilities. AD is mainly characterized by misfolding and aggregation of amyloid-β (Aβ) peptides and Tau proteins into amyloid plaques and neurofibrillary tangles [1,2]. For decades, these deposits were considered the primary cause of disease onset and progression. However, it is increasingly recognized that the soluble oligomeric species formed during the aggregation process are the major neurotoxic species of AD [3–6]. Consequently, these oligomers represent a primary drug target and a promising biomarker candidate for early AD diagnostics. The minute amounts of oligomeric Aβ in body fluids such as cerebrospinal fluid (CSF, aM-fM) [5] and excessive concentrations of Aβ monomers and matrix components require extremely sensitive and specific quantitation technologies [5–7].

We previously developed the surface-based fluorescence intensity distribution analysis (sFIDA) technology as an oligomer-specific quantitation method with single-particle

sensitivity [8–12]. Although the biochemical setup of the sFIDA assay is similar to sandwich ELISA (Figure 1), the readout is microscopy-based with sub-femtomolar sensitivity [7]. In sFIDA, Aβ species are captured on a glass surface by an N-terminal anti-Aβ antibody; subsequently, Aβ oligomers are detected by two different fluorescence-labeled antibodies. Monomeric Aβ is not detected because capture and detection antibodies compete for the same or overlapping epitopes [11]. Using linear epitopes, all subtypes of aggregated protein, including low- and high-molecular-weight oligomers, are detected [8]. The glass surface is imaged by dual-color total internal reflection fluorescence microscopy (TIRFM) to count the number of oligomers in a sample. Background noise is reduced by applying a cutoff, which is a predefined intensity value, and only signals above the cutoff are evaluated. Moreover, signal colocalization of both fluorescently labeled detection antibodies (called sFIDA readout) increases specificity and directly correlates with the Aβ oligomer concentration in the sample [11].

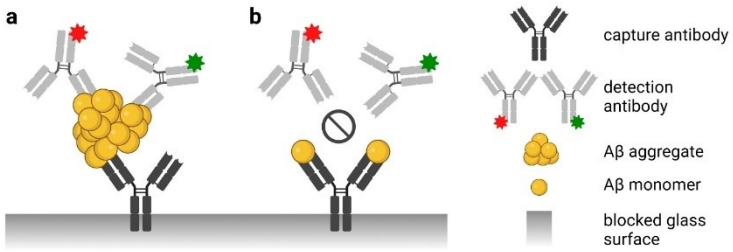

Figure 1. Scheme of the sFIDA principle. The biochemical principle of sFIDA is similar to a sandwich ELISA with capture and detection antibodies directed against the same or overlapping epitopes of the N-terminus of Aβ. Monomeric and oligomeric Aβ species of the sample bind to the capture antibodies. (**a**) However, the red or green fluorescently labeled detection antibodies only detect aggregated Aβ species such as oligomers because the assay antibodies bind to the same or overlapping epitope. (**b**) Therefore, the red or green labeled detection antibody cannot bind monomers because the capture antibody already masks the epitope. Subsequently, the assay surface is imaged using dual-color fluorescence microscopy (excitation at 635 and 488 nm), and only colocalized pixels above a defined cutoff threshold are counted by image data analysis. Abbreviations: Aβ, amyloid-β; sFIDA, surface-based fluorescence intensity distribution analysis. Created with BioRender.com (accessed on 26 April 2023).

Moreover, oligomer quantification is challenging because reliable calibration standards are required [4,5,13]. To address this issue, we recently developed and characterized stable silica nanoparticles (SiNaPs) coated with Aβ peptides, which serve as calibration standards for translating pixel-based readouts into molar particle concentrations [13]. In contrast to natural oligomers that can undergo structural changes and epitope masking in response to changes in buffer conditions or matrix effects [14,15], SiNaPs are very robust because of their artificial, silica-based nature. Nevertheless, it is necessary to have an Aβ oligomer-based internal quality control (IQC) sample that sensitively detects unfavorable or declining assay performance in response to analytical, biological, or clinical changes [16,17]. In addition, monitoring the day-to-day (between-run) precision and accuracy of the IQC sample improves assay comparability and standardizes oligomer-based diagnostic methods for routine applications [18].

Soluble Aβ oligomers are transient and very heterogeneous in size and shape. Thus, investigators have struggled to prepare a reliable Aβ oligomer sample for in vitro and in vivo studies [4,5,13,19]. Firstly, Aβ oligomers must be sufficiently stable during the assay procedure, i.e., must not dissociate to monomers or grow further into insoluble structures such as fibrils. In this context, the ease of the aggregation protocol would also be important, as it should not require complex pretreatments for stabilization, such as crosslinking or protein engineering [20]. Secondly, a suitable characterization method

must be applied to investigate the shape and size of Aβ oligomers. Several methods are described in the literature, whereby atomic force microscopy (AFM) enables size and shape characterization because of its insensitivity to buffer components and matrix effects while providing high-resolution three-dimensional morphological images [21]. Thirdly, Aβ oligomers should be stable for in vitro studies such as oligomer-based diagnostic methods to facilitate reproducibility that is evaluated using quality assurance tools such as control sheets, Shewhart charts, or Cusum charts [16–18].

In the present study, we describe detailed methods to consistently generate an Aβ1–42 oligomer-based IQC sample and characterize its shape and size using atomic force microscopy. We then demonstrate IQC applicability and monitoring using sFIDA for in vitro oligomer-based diagnostic methods. We investigated several validation parameters, such as detection and quantification limits, intra-assay variability, dilution linearity, and assay selectivity. Lastly, we demonstrate the use of Shewhart charts for monitoring the IQC performance over time at three IQC sample concentrations.

2. Materials and Methods

2.1. Monomerization Aβ1–42 Peptide Stock and Aggregation Protocol

The monomerization and aggregation protocol used to generate oligomeric Aβ species was established by considering the findings of Aβ aggregation studies [19–23]. For a graphical illustration of the preparation methods, including the monomerization and aggregation procedure, see Figure S1.

Monomerization of the Aβ1–42 peptide stock is essential for generating homogeneous oligomers [19,21]. Thus, we used a strong fluorinated alcohol, 1,1,1,3,3,3-hexafluoro-2-propanol (HFIP, Sigma-Aldrich, St. Louis, MO, USA), to remove any preexisting β-sheet secondary structure or seeds. All preparation steps that use HFIP should be performed under a fume hood or clean bench because of its volatility. We reduced the lyophilized starting material per aliquot because Aβ1–42 aggregates more spontaneously at a stock concentration higher than 90 nM. Thus, we first prepared aliquots containing 50 µg of Aβ1–42 by adding 550 µL of HFIP directly into the original vial containing 1 mg of Aβ1–42 (Bachem AG, Bubendorf, Switzerland). Complete dissolution of the Aβ1–42 peptide was achieved by 30 min incubation at room temperature (RT) and agitated at 650 rpm. The solution was then transferred into a protein low-binding reaction tube (Eppendorf, Hamburg, Germany), and the original vial was rinsed with 550 µL of HFIP. Next, this solution was quickly divided into 20 aliquots of 50 µL each using a repeating pipette or cooled Hamilton syringe (Figure S1, step 1). Subsequently, tubes were transferred into a SpeedVac and dried for ~1 h without heating until all HFIP and H_2O were removed. The monomeric stock tubes containing 50 µg of Aβ1–42 were sealed and stored at RT (Figure S1, step 2). To further reduce the initial amount of Aβ1–42, we repeated this step by adding 550 µL of HFIP to a 50 µg Aβ1–42 tube and creating 10 new aliquots of 5 µg each. These were dried and stored as described above (Figure S1, step 3).

For the preparation of the IQC sample stock solution, 5 µg of monomeric Aβ1–42 was solved in 5 µL of dimethyl sulfoxide (DMSO, Sigma-Aldrich), briefly mixed, spun down, and agitated for 10 min at 650 rpm (Thermomixer, Eppendorf) at RT (Figure S1, step 4). This step should be scheduled immediately prior to further use because a prolonged residence time of Aβ in the DMSO stock solution can lead to spontaneous protofibril formation [21]. Because physiological conditions such as salt concentration and pH facilitate the aggregation of oligomeric Aβ species [21], we subsequently diluted the DMSO stock solution with 1× phosphate-buffered saline, pH 7.4 (PBS, Sigma-Aldrich) containing 0.04% sodium azide (NaN_3, AppliChem, Darmstadt, Germany) to a concentration of 10 µM (Figure S1, step 5). The IQC sample stock solution was again briefly mixed, spun down, and agitated for 16 h at 650 rpm at RT to promote oligomerization (Figure S1, step 6).

2.2. Atomic Force Microscopy

AFM is insensitive to matrix effects and solution conditions, and it generates detailed surface information at a nanometer scale [21]. Therefore, AFM was used for the size and shape characterization of the synthesized Aβ oligomers.

The 10 µM IQC sample stock solution containing oligomeric species was diluted to 1 µM in PBS. As a control, 10 µM monomeric IQC sample stock solution was prepared analogously, but incubation after adding PBS was not performed (Section 2.1). Ten microliters of each sample was loaded onto a mica slide and incubated for 30 min at RT in a closed petri dish. A wet tissue was added to prevent drying artefacts. The slide was washed 3× with 100 µL of ddH_2O and dried with N_2 gas. The samples were measured using NanoWizard III (JPK BioAFM, Bruker Corporation, Billerica, MA, USA) with an OMCL-AC160TS cantilever (Olympus Corporation, Tokyo, Japan) in the intermittent contact mode (AC mode) in air. For size determination, three images (2 × 2 µm with a resolution of 512 × 512 pixels) were recorded with a frequency of 0.5 Hz. Assuming the oligomers are globular, the height profile of 1300 oligomers was further analyzed with ImageJ using the "Find Maxima" tool. The determined height was equated to the size of the oligomers.

2.3. sFIDA

2.3.1. Synthesis of SiNaPs Coated with Aβ1–15

In this study, SiNaPs coated with Aβ1–15 were synthesized, functionalized, and activated, as described previously [7,8,13]. Briefly, SiNaPs were synthesized via the Stöber process and silanized with 3-aminopropyl(triethoxysilane) (APTES, Sigma-Aldrich) to functionalize the surface with primary amino groups. The carboxy groups of maleimidohexanoic acid (MIHA, abcr GmbH, Karlsruhe, Germany) were then activated by 1-ethyl-3-(3-dimethylaminopropyl) carbodiimide (EDC, Sigma-Aldrich) and N-hydroxysuccinimide (NHS, Sigma-Aldrich) and coupled covalently to the amines. Aβ and maleimide groups were crosslinked using C-terminal functionalized Aβ1–15 peptides with cysteamine (Peptides and Elephants, Henningsdorf, Germany). Lastly, the molar SiNaP concentration was calculated on the basis of the silicon concentration, which was determined by inductively coupled plasma mass spectrometry, and the size, density, and shape of the particles were determined by transmission electron microscopy.

2.3.2. Labeling of Antibodies

The anti-Aβ antibody IC16 (mouse, monoclonal, amino acids (aa)2–8, Heinrich-Heine-University Düsseldorf, Düsseldorf, Germany) labeled with CF633 dye (Biotium, Freemont, CA, USA) and the anti-Aβ antibody Nab228 (mouse, monoclonal, aa1–11, Sigma-Aldrich) labeled with CF488A dye (Biotium) were used as detection probes for TIRFM. Labeling was performed according to the manufacturer's protocol. After purification via size exclusion using a polyacrylamide bead suspension (Bio-Gel P-30 Gel, Bio-Rad Laboratories, Hercules, CA, USA), the concentration and degree of labeling of both detection probes were calculated according to the manufacturer's protocols.

2.3.3. Assay Protocol

In the present study, 384-well plates (Sensoplate Plus, Greiner Bio-One, Frickenhausen, Germany) were functionalized with the Nab228 antibody (2.5 µg/mL in 0.1 M carbonate solution pH 8.4, 40 µL per well). After overnight incubation at 4 °C, plates were washed five times with Tris-buffered saline containing Tween (TBST, 1× TBS (Serva, Duisburg, Germany) and 0.05% Tween-20 (AppliChem)) and five times with 1× TBS and blocked with 0.5% bovine serum albumin (BSA, AppliChem) in 1× TBS containing 0.03% ProClin (Sigma-Aldrich,) for 1.5 h at RT. After washing the wells, as described above, 20 µL per well of SiNaPs (3.16-fold dilution, 10.26 pM–0.3 fM), assay controls, or IQC samples were applied in fourfold determination and incubated for 2 h at RT. For sample dilution, 1× PBS containing 0.05% Tween, 0.5% BSA, and 0.095% NaN_3 was used. Using the oligomeric IQC sample stock solution, a 3.16-fold dilution series ranging from 100 nM (IQC-15) to

0.01 pM (IQC-1) was used for validation studies, whereas, for the QC chart, 20 replicates of 316 pM (IQC-10), 31.6 pM (IQC-8), and 3.16 pM (IQC-6) were used. Wells were then washed five times with 1× TBS before adding 20 µL per well of the centrifuged (100,000× *g*, 4 °C, 1 h) detection antibodies mixture (IC16-CF633 + Nab228-CF488A, each at 0.625 µg/mL, in TBST + 0.1% BSA) for 1 h at RT. Lastly, wells were washed again, and the buffer was changed to 1× TBS with 0.03% ProClin. A microplate washer (405LS Microplate Washer, BioTek, Winnoski, VT, USA) was used for all washing steps.

2.3.4. Image Data Acquisition

The well surface was imaged in two different channels (channel 633: excitation 635 nm, emission filter 705/72 nm, exposure time 1000 ms, gain 1000; channel 488: excitation 488 nm, emission filter 525/36 nm, exposure time 1000 ms, gain 500) using TIRFM (Leica DMI6000B, Wetzlar, Germany). Twenty-five images per well with 1000 × 1000 pixels each were measured, representing 3.14% of the well surface.

2.4. Statistics

General statistical analyses were performed using Microsoft Excel (Microsoft, Redmond, WA, USA), and OriginPro (OriginLab Corporation, Northampton, MA, USA) and matlab2019b (The MathWorks, Natick, MA, USA) were used for calculations and graphs. Data were further analyzed for normal distributions using the Shapiro–Wilk test; for non-normal distributions, a non-parametric test was used, i.e., the Mann–Whitney U test.

2.4.1. Analysis of Image Data

Images were analyzed using in-house developed software that features artefact filtering and an automated sFIDA readout calculation [7,8]. To reduce background noise, intensity cutoffs were defined as the signal intensity exceeding 0.05% of the total pixels of the individual channels of the used blank control (dilution buffer, BC). Lastly, the number of pixels that had intensities above the defined cutoff and were colocalized in both fluorescence channels was calculated as the sFIDA readout. sFIDAta calculated the sFIDA readout on the basis of the mean value, standard deviation, and coefficient of variation (CV%) for each sample and the respective replicates.

2.4.2. Calibration

For calibrating the received sFIDA readouts, a weighted linear regression analysis with respective weights calculated as one per readout was performed with matlab2019b (The MathWorks). Therefore, all data points of the SiNaP calibration curve that differed significantly from BC and were above the limit of detection (Section 2.4.1) were included. For all further analyses, only the calibrated sFIDA readouts were shown.

2.4.3. Analytical Validation: Detection and Quantification Limits

For the calculation of the limit of blank (LoB) and limit of detection (LoD), 24 BC samples were analyzed, and parameters were calculated according to Armbruster et al. [24] using Equations (1) and (2). Afterward, values were translated into particle concentrations using the calculated calibration curve.

$$\text{LoB} = \text{mean sFIDA reaodut}_{\text{BC}} + 1.645 \times \text{standard deviation}_{\text{BC}}. \quad (1)$$

$$\text{LoD} = \text{mean sFIDA readout}_{\text{BC}} + 2 \times \text{standard deviation}_{\text{BC}}. \quad (2)$$

Using the calibrated particle concentrations of the Aβ oligomer dilution series, the linear working range was defined by calculating the lower and the upper endpoint and the dilution linearity. Therefore, the concentrations that differed significantly from the next lower concentration were determined using the one-sided Mann–Whitney U test with a confidence interval of 5%. Before calculating dilution linearity, background correction was

performed by subtracting the BC value from each IQC sample value. Subsequently, the percentage dilution linearity of each dilution step was calculated using Equation (3).

$$\text{Dilution linearity}[\%] = \frac{\text{observed value}}{(\text{expected value}/\text{dilution factor})} \times 100\% \quad (3)$$

Within the working range, the mean dilution linearity should be 80–120%, and the coefficient of determination should be higher than 0.95 to be accepted. The CV% of the four replicates of the same sample within the same run was calculated to assess intra-assay variability (within-run precision).

2.4.4. Analytical Validation: Analytical Selectivity

The selectivity of sFIDA indicated by the percentage signal reduction (Equation (4)) was carried out by measuring the IQC-13 (10 nM monomer concentration) sample in different assay setups. Nonspecific binding to the blocking agent used was excluded by performing capture control, where the capture antibody was omitted. As an autofluorescence control, the assay was performed using only TBST + 0.1% BSA without detection probes. In addition, the cross-reactivity of anti-Tau antibodies against the produced Aβ oligomers was tested. To this end, the Tau12 antibody (mouse, monoclonal, aa6–18, Biolegend, San Diego, CA, USA) was conjugated with CF633 and CF488A according to the protocol in Section 2.3.2 and diluted in TBST + 0.1% BSA to 0.625 µg/mL. The insensitivity of sFIDA against monomeric Aβ species was evaluated by applying 10 nM of freshly diluted monomeric Aβ1–42. IQC-13 was spiked in bovine CSF to simulate matrix effects, and the sFIDA readouts, generated using 0.05% cutoff-based CSF-blank, were compared to an equal concentration in the dilution buffer.

$$\text{Signal reduction}[\%] = \left(1 - \frac{\text{observed readout assay control}}{\text{readout reference}}\right) \times 100\% \quad (4)$$

Furthermore, sFIDA readouts of the respective assay control were compared to the readouts of the standard assay setup using the one-sided Mann–Whitney U test with a confidence interval of 5%.

2.4.5. Establishment of QC-Tool

A Shewhart chart, the most widely used tool for IQC [18], was used to monitor the readouts of IQC-10, IQC-8, and IQC-6. The oligomeric IQC sample stock solution (Section 2.1) was serially diluted 20 times to corresponding monomer concentrations of 316 pM (IQC-10), 31.6 pM (IQC-8), and 3.16 pM (IQC-6) to simulate 20 observations of each IQC sample. Subsequently, each dilution underwent a fourfold sFIDA analysis, and the observed sFIDA readouts were calibrated into particle concentrations. Lastly, observed particle concentrations were plotted as absolute values against the number of analyses. Using the mean and the standard deviation of the 20 observations, the lower and upper control limits (LCL/UCL) and action limits (LAL/UAL), respectively, were calculated according to Equations (5)–(8) and were integrated into the control chart.

$$\text{LCL} = \text{mean} - 2 \times \text{standard deviation} \quad (5)$$

$$\text{UCL} = \text{mean} + 2 \times \text{standard deviation} \quad (6)$$

$$\text{LAL} = \text{mean} - 3 \times \text{standard deviation} \quad (7)$$

$$\text{UAL} = \text{mean} + 3 \times \text{standard deviation} \quad (8)$$

In general, values within the control limits are considered satisfactory. Even if values are located between control and action limits, they are still accepted if they do not affect more than 10% of the measured values. However, if one result of a sample occurs outside the action limit, or if nine consecutive results create a trend (decreasing or increasing) or lie on

one side of the central line, the operator's intervention becomes necessary [18,25]. Between-run precision was considered satisfactory when all results were unbiased, all results lay within the warning limits, and the mean CV% of the 20 replicates was below 20%.

3. Results

The aim of this study was to develop and characterize an IQC sample for oligomer-based diagnostic assays. The first part of the results describes the characterization of the IQC sample, which was prepared using the protocol established in Section 2.1. In the second part, we used the IQC sample in the sFIDA assay and determined several validation parameters. Lastly, application of the Shewhart chart to monitor IQC performance was demonstrated with three IQC samples.

3.1. Aβ Oligomer-Based IQC Sample Displays High Homogeneity

The size distribution and morphology of the Aβ oligomers were determined by AFM. The analysis showed that the oligomers were monodisperse and globular in shape (Figure 2a). In contrast, we observed no particles in the monomer control containing a 10-fold higher protein concentration. Size distribution analysis revealed that the median height of all 1300 oligomers was 2.67 nm, with a minimum size of 1.07 nm. Only 2% of the detected oligomers were ≥5 nm (Figure 2b).

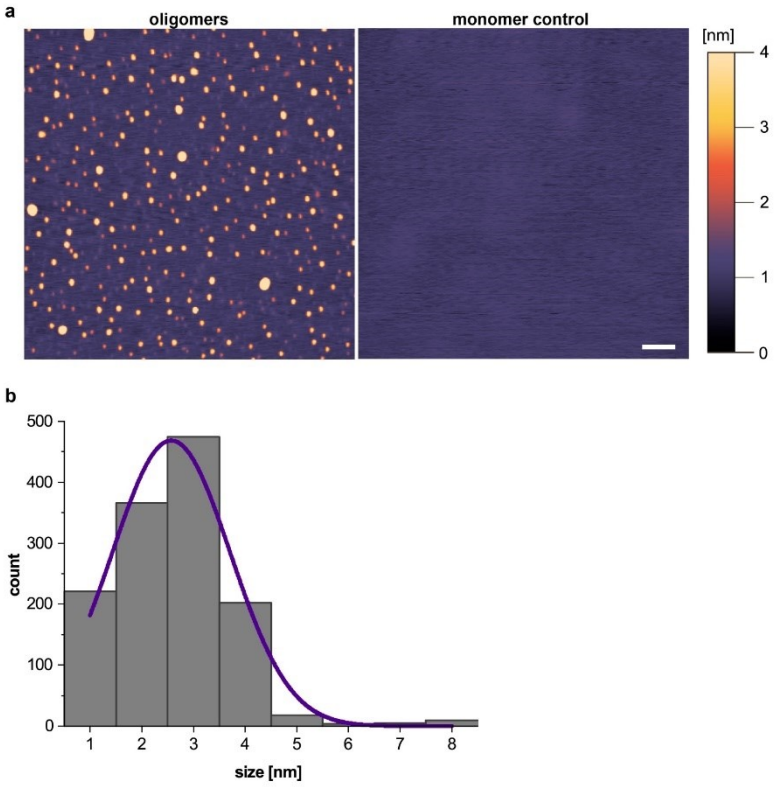

Figure 2. Analysis of the Aβ oligomers measured by AFM. (**a**) AFM images of the monomer control and Aβ oligomer samples. The color scale indicates the height profile. Scale bar = 200 nm. (**b**) Histogram showing the size distribution of 1300 oligomers. Abbreviations: Aβ, amyloid-β; AFM, atomic force microscopy.

3.2. Successful Application of the Aβ Oligomer-Based IQC Sample in the sFIDA Assay

The applicability of the prepared Aβ oligomers as an IQC sample for in vitro oligomer-based diagnostic methods using the sFIDA assay was investigated. We prepared a 3.16-fold concentration series of the oligomers in dilution buffer and subjected each sample to sFIDA analysis in quadruplicate determination. The molar concentrations represent monomer concentrations ranging from 0.01 pM (IQC-1) to 100 nM (IQC-15). Using the SiNaPs calibration curve (y = 5.08x − 0.25), we calculated the Aβ oligomer concentrations in each IQC sample from the sFIDA readouts. Individual sFIDA readouts and calibrated particle concentrations for each IQC sample are listed in Table S1.

Figure 3 illustrates the sFIDA IQC performance, which exhibits a 5 log dynamic range and an analytical sensitivity below the femtomolar level (LoB: 0.25 fM, LoD: 0.28 fM). The lower limit of quantification (LLoQ), upper limit of quantification (ULoQ), and acceptable dilution linearity (acceptance range of 80–120%, Section 2.4.1) defined the working range of the used IQC samples. Data were not normally distributed (p-value: 6.97×10^{-6}). Thus, the two quantification limits were identified using the one-sided Mann–Whitney U test with a confidence interval of 5% (Table S1) and were set to a particle concentration of 0.36 fM (IQC-3) and 197 pM (IQC-14). Within this range, a mean percentage dilution linearity of 107% was determined (Table S2). Interestingly, a coefficient of determination of 0.73 indicated that the dilution linearity could be improved. A closer inspection of the data indicated that the IQC-14 readout was an outlier with a similar readout to that of IQC-13. Removing IQC-14 from the fit yielded a coefficient of determination of 0.99. This refit resulted in a change in the percentage dilution linearity; however, the value of 109% was still acceptable. Furthermore, within this linear working range of 0.36 fM–196 pM, a mean CV% of 18.4% was determined, indicating acceptable intra-assay variance for single-particle analysis.

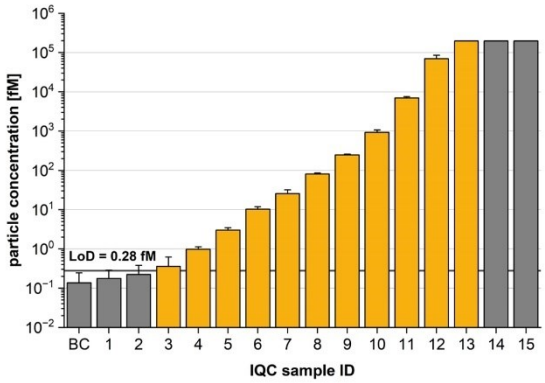

Figure 3. Molar particle concentration of internal quality control (IQC) samples and blank control (BC). On the basis of 24 replicates of the BC, the limit of detection (LoD) was calculated and translated into a particle concentration of 0.28 fM using the calibration curve. The linear working range (yellow) was identified by acceptable dilution linearity between the upper (196 pM) and lower (0.36 fM) limits of quantification. Note the logarithmic scale. Data are presented as the mean and standard deviation of four replicates.

3.3. sFIDA Features High Selectivity for the Aβ Oligomer-Based IQC Sample

Testing different assay controls confirmed that sFIDA is highly selective for aggregated Aβ species and robust against false-positive signals because of matrix interference and cross-reactivities. Figure 4a shows sFIDA readouts of IQC-13 applied on different assay setups. For all controls, a signal reduction of almost 100% was observed (Table S3a). Because data showed a non-normal distribution (Shapiro–Wilk test p-value: 2.53×10^{-4}), we applied the nonparametric one-sided Mann–Whitney U test with a confidence interval of 5% to

investigate differences between the sFIDA readouts of the respective assay control and the reference. For all controls, significantly lower sFIDA readouts were observed compared to the reference (for individual *p*-values, see Table S3). Aβ oligomers were only detected when captured on the assay surface via the anti-Aβ antibodies, whereas no detection was observed in the absence of the capture antibody. In addition, the capture control readout was significantly lower than the reference values (*p*-value: 0.0152). Moreover, false-positive signals generated by the autofluorescence of chemicals and buffers were not detected because the sFIDA readout of the autofluorescence control was significantly lower than the sFIDA readout of the reference, as indicated by the *p*-value of 0.0147. Using anti-Tau antibodies as the detection probe or monomers (Figure 4b, Table S3b) as the target yielded no false-positive signals caused by cross-reactivity. For both controls, significantly lower sFIDA readouts compared to the reference were observed (*p*-value of 0.0152).

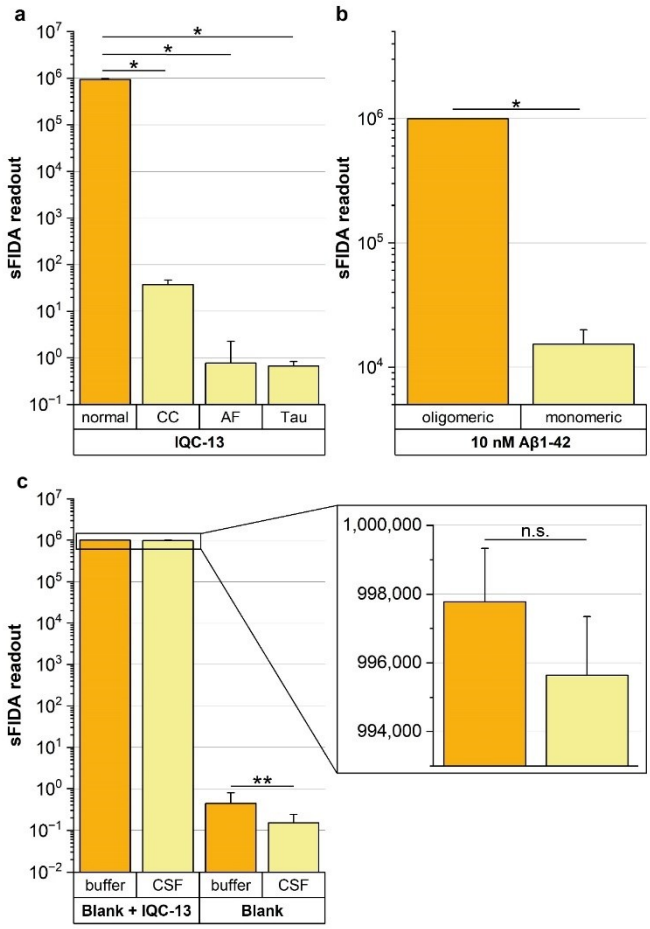

Figure 4. Comparison of sFIDA readout of IQC-13 applied on different assay setups. (**a**) sFIDA readouts of the normal assay setup were compared to assay setups without the capture antibody (capture control, CC), without Aβ-specific detection probes (TBST + 0.1% BSA without any detection probes, autofluorescence control, AF) or with Tau-specific detection probes (equimolar mixture of Tau12 antibodies labeled with CF633 and CF488A in TBST + 0.1% BSA, Tau). A signal reduction of almost 100% and significantly lower sFIDA readouts compared to the standard assay setup (normal,

p-values between 0.0152 and 0.0147) were observed for all controls. (**b**) In addition, equal molar concentrations of monomeric Aβ1–42 were applied on the assay surface to demonstrate that the assay is insensitive toward monomers. A signal reduction of nearly 99% and significantly lower sFIDA readouts compared to the standard assay setup were observed (*p*-value: 0.0152), showing that interference from monomeric Aβ can be excluded. (**c**) To evaluate the matrix effects of CSF, IQC-13 was spiked into bovine CSF, and sFIDA readouts were calculated on the basis of the background signal of the additionally applied bovine CSF-blank. For IQC-13, no significant difference in the sFIDA readouts was observed (*p*-value: 0.108), and only a slight signal reduction of 0.2% was observed. In contrast, the sFIDA readout of CSF-blank was significantly lower compared to the buffer control (*p*-value: 0.002, signal reduction: 67%). Note the logarithmic scale. Data are presented as the mean and standard deviation of four replicates. Significant differences between groups were calculated using the one-sided Mann–Whitney U test with a confidence interval of 5%. Significant differences are marked as follows: * $0.01 \leq p < 0.05$; ** $0.001 \leq p < 0.01$; n.s. not significant. Abbreviations: CSF, cerebrospinal fluid; IQC, internal quality control.

Furthermore, after spiking the Aβ oligomers in CSF, only negligible matrix effects were observed, with a minor signal reduction of 0.2% and no significant difference in the readouts (*p*-value: 0.108) (Figure 4c, Table S3c). In addition, matrix components in the CSF-blank reduced the background signal more efficiently than the dilution buffer, indicated by a signal reduction of approximately 67% and significantly lower readouts indicated by a *p*-value of 0.002 (CSF-blank vs. BC). Consequently, the signal-to-noise ratio between IQC-13 and the respective blank was three times higher in CSF than in the dilution buffer.

3.4. Shewhart Chart as a Reliable QC-Tool for Monitoring IQC Performance

Control charts are a valuable tool for monitoring assay performance and can be used by any laboratory [25]. In this work, we demonstrated the use of a Shewhart chart to monitor the performance of three IQC samples in sFIDA (for respective TIRFM images showing co-localized pixel above cutoff values, see Figure S2) by integrating values of 20 observations of each IQC sample into a separate chart (Table S4). Charts were then interpreted analogously to defined rules (Section 2.4.3).

All three IQC samples showed low inter-assay variability as the calculated mean CV% of the respective 20 observations was below 20% (IQC-6 = 16.2%, IQC-8 = 16.5%, IQC-10 = 17.6%). As illustrated in Figure 5, none of the IQC samples exceeded the action limit. In addition, neither IQC-6 nor IQC-8 exceeded the control limits, but one value of sample IQC-10 occurred between the control and action limit. Nonetheless, assay performance was considered acceptable within the predefined range because this was the only deviation. No ascending or descending trend of the nine consecutive observation points was seen in IQC samples. Even if no out-of-control situation could be determined in IQC samples, IQC-6 should be monitored further as a general downward progression became apparent. Moreover, an out-of-control situation may arise in the foreseeable future if the next three observation points of IQC-6 also occur between the central line and the lower control limit.

In particular, for those assays subjected to quality management, such as sFIDA technology, troubleshooting out-of-order situations can be monitored rapidly, as possible causes related to the operator, instruments, manufacturing protocols, and/or lot numbers of assay components are regularly documented.

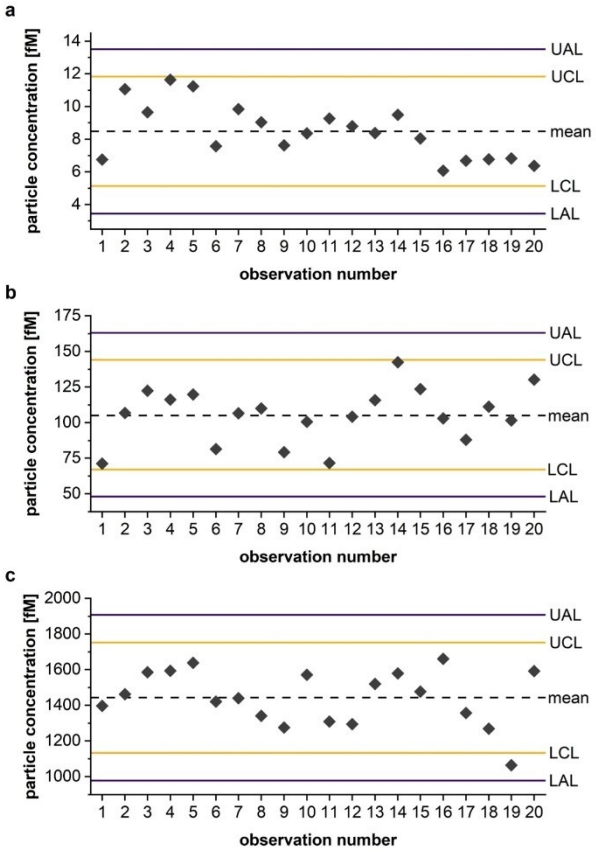

Figure 5. Shewhart chart monitoring the performance of IQC-6 (**a**), IQC-8 (**b**) and IQC-10 (**c**). The calibrated particle concentrations of 20 observations of each IQC sample (gray dots) were plotted to simulate assay performance in chronological order. Mean: central dashed line; upper and lower control limit (UCL, LCL): yellow line; upper and lower action limit (UAL, LAL): purple line. Data are presented as the mean of four replicates (gray data points). Abbreviation: IQC, internal quality control.

4. Discussion

In the present study, we developed a homogeneous and reproducible Aβ oligomer-based IQC sample for sFIDA and established a QC-tool for monitoring assay performance.

We characterized the formation of Aβ oligomers by AFM, which revealed globular-shaped oligomers with a median size of 2.67 nm, whereby AFM analysis revealed the size of a dried oligomer and not the hydrodynamic size. Oligomers are in thermodynamic equilibrium with monomers and larger aggregates, such as amyloid fibrils. In vitro produced oligomers have been shown to dissociate into monomers within a few hours, with only a small fraction of oligomers converting to fibrils [26]. Conversion to fibrils can be excluded herein because no fibrillary morphologies were detected by AFM. Noteworthily, the sFIDA assay currently does not discriminate oligomers from larger yet still soluble aggregates because of the diffraction limit of the optical detection system. However, as larger particles bind more fluorescent probes, a size determination of sub-resolution particles should be possible based on pixel intensity. For this purpose, the oligomers developed can serve as a size standard. In addition to established AD biomarkers, such as monomeric Aβ1–42, the ratio of Aβ1–42 to Aβ1–40, phosphorylated Tau, and total Tau in CSF, and magnetic

resonance imaging and positron emission tomography (PET), i.e., Amyloid-PET or Tau-PET [2,27,28], oligomeric forms of Aβ represent a promising biomarker candidate for early AD diagnosis [5,6,29]. Consequently, in vitro, oligomer-based diagnostics are the subject of current biomarker research.

We detected and quantified oligomers at sub-femtomolar concentrations, down to 0.28 fM (LoD), which qualifies the sFIDA assay for biofluid-based in vitro oligomer-based diagnostic methods [5]. We previously showed that Aβ oligomers and aggregates are detectable in human CSF samples [10] and complex matrices such as murine and human brain homogenate samples [9] using sFIDA. Due to further development of the assay protocol, including the use of synthetic Aβ oligomers shown herein, the analytical sensitivity was further improved compared to our previously published data [7]. The potential of this analytical sensitivity to improve diagnostic performance must be validated using a large set of clinical samples. In comparison to other oligomer-specific Aβ assays, sFIDA ensures single-particle sensitivity. Although a direct comparison of sensitivity among different assays is challenging because of variations in assay design, calibration standards, and detection limit calculations, we evaluated the sensitivity ranges of various assays (Table 1).

Table 1. Comparison of several Aβ oligomer quantification assays according to their sensitivity level. For this purpose, the respective weight concentrations pg/mL were converted into femtomolar oligomer concentrations using the approximate molecular weights of the used calibration standards.

Reference	Assay Setup	Calibration Standard	Sensitivity [fM]
sFIDA	Single-particle analysis with fluorescence microscopy, overlapping epitopes capture: Nab228 aa1–11 detection: IC16 aa2–8 + Nab228 aa1–11	Aβ1–15 SiNaPs	LoD = 0.28
Savage et al. [30]	Single particle analysis with bead-based assay capture: 19.3 oligomer-specific detection: 82E1 aa1–16	Aβ1–42 oligomers (MW 1117 kDa)	LoD = 0.08
IBL [31]	ELISA capture: 82E1 aa1–16 detection: 24B3 oligomer-specific	E22P–Aβ40 Dimer	31.4 (N/A)
Hölttä et al. [32]	ELISA, overlapping epitopes capture and detection: 82E1 aa1–16	Dimer Aβ1–11	LLoQ = 90.9
Kasai et al. [33]	ELISA, overlapping epitopes capture and detection: Ban50 aa1–10	MAP 16-mer (lysine core)	LoD = 190
Esparza et al. [34]	Single particle analysis with bead-based assay overlapping epitopes capture and detection: HJ3.4 aa1–13	Aβ1–40Ser26Cys dimer	LLoQ = 720

Only the assay described by Savage et al. (0.08 fM) [30] or the commercial ELISA assay from Immuno-Biological Laboratories Co. Ltd. (IBL, Fujioka, Japan) [31] (31.4 fM), which also claims to detect single particles, offers sensitivity in the low femtomolar range, which is presumably because of the combined use of N-terminal and oligomer-specific assay antibodies. In contrast, all listed homotypic assays, using the same antibody for capture and detection, showed insufficient sensitivity levels between 91 and 720 fM. However, because of epitope competition, these assays [32–34] and the sFIDA assay are insensitive toward monomers.

Through our experiments, we demonstrated that Aβ oligomer-based IQC samples are reproducible, homogeneous, and suitable in oligomer-based diagnostic methods such as sFIDA. However, as our studies were performed in an artificial sample matrix, further

validation data from authentic biological sample matrices such as the plasma or CSF should be obtained, including extensive recovery and parallelism studies [35]. In addition, the critical concentration at which endogenous components compromise the readout and lead to false-positive or false-negative results must be investigated. For sFIDA analysis of α-synuclein and Tau aggregates in CSF, we showed that blood contamination and HAMAs can affect the sFIDA readout [8]. In particular, for CSF, validation should be straightforward because we determined a signal loss of only 0.2% for IQC-15 due to matrix effects. The Aβ oligomer IQC can also facilitate the development of a blood-based sFIDA assay, which is currently in progress. However, the complex plasma matrix could make validation more challenging, as strong matrix effects such as interference between Aβ and human serum albumin or between circulating human antibodies with the assay antibodies are expected [6,15,36,37]. In addition to matrix effects, sample stability and sample tubing can also influence the measurement signal [38,39]. For future routine applications and regulatory approval of the sFIDA technology, the IQC sample should ideally be available as a ready-to-use kit component. Hence, the benchtop stability and long-term stability of the IQC sample should be investigated by testing different sample tubes, storage temperatures and durations, and the effects of repetitive freeze–thaw cycles [2,35,40].

5. Conclusions

Since protein misfolding and aggregation are pathological hallmarks for a variety of neurodegenerative diseases, it is necessary to establish additional IQC samples, e.g., based on Tau or α-synuclein oligomers that improve the routine application of oligomer-based diagnostic methods such as sFIDA. Transitioning from research use to in vitro diagnostics (IVD) has various regulatory requirements [11]. The Aβ oligomer-based IQC sample implemented represents an important step toward the standardization, routine application and ultimately, registration of sFIDA as a diagnostic tool of AD for the IVD market.

Supplementary Materials: The following supporting information can be downloaded at https://www.mdpi.com/article/10.3390/diagnostics13101702/s1: Figure S1. Scheme of monomerization and oligomerization procedure; Figure S2. TIRFM-images of colocalized pixels of IQC-6, IQC-8, and IQC-10 samples with intensities above blank control-based cutoff; Table S1. Individual sFIDA readouts, calibrated molar particle concentrations, and CV% for each IQC sample; Table S2. Calculation of dilution linearity of Aβ oligomer-based IQC samples within working range; Table S3. Selectivity and recovery of the sFIDA assay to IQC-13; Table S4. Raw data used to generate Shewhart charts in Figure 5.

Author Contributions: Conceptualization, M.P., A.D. and O.B.; formal analysis, M.P., A.D. and F.R.; funding acquisition, D.W. and O.B.; investigation, M.P. and A.D.; methodology, M.P., A.D., L.B., T.B. and V.K.-S.; project administration, D.R., D.W. and O.B.; supervision, D.R., D.W. and O.B.; validation, M.P. and A.D.; writing—original draft, M.P. and A.D.; writing—review and editing, W.H., D.R., D.W. and O.B. All authors have read and agreed to the published version of the manuscript.

Funding: This research was funded by the Helmholtz Association, grant number HVF0079.

Institutional Review Board Statement: Not applicable.

Data Availability Statement: The data presented in this study are available in the article and its Supplementary Materials.

Acknowledgments: The authors thank Volker Nischwitz (Central Institute for Engineering, Electronics and Analytics, Analytics (ZEA-3), Forschungszentrum Jülich, 52428, Jülich, Germany) for determining silicon concentrations in the Aβ1–15 SiNaPs using inductively coupled plasma mass spectrometry. The authors also thank Carsten Korth (Institute of Neuropathology, Universitätsklinikum Düsseldorf, 40225 Düsseldorf, Germany) for providing the IC16 antibody. Jürgen Rehage, Maike Heppelmann, and Ioannis Proios (University of Veterinary Medicine Hannover, 30559 Hannover, Germany) kindly provided the bovine CSF used for the spiking experiment. Lastly, the authors thank Andrew Dingley for proofreading the manuscript.

Conflicts of Interest: Dieter Willbold and Oliver Bannach are cofounders and shareholders of attyloid GmbH. Dieter Willbold and Detlev Riesner are members of attyloid's supervisory board. These factors did not influence the interpretation of the data. The remaining authors declare no conflicts of interest.

References

1. Brettschneider, J.; Del Tredici, K.; Lee, V.M.; Trojanowski, J.Q. Spreading of pathology in neurodegenerative diseases: A focus on human studies. *Nat. Rev. Neurosci.* **2015**, *16*, 109–120. [CrossRef] [PubMed]
2. Dulewicz, M.; Kulczyńska-Przybik, A.; Mroczko, P.; Kornhuber, J.; Lewczuk, P.; Mroczko, B. Biomarkers for the Diagnosis of Alzheimer's Disease in Clinical Practice: The Role of CSF Biomarkers during the Evolution of Diagnostic Criteria. *Int. J. Mol. Sci.* **2022**, *23*, 8598. [CrossRef] [PubMed]
3. Tolar, M.; Abushakra, S.; Sabbagh, M. The path forward in Alzheimer's disease therapeutics: Reevaluating the amyloid cascade hypothesis. *Alzheimers Dement.* **2020**, *16*, 1553–1560. [CrossRef] [PubMed]
4. Lotz, G.P.; Legleiter, J. The role of amyloidogenic protein oligomerization in neurodegenerative disease. *J. Mol. Med.* **2013**, *91*, 653–664. [CrossRef]
5. Kulenkampff, K.; Wolf Perez, A.-M.; Sormanni, P.; Habchi, J.; Vendruscolo, M. Quantifying misfolded protein oligomers as drug targets and biomarkers in Alzheimer and Parkinson diseases. *Nat. Rev. Chem.* **2021**, *5*, 277–294. [CrossRef]
6. Mroczko, B.; Groblewska, M.; Litman-Zawadzka, A.; Kornhuber, J.; Lewczuk, P. Amyloid β oligomers (AβOs) in Alzheimer's disease. *J. Neural. Transm.* **2018**, *125*, 177–191. [CrossRef]
7. Herrmann, Y.; Kulawik, A.; Kühbach, K.; Hülsemann, M.; Peters, L.; Bujnicki, T.; Kravchenko, K.; Linnartz, C.; Willbold, J.; Zafiu, C.; et al. sFIDA automation yields sub-femtomolar limit of detection for Aβ aggregates in body fluids. *Clin. Biochem.* **2017**, *50*, 244–247. [CrossRef]
8. Blömeke, L.; Pils, M.; Kraemer-Schulien, V.; Dybala, A.; Schaffrath, A.; Kulawik, A.; Rehn, F.; Cousin, A.; Nischwitz, V.; Willbold, J.; et al. Quantitative detection of α-Synuclein and Tau oligomers and other aggregates by digital single particle counting. *NPJ Parkinsons Dis.* **2022**, *8*, 68. [CrossRef]
9. Kass, B.; Schemmert, S.; Zafiu, C.; Pils, M.; Bannach, O.; Kutzsche, J.; Bujnicki, T.; Willbold, D. Aβ oligomer concentration in mouse and human brain and its drug-induced reduction ex vivo. *Cell. Rep. Med.* **2022**, *3*, 100630. [CrossRef]
10. Wang-Dietrich, L.; Funke, S.A.; Kühbach, K.; Wang, K.; Besmehn, A.; Willbold, S.; Cinar, Y.; Bannach, O.; Birkmann, E.; Willbold, D. The amyloid-β oligomer count in cerebrospinal fluid is a biomarker for Alzheimer's disease. *J. Alzheimers Dis.* **2013**, *34*, 985–994. [CrossRef]
11. Kulawik, A.; Heise, H.; Zafiu, C.; Willbold, D.; Bannach, O. Advancements of the sFIDA method for oligomer-based diagnostics of neurodegenerative diseases. *FEBS Lett.* **2018**, *592*, 516–534. [CrossRef] [PubMed]
12. Schaffrath, A.; Schleyken, S.; Seger, A.; Jergas, H.; Özdüzenciler, P.; Pils, M.; Blömeke, L.; Cousin, A.; Willbold, J.; Bujnicki, T.; et al. Patients with isolated REM-sleep behavior disorder have elevated levels of alpha-synuclein aggregates in stool. *NPJ Parkinsons Dis.* **2023**, *9*, 14. [CrossRef] [PubMed]
13. Hülsemann, M.; Zafiu, C.; Kühbach, K.; Lühmann, N.; Herrmann, Y.; Peters, L.; Linnartz, C.; Willbold, J.; Kravchenko, K.; Kulawik, A.; et al. Biofunctionalized Silica Nanoparticles: Standards in Amyloid-β Oligomer-Based Diagnosis of Alzheimer's Disease. *J. Alzheimers Dis.* **2016**, *54*, 79–88. [CrossRef] [PubMed]
14. Zielinski, M.; Röder, C.; Schröder, G.F. Challenges in sample preparation and structure determination of amyloids by cryo-EM. *J. Biol. Chem.* **2021**, *297*, 100938. [CrossRef] [PubMed]
15. Vanderstichele, H.; Stoops, E.; Vanmechelen, E.; Jeromin, A. Potential sources of interference on Abeta immunoassays in biological samples. *Alzheimers Res. Ther.* **2012**, *4*, 39. [CrossRef]
16. Blacksell, S.D.; Cameron, A.R.; Chamnanpood, C.; Chamnanpood, P.; Tatong, D.; Monpolsiri, M.; Westbury, H.A. Implementation of internal laboratory quality control procedures for the monitoring of ELISA performance at a regional veterinary laboratory. *Vet. Microbiol.* **1996**, *51*, 1–9. [CrossRef]
17. Sturgeon, C.M. Chapter 6.2—Quality Assurance. In *The Immunoassay Handbook*, 4th ed.; Wild, D., Ed.; Elsevier: Oxford, UK, 2013; pp. 441–454.
18. Lock, R.J. My approach to internal quality control in a clinical immunology laboratory. *J. Clin. Pathol.* **2006**, *59*, 681–684. [CrossRef]
19. Ryan, D.A.; Narrow, W.C.; Federoff, H.J.; Bowers, W.J. An improved method for generating consistent soluble amyloid-beta oligomer preparations for in vitro neurotoxicity studies. *J. Neurosci. Methods* **2010**, *190*, 171–179. [CrossRef]
20. Kotler, S.A.; Ramamoorthy, A. Preparation of Stable Amyloid-β Oligomers Without Perturbative Methods. *Methods Mol. Biol.* **2018**, *1777*, 331–338. [CrossRef]
21. Stine, W.B.; Jungbauer, L.; Yu, C.; LaDu, M.J. Preparing synthetic Aβ in different aggregation states. *Methods Mol. Biol.* **2011**, *670*, 13–32. [CrossRef]
22. Brener, O.; Dunkelmann, T.; Gremer, L.; van Groen, T.; Mirecka, E.A.; Kadish, I.; Willuweit, A.; Kutzsche, J.; Jürgens, D.; Rudolph, S.; et al. QIAD assay for quantitating a compound's efficacy in elimination of toxic Aβ oligomers. *Sci. Rep.* **2015**, *5*, 13222. [CrossRef]
23. Novo, M.; Freire, S.; Al-Soufi, W. Critical aggregation concentration for the formation of early Amyloid-β(1–42) oligomers. *Sci. Rep.* **2018**, *8*, 1783. [CrossRef] [PubMed]

24. Armbruster, D.A.; Pry, T. Limit of blank, limit of detection and limit of quantitation. *Clin. Biochem. Rev.* **2008**, *29* (Suppl. S1), S49–S52. [PubMed]
25. Reichenbächer, M.; Einax, J.W. *Challenges in Analytical Quality Assurance*; Springer: Berlin/Heidelberg, Germany, 2011.
26. Michaels, T.C.T.; Šarić, A.; Curk, S.; Bernfur, K.; Arosio, P.; Meisl, G.; Dear, A.J.; Cohen, S.I.A.; Dobson, C.M.; Vendruscolo, M.; et al. Dynamics of oligomer populations formed during the aggregation of Alzheimer's Aβ42 peptide. *Nat. Chem.* **2020**, *12*, 445–451. [CrossRef] [PubMed]
27. Jack, C.R., Jr.; Bennett, D.A.; Blennow, K.; Carrillo, M.C.; Dunn, B.; Haeberlein, S.B.; Holtzman, D.M.; Jagust, W.; Jessen, F.; Karlawish, J.; et al. NIA-AA Research Framework: Toward a biological definition of Alzheimer's disease. *Alzheimers Dement.* **2018**, *14*, 535–562. [CrossRef] [PubMed]
28. Lewczuk, P.; Łukaszewicz-Zając, M.; Mroczko, P.; Kornhuber, J. Clinical significance of fluid biomarkers in Alzheimer's Disease. *Pharmacol. Rep.* **2020**, *72*, 528–542. [CrossRef]
29. Shea, D.; Colasurdo, E.; Smith, A.; Paschall, C.; Jayadev, S.; Keene, C.D.; Galasko, D.; Ko, A.; Li, G.; Peskind, E.; et al. SOBA: Development and testing of a soluble oligomer binding assay for detection of amyloidogenic toxic oligomers. *Proc. Natl. Acad. Sci. USA* **2022**, *119*, e2213157119. [CrossRef]
30. Savage, M.J.; Kalinina, J.; Wolfe, A.; Tugusheva, K.; Korn, R.; Cash-Mason, T.; Maxwell, J.W.; Hatcher, N.G.; Haugabook, S.J.; Wu, G.; et al. A sensitive aβ oligomer assay discriminates Alzheimer's and aged control cerebrospinal fluid. *J. Neurosci.* **2014**, *34*, 2884–2897. [CrossRef]
31. IBL-International. Human Amyloid β Toxic Oligomer Assay Kit—IBL. Instruction for Use Code No. 27709. Available online: https://www.ibl-japan.co.jp/files/topics/4751_ext_02_en_0.pdf (accessed on 29 March 2023).
32. Hölttä, M.; Hansson, O.; Andreasson, U.; Hertze, J.; Minthon, L.; Nägga, K.; Andreasen, N.; Zetterberg, H.; Blennow, K. Evaluating amyloid-β oligomers in cerebrospinal fluid as a biomarker for Alzheimer's disease. *PLoS ONE* **2013**, *8*, e66381. [CrossRef]
33. Kasai, T.; Tokuda, T.; Taylor, M.; Nakagawa, M.; Allsop, D. Utilization of a multiple antigenic peptide as a calibration standard in the BAN50 single antibody sandwich ELISA for Aβ oligomers. *Biochem. Biophys Res. Commun.* **2012**, *422*, 375–380. [CrossRef]
34. Esparza, T.J.; Zhao, H.; Cirrito, J.R.; Cairns, N.J.; Bateman, R.J.; Holtzman, D.M.; Brody, D.L. Amyloid-β oligomerization in Alzheimer dementia versus high-pathology controls. *Ann. Neurol.* **2013**, *73*, 104–119. [CrossRef] [PubMed]
35. Andreasson, U.; Perret-Liaudet, A.; van Waalwijk van Doorn, L.J.; Blennow, K.; Chiasserini, D.; Engelborghs, S.; Fladby, T.; Genc, S.; Kruse, N.; Kuiperij, H.B.; et al. A Practical Guide to Immunoassay Method Validation. *Front. Neurol.* **2015**, *6*, 179. [CrossRef] [PubMed]
36. Kuo, Y.M.; Kokjohn, T.A.; Kalback, W.; Luehrs, D.; Galasko, D.R.; Chevallier, N.; Koo, E.H.; Emmerling, M.R.; Roher, A.E. Amyloid-beta peptides interact with plasma proteins and erythrocytes: Implications for their quantitation in plasma. *Biochem. Biophys Res. Commun.* **2000**, *268*, 750–756. [CrossRef] [PubMed]
37. Sehlin, D.; Söllvander, S.; Paulie, S.; Brundin, R.; Ingelsson, M.; Lannfelt, L.; Pettersson, F.E.; Englund, H. Interference from heterophilic antibodies in amyloid-β oligomer ELISAs. *J. Alzheimers Dis.* **2010**, *21*, 1295–1301. [CrossRef] [PubMed]
38. Vanderstichele, H.M.; Janelidze, S.; Demeyer, L.; Coart, E.; Stoops, E.; Herbst, V.; Mauroo, K.; Brix, B.; Hansson, O. Optimized Standard Operating Procedures for the Analysis of Cerebrospinal Fluid Aβ42 and the Ratios of Aβ Isoforms Using Low Protein Binding Tubes. *J. Alzheimers Dis.* **2016**, *53*, 1121–1132. [CrossRef]
39. Schoonenboom, N.S.; Mulder, C.; Vanderstichele, H.; Van Elk, E.J.; Kok, A.; Van Kamp, G.J.; Scheltens, P.; Blankenstein, M.A. Effects of processing and storage conditions on amyloid β(1–42) and tau concentrations in cerebrospinal fluid: Implications for use in clinical practice. *Clin. Chem.* **2005**, *51*, 189–195. [CrossRef]
40. van de Merbel, N.; Savoie, N.; Yadav, M.; Ohtsu, Y.; White, J.; Riccio, M.F.; Dong, K.; de Vries, R.; Diancin, J. Stability: Recommendation for best practices and harmonization from the Global Bioanalysis Consortium Harmonization Team. *Aaps J.* **2014**, *16*, 392–399. [CrossRef]

4 Zusammenfassung und Diskussion

Die früheren Entwicklungen der sFIDA-Technologie fokussierten sich auf die Chemie der Glasoberfläche, der Anwendung der Fluoreszenzmikroskopie, auf der Entwicklung eines Kalibrationsstandards und der Automatisierung der Methode [105, 107, 112, 113, 134]. Außerdem wurden erste Experimente mit CSF und Plasma als Matrix durchgeführt [108, 109, 111, 114, 115]. Die darauf aufbauenden Schritte in dieser Arbeit lagen in der Weiterentwicklung des sFIDA für verschiedene Matrices im Hinblick auf eine ausreichende analytische Sensitivität und Selektivität und der Überprüfung ebendieser. Abschließend wurde die Eignung der Quantifizierung von Proteinaggregaten für die Diagnose von neurodegenerativen Erkrankungen anhand der Messung von klinischen Proben eruiert.

4.1 Entwicklung sensitiver und selektiver sFIDA-Assays

Die Entwicklung eines Assays zum Nachweis von Proteinaggregaten in Körperflüssigkeiten ist an verschiedene Herausforderungen gekoppelt. Entscheidend ist eine ausreichende Sensitivität des Assays, um die geringen Oligomerkonzentrationen in Körperflüssigkeiten quantitativ nachzuweisen, sowie besonders bei komplexen Matrices wie Plasma und Stuhl eine hohe Selektivität für den Analyten gegenüber anderen Matrixbestandteilen [97, 133]. Die Bestimmung der Sensitivität und Selektivität eines Verfahrens sind außerdem wichtige Bestandteile einer Assay-Validierung. Weitere Parameter, die bei einer vollständigen Validierung gefordert sind, wie Präzision, Wiederfindungsrate und Probenstabilität, sind für die Zulassung notwendig und wurden bei der Etablierung einzelner Assays untersucht, um hierüber Rückschlüsse über die technische Leistung des sFIDA treffen zu können [135-137].

Sensitivität

Der sFIDA unterscheidet sich von einem ELISA durch die Verwendung von fluoreszenzmarkierten Antikörpern und die fluoreszenzmikroskopische Analyse von Aggregaten und Oligomeren. Dieses Vorgehen hat den Vorteil, dass einzelne Partikel auf der Oberfläche detektiert und gezählt werden können, die bei Messung der Gesamtfluoreszenz im Rauschen untergehen würden. Die Sensitivität eines Assays wird durch die Detektionsgrenze (*limit of detection*, LOD) bzw. die Quantifizierungsgrenze (*lower limit of quantification,* LLOQ) angegeben [138]. Der LOD bzw. LLOQ kann auf verschiedene Weisen bestimmt werden und gibt an, wie hoch die Konzentration in einer Probe sein muss, um mit ausreichender Richtigkeit und Präzision nachgewiesen bzw. quantifiziert werden zu können [135, 138]. Die Sensitivität des sFIDA wird in der Regel mithilfe der SiNaPs

bestimmt. Hierzu wird eine Verdünnungsreihe gemessen, der LOD anhand der Negativkontrolle und der Standardabweichung der Negativkontrolle berechnet und anschließend durch die Kalibration in eine molare Konzentration umgerechnet (s. beispielsweise das Manuskript in Kapitel 3.7). Für die Sensitivität der in dieser Arbeit verwendeten Assays konnte je nach Analyt und Matrix ein subfemtomolarer bis femtomolarer LOD erreicht werden (Tabelle 6), was einem zu erwartenden Konzentrationsbereich für Proteinaggregate entspricht [97].

Tabelle 6 Nachweisgrenzen (LODs) der entwickelten sFIDA-Assays für die Quantifizierung von Aβ-, Tau- und αSyn-SiNaPs

Analyt	Assay Matrix	LOD [fM]	Manuskript in Kapitel
Aβ	Puffer	0,3	3.7
	Plasma	1,8	3.4
	Stuhl*	1,7	3.5
Tau	CSF*	33,7	3.1
αSyn	CSF*	6,7	3.1
	Stuhl*	0,3	3.6

* SiNaPs wurden zur Bestimmung des LODs in den jeweiligen Verdünnungspuffer gegeben

Eine ausreichende Sensitivität des sFIDA für die Quantifizierung von Proteinaggregaten in verschiedenen Körperflüssigkeiten konnte durch die Messung von Patientenproben bestätigt werden, da in den jeweiligen Studien die Mehrheit der Proben oberhalb des LODs lag (siehe z.B. Manuskripte in Kapitel 3.1 und 3.4). Der große dynamische Messbereich des sFIDA konnte nicht nur durch Verdünnungsreihen der SiNaPs und Aggregate, sondern auch durch die Konzentrationsunterschiede der gemessenen Aβ, αSyn und Tau-Oligomere in den verschiedenen Körperflüssigkeiten gezeigt werden (< 1 fM bis > 10 pM je nach Analyten und Matrix, s. Manuskripte in Kapitel 3.1, 3.2, 3.4, 3.5 und 3.6).

Trotz der hohen Sensitivität der Verfahren lagen einige Proben unter dem LOD, wodurch die Notwendigkeit betont wird, die Sensitivität der Assays weiter zu erhöhen. Die theoretisch erreichbare Sensitivitätsgrenze des sFIDA wird u.a. durch die gemessene Fläche eines Wells begrenzt. Um bei der Vermessung von 25 Bildern pro Well im TIRF noch mindestens einen Partikel zu detektieren, muss die Konzentration in der Probe bei ca. 3 aM liegen. Um sich dieser Sensitivität auch in der Praxis zu nähern, können die Assays unter anderem bezüglich der intra-Assay-Präzision, des Hintergrundsignals und der Verwendung hoch-affiner Antikörper weiter optimiert werden. Eine Erhöhung der Sensitivität bewirkt eine zuverlässigere Quantifizierung aller Proben und eine bessere Differenzierung der Proben im niedrigen Konzentrationsbereich. Außerdem können so bereits kleine

Unterschiede z.B. in longitudinalen Studien oder durch den Effekt von anti-Oligomeren Therapien, quantifiziert werden.

Zur Kalibration wurden in dieser Arbeit SiNaPs verwendet. Diese haben den Vorteil, dass sie auf Vorrat herstellbar, stabil und hinsichtlich ihrer Struktur, der zugänglichen Epitope und der Konzentration definierbar sind. Hierzu wurde in einem Kooperationsprojekt die Konzentrationsbestimmung der SiNaPs von einer gravimetrischen Methode auf die Massenspektrometrie mit induktiv gekoppeltem Plasma (*inductively coupled plasma – mass spectrometry,* ICP-MS) umgestellt (erstmals verwendet in der Arbeit in Kapitel 3.1). Bei der ICP-MS wird die Konzentration von Silizium in einer Probe bestimmt und durch Kenntnis der Größe, Form und des Molekulargewichts der SiNaPs in eine Partikelkonzentration umgerechnet. Der Vorteil der ICP-MS-Methode im Vergleich zur Gravimetrie liegt in einer höheren Genauigkeit und einer Reduktion des Probenvolumens um >95 %.

Außerdem wurde das Protokoll für die Proteinkonjugation der Aβ-SiNaPs im Hinblick auf die apparente Partikelgröße im sFIDA optimiert. Durch Reduktion der Anzahl an Epitopen wurden die SiNaPs so angepasst, dass sie der Größe der Oligomere in Patientenproben entsprechen (s. Manuskript in 3.4). Hierdurch kann die Genauigkeit der Umrechnung des pixelbasierten Readouts in eine molare Partikelkonzentration erhöht werden.

Da die SiNaPs speziell für die Anwendung im sFIDA entwickelt wurden, der lineare Epitope in den Proteinen nachweist, sind sie allerdings nicht für die Kalibration von Assays mit strukturspezifischen Antikörpern geeignet. Im Gegensatz zu den SiNaPs sind aus rekombinantem Protein hergestellte Aggregate heterogen in der Anzahl an Monomereinheiten und dadurch hinsichtlich ihrer molaren Partikelkonzentration nicht bestimmbar. Allerdings sind diese Aggregate aufgrund ihrer Ähnlichkeit zu *in vivo*-Oligomeren für die Entwicklung der Methoden insbesondere in komplexen Matrices wie Stuhl und Plasma durchaus hilfreich. Daher wurden in der vorliegenden Arbeit Protokolle für die Verwendung von rekombinant hergestelltem Aβ, αSyn und Tau-Aggregaten im sFIDA etabliert. Ein besonderes Augenmerk lag auf der Weiterentwicklung und der Charakterisierung reproduzierbarer Aβ-Aggregate als Qualitätskontrolle (und alternativ als Kalibrationsstandard) im sFIDA (Manuskript in Kapitel 3.7). Hierbei zeigt sich der Einfluss der Auswahl des Kalibrationsstandards auf die Bestimmung des LODs, wie man am Beispiel von Aβ-Oligomeren in Plasma erkennen kann. Im Gegensatz zu Aβ-SiNaPs mit einem LOD von ca. 1,8 fM, konnte mit den Aβ-Aggregaten ein LOD von 0,42 pM (≙1,9 pg/ml $Aβ_{1-42}$) bezogen auf die Monomerkonzentration erreicht werden (Manuskript in Kapitel 3.4). Um die Partikelkonzentration der Aggregate zu bestimmen und dadurch einen Vergleich der Sensitivitäten von SiNaPs und Aggregaten zu ermöglichen, ist die Kenntnis über die Anzahl

von Monomeren pro Aggregat erforderlich. Diese wiederum hängt vom verwendeten Aggregationsprotokoll ab. Unter der Annahme von 18 Monomeren pro Aggregat (entspricht der theoretischen Anzahl an Epitopen auf den SiNaPs) lässt sich die Monomerkonzentration von 0,42 pM in eine Partikelkonzentration von 23 fM bei Verwendung der Aβ-Aggregate als Kalibrationsstandard umrechnen. Mögliche Ursachen für den zehnfachen Unterschied zu den SiNaPs liegen in einer unvollständigen Aggregation, einer größeren Anzahl von Monomereinheiten pro Aggregat oder am wahrscheinlichsten in einer eingeschränkten Zugänglichkeit der Epitope in den Aggregaten.

Ein direkter Vergleich der Sensitivität des sFIDA mit anderen aggregatspezifischen Assays ist aus mehreren Gründen nur schwer bis gar nicht möglich. Neben der unterschiedlichen Berechnung des LODs bzw. LLOQs liegt das Hauptproblem in unterschiedlichen Kalibrationsstandards. Während die meisten Assays $A\beta_{1-42}$-Aggregate zur Kalibration verwenden, nutzen andere beispielsweise $A\beta_{1-11}$-Dimere [98, 139]. Zusätzlich ist die genaue Struktur der Aggregate, die Ausbeute und die Anzahl an Monomereinheiten pro Aggregat abhängig vom gewählten Aggregationsprotokoll [121, 140].

Da sich die angegebenen Sensitivitäten anderer Assays allerdings über mehr als drei Größenordnungen erstrecken (Tabelle 7), kann man zwar keinen direkten Vergleich, aber eine ungefähre Einordnung des sFIDA gegenüber anderen Verfahren durchführen.

Tabelle 7 Übersicht über das Prinzip und die Sensitivität von Oligomer-Assays

Analyt	Matrix	Name	Prinzip	Sensitivität	Quelle
Aβ	CSF	Erenna	Überlappende Epitope	LOD: 90 fg/ml	[99]
	CSF	ELISA	Überlappende Epitope	LLOQ: 200 fg/ml	[98]
		ELISA	Überlappende Epitope	LOD: 90 pg/ml	[141]
	CSF, Plasma	SMCxPro	Oligomer-spezifischer Antikörper	LLOQ: 600 fg/ml	[142]
	Plasma	MDS	Oligomerisierung	LLOQ: 239 pg/ml	[143]
		SOBA	Nachweis des α-Sheet-Anteils	LLOQ: 1 fM	[144]
αSyn	CSF	ELISA	Überlappende Epitope	-	[102, 145, 146]
		ELISA	Oligomer/Aggregat-spezifischer Antikörper	LOD: 10 pg/ml	[103]
	Plasma	ELISA	Überlappende Epitope	LOD: 14,3 ng/Well	[147]
Tau	CSF	ELISA	Oligomer-spezifischer Antikörper	-	[148]

Der sensitivste Assay zum Nachweis von Aβ-Oligomeren in Tabelle 7 ist der Erenna-Assay mit einer Sensitivität von 90 fg/ml. Zur Kalibration werden in diesem Assay High-Molecular-Weight-Oligomere mit einem durchschnittlichen Molekulargewicht von 1117 kDa verwendet (entspricht ca. 250 Monomereinheiten). Mithilfe dieser Angaben lässt sich der LOD in eine molare Partikelkonzentration von 0,08 fM umrechnen [99]. Die Sensitivität des sFIDA für den Nachweis von Aβ-Oligomeren liegt ebenfalls im sub-femtomolaren Bereich und kann daher zu den sensitivsten Verfahren gezählt werden (Manuskript in Kapitel 3.7). Analog verhält es sich bei der Quantifizierung von αSyn-Oligomeren. Der ELISA mit einem LOD von 10 pg/ml entspricht unter Annahme von 20 Monomeren pro Aggregat einer molaren Partikelkonzentration von 34,7 fM. Mit dem sFIDA konnte ein LOD von 0,3 fM im Stuhlassay (Manuskript in Kapitel 3.6) bzw. 6,7 fM beim gleichzeitigen Nachweis von Tau-Aggregaten (Manuskript in Kapitel 3.1) erreicht werden.

Um verschiedene Assays zukünftig miteinander zu vergleichen und um eine zuverlässige Konzentration von Aggregaten in den Körperflüssigkeiten über verschiedene Assays hinweg angeben zu können, ist die Einführung eines Referenzstandards notwendig [23]. Für $A\beta_{1-42}$-Immunoasssays in CSF konnte beispielsweise gezeigt werden, dass durch die Re-Kalibration des Assays mit einem Referenzstandard die Unterschiede zwischen verschiedenen Assays ausgeglichen werden können [149]. Einen möglichen Referenzstandard stellen die in dieser Arbeit entwickelten Aβ-Oligomere dar (Manuskript in Kapitel 3.7).

Selektivität

Der zweite entscheidende Punkt bei der Entwicklung eines Assays, insbesondere für den Nachweis in Körperflüssigkeiten, ist die Selektivität für den entsprechenden Analyten. Hierbei gilt es insbesondere sicherzustellen, dass der Assay das richtige Target erkennt und nicht durch Probenbestandteile beeinflusst wird (für mögliche Einflüsse der Matrix s. Kapitel 1.3.5). Für den Nachweis der Selektivität wurden verschiedenen Kontrollen durchgeführt:

- Hinzugeben (Spiken) möglicher kreuzreagierender Substanzen (z.B. Monomer, heterophile Antikörper)
- Weglassen oder Austauschen des Capture- und Detektionsantikörpers
- Abreicherung des Analyten durch Immundepletion
- Spiken des Kalibrationsstandards in die Matrix

Das Prinzip des sFIDA mit Antikörpern gegen die gleichen oder überlappende Epitope schließt den Nachweis von Monomeren in der Theorie aus. Durch das Spiking mit Aβ, αSyn und Tau-Monomeren konnte bestätigt werden, dass die Anwesenheit von Monomeren die

Quantifizierung von Aggregaten dieser Proteine auch in der Praxis nicht beeinträchtigt (Manuskripte in Kapitel 3.1, 3.2, 3.4, 3.5 und 3.6). Somit kann das Ergebnis selbst bei einer unspezifischen Bindung des Analyten an die Assayoberfläche, wie es für Tau-Oligomere allgemein oder für Aβ-Oligomere in Plasma beobachtet wurde, nicht auf den Einfluss von Monomeren zurückgeführt werden (Manuskripte in Kapitel 3.1 und 3.4).

Eine unspezifische Bindung an Oberflächen zeigte sich nicht nur durch ein Signal im sFIDA, obwohl kein Captureantikörper pipettiert wurde (Capturekontrolle), sondern auch bei der Immundepletion. Hierbei werden magnetische Beads, an die ein Antikörper gegen den Analyten gekoppelt ist, mit der Probe inkubiert, wodurch der Analyt an die Beads binden kann. Durch die paramagnetischen Eigenschaften können die Beads und dadurch der Analyt durch einen Magneten aus der Probe entfernt werden. Sowohl für αSyn und Tau in CSF, αSyn und Aβ in Stuhl und Aβ in Plasma konnte in biologischen Proben eine Reduktion des Signals im sFIDA durch Entfernen des Analyten gezeigt werden (Manuskripte in Kapitel 3.1, 3.4, 3.5 und 3.6). Hieraus lässt sich schließen, dass die gemessenen Signale nicht durch störende Effekte der jeweiligen Matrix, sondern durch das nachzuweisende Protein hervorgerufen werden. Allerdings ergab sich bei Tau-Oligomeren in CSF und Aβ-Oligomeren in Plasma analog zur Capturekontrolle eine unspezifische Bindung der Probenbestandteile an den Bead-Grundkörper ohne Antikörper und damit eine unspezifische Signalreduktion (Manuskripte in Kapitel 3.1 und 3.4). Da die antikörperbasierte Signalreduktion aber höher war als die unspezifische Signalreduktion, kann trotzdem von einem selektiven Nachweis des Analyten ausgegangen werden. Durch die Entwicklung eines Protokolls für die Immundepletion von biologischen Proben in Kombination mit dem sFIDA konnte eine wertvolle Methode entwickelt werden, um die Selektivität des Assays nicht nur für rekombinante Aggregate, sondern auch für biologische Proben selbst zu analysieren. Mögliche Optimierungen der Assays, die auf eine Reduktion der unspezifischen Bindung an Probenbestandteile abzielen, betreffen unter anderem den Blockierungsschritt und Probenverdünnungen.

Für die Quantifizierung von Analyten in Plasma ist die Interferenz mit heterophilen Antikörpern, insbesondere HAMAs, ein häufig beobachteter Störfaktor in 5-40 % der Proben. Heterophile Antikörper können aber in geringerer Konzentration auch im CSF vorkommen [133]. In einem Oligomer-ELISA wurde gezeigt, dass durch Blockierung der HAMAs das Signal in CSF- und Plasmaproben reduziert bzw. eliminiert wurde [150]. Zwar konnte in dieser Arbeit ebenfalls ein theoretischer Einfluss von HAMAs auf das Signal im sFIDA beobachtet werden, das Abfangen möglicher HAMAs in CSF-Proben durch Zugabe eines Maus-Antikörpers resultierte allerdings nicht in einer Signalreduktion. Für CSF-Proben kann aus diesem Grund ein Einfluss von HAMAs auf die Quantifizierung von αSyn und Tau-Oligomeren nicht bestätigt werden (Manuskript in Kapitel 3.1). Um für die

Bestimmung von Aβ-Oligomeren in Plasma eine HAMA-Interferenz zu kompetieren, wurde in diesem Assay der Maus-Capture-Antikörper Nab288 gegen den humanisierten Antikörper Bapineuzumab ausgetauscht, wodurch eine Quervernetzung zwischen Capture- und Detektionsantikörper durch HAMAs verhindert werden konnte (Manuskript in Kapitel 3.4). Durch diese Maßnahme konnte die Selektivität des Assays erhöht und falsch-positive Signale reduziert werden.

Zusätzlich wurde für CSF- und Plasma der Einfluss der Matrix auf den Nachweis und die Quantifizierung von SiNaPs untersucht. Für CSF-Analysen wurde hierfür die Wiederfindungsrate (*recovery*) von SiNaPs in CSF im Vergleich zur Pufferkontrolle bestimmt. Für αSyn- und Aβ-SiNaPs konnte eine Wiederfindungsrate von 79 % bzw. 100 % erreicht werden, während die Wiederfindungsrate für Tau-SiNaPs bei 36 % lag (Manuskripte in Kapitel 3.1 und 3.7). Die geringe Wiederfindungsrate bei den Tau-SiNaPs kann zu einem Fehler in der Berechnung der Oligomerkonzentration führen, der vertiefend analysiert werden sollte, z.B. durch Bestimmung der Wiederfindungsrate von Tau-Aggregaten in CSF. Sollte sich ein Einfluss der CSF-Matrix auf die Quantifizierung der Tau-Oligomerkonzentrationen bestätigen, kann in zukünftigen Studien ein Korrekturfaktor für die berechneten Oligomerkonzentrationen angewendet werden. Für die Quantifizierung von Aβ-Oligomeren wurde die Wiederfindungsrate nicht im Vergleich zur Pufferkontrolle, sondern zum Referenzplasma bestimmt, um hierüber festzustellen, ob die individuelle Plasmamatrix die Quantifizierung beeinflusst. Da die durchschnittliche Wiederfindungsrate bei 92 % lag, kann eine zuverlässige Quantifizierung unabhängig von der Matrix angenommen werden (Manuskript in Kapitel 3.4).

Präanalytik

Um reproduzierbare Ergebnisse aus unabhängigen Assays zu erzielen, ist nicht nur eine geeignete Kalibration entscheidend, sondern auch die Analyse von möglichen Einflussfaktoren sowohl während der Präparation als auch präanalytisch. In Robustheitsstudien werden kleine Änderungen in den Methodenparametern wie Inkubationszeiten oder Temperaturen vorgenommen, um Bereiche festzulegen, in denen das Messergebnis nicht beeinflusst wird [135]. Zu den präanalytischen Einflussfaktoren zählen z.B. Gefrier-Tau-Zyklen, Lagerung und Probenvorbehandlungen. Welche Faktoren relevant sind, kann sowohl vom Protein als auch von der Matrix abhängen und sich für den jeweiligen Analyten unterscheiden.

Studien zu präanalytischen Einflussfaktoren liegen bisher hauptsächlich für die ausführlicher untersuchten Monomere in CSF vor. Hier konnte gezeigt werden, dass die Konzentrationen vom Probengefäß, tageszeitlichen Schwankungen und der Anzahl an Überführungsschritten in neue Gefäße abhängt [151, 152]. Im Gegensatz dazu blieb die

Konzentration von αSyn-Oligomeren durch Überführen in ein neues Probengefäß oder durch längere Lagerung bei Raumtemperatur oder 4 °C konstant, nahm aber durch wiederholtes Einfrieren und Auftauen ab [152]. Für allgemeine Proteinbestimmungen in CSF wurden außerdem Einflüsse durch das entnommene CSF-Volumen und die Reihenfolge der Einzelproben, die Punktionsstelle, die Zeit bis zum Zentrifugieren und Einfrieren und die Zentrifugationsdauer- und Geschwindigkeit festgestellt [127].

Für Bestimmungen von Aβ- und Tau-Monomeren in Plasma wurden vor allem Einflüsse des Antikoagulanz, aber auch der Dauer bis zum Zentrifugieren und der Lagerung berichtet [153, 154]. Im Gegensatz dazu war die Wiederfindungsrate der Aβ-Oligomere in einer weiteren Studie nur vom verwendeten Antikoagulanz abhängig [155]. Der Einfluss des Antikoagulanz auf das Signal im sFIDA wurde im Vorfeld von Kravchenko et al. untersucht. Die verwendeten Antikoagulanzen unterschieden sich in der Sensitivität und Präzision der Bestimmung von Aβ-SiNaPs, wobei mit EDTA-Plasma die höchste Sensitivität von 16 fM bei gleichzeitig geringstem Variationskoeffizienten erreicht werden konnte [114]. In der vorliegenden Arbeit wurde ausschließlich mit EDTA-Plasma gearbeitet, wobei sowohl die Nachweisgrenze reduziert als auch die Präzision im Vergleich zu vorherigen Studien erhöht werden konnten. Außerdem wurde ein Einfluss von der Anzahl der Überführschritte, der Gefrier-Tau-Zyklen und von der Hämolyse von roten Blutkörperchen auf den sFIDA Readout festgestellt (s. Manuskript in Kapitel 3.4).

Da es sich bei der Bestimmung von Aβ- und αSyn-Oligomeren in Stuhlproben um ein neuartiges Verfahren handelt, liegen hier bisher keine Studien zu präanalytischen Einflussfaktoren vor. Für Proteinbestimmungen in Stuhl wurde allgemein berichtet, dass Extrakte über einen längeren Zeitraum gelagert werden können als die unbehandelte Probe. Auch die Temperatur der Lagerung und der Lagerungspuffer können die Wiederfindung der Proteine beeinflussen [156, 157]. Die in dieser Arbeit bestimmten Aβ-Oligomere zeigten ein vergleichbares Verhalten mit höherer Stabilität durch das Extrahieren und Lagerung bei geringerer Temperatur (s. Manuskript in Kapitel 3.5).

Um reproduzierbare Ergebnisse zu erzielen und um die Ergebnisse unterschiedlicher Studien miteinander vergleichen zu können, ist eine Vereinheitlichung präanalytischer Vorgehensweisen essenziell. Daher wurden sowohl für CSF als auch für Blut entsprechende Protokolle vorgeschlagen, die Faktoren wie z.B. Probengefäße, Zentrifugationsgeschwindigkeiten und Dauer bis zum Einfrieren regeln [127, 153]. Allerdings sind solche Protokolle nur für neu gesammelte Proben anwendbar, während viele Studien auf Proben aus Biobanken zurückgreifen, die teilweise vor der Etablierung einheitlicher Protokolle gesammelt wurden. Außerdem können für die Bestimmung von Oligomeren andere oder zusätzliche Einflussfaktoren gelten, weshalb die Gültigkeit der Protokolle für den entsprechenden Analyten bestätigt werden muss.

Um die Robustheit und dadurch die Reproduzierbarkeit der Assays zu erhöhen, sollten in zukünftigen Studien aufbauend auf den bisherigen Erkenntnissen sowohl präanalytische als auch methodische Einflussfaktoren ausführlicher untersucht werden.

Zusammenfassend konnte durch die Weiterentwicklung des sFIDA für verschiedene Analyten und verschiedene Matrices gezeigt werden, dass die Technologie eine hohe Sensitivität und Selektivität für den Analyten aufweist und daher sowohl für die gleichzeitige Quantifizierung von Proteinaggregaten in CSF als auch für komplexe Matrices wie Plasma geeignet ist. Da sich *in-vivo* vorkommende Aggregate von *in-vitro* Aggregaten und SiNaPs unterscheiden, ist insbesondere die Messung von biologischen Proben und die Überprüfung der Selektivität anhand dieser Proben ein wichtiger Schritt, um die Eignung des sFIDA zu zeigen.

4.2 Eignung der Quantifizierung von Oligomeren zur Diagnose von neurodegenerativen Erkrankungen

Im ersten Teil dieser Arbeit konnte gezeigt werden, dass der sFIDA-Assay technisch in der Lage ist, selbst geringe Konzentrationen der Oligomere in den verschiedenen Körperflüssigkeiten nachzuweisen. Darauf aufbauend wurde anhand von Patientenproben überprüft, ob sich die Oligomerkonzentrationen in den Körperflüssigkeiten in Abhängigkeit der Erkrankung bzw. des Erkrankungsfortschrittes unterscheiden. Im Folgenden sind daher die Ergebnisse der verschiedenen Studien kurz zusammengefasst und Zusammenhänge zwischen den Studien erörtert worden. Eine ausführliche Diskussion der einzelnen Studien erfolgte in den Manuskripten selbst. Außerdem werden in diesem Abschnitt Unterschiede zu anderen Verfahren erläutert, um abschließend eine Aussage über die Eignung der Quantifizierung von Oligomeren mittels sFIDA zur Diagnose neurodegenerativer Erkrankungen treffen zu können.

Oligomerkonzentrationen in verschiedenen neurodegenerativen Erkrankungen

Erste diagnostische sFIDA-Analysen fokussierten sich auf CSF, da hier durch die direkte Verbindung mit dem Gehirnparenchym höhere Konzentrationen erwartet und Veränderungen direkt widergespiegelt werden können [158]. Aufgrund der Invasivität der Liquorpunktion und der damit verbundenen möglichen Nebenwirkungen wurden aufbauend auf den in CSF gewonnen Erkenntnissen weniger oder nicht invasive Verfahren wie die Bestimmung der Oligomere in Plasma bzw. Stuhl entwickelt.

Für AD wurden in dieser Arbeit erhöhte Aβ- und αSyn-, allerdings keine erhöhten Tau-Oligomer-Konzentrationen im CSF gemessen (Manuskript in Kapitel 3.1 und 3.2). Eine Erhöhung der Aβ-Oligomerkonzentration konnte dabei nur bei Amyloid-positiven

Patienten in Frühstadien wie SCD und MCI, allerdings nicht in AD-Patienten festgestellt werden. Daraus ergibt sich ein glockenförmiger Verlauf der Aβ-Oligomerkonzentration mit dem Fortschreiten der Erkrankung mit den höchsten Oligomerkonzentrationen in MCI-Patienten (Abbildung 4 im Manuskript in Kapitel 3.2). Zusätzlich wurde festgestellt, dass höhere Oligomerkonzentrationen im CSF von ApoE ε4-positiven Patienten zu finden sind, die außerdem zu einem späteren Zeitpunkt im Krankheitsverlauf ein Maximum erreichen. Diese erhöhten Aβ-Oligomerkonzentrationen im CSF von ApoE ε4-Carriern lassen sich unter anderem durch eine weniger effektive Clearance von Aβ-Oligomeren erklären. Mögliche Mechanismen einer eingeschränkten Clearance sind sowohl eine geringere Degradierung durch Mikroglia, als auch ein verminderter Abtransport von Aβ über die Blut-Hirn- bzw. Blut-CSF-Schranke [159, 160].

Für die Interpretation der Aβ-Oligomerkonzentrationen in Plasma ist die Betrachtung der Clearance ebenfalls von Bedeutung. Hier wurden geringere Aβ-Oligomerkonzentrationen in SCD und AD-Patienten im Vergleich zur Kontrolle gemessen (s. Manuskript in Kapitel 3.4). Betrachtet man nur Patienten mit vorliegender Amyloid-Pathologie, zeigten sowohl SCD, MCI als auch AD-Patienten signifikant geringere Aβ-Oligomerkonzentrationen im Plasma. Im Gegensatz dazu waren die Aβ-Oligomerkonzentrationen bei Amyloid-negativen Patienten nicht verändert. Korrelationsanalysen legen auch hier einen Einfluss der Clearance der Aβ-Oligomere nahe: während die Aβ-Oligomerkonzentrationen in CSF und Plasma von Angehörigen, Kontroll- und SCD-Patienten direkt korrelierten, wurde bei MCI- und AD-Patienten eine inverse Korrelation festgestellt. Betrachtet man nur die Amyloid-positiven Patienten, gehen diese Korrelationen verloren. Eine mögliche Erklärung liegt in der bevorzugten Ablagerung der Aβ-Oligomere in unlöslichen Plaques, wodurch die Konzentration im Blut nicht mehr von der CSF-Konzentration abhängig ist. Für den Transport von Aβ-Monomeren ins Blut ist bereits eine Abhängigkeit vom ApoE-Status beschrieben worden [160]. Korrelationsanalysen der Oligomere zwischen CSF und Plasma legen ebenfalls einen Einfluss des ApoE-Status auf die Clearance auch für Aβ-Oligomere nahe, da im Gegensatz zu ApoE ε4-negativen Patienten bei ApoE ε4-positiven Patienten kein Zusammenhang der Aβ-Oligomerkonzentrationen zwischen CSF- und Plasma gefunden werden konnte. Ein möglicher Ansatzpunkt für die Erklärung der reduzierten Aβ-Oligomerkonzentrationen im Plasma ist daher ein verminderter Abtransport aus dem Gehirn ins Blut.

Trotz der reduzierten Konzentrationen der Aβ-Oligomere im Plasma von AD-Patienten, wurden im Stuhl erhöhte Aβ-Oligomerkonzentrationen gegenüber den Kontrollen beobachtet (Manuskript in Kapitel 3.5). Hierfür kommen verschiedene Erklärungen infrage. Die Clearance von Aβ erfolgt in der Peripherie zum größten Teil in der Leber, von wo aus die Ausscheidung über die Galle und den Stuhl erfolgen kann [77]. Fehlfunktionen der Leber

resultieren in einer reduzierten Clearance von Aβ und stehen möglicherweise im Zusammenhang mit AD [77]. Eine potenzielle Erklärung für die erhöhten Oligomerkonzentrationen in Stuhl ist daher ein reduzierter Abbau der Oligomere in der Leber. Außerdem wurde ein Zusammenhang des Magen-Darm-Mikrobioms mit AD bzw. Aβ-Ablagerungen berichtet [77], sodass auch Bakterien im Magen-Darm-Trakt zur Konzentration der Aβ-Oligomere im Stuhl beitragen könnten. Außerdem wurden für Aβ-Monomere Plasma- unabhängige Transportmechanismen z.B. durch Neuron-Neuron-Transport und eine Produktion von APP im enterischen Nervensystem beobachtet [161]. Um mögliche Clearance-Mechanismen und den Ursprung der Oligomere im Stuhl besser zu verstehen, können in zukünftigen Studien Proben derselben Patienten in allen drei Matrices gemessen und die Zusammenhänge analysiert werden.

Da nicht nur Ablagerungen des Aβ, sondern auch des Tau-Proteins für AD charakteristisch sind, wurden die Tau-Oligomer-Konzentrationen im CSF von AD-Patienten in zwei Studien untersucht. Trotz eines starken positiven Zusammenhangs zwischen den αSyn- und Tau- bzw. die Aβ- und Tau-Oligomerkonzentrationen konnten in beiden Studien keine erhöhten Tau-Oligomerkonzentrationen im CSF von AD-Patienten gemessen werden (Manuskripte in Kapitel 3.1 und 3.2). Im Gegensatz dazu zeigten Patienten mit der primären 4R-Tauopathie PSP deutlich erhöhte Tau-Oligomerkonzentrationen (Manuskript in Kapitel 3.1). Unterschiede lassen sich u.a. durch unterschiedliche Tau-Strukturen und das Fortschreiten der Erkrankung erklären: Vorherige Studien konnten erhöhte Tau-Oligomerkonzentrationen nur in fortgeschrittenen Stadien der AD messen [148], während sich Patienten in der DELCODE-Studie (*DZNE-longitudinal cognitive impairment and dementia study)* in frühen Erkrankungsstadien befanden. Der Erkrankungsfortschritt der AD-Patienten und der PSP-Patienten in der ersten Studie ist nicht weiter definiert. Allerdings handelt es sich bei PSP um eine schnell voranschreitende Erkrankung mit einer durchschnittlichen Lebenserwartung von 8 Jahren nach der Diagnose [55], wodurch Tau-Oligomerkonzentrationen möglicherweise früher erhöht sind. Eine longitudinale Beobachtung über einen längeren Zeitraum (z.B. 5-10 Jahre) und bei AD insbesondere bis in fortgeschrittene Stadien der Erkrankung kann zum Verständnis der Tau-Oligomerkonzentrationen im CSF beitragen.

Obwohl AD-Patienten keine erhöhten Tau-Oligomere im CSF zeigten, konnte durch die Gabe des Aβ-eliminierenden Medikaments RD2 in Hunden dosisabhängig die Zunahme der Tau-Oligomerkonzentration in CSF gestoppt werden, während die Aβ-Oligomer-Konzentrationen zwischen Baseline und Follow-Up keine signifikanten Unterschiede zwischen Placebo und Behandlung ergeben haben (Manuskript in Kapitel 3.3). Als mögliche Ursache für den fehlenden messbaren Effekt auf die Aβ-Oligomerkonzentrationen kommen u.a. Limitierungen in der Rekrutierung der Hunde infrage, da in vorherigen Studien die

Wirkung des Medikaments auf die Aβ-Oligomere bereits gezeigt werden konnte [39, 162]. Analog zu den anderen Studien zur Bestimmung der Tau-Oligomerkonzentrationen mittels sFIDA konnte aber auch hier eine Korrelation zwischen den Aβ- und Tau-Oligomerkonzentrationen im CSF festgestellt werden.

Neben AD lag ein weiteres Anwendungsfeld des sFIDA in der Analyse der Oligomerkonzentrationen in Patienten mit Synucleinopathien. Hierbei zeigten PD und DLB-Patienten gegenüber den Kontrollen erhöhte αSyn-Oligomerkonzentrationen im CSF (Manuskript in Kapitel 3.1). Obwohl auch für PD die αSyn- und Tau-Oligomerkonzentrationen korrelierten, konnten erhöhte Tau-Oligomer-Konzentrationen nur bei DLB-Patienten gefunden werden. Bei der Vermessung der CSF-Proben der PD-Patienten wurde nicht zwischen einem möglichen Ursprung im zentralen oder enterischen Nervensystem unterschieden, wohingegen bei der Untersuchung der Oligomerkonzentrationen im Stuhl iRBD-Patienten eingeschlossen waren, bei denen der Ursprung im enterischem Nervensystem vermutet wird [46]. Für diese iRBD-Patienten, allerdings nicht für PD-Patienten, konnten signifikant erhöhte αSyn-Oligomerkonzentrationen im Stuhl gemessen werden. Für zukünftige Studien wäre auch hier eine vergleichende Messung der Oligomerkonzentrationen in verschiedenen Matrices unter Berücksichtigung des Ursprungstyp und des Fortschreitens der Erkrankung interessant. Erhöhte Oligomerkonzentrationen im Stuhl bei der *gut-first*-Gruppe und erhöhte Konzentrationen im CSF bei der *brain-first*-Gruppe würden die These der Ursprungstypen unterstützen und bei der Auswahl geeigneter Patienten für klinische Studien helfen.

Neben dem sFIDA gibt es weitere Verfahren, mit denen die Oligomerkonzentrationen in neurodegenerativen Erkrankungen bestimmt werden. Die Ergebnisse sind allerdings nicht einheitlich: Während in manchen Studien erhöhte Oligomerkonzentrationen in erkrankten Patienten berichtetet wurden, konnten andere keine Unterschiede feststellen, wie z.B. für die Bestimmung von Aβ-Oligomeren in AD [98, 141] oder αSyn-Oligomeren in DLB [145, 163]. Zusätzlich zu den Unterschieden zwischen verschiedenen Verfahren, zeigten viele Studien, so auch die in dieser Arbeit gemessenen Proben, sowohl in der Abgrenzung zwischen Erkrankten und Kontrollen als auch differenzialdiagnostisch zur Abgrenzung unterschiedlicher Erkrankungen eine große Überlappung in der Konzentration der Oligomere [99, 139, 145, 163]. Für die Unterschiede zwischen den Studien und den großen Überlapp kommen insbesondere Unterschiede in der Präanalytik, im Assaydesign, in der Struktur der Oligomere und Co-Pathologien infrage.

Diversität der Oligomerstrukturen

Sowohl für Aβ als auch für αSyn und Tau wurde ein heterogener Pool an Aggregatstrukturen beschrieben. Diese Aggregate unterscheiden sich in der Größe bzw. dem Molekulargewicht, posttranslationalen Modifikationen und der dreidimensionalen Konformation. Unterschiede wurden dabei sowohl inter-individuell als auch intra-individuell und in Abhängigkeit des Erkrankungsstadiums beobachtet [89, 164-166]. Wie in Kapitel 1.3.1 erläutert, verwenden die meisten Assays spezifische Antikörper, die entweder gegen ein lineares oder ein oligomerspezifisches Epitop gerichtet sind (s. auch Tabelle 7). Während Assays mit Antikörpern gegen überlappende Epitope wie dem sFIDA die Gesamtheit der Oligomere unabhängig von ihrer Struktur erkennen, wird bei Verfahren mit oligomerspezifischen Antikörpern eine Untergruppe detektiert. Aufgrund der Vielzahl verschiedener Oligomerstrukturen und Antikörper ist eine unterschiedliche Sensitivität der Assays gegenüber einzelnen Subtypen naheliegend. Der Einfluss der Antikörperauswahl lässt sich an einer Studie von Yang et al. erkennen, der gezeigt hat, dass dieselben Proben mit unterschiedlichen Antikörpern gemessen zu nur schwach korrelierenden Ergebnissen geführt haben [167]. Welche Oligomerstrukturen bei den jeweiligen neurodegenerativen Erkrankungen das höchste neurotoxische Potential haben, am spezifischsten mit der Erkrankung zusammenhängen und folglich für eine Diagnose ebendieser am besten geeignet sind, ist zum jetzigen Zeitpunkt noch nicht geklärt. Zusätzlich ist zu beachten, dass verschiedene Fragestellungen möglicherweise verschiedene Assays erfordern. Zum einen hängt die Struktur der Oligomere u.a. mit dem Erkrankungsfortschritt zusammen [165], sodass für eine Diagnose in Frühstadien ein anderer Assayaufbau oder Antikörper entscheidend sein kann als in fortgeschrittenen Stadien. Zum anderen ist die Aufgabe des Assays entscheidend. Beim *Target Engagement* in klinischen Studien kann beispielsweise ein Verfahren von Vorteil sein, dass die Gesamtheit der Oligomere quantifiziert, da bei strukturspezifischen Assays unklar bleibt, ob es zur Eliminierung der Oligomere oder nur zu einer Änderung der Struktur gekommen ist, die der Assay nicht detektieren kann. Außerdem adressieren die anti-Oligomeren Therapien möglicherweise verschiedene Strukturen gleichzeitig, was nur durch einen Assay wie dem sFIDA abgebildet werden kann, der die Gesamtheit der Oligomere quantifiziert.

Ein großer Vorteil der sFIDA Technologie ist außerdem die Möglichkeit der Variabilität und der zeitgleichen Detektion mehrerer Strukturen, wie es anhand des simultanen Nachweises zweier Proteine gezeigt werden konnte (Manuskripte in Kapitel 3.1, 3.2 und 3.3). Diese Flexibilität kann zukünftig auf die Bestimmung unterschiedlicher Strukturen in einem Oligomer erweitert werden: Durch die Anwendung mehrerer Fluoreszenzkanäle und die Auswertung der Kolokalisation kann beispielsweise für den einen Kanal der normale

sFIDA-Aufbau mit überlappenden Epitopen gewählt werden, wodurch die Gesamtheit der Oligomere quantifiziert wird. Gleichzeitig kann in einem weiteren Kanal ein strukturspezifischer Antikörper vermessen werden, um damit die Spezifität zu erhöhen, bzw. einen strukturellen Subtyp eines Oligomers zu analysieren. Das Verhältnis zwischen einer bestimmten Oligomerstruktur und der Gesamtzahl an Oligomeren kann, ähnlich wie bei dem Verhältnis von $A\beta_{1-42}/A\beta_{1-40}$ eine zusätzliche Information liefern und durch den Ausgleich präanalytischer und individueller Unterschiede die Robustheit erhöhen. Zusätzlich kann man bei Studien zur Bestimmung des *Target Engagement* in einem Kanal das Oligomer, in einem anderen das Medikament markieren, um durch die Kolokalisation die Bindung des Medikaments an die Oligomere zu zeigen. Dazu muss lediglich sichergestellt sein, dass Wirkstoff und Assayantikörper unterschiedliche Epitope erkennen.

Co-Pathologien

Während präanalytische Einflussfaktoren, das Assaydesign und die Diversität der Oligomerstrukturen die unterschiedlichen Ergebnisse diagnostischer Studien erklären, lässt sich die Überlappung der Oligomerkonzentrationen in Körperflüssigkeiten u.a. auf eine verzögerte Diagnose im Vergleich zu pathophysiologischen Veränderungen im Gehirn und Co-Pathologien zwischen neurodegenerativen Erkrankungen zurückführen. Ablagerungen von Aβ, αSyn und Tau lassen sich bereits Jahre oder Jahrzehnte vor dem Auftreten der Symptome feststellen [16, 44]. Die Diagnosestellung erfolgt allerdings erst nach dem Auftreten von Symptomen und in der Routinediagnostik primär anhand der Symptomatik [44, 56]. Dieses Vorgehen resultiert in einer falschen Diagnose bei ca. 25-30 % der Alzheimer-, 20 % der Parkinson- und DLB-Patienten und 15 % der PSP-Patienten, wie sich durch histopathologische Untersuchungen nach dem Tod feststellen lässt [51, 58, 96, 168]. Obwohl die Genauigkeit der Diagnose in spezialisierten Zentren durch die Erfahrung der verantwortlichen Kliniker und der Verwendung von Biomarkern und bildgebenden Verfahren erhöht wird, beeinflusst eine Fehldiagnose nicht nur das Leben des Patienten, sondern auch die Entwicklung neuer diagnostischer Methoden und Medikamente [51]. Die Berechnung der Spezifität und Sensitivität von Biomarkern erfolgt in der Regel im Vergleich zur (symptombasierten) Primärdiagnose, sodass fehldiagnostizierte Patienten die berechnete Genauigkeit der neuen Verfahren reduzieren können. Auch für die Bewertung der Eignung der mittels sFIDA gemessenen Oligomerkonzentrationen zur Diagnose ist eine akkurate Primärdiagnose entscheidend, wie man am Beispiel der Bestimmung der Aβ-Oligomere in CSF in der DELCODE-Studie (Manuskript in Kapitel 3.2) erkennen kann. Während bei Betrachtung aller Patienten signifikante Unterschiede nur zwischen MCI-Patienten und Kontrollen beobachtet werden konnten, zeigten sowohl SCD- als auch MCI-Patienten unter Berücksichtigung der aktualisierten Definition von AD (Biomarker-Evidenz

für Aβ-Ablagerungen, s. Kapitel 1.1.1) signifikant erhöhte Oligomerkonzentrationen. Erfolgte die Gruppierung der Patienten in der DELCODE-Studie ausschließlich nach dem AT(N)-System anstatt der klinischen Beurteilung, konnte die Unterscheidbarkeit zwischen Frühstadien (A+T-) und Kontrollen (A-T-) weiter erhöht werden. Ursachen hierfür sind, dass für 7,5 % der AD und > 25 % der MCI-Patienten keine Amyloid-Pathologie nachgewiesen werden konnte, während sich > 25 % der Kontrollen aufgrund auffälliger $Aβ_{1-42}$-Werte zu Frühstadien innerhalb des Alzheimer-Kontinuums zuordnen lassen und daher keine geeignete Kontrollgruppe darstellen.

Die Relevanz der Co-Pathologien wurde insbesondere in der Studie in Kapitel 3.1 erörtert. In dieser Studie wurden die αSyn- und Tau-Oligomerkonzentrationen in PD, DLB, PSP und AD-Patienten untersucht. Obwohl AD-Patienten durch die Anwesenheit von Aβ und Tau-Oligomeren und nicht primär durch αSyn-Pathologie charakterisiert sind, zeigten diese Patienten signifikant erhöhte αSyn-Oligomer-Konzentrationen im Vergleich zur Kontrolle und ließen sich nicht von Synucleinopathien wie PD und DLB unterscheiden. Zusätzlich wurden erhöhte Tau-Oligomerkonzentrationen in DLB-Patienten gemessen. Diese Ergebnisse stehen im Einklang mit anderen Studien, die Lewy-Körperchen in Gehirnen von AD-Patienten gefunden haben [169, 170]. Umgekehrt zeigen PD und DLB-Patienten häufig auffällige AD-Pathologien wie Aβ- und Tau-Ablagerungen [48, 171]. Weitere Studien haben gezeigt, dass bei der Mehrheit der Patienten Co-Pathologien zwischen Aβ, αSyn, Tau und TDP-43-Ablagerungen gefunden wurden, die unter anderem abhängig von der Primärerkrankung, dem Alter und dem ApoE-Status waren [172, 173].

Die Bestimmung der Oligomerkonzentration eines einzelnen Proteins, z.B. αSyn, kann daher zwar auf eine entsprechende Pathologie hindeuten, allerdings wird eine zuverlässige differenzialdiagnostische Abgrenzung zwischen neurodegenerativen Erkrankungen aufgrund der Möglichkeit einer Co-Pathologie erschwert (Abbildung 15A). Eine zusätzliche Bestimmung weiterer Protein-Oligomere, z.B. Tau, resultierte in der vorliegenden Studie in einer deutlicheren Abgrenzung der Krankheitsbilder, da insbesondere PSP-Patienten erhöhte Tau-Oligomere in CSF zeigten (Abbildung 15B in Anlehnung an Kapitel 3.1). Die absoluten Oligomerkonzentrationen geben hierbei möglicherweise Rückschlüsse auf die primäre Erkrankung, z.B. waren die Tau-Oligomerkonzentrationen in der primären Tauopathie PSP am höchsten, während DLB-Patienten zwar ebenfalls signifikant erhöhte Tau-Oligomerkonzentrationen zeigten, diese waren allerdings geringer als bei PSP. Zieht man weitere Biomarker wie Aβ-Oligomere in CSF hinzu, könnte eine deutlichere Differenzierung der neurodegenerativen Erkrankungen erreicht werden (Abbildung 15C). Die Berücksichtigung zusätzlicher Dimensionen, z.B. von TDP-43-Oligomeren zur Abgrenzung der frontotemporalen Demenz, ergänzt das individuelle Erkrankungsprofil eines Patienten weiter. Um zwischen Co-Pathologien und der zugrunde liegenden

Erkrankung zu unterscheiden, bietet sich auch hier die Analyse unterschiedlicher Strukturen an, da diese sich in Abhängigkeit der Erkrankung unterscheiden können (s. Diversität der Oligomerstrukturen).

Die ganzheitliche Betrachtung der Pathologien ist dabei nicht nur entscheidend für eine korrekte Diagnosestellung, sondern auch für die Therapie der Patienten. Beginnt beispielsweise eine Therapie bei AD in Frühstadien, in denen noch keine Tau-Pathologie vorliegt, ist eine Adressierung der Aβ-Oligomere möglicherweise ausreichend, während bei gleichzeitig vorliegender Tau-Pathologie auch Tau medikamentös adressiert werden muss, um Downstream-Prozesse und eine weitere, durch Tau-ausgelöste Neurodegeneration zu verhindern [34, 96]. Außerdem ist eine Charakterisierung des Biomarkerprofils der Patienten sowohl während der klinischen Studien als auch in der routinemäßigen Anwendung sinnvoll, um Therapien gegen alle neurotoxischen Proteinaggregate zu starten [172].

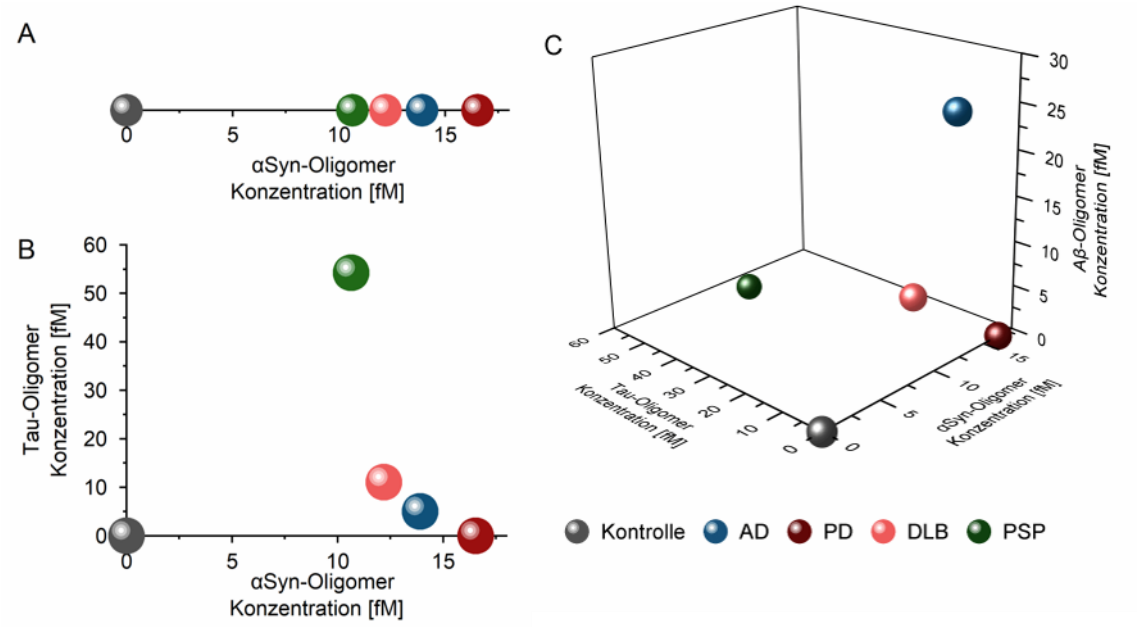

Abbildung 15 Modell zur Erhöhung der Unterscheidbarkeit der Erkrankungen bei Bestimmung mehrerer Biomarker
Bei der Untersuchung eines einzelnen Biomarkers (z.B. αSyn-Oligomere) muss eine klare Abtrennung der verschiedenen diagnostischen Gruppen vorliegen, um eine richtige Diagnose zu ermöglichen (A). Durch das Hinzuziehen eines zweiten (B, Tau-Oligomere) oder dritten Biomarkers (C, Aβ-Oligomere) kann ein erkrankungsspezifisches Biomarker-Profil mit erhöhter Abgrenzung der diagnostischen Gruppen erstellt werden. Abbildung in Anlehnung an Kapitel 3.1.

5 Fazit und Ausblick

Die vorliegende Arbeit konnte zeigen, dass sowohl αSyn- als auch Aβ- und Tau-Oligomere in verschiedenen Matrices mittels sFIDA quantifiziert werden können.

Aus technologischer Sicht ist die Etablierung eines Referenzstandards wichtig, um verschiedene Assays und Technologien miteinander zu vergleichen und eine verlässliche Quantifizierung zu ermöglichen. Für diesen Vergleich sind insbesondere Standardprotokolle zur Probengewinnung entscheidend, damit präanalytische Einflussfaktoren auf die Ergebnisse verschiedener Studien ausgeschlossen werden können. Außerdem konnte in vorherigen sFIDA-Studien gezeigt werden, dass durch Automatisierung der Präparation des Assays die Standardabweichung reduziert und die Sensitivität erhöht werden kann [134].

Die größte Limitierung der Quantifizierung von Oligomeren zur Diagnose der neurodegenerativen Erkrankungen liegt in der Überlappung der diagnostischen Gruppen. Die Trennschärfe könnte zukünftig durch zeitgleiche Messung verschiedener Proteinoligomere im klassischen sFIDA-Prinzip mit Epitop-überlappenden Antikörpern oder durch Hinzufügen strukturspezifischer Antikörper erhöht werden. Hierfür ist es erforderlich, dieselben Proben mit verschiedenen Antikörperkombinationen zu messen, um darüber Rückschlüsse auf die beste Antikörperkombination für eine spezielle Fragestellung zu ziehen. Außerdem kann eine vertiefende Analyse der Bilddaten in Hinblick auf die apparente Partikelgröße und Intensität Aufschlüsse über unterschiedliche Oligomerstrukturen geben, da größere Partikel möglicherweise mehr Detektionssonden binden können, dadurch heller leuchten und einen größeren Lichthof erzeugen.

Für die Entwicklung von Oligomer-Assays ist ein tieferes Verständnis der strukturellen Eigenschaften von Oligomeren essenziell, um neue struktur-spezifische Antikörper zu entwickeln und dadurch die Spezifität für eine bestimmte Erkrankung zu erhöhen. In Anbetracht der Beobachtung, dass die Oligomerkonzentrationen insbesondere in Frühstadien wie der iRBD oder MCI, allerdings nicht in fortgeschrittenen Stadien erhöht sind, werden vor allem longitudinale Studien dabei helfen, das Verständnis über Änderungen in den Oligomerkonzentrationen zu erhöhen. Außerdem sollten, ähnlich wie im Manuskript in Kapitel 3.4, verschiedene Körperflüssigkeiten derselben Patienten untersucht werden, um dadurch das Verständnis für die Ursprünge und Verteilung der Oligomere in peripheren Körperflüssigkeiten wie Blut oder Stuhl zu erhöhen.

Obwohl die Überlappung zwischen den diagnostischen Gruppen zum jetzigen Zeitpunkt keine individuelle Diagnosestellung ermöglicht, ist die Bestimmung der Oligomerkonzentrationen für die Behandlung von neurodegenerativen Erkrankungen ein wichtiger Aspekt. Im Rahmen der Entwicklung neuer Medikamente kann die Bestimmung

der Oligomer-Konzentration im CSF zur Rekrutierung geeigneter Patienten (diskutiert im Manuskript in Kapitel 3.1) und zum Monitoring der Wirkung eines Medikaments herangezogen werden (s. Manuskript in Kapitel 3.3). Außerdem kann die longitudinale Bestimmung der Oligomerkonzentrationen im Verlauf der Behandlung eine individuelle Dosistitration ermöglichen. Durch nicht-invasive Verfahren wie der Bestimmung von αSyn- und Aβ-Oligomeren (Kapitel 3.5 und 3.6) in Stuhl könnte zukünftig ein breit aufgestelltes Pre-Screening erfolgen, da eine Stuhlanalyse im Gegensatz zur CSF-Analyse keine Risiken für den Patienten birgt und routinemäßig auch in Hausarztpraxen durchgeführt werden kann.

Eine Abhängigkeit der Oligomerkonzentrationen von der Erkrankung bzw. vom Erkrankungsfortschritt in allen sFIDA-Studien unterstreicht trotz der Überlappungen der individuellen Gruppen das Potential der Quantifizierung dieser Oligomere. Anhand der Vielzahl an Anwendungen sowohl in Bezug auf den Analyten als auch auf die Matrix, gekoppelt mit der hohen Sensitivität der Verfahren aufgrund der Einzelpartikelanalyse, stellt der sFIDA eine flexible Technologie dar, die zukünftig sowohl für diagnostische Studien als auch zur Unterstützung von klinischen Studien angewendet werden kann.

6 Literaturverzeichnis

1. Peplow, P.V., B. Martinez, and T.A. Gennarelli, *Prevalence, NeedsNeeds, StrategiesStrategies, and Risk FactorsRisk factorsfor Neurodegenerative DiseasesNeurodegenerative diseases*, in *Neurodegenerative Diseases Biomarkers: Towards Translating Research to Clinical Practice*, P.V. Peplow, B. Martinez, and T.A. Gennarelli, Editors. 2022, Springer US: New York, NY. p. 3-8.
2. Forman, M.S., J.Q. Trojanowski, and V.M.Y. Lee, *Neurodegenerative diseases: a decade of discoveries paves the way for therapeutic breakthroughs.* Nature Medicine, 2004. **10**(10): p. 1055-1063.
3. Soto, C. and S. Pritzkow, *Protein misfolding, aggregation, and conformational strains in neurodegenerative diseases.* Nat Neurosci, 2018. **21**(10): p. 1332-1340.
4. Dugger, B.N. and D.W. Dickson, *Pathology of Neurodegenerative Diseases.* Cold Spring Harb Perspect Biol, 2017. **9**(7).
5. Reith, W., *Neurodegenerative Erkrankungen.* Der Radiologe, 2018. **58**(3): p. 241-258.
6. Deutsche Alzheimer-Gesellschaft e.V. *Die Häufigkeit von Demenzerkrankungen*. 2022 29.09.22 8:36]; Available from: https://www.deutsche-alzheimer.de/fileadmin/Alz/pdf/factsheets/infoblatt1_haeufigkeit_demenzerkrankungen_dalzg.pdf.
7. Radtke, R. *Statistiken zum Thema Demenz weltweit*. 2022; Available from: https://de.statista.com/themen/2032/demenzerkrankungen-weltweit/#topicHeader__wrapper.
8. Alzheimer's Association, *2022 Alzheimer's disease facts and figures.* Alzheimers Dement, 2022. **18**(4): p. 700-789.
9. Hippius, H. and G. Neundörfer, *The discovery of Alzheimer's disease.* Dialogues Clin Neurosci, 2003. **5**(1): p. 101-8.
10. Albert, M.S., et al., *The diagnosis of mild cognitive impairment due to Alzheimer's disease: recommendations from the National Institute on Aging-Alzheimer's Association workgroups on diagnostic guidelines for Alzheimer's disease.* Alzheimers Dement, 2011. **7**(3): p. 270-9.
11. DGN, D.G.f.N.e.V. and D.G.f.P.u.P.P.u.N.e.V. DGPPN, *S3-Leitlinie Demenzen*. 2016, https://register.awmf.org/de/leitlinien/detail/038-013: AWMF.
12. Jack, C.R., Jr., et al., *NIA-AA Research Framework: Toward a biological definition of Alzheimer's disease.* Alzheimers Dement, 2018. **14**(4): p. 535-562.
13. d'Abramo, C., L. D'Adamio, and L. Giliberto, *Significance of Blood and Cerebrospinal Fluid Biomarkers for Alzheimer's Disease: Sensitivity, Specificity and Potential for Clinical Use.* J Pers Med, 2020. **10**(3).

14. Trejo-Lopez, J.A., A.T. Yachnis, and S. Prokop, *Neuropathology of Alzheimer's Disease.* Neurotherapeutics, 2022. **19**(1): p. 173-185.
15. Braak, H. and E. Braak, *Neuropathological stageing of Alzheimer-related changes.* Acta Neuropathol, 1991. **82**(4): p. 239-59.
16. Hampel, H., et al., *The Amyloid-β Pathway in Alzheimer's Disease.* Molecular Psychiatry, 2021. **26**(10): p. 5481-5503.
17. Mroczko, B., et al., *Amyloid beta oligomers (AbetaOs) in Alzheimer's disease.* J Neural Transm (Vienna), 2018. **125**(2): p. 177-191.
18. Ullah, R., et al., *Abnormal amyloid beta metabolism in systemic abnormalities and Alzheimer's pathology: Insights and therapeutic approaches from periphery.* Ageing Res Rev, 2021. **71**: p. 101451.
19. Kanekiyo, T., H. Xu, and G. Bu, *ApoE and Aβ in Alzheimer's disease: accidental encounters or partners?* Neuron, 2014. **81**(4): p. 740-54.
20. McKhann, G.M., et al., *The diagnosis of dementia due to Alzheimer's disease: recommendations from the National Institute on Aging-Alzheimer's Association workgroups on diagnostic guidelines for Alzheimer's disease.* Alzheimers Dement, 2011. **7**(3): p. 263-9.
21. Chen, G.-f., et al., *Amyloid beta: structure, biology and structure-based therapeutic development.* Acta Pharmacologica Sinica, 2017. **38**(9): p. 1205-1235.
22. Olsson, B., et al., *CSF and blood biomarkers for the diagnosis of Alzheimer's disease: a systematic review and meta-analysis.* Lancet Neurol, 2016. **15**(7): p. 673-684.
23. Mattsson, N., *CSF biomarkers in neurodegenerative diseases.* Clin Chem Lab Med, 2011. **49**(3): p. 345-52.
24. Khoury, R. and E. Ghossoub, *Diagnostic biomarkers of Alzheimer's disease: A state-of-the-art review.* Biomarkers in Neuropsychiatry, 2019. **1**: p. 100005.
25. Chávez-Fumagalli, M.A., et al., *Diagnosis of Alzheimer's Disease in Developed and Developing Countries: Systematic Review and Meta-Analysis of Diagnostic Test Accuracy.* Journal of Alzheimer's Disease Reports, 2021. **5**: p. 15-30.
26. Marcus, C., E. Mena, and R.M. Subramaniam, *Brain PET in the diagnosis of Alzheimer's disease.* Clin Nucl Med, 2014. **39**(10): p. e413-22; quiz e423-6.
27. Andreasson, U., K. Blennow, and H. Zetterberg, *Method and Clinical Validation of Biomarkers for Neurodegenerative Diseases*, in *Cerebrospinal Fluid Biomarkers*, C.E. Teunissen and H. Zetterberg, Editors. 2021, Springer US: New York, NY. p. 163-173.
28. Bloudek, L.M., et al., *Review and Meta-Analysis of Biomarkers and Diagnostic Imaging in Alzheimer's Disease.* Journal of Alzheimer's Disease, 2011. **26**: p. 627-645.

29. Lewczuk, P., et al., *Amyloid-β 42/40 Cerebrospinal Fluid Concentration Ratio in the Diagnostics of Alzheimer's Disease: Validation of Two Novel Assays.* Journal of Alzheimer's Disease, 2015. **43**: p. 183-191.
30. Hansson, O., et al., *Advantages and disadvantages of the use of the CSF Amyloid β (Aβ) 42/40 ratio in the diagnosis of Alzheimer's Disease.* Alzheimer's Research & Therapy, 2019. **11**(1): p. 34.
31. Mo, J.A., et al., *Cerebrospinal fluid beta-amyloid1-42 levels in the differential diagnosis of Alzheimer's disease--systematic review and meta-analysis.* PLoS One, 2015. **10**(2): p. e0116802.
32. Morris, E., et al., *Diagnostic accuracy of 18F amyloid PET tracers for the diagnosis of Alzheimer's disease: a systematic review and meta-analysis.* European Journal of Nuclear Medicine and Molecular Imaging, 2016. **43**(2): p. 374-385.
33. Jessen, F., et al., *The characterisation of subjective cognitive decline.* Lancet Neurol, 2020. **19**(3): p. 271-278.
34. Tolar, M., S. Abushakra, and M. Sabbagh, *The path forward in Alzheimer's disease therapeutics: Reevaluating the amyloid cascade hypothesis.* Alzheimers Dement, 2020. **16**(11): p. 1553-1560.
35. Tampi, R.R., B.P. Forester, and M. Agronin, *Aducanumab: evidence from clinical trial data and controversies.* Drugs Context, 2021. **10**.
36. Food and Drug Administration, *BLA accelerated approvel of Leqembi*. 2023, Biologic License Application (BLA): 761269; EISAI INC: https://www.accessdata.fda.gov/scripts/cder/daf/index.cfm?event=overview.process&ApplNo=761269.
37. Sims, J.R., et al., *Donanemab in Early Symptomatic Alzheimer Disease: The TRAILBLAZER-ALZ 2 Randomized Clinical Trial.* JAMA, 2023. **330**(6): p. 512-527.
38. van Dyck, C.H., et al., *Lecanemab in Early Alzheimer's Disease.* New England Journal of Medicine, 2022.
39. van Groen, T., et al., *The Aβ oligomer eliminating D-enantiomeric peptide RD2 improves cognition without changing plaque pathology.* Scientific Reports, 2017. **7**(1): p. 16275.
40. Kutzsche, J., et al., *Safety and pharmacokinetics of the orally available antiprionic compound PRI-002: A single and multiple ascending dose phase I study.* Alzheimers Dement (N Y), 2020. **6**(1): p. e12001.
41. Cummings, J., et al., *Alzheimer's disease drug development pipeline: 2022.* Alzheimers Dement (N Y), 2022. **8**(1): p. e12295.
42. Du, X.Y., X.X. Xie, and R.T. Liu, *The Role of α-Synuclein Oligomers in Parkinson's Disease.* Int J Mol Sci, 2020. **21**(22).

43. Emin, D., et al., *Small soluble α-synuclein aggregates are the toxic species in Parkinson's disease.* Nat Commun, 2022. **13**(1): p. 5512.
44. Poewe, W., et al., *Parkinson disease.* Nat Rev Dis Primers, 2017. **3**: p. 17013.
45. James Parkinson, Member of the Royal College of Surgeons, *An Essay on the Shaking Palsy.* The Journal of Neuropsychiatry and Clinical Neurosciences, 2002. **14**(2): p. 223-236.
46. Borghammer, P. and N. Van Den Berge, *Brain-First versus Gut-First Parkinson's Disease: A Hypothesis.* J Parkinsons Dis, 2019. **9**(s2): p. S281-s295.
47. Outeiro, T.F., et al., *Dementia with Lewy bodies: an update and outlook.* Mol Neurodegener, 2019. **14**(1): p. 5.
48. Irwin, D.J., V.M. Lee, and J.Q. Trojanowski, *Parkinson's disease dementia: convergence of alpha-synuclein, tau and amyloid-beta pathologies.* Nat Rev Neurosci, 2013. **14**(9): p. 626-36.
49. Höglinger, G.U., et al., *Differentiation of atypical Parkinson syndromes.* J Neural Transm (Vienna), 2017. **124**(8): p. 997-1004.
50. DGN, Deutsche Gesellschaft für Neurologie e.V., *S3-Leitlinie Parkinson-Syndrom, idiopathisch*. Vol. 7.0 (in Überarbeitung). 2016, https://register.awmf.org/de/leitlinien/detail/030-010: AWMF. 312.
51. Rizzo, G., et al., *Accuracy of clinical diagnosis of Parkinson disease.* A systematic review and meta-analysis, 2016. **86**(6): p. 566-576.
52. Braak, H., et al., *Staging of brain pathology related to sporadic Parkinson's disease.* Neurobiology of Aging, 2003. **24**(2): p. 197-211.
53. *30.1 Einleitung*, in *Parkinson-Syndrome und andere Bewegungsstörungen*. 2012, Georg Thieme Verlag KG: Stuttgart.
54. McFarthing, K., et al., *Parkinson's Disease Drug Therapies in the Clinical Trial Pipeline: 2022 Update.* J Parkinsons Dis, 2022. **12**(4): p. 1073-1082.
55. Levin, J., et al., *The Differential Diagnosis and Treatment of Atypical Parkinsonism.* Dtsch Arztebl Int, 2016. **113**(5): p. 61-9.
56. Höglinger, G.U., et al., *Clinical diagnosis of progressive supranuclear palsy: The movement disorder society criteria.* Mov Disord, 2017. **32**(6): p. 853-864.
57. Litvan, I., et al., *Clinical research criteria for the diagnosis of progressive supranuclear palsy (Steele-Richardson-Olszewski syndrome): report of the NINDS-SPSP international workshop.* Neurology, 1996. **47**(1): p. 1-9.
58. Ali, F., et al., *Sensitivity and Specificity of Diagnostic Criteria for Progressive Supranuclear Palsy.* Mov Disord, 2019. **34**(8): p. 1144-1153.

59. Wagshal, D., et al., *Divergent CSF tau alterations in two common tauopathies: Alzheimer's disease and progressive supranuclear palsy.* J Neurol Neurosurg Psychiatry, 2015. **86**(3): p. 244-50.
60. Magdalinou, N.K., et al., *A panel of nine cerebrospinal fluid biomarkers may identify patients with atypical parkinsonian syndromes.* Journal of Neurology, Neurosurgery & Psychiatry, 2015. **86**(11): p. 1240-1247.
61. Ross, C.A. and M.A. Poirier, *Protein aggregation and neurodegenerative disease.* Nat Med, 2004. **10 Suppl**: p. S10-7.
62. Iadanza, M.G., et al., *A new era for understanding amyloid structures and disease.* Nature Reviews Molecular Cell Biology, 2018. **19**(12): p. 755-773.
63. Willbold, D., et al., *Amyloid-type Protein Aggregation and Prion-like Properties of Amyloids.* Chem Rev, 2021. **121**(13): p. 8285-8307.
64. Meinhardt, J. and M. Fändrich, *Struktur von Amyloidfibrillen.* Der Pathologe, 2009. **30**(3): p. 175-181.
65. Adamcik, J. and R. Mezzenga, *Amyloid Polymorphism in the Protein Folding and Aggregation Energy Landscape.* Angewandte Chemie International Edition, 2018. **57**(28): p. 8370-8382.
66. Prusiner, S.B., *Novel proteinaceous infectious particles cause scrapie.* Science, 1982. **216**(4542): p. 136-44.
67. Cline, E.N., et al., *The Amyloid-β Oligomer Hypothesis: Beginning of the Third Decade.* J Alzheimers Dis, 2018. **64**(s1): p. S567-s610.
68. Schaffert, L.-N. and W.G. Carter, *Do post-translational modifications influence protein aggregation in neurodegenerative diseases: a systematic review.* Brain sciences, 2020. **10**(4): p. 232.
69. Kuo, Y.M., et al., *Amyloid-beta peptides interact with plasma proteins and erythrocytes: implications for their quantitation in plasma.* Biochem Biophys Res Commun, 2000. **268**(3): p. 750-6.
70. Sengupta, U., A.N. Nilson, and R. Kayed, *The Role of Amyloid-β Oligomers in Toxicity, Propagation, and Immunotherapy.* EBioMedicine, 2016. **6**: p. 42-49.
71. Xin, S.H., et al., *Clearance of Amyloid Beta and Tau in Alzheimer's Disease: from Mechanisms to Therapy.* Neurotox Res, 2018. **34**(3): p. 733-748.
72. Jessen, N.A., et al., *The Glymphatic System: A Beginner's Guide.* Neurochem Res, 2015. **40**(12): p. 2583-99.
73. Walker, L.C., J. Schelle, and M. Jucker, *The Prion-Like Properties of Amyloid-β Assemblies: Implications for Alzheimer's Disease.* Cold Spring Harb Perspect Med, 2016. **6**(7).

74. Hladky, S.B. and M.A. Barrand, *Mechanisms of fluid movement into, through and out of the brain: evaluation of the evidence.* Fluids Barriers CNS, 2014. **11**(1): p. 26.
75. Wakamatsu, K., et al., *Metabolites and Biomarker Compounds of Neurodegenerative Diseases in Cerebrospinal Fluid.* Metabolites, 2022. **12**(4).
76. Natale, G., et al., *Glymphatic System as a Gateway to Connect Neurodegeneration From Periphery to CNS.* Front Neurosci, 2021. **15**: p. 639140.
77. Wang, J., et al., *A systemic view of Alzheimer disease - insights from amyloid-β metabolism beyond the brain.* Nat Rev Neurol, 2017. **13**(10): p. 612-623.
78. Josephs, K.A., *Current Understanding of Neurodegenerative Diseases Associated With the Protein Tau.* Mayo Clin Proc, 2017. **92**(8): p. 1291-1303.
79. Avila, J., et al., *Tau Structures.* Front Aging Neurosci, 2016. **8**: p. 262.
80. Wang, Y. and E. Mandelkow, *Tau in physiology and pathology.* Nat Rev Neurosci, 2016. **17**(1): p. 5-21.
81. Vogels, T., et al., *Propagation of Tau Pathology: Integrating Insights From Postmortem and In Vivo Studies.* Biol Psychiatry, 2020. **87**(9): p. 808-818.
82. Goedert, M., D.S. Eisenberg, and R.A. Crowther, *Propagation of Tau Aggregates and Neurodegeneration.* Annu Rev Neurosci, 2017. **40**: p. 189-210.
83. Gerson, J.E. and R. Kayed, *Formation and propagation of tau oligomeric seeds.* Front Neurol, 2013. **4**: p. 93.
84. Goedert, M. and M.G. Spillantini, *Propagation of Tau aggregates.* Mol Brain, 2017. **10**(1): p. 18.
85. Emamzadeh, F.N., *Alpha-synuclein structure, functions, and interactions.* J Res Med Sci, 2016. **21**: p. 29.
86. Uversky, V.N., *Neuropathology, biochemistry, and biophysics of alpha-synuclein aggregation.* J Neurochem, 2007. **103**(1): p. 17-37.
87. Marques, O. and T.F. Outeiro, *Alpha-synuclein: from secretion to dysfunction and death.* Cell Death Dis, 2012. **3**(7): p. e350.
88. Ma, L.-Y., et al., *Alpha-Synuclein in Peripheral Tissues in Parkinson's Disease.* ACS Chemical Neuroscience, 2019. **10**(2): p. 812-823.
89. Bengoa-Vergniory, N., et al., *Alpha-synuclein oligomers: a new hope.* Acta Neuropathol, 2017. **134**(6): p. 819-838.
90. Rocha Cabrero, F. and E.H. Morrison, *Lewy Bodies*, in *StatPearls*. 2022, StatPearls Publishing

Copyright © 2022, StatPearls Publishing LLC.: Treasure Island (FL).

91. Galpern, W.R. and A.E. Lang, *Interface between tauopathies and synucleinopathies: a tale of two proteins.* Ann Neurol, 2006. **59**(3): p. 449-58.

92. Hijaz, B.A. and L.A. Volpicelli-Daley, *Initiation and propagation of α-synuclein aggregation in the nervous system.* Mol Neurodegener, 2020. **15**(1): p. 19.
93. Stefanis, L., et al., *How is alpha-synuclein cleared from the cell?* J Neurochem, 2019. **150**(5): p. 577-590.
94. Oueslati, A., *Implication of Alpha-Synuclein Phosphorylation at S129 in Synucleinopathies: What Have We Learned in the Last Decade?* J Parkinsons Dis, 2016. **6**(1): p. 39-51.
95. Bates, C.A. and W. Zheng, *Brain disposition of α-Synuclein: roles of brain barrier systems and implications for Parkinson's disease.* Fluids and Barriers of the CNS, 2014. **11**(1): p. 17.
96. Hansson, O., et al., *The Alzheimer's Association appropriate use recommendations for blood biomarkers in Alzheimer's disease.* Alzheimers Dement, 2022.
97. Kulenkampff, K., et al., *Quantifying misfolded protein oligomers as drug targets and biomarkers in Alzheimer and Parkinson diseases.* Nature Reviews Chemistry, 2021. **5**(4): p. 277-294.
98. Holtta, M., et al., *Evaluating amyloid-beta oligomers in cerebrospinal fluid as a biomarker for Alzheimer's disease.* PLoS One, 2013. **8**(6): p. e66381.
99. Savage, M.J., et al., *A sensitive abeta oligomer assay discriminates Alzheimer's and aged control cerebrospinal fluid.* J Neurosci, 2014. **34**(8): p. 2884-97.
100. Wang, M.J., et al., *Oligomeric forms of amyloid-β protein in plasma as a potential blood-based biomarker for Alzheimer's disease.* Alzheimers Res Ther, 2017. **9**(1): p. 98.
101. Zhou, L., et al., *Plasma amyloid-β oligomers level is a biomarker for Alzheimer's disease diagnosis.* Biochem Biophys Res Commun, 2012. **423**(4): p. 697-702.
102. Tokuda, T., et al., *Detection of elevated levels of alpha-synuclein oligomers in CSF from patients with Parkinson disease.* Neurology, 2010. **75**(20): p. 1766-72.
103. Majbour, N.K., et al., *Oligomeric and phosphorylated alpha-synuclein as potential CSF biomarkers for Parkinson's disease.* Mol Neurodegener, 2016. **11**: p. 7.
104. Birkmann, E., et al., *A highly sensitive diagnostic assay for aggregate-related diseases, including prion diseases and Alzheimer's disease.* Rejuvenation Res, 2008. **11**(2): p. 359-63.
105. Birkmann, E., et al., *Counting of single prion particles bound to a capture-antibody surface (surface-FIDA).* Vet Microbiol, 2007. **123**(4): p. 294-304.
106. Birkmann, E., et al., *Detection of prion particles in samples of BSE and scrapie by fluorescence correlation spectroscopy without proteinase K digestion.* Biol Chem, 2006. **387**(1): p. 95-102.

107. Funke, S.A., et al., *Single-particle detection system for Abeta aggregates: adaptation of surface-fluorescence intensity distribution analysis to laser scanning microscopy.* Rejuvenation Res, 2010. **13**(2-3): p. 206-9.
108. Bannach, O., et al., *Detection of prion protein particles in blood plasma of scrapie infected sheep.* PLoS One, 2012. **7**(5): p. e36620.
109. Funke, S.A., et al., *Single particle detection of Aβ aggregates associated with Alzheimer's disease.* Biochemical and Biophysical Research Communications, 2007. **364**(4): p. 902-907.
110. Funke, S.A., et al., *An ultrasensitive assay for diagnosis of Alzheimer's disease.* Rejuvenation Res, 2008. **11**(2): p. 315-8.
111. Wang-Dietrich, L., et al., *The amyloid-beta oligomer count in cerebrospinal fluid is a biomarker for Alzheimer's disease.* J Alzheimers Dis, 2013. **34**(4): p. 985-94.
112. Herrmann, Y., et al., *Nanoparticle standards for immuno-based quantitation of alpha-synuclein oligomers in diagnostics of Parkinson's disease and other synucleinopathies.* Clin Chim Acta, 2017. **466**: p. 152-159.
113. Hülsemann, M., et al., *Biofunctionalized Silica Nanoparticles: Standards in Amyloid-beta Oligomer-Based Diagnosis of Alzheimer's Disease.* J Alzheimers Dis, 2016. **54**(1): p. 79-88.
114. Kravchenko, K., et al., *Analysis of anticoagulants for blood-based quantitation of amyloid beta oligomers in the sFIDA assay.* Biol Chem, 2017. **398**(4): p. 465-475.
115. Kühbach, K., et al., *Application of an Amyloid Beta Oligomer Standard in the sFIDA Assay.* Front Neurosci, 2016. **10**: p. 8.
116. He, J., *Practical Guide to ELISA Development.* The Immunoassay Handbook, 2013: p. 381-393.
117. Raem, A. and P. Rauch, *Immunoassay*, ed. P.R. Arnold Raem. Vol. 1. 2007: Spektrum Akademischer Verlag, Heidelberg. 370.
118. Bannach, O., K. Kühbach, and D. Willbold, *Ein neues Verfahren zur Früh diagnose der Alzheimerschen Demenz.* BIOspektrum, 2015. **21**(7): p. 728-730.
119. Klebe, G., *Protein-Ligand-Wechselwirkungen als Grundlage der Arzneistoffwirkung*, in *Wirkstoffdesign: Entwurf und Wirkung von Arzneistoffen*. 2009, Spektrum Akademischer Verlag: Heidelberg. p. 49-67.
120. Kulawik, A., et al., *Advancements of the sFIDA method for oligomer-based diagnostics of neurodegenerative diseases.* FEBS Lett, 2018. **592**(4): p. 516-534.
121. Stine, W.B., et al., *Preparing synthetic Aβ in different aggregation states.* Methods Mol Biol, 2011. **670**: p. 13-32.
122. Poulter, N.S., et al., *The physical basis of total internal reflection fluorescence (TIRF) microscopy and its cellular applications.* Methods Mol Biol, 2015. **1251**: p. 1-23.

123. Mahlke, C., *Mikroskopie*, in *Der Experimentator: Neurowissenschaften*. 2011, Spektrum Akademischer Verlag: Heidelberg. p. 145-156.
124. Aescht, E., et al., *Mikroskopische Verfahren*, in *Romeis Mikroskopische Technik*, M. Mulisch and U. Welsch, Editors. 2010, Spektrum Akademischer Verlag: Heidelberg. p. 1-38.
125. Mutschler, E., H.G. Schaible, and P. Vaupel, *Anatomie, Physiologie und Pathophysiologie des Menschen*. Vol. 6. 2007: Wissenschaftliche Verlagsgesellschaft mbH Stuttgart. 981.
126. Tumani, H., et al., *S1-Leitlinie: Lumbalpunktion und Liquordiagnostik.* DGNeurologie, 2019. **2**(6): p. 456-480.
127. Teunissen, C.E., et al., *A consensus protocol for the standardization of cerebrospinal fluid collection and biobanking.* Neurology, 2009. **73**(22): p. 1914-22.
128. *Blut*, in *Biochemie für Mediziner: Ein Lern- und Arbeitsbuch mit klinischem Bezug*. 2005, Springer Berlin Heidelberg: Berlin, Heidelberg. p. 721-752.
129. Tuck, M.K., et al., *Standard operating procedures for serum and plasma collection: early detection research network consensus statement standard operating procedure integration working group.* J Proteome Res, 2009. **8**(1): p. 113-7.
130. Greco, V., et al., *Direct Assessment of Plasma/Serum Sample Quality for Proteomics Biomarker Investigation*, in *Serum/Plasma Proteomics: Methods and Protocols*, D.W. Greening and R.J. Simpson, Editors. 2017, Springer New York: New York, NY. p. 3-21.
131. Cruz, A., et al., *Faecal Diagnostic Biomarkers for Colorectal Cancer.* Cancers, 2021. **13**(21): p. 5568.
132. Rose, C., et al., *The Characterization of Feces and Urine: A Review of the Literature to Inform Advanced Treatment Technology.* Crit Rev Environ Sci Technol, 2015. **45**(17): p. 1827-1879.
133. Vanderstichele, H., et al., *Potential sources of interference on Abeta immunoassays in biological samples.* Alzheimers Res Ther, 2012. **4**(5): p. 39.
134. Herrmann, Y., et al., *sFIDA automation yields sub-femtomolar limit of detection for Abeta aggregates in body fluids.* Clin Biochem, 2017. **50**(4-5): p. 244-247.
135. Andreasson, U., et al., *A Practical Guide to Immunoassay Method Validation.* Front Neurol, 2015. **6**: p. 179.
136. Food and Drug Administration, *Bioanalytical Method Validation Guidance for Industry*, in *FDA-2013-D-1020*. 2018: https://www.fda.gov/regulatory-information/search-fda-guidance-documents/bioanalytical-method-validation-guidance-industry

137. EMA, CHMP, and ICH, *ICH guideline M10 on bioanalytical method validation and study sample analysis - Step 5*, in *EMA/CHMP/ICH/172948/2019*. 2019: https://www.ema.europa.eu/en/ich-m10-bioanalytical-method-validation-scientific-guideline#current-version-section.

138. Sheehan, C., J. He, and M. Smith, *Chapter 5.2 - Method Evaluation—A Practical Guide*, in *The Immunoassay Handbook (Fourth Edition)*, D. Wild, Editor. 2013, Elsevier: Oxford. p. 395-402.

139. Fukumoto, H., et al., *High-molecular-weight beta-amyloid oligomers are elevated in cerebrospinal fluid of Alzheimer patients.* FASEB J, 2010. **24**(8): p. 2716-26.

140. Novo, M., S. Freire, and W. Al-Soufi, *Critical aggregation concentration for the formation of early Amyloid-β (1–42) oligomers.* Scientific Reports, 2018. **8**(1): p. 1783.

141. Jongbloed, W., et al., *Amyloid-beta oligomers relate to cognitive decline in Alzheimer's disease.* J Alzheimers Dis, 2015. **45**(1): p. 35-43.

142. Liu, L., et al., *An ultra-sensitive immunoassay detects and quantifies soluble Aβ oligomers in human plasma.* Alzheimers Dement, 2022. **18**(6): p. 1186-1202.

143. Babapour Mofrad, R., et al., *Plasma amyloid-β oligomerization assay as a pre-screening test for amyloid status.* Alzheimers Res Ther, 2021. **13**(1): p. 133.

144. Shea, D., et al., *SOBA: Development and testing of a soluble oligomer binding assay for detection of amyloidogenic toxic oligomers.* Proc Natl Acad Sci U S A, 2022. **119**(50): p. e2213157119.

145. Hansson, O., et al., *Levels of cerebrospinal fluid alpha-synuclein oligomers are increased in Parkinson's disease with dementia and dementia with Lewy bodies compared to Alzheimer's disease.* Alzheimers Res Ther, 2014. **6**(3): p. 25.

146. Parnetti, L., et al., *Differential role of CSF alpha-synuclein species, tau, and Abeta42 in Parkinson's Disease.* Front Aging Neurosci, 2014. **6**: p. 53.

147. El-Agnaf, O.M.A., et al., *Detection of oligomeric forms of α-synuclein protein in human plasma as a potential biomarker for Parkinson's disease.* 2006. **20**(3): p. 419-425.

148. Sengupta, U., et al., *Tau oligomers in cerebrospinal fluid in Alzheimer's disease.* Ann Clin Transl Neurol, 2017. **4**(4): p. 226-235.

149. Boulo, S., et al., *First amyloid β1-42 certified reference material for re-calibrating commercial immunoassays.* Alzheimers Dement, 2020. **16**(11): p. 1493-1503.

150. Sehlin, D., et al., *Interference from heterophilic antibodies in amyloid-beta oligomer ELISAs.* J Alzheimers Dis, 2010. **21**(4): p. 1295-301.

151. Slats, D., et al., *Hourly variability of cerebrospinal fluid biomarkers in Alzheimer's disease subjects and healthy older volunteers.* Neurobiology of Aging, 2012. **33**(4): p. 831.e1-831.e9.

152. Abdi, I.Y., et al., *Preanalytical Stability of CSF Total and Oligomeric Alpha-Synuclein.* Front Aging Neurosci, 2021. **13**: p. 638718.
153. Rózga, M., et al., *Preanalytical sample handling recommendations for Alzheimer's disease plasma biomarkers.* Alzheimer's & Dementia: Diagnosis, Assessment & Disease Monitoring, 2019. **11**(1): p. 291-300.
154. Ashton, N.J., et al., *Effects of pre-analytical procedures on blood biomarkers for Alzheimer's pathophysiology, glial activation, and neurodegeneration.* Alzheimer's & Dementia: Diagnosis, Assessment & Disease Monitoring, 2021. **13**(1): p. e12168.
155. Verberk, I.M.W., et al., *Characterization of pre-analytical sample handling effects on a panel of Alzheimer's disease-related blood-based biomarkers: Results from the Standardization of Alzheimer's Blood Biomarkers (SABB) working group.* Alzheimers Dement, 2022. **18**(8): p. 1484-1497.
156. Hamer, H.M., et al., *Impact of Preanalytical Factors on Calprotectin Concentration in Stool: A Multiassay Comparison* The Journal of Applied Laboratory Medicine, 2022. **7**(6): p. 1401-1411.
157. Morris, L.S. and J.R. Marchesi, *Assessing the impact of long term frozen storage of faecal samples on protein concentration and protease activity.* J Microbiol Methods, 2016. **123**: p. 31-8.
158. Blennow, K. and H. Zetterberg, *The Past and the Future of Alzheimer's Disease Fluid Biomarkers.* Journal of Alzheimer's Disease, 2018. **62**: p. 1125-1140.
159. Gratuze, M., C.E.G. Leyns, and D.M. Holtzman, *New insights into the role of TREM2 in Alzheimer's disease.* Mol Neurodegener, 2018. **13**(1): p. 66.
160. Yamazaki, Y., et al., *Apolipoprotein E and Alzheimer disease: pathobiology and targeting strategies.* Nat Rev Neurol, 2019. **15**(9): p. 501-518.
161. Kowalski, K. and A. Mulak, *Brain-Gut-Microbiota Axis in Alzheimer's Disease.* J Neurogastroenterol Motil, 2019. **25**(1): p. 48-60.
162. Kass, B., et al., *Abeta oligomer concentration in mouse and human brain and its drug-induced reduction ex vivo.* Cell Rep Med, 2022. **3**(5): p. 100630.
163. van Steenoven, I., et al., *alpha-Synuclein species as potential cerebrospinal fluid biomarkers for dementia with lewy bodies.* Mov Disord, 2018. **33**(11): p. 1724-1733.
164. Wildburger, N.C., et al., *Diversity of Amyloid-beta Proteoforms in the Alzheimer's Disease Brain.* Sci Rep, 2017. **7**(1): p. 9520.
165. De, S., et al., *Soluble aggregates present in cerebrospinal fluid change in size and mechanism of toxicity during Alzheimer's disease progression.* Acta Neuropathol Commun, 2019. **7**(1): p. 120.
166. Mroczko, B., M. Groblewska, and A. Litman-Zawadzka, *The Role of Protein Misfolding and Tau Oligomers (TauOs) in Alzheimer's Disease (AD).* Int J Mol Sci, 2019. **20**(19).

167. Yang, T., et al., *A highly sensitive novel immunoassay specifically detects low levels of soluble Abeta oligomers in human cerebrospinal fluid.* Alzheimers Res Ther, 2015. **7**(1): p. 14.

168. Rizzo, G., et al., *Accuracy of clinical diagnosis of dementia with Lewy bodies: a systematic review and meta-analysis.* Journal of Neurology, Neurosurgery & Psychiatry, 2018. **89**(4): p. 358-366.

169. Irwin, D.J. and H.I. Hurtig, *The Contribution of Tau, Amyloid-Beta and Alpha-Synuclein Pathology to Dementia in Lewy Body Disorders.* J Alzheimers Dis Parkinsonism, 2018. **8**(4).

170. Wakabayashi, K., et al., *The Lewy body in Parkinson's disease and related neurodegenerative disorders.* Mol Neurobiol, 2013. **47**(2): p. 495-508.

171. Cong, C., et al., *Significant Overlap of α-Synuclein, Amyloid-β, and Phospho-Tau Pathologies in Neuropathological Diagnosis of Lewy-related Pathology: Evidence from China Human Brain Bank.* Journal of Alzheimer's Disease, 2021. **80**: p. 447-458.

172. Robinson, J.L., et al., *Neurodegenerative disease concomitant proteinopathies are prevalent, age-related and APOE4-associated.* Brain, 2018. **141**(7): p. 2181-2193.

173. Robinson, J.L., et al., *The development and convergence of co-pathologies in Alzheimer's disease.* Brain, 2021. **144**(3): p. 953-962.

7 Anhänge der Manuskripte

7.1 Quantitative Detection of α-Synuclein and Tau oligomers and other aggregates by Digital Single Particle Counting

Autoren:	Lara Blömeke, Marlene Pils, Victoria Kraemer-Schulien, Alexandra Dybala, Anja Schaffrath, Andreas Kulawik, Fabian Rehn, Anne Cousin, Volker Nischwitz, Johannes Willbold, Rebecca Zack, Thomas F. Tropea, Tuyen Bujnicki, Gültekin Tamgüney, Daniel Weintraub, David Irwin, Murray Grossman, David A. Wolk, John Q. Trojanowski, Oliver Bannach, Alice Chen-Plotkin, Dieter Willbold
Journal:	npj parkinson's disease (veröffentlicht)
DOI:	10.1038/s41531-022-00330-x
Impact-Faktor:	8,7 (2022)
Beitrag:	Eigenanteil: 70 % Entwicklung des Assays Messung und Auswertung der Proben Anfertigung der Abbildungen Statistische Auswertung Hauptverfasserin des Manuskripts

Quantitative Detection of α-Synuclein and Tau Oligomers and other Aggregates by Digital Single Particle Counting

Lara Blömeke, Marlene Pils, Victoria Kraemer-Schulien, Alexandra Dybala, Anja Schaffrath, Andreas Kulawik, Fabian Rehn, Anne Cousin, Volker Nischwitz, Johannes Willbold, Rebecca Zack, Thomas F. Tropea, Tuyen Bujnicki, Gültekin Tamgüney, Daniel Weintraub, David Irwin, Murray Grossman, David A. Wolk, John Q. Trojanowski, Oliver Bannach, Alice Chen-Plotkin, Dieter Willbold

Supplementary Information

Supplementary Table 1 CV% values of each experiment for SiNaPs and CSF samples

	aSyn		Tau	
Experiment	Calibration	Samples	Calibration	Samples
1	18.05	22.08	20.42	18.62
2	22.18	32.86	30.27	19.45
3	17.33	20.71	23.00	15.66
4	14.63	12.58	18.60	10.81
5	11.71	9.16	12.54	8.66
6	14.87	12.70	16.01	9.58
7	16.99	13.86	15.15	10.15
8	10.29	10.58	16.77	10.84
Mean	15.76	16.82	19.10	12.97

Supplementary Table 2 LOD values for aSyn- and Tau silica nanoparticles [fM] for each experiment

Experiment	aSyn	Tau
1	9.59	36.69
2	20.72	70.09
3	6.76	32.04
4	1.67	10.09
5	6.08	-
6	2.43	-
7	3.53	-
8	2.98	19.41
Mean	6.72	33.7

Supplementary Table 3 Number of samples above the LOD for each individual experiment

Experiment	aSyn	Tau
1	11	8
2	13	6
3	18	19
4	23	9
5	17	5
6	27	24
7	20	15
8	27	18
Sum	156	104

Supplementary Table 4 Demographic information, aSyn and Tau aggregate concentrations and blood contamination level of each individual patient CSF sample

Sample	*Diagnosis*	*Sex*	*Deceased*	*Education (years)*	*Age at Sample*	*aSyn aggregate concentration [fM]*	*StdDev aSyn*	*Tau aggregate concentration [fM]*	*StdDev Tau*	*Blood contamination level*
1	AD	Male	True	16	72.00	0.00	0.00	0.00	0.00	0
2	AD	Female	True	12	68.00	3.51	0.30	1.60	0.23	0
3	AD	Male	False	18	75.00	8.84	0.36	0.00	0.00	0
4	AD	Male	True	18	75.00	24.20	3.20	0.00	0.00	0
5	AD	Female	False	6	65.00	75.75	12.31	12.70	0.38	0
6	AD	Female	True	15	65.00	0.00	0.00	0.00	0.00	0
7	AD	Female	False	18	65.00	521.47	116.08	20.11	2.04	4
8	AD	Male	False	11	77.00	9.52	1.14	0.00	0.00	0
9	AD	Female	False	16	76.00	18.48	1.37	0.00	0.00	4
10	AD	Male	True	16	61.00	144.55	14.95	0.00	0.00	0
11	AD	Male	True	12	68.00	0.00	0.00	0.00	0.00	0
12	AD	Male	False	18	66.00	66.46	7.84	0.00	0.00	0
13	AD	Male	False	20	81.00	202.30	16.43	22.69	2.87	0
14	AD	Female	False	16	75.00	156.65	32.57	16.87	2.12	0
15	AD	Male	True	12	69.00	15.41	1.25	0.00	0.00	2
16	AD	Female	False	18	70.00	0.00	0.00	0.00	0.00	1
17	AD	Female	False	20	75.00	0.00	0.00	0.00	0.00	0
18	AD	Male	False	12	64.00	0.00	0.00	0.00	0.00	3
19	AD	Male	False	12	73.00	221.12	31.78	19.19	1.78	4
20	AD	Male	False	12	63.00	12.42	2.29	6.79	0.53	4
21	AD	Male	True	16	66.00	37.81	6.06	9.82	0.83	0
22	AD	Male	False	18	68.00	33.69	2.30	35.38	3.16	1
23	AD	Female	False	15	69.00	0.00	0.00	4.93	0.50	4
24	AD	Male	False	12	56.00	0.00	0.00	0.99	0.06	1
25	AD	Male	True	14	55.00	11.58	1.01	10.33	1.09	0
26	AD	Female	False	12	68.00	120.74	16.88	8.98	0.83	0
27	AD	Male	False	16	66.00	8.32	0.66	12.36	0.66	2
28	AD	Male	False	16	59.00	85.40	9.02	20.72	1.71	4

29	DLB	Male	True	12	73.00	12.20	1.76	11.07	1.02	0
30	DLB	Male	False	12	67.00	8.52	1.31	0.00	0.00	0
31	DLB	Female	False	18	68.00	2.57	0.36	0.00	0.00	3
32	DLB	Male	False	16	79.00	886.05	65.57	75.02	4.34	0
33	DLB	Female	False	20	58.00	0.00	0.00	12.05	0.74	0
34	DLB	Female	True	12	66.00	13.02	1.20	14.56	2.10	0
35	DLB	Female	False	14	87.00	2.38	0.22	0.00	0.00	2
36	DLB	Male	False	18	66.00	70.49	6.04	0.00	0.00	0
37	DLB	Male	True	20	66.00	3.75	0.15	0.00	0.00	0
38	DLB	Male	False	14	74.00	0.00	0.00	3.14	0.51	2
39	DLB	Male	True	19	65.00	7.88	0.84	12.38	0.96	0
40	DLB	Male	True	12	70.00	0.00	0.00	13.39	0.53	0
41	DLB	Male	False	12	72.00	370.27	51.32	27.96	3.86	0
42	DLB	Male	False	16	68.00	22.03	3.69	12.43	0.76	0
43	DLB	Male	True	18	63.00	78.99	3.33	8.12	0.60	2
44	DLB	Male	False	14	84.00	13.47	1.75	1.89	0.14	1
45	DLB	Male	False	16	68.00	2949.10	470.68	153.28	17.66	0
46	DLB	Male	False	16	63.00	136.01	24.98	10.69	1.15	2
47	DLB	Female	False	16	68.00	11.73	1.42	12.32	0.51	0
48	N	Female	False	18	70.00	0.00	0.00	0.00	0.00	3
49	N	Female	False	18	73.00	81.98	22.45	0.00	0.00	0
50	N	Male	False	16	57.00	0.00	0.00	0.00	0.00	0
51	N	Male	False	12	61.00	0.00	0.00	36.89	7.70	2
52	N	Male	False	18	74.00	0.00	0.00	0.00	0.00	0
53	N	Female	True	20	70.00	0.00	0.00	0.00	0.00	0
54	N	Male	True	19	83.00	0.00	0.00	0.00	0.00	4
55	N	Female	False	18	74.00	0.00	0.00	24.30	4.41	1
56	N	Male	False	18	75.00	0.00	0.00	0.00	0.00	3
57	N	Female	False	16	58.00	43.36	8.97	0.00	0.00	0
58	N	Male	False	16	67.00	119.16	46.24	37.25	5.88	1
59	N	Female	False	20	69.00	0.00	0.00	0.00	0.00	3
60	N	Male	False	20	60.00	72.13	8.67	7.79	0.62	0
61	N	Male	False	12	62.00	0.00	0.00	0.00	0.00	0
62	N	Male	False	20	77.00	0.00	0.00	0.00	0.00	0

63	N	Female	False	18	63.00	0.00	0.00	0.00	0.00	0
64	N	Female	False	12	59.00	602.80	231.60	110.63	16.15	3
65	N	Female	False	20	57.00	13.13	2.78	0.00	0.00	1
66	N	Male	True	12	93.00	0.00	0.00	0.00	0.00	4
67	N	Female	False	18	80.00	0.00	0.00	0.00	0.00	2
68	N	Male	False	20	70.00	5.00	0.27	0.00	0.00	0
69	N	Male	False	20	71.00	0.00	0.00	0.00	0.00	1
70	N	Female	False	20	71.00	17.92	1.72	30.74	1.94	2
71	N	Female	False	20	71.00	0.00	0.00	0.00	0.00	1
72	N	Female	True	14	89.00	0.00	0.00	0.00	0.00	0
73	N	Female	False	20	66.00	0.00	0.00	0.00	0.00	4
74	N	Female	False	16	64.00	0.00	0.00	0.00	0.00	0
75	N	Male	False	18	70.00	0.00	0.00	0.00	0.00	4
76	N	Male	True	20	90.00	112.50	45.08	0.00	0.00	4
77	N	Male	False	12	71.00	0.00	0.00	0.00	0.00	0
78	N	Male	False	4	56.00	0.00	0.00	0.00	0.00	0
79	N	Male	False	20	74.00	0.00	0.00	0.00	0.00	3
80	N	Male	False	9	66.00	0.00	0.00	0.00	0.00	0
81	N	Male	True	20	80.00	1536.16	572.99	142.57	33.72	4
82	N	Female	False	16	57.00	16.57	1.15	0.00	0.00	0
83	N	Male	False	18	70.00	0.00	0.00	0.00	0.00	4
84	N	Female	False	18	66.00	6.64	1.21	0.00	0.00	4
85	N	Male	False	18	69.00	29.53	5.15	0.00	0.00	3
86	N	Female	False	14	65.00	7.74	0.55	33.95	2.42	0
87	N	Female	False	18	64.00	5.78	0.41	25.09	2.54	3
88	N	Male	False	12	62.00	0.00	0.00	0.00	0.00	2
89	N	Female	False	14	66.00	2.25	0.23	0.00	0.00	4
90	N	Male	False	12	57.00	6.19	0.34	30.29	3.81	4
91	N	Male	False	16	74.00	3742.12	361.11	202.57	17.10	4
92	N	Male	False	18	63.00	6.47	0.46	0.00	0.00	4
93	PD	Female	False	16	63.00	0.00	0.00	34.76	12.08	0
94	PD	Male	True	16	76.00	49.27	9.72	0.00	0.00	0
95	PD	Male	True	12	75.00	10229.34	5666.03	1117.47	181.59	4

96	PD	Male	False	16	63.00	621.44	232.23	0.00	0.00	0
97	PD	Male	True	16	64.00	0.00	0.00	0.00	0.00	1
98	PD	Male	False	18	64.00	3.75	0.43	0.00	0.00	0
99	PD	Female	True	18	80.00	147.24	46.97	32.26	5.74	4
100	PD	Male	True	12	84.00	86.24	19.19	0.10	0.02	4
101	PD	Male	True	14	62.00	131.68	14.47	16.11	1.62	0
102	PD	Female	False	18	66.00	248.19	44.48	16.14	1.21	4
103	PD	Male	False	20	58.00	193.78	91.25	0.00	0.00	4
104	PD	Male	False	16	62.00	75.01	15.85	302.30	78.63	0
105	PD	Male	False	18	87.00	52.49	6.61	0.08	0.01	0
106	PD	Female	False	18	59.00	10.72	1.55	0.00	0.00	4
107	PD	Male	True	16	72.00	146.89	17.61	17.27	1.07	2
108	PD	Male	True	11	77.00	107.68	22.31	10.75	0.51	0
109	PD	Female	False	16	57.00	53.46	6.75	20.61	2.53	3
110	PD	Male	False	18	64.00	4.85	0.54	0.00	0.00	4
111	PD	Male	False	18	67.00	0.00	0.00	0.00	0.00	4
112	PD	Male	False	18	64.00	17.19	5.94	0.00	0.00	0
113	PD	Male	False	16	65.00	766.49	320.78	47.45	4.65	0
114	PD	Male	True	14	79.00	0.00	0.00	0.00	0.00	3
115	PD	Male	False	13	67.00	372.84	98.84	61.82	10.50	2
116	PD	Female	False	19	60.00	138.14	46.83	51.90	10.04	0
117	PD	Male	False	16	66.00	289.85	75.62	0.00	0.00	1
118	PD	Male	False	13	59.00	83.84	18.40	0.00	0.00	2
119	PD	Male	False	18	60.00	0.00	0.00	0.00	0.00	0
120	PD	Male	False	16	59.00	40.33	19.68	0.00	0.00	4
121	PD	Male	False	14	56.00	0.00	0.00	0.00	0.00	1
122	PD	Female	True	18	63.00	8.36	1.42	0.00	0.00	2
123	PD	Male	True	16	73.00	0.00	0.00	0.00	0.00	1
124	PD	Female	False	17	70.00	0.00	0.00	0.00	0.00	4
125	PD	Female	False	16	63.00	0.00	0.00	0.00	0.00	0
126	PD	Male	True	20	70.00	0.00	0.00	0.00	0.00	0
127	PD	Female	False	18	67.00	0.00	0.00	0.00	0.00	0
128	PD	Male	False	18	68.00	0.00	0.00	0.00	0.00	0
129	PD	Male	False	16	62.00	16.54	1.44	85.32	5.46	0

130	PD	Female	False	14	61.00	205.19	88.91	0.00	0.00	4
131	PD	Male	True	18	72.00	0.00	0.00	0.00	0.00	3
132	PD	Male	True	12	64.00	84.34	12.81	21.78	2.25	0
133	PD	Female	False	16	63.00	0.00	0.00	0.00	0.00	1
134	PD	Male	False	13	57.00	0.00	0.00	0.00	0.00	0
135	PD	Male	False	16	67.00	587.52	134.89	137.76	17.80	0
136	PD	Female	False	18	62.00	0.00	0.00	0.00	0.00	0
137	PD	Male	False	14	54.00	0.00	0.00	0.00	0.00	0
138	PD	Male	True	14	55.00	90.61	15.76	0.00	0.00	4
139	PD	Male	False	20	59.00	51.37	18.63	0.00	0.00	4
140	PD	Male	False	20	66.00	0.00	0.00	0.00	0.00	0
141	PD	Male	False	12	57.00	375.96	64.21	36.13	6.35	3
142	PD	Male	False	16	56.00	11.37	0.76	0.00	0.00	0
143	PD	Male	True	16	72.00	114.05	17.52	9.66	1.37	1
144	PD	Female	False	16	63.00	0.00	0.00	0.00	0.00	0
145	PD	Male	False	18	68.00	229.91	34.62	55.16	7.03	2
146	PD	Female	False	16	65.00	4.95	0.28	19.55	2.14	0
147	PD	Female	False	18	68.00	45.25	5.94	3.94	0.41	4
148	PD	Male	False	18	65.00	11.96	1.18	0.00	0.00	0
149	PD	Male	False	14	76.00	10.05	1.21	0.00	0.00	0
150	PD	Male	False	14	58.00	0.00	0.00	3.79	0.25	0
151	PD	Male	False	16	54.00	24.73	3.97	0.00	0.00	0
152	PD	Female	False	16	72.00	0.00	0.00	0.00	0.00	4
153	PD	Male	False	20	57.00	10.63	1.11	0.00	0.00	0
154	PD	Male	False	20	71.00	17.15	3.21	0.00	0.00	0
155	PD	Male	False	12	59.00	11.32	1.76	0.00	0.00	0
156	PD	Male	False	20	54.00	76.96	14.31	1.12	0.16	0
157	PD	Female	False	14	71.00	15.56	1.66	32.06	3.42	0
158	PD	Male	False	20	64.00	407.13	62.90	23.01	3.30	0
159	PD	Male	False	18	65.00	4.14	0.22	0.00	0.00	0
160	PD	Female	False	18	65.00	16.94	2.62	0.00	0.00	0
161	PD	Female	False	18	59.00	33.96	5.75	33.04	2.29	0
162	PD	Male	False	18	74.00	21.90	2.51	0.00	0.00	0
163	PD	Female	False	19	67.00	19.12	1.82	19.73	2.60	0

164	PD	Female	False	16	70.00	24.10	1.16	0.00	0.00	0
165	PD	Female	False	16	62.00	73.93	8.92	7.12	0.70	0
166	PD	Female	False	16	58.00	3.32	0.30	0.00	0.00	1
167	PD	Male	False	18	66.00	80.83	7.37	37.98	2.23	0
168	PD	Male	True	16	70.00	23.47	1.86	2.02	0.16	0
169	PD	Female	False	18	52.00	132.21	22.41	0.00	0.00	0
170	PD	Male	False	18	68.00	29.28	6.21	5.66	0.63	3
171	PD	Male	True	12	63.00	0.00	0.00	0.00	0.00	0
172	PD	Male	False	15	75.00	12.28	1.22	0.00	0.00	0
173	PD	Female	False	11	54.00	0.00	0.00	0.00	0.00	0
174	PD	Male	False	13	60.00	14.62	1.33	22.73	2.62	0
175	PD	Male	False	19	62.00	67.99	4.77	0.00	0.00	0
176	PD	Male	False	18	67.00	0.00	0.00	0.00	0.00	4
177	PD	Male	False	15	62.00	2.81	0.28	0.00	0.00	4
178	PD	Male	False	16	72.00	44.98	4.20	38.38	3.88	3
179	PD	Female	False	14	69.00	8.09	1.20	0.00	0.00	0
180	PD	Male	False	18	63.00	555.58	96.28	33.51	5.21	1
181	PD	Female	False	16	54.00	99.96	22.01	0.00	0.00	0
182	PD	Male	False	18	79.00	13.82	0.93	20.54	4.27	1
183	PD	Female	False	18	77.00	0.00	0.00	0.00	0.00	0
184	PD	Male	False	16	55.00	8.52	0.85	30.14	5.21	0
185	PD	Female	False	18	69.00	7.62	0.88	0.00	0.00	0
186	PD	Female	False	16	77.00	0.00	0.00	0.00	0.00	0
187	PD	Female	False	16	59.00	4.07	0.34	0.41	0.05	0
188	PD	Female	True	12	80.00	35.02	2.98	8.29	0.68	0
189	PD	Female	False	18	69.00	0.00	0.00	0.00	0.00	4
190	PD	Male	False	16	69.00	0.00	0.00	0.00	0.00	0
191	PD	Male	False	12	69.00	26.32	1.54	0.00	0.00	4
192	PD	Female	False	14	80.00	182.85	20.13	45.89	6.23	1
193	PD	Male	False	13	59.00	35.76	4.22	0.00	0.00	0
194	PD	Male	False	16	75.00	0.00	0.00	0.00	0.00	4
195	PD	Female	False	14	57.00	19.59	2.02	0.00	0.00	0
196	PD	Male	False	18	74.00	4490.78	1154.13	60.32	4.69	1
197	PD	Male	False	18	70.00	201.21	27.67	0.00	0.00	0

198	PD	Female	True	16	71.00	4384.64	901.04	142.69	16.95	0
199	PD	Female	False	20	77.00	13.83	1.27	0.00	0.00	0
200	PD	Male	False	16	65.00	8.23	0.45	0.00	0.00	0
201	PD	Male	False	18	74.00	187.24	15.78	3.85	0.32	4
202	PD	Female	False	16	54.00	7.15	0.35	0.00	0.00	1
203	PD	Female	False	18	50.00	0.00	0.00	0.00	0.00	0
204	PD	Female	False	20	55.00	40.55	9.22	0.00	0.00	0
205	PD	Male	False	18	74.00	3.64	0.13	0.00	0.00	1
206	PD	Male	False	14	65.00	9.55	0.74	0.00	0.00	0
207	PD	Male	False	18	76.00	0.00	0.00	0.00	0.00	2
208	PSP	Female	False	12	72.00	1540.61	581.89	480.18	76.40	0
209	PSP	Male	True	10	71.00	0.00	0.00	0.00	0.00	0
210	PSP	Male	True	18	58.00	0.00	0.00	0.00	0.00	0
211	PSP	Male	True	12	56.00	0.00	0.00	0.00	0.00	4
212	PSP	Male	True	12	72.00	0.00	0.00	50.59	16.29	0
213	PSP	Male	False	12	56.00	2339.34	1093.41	262.56	72.65	0
214	PSP	Male	True	20	71.00	10.56	2.99	53.03	16.28	3
215	PSP	Male	False	20	70.00	0.00	0.00	0.00	0.00	0
216	PSP	Female	False	16	72.00	0.00	0.00	0.00	0.00	1
217	PSP	Female	False	16	66.00	11.74	1.35	55.46	26.30	0
218	PSP	Female	True	16	64.00	0.00	0.00	0.00	0.00	0
219	PSP	Female	True	19	59.00	288.40	164.91	0.00	0.00	0
220	PSP	Female	False	16	68.00	59.56	26.04	0.00	0.00	1
221	PSP	Male	False	12	68.00	227.69	90.53	87.52	21.84	2
222	PSP	Female	False	12	64.00	9.07	1.28	32.81	2.97	0
223	PSP	Female	False	15	72.00	11.25	2.11	75.38	15.20	0
224	PSP	Female	False	15	71.00	44.69	8.89	65.87	12.89	0
225	PSP	Female	False	16	68.00	0.00	0.00	58.53	1.30	0
226	PSP	Female	False	14	60.00	0.00	0.00	39.49	5.90	0
227	PSP	Female	True	16	63.00	0.00	0.00	155.77	23.57	4
228	PSP	Male	True	18	75.00	0.00	0.00	0.00	0.00	0
229	PSP	Female	False	18	65.00	0.00	0.00	64.98	10.51	1
230	PSP	Female	False	19	72.00	18.51	6.31	112.82	17.52	3
231	PSP	Male	True	14	72.00	70.30	11.02	207.12	23.09	4

232	PSP	Male	False	16	67.00	603.26	166.08	104.81	24.00	0
233	PSP	Female	False	12	78.00	0.00	0.00	32.11	3.07	0
234	PSP	Male	False	16	58.00	17.12	2.93	117.12	23.41	1
235	PSP	Male	False	12	77.00	10.73	0.29	52.67	4.95	3
236	PSP	Male	False	16	65.00	720.76	132.26	156.15	15.01	0
237	PSP	Male	True	16	74.00	21.00	6.02	98.61	10.14	0

Supplementary Table 5 p-values of tests on normal distribution for aSyn and Tau aggregates in CSF

		PD	DLB	AD	PSP	N
aSyn	Shapiro Wilk	0	$7.37*10^{-8}$	$2.44*10^{-7}$	$1.81*10^{-9}$	$9.16*10^{-14}$
	Lilliefors	$7.91*10^{-57}$	$5.73*10^{-9}$	$13.85*10^{-6}$	$1.20*10^{-13}$	$5.24*10^{-26}$
	Kolmogorov Smirnov	$5.72*10^{-18}$	0.0027	0.018	$7.76*10^{-5}$	$8.45*10^{-9}$
	Anderson Darling	$4.18*10^{-76}$	$2.35*10^{-12}$	$5.94*10^{-9}$	$3.00*10^{-17}$	$1.59*10^{-33}$
Tau	Shapiro Wilk	0	$9.03*10^{-7}$	$5.54*10^{-5}$	$4.72*10^{-6}$	$6.85*10^{-12}$
	Lilliefors	$6.56*10^{-57}$	$1.40*10^{-8}$	$3.70*10^{-5}$	$9.74*10^{-4}$	$9.8*10^{-21}$
	Kolmogorov Smirnov	$5.4*10^{-18}$	0.004	0.036	0.103	$4.03*10^{-7}$
	Anderson Darling	$2.12*10^{-69}$	$3.60*10^{-9}$	$4.97*10^{-6}$	$1.35*10^{-5}$	$4.42*10^{-25}$

Supplementary Table 6 Pearson coefficient of correlation values for analysis between aSyn and Tau aggregate concentrations and age, education, sex, disease duration, and death

		All cohorts	PD	DLB	AD	PSP	N
aSyn	Age	0.096	0.157	0.026	0.049	-0.256	0.130
	Education	-0.074	-0.133	0.025	0.183	-0.268	0.009
	Sex	-0.081	-0.061	-0.210	0.179	-0.134	-0.155
	Disease duration	0.093	0.012	0.073	0.130	-0.115	–
	Deceased	0.095	0.226*	-0.225	-0.235	-0.248	0.087
Tau	Age	0.070	0.166	0.031	-0.024	0.016	0.074
	Education	-0.144*	-0.182	-0.001	0.150	-0.258	-0.060
	Sex	-0.043	-0.081	-0.195	-0.060	-0.006	-0.089
	Disease duration	0.068	-0.006	0.106	0.047	0.055	–
	Deceased	0.070	-0.193*	-0.181	-0.357	-0.211	0.085

* indicates a significant correlation with p-values between 0.01–0.05

Supplementary Figure 1 TEM image (a) and size distribution (b) of silica nanoparticles

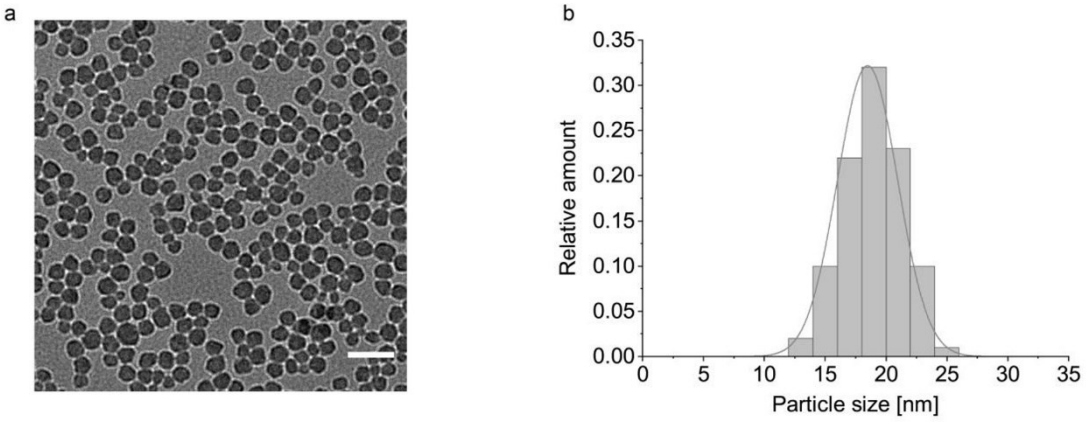

The exemplary image of an aSyn silica nanoparticle (a) shows the typical particle shape of the calibration standard. The scale bar is 50 nm. Aminated silica nanoparticles, which are the basis for peptide conjugation, show a normally distributed particle size with a mean of 18.5 nm (b, normal distribution analysed using Kolmogorov Smirnoff).

Supplementary Figure 2 aSyn (a) and Tau (b) aggregate concentrations grouped by blood-contamination levels

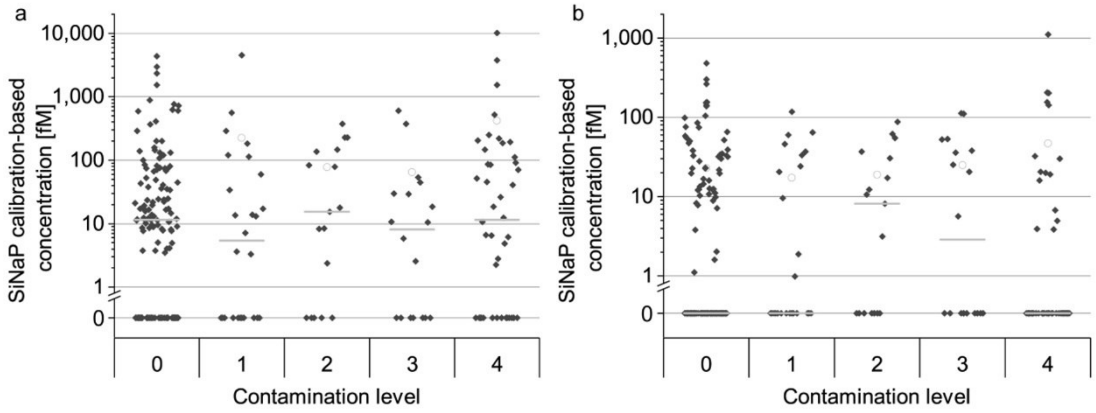

Blood contamination in CSF samples were measured with Combur10 stripes and grouped in 5 contamination levels (0: no contamination, 1: ~10 Ery/µL, 2: ~25 Ery/µL, 3: ~50 Ery/µL, 4: >250 Ery/µL). Higher contamination levels did not result in significant differences in aggregate concentrations (Kruskal-Wallis ANOVA: $p = 0.78$ for aSyn aggregates and $p = 0.63$ for Tau aggregates).

7.2 Aβ oligomers peak in early stages of Alzheimer's disease preceding Tau pathology

Autoren:	Lara Blömeke*, Fabian Rehn*, Victoria Kraemer-Schulien*, Janine Kutzsche, Marlene Pils, Tuyen Bujnicki, Piotr Lewczuk, Johannes Kornhuber, Silka D. Freiesleben Luisa-Sophie Schneider, Lukas Preis, Josef Priller, Eike J. Spruth, Slawek Altenstein, Andrea Lohse, Anja Schneider, Klaus Fliessbach, Jens Wiltfang, Niels Hansen, Ayda Rostamzadeh, Emrah Düzel, Wenzel Glanz, Enise I. Incesoy, Michaela Butryn, Katharina Buerger, Daniel Janowitz, Michael Ewers, Robert Perneczky, Boris-Stephan Rauchmann, Stefan Teipel, Ingo Kilimann, Doreen Goerss, Christoph Laske, Matthias H. Munk, Carolin Sanzenbacher, Annika Spottke, Nina Roy-Kluth, Michael T. Heneka, Frederic Brosseron, Michael Wagner, Steffen Wolfsgruber, Luca Kleineidam, Melina Stark, Matthias Schmid, Frank Jessen, Oliver Bannach, Dieter Willbold, Oliver Peters *Autoren sind gleichberechtigt
Journal:	Alzheimer's and Dementia- Diagnosis, Assessment & Disease Monitoring (veröffentlicht)
DOI:	10.1002/dad2.12589
Impact-Faktor:	16,655 (2021)
Beitrag:	Eigenanteil: 25 % Entwicklung des Assays Auswertung der Ergebnisse Anfertigung der Abbildungen Verfassen des Manuskripts

Aβ oligomers peak in early stages of Alzheimer's disease preceding Tau pathology

Supplementary Information

Authors: Lara Blömeke, Fabian Rehn, Victoria Kraemer-Schulien, Janine Kutzsche, Marlene Pils, Tuyen Bujnicki, Piotr Lewczuk, Johannes Kornhuber, Silka D. Freiesleben Luisa-Sophie Schneider, Lukas Preis, Josef Priller, Eike J. Spruth, Slawek Altenstein, Andrea Lohse, Anja Schneider, Klaus Fliessbach, Jens Wiltfang, Niels Hansen, Ayda Rostamzadeh, Emrah Düzel, Wenzel Glanz, Enise I. Incesoy, Michaela Butryn, Katharina Buerger, Daniel Janowitz, Michael Ewers, Robert Perneczky, Boris-Stephan Rauchmann, Stefan Teipel, Ingo Kilimann, Doreen Goerss, Christoph Laske, Matthias H. Munk, Carolin Sanzenbacher, Annika Spottke, Nina Roy-Kluth, Michael T. Heneka, Frederic Brosseron, Michael Wagner, Steffen Wolfsgruber, Luca Kleineidam, Melina Stark, Matthias Schmid, Frank Jessen, Oliver Bannach, Dieter Willbold, Oliver Peters

Supplementary Table 1. Mean coefficient of variation (CV%) values of the SiNaPs and the samples over the four replicates for Aβ and Tau.

	Aβ		Tau	
Experiment	SiNaPs [%]	Samples [%]	SiNaPs [%]	Samples [%]
1	15.6	15.6	13.5	10.4
2	11.2	12.8	10.8	8.6
3	14.8	12.0	12.7	8.5
4	12.1	13.0	10.7	9.8
5	15.6	12.0	17.1	13.7
6	10.5	11.5	8.9	9.2
7	14.3	13.3	15.0	11.2
8	15.0	13.8	12.7	9.7
9	12.3	13.9	12.0	8.7
10	12.5	14.2	9.6	8.0
11	18.2	12.7	14.5	8.9
12	12.3	11.4	10.2	7.2
13	10.5	13.0	9.5	6.6
14	17.6	13.5	11.3	8.9
15	12.1	12.8	9.9	7.1
16	14.5	11.9	12.4	8.4
Mean	13.7	13.0	11.9	9.1

Supplementary Fig. 1. Assay controls for measurement of Aβ (A, C) and Tau (B, D) oligomer levels.

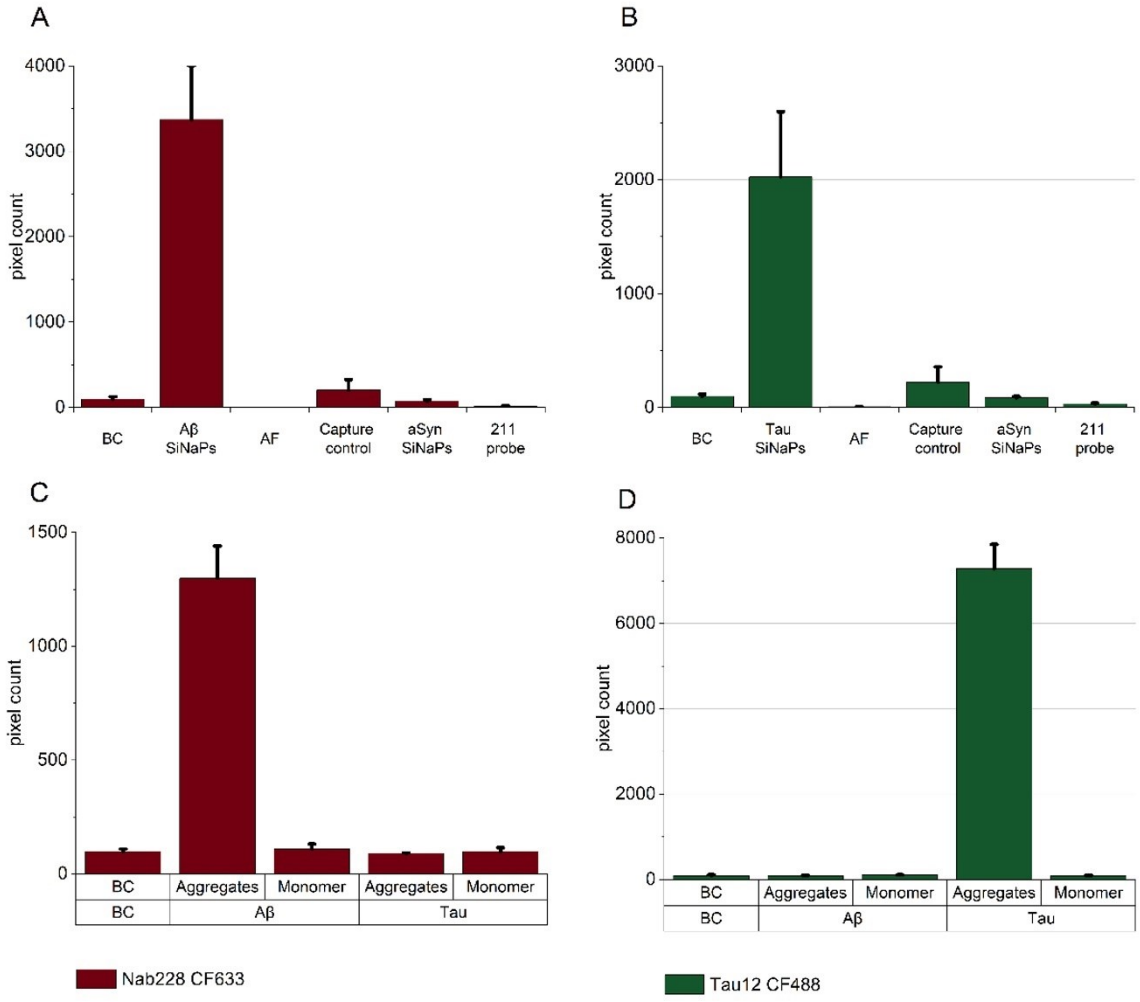

For Aβ (A) as well as for Tau (B), none of the assay components showed an autofluorescence signal (AF, signal < 0.1%). The signal of SiNaPs when leaving of the capture antibody was reduced to 2.8% for Aβ and 7.4% for Tau, respectively. When applying α-Synuclein (αSyn) SiNaPs or when detecting Aβ and Tau SiNaPs with an αSyn specific antibody (211), pixel counts were at blank control (BC) level. Recombinant Aβ aggregates of 1 nM (concentration depends on the monomer concentration) showed an increased fluorescence signal for detection with Nab228 CF633 (C), but were not detected with Tau12 CF488A (D). Likewise, Tau aggregates of 250 pM

(concentration depends on the monomer concentration) were detected with Tau12 CF488A, but not with Nab228 CF633. Neither presence of monomeric Aβ nor the presence of monomeric Tau showed a fluorescence signal above the blank control when applied in the same concentration like the aggregates with a signal reduction by more than 99% compared to the same concentration of monomer units in aggregates. Standard deviation was determined across the four replicates

Supplementary Table 2. Scaling factors of the individual experiments for Aβ and Tau oligomer pixel counts used to perform scaling.

Experiment	Scale Factor Aβ	Scale Factor Tau
1	1.459	1.224
2	0.938	0.977
3	0.938	0.977
4	1.236	1.597
5	1.300	1.688
6	1.108	1.510
7	1.077	1.306
8	0.798	1.129
9	1.237	0.689
10	1.084	0.934
11	0.965	0.985
12	1.020	1.037
13	0.893	0.850
14	1.004	0.723
15	0.810	0.643
16	0.822	0.998

Supplementary Fig 2. Measured Aβ (A, C) and Tau (B, D) pixel counts before scaling. To increase readability, the y-axis was limited to the range between 20−350 for Aβ (C) and 20−200 for Tau (D). Especially for Tau considerable fluorescence fluctuations between the 16 individual plates can be observed. As the samples were applied in the blinded state, the distribution of the diagnostic groups on the plates is not uniform and consequently a distortion of statistical results could occur if values are used without scaling.

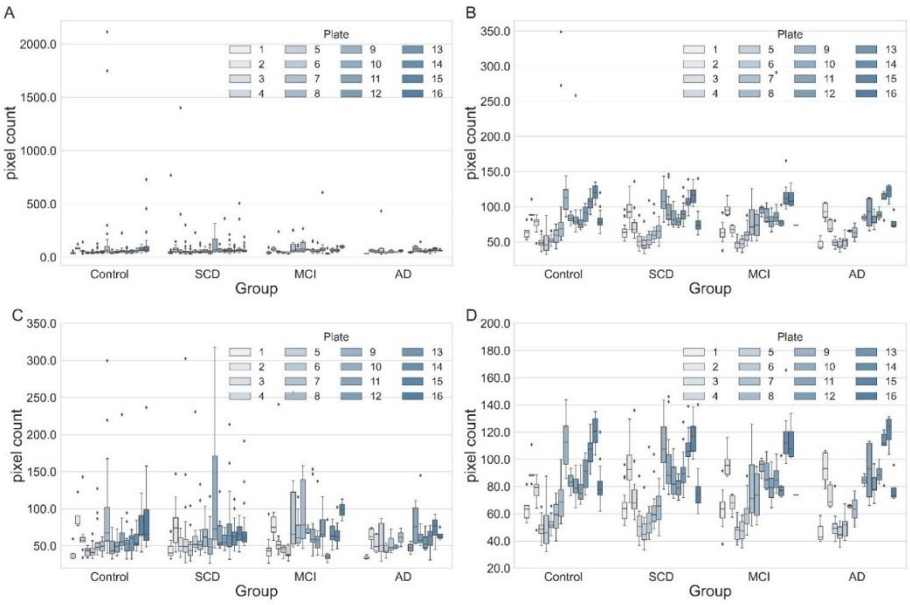

Supplementary Fig 3. Measured Aβ (A, C) and Tau (B, D) oligomer pixel counts after scaling. To increase readability, the y-axis was limited to the range between 20−350 for Aβ (C) and 20−200 for Tau. Since the fluorescence fluctuations between the individual plates are now reduced to an acceptable level, it is now possible to carry out statistical analyses without distorting the results.

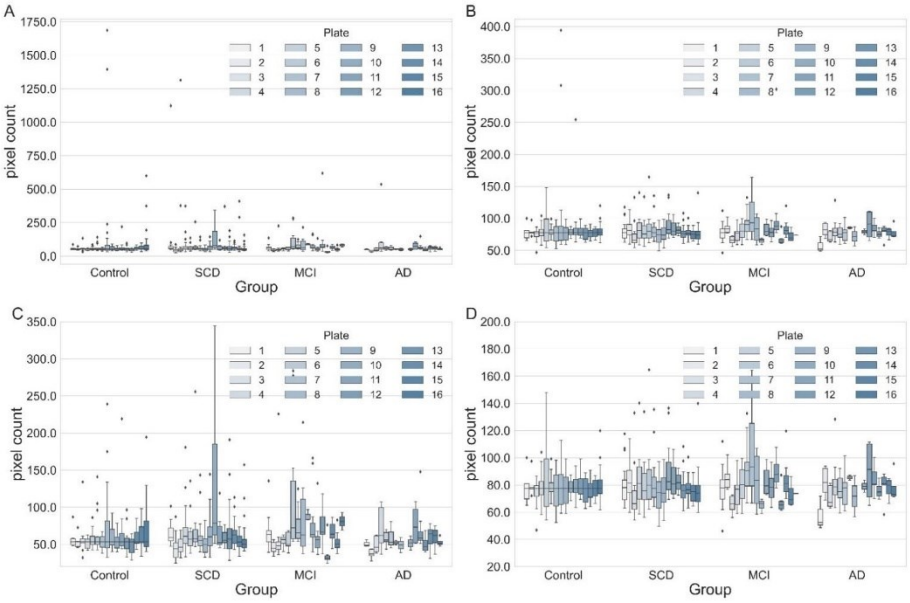

51 **Supplementary Table 3. Effect size, among groups significantly differing from each other**

Groups	Median Difference Ratio [%]
Control vs. MCI	8.57
Control [A-] vs. SCD [A+]	8.65
Control [A-] vs. MCI [A+]	13.26
SCD [A-] vs. SCD [A+]	5.06
A-T- vs. A+T-	9.31
A+T- vs. A+T+	-8.65

52

53 **Supplementary Table. 4. Bootstrapped median AUC scores.**

Groups	Bootstrapped median AUC score
Control vs. MCI	0.54
Control [A-] vs. SCD [A+]	0.56
Control [A-] vs. MCI [A+]	0.57
SCD [A-] vs. SCD [A+]	0.57
A-T- vs. A+T-	0.60
A+T- vs. A+T+	0.60

54

55

Supplementary Fig. 4. ROC-Curves of classifications between groups significantly differing from each other.

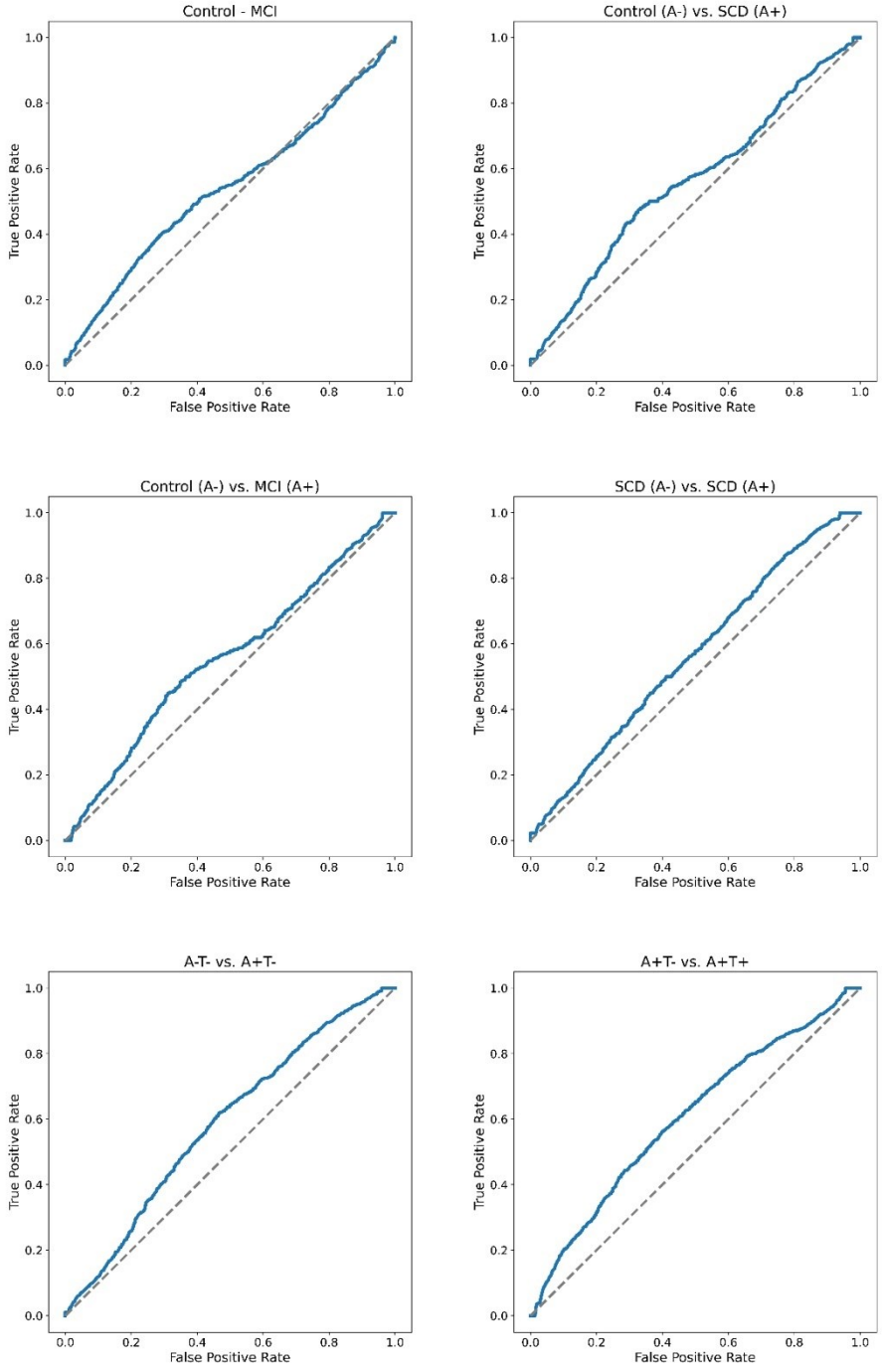

For all group pairs showing a significant difference according to Mann-Whitney-U a ROC-Curve and AUC-Score was calculated. To account for the variance and consequent uncertainty arising from a train-test split, a strictly stratified bootstrapping approach with N=500 was chosen, where for each iteration, a randomized subset of data was determined using random sampling with replacement. This subset was then divided into training and test sets, and a logistic regression was trained and used to classify the test data. For each of the N regressions, an ROC curve and AUC were computed. Since the dispersion of the AUC scores was very high, the median of all scores was used to avoid the inclusion of outliers. To visualize a single curve, the FPR and TPR values were calculated for each of the N iterations, interpolated at intervals of 0.001 steps, and then the median of all N FPR values for each TPR value was computed.

The AUC scores were found to be in a range between 0.54 and 0.57, which, while not particularly high, was not unexpected. This can be partly attributed to the considerable overlap among the groups, together with the illustrated progression of Aβ oligomers depicted in Figure 4. The values do not monotonically increase but instead reach their maximum in the SCD (ApoE4-) or MCI (ApoE4+) stage before subsequently decreasing. However, logistic regression, building the foundation of ROC analysis, need constantly increasing or decreasing levels over the disease progression and therefore cannot accurately depict the described development.

Supplementary Table 5. Regression Error

Model	nMAE
All Data	0.16
ApoeE4+	0.24
ApoE4-	0.15

The MAE was normalized by the standard deviation.

Supplementary Fig. 5. Binned Aβ oligomer pixel counts plotted as a function of Aβ42 and pTau concentrations.

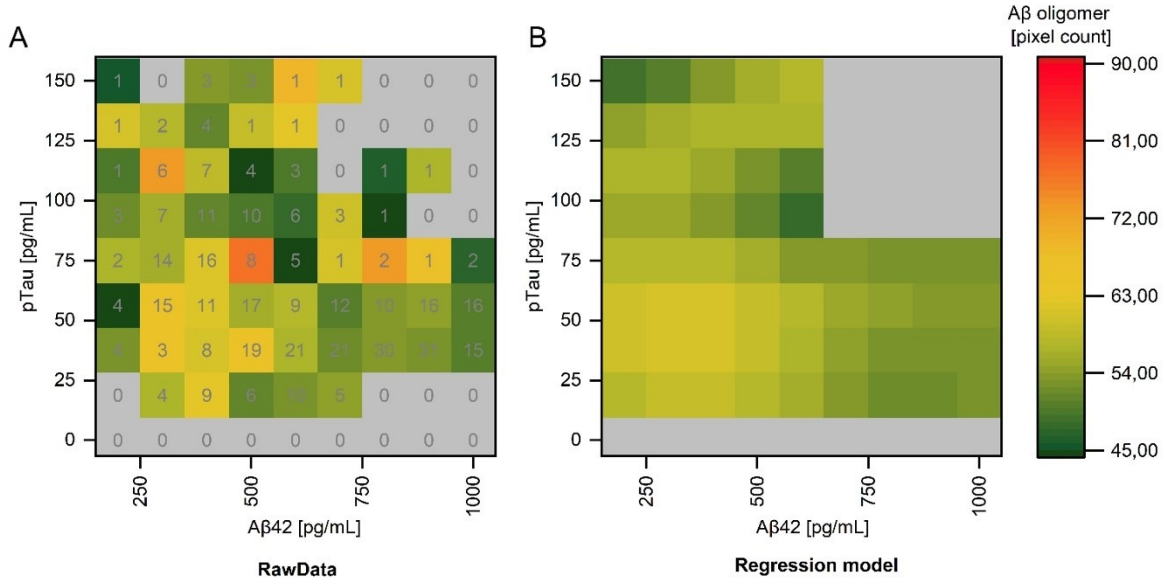

The heatmap shows a 2D plot with Aβ42 and pTau concentrations on the x any y axis, respectively. (A) measured Aβ oligomer pixel counts were binned and median oligomer pixel counts were plotted based on Aβ42 and pTau concentrations. Numbers in the squares represent the number of measurement points. (B) Results of the regression model were binned and plotted equal to (A). Highest Aβ oligomer pixel counts are found at low Aβ42 and pTau concentrations for the raw data as well as for the regression data.

7.3 Oral treatment with all-D-peptide RD2 enhances cognition in aged beagle dogs – a model of sporadic Alzheimer's disease

Autoren:	Janine Kutzsche*, Sarah Schemmert*, Tuyen Bujnicki*, Christian Zafiu, Steffen Halbgebauer, Victoria Kraemer-Schulien, Marlene Pils, Lara Blömeke, Julia Post, Andreas Kulawik, Dagmar Jürgens, Wolfgang M. Rossberg, Michael Hümpel, Oliver Bannach, Markus Otto, Joseph A. Araujo, Antje Willuweit, Dieter Willbold *Autoren sind gleichberechtigt
Journal:	Heliyon (veröffentlicht)
DOI:	10.1016/j.heliyon.2023.e18443
Impact-Faktor:	3,776 (2022)
Beitrag:	Eigener Anteil: 5 % Entwicklung des sFIDA-Assays Diskussion der Ergebnisse Prüfen des Manuskripts

SUPPLEMENTAL INFORMATION

Table S1: Complete Blood Count (mean values and standard deviation) - baseline and after three months of treatment

Parameter	Units	Normal Range	Placebo		RD2 acetate 3 mg/kg		RD2 acetate 30 mg/kg	
			baseline	treatment	baseline	treatment	baseline	treatment
WBC	10^9/l	4.0-16	6.4 ± 3.9	5.7 ± 3.1	4.6 ± 1.9	5.1 ± 1.4	4.4 ± 1.4	4.0 ± 1.2
RBC	10^{12}/l	4.8-9.3	5.3 ± 0.45	5.4 ± 0.38	5.4 ± 0.31	5.4 ± 0.35	5.5 ± 0.67	5.6 ± 0.65
Hemoglobin	g/l	121-203	123 ± 11	123 ± 9.4	128 ± 8.8	128 ± 8.2	131 ± 16	132 ± 16
Hematocrit	%	36-60	37 ± 3.1	38 ± 2.7	47 ± 28	47 ± 28	40 ± 4.6	41 ± 4.7
MCV	Fl	58-79	71 ± 1.7	72 ± 2.6	70 ± 9.3	70 ± 9.3	72 ± 2.1	73 ± 1.7
MCH	Pg	19-28	23 ± 0.86	23 ± 0.97	28 ± 15	28 ± 15	24 ± 0.47	24 ± 0.42
MCHC	g/l	300-380	329 ± 8.6	321 ± 3.8	301 ± 88	299 ± 87	332 ± 8.1	324 ± 5.3
Platelet count	10^9/l	170-400	394 ± 165	384 ± 146	343 ± 94	335 ± 85	301 ± 111	327 ± 108
Neutrophils	10^9/l	2.06-10.60	4.5 ± 3.4	4.0 ± 2.5	2.8 ± 1.6	3.5 ± 1.1	2.8 ± 1.0	2.6 ± 0.92
Lymphocytes	10^9/l	0.69-4.50	1.3 ± 0.30	1.2 ± 0.36	1.2 ± 0.45	1.2 ± 0.36	1.2 ± 0.36	1.1 ± 0.28
Monocytes	10^9/l	0-0.84	0.29 ± 0.23	0.28 ± 0.18	0.18 ± 0.08	0.23 ± 0.09	0.19 ± 0.07	0.19 ± 0.05
Eosinophils	10^9/l	0-1.20	0.29 ± 0.19	0.26 ± 0.17	0.27 ± 0.11	0.18 ± 0.08	0.21 ± 0.10	0.22 ± 0.19
Basophils	10^9/l	0-0.15	0	0	0	0	0	0
Total Protein	g/l	50-74	54 ± 3.1	57 ± 6.6	53 ± 2.1	56 ± 2.9	54 ± 5.3	57 ± 6.0
Albumin	g/l	27-44	31 ± 2.1	31 ± 2.8	30 ± 2.7	30 ± 2.5	29 ± 2.3	30 ± 2.6
Globulin	g/l	16-36	23 ± 3.3	25 ± 4.1	24 ± 2.0	26 ± 2.6	25 ± 3.8	28 ± 4.5
A/G Ratio		0.8-2.0	1.4 ± 0.25	1.3 ± 0.27	1.3 ± 0.20	1.2 ± 0.18	1.2 ± 0.14	1.1 ± 0.18

Table S2: Clinical chemistry (mean values and standard deviation) - baseline and after three months of treatment. Mean results of the clinical chemistry for placebo and RD2 treated animals. There were no significant changes in any of the listed measures except for the triglyceride concentration, which was significantly increased after dosing with 3 mg/kg or 30 mg/kg, but still in the normal range of historical controls.

Parameter	Units	Normal Range	Placebo		RD2 acetate 3 mg/kg		RD2 acetate 30 mg/kg	
			baseline	treatment	baseline	treatment	baseline	treatment
Phosphorus	mmol/l	0.81-1.9	1.3 ± 0.21	1.7 ± 0.95	1.4 ± 0.27	1.5 ± 0.25	1.4 ± 0.32	1.6 ± 0.35
Glucose	mmol/l	3.9-7.7	5.0 ± 0.52	5,3 ± 0.49	4.9 ± 0,29	5.2 ± 0.33	5.0 ± 0.41	5.1 ± 0.54
Calcium	mmol/l	2.2-2.9	2.4 ± 0.06	2.4 ± 0.04	2.3 ± 0.08	2.4 ± 0.11	2.3 ± 0.11	2.4 ± 0.12

Magnesium	mmol/l	0.7-1.3	0.70 ± 0.05	0.77 ± 0.06	0.74 ± 0.05	0.78 ± 0.06	0.73 ± 0.07	0.76 ± 0.05
Sodium	mmol/l	139-154	145 ± 3.9	147 ± 1.0	146 ± 3.8	147 ± 1.5	145 ± 3.6	148 ± 2.3
Potassium	mmol/l	3.6-5.5	4.3 ± 0.31	4.4 ± 0.28	4.2 ± 0.29	4.3 ± 0.25	4.1 ± 0.32	4.3 ± 0.40
Sodium/Potassium Ratio		27-38	34 ± 2.5	34 ±2.1	35 ± 2.0	34 ± 1.8	35 ± 2.7	35 ± 3.1
Chloride	mmol/l	102-120	112 ± 3.9	113 ± 1.7	113 ± 2.3	113 ± 2.5	112 ± 3.7	113 ± 2.8
Cholesterol	mmol/l	2.4-10	4.9 ± 0.95	5.2 ± 0.68	5.2 ± 0.83	5.5 ± 0.86	5.3 ± 1.2	5.4 ± 1.2
Triglycerides	mmol/l	0.33-3.3	2.0 ± 0.33	2.0 ± 0.47	2.7 ± 1.4	3.2 ± 1.8	2.2 ± 0.37	2.6 ± 0.39
Amylase	U/l	290-1125	475 ± 203	503 ± 229	494 ± 164	511 ± 159	434 ± 142	465 ± 182
Precision PSL	U/l	24-140	60 ± 21	44 ± 16	68 ± 50	52 ± 31	66 ± 29	57 ± 26
CPK total	U/l	59-895	84 ± 18	88 ± 13	96 ± 33	92 ± 32	92 ± 21	103 ± 43

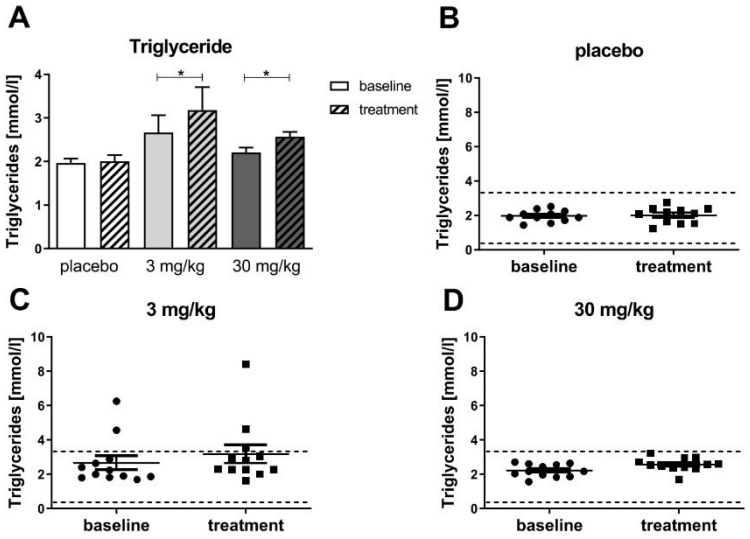

Figure S1: Blood concentration of triglycerides of placebo (B), 3 mg/kg RD2 (C) and 30 mg/kg RD2 (D) treated animals was analyzed using a paired t-test with timepoints serving as a within-subject measure. A significantly increased concentration of triglycerides was detected after three-month RD2 treatment (3 mg/kg and 30 mg/kg) compared to baseline, but not in the placebo treated animals (A). With two exceptions (in 3 mg/kg group), all measured values are within the normal reference range. Without these two animals, which are already out of the normal range at baseline, there is no significant difference between baseline and treatment any more in the 3 mg/kg group. Area between the dashed lines represent the normal reference range. (*$p < 0.05$). Data is presented as mean ± SEM; n = 11 to 12

Table S3: Liver function blood test. To assess potential effects of RD2 on liver function, aspartate aminotransferase (AST), alanine transaminase (ALT), alkaline phosphatase (Alk), gamma-glutamyl transpeptidase (GGTP), albumin, and total bilirubin were determined. There were no significant treatment related changes in any of the listed measures.

Parameter	Units	Normal Range	Placebo		RD2 acetate 3 mg/kg		RD2 acetate 30 mg/kg	
			baseline	treatment	baseline	treatment	baseline	treatment
AST	U/l	15-66	22 ± 5.2	22 ± 4.7	23 ± 4.5	22 ± 7.3	25 ± 4.1	25 ± 3.2
ALT	U/l	12-118	45 ± 25	98 ± 132	33 ± 23	29 ± 13	32 ± 15	32 ± 19
Alk	U/l	5-131	53 ± 30	134 ± 200	113 ± 136	121 ± 140	93 ± 91	84 ± 77
GGTP	U/l	1-12	3.9 ± 1.3	9.0 ± 6.4	3.5 ± 4.5	6.4 ± 2.0	3.6 ± 1.2	6.1 ± 1.5
Bilirubin	µmol/l	0.0-5.1	2.5 ±0.53	3.1 ± 1.2	2.5 ± 0.63	2.4 ± 0.57	2.2 ± 0.44	2.4 ± 0.54
BUN	mmol/l	2.1-11	5.2 ± 1.7	5.7 ± 4.0	5.4 ± 0.79	5.8 ± 0.99	5.2 ± 1.1	5.9 ± 1.6
Creatinine	µmol/l	44-141	56 ± 20	59 ± 26	51 ± 9.3	54 ± 11	54 ± 10	61 ± 12
Creatinine/BUN ratio			96 ± 23	93 ± 22	108 ± 18	110 ± 16	97 ± 15	96 ± 8.7

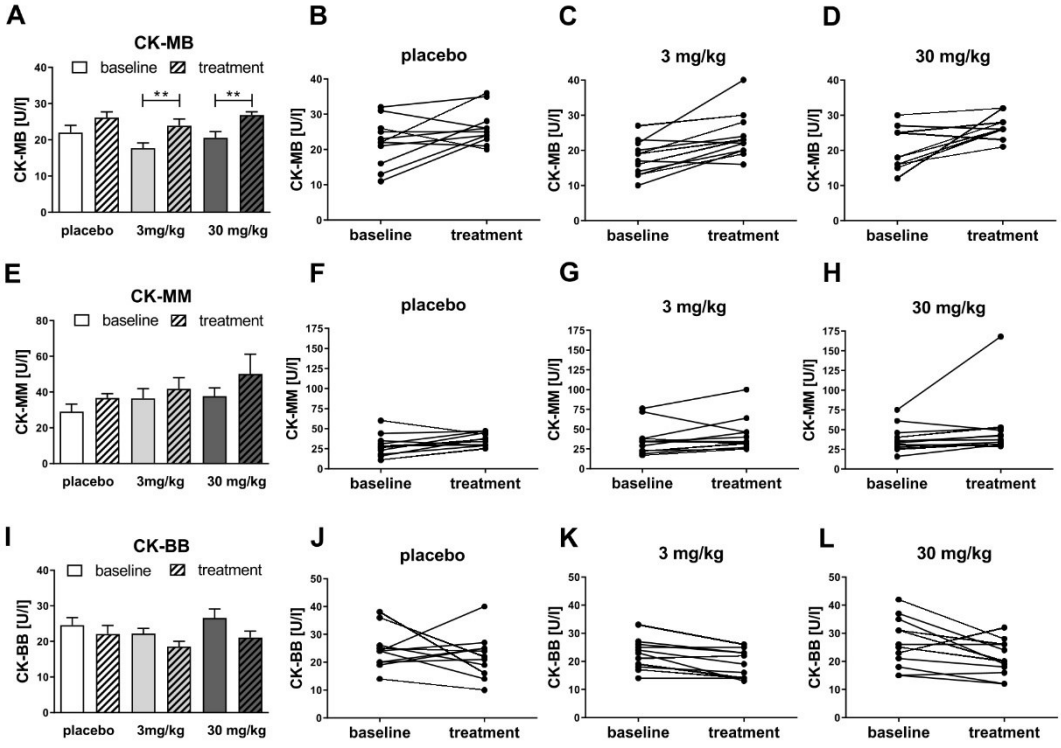

Figure S2: Blood concentration of the creatinine kinase isoenzymes (CK-MB (A-D), CK-MM (E-F) and CK-BB (I-L) were each analyzed using a paired t-test with timepoints serving as a within-subject measure. A significantly increased concentration of CK-MB was detected after three-month treatment

with RD2 (3 mg/kg and 30 mg/kg) compared to baseline, but not in the placebo treated animals. (**p < 0.01) (A). Data are presented as mean ± SEM; n = 11 to 12.

Other correlations

We found a significant and positive correlation between the results of the DNMP and the selective attention tests in the dogs of the placebo cohort at all time points available (Fig. S3F). This indicates that both tests are robustly measuring memory and cognition deficits in dogs. We found a positive and significant correlation between selective attention accuracy and total Aβ42 concentration in CSF (Fig. S3D). We examined the correlation of changes (after three months treatment versus baseline) of CSF Aβ42 total concentrations with changes (after three months treatment versus baseline) of CSF Aβ oligomer concentrations and found a significant and inverse correlation (Fig. S3F, Pearson -0.496 p-value 0.00287). This does not necessarily mean that Aβ42 levels are increased due to Aβ oligomer disassembly. Disassembly of 100 fM Aβ oligomers, even if we anticipate 100 monomer building blocks per oligomer, would yield 10 pM amounts of additional Aβ monomers equal to 40 pg/ml, a concentration increase that may not contribute significantly to the total Aβ42 concentration (Fig. S3E).

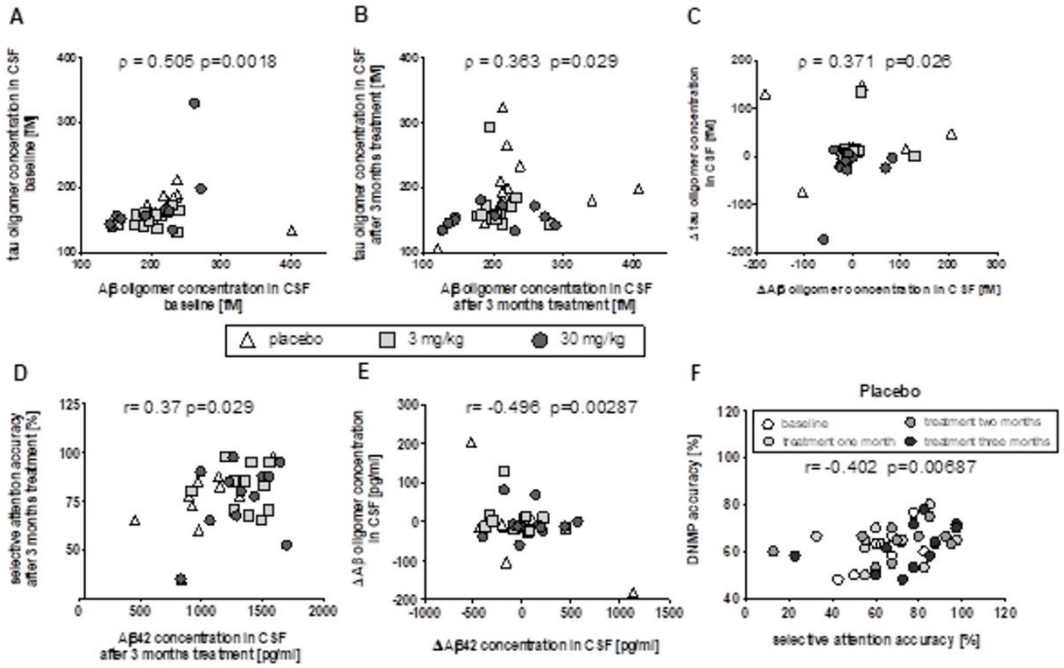

Figure S3: Correlations between Aβ42 and Aβ oligomer concentrations as well as with cognitive testing. A: Correlation of CSF Aβ oligomer concentration vs. CSF tau oligomer concentration at baseline. B: Correlation of CSF Aβ oligomer concentration vs. CSF tau oligomer concentration after 3 months treatment with RD2. C: Correlation of changes of CSF Aβ oligomer concentration vs. changes of CSF tau oligomer concentration. Changes (Δ) were calculated by subtracting baseline value from three-month treatment value. D: Correlation of CSF Aβ42 concentration with selective attention accuracy after 3 months treatment. E: Correlation of changes of CSF Aβ42 concentration with changes of CSF Aβ oligomer concentration. Changes (Δ) were calculated by subtracting baseline value from

three-month treatment value. F: Correlation of selective attention accuracy and DNMP accuracy of the placebo group from all available different time points. Correlations were performed with Pearson (r) and Spearman (ρ) analysis at alpha level 0.05 with n = 11 to 12.

7.4 Blood-based quantification of Aβ oligomers indicates impaired clearance from brain in ApoE ε4 positive subjects

Autoren:	Lara Blömeke, Fabian Rehn, Marlene Pils, Victoria Kraemer-Schulien, Anne Cousin, Janine Kutzsche, Tuyen Bujnicki, Silke Dawn Freiesleben, Luisa-Sophie Schneider, Lukas Preis, Josef Priller, Eike Jakob Spruth, Slawek Altenstein, Anja Schneider, Klaus Fliessbach, Jens Wiltfang, Niels Hansen, Ayda Rostamzahdeh, Emrah Düzel, Wenzel Glanz, Enise I. Incesoy, Katharina Buerger, Daniel Janowitz, Michael Ewers, Robert Perneczky, Boris-Stephan Rauchmann, Stefan Teipel, Ingo Kilimann, Christoph Laske, Matthias H. Munk, Annika Spottke, Nina Roy, Michael T. Heneka, Frederic Brosseron, Michael Wagner, Sandra Roeske, Alfredo Raminez, Matthias Schmid, Frank Jessen, Oliver Bannach, Oliver Peter, Dieter Willbold
Journal:	Communications Medicine (im Review)
DOI:	/
Impact-Faktor:	Gegründet 2021, noch kein Impact-Faktor verfügbar
Beitrag:	Eigenanteil: 75 % Entwicklung des Assays Synthese und Weiterentwicklung der Silikananopartikel Planung, Durchführung und Auswertung der Validierungsexperimente Durchführung und Auswertung der Plasmaprobenmessungen Anfertigung der Abbildungen Statistische Auswertung Hauptverfasserin des Manuskripts

Blood-based quantification of Aβ oligomers indicates impaired clearance from brain in ApoE ε4 positive subjects

Lara Blömeke, Fabian Rehn, Marlene Pils, Victoria Kraemer-Schulien, Anneliese Cousin, Janine Kutzsche, Tuyen Bujnicki, Silka D. Freiesleben, Luisa-Sophie Schneider, Lukas Preis, Josef Priller, Eike J. Spruth, Slawek Altenstein, Anja Schneider, Klaus Fliessbach, Jens Wiltfang, Niels Hansen, Ayda Rostamzadeh, Emrah Düzel, Wenzel Glanz, Enise I. Incesoy, Katharina Buerger, Daniel Janowitz, Michael Ewers, Robert Perneczky, Boris-Stephan Rauchmann, Stefan Teipel, Ingo Kilimann, Christoph Laske, Matthias H. Munk, Annika Spottke, Nina Roy, Michael T. Heneka, Frederic Brosseron, Michael Wagner, Sandra Roeske, Alfredo Ramirez, Matthias Schmid, Frank Jessen, Oliver Bannach, Oliver Peters, Dieter Willbold

Supplementary Figures and Tables

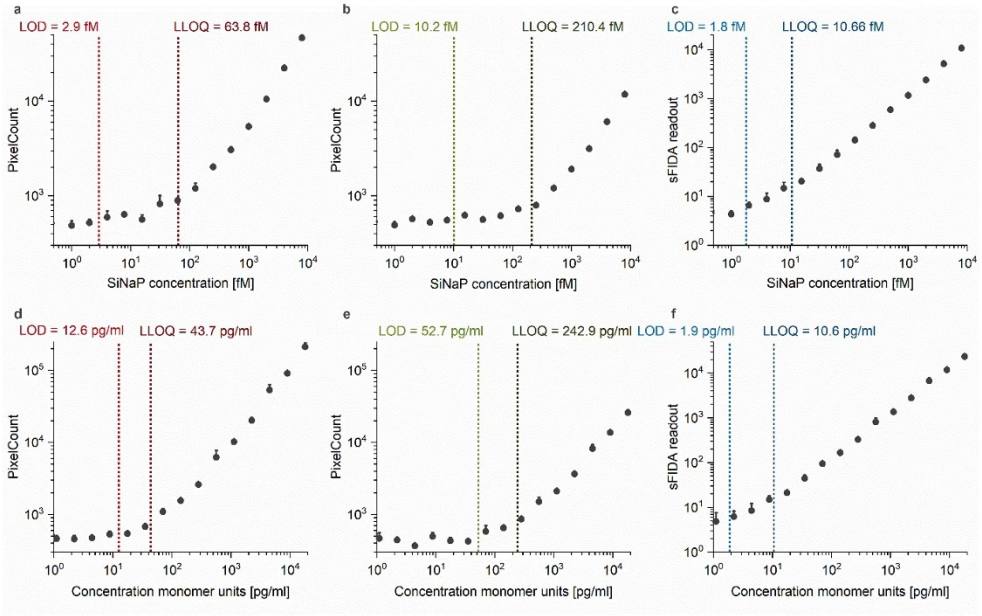

Supplementary Fig. 1 Linear dilution of $A\beta_{1-15}$ SiNaPs and $A\beta_{1-42}$ aggregates spiked in plasma. Shown are dilution series for $A\beta_{1-15}$ SiNaPs for the red (CF 633) (**a**) and green (CF488) (**b**) fluorescence channels, and the colocalization (**c**) and the corresponding limit of detection (LOD) and lower limit of quantification (LLOQ). Similarly, dilution series of synthetic $A\beta_{1-42}$ aggregates for the red (CF633) (**d**) and green (CF488) (**e**) fluorescence channels and colocalization (**f**) with calculated LOD and LLOQs are shown. The standard deviation was calculated across the four replicates. Please, note the logarithmic scale.

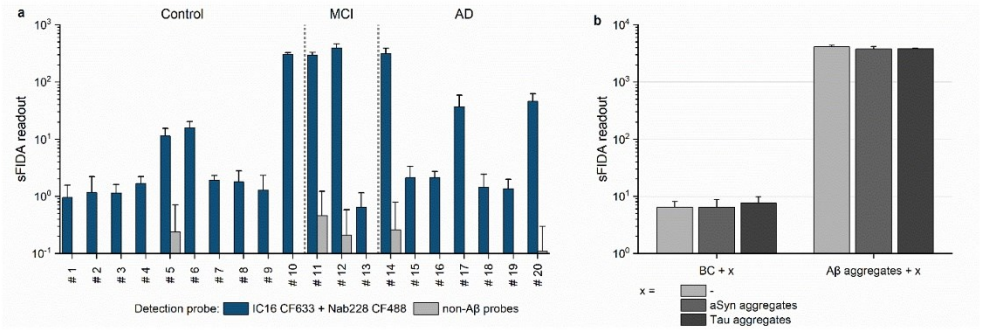

Supplementary Fig. 2 Assay controls with non-Aβ probes (a) and αSyn and Tau aggregates. a sFIDA readouts of the samples (#1 to #20) of the validation cohort for detection with anti-Aβ detection antibodies IC16 CF633 in combination with Nab228 CF488 (blue) and non-Aβ probes MOPC-21 CF633 in combination with 211 CF488 (grey). While the samples detected with anti-Aβ antibodies showed an sFIDA readout ranging from approximately 1 pixel to 500 pixels, the samples did not give a signal when detected with antibodies who do not recognize Aβ. **b** Neat plasma and 1 nM (18 ng/ml) Aβ aggregates (concentration based on the monomer unit concentration) were spiked with 1 nM of αSyn and Tau aggregates, respectively. Standard deviation was calculated across the four replicates. Please, note the logarithmic scaling.

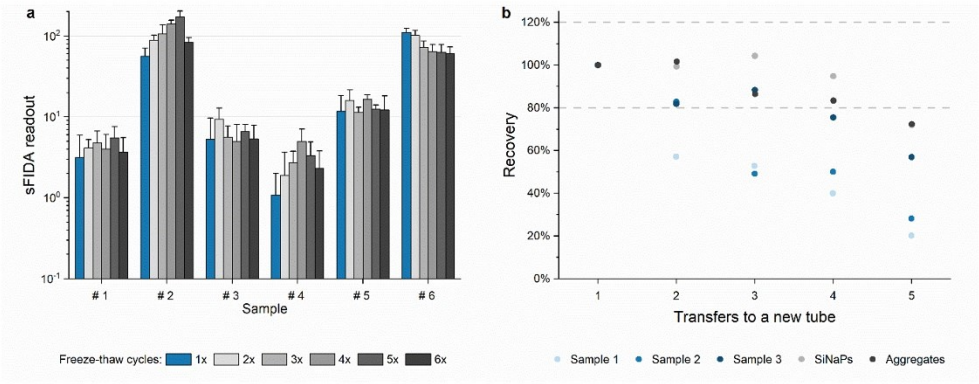

Supplementary Fig. 3 Evaluation of freeze-thaw cycles (a) and influence of tube transfers (b). a Six patient plasma samples were thawed for 2 h at RT and then refrozen. The sFIDA readout for half of the samples remained unaffected (mean recovery 103%–129%), whereas additional freeze-thaw cycles caused an increase in the sFIDA readout for two samples and a decrease in the readout for one sample. Please, note the logarithmic scaling. Standard deviation is calculated across the four replicates. **b** After centrifugation, the supernatants of the plasma samples were transferred to a new tube (one transfer). One additional transfer reduced the sFIDA readout for the samples, whereas that of SiNaPs and recombinant aggregates remains constant for at least two additional transfers.

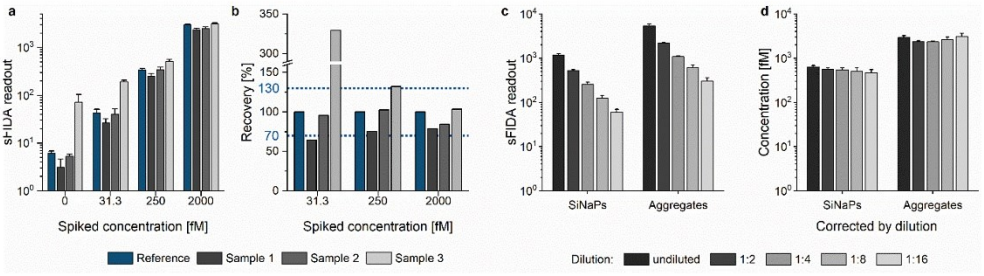

Supplementary Fig. 4 Recovery of SiNaPs in different matrices (a, b) and dilution of SiNaPs and aggregates spiked in plasma (c, d). a Three samples with an initial low (sample 1), medium (sample 2) and high concentration (sample 3) of Aβ oligomers were spiked with three different concentrations of SiNaPs to examine whether the recovery of SiNaPs is dependent on the individual plasma matrix. **b** The obtained sFIDA readouts were initially normalized with the non-spiked sample and then compared to the readout of the same concentration of SiNaPs in the reference plasma sample. Samples 1 and 2 showed a mean recovery of 73% and 94%, respectively. For sample 3, the lowest concentration of 31.3 fM was beyond the acceptable range (dashed blue line), whereas medium and high concentrations of SiNaPs spiked in sample 3 showed a mean recovery of 118%. Mean recovery of all samples and concentrations (except sample 3 spiked with a low concentration) was 92%. **c** SiNaPs and recombinant $A\beta_{1-42}$ aggregates were spiked in plasma and diluted two-fold with TBS. **d** After calibration and correction for dilution, calculated stock concentrations for SiNaPs and aggregates differed on average by 15.9% and 8.9%, respectively. Standard deviations are calculated across the four replicates. Please, note the logarithmic scaling in a, c and d.

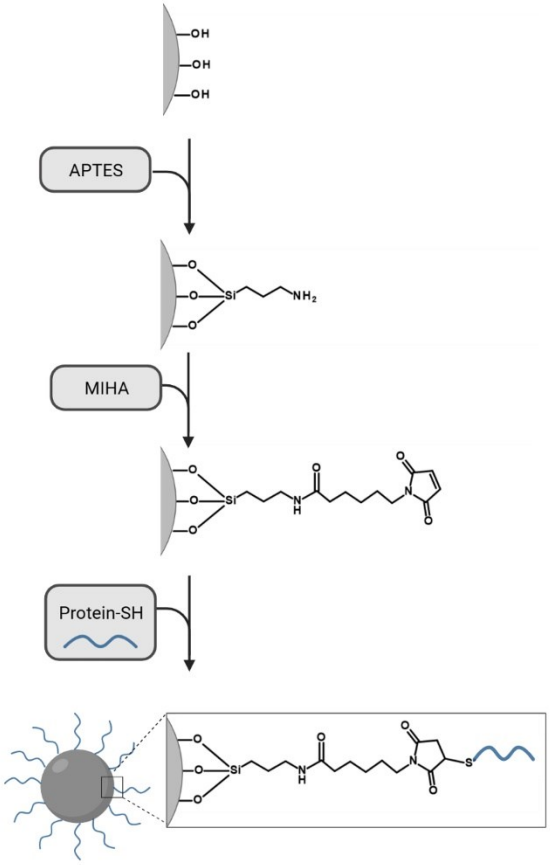

Supplementary Fig. 5 Synthesis of protein conjugated SiNaPs. The process of protein conjugation of SiNaPs consists of three main steps. First, the silica core is functionalized with APTES. As a second step, MIHA is added as a crosslinker between the SiNaPs core and the protein. The use of maleimide as functional group in combination with the reaction conditions allows a directed coupling with the thiol group at the modified C-terminus of the protein. The resulting protein conjugated SiNaPs imitate a protein aggregate with multiple binding sites for the antibody but showing a unique size distribution, high stability, and defined epitope number [1].

Supplementary Table 1 Mean Spearman coefficient of correlation r of the bootstrapping analysis of Aβ oligomers in plasma with demographics and biomarkers in CSF and plasma (*p*-value of Spearman distribution * 0.01 – 0.05, ** *p*-value 0.001 – 0.01)

		Control/Relatives/SCD	MCI/AD
	Age	−0.100	0.047
	MMSE	−0.053	0.011
CSF	$A\beta_{1-40}$	−0.037	0.219*
	$A\beta_{1-42}$	0.103	0.236**
	$A\beta_{1-42}/A\beta_{1-40}$	0.166*	0.196*
	tTau	−0.160*	0.023
	pTau	−0.203**	0.051
	Aβ Oligomers	0.186**	−0.217**
	Tau Oligomers	0.201**	−0.096
Plasma	$A\beta_{1-40}$	−0.067	0.148
	$A\beta_{1-42}$	−0.044	0.054
	$A\beta_{1-42}/A\beta_{1-40}$	0.034	−0.233*

1 Herrmann, Y. *et al.* Nanoparticle standards for immuno-based quantitation of alpha-synuclein oligomers in diagnostics of Parkinson's disease and other synucleinopathies. *Clin Chim Acta* **466**, 152-159 (2017). https://doi.org:10.1016/j.cca.2017.01.010

7.5 Elevated Aβ aggregates in feces from Alzheimer's disease patients: a proof-of-concept study

Autoren:	Marlene Pils, Alexandra Dybala, Anja Schaffrath, Fabian Rehn, Janine Kutzsche, Lara Blömeke, Markus Tusche, Pelin Özdüzenciler, Tuyen Bujnicki, Victoria Kraemer-Schulien, Hannes Gramespacher, Maximilian H.T. Schmieschek, Michael T. Barbe, Oezguer A. Onur, Gereon R. Fink, Gültekin Tamgüney, Oliver Bannach und Dieter Willbold
Journal:	Alzheimer's Research and Therapy (im Review)
DOI:	/
Impact-Faktor:	9.0 (2022)
Beitrag:	Eigenanteil: 10 % Etablierung des Aggregationsprotokolls und des Protokolls für die Immunodepletion im sFIDA Unterstützung bei der analytischen Validierung und Statistik Diskussion der Ergebnisse Prüfung des Manuskripts

Elevated Aβ aggregates in feces from Alzheimer's disease patients - a proof-of-concept study

Supplementary Information

Marlene Pils, Alexandra Dybala, Anja Schaffrath, Fabian Rehn, Janine Kutzsche, Lara Blömeke, Markus Tusche, Pelin Özdüzenciler, Tuyen Bujnicki, Victoria Kraemer-Schulien, Hannes Gramespacher, Maximilian H.T. Schmieschek, Michael T. Barbe, Oezguer A. Onur, Gereon R. Fink, Gültekin Tamgüney[3], Oliver Bannach and Dieter Willbold[*]

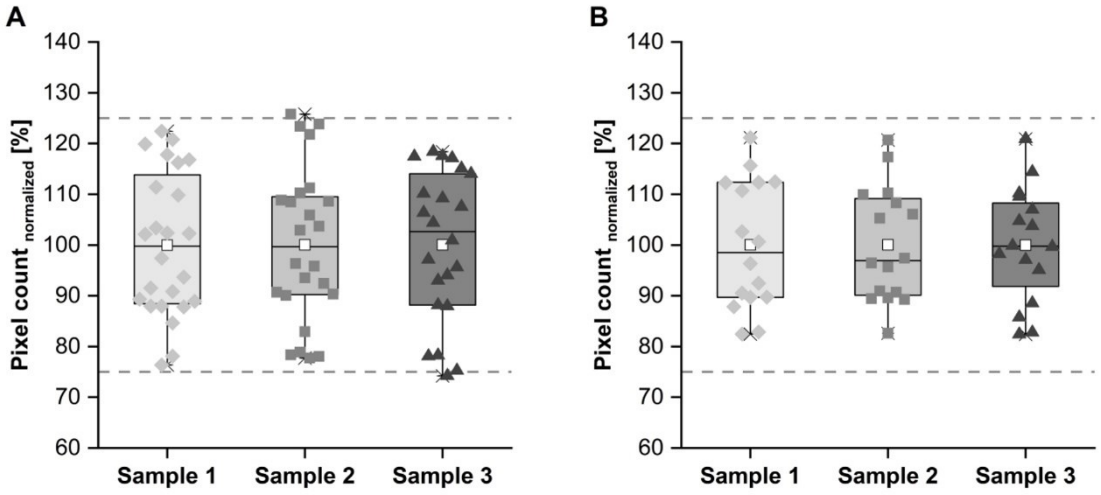

Figure S1. Evaluation of the reproducibility of sample homogenization and dilution for three different fecal samples, related to Results. (**A**) To evaluate the reproducibility of sample homogenization, we prepared six identical aliquots from each of three different fecal samples. Each homogenate was diluted 1:5 and was measured by sFIDA in 4-fold replicates, and reproducibility was determined based on normalized pixel counts. Consequently, there were 24 data points per box for each of the three samples (except for sample 3, where only 22 data points were available due to measurement artifacts in the affected wells). Intra-assay variances described by CV% of about 15% were recorded for all three samples confirming the reproducibility of the homogenization procedure. Based on documented sample weight, a precision of 98.6% and a trueness of 99.4% were calculated for the Simplix tubes. (**B**) We prepared a 1:5 dilution of each sample homogenate four times and subjected each dilution to sFIDA in quadruplicates. In general, we observed a high reproducibility with normalized pixel counts of the three fecal samples not exceeding the predefined tolerance range of ± 25% and showing low intra-assay variance (CV% of sample 1: 12.6%, samples 2 and 3: 11.3% each). For all replicates, a precision of 88.3% was determined, indicating a high reproducibility of the sample dilution (tolerance range 80−120%). Box plots include the median as a line and the mean as a square. The tolerance range of ± 25% is depicted as dashed gray lines. sample 1 = diamonds, low readout; sample 2 = squares, intermediate readout, and sample 3 = triangles, high readout.

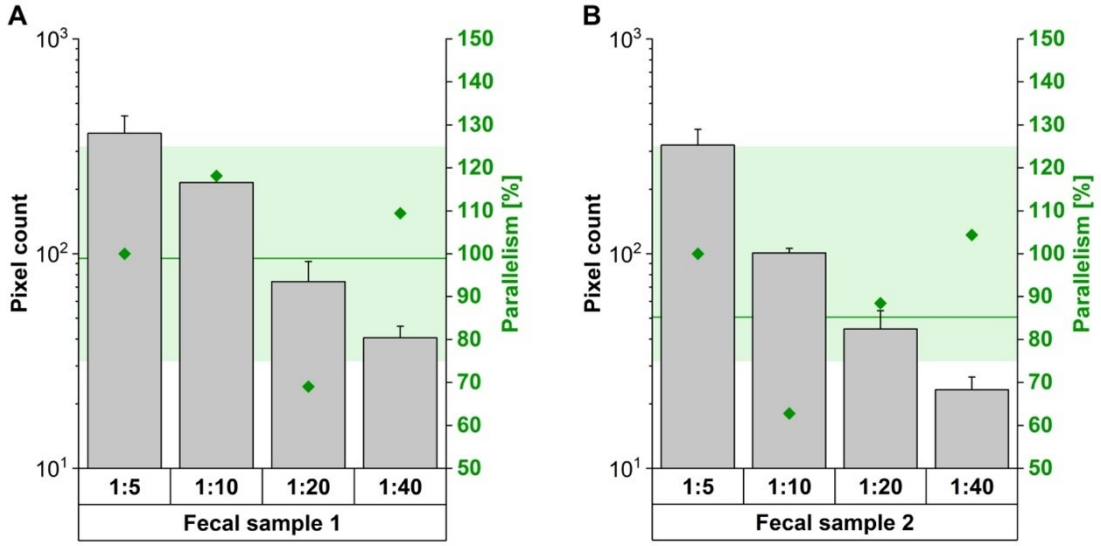

Figure S2. Parallelism of endogenous Aβ aggregates in fecal sample 1 and sample 2, related to Results. We performed a parallelism study using two fecal samples (sample 1 (**A**), sample 2 (**B**) with high endogenous Aβ aggregate concentrations to test whether samples can be diluted linearly. The pixel counts (left y-axis, gray bars) and the calculated percent parallelism (dilution linearity, right y-axis, dark green diamonds) were plotted against the used sample dilution. The acceptance range for percent parallelism was 75−125%, indicated by light green background shading. Mean percent dilution linearities of 99.9%, for sample 1, and 85.2%, for sample 2, were observed, although two values exceeded the lower tolerance limit (1:20 dilution of sample 1, 1:10 dilution of sample 2). Thus, we can exclude strong interferences due to, e.g., heterophilic antibodies, which typically affect dilution linearity (Park & Kricka, 2013). Consequently, samples with a high Aβ aggregate level can be diluted within a linear range and yield reliable results. Data are represented as mean with standard deviation.

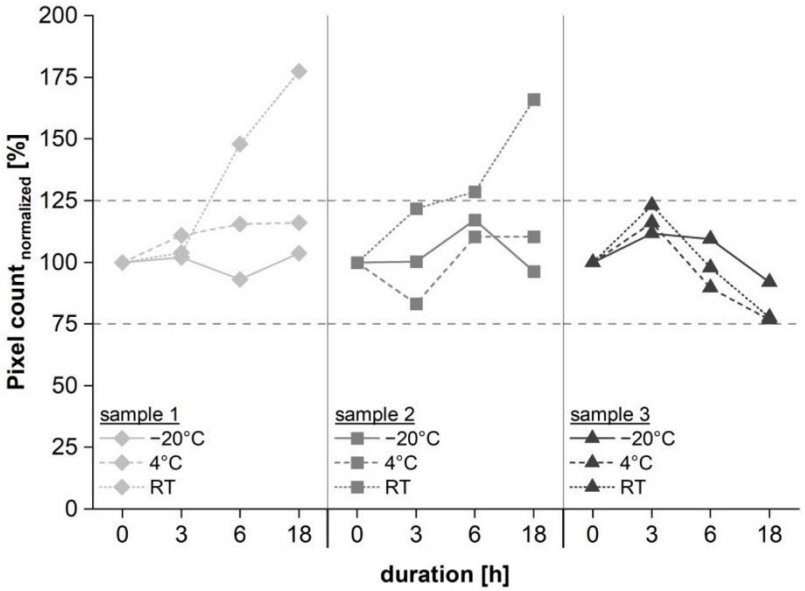

Figure S3. Evaluation of thermostability during transport or bench-top handling, related to Results and Figure 2. To investigate thermostability, three crude fecal samples (sample 1 = diamonds, low readout; sample 2 = square, intermediate readout; sample 3 = triangle, high readout) were stored at −20 °C, 4 °C or 20 °C for 3, 6, or 18 h before they were frozen at −80 °C. Afterward, crude samples were homogenized, diluted 1:5 with sample buffer, and subjected to sFIDA analysis in quadruplicates. Normalized pixel counts were calculated using a non-stressed reference sample and plotted against storage time. Dashed lines indicate the tolerance range of ± 25%. Because none of the samples showed normalized pixel counts outside the tolerance, we assumed that sample stability at −20 °C and 4 °C is not affected within the analyzed time period of 3 to 18h. In contrast, simulated transport or bench-top handling at 20 °C exceeded the tolerance limit after 3 h (sample 1 and sample 2). A signal increase was observed for both samples, which can be explained by increasing autofluorescence caused by decay processes and bacterial growth at this temperature. Consequently, we have decided not to transport or handle the sample at RT and adapted the sFIDA procedure accordingly, i.e., by sufficiently cooling the fecal samples during the preanalytics.

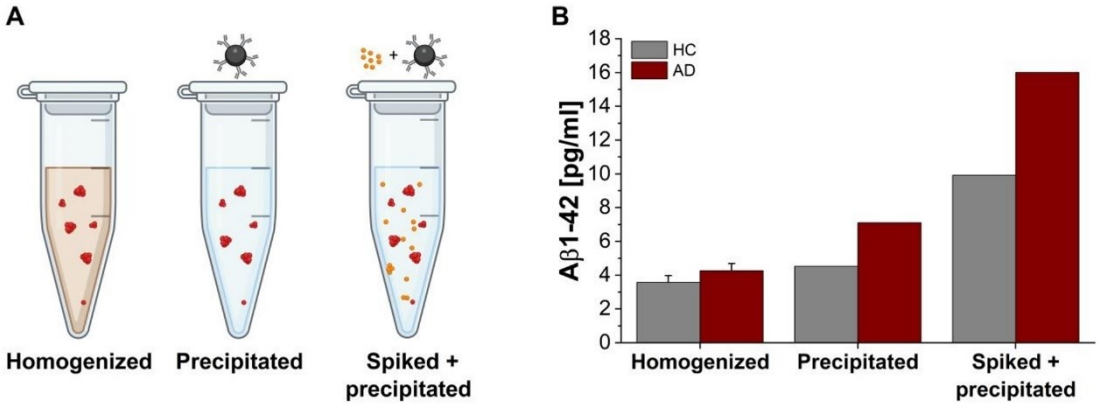

Figure S4. Schematic illustration of sample treatment and confirming the presence of fecal Aβ species in those samples using ELISA, related to Results. To determine total Aβ (monomers and aggregates) in feces, two samples (gray: HC, red: AD patient) were analyzed using a human amyloid β (1−42) ELISA Assay kit (IBL International, Hamburg, Germany). While this ELISA was developed for plasma, CSF, and cell culture supernatants (IBL-international, 2016), it should at least be applicable for the qualitative detection of Aβ in the feces. We tested the effect of different sample treatments ("homogenized", "precipitated", and "spiked + precipitated", schematic illustration in (**A**), *created with BioRender.com*.) on the discrimination between AD and HC. Signals (**B**) could be detected in those samples that were only homogenized, but no differentiation between both samples was possible. Sensitivity could only be increased by accumulation and elimination of the matrix by immunoprecipitation. This difference between control and AD could be further enhanced by adding Aβ1−42 as the substrate for the seeding process. NOTE. For the immunoprecipitation, a total of 1.5 g feces per donor were required to obtain 100 µL supernatant. Due to the limited amount of feces, only a single determination by ELISA was possible. Therefore, no standard deviation is shown. In case of homogenized samples, data are represented as mean with standard deviation.

Table S1. Results of normal distribution tests for molar Aβ aggregate concentrations in fecal samples, related to Results.

Normal distribution test	All samples	AD samples	HC samples
Shapiro−Wilk	$2.51*10^{-14}$	$3.37*10^{-8}$	0.003
Lilliefors	$3.99*10^{-19}$	$9.71*10^{-7}$	0.109
Kolmogorov Smirnov	$1.24*10^{-6}$	0.012	0.513
Anderson−Darling	$7.11*10^{-31}$	$6.43*10^{-12}$	0.018

[a]Abbreviations: AD, Alzheimer's disease; HC, healthy controls

Table S2. The coefficient of variation, calculated calibration curve, coefficient of determination and the limit of detection of each experiment for Aβ-coated SiNaPs, IQC samples, and fecal samples, related to Results.

	Experiment 1	**Experiment 2**	**Mean**
CV%	S: 11.54	S: 15.15	S: 13.35
	I: 10.91	I: 11.30	I: 11.11
	F: 19.36	F: 18.13	F: 18.74
Calibration curve	Range: 0.32 fM − 1026 fM	Range: 1.03 fM − 1026 fM	-
	y = 1.536x + 6.984	y = 1.118x + 10.88	-
	R^2 = 0.9709	R^2 = 0.9886	R^2 = 0.9798
LoD [fM]	2.27	1.09	1.68

[a]NOTE. CV% are defined as the ratio of standard deviation and the mean of the respective sample quadruplicates. The calibration curve was calculated based on the pixel counts of Aβ-coated SiNaPs using linear regression (readouts were weighted with 1/readout).

[b]Abbreviations: CV%, coefficient of variation; S, Aβ-coated SiNaPs; I, IQC samples; F, fecal samples; R^2, coefficients of determination; LoD, the limit of detection.

Table S3. Clinical information, Bristol scale scores, and mean Aβ-aggregate concentrations with the standard deviation of the individual subjects, related to Results, Figure 5B and Figure 5C.

Sample	Cohort	Cognition	Clinical symptoms	Bristol scale	Fecal Aβ aggregate concentration ± SD [fM]
1	AD	impaired	MCI	5	1852.5 ± 174.7
2	AD	impaired	dementia	4	3430.8 ± 773.7
3	AD	impaired	MCI	4	50.9 ± 3.53
4	AD	impaired	MCI	5	49 ± 6.31
5	AD	impaired	MCI	3	49.4 ± 8.63
6	AD	impaired	dementia	3	798.9 ± 364.6
7	AD	impaired	MCI	5	322.4 ± 45.6
8	AD	impaired	MCI	5	273.3 ± 33.9
9	AD	impaired	MCI	5	40.1 ± 3.78
10	AD	impaired	MCI	3	28.7 ± 3.97
11	AD	impaired	MCI	4	139.7 ± 44.1
12	AD	impaired	dementia	4	215.3 ± 26.2
13	AD	impaired	MCI	5	462.9 ± 143.9
14	AD	impaired	MCI	3	120.6 ± 15.7
15	AD	impaired	MCI	5	45.5 ± 6.66
16	AD	impaired	MCI	4	53.6 ± 12.4
17	AD	impaired	dementia	4	387.1 ± 46.2
18	AD	impaired	MCI	4	268.7 ± 48.4
19	AD	impaired	MCI	4	665.9 ± 312.8
20	AD	impaired	MCI	5	65.6 ± 4.59
21	AD	impaired	MCI	3	15.5 ± 1.66
22	AD	impaired	MCI	6	165.2 ± 46.4
23	AD	impaired	MCI	6	40.3 ± 4.51
24	AD	impaired	MCI	4	111.5 ± 11.6
25	AD	impaired	MCI	5	62.6 ± 12.5
26	AD	impaired	MCI	6	2.2 ± 0.24
27	HC	normal	-	5	104 ± 25.7
28	HC	normal	-	6	190.7 ± 53.2
29	HC	normal	-	5	49.2 ± 8
30	HC	normal	-	5	73.3 ± 6.7
31	HC	normal	-	5	73.6 ± 7.9
32	HC	normal	-	5	72.9 ± 22.2
33	HC	normal	-	4	27.4 ± 3.9
34	HC	normal	-	4	114.9 ± 27.3
35	HC	normal	-	3	46.2 ± 14.5
36	HC	normal	-	5	45.7 ± 9

37	HC	normal	-	5	89.6 ± 15.4
38	HC	normal	-	5	64 ± 12.4
39	HC	normal	-	6	45.4 ± 5.7
40	HC	normal	-	6	86.7 ± 15
41	HC	normal	-	6	62.7 ± 12.1
42	HC	normal	-	5	22.6 ± 4.4
43	HC	normal	-	6	23.9 ± 7.1
44	HC	normal	-	6	56.6 ± 12.7
45	HC	normal	-	5	58 ± 14.7
46	HC	normal	-	6	198.5 ± 49.6
47	HC	normal	-	4	67.1 ± 7.4
48	HC	normal	-	6	32.9 ± 5.8
49	HC	normal	-	5	99.3 ± 20.2
50	HC	normal	-	4	11.3 ± 3.2
51	HC	normal	-	5	5.1 ± 1.2
52	HC	normal	-	5	96.4 ± 16.6
53	HC	normal	-	6	15.6 ± 2
54	HC	normal	-	6	33.2 ± 4.6
55	HC	normal	-	6	36.3 ± 6.5
56	HC	normal	-	5	13.6 ± 1.6
57	HC	normal	-	4	1.3 ± 0.5

[a]Abbreviations: AD, Alzheimer's disease; MCI, mild cognitive impairment; HC, healthy controls; SD, standard deviation.

Table S4. Spearman coefficient of correlation values for the analyses between fecal Aβ aggregate levels and seven fecal biomarkers indicating gut inflammation and increased permeability of intestinal membranes (bile acid, lipids, calprotectin, IgA, α-1-antitrypsin, hemoglobin, and albumin), related to Results.

Biomarker	Bile acid	Lipids	Calpro-tectin	IgA	α1-Anti-trypsin	Hemo-globin	Albumin	Aβ aggregates
Bile acid	1	0.5181*	−0.1580	−0.1596	−0.0164	0.2236	0.0039	−0.1108
Lipids		1	−0.2998	0.0778	−0.2737	0.0854	0.1134	−0.3805
Calprotectin			1	0.5941*	0.5845*	0.4669	0.5911*	0.1489
IgA				1	0.2336	0.2423	0.6071*	−0.0118
α1-Antitrypsin					1	0.3872	0.0731	0.3564
Hemoglobin						1	0.5965*	−0.0121
Albumin							1	−0.3665
Aβ aggregates								1

[a]NOTE. Significant correlations are indicated by * p: ≤ 0.05.

Table S5. *p*-values of two-sided Mann−Whitney U test for pairwise comparisons of measured fecal biomarker concentrations, related to Results.

Biomarker	AD (n = 7)	HC (n = 8)	*p*-value
Bile acid [mmol/100 g]	350 ± 91.7	272 ± 70.5	0.1321
Lipids wt%	1.6 ± 0.7	1.6 ± 0.6	0.8608
Calprotectin [µg/g]	40.3 ± 27.5	53.5 ± 32.5	0.3524
IgA [µg/g]	1444 ± 2041	1716 ± 1433	0.2699
α1-Antitrypsin [µg/g]	39.1 ± 22.7	61.8 ± 47.6	0.1753
Hemoglobin [µg/g]	0.3 ± 0	0.4 ± 0.3	0.2036
Albumin [µg/g]	4.1 ± 2.0	9.8 ± 10.9	0.1870

[a]NOTE. No significant differences of fecal biomarker concentrations between AD patients and HC were found. [b]Abbreviations: AD, Alzheimer's disease; HC, healthy controls.

Supplemental References

IBL-international. (2016). *Amyloid-beta (1-42) (FL) ELISA Instruction for use Code No. 27719, version 2.*

Park, J. Y., & Kricka, L. J. (2013). Chapter 5.3 - Interferences in Immunoassay. In D. Wild (Ed.), *The Immunoassay Handbook (Fourth Edition)* (pp. 403-416). Elsevier. https://doi.org/https://doi.org/10.1016/B978-0-08-097037-0.00027-0

7.6 Patients with isolated REM-sleep behavior disorder have elevated levels of alpha-synuclein aggregates in stool

Autoren:	Anja Schaffrath, Sophia Schleyken, Aline Seger, Hannah Jergas, Pelin Özdüzenciler, Marlene Pils, Lara Blömeke, Annelise Cousin, Johannes Willbold, Tuyen Bujnicki, Oliver Bannach, Gereon R. Fink, Dieter Willbold, Michael Sommerauer, Michael T. Barbe, Gültekin Tamgüney
Journal:	npj parkinson's disease (veröffentlicht)
DOI:	10.1038/s41531-023-00458-4
Impact-Faktor:	8,7 (2022)
Beitrag:	Eigenanteil: 10 % Etablierung des Protokolls der Immundepletion im sFIDA Synthese der Silika-Nanopartikel Diskussion der Ergebnisse Prüfung des Manuskripts

Patients with isolated REM-sleep behavior disorder have elevated levels of alpha-synuclein aggregates in stool

Anja Schaffrath[1], Sophia Schleyken[2], Aline Seger[2], Hannah Jergas[2], Pelin Özdüzenciler[1], Marlene Pils[1,3], Lara Blömeke[1,3], Anneliese Cousin[1], Johannes Willbold[1], Tuyen Bujnicki[1], Oliver Bannach[1,3,4], Gereon R. Fink[2,5], Dieter Willbold[1,4], Michael Sommerauer[2,5], Michael T. Barbe[2], Gültekin Tamgüney[1,4]

SUPPLEMENTARY RESULTS

Supplementary Table 1 Demographic and clinical information and concentrations of α-synuclein aggregates in stool of individual subjects

Sample	*Diagnosis*	*Sex*	*Age at sampling [years]*	*Age at onset [years]*	*Disease duration [years]*	*Education [years]*	*CCCSS score*	*DemTect score*	*NMSS score*	*MDS-UDPRS III score*	*Scent score*	*Hoehn and Yahr score*	*Levodopa challenge test [% change]*	*DaTSCAN score*	*Screening questionnaire PD score*	*RBDSQ score*	*α-Synuclein aggregate concentration ± SD [fM]*
1	PD	Male	73	60	13	18	9	13	37	22	4	4	0.692	+	5	7	1.38 ± 0.22
2	PD	Male	68	54	14	10	10	13	17	27	6	3	0.333	N/A	6	10	0.88 ± 1.07
3	PD	Male	56	45	11	12	3	17	51	35	7	4	0.529	+	5	8	9.20 ± 2.85
4	PD	Male	71	61	10	17	1	11	67	65	8	5	0.239	+	9	6	104.73 ± 17.43
5	PD	Male	46	41	5	12	0	14	103	21	3	3	0.438	N/A	6	2	0.26 ± 0.25
6	PD	Male	72	57	15	19	6	14	54	28	5	5	0.469	N/A	4	5	0.98 ± 0.55
7	PD	Male	54	50	4	16	0	18	20	19	2	2	0.467	+	7	0	1.51 ± 0.88
8	PD	Female	71	49	22	12	4	9	67	20	9	3	0.481	N/A	9	4	5.58 ± 2.07
9	PD	Male	56	52	4	16	2	15	9	33	7	5	0.320	N/A	7	5	2.97 ± 0.73
10	PD	Male	62	50	12	20	0	18	9	10	2	2	0.462	+	8	3	4.28 ± 0.51
11	PD	Male	80	78	2	8	3	14	4	17	3	2	N/A	N/A	1	0	4.28 ± 1.87
12	PD	Female	78	63	15	11	18	17	48	76	2	5	0.431	N/A	6	4	108.40 ± 20.31
13	PD	Male	68	58	10	18	9	16	4	17	3	4	0.632	N/A	5	2	1.53 ± 0.73

14	PD	Female	80	66	14	13	11	13	34	25	7	4	0.528	+	7	1	0.40 ± 0.33
15	PD	Female	52	35	17	19	1	12	27	23	4	4	0.577	N/A	5	7	0.19 ± 0.08
16	PD	Female	74	60	14	17	9	10	21	50	2	5	0.323	N/A	9	6	4.28 ± 0.75
17	PD	Male	63	54	9	13	1	12	12	15	4	2	0.639	+	7	4	5.72 ± 0.89
18	PD	Male	74	62	12	12	3	11	21	8	0	2	0.320	N/A	2	3	10.52 ± 3.99
19	PD	Male	82	73	9	12	0	9	46	23	8	4	0.378	N/A	7	5	2.22 ± 0.39
20	PD	Female	50	39	11	14	2	11	16	22	7	2	0.459	+	5	2	1.14 ± 0.11
21	PD	Female	56	51	5	12	0	15	4	30	9	3	0.321	+	7	5	1.04 ± 0.48
22	PD	Female	60	51	9	17	3	17	16	16	7	2	0.423	+	7	2	0.60 ± 0.25
23	PD	Male	60	40	20	12	7	18	15	30	3	3	0.474	N/A	5	3	462.07 ± 46.48
24	PD	Male	57	39	18	15	7	12	42	41	6	3	0.400	+	5	8	7.56 ± 1.15
25	PD	Male	59	56	3	17	13	18	46	7	4	2	0.483	N/A	7	9	673.25 ± 19.52
26	PD	Female	58	58	0	20	2	18	52	16	1	2	N/A	+	0	11	2.52 ± 0.37
27	PD	Male	68	62	6	20	1	17	10	5	6	2	N/A	+	4	2	0.07 ± 0.06
28	PD	Male	76	74	2	13	1	11	21	35	6	3	N/A	N/A	6	8	2.49 ± 0.76
29	PD	Male	60	51	9	21	4	14	56	22	1	3	0.486	N/A	8	5	1.19 ± 0.30
30	PD	Male	59	54	5	19	4	18	28	33	6	3	N/A	+	7	12	3.87 ± 1.14
31	PD	Male	65	63	2	15	6	12	28	42	5	4	0.431	N/A	9	8	7.09 ± 0.54
32	PD	Male	41	40	1	22	2	18	7	11	10	2	N/A	+	2	3	6.89 ± 0.60
33	PD	Male	66	45	21	15	5	18	14	11	6	2	0.000	+	4	4	1.57 ± 0.52
34	PD	Female	60	50	10	13	12	13	27	19	6	3	0.429	+	8	7	3.51 ± 0.72

35	PD	Male	71	66	5	12	2	8	30	42	9	4	0.250	+	4	1	0.27 ± 0.09
36	PD	Male	58	54	4	15	2	11	42	10	8	3	0.692	N/A	7	6	1.30 ± 0.92
37	PD	Female	70	57	13	8	11	11	25	22	8	3	0.441	N/A	6	4	0.19 ± 0.03
38	PD	Male	55	41	14	9	12	7	30	50	6	4	0.447	N/A	8	6	1.32 ± 0.29
39	PD	Male	68	64	4	13	6	9	65	21	3	3	N/A	+	9	6	2.19 ± 0.35
40	PD	Male	78	71	7	18	7	10	10	19	7	3	N/A	+	8	12	45.51 ± 12.8
41	PD	Male	55	50	5	16	1	14	1	5	8	2	0.538	N/A	3	5	5.79 ± 2.57
42	PD	Female	49	44	5	15	5	18	13	9	8	3	0.000	N/A	7	3	1.47 ± 0.11
43	PD	Female	65	50	15	25	4	17	22	N/A	5	4	0.219	N/A	5	11	4.01 ± 0.43
44	PD	Male	41	37	4	20	3	14	17	18	6	3	N/A	+	6	1	2.78 ± 0.30
45	PD	Male	69	58	11	16	3	10	20	21	6	3	0.517	N/A	5	5	2.42 ± 0.28
46	PD	Male	63	53	10	13	8	14	21	13	10	2	0.313	+	7	8	4.61 ± 0.73
47	PD	Male	71	65	6	12	3	10	26	48	4	3	0.163	+	7	1	0.61 ± 0.38
48	PD	Female	78	64	14	20	6	18	23	30	4	3	0.286	N/A	7	2	28.42 ± 1.67
49	PD	Male	76	60	16	12	11	13	90	31	6	4	0.300	N/A	6	9	1.72 ± 0.22
50	PD	Male	55	55	0	30	0	17	2	5	7	2	N/A	+	1	3	10.82 ± 1.36
51	PD	Male	77	65	12	18	3	13	26	26	7	3	-0.023	N/A	4	8	57.33 ± 12.05
52	PD	Male	64	52	12	22	9	16	20	25	7	2	0.933	N/A	8	4	6.72 ± 1.13
53	PD	Male	83	73	10	22	8	18	36	54	5	4	N/A	N/A	6	7	28.19 ± 3.40
54	PD	Male	62	53	9	18	3	15	44	6	2	2	0.333	+	5	6	1.03 ± 1.01
55	PD	Female	70	63	7	14	0	12	18	13	6	3	0.368	N/A	8	4	3.82 ± 0.35

56	PD	Female	74	61	13	8	3	12	19	63	4	5	N/A	N/A	7	7	15.3 ± 0.73
57	PD	Female	77	50	27	13	1	18	67	30	2	4	0.567	N/A	9	7	48.39 ± 6.44
58	PD	Female	62	48	14	23	7	18	11	40	7	5	0.093	+	6	4	21.84 ± 2.24
59	PD	Female	75	49	26	16	2	9	36	25	2	3	N/A	N/A	5	4	2.97 ± 1.59
60	PD	Male	59	57	2	14	1	14	29	41	9	3	N/A	N/A	4	3	0.98 ± 0.48
61	PD	Male	68	58	10	14	0	18	24	24	0	2	0.609	N/A	7	4	16.89 ± 0.56
62	PD	Male	73	68	5	18	0	18	14	22	7	3	N/A	+	3	4	1.07 ± 0.07
63	PD	Male	57	49	8	15	1	14	13	10	9	2	0.545	N/A	3	2	10.23 ± 1.20
64	PD	Female	54	45	9	16	2	18	15	9	10	3	0.686	+	7	3	24.45 ± 9.80
65	PD	Female	57	45	12	12	2	18	122	26	7	2	0.720	N/A	8	7	27.74 ± 1.61
66	PD	Female	68	51	17	12	0	17	19	19	8	4	0.318	N/A	2	8	3.70 ± 0.30
67	PD	Female	64	57	7	20	8	13	59	21	8	3	0.629	N/A	8	11	0.23 ± 0.15
68	PD	Male	56	48	8	13	10	12	39	22	4	3	0.310	+	6	6	1.34 ± 0.68
69	PD	Female	74	73	1	17	2	15	15	16	8	3	N/A	+	6	9	119.51 ± 12.54
70	PD	Male	46	36	10	24	1	15	22	16	9	2	0.667	+	6	3	3.34 ± 0.58
71	PD	Female	69	56	13	11	7	15	51	28	4	3	0.415	N/A	7	6	0.43 ± 0.19
72	PD	Male	55	53	2	18	12	14	50	17	3	2	N/A	N/A	8	6	14.38 ± 9.20
73	PD	Male	78	60	18	17	2	12	36	59	3	5	N/A	N/A	7	5	14.16 ± 1.74
74	PD	Male	52	45	7	16	7	9	51	21	8	3	0.346	+	6	2	1.09 ± 0.48
75	PD	Female	57	55	2	15	2	18	12	6	6	3	0.733	+	1	1	49.21 ± 4.31
76	PD	Male	55	45	10	N/A	N/A	7	79	22	7	3	0.478	+	N/A	N/A	3.56 ± 1.25

77	PD	Male	60	57	3	10	0	12	55	36	2	3	N/A	+	1	1	7.97 ± 1.47
78	PD	Male	52	46	6	18	6	13	0	5	6	2	0.000	N/A	3	1	1.10 ± 0.57
79	PD	Male	51	40	11	14	7	8	10	31	4	4	0.485	+	5	5	10.30 ± 1.23
80	PD	Male	73	72	1	14	15	15	62	23	1	3	N/A	N/A	5	1	57.08 ± 5.86
81	PD	Male	66	55	11	12	0	14	51	13	7	2	N/A	+	4	2	4.46 ± 0.90
82	PD	Female	67	53	14	12	3	15	57	31	8	4	0.341	N/A	9	10	11.45 ± 1.64
83	PD	Male	72	66	6	13	1	15	13	12	5	3	N/A	N/A	7	9	20.57 ± 0.95
84	PD	Male	59	49	10	13	3	14	29	13	3	2	0.474	N/A	7	2	1.81 ± 0.66
85	PD	Male	74	68	6	8	2	9	6	42	6	N/A	0.543	N/A	4	1	0.13 ± 0.12
86	PD	Female	62	56	6	16	0	13	13	10	2	2	N/A	N/A	2	6	8.78 ± 0.89
87	PD	Male	71	64	7	19	0	18	18	29	3	3	N/A	N/A	5	1	0.60 ± 0.28
88	PD	Male	51	51	0	13	1	17	12	11	3	2	N/A	+	4	11	15.51 ± 2.65
89	PD	Female	57	56	1	14	3	13	24	6	8	2	N/A	+	5	4	1.34 ± 0.91
90	PD	Male	78	72	6	13	0	17	11	14	6	3	0.444	+	2	1	0.80 ± 0.41
91	PD	Male	62	59	3	22	1	14	13	7	7	2	N/A	+	2	3	40.25 ± 2.04
92	PD	Male	81	69	12	13	4	2	64	55	1	5	N/A	N/A	7	4	21.44 ± 1.33
93	PD	Male	64	63	1	18	0	13	12	4	2	2	N/A	+	3	3	151.19 ± 19.38
94	PD	Male	80	77	3	10	1	13	31	17	1	2	0.143	+	4	3	8.73 ± 1.92
95	iRBD	Male	56	N/A	N/A	21	2	17	6	1	11	N/A	N/A	N/A	0	6	10.01 ± 2.42
96	iRBD	Male	72	60	12	3	N/A	16	1	4	11	N/A	N/A	N/A	2	6	2.83 ± 1.15
97	iRBD	Male	61	N/A	N/A	16	N/A	14	4	5	11	N/A	N/A	N/A	0	6	10.99 ± 2.60

98	iRBD	Female	59	55	4	20	4	17	14	0	6	N/A	N/A	N/A	0	10	15.96 ± 1.49
99	iRBD	Male	78	N/A	N/A	14	N/A	17	15	4	8	N/A	N/A	N/A	0	10	6.04 ± 2.12
100	iRBD	Female	67	50	17	12	3	13	N/A	8	5	N/A	N/A	N/A	0	9	5.54 ± 1.44
101	iRBD	Male	63	63	0	16	2	17	3	5	10	N/A	N/A	N/A	0	8	0.74 ± 0.86
102	iRBD	Male	58	54	4	16	0	13	N/A	6	9	N/A	N/A	N/A	0	10	8.37 ± 1.95
103	iRBD	Female	64	61	3	21	0	15	N/A	3	3	N/A	N/A	N/A	0	7	4.34 ± 0.80
104	iRBD	Male	64	63	1	15	4	11	N/A	2	7	N/A	N/A	+	0	8	4.12 ± 0.80
105	iRBD	Male	70	60	10	N/A	0	14	12	5	10	N/A	N/A	N/A	0	12	5.11 ± 1.11
106	iRBD	Male	66	52	14	17	0	12	4	5	7	N/A	N/A	+	0	11	5.9 ± 0.68
107	iRBD	Male	73	71	2	N/A	N/A	12	2	4	6	N/A	N/A	N/A	N/A	N/A	24.42 ± 5.82
108	iRBD	Female	65	60	5	16	1	17	6	3	5	N/A	N/A	+	0	9	2.90 ± 0.83
109	iRBD	Male	72	62	10	11	2	14	N/A	5	9	N/A	N/A	+	0	N/A	7.87 ± 1.34
110	iRBD	Male	75	72	3	18	2	14	8	7	3	N/A	N/A	N/A	0	7	126.81 ± 19.12
111	iRBD	Male	69	64	5	14	0	17	9	4	8	N/A	N/A	+	0	12	1.10 ± 0.33
112	iRBD	Female	66	62	4	15	5	18	2	3	9	N/A	N/A	N/A	0	5	18.92 ± 2.02
113	iRBD	Male	59	56	3	19	3	9	22	5	7	N/A	N/A	+	0	9	32.97 ± 3.34
114	iRBD	Male	75	66	9	18	0	17	1	5	7	N/A	N/A	N/A	0	11	16.64 ± 2.23
115	iRBD	Male	55	40	15	21	0	11	0	8	12	N/A	N/A	N/A	0	5	6.29 ± 0.68
116	iRBD	Male	69	66	3	15	8	12	N/A	13	7	N/A	N/A	+	0	11	3.26 ± 0.44
117	iRBD	Male	54	49	5	12	5	12	48	3	8	N/A	N/A	+	5	13	19.17 ± 4.96
118	iRBD	Male	74	72	2	16	0	15	N/A	6	7	N/A	N/A	N/A	0	10	3.82 ± 0.69

119	iRBD	Male	66	61	5	15	3	18	21	7	6	N/A	N/A	N/A	0	10	0.93 ± 0.28
120	iRBD	Male	70	63	7	20	2	13	31	8	1	N/A	N/A	N/A	1	5	6.08 ± 0.29
121	iRBD	Male	67	50	17	13	0	17	2	10	7	N/A	N/A	N/A	0	10	4.15 ± 1.32
122	iRBD	Male	67	56	11	17	0	17	3	4	9	N/A	N/A	+	0	10	8.14 ± 1.95
123	iRBD	Male	62	47	15	31	4	14	N/A	5	9	N/A	N/A	+	1	9	7.49 ± 1.43
124	iRBD	Male	70	N/A	N/A	15	0	18	1	4	7	N/A	N/A	N/A	0	5	4.10 ± 0.48
125	iRBD	Female	63	62	1	19	12	14	N/A	0	4	N/A	N/A	N/A	0	8	4.64 ± 4.76
126	iRBD	Male	75	55	20	15	6	13	N/A	4	8	N/A	N/A	+	1	8	35.60 ± 2.14
127	iRBD	Male	67	61	6	16	5	13	23	1	3	N/A	N/A	N/A	0	11	17.04 ± 3.11
128	iRBD	Male	70	67	3	22	3	14	N/A	3	3	N/A	N/A	+	1	10	64.72 ± 3.37
129	iRBD	Male	74	72	2	12	2	11	N/A	5	5	N/A	N/A	N/A	0	7	5.35 ± 1.06
130	iRBD	Male	58	53	5	13	9	14	N/A	7	5	N/A	N/A	+	3	11	2.55 ± 0.47
131	iRBD	Female	77	66	11	16	1	15	4	5	10	N/A	N/A	N/A	0	12	15.40 ± 2.58
132	iRBD	Female	59	55	4	16	1	15	N/A	4	10	N/A	N/A	N/A	0	7	24.68 ± 1.03
133	iRBD	Male	68	60	8	18	2	18	N/A	4	7	N/A	N/A	N/A	0	9	4.34 ± 0.84
134	iRBD	Male	63	N/A	N/A	N/A	N/A	18	N/A	2	7	N/A	N/A	N/A	N/A	N/A	5.34 ± 0.62
135	iRBD	Male	64	62	2	12	5	14	102	5	10	N/A	N/A	N/A	0	13	2.89 ± 0.53
136	iRBD	Male	61	50	11	16	6	18	76	5	9	N/A	N/A	+	0	12	147.61 ± 8.84
137	iRBD	Male	64	60	4	N/A	N/A	11	9	2	5	N/A	N/A	N/A	N/A	N/A	96912.87 ± 14905.2
138	iRBD	Male	66	63	3	12	3	13	2	5	7	N/A	N/A	N/A	0	4	10.42 ± 1.18
139	iRBD	Male	63	62	1	15	2	14	9	0	3	N/A	N/A	N/A	0	5	46.81 ± 3.15

140	iRBD	Male	61	51	10	25	1	15	6	3	5	N/A	N/A	+	1	12	223.93 ± 16.15
141	iRBD	Male	58	54	4	15	2	17	6	1	6	N/A	N/A	+	0	3	5.30 ± 0.66
142	iRBD	Male	63	55	8	13	9	11	8	3	0	N/A	N/A	N/A	0	11	12.89 ± 0.74
143	iRBD	Male	59	47	12	22	2	14	5	2	9	N/A	N/A	N/A	0	11	1.99 ± 1.39
144	iRBD	Male	73	63	10	17	0	12	1	1	8	N/A	N/A	N/A	0	8	36.79 ± 4.54
145	iRBD	Male	69	54	15	18	8	18	14	0	6	N/A	N/A	+	0	10	30.49 ± 7.58
146	iRBD	Male	60	N/A	N/A	N/A	N/A	12	15	3	7	N/A	N/A	N/A	N/A	N/A	10.48 ± 4.54
147	iRBD	Male	63	53	10	17	0	18	25	3	2	N/A	N/A	N/A	0	7	1.46 ± 0.83
148	iRBD	Male	60	50	10	15	2	17	7	2	7	N/A	N/A	+	0	2	28.32 ± 4.72
149	iRBD	Male	74	71	3	19	1	18	18	9	9	N/A	N/A	+	0	12	6.67 ± 1.46
150	iRBD	Male	56	53	3	N/A	N/A	14	17	2	10	N/A	N/A	N/A	N/A	N/A	7.65 ± 0.55
151	iRBD	Male	72	58	14	8	1	17	12	1	5	N/A	N/A	N/A	0	12	59941.25 ± 16328
152	iRBD	Male	65	61	4	13	1	18	6	3	4	N/A	N/A	N/A	0	7	30.55 ± 1.42
153	iRBD	Male	74	68	6	12	6	15	13	2	6	N/A	N/A	N/A	0	10	19.34 ± 2.84
154	iRBD	Male	72	57	15	17	0	14	19	5	5	N/A	N/A	N/A	0	10	59.57 ± 4.69
155	iRBD	Male	67	65	2	11	4	12	11	1	3	N/A	N/A	+	0	6	24.92 ± 4.06
156	iRBD	Male	80	60	20	19	0	14	15	7	6	N/A	N/A	N/A	0	7	5.98 ± 2.15
157	iRBD	Male	68	63	5	18	6	15	40	2	4	N/A	N/A	+	0	12	18.98 ± 4.67
158	iRBD	Female	77	70	7	13	6	14	24	4	6	N/A	N/A	+	1	7	24.75 ± 1.54
159	iRBD	Male	74	69	5	17	1	14	16	2	0	N/A	N/A	N/A	0	11	100.09 ± 8.34
160	iRBD	Male	69	64	5	13	4	15	21	7	4	N/A	N/A	N/A	0	10	23.66 ± 1.97

161	iRBD	Male	60	59	1	11	3	16	29	1	4	N/A	N/A	N/A	1	13	0.94 ± 0.82
162	iRBD	Male	61	59	2	N/A	N/A	18	15	2	8	N/A	N/A	N/A	N/A	N/A	58.18 ± 5.88
163	iRBD	Male	57	38	19	17	0	15	38	3	7	N/A	N/A	N/A	0	12	10.91 ± 1.89
164	iRBD	Female	56	50	6	13	4	17	27	2	9	N/A	N/A	N/A	1	12	2.87 ± 0.87
165	iRBD	Male	68	48	20	N/A	N/A	11	40	N/A	7	N/A	N/A	N/A	N/A	N/A	1.29 ± 0.14
166	iRBD	Male	76	70	6	15	3	15	18	12	10	N/A	N/A	N/A	1	11	146.32 ± 6.96
167	HC	Male	18	N/A	N/A	12	3	15	N/A	N/A	10	N/A	N/A	N/A	0	2	4.29 ± 2.43
168	HC	Male	62	N/A	N/A	18	0	14	N/A	N/A	10	N/A	N/A	N/A	0	3	3.57 ± 2.43
169	HC	Male	70	N/A	N/A	16	7	10	N/A	N/A	11	N/A	N/A	N/A	0	0	33.19 ± 3.44
170	HC	Female	58	N/A	N/A	16	0	17	N/A	N/A	11	N/A	N/A	N/A	0	0	80.06 ± 24.21
171	HC	Female	74	N/A	N/A	11	4	12	N/A	N/A	10	N/A	N/A	N/A	1	1	73.96 ± 4.57
172	HC	Male	70	N/A	N/A	12	0	12	N/A	N/A	10	N/A	N/A	N/A	0	1	45.82 ± 2.48
173	HC	Female	55	N/A	N/A	15	1	18	N/A	N/A	11	N/A	N/A	N/A	0	1	2.03 ± 1.35
174	HC	Female	20	N/A	N/A	14	4	15	N/A	N/A	11	N/A	N/A	N/A	0	1	5.24 ± 0.46
175	HC	Female	20	N/A	N/A	14	5	16	N/A	N/A	10	N/A	N/A	N/A	0	3	6.01 ± 1.70
176	HC	Female	78	N/A	N/A	12	4	18	N/A	N/A	11	N/A	N/A	N/A	0	3	28.93 ± 4.84
177	HC	Female	66	N/A	N/A	14	0	17	N/A	N/A	11	N/A	N/A	N/A	0	3	13.36 ± 2.41
178	HC	Male	75	N/A	N/A	18	0	14	27	N/A	11	N/A	N/A	N/A	0	0	17.56 ± 1.81
179	HC	Male	74	N/A	N/A	10	2	13	8	N/A	10	N/A	N/A	N/A	0	0	1.74 ± 0.19
180	HC	Female	70	N/A	N/A	11	0	18	9	N/A	11	N/A	N/A	N/A	3	2	5.78 ± 1.81
181	HC	Female	63	N/A	N/A	20	4	18	1	N/A	11	N/A	N/A	N/A	0	2	4.15 ± 0.37

182	HC	Female	66	N/A	N/A	18	7	18	10	N/A	12	N/A	N/A	N/A	0	2	6.66 ± 0.43
183	HC	Male	34	N/A	N/A	16	7	17	1	N/A	11	N/A	N/A	N/A	0	1	51.35 ± 0.81
184	HC	Female	72	N/A	N/A	18	1	18	10	N/A	10	N/A	N/A	N/A	1	0	13.00 ± 2.49
185	HC	Male	77	N/A	N/A	23	5	15	0	N/A	11	N/A	N/A	N/A	0	2	6.84 ± 0.90
186	HC	Female	60	N/A	N/A	16	0	18	18	N/A	12	N/A	N/A	N/A	0	4	2.93 ± 1.01
187	HC	Female	64	N/A	N/A	13	2	18	N/A	N/A	N/A	N/A	N/A	N/A	1	2	19.37 ± 1.97
188	HC	Female	61	N/A	N/A	14	2	17	3	N/A	8	N/A	N/A	N/A	0	1	12.08 ± 1.34
189	HC	Male	36	N/A	N/A	20	0	18	4	N/A	11	N/A	N/A	N/A	0	1	0.84 ± 0.25
190	HC	Male	62	N/A	N/A	13	1	N/A	N/A	N/A	N/A	N/A	N/A	N/A	2	2	0.68 ± 0.22
191	HC	Female	60	N/A	N/A	20	0	18	18	N/A	2	N/A	N/A	N/A	0	0	0.86 ± 0.38
192	HC	Male	52	N/A	N/A	15	0	14	4	N/A	10	N/A	N/A	N/A	0	0	2.01 ± 0.23
193	HC	Female	66	N/A	N/A	19	2	15	1	N/A	10	N/A	N/A	N/A	0	0	38.59 ± 4.2
194	HC	Female	63	N/A	N/A	12	4	17	34	N/A	11	N/A	N/A	N/A	0	0	1.20 ± 0.10
195	HC	Male	59	N/A	N/A	16	1	N/A	11	N/A	11	N/A	N/A	N/A	0	2	0.30 ± 0.24
196	HC	Female	71	N/A	N/A	16	11	18	15	N/A	11	N/A	N/A	N/A	0	4	14.93 ± 4.15
197	HC	Female	70	N/A	N/A	12	0	17	16	N/A	6	N/A	N/A	N/A	0	4	70.07 ± 10.59
198	HC	Female	48	N/A	N/A	17	1	18	1	N/A	11	N/A	N/A	N/A	0	0	3.55 ± 1.91
199	HC	Male	65	N/A	N/A	18	2	18	4	N/A	11	N/A	N/A	N/A	0	2	0.40 ± 0.09
200	HC	Male	72	N/A	N/A	22	1	13	14	N/A	7	N/A	N/A	N/A	0	3	1.58 ± 0.47
201	HC	Female	50	N/A	N/A	15	2	18	18	N/A	11	N/A	N/A	N/A	0	5	1.42 ± 0.82
202	HC	Male	43	N/A	N/A	21	0	14	0	N/A	10	N/A	N/A	N/A	0	0	7.07 ± 1.02

203	HC	Male	57	N/A	N/A	22	0	15	3	N/A	11	N/A	N/A	N/A	0	1	1.56 ± 0.16
204	HC	Female	69	N/A	N/A	21	0	16	2	N/A	7	N/A	N/A	N/A	0	0	1.47 ± 0.14
205	HC	Female	48	N/A	N/A	13	3	17	3	N/A	12	N/A	N/A	N/A	0	0	10.77 ± 1.16
206	HC	Female	39	N/A	N/A	18	4	15	3	N/A	11	N/A	N/A	N/A	0	0	119.64 ± 11.56
207	HC	Female	42	N/A	N/A	17	3	18	21	N/A	11	N/A	N/A	N/A	0	0	3.28 ± 0.34
208	HC	Female	53	N/A	N/A	15	1	17	2	N/A	11	N/A	N/A	N/A	0	3	2.67 ± 0.43
209	HC	Female	24	N/A	N/A	18	6	17	18	N/A	11	N/A	N/A	N/A	2	1	1.15 ± 0.58
210	HC	Female	52	N/A	N/A	15	4	13	46	N/A	11	N/A	N/A	N/A	0	4	1.14 ± 1.24
211	HC	Female	20	N/A	N/A	14	8	18	10	N/A	12	N/A	N/A	N/A	0	5	5.54 ± 1.23
212	HC	Male	78	N/A	N/A	12	0	13	32	N/A	N/A	N/A	N/A	N/A	1	5	2.82 ± 0.96
213	HC	Male	26	N/A	N/A	13	0	18	2	N/A	11	N/A	N/A	N/A	0	0	4.18 ± 0.92
214	HC	Male	38	N/A	N/A	17	3	17	0	N/A	12	N/A	N/A	N/A	0	3	292.79 ± 91.38
215	HC	Female	81	N/A	N/A	13	4	10	71	N/A	12	N/A	N/A	N/A	4	5	35.53 ± 9.47
216	HC	Female	61	N/A	N/A	23	5	18	16	N/A	9	N/A	N/A	N/A	1	1	6.87 ± 1.11
217	HC	Male	64	N/A	N/A	18	3	13	20	N/A	11	N/A	N/A	N/A	0	2	0.93 ± 0.45

PD, Parkinson's disease; iRBD, isolated rapid eye movement sleep behavior disorder; HC, healthy control; CCCSS, Cleveland Clinic Constipation Scoring System; NMSS, Non-Motor Symptoms Scale; MDS-UPDRS III, Movement Disorder Society's Unified Parkinson's Disease Rating Scale Part III; RBDSQ, iRBD screening questionnaire; SD, standard deviation; N/A, not available

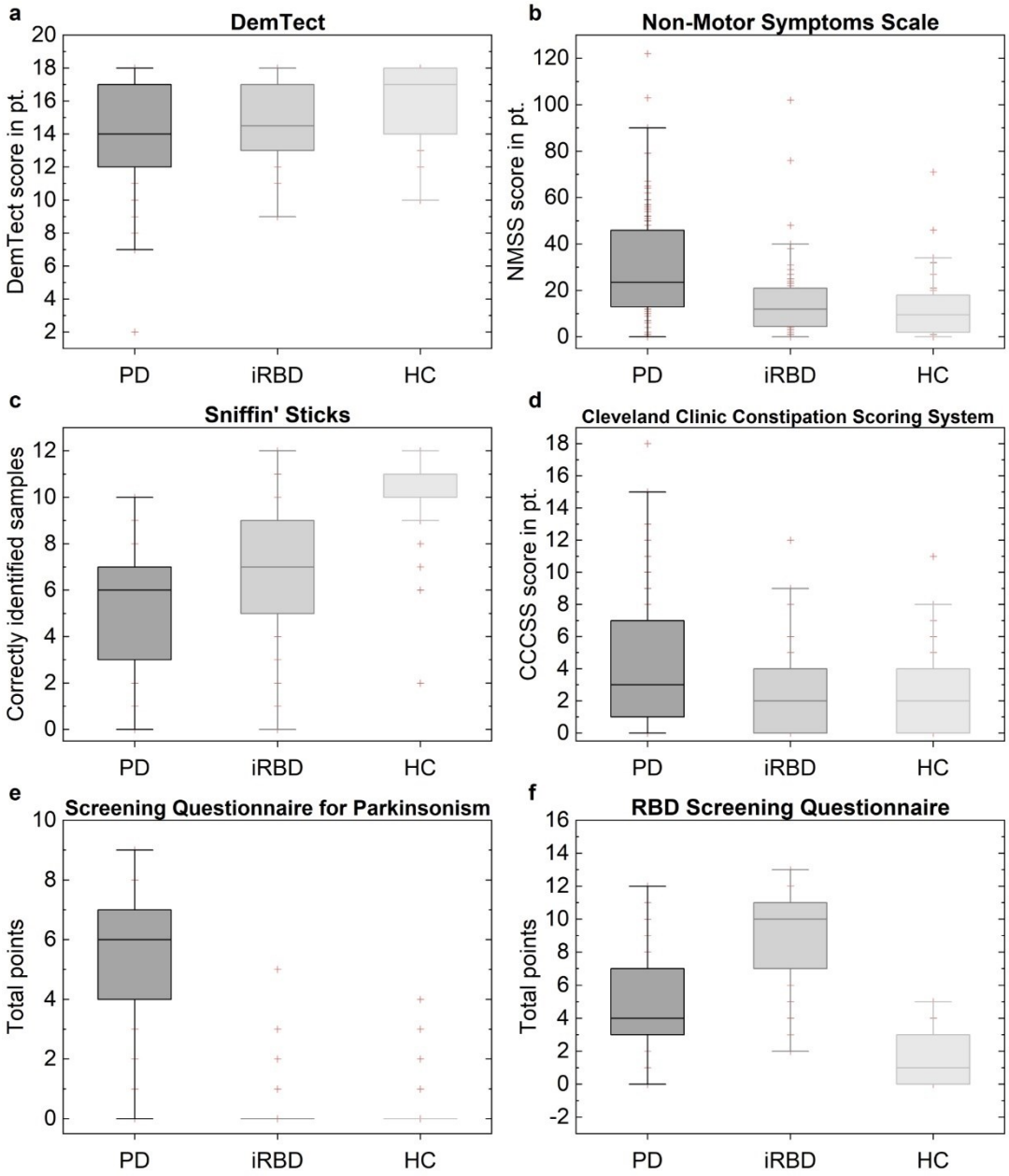

Supplementary Fig. 1 Results for PD and iRBD patients and healthy controls based on their performance in various tests and screening questionnaires.

a The DemTect score showed that the cognitive performance of healthy controls (15.9 ± 2.3) was significantly higher than that of PD (13.8 ± 3.3, $p < 0.001$) and iRBD patients (14.8 ± 2.3, $p = 0.020$). **b** Based on the Non-Motor Symptoms Scale (NMSS), the performance of PD patients was significantly worse than that of iRBD patients (30.6 ± 23.1 vs. 16.2 ± 18.0, $p < 0.001$) and healthy controls (12.5 ± 14.4, $p < 0.001$). **c** Also, the olfactory performance of PD patients (5.3 ± 2.6) was significantly worse ($p < 0.01$) than that of iRBD patients (6.6 ± 2.7) and healthy controls (10.4 ± 1.7), based on correctly

identified sniffin' sticks. **d** Based on the Cleveland Clinic Constipation Scoring System (CCCSS), PD patients (4.1 ± 4.0) were significantly more ($p < 0.05$) constipated than iRBD patients (2.8 ± 2.7) and healthy controls (2.5 ± 2.5). **e** PD patients (5.6 ± 2.2) scored significantly higher ($p < 0.001$) than iRBD patients (0.3 ± 0.8) and healthy controls (0.3 ± 0.8) on the Screening Questionnaire for Parkinsonism. **f** The RBD Screening Questionnaire (RBDSQ) revealed significant differences ($p < 0.001$) between iRBD (9.0 ± 2.7) and PD patients (4.9 ± 3.0) or healthy controls (1.7 ± 1.6), and between PD patients and healthy controls.

Supplementary Table 2 The coefficient of variation of each experiment for α-synuclein SiNaPs and stool samples

	Coefficient of variation [%]	
Experiment	α-synuclein SiNaPs	Stool samples
1	27.22	40.53
2	16.74	25.32
3	17.41	19.34
4	37.19	27.92
5	33.25	22.12
6	25.32	22.11
7	33.05	28.82
8	28.50	25.50
9	36.98	25.31
Mean	28.41	26.33

Supplementary Table 3 LOD values for α-synuclein SiNaPs for each experiment

Experiment	LOD [fM]
1	0.06
2	–
3	0.05
4	0.72
5	0.15
6	0.11
7	0.22
8	0.69
9	0.43
Mean	0.30

LOD, limit of detection

Supplementary Table 4 Number of stool samples above the LOD for each individual experiment

Experiment	Number of samples measured / number of samples above the LOD
1	27 / 27
2	27 / 27
3	24 / 24
4	27 / 27
5	26 / 26
6	26 / 26
7	26 / 26
8	25 / 25
9	9 /9
Sum	**217 / 217**

LOD, limit of detection

Supplementary Table 5 P-values of tests on normal distribution for α-synuclein aggregate concentrations in stool

	PD	iRBD	HC
Shapiro Wilk	0	0	$2.0*10^{-12}$
Lilliefors	$3.5*10^{-39}$	$5.4*10^{-59}$	$5.1*10^{-15}$
Kolmogorov Smirnov	$6.0*10^{-13}$	$1.7*10^{-19}$	$2.5*10^{-5}$
Anderson Darling	$3.7*10^{-54}$	$9.7*10^{-61}$	$1.2*10^{-21}$

PD, Parkinson's disease; iRBD, isolated rapid eye movement sleep behavior disorder; HC, healthy control

Supplementary Table 6 Spearman coefficient of correlation for α-synuclein aggregate concentrations in stool and age, education, sex, DemTect score, disease duration, MDS-UPDRS III, or questionnaires for PD or iRBD

	All cohorts	PD	iRBD	HC
Age	0.183*	0.125	0.155	0.195
Education	0.041	0.088	0.124	−0.187
Sex	0.008	0.007	−0.074	0.202
DemTect	0.074	0.221*	−0.166	−0.140
Disease duration	−0.050	−0.003	0.069	N/A
MDS-UPDRS III	−0.282*	−0.0004	−0.210	N/A
Screening questionnaire for parkinsonism	−0.154*	0.057	0.031	0.066
RBDSQ	0.188*	0.223*	−0.020	−0.054

PD, Parkinson's disease; iRBD, isolated rapid eye movement sleep behavior disorder; HC, healthy control; MDS-UPDRS, Movement Disorder Society's Unified Parkinson's Disease Rating Scale Part III; N/A, not applicable; RBDSQ, REM sleep behavior disorder screening questionnaire; * $p < 0.05$

7.7 Development and Implementation of an Internal Quality Control Sample to Standardize Oligomer-Based Diagnostics of Alzheimer's Disease

Autoren:	Marlene Pils, Alexandra Dybala, Fabian Rehn, Lara Blömeke, Tuyen Bujnicki, Victoria Kraemer-Schulien, Wolfgang Hoyer, Detlev Riesner, Dieter Willbold und Oliver Bannach
Journal:	Diagnostics (veröffentlicht)
DOI:	10.3390/diagnostics13101702
Impact-Faktor:	3,6 (2022)
Beitrag:	Eigenanteil: 10 % Etablierung des Aggregationsprotokolls Diskussion der Ergebnisse Prüfung des Manuskripts

Development and Implementation of an Internal Quality Control Sample to Standardize Oligomer-Based Diagnostics of Alzheimer's Disease

Supplementary Material

Marlene Pils, Alexandra Dybala, Fabian Rehn, Lara Blömeke, Tuyen Bujnicki, Victoria Kraemer-Schulien, Wolfgang Hoyer, Detlev Riesner, Dieter Willbold and Oliver Bannach

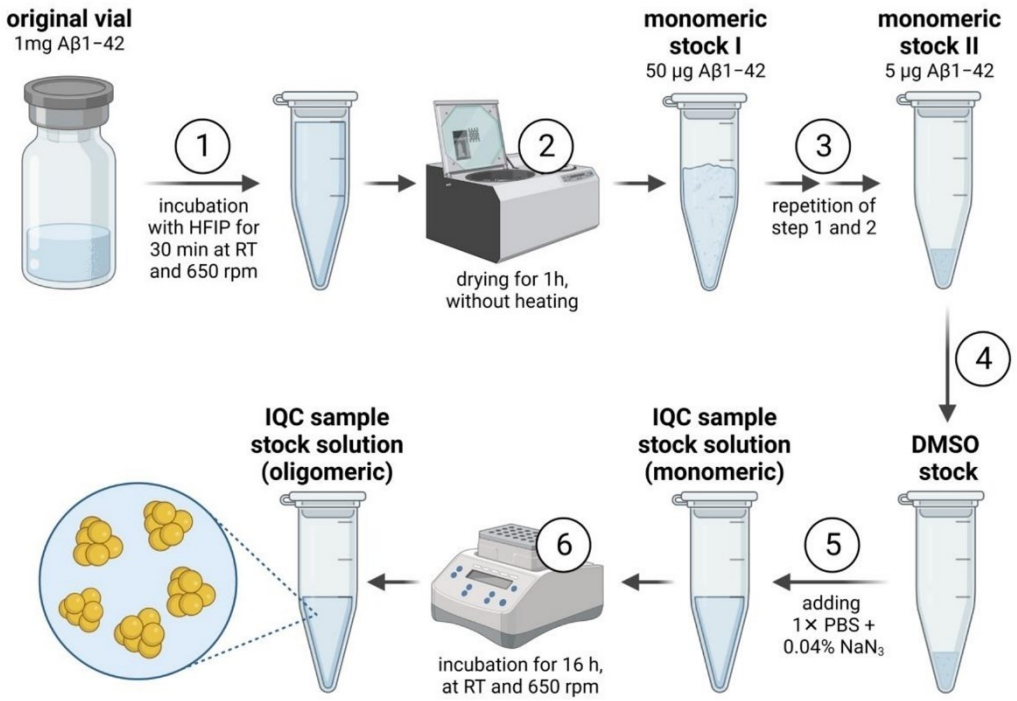

Figure S1. Scheme of monomerization and oligomerization procedure. Step 1: 1 mg Aβ1−42 is dissolved 550 µl HFIP for 1 h at RT with mixing at 650 rpm. The original sample tube is rinsed with an additional 550 µl HFIP, and the combined sample is divided into twenty aliquots containing 50 µg Aβ1−42. Step 2: aliquots are transferred to a SpeedVac and dried for ~1 h without heating until all HFIP and H_2O are removed. Step 3: the initial amount of Aβ1−42 is reduced by dissolving 50 µg Aβ1−42 with 550 µl HFIP and dividing this sample into ten aliquots containing 5 µg Aβ1−42. These aliquots are dried using a SpeedVac. Step 4: for oligomerization, 5 µg Aβ1−42 is dissolved in 5 µl DMSO, mixed briefly, centrifuged, and agitated for 10 min at RT and 650 rpm. Step 5: An IQC stock solution is prepared by adding 1× PBS containing 0.04% NaN_3. Step 6: the monomeric solution is mixed briefly, centrifuged and agitated for 16 h at 650 rpm and RT to promote oligomerization. Abbreviations: Aβ, amyloid-β; DMSO, dimethyl sulfoxide; HFIP, 1,1,1,3,3,3-hexafluoro-2-propanol; IQC, internal quality control; NaN_3, sodium azide; PBS, phosphate-buffered saline; RT, room temperature. Created with Biorender.com (accessed on 10 May 2023).

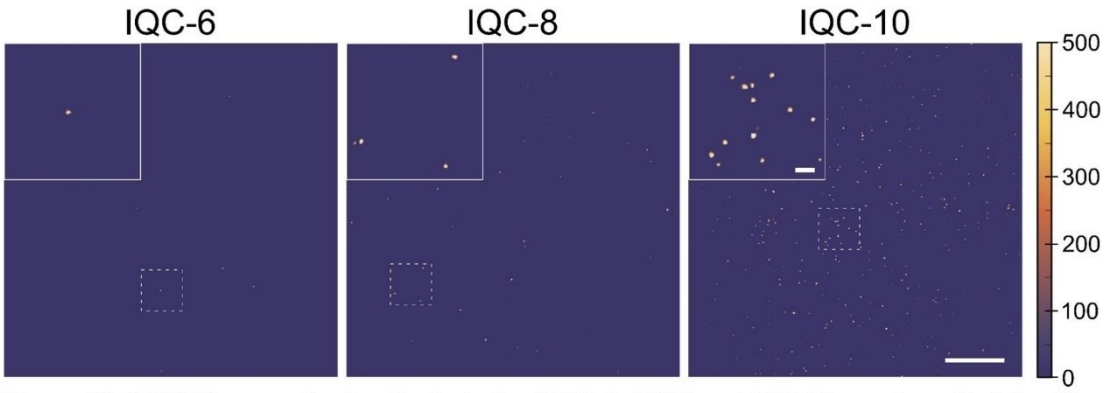

Figure S2. TIRFM-images of colocalized pixels of IQC-6, IQC-8 and IQC-10 samples with intensities above the blank control-based cutoff. The colocalized TIRFM images were created using a multi-step process. First, a global cutoff value was selected for each channel based on the blank control (0.05%). Only signals exceeding this value were considered in the consecutive analysis, enabling a distinction between signals and background noise, thereby increasing the measurement accuracy. In the next step, the matrices of both channels, representing the same area of a well, were used to create two supportive matrices. A binary matrix was generated that contains a one for all pixels whose intensity in both channel matrices is above the respective cutoff and a zero otherwise. The second matrix was the product of both channel matrices, which was scaled to the original range of values by dividing through by the maximum possible intensity value. The cutoffs were considered by multiplying the two generated supportive matrices, and the colocalization matrix for a distinct area of the well was created. For each image, a section was selected and enlarged (10×) to demonstrate differences in particle concentrations among the tested IQC samples. The color scaling was created using matlab2019b, where all pixels with an intensity equal to or higher than 500 were colored yellow. Scale bar image: 20 µm; scale bar enlarged image: 2 µm. Abbreviations: IQC, internal quality control; TIRFM, total internal reflection fluorescence microscopy.

Table S1. Individual sFIDA readouts, calibrated molar particle concentrations and CV% for each IQC sample. sFIDA readouts of each IQC sample were converted into femtomolar concentrations using the linear equation y = 5.08x – 0.25. Using the one-sided Mann-Whitney U test with a confidence interval of 5%, the molar particle concentrations of IQC samples that differed significantly from the next lower concentration were determined (marked green), and thus the lower limit of quantification (LLoQ, italic, *) and upper limit of quantification (ULoQ, italic, **) were identified. Observed sFIDA readouts are presented as the means of four replicates.

IQC sample	Monomer concentration [pM]	sFIDA readout	Particle concentration [fM]	CV%	One-sided Mann-Whitney U test *p*-value
IQC-1	0.01	0.7	0.18	61.3	0.1252
IQC-2	0.03	0.9	0.22	68.8	0.3429
IQC-3	0.1	1.6	0.36	73.3	*0.1714**
IQC-4	0.3	4.7	0.98	16.4	0.0286
IQC-5	1.0	15	3.0	15.7	0.0286
IQC-6	3.2	52	10.3	13.8	0.0143
IQC-7	10	130	25.7	24.1	0.0143
IQC-8	31.6	409	80.6	7.3	0.0143
IQC-9	100	1253	247	4.6	0.0143
IQC-10	316	4701	925	16.2	0.0143
IQC-11	1000	35,723	7031	7.7	0.0143
IQC-12	3162	351,702	69,219	23.3	0.0143
IQC-13	10,000	997,783	196,375	0.2	0.0143
IQC-14	31,622	1,000,000	196,812	0	*0.0143***
IQC-15	100,000	1,000,000	196,812	0	1

*LLoQ, ** ULoQ

Table S2. Calculation of the dilution linearity of Aβ oligomer-based internal quality control (IQC) samples within the working range. Data are presented as the means of four replicates. Molar particle concentrations were background corrected, and the percent dilution linearity of each IQC sample was calculated according to Equation (3). In addition, the average of all IQC samples (mean) was calculated. *IQC-14 was excluded from the analysis. Tolerance range: 80–120%.

IQC sample	Particle concentration [fM]	Particle concentration after background correction [fM]	Linearity [%]
IQC-3	0.36	0.22	84
IQC-4	0.98	0.84	93
IQC-5	3.0	2.9	89
IQC-6	10.3	10.2	126
IQC-7	25.7	25.5	100
IQC-8	80.6	80.5	103
IQC-9	247	247	84
IQC-10	925	925	42
IQC-11	7031	7031	32
IQC-12	69,219	69,219	111
IQC-13	196,375	196,375	316
IQC-14	196,812	196,812	316
		Mean	**107 | 109***
		Coefficient of determination	**0.73 | 0.99***

Table S3. Selectivity and recovery of the sFIDA assay to IQC-13. (**a**) sFIDA readouts of the IQC-13 sample were applied on different assay control setups, and the calculated percentage signal reduction was compared to the standard assay setup (normal). (**b**) Investigation of monomeric interference. (**c**) Influence of matrix effects on sFIDA readouts of the IQC-13 sample spiked in buffer or bovine CSF. Observed sFIDA readouts are presented as the means of four replicates. Using the one-sided Mann-Whitney U test with a confidence interval of 5%, the sFIDA readout of the respective assay control was compared to the readout of the standard assay setup. Abbreviations: CSF, cerebrospinal fluid; IQC, internal quality control.

(a)

Assay control setup	Observed sFIDA readout	Signal reduction [%]	One-sided Mann-Whitney U test *p*-value
Normal	941,271	-	-
Capture Control (CC)	37.27	100	0.0152
Autofluorescence control (AF)	0.77	100	0.0147
Cross-reactivity anti-Tau antibodies (Tau)	0.67	100	0.0152

(b)

Assay control setup	Observed sFIDA readout	Signal reduction [%]	One-sided Mann-Whitney U test *p*-value
Normal	941,271	-	-
Monomer control	15,231	98.38	0.0152

(c)

Assay control setup		Observed sFIDA readout	Signal reduction [%]	One-sided Mann-Whitney U test *p*-value	Signal-to-noise ratio IQC/blank
Blank	buffer	0.45	66.67	-	-
	CSF	0.15		0.002	-
Blank + IQC-13	buffer	997,783	0.21	-	2,217,295
	CSF	995,639		0.108	6,637,597

Table S4. Raw data used to generate Shewhart charts in Figure 5. Listed are the calibrated particle concentrations of 20 observations of each applied internal quality control (IQC) sample (IQC-6, IQC-8 and IQC-10) and the determined intra-assay variance described as CV%. The respective values were used to calculate the mean, standard deviation (SD) and upper/lower control (UCL/LCL) and action limits (UAL/LAL). Data from each observation represent the mean of four replicates.

	IQC-6		IQC-8		IQC-10	
Observation	**Particle concentration [fM]**	**CV%**	**Particle concentration [fM]**	**CV%**	**Particle concentration [fM]**	**CV%**
1	6.8	3.4	71.3	16.2	1397.7	24.2
2	11.1	18.5	106.8	19.9	1463.0	9.6
3	9.6	33.9	122.5	15.5	1585.6	16.5
4	11.6	10.2	116.3	24.4	1593.7	11.8
5	11.2	14.7	119.8	17.0	1638.6	20.3
6	7.6	36.2	81.4	20.8	1421.9	24.3
7	9.8	14.1	106.7	20.4	1439.7	22.6
8	9.0	11.0	110.1	15.3	1340.8	9.5
9	7.6	15.7	79.3	17.8	1276.4	20.6
10	8.4	22.9	100.7	27.6	1571.9	16.4
11	9.3	14.4	71.7	4.3	1309.4	11.8
12	8.8	29.6	104.3	25.1	1295.2	5.6
13	8.4	8.5	115.8	8.5	1520.7	32.0
14	9.5	8.4	142.3	7.9	1579.4	21.0
15	8.0	9.9	123.6	13.8	1476.9	21.9
16	6.1	8.7	103.1	18.8	1661.7	14.8
17	6.7	12.2	88.1	12.8	1356.5	12.6
18	6.8	19.5	111.2	14.2	1269.8	16.2
19	6.8	20.2	101.6	18.3	1064.7	10.8
20	6.4	12.1	130.3	10.6	1592.7	28.8
Mean	**8.5**		**105**		**1443**	
SD	**1.7**		**19**		**155**	
UCL	**11.8**		**144**		**1752**	
LCL	**5.1**		**67**		**1133**	
UAL	**13.5**		**163**		**1907**	
LAL	**3.5**		**48**		**978**	